frontiers | Research Topics

Protein lipidation in health and disease

Edited by
Rebeca M. Mejias Estevez and William Fuller

Published in
Frontiers in Physiology

ISSN 1664-8714
ISBN 978-2-8325-3912-5
DOI 10.3389/978-2-8325-3912-5

About Frontiers

Frontiers is more than just an open access publisher of scholarly articles: it is a pioneering approach to the world of academia, radically improving the way scholarly research is managed. The grand vision of Frontiers is a world where all people have an equal opportunity to seek, share and generate knowledge. Frontiers provides immediate and permanent online open access to all its publications, but this alone is not enough to realize our grand goals.

Frontiers journal series

The Frontiers journal series is a multi-tier and interdisciplinary set of open-access, online journals, promising a paradigm shift from the current review, selection and dissemination processes in academic publishing. All Frontiers journals are driven by researchers for researchers; therefore, they constitute a service to the scholarly community. At the same time, the *Frontiers journal series* operates on a revolutionary invention, the tiered publishing system, initially addressing specific communities of scholars, and gradually climbing up to broader public understanding, thus serving the interests of the lay society, too.

Dedication to quality

Each Frontiers article is a landmark of the highest quality, thanks to genuinely collaborative interactions between authors and review editors, who include some of the world's best academicians. Research must be certified by peers before entering a stream of knowledge that may eventually reach the public - and shape society; therefore, Frontiers only applies the most rigorous and unbiased reviews. Frontiers revolutionizes research publishing by freely delivering the most outstanding research, evaluated with no bias from both the academic and social point of view. By applying the most advanced information technologies, Frontiers is catapulting scholarly publishing into a new generation.

What are Frontiers Research Topics?

Frontiers Research Topics are very popular trademarks of the *Frontiers journals series*: they are collections of at least ten articles, all centered on a particular subject. With their unique mix of varied contributions from Original Research to Review Articles, Frontiers Research Topics unify the most influential researchers, the latest key findings and historical advances in a hot research area.

Find out more on how to host your own Frontiers Research Topic or contribute to one as an author by contacting the Frontiers editorial office: frontiersin.org/about/contact

Protein lipidation in health and disease

Topic editors

Rebeca M. Mejias Estevez — Sevilla University, Spain

William Fuller — University of Glasgow, United Kingdom

Citation

Estevez, R. M. M., Fuller, W., eds. (2023). *Protein lipidation in health and disease*. Lausanne: Frontiers Media SA. doi: 10.3389/978-2-8325-3912-5

Table of contents

frontiers | Frontiers in Physiology

TYPE Editorial
PUBLISHED 30 October 2023
DOI 10.3389/fphys.2023.1317031

OPEN ACCESS

EDITED AND REVIEWED BY
Nada A. Abumrad,
Washington University in St. Louis,
United States

*CORRESPONDENCE
William Fuller,
will.fuller@glasgow.ac.uk
Rebeca Mejías,
rmejias@us.es

RECEIVED 10 October 2023
ACCEPTED 20 October 2023
PUBLISHED 30 October 2023

CITATION
Fuller W and Mejías R (2023), Editorial: Protein lipidation in health and disease. *Front. Physiol.* 14:1317031.
doi: 10.3389/fphys.2023.1317031

Editorial: Protein lipidation in health and disease

William Fuller[1]* and Rebeca Mejías[2,3]*

[1]Institute of Cardiovascular and Medical Sciences, University of Glasgow, Glasgow, United Kingdom, [2]Department of Physiology, School of Biology, Universidad de Sevilla, Seville, Spain, [3]Instituto de Biomedicina de Sevilla-IBiS, Hospital Universitario Virgen Del Rocío, Consejo Superior de Investigaciones Científicas, Universidad de Sevilla, Seville, Spain

KEYWORDS

palmitoylation, lipidation, post-translational modifications, human pathologies, palmitoyl acyltransferase (PAT)

Editorial on the Research Topic
Protein lipidation in health and disease

Protein lipidation, the attachment of lipids to proteins, influences how proteins fold, their stability, trafficking, interaction with other proteins, and association with specific domains on cellular membranes. Various types of lipids, such as phospholipids, isoprenoids, fatty acids, cholesterol, GPI (glycosylphosphatidylinositol)-anchors, and LDEs (lipid-derived electrophiles), modify proteins covalently. S-palmitoylation or S-acylation is a reversible type of lipidation where a fatty acid called palmitate attaches to specific cysteine residues through a labile thioester bond. N-palmitoylation (via a stable amine bond) and O-palmitoylation (via a stable ester bond) are less common and irreversible kinds of palmitoylation (Chen et al., 2018). S-palmitoylation (called palmitoylation for simplicity in this editorial) is catalysed in mammals by a family of 23–24 proteins called palmitoyl acyltransferases (zDHHC-PATs), and de-acylation is mediated by α/β serine hydrolases and thioesterases, including APT1 (acyl-protein thiosterase 1) and ABHD17 thioesterases, among others (Zhou et al., 2023). Additionally, several PAT-interacting proteins have been identified that regulate their function and localization (Salaun et al., 2020).

The objective of this Research Topic is to compile the most recent insights on the impact of protein lipidation on protein function and explore how alterations in these modifications are linked to the pathophysiology of human diseases, paving the way for the development of novel therapeutic strategies.

One important feature of many post-translational modifications (PTMs) is how they can be regulated by gene-splicing variants. For example, the splice variant of the AMPA scaffolding protein GRIP1, GRIP1b, can be palmitoylated, whereas GRIP1a cannot, affecting its subcellular distribution (Hanley and Henley, 2010). In this line, Wirth and Ponimaskin review the literature describing that the small GTPase Cdc42 splice variant which is palmitoylated (Cdc42-palm) is mainly expressed in the brain, in contrast to its prenylated ubiquitous form (Cdc42-prenyl). It would be interesting to further explore in the future whether these are anecdotal cases or whether the regulation of splice variants and protein isoforms are more widespread modulators of protein palmitoylation.

Recent studies have revealed that numerous immune-associated proteins undergo S-palmitoylation. These findings have shed light on the vital roles played by palmitoylation in immune function, particularly in directing immune signalling proteins to the membrane and lipid rafts. Furthermore, alterations in PAT activity and variations in

palmitoylation have been linked to human immunological disorders (Zhang et al., 2021). To strengthen the functional importance of lipidation in the immune system, Wirth and Ponimaskin discuss the possible association between aberrant palmitoylation of Cdc42 and activation of inflammatory responses and autoinflammatory diseases. Furthermore, West et al. introduce PATs as novel regulators of T-cell function in their literature review. For example, zDHHC7 and zDHHC21 have been shown to be critical for T-helper cells differentiation, and key proteins in T-cell signalling such as CD4 and CD8 are palmitoylated. Despite these advances, the role of lipidation in the immune system remains mostly unknown.

Diverse findings point to a complex interrelationship of palmitoylation and other PTMs such as phosphorylation, S-nitrosylation, acetylation and ubiquitination. Thus, for example, palmitoylation may inhibit, compete with, or facilitate another PTM, and palmitoylation/depalmitoylation can also regulate subsequent phosphorylation of certain substrates [reviewed by (Ramzan et al.)]. In the future it will be pivotal to further investigate the crosstalk between lipidation and other PTMs to understand the consequences for protein localization and function, as well as the impact on organelle function.

A fundamental limitation in the lipidation field, is the limited availability of assays to assess palmitoylation. Schek et al. describe a methodological advance for detecting palmitoylated proteins on paraffin-embedded samples. This approach could provide important insights into the role of palmitoylation in the pathology of human diseases and be extended to detect additional PTMs. An additional drawback has been the relatively unexplored pattern of expression of different PATs and their interacting/regulatory proteins. To address this, Wild et al. have generated databases of the expression of palmitoylation and depalmitoylation enzymes, and accessory proteins, in mouse brain (BrainPalmSeq) (Wild et al., 2022) and human cell types (CellPalmSeq). These tools will help both clinicians and researchers to interrogate the implications of palmitoylation in physiology and pathology. CellPalmSeq, described in this Research Topic, is an important resource that will support the field to select the most appropriate cellular models to interrogate how palmitoylation regulates pathways and individual proteins.

Dysregulation of lipid metabolism and protein lipidation is associated with different pathologies, but understanding the underlying molecular mechanisms remains a challenge. This is partly due to limited knowledge regarding how lipidation and its regulating enzymes are controlled by cellular signalling pathways. While lipidation-targeted therapies are being investigated for cancer treatment, for example, their application to other diseases is still largely unexplored. Furthermore, while certain forms of protein lipidation, like S-palmitoylation, have garnered substantial attention in recent years, others, such as N-palmitoylation, remain relatively unexplored. Therefore, it is crucial to advance the knowledge of the regulatory mechanisms that control lipidation, the interplay between lipidation and other post-translational modifications, methodologies to detect, measure, and manipulate protein lipidation, the interplay between lipid metabolism and protein lipidation, and less common or studied varieties of lipidation. Besides, it is worth to highlight the importance of prioritising studies investigating putative sex difference in palmitoylation (Ramzan et al.) and palmitoylation-independent functions of PATs in future studies.

The contribution of aberrant palmitoylation to development of human pathologies is an important consideration for this field. This Research Topic gives a broad overview of the importance of these PTMs in neurodegeneration, X-linked intellectual disability, metabolic disease, cancer, and cardiac pathologies (Lemarié et al.; Main et al.; Nguyen et al.; Pierce and Hougland; Ramzan et al.). Main et al. used publicly-available RNA-seq datasets from patients with heart failure to evaluate how palmitoylation and depalmitoylation pathways remodel in these patients as well as in animal models and clinical biopsies. A complex picture emerges in which the surface-membrane acyl transferase zDHHC5 expression increases significantly during early remodeling but declines once heart failure is established. These expression changes correlate very poorly with substrate palmitoylation, highlighting the continuing paucity in our understanding of how zDHHC-PAT activity is controlled.

With this in mind, the findings of Nguyen et al. that several zDHHC-PATs are stabilised by accessory proteins, is important for the field. Although zDHHC20, the first zDHHC enzyme to be crystallized is clearly functional without such a partner, Nguyen et al. find that zDHHCs 5, 8, 9, 14, and 18 (but not 3 and 20) can be stabilized by GCP16 to support enhanced enzymatic activity. This suggests an additional layer of control for activity of some of these enzymes than has hitherto been under-appreciated. Clearly the expression level of the accessory protein, as well as the expression level of the enzyme itself, will be an important determinant of substrate palmitoylation.

Numerous ion transporters and channels in excitable tissues are regulated by palmitoylation. Congreve et al. focused on the cardiac voltage sensitive ion channel HCN4, which is expressed in the sino atrial node and cardiac conduction system, and has the unique property of being activated by hyperpolarization. HCN4 controls heart rate by controlling the rate of depolarization in nodal tissue, and its activity is significantly enhanced by palmitoylation of two cysteines in the channel's amino terminus. This raises the intriguing possibility that a fundamental feature of multicellular organisms, the heartbeat, is controlled by the coordinated activities of palmitoylating and depalmitoylating enzymes on a single ion channel.

The scaffolding protein ankyrin B, the small cousin of the giant ankyrin G, controls the localization of ion channels and transporters in numerous tissues. Gupta and Jenkins identified numerous palmitoylation sites in ankyrin B which are palmitoylated by zDHHC17. When ankyrin B is not palmitoylated it loses its ability to correctly localize voltage sensitive sodium channels to dendritic membranes, highlighting the importance of palmitoylation not only of ion channels but also of their targeting partners for the control of tissue excitability.

In the last 20 years, progress has been made in the study of regulatory mechanisms of palmitoylation, the role of this posttranslational modification in physiology and diseases, and the methodology for its study. However, there is still much research to be performed in these aspects and the interplay of the findings with the overall regulation of lipid metabolism in the organism.

Author contributions

WF: Conceptualization, Investigation, Writing–original draft, Writing–review and editing. RM: Conceptualization, Investigation, Writing–original draft, Writing–review and editing.

Funding

The author(s) declare that no financial support was received for the research, authorship, and/or publication of this article.

Acknowledgments

We thank the authors and reviewers who contributed to this Research Topic.

Conflict of interest

The authors declare that the research was conducted in the absence of any commercial or financial relationships that could be construed as a potential conflict of interest.

Publisher's note

References

Chen, B., Sun, Y., Niu, J., Jarugumilli, G. K., and Wu, X. (2018). Protein lipidation in cell signaling and diseases: function, regulation, and therapeutic opportunities. *Cell. Chem. Biol.* 25, 817–831. doi:10.1016/J.CHEMBIOL.2018.05.003

Hanley, L. J., and Henley, J. M. (2010). Differential roles of GRIP1a and GRIP1b in AMPA receptor trafficking. *Neurosci. Lett.* 485, 167–172. doi:10.1016/J.NEULET.2010.09.003

Salaun, C., Locatelli, C., Zmuda, F., González, J. C., and Chamberlain, L. H. (2020). Accessory proteins of the zDHHC family of S-acylation enzymes. *J. Cell. Sci.* 133, 251819. doi:10.1242/JCS.251819

Wild, A. R., Hogg, P. W., Flibotte, S., Nasseri, G., Hollman, R., Abazari, D., et al. (2022). Exploring the expression patterns of palmitoylating and de-palmitoylating enzymes in the mouse brain using the curated RNA-seq database BrainPalmSeq. *Elife* 11, 75804. doi:10.7554/ELIFE.75804

Zhang, Y., Qin, Z., Sun, W., Chu, F., and Zhou, F. (2021). Function of protein S-palmitoylation in immunity and immune-related diseases. *Front. Immunol.* 12, 661202. doi:10.3389/FIMMU.2021.661202

Zhou, B., Hao, Q., Liang, Y., and Kong, E. (2023). Protein palmitoylation in cancer: molecular functions and therapeutic potential. *Mol. Oncol.* 17, 3–26. doi:10.1002/1878-0261.13308

frontiers | Frontiers in Physiology

TYPE Original Research
PUBLISHED 05 October 2022
DOI 10.3389/fphys.2022.1023237

OPEN ACCESS

EDITED BY
Vincenza Cifarelli,
Saint Louis University, United States

REVIEWED BY
Paul M. Jenkins,
University of Michigan, United States
Matthew J. Brody,
University of Michigan, United States

*CORRESPONDENCE
William Fuller,
will.fuller@glasgow.ac.uk

SPECIALTY SECTION
This article was submitted to Lipid and Fatty Acid Research, a section of the journal Frontiers in Physiology

RECEIVED 19 August 2022
ACCEPTED 20 September 2022
PUBLISHED 05 October 2022

CITATION
Main A, Boguslavskyi A, Howie J, Kuo C-W, Rankin A, Burton FL, Smith GL, Hajjar R, Baillie GS, Campbell KS, Shattock MJ and Fuller W (2022), Dynamic but discordant alterations in zDHHC5 expression and palmitoylation of its substrates in cardiac pathologies. *Front. Physiol.* 13:1023237. doi: 10.3389/fphys.2022.1023237

Dynamic but discordant alterations in zDHHC5 expression and palmitoylation of its substrates in cardiac pathologies

Alice Main[1], Andri Boguslavskyi[2], Jacqueline Howie[1], Chien-Wen Kuo[1], Aileen Rankin[1], Francis L. Burton[1], Godfrey L. Smith[1], Roger Hajjar[3], George S. Baillie[1], Kenneth S. Campbell[4], Michael J. Shattock[2] and William Fuller[1]*

[1]Institute of Cardiovascular and Medical Sciences, University of Glasgow, Glasgow, United Kingdom, [2]School of Cardiovascular and Metabolic Medicine and Sciences, King's College London, London, United Kingdom, [3]Flagship Pioneering, Cambridge, MA, United States, [4]Division of Cardiovascular Medicine, University of Kentucky, Lexington, KY, United States

S-palmitoylation is an essential lipid modification catalysed by zDHHC-palmitoyl acyltransferases that regulates the localisation and activity of substrates in every class of protein and tissue investigated to date. In the heart, S-palmitoylation regulates sodium-calcium exchanger (NCX1) inactivation, phospholemman (PLM) inhibition of the Na^+/K^+ ATPase, Nav1.5 influence on membrane excitability and membrane localisation of heterotrimeric G-proteins. The cell surface localised enzyme zDHHC5 palmitoylates NCX1 and PLM and is implicated in injury during anoxia/reperfusion. Little is known about how palmitoylation remodels in cardiac diseases. We investigated expression of zDHHC5 in animal models of left ventricular hypertrophy (LVH) and heart failure (HF), along with HF tissue from humans. zDHHC5 expression increased rapidly during onset of LVH, whilst HF was associated with decreased zDHHC5 expression. Paradoxically, palmitoylation of the zDHHC5 substrate NCX1 was significantly reduced in LVH but increased in human HF, while palmitoylation of the zDHHC5 substrate PLM was unchanged in all settings. Overexpression of zDHHC5 in rabbit ventricular cardiomyocytes did not alter palmitoylation of its substrates or overall cardiomyocyte contractility, suggesting changes in zDHHC5 expression in disease may not be a primary driver of pathology. zDHHC5 itself is regulated by post-translational modifications, including palmitoylation in its C-terminal tail. We found that in HF palmitoylation of zDHHC5 changed in the same manner as palmitoylation of NCX1, suggesting additional regulatory mechanisms may be involved. This study provides novel evidence that palmitoylation of cardiac substrates is altered in the setting of HF, and that expression of zDHHC5 is dysregulated in both hypertrophy and HF.

KEYWORDS

palmitoylation, hypertrophy, heart failure, ZDHHC5, cardiac muscle, depalmitoylation, ion transporter

Introduction

Heart failure (HF) represents a major economic and global burden affecting over 26 million people worldwide, with ~3.6 million patients newly diagnosed every year (Ambrosy et al., 2014; Simmonds et al., 2020). All clinical therapies currently aim to reduce myocardial demand by either reducing peripheral resistance and pre-load [i.e., angiotensin-converting enzyme inhibitors (ACEi)] or ventricular after-load and remodelling (i.e., β-blockers; Shah A. et al., 2017). This largely helps to compensate for reduced ejection fraction and systolic dysfunction [as seen in HF with reduced ejection fraction (HFrEF)] and is therefore more effective for management of HFrEF than for HF with preserved ejection fraction (HFpEF). However, even though improved therapeutic recommendations for HFrEF significantly reduce morbidity and mortality rates in clinical trials, prognosis is still poor in this group with a trial of 40,000 hospitalised HF patients demonstrating a 5-year mortality rate of 75%, independent of LVEF (McMurray et al., 2014; Shah K. S. et al., 2017). As such, there remains a pressing and largely unmet clinical need for HF therapies.

Understanding the molecular basis of HF, in both humans and animal models, is essential to developing and directing appropriate therapies. However, this task is complicated by the fact that compensatory cardiac hypertrophy, leading to normal or even enhanced systolic function and left ventricular (LV) enlargement, often precedes decompensated HF and eventual LV dilatation and dysfunction (Kemp and Conte, 2012). The biochemical and molecular changes in both these phases of the disease are distinct, and currently available animal models are often better at modelling hypertrophy than the complex clinical syndrome of HF (Houser et al., 2012). Interestingly, a key component of cardiac dysfunction associated with both cardiac hypertrophy and HF is the dysregulation in expression, modification and function of proteins involved in excitation contraction coupling (ECC). Many of the pathological changes in protein function in ECC during cardiac disease can be attributed to changes in post-translational modification (PTM) regulation, including phosphorylation (Ramila et al., 2015; Sequeira and Maack, 2018) and redox modifications like S-glutathionylation (Pastore and Piemonte, 2013). The majority of proteins involved in ECC have been reported to be regulated by the lipid post-translational modification palmitoylation (see review by Essandoh et al., 2020) with recent proteomic analysis suggesting over 450 cardiac proteins are palmitoylated (Miles et al., 2021). Palmitoylation is a reversible modification involving the attachment of a fatty acid (most commonly palmitoyl derived from palmitoyl-CoA) to the thiol of a cysteine residue. This has a wide range of physiological effects, including regulating the location of the palmitoylated substrate, altering its conformation and consequently activity, or regulating protein-protein interactions. The modification is catalysed by a group of structurally related zDHHC-palmitoyl acyltransferases (zDHHC-PATs) which are integral membrane proteins located throughout the secretory pathway (Main and Fuller, 2021).

Although important in regulating ECC substrate activity, the role of palmitoylation in cardiac disease and HF remains largely unknown. There have been limited studies conducted in zDHHC knock-out animals, but zDHHCs show redundancy and therefore determining individual enzyme characteristics *via* this route is challenging (Main and Fuller, 2021). The most well characterised cardiac zDHHC-PAT is cell surface localised zDHHC5 (see review by Woodley and Collins, 2021). NCX1 and Na^+/K^+ ATPase both interact with zDHHC5 after its fourth transmembrane domain, in a site that also interacts with its accessory proteins Golga7 and Golga7b (Ko et al., 2019; Plain et al., 2020; Woodley and Collins, 2021). zDHHC5 directly palmitoylates ECC substrates NCX1 and PLM (Howie et al., 2014; Gök et al., 2020). ZDHHC5 has attracted attention in cardiac physiology as it is a key contributor to massive endocytosis (MEND) of the cellular membrane in anoxia/reperfusion (A/R) injury, with zDHHC5 knock-out hearts showing enhanced functional recovery from A/R injury (Hilgemann et al., 2013; Lin et al., 2013). In the present study, we evaluated changes in zDHHC5 expression in animal models of left ventricular hypertrophy and heart failure, as well as in human ischaemic heart failure samples. We provide the evidence that palmitoylation of cardiac substrates is altered in the setting of HF, and that expression of zDHHC5 is dysregulated in both hypertrophy and HF.

Materials and methods

Human organ donor and ischaemic heart failure samples

Samples from organ donors (non-failing) and human heart failure patients were obtained from the Gill Cardiovascular Biorepository at the University of Kentucky, of which patients and families of organ donors provided written consent. All procedures were approved by the local IRB and details of the collection procedures have been published previously (Blair et al., 2016). The study conformed with the principles in the Declaration of Helsinki. Samples in this study were taken

from the ventricular endocardium of each heart with details in Supplementary Table S1.

Mouse model of cardiac hypertrophy induced by pressure overload

Ventricular hypertrophy was induced by pressure overload *via* aortic constriction in 6-week old C57BL/6J mice, as has been previously described (Boguslavskyi et al., 2014).

Porcine model of heart failure

Pigs were subjected to left anterior descending artery balloon occlusion to induce a myocardial infarction, as has been described previously (Tilemann et al., 2013). Tissue was harvested for molecular analysis after the development of heart failure (3 months post-MI) along with sham controls.

Ethical statement

Animals were handled in accordance with the UK Animals (Scientific Procedures) Act of 1986. All procedures were approved by the UK Home Office (PP7088535) and Glasgow University Ethics Review Committee. The animal studies were reviewed and approved by the Animal Welfare and Ethical Review Body, University of Glasgow and the Animal Welfare and Ethical Review Body, King's College London.

Rabbit model of myocardial infarction and heart failure

Adult male New Zealand White rabbits (12 weeks old, ~3–4 kg) were given premedication with 0.4 ml/kg intramuscular Hypnorm (fentanyl citrate, 0.315 mg/ml: fluanisone 10 mg/ml, Janssen Pharmaceuticals). Anaesthesia was induced with 0.25–0.5 mg/kg midazolam (Hypnovel, Roche) *via* a cannula in the marginal ear vein. Rabbits were intubated and ventilated using a Harvard small animal ventilator with a 1:1 mixture of nitrous oxide and oxygen containing 1% halothane at a tidal volume of 50 ml and a frequency of 40 min^{-1}. Preoperative antibiotic prophylaxis was given with 1 ml Amfipen (ampicillin 100 mg/ml, Mycofarm UK Ltd.) intramuscularly. A left thoracotomy was performed through the fourth intercostal space. Quinidine hydrochloride (10 mg/kg; Sigma Pharmaceuticals), a class IA antiarrhythmic (potassium channel blocker) was administered intravenously prior to coronary artery ligation to reduce the incidence of ventricular fibrillation. The marginal branch of the left circumflex coronary artery, which supplies most of the LV free wall, was ligated to produce an ischaemic area of 30%–40% of the LV (Nisbet et al., 2016). Animals were maintained for 8 weeks during which ischaemic cardiomyopathy developed (confirmed by echocardiography measurement) before cells were isolated for molecular analysis.

Rabbit cardiomyocyte isolation

Adult rabbit ventricular myocytes (ARVM) were isolated from male New Zealand white rabbits as previously described. Isolation of adult rabbit ventricular cardiomyocytes (ARVM) was completed as described previously (Kettlewell et al., 2013). Briefly, New Zealand White male rabbits (12 weeks old, ~3–4 kg) were euthanised with a terminal dose of sodium pentobarbital (100 mg/kg) with heparin (500IU), following which the heart was removed and retrogradely perfused on a Langendorff system. Enzymatic digestion of the tissue using a protease and collagenase solution occurred for ~15 min before heart was removed from the system and cut into sections (left atria, right atria, right ventricle, left ventricle and septal regions) and each was finely dissected in Krafte-Brühe solution. The mixture was then triturated and agitated for 10 min before filtering and the cell suspension was centrifuged manually for a minute before the pellet was re-suspended in fresh KB. For experiments, cells were stepped up to physiological calcium in modified Krebs-Henseleit solution, initially containing 100 μM of $CaCl_2$ and left to settle for before the process was repeated using 200 μM, 500 μM, 1 mM, and 1.8 mM concentrations of $CaCl_2$. Cells were then snap frozen and kept at -80°C or used for functional experiments.

Viral infection

Adenoviruses expressing zDHHC5 and zDHHS5 were produced in house using the AdEasy system (Agilent). Rabbit ARVM were infected for 18–24 h by adding virus directly to the culture medium.

Sucrose gradient fractionation

Rabbit cardiomyocytes were homogenised 18–24 h post-infection in 0.5 M Na_2CO_3 (pH11) containing Protease Inhibitor Cocktail Set III (1:1,000; #539134, Calbiochem). Samples were sonicated at 5 μm amplitude 3 times in 20 s on/off bursts. The cell lysates were then mixed with an equal volume of 90% sucrose in MES-buffered saline (MBS, 50 mM MES buffer with 1.5 M NaCl, pH 6.5) to make a 45% sucrose component, and 4 ml of this solution was then added to the bottom of a polypropylene centrifuge tube. To this, a layer of

4 ml 35% sucrose in MBS was added by slowly pipetting down the side of the tube, followed by an additional layer of 4 ml 5% sucrose in MBS in a similar fashion. The samples were then centrifuged in a Beckman Optima XL-80k Ultracentrifuge using a SW40.1Ti swinging bucket rotor at 39000RPM for 18 h at 4°C. Following centrifugation, twelve 1 ml fractions were removed from each centrifuge tube. Fractions 4-5 are reported to contain buoyant caveolae membranes where zDHHC5 and Caveolin-3 predominantly localise (Howie et al., 2014), therefore these were combined and the membranes pelleted at 100,000 g for 60 min, and pellet resuspended in SDS-PAGE loading buffer. The same method was used to combine non-caveolae membrane (fractions 8–12).

Acyl-resin assisted capture

Acyl-resin assisted capture was used to purify palmitoylated proteins in a sample and adapted from a method published previously (Forrester et al., 2011). Cultured and pelleted cells were lysed in blocking buffer containing 1% methyl methanethiosulfonate (MMTS) to methylate free cysteines. Proteins were then precipitated using acetone and the resulting pellet subsequently washed using 70% acetone to remove excess MMTS. The pellets were then re-suspended in binding buffer before a portion of the sample was taken (unfractionated sample, total protein). To the remaining solution, 250 mM NH_2OH [hydroxylamine (HA), pH 7.5] was added to hydrolyse thioester bonds, with the same concentration of sodium chloride (NaCl, pH 7.5) added in its place for negative control samples. The proteins with free cysteines were the purified using thiopropyl sepharose beads. Palmitoylation of substrates was determined by relative quantity in HA samples compared to unfractionated.

Immunoblotting

Standard western blotting was carried out using 6%–20% gradient gels. The primary antibodies used were as follows: zDHHC5 (1:1,000, Sigma, HPA014670), NCX1 (1:1,000, Swant, R3F1), PLM (FXYD1, 1:1,000, Abcam, ab76597), Flotillin-2 (1:1,000, BD Biosciences, 610383), Caveolin-3 (1:4,000, BD Biosciences, 610420), HA-tag (1:5,000, Roche, 11867423001). The secondary antibodies used were as follows: Rabbit anti-mouse HRP (1:2,000, Jackson ImmunoResearch 111-035-144), Goat anti-rabbit HRP (1:2,000, Jackson ImmunoResearch 315-035-003), Goat anti-rat HRP (1:2,000, Jackson ImmunoResearch, 313-035-003), Donkey anti-guinea pig (1:2,000, Jackson ImmunoResearch, 106-035-003).

Confocal microscopy

Cardiomyocytes on 16 mm glass coverslips were fixed with 4% paraformaldehyde (PFA) for 15 min at room temperature. Cells were permeabilised with 0.1% Triton-X100 in PBS for 10 min at room temperature before blocking with 3% BSA in PBS for at least 1 h. Coverslips were incubated with HA-tag primary antibody (1:200, Roche, 11867423001) in 0.1% BSA in PBS for 1 h before subsequent incubation with anti-rat Alexa Fluor 546 secondary antibody (1:400, Thermofisher, A-11081) for an additional hour. Coverslips were then mounted onto glass slides using Dako Fluorescence Mounting Medium with 1 µl/ml 4′,6-diamidino-2-phenylindole (DAPI). Cells were then visualised using a Zeiss LSM 510 META Confocal Microscope with a ×40 objective.

Contractility measurements

CellOPTIQ® is an *in vitro* system designed by Clyde Biosciences which allows measurements of contractility, voltage and calcium to be carried out in individual adult cardiomyocytes (Clyde Biosciences Ltd.; Glasgow, UK). Following culture and infection of cardiomyocytes for 18–24 h, cells were transferred to a modified Krebs-Henseleit solution containing 1.8 mM $CaCl_2$ and incubated at 37°C using a heated stage. Cells were paced using electrodes with 40 V pulses of 0.2 ms duration at a frequency of 2 Hz. Five second recordings at 100 fps were then taken of individual cells using a ×60 objective. Contractility recordings were analysed using an ImageJ Macro prepared by Dr Francis Burton which analyses the changes in sarcomere length as a measurement of cardiomyocyte contractility by determining the spatial frequency of the intensity profile of sarcomere bands over time. Each recording produced roughly 10 contractile peaks which were averaged to give one trace per cell which was analysed for contractility parameters of amplitude, time to up and down 90% of peak, contractile duration at 50% and 90% of peak and overall time to peak (Rocchetti et al., 2014).

Statistics

Statistical analysis was completed using GraphPad Prism (Version 7; California, United States) and was performed on groups with three biological replicates or more. For comparisons in data sets with more than two groups, a one-way analysis of variance (ANOVA) with a Sidak's or Dunnett's post-hoc test was used, with comparisons detailed in the figure legend. For comparisons of two groups, a paired or unpaired Student's *t*-test was used. All samples were tested for the presence of significant outliers (Rout's test). A probability of $p < 0.05$ was considered to be statistically significant.

Results

Remodelling of the cellular palmitoylation machinery in heart failure

There remains a pressing need to understand the gene and protein expression changes in the failing myocardium in HFpEF and HFrEF in order to tailor existing, and develop new, therapeutic options. Despite the knowledge that zDHHC5 is involved in A/R injury and regulates activity of several important cardiac substrates, the expression or activity of zDHHC5, or any other palmitoylating or depalmitoylating enzymes, has not been investigated in a HF setting. Recently, Hahn and Knotsdottier et al. completed a comprehensive study of RNA transcript changes in HFpEF and HFrEF compared to organ donor controls. To investigate the relevance of palmitoylation as a modification in heart failure, using the available data, we plotted the change in relative abundance in HFpEF and HFrEF compared to organ donor controls of all available palmitoylating enzymes (zDHHC-PATs), depalmitoylating enzymes (LYPLAs, PPTs and ABHDs), accessory proteins [Selenoprotein-K (Fredericks et al., 2017) and Golga7 (Ko et al., 2019)] and proteins involved in fatty acyl CoA production [acyl-CoA synthases (ACSL) and fatty acid synthase (FASN)]. Several of these were found to be both up and down regulated in the failing myocardium, although many to a modest extent, with some changes unique to one phenotype. This included zDHHC5 which was significantly reduced in HFpEF but not HFrEF. Fatty acid and fatty acyl CoA availability have recently emerged as regulators of protein palmitoylation (Main and Fuller, 2021). For example, acyl-CoA synthase (ACSL) isoforms physically associate with zDHHC5, and acyl-CoA synthase activity is required for insulin-induced palmitoylation of NCX1 (Plain et al., 2020; Gök et al., 2022). ACSLs 1 and 4 were significantly downregulated in both HFpEF and HFrEF, with significant changes in all other isoforms and fatty acid synthase in HFpEF only (Figure 1; Hahn et al., 2021).

zDHHC5 expression and substrate palmitoylation in cardiac hypertrophy

Cardiac hypertrophy and associated remodelling of the left ventricle precedes many forms of cardiac disease, including heart failure, and is recognised as a crucial step in its pathophysiology (Rame and Dries, 2007). Left ventricular hypertrophy (LVH) induced by pressure overload *via* aortic constriction ("banding") is commonly used to investigate early molecular changes associated with pathological remodelling. This mouse model (described in Boguslavskyi et al., 2014) displays a 50% increase in LV mass 2 weeks after banding the thoracic aorta and reduced ejection fraction 8 weeks after surgery. We investigated changes in zDHHC5 expression associated with the onset of LVH. Compared to sham operated control mice, zDHHC5 expression was modestly increased from the earliest timepoint investigated (3 days post-banding) and was significantly elevated 2-week and 8-week after surgery. Unexpectedly, whilst zDHHC5 expression was increased 8-week post injury, palmitoylation of zDHHC5 substrate NCX1 was significantly reduced, whilst palmitoylation of its substrate PLM remained unchanged (Figure 2).

As elevated zDHHC5 expression but paradoxically reduced levels of NCX1 palmitoylation were associated with the development of LVH, we investigated whether increasing zDHHC5 expression in cardiomyocytes could be directly contributing to the contractile dysfunction observed in this phenotype. We engineered adenoviruses expressing HA-tagged zDHHC5 and catalytically inactive zDHHS5, and infected adult rabbit ventricular cardiomyocytes, achieving dose dependent increases in zDHHC5 expression levels (Figure 3A). Confocal microscopy revealed localisation of HA-tagged zDHHC5 in intercalated discs, cell surface and perinuclear membrane, whilst sucrose gradient fractionation indicated that virally encoded HA-zDHHC5 localised to buoyant membranes prepared using sucrose gradients alongside Caveolin-3, in a similar manner to endogenous zDHHC5 (Howie et al., 2014; Supplementary Figure S1). Changes in contractile function were investigated using the CellOPTIQ® contractility system (Clyde Biosciences Ltd.), and contractility parameters measured by determining the spatial frequency of the intensity profile of sarcomere bands over time (Supplementary Figure S2; Rocchetti et al., 2014). Overexpression of zDHHC5 or zDHHS5 had no effect on contractile force (as determined by sarcomere shortening (Figure 3B) or on any other parameters of contractility (Supplementary Figure S3). Viral overexpression of zDHHC5 did not lead to changes in palmitoylation of its substrates NCX1 or PLM (Figure 3C).

zDHHC5 expression and substrate palmitoylation in heart failure

We investigated whether the differences in zDHHC5 expression and substrate palmitoylation identified early in cardiac hypertrophy persists in HF by analysing two experimental models (rabbit and pig) of myocardial infarction (MI) induced HF, as well as samples from ischaemic human HF patients (classified as reduced ejection fraction, details in Supplementary Table S1). In contrast to LVH, zDHHC5 expression was unchanged or modestly reduced in post-MI samples compared to control. Additionally, despite RNA sequencing data suggesting zDHHC5 expression levels are reduced in HFpEF but unchanged in HFrEF (Figure 1; Hahn et al., 2021) we found that protein expression of

zDHHC5 was significantly reduced in ischaemic HF samples compared to organ donors. Interestingly, whilst PLM palmitoylation remained unchanged in all cases, NCX1 palmitoylation was significantly reduced in animal models of HF but increased in human heart failure (Figure 4).

zDHHC5 palmitoylation in heart failure

The results thus far suggest zDHHC5 expression levels correlate poorly with palmitoylation of its substrates, and that in ventricular muscle changes in zDHHC5 expression alone may not be sufficient to increase changes in palmitoylation of its substrates. ZDHHC5 is the target of PTMs itself, including palmitoylation, which occurs on its active site cysteine during autopalmitoylation before transferring the palmitate to a substrate cysteine (Brigidi et al., 2015). Additionally, zDHHC5 is palmitoylated at additional sites in its C-terminal tail, which is key to mediating its response to β-adrenergic signalling and facilitating its interaction with the Na^+/K^+ ATPase, which regulates recruitment and palmitoylation of PLM (Yang et al., 2010; Chen et al., 2020; Plain et al., 2020). As such, we investigated whether palmitoylation of zDHHC5 was changed in HF. Interestingly, zDHHC5 palmitoylation was

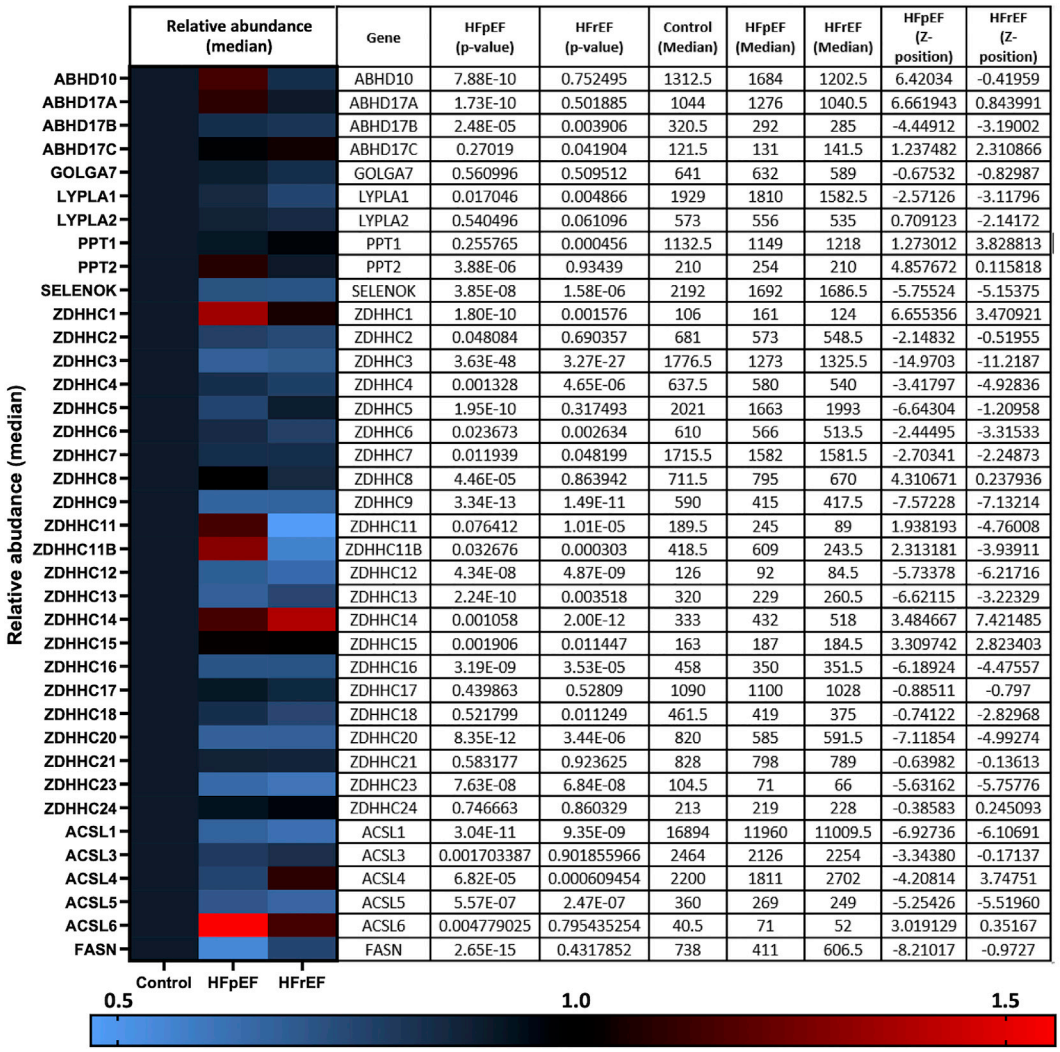

Relative abundance (median)	Gene	HFpEF (p-value)	HFrEF (p-value)	Control (Median)	HFpEF (Median)	HFrEF (Median)	HFpEF (Z-position)	HFrEF (Z-position)
ABHD10	ABHD10	7.88E-10	0.752495	1312.5	1684	1202.5	6.42034	-0.41959
ABHD17A	ABHD17A	1.73E-10	0.501885	1044	1276	1040.5	6.661943	0.843991
ABHD17B	ABHD17B	2.48E-05	0.003906	320.5	292	285	-4.44912	-3.19002
ABHD17C	ABHD17C	0.27019	0.041904	121.5	131	141.5	1.237482	2.310866
GOLGA7	GOLGA7	0.560996	0.509512	641	632	589	-0.67532	-0.82987
LYPLA1	LYPLA1	0.017046	0.004866	1929	1810	1582.5	-2.57126	-3.11796
LYPLA2	LYPLA2	0.540496	0.061096	573	556	535	0.709123	-2.14172
PPT1	PPT1	0.255765	0.000456	1132.5	1149	1218	1.273012	3.828813
PPT2	PPT2	3.88E-06	0.93439	210	254	210	4.857672	0.115818
SELENOK	SELENOK	3.85E-08	1.58E-06	2192	1692	1686.5	-5.75524	-5.15375
ZDHHC1	ZDHHC1	1.80E-10	0.001576	106	161	124	6.655356	3.470921
ZDHHC2	ZDHHC2	0.048084	0.690357	681	573	548.5	-2.14832	-0.51955
ZDHHC3	ZDHHC3	3.63E-48	3.27E-27	1776.5	1273	1325.5	-14.9703	-11.2187
ZDHHC4	ZDHHC4	0.001328	4.65E-06	637.5	580	540	-3.41797	-4.92836
ZDHHC5	ZDHHC5	1.95E-10	0.317493	2021	1663	1993	-6.64304	-1.20958
ZDHHC6	ZDHHC6	0.023673	0.002634	610	566	513.5	-2.44495	-3.31533
ZDHHC7	ZDHHC7	0.011939	0.048199	1715.5	1582	1581.5	-2.70341	-2.24873
ZDHHC8	ZDHHC8	4.46E-05	0.863942	711.5	795	670	4.310671	0.237936
ZDHHC9	ZDHHC9	3.34E-13	1.49E-11	590	415	417.5	-7.57228	-7.13214
ZDHHC11	ZDHHC11	0.076412	1.01E-05	189.5	245	89	1.938193	-4.76008
ZDHHC11B	ZDHHC11B	0.032676	0.000303	418.5	609	243.5	2.313181	-3.93911
ZDHHC12	ZDHHC12	4.34E-08	4.87E-09	126	92	84.5	-5.73378	-6.21716
ZDHHC13	ZDHHC13	2.24E-10	0.003518	320	229	260.5	-6.62115	-3.22329
ZDHHC14	ZDHHC14	0.001058	2.00E-12	333	432	518	3.484667	7.421485
ZDHHC15	ZDHHC15	0.001906	0.011447	163	187	184.5	3.309742	2.823403
ZDHHC16	ZDHHC16	3.19E-09	3.53E-05	458	350	351.5	-6.18924	-4.47557
ZDHHC17	ZDHHC17	0.439863	0.52809	1090	1100	1028	-0.88511	-0.797
ZDHHC18	ZDHHC18	0.521799	0.011249	461.5	419	375	-0.74122	-2.82968
ZDHHC20	ZDHHC20	8.35E-12	3.44E-06	820	585	591.5	-7.11854	-4.99274
ZDHHC21	ZDHHC21	0.583177	0.923625	828	798	789	-0.63982	-0.13613
ZDHHC23	ZDHHC23	7.63E-08	6.84E-08	104.5	71	66	-5.63162	-5.75776
ZDHHC24	ZDHHC24	0.746663	0.860329	213	219	228	-0.38583	0.245093
ACSL1	ACSL1	3.04E-11	9.35E-09	16894	11960	11009.5	-6.92736	-6.10691
ACSL3	ACSL3	0.001703387	0.901855966	2464	2126	2254	-3.34380	-0.17137
ACSL4	ACSL4	6.82E-05	0.000609454	2200	1811	2702	-4.20814	3.74751
ACSL5	ACSL5	5.57E-07	2.47E-07	360	269	249	-5.25426	-5.51960
ACSL6	ACSL6	0.004779025	0.795435254	40.5	71	52	3.019129	0.35167
FASN	FASN	2.65E-15	0.4317852	738	411	606.5	-8.21017	-0.9727

FIGURE 1
RNA transcript changes of palmitoylating and depalmitoylating enzymes and accessory proteins in heart failure. Hahn and Knutsdottir et al. (2020) performed RNA sequencing on biopsies from heart failure patients with preserved ejection fraction (HFpEF, n = 41), reduced ejection fraction (HFrEF, n = 30) and donor controls (n = 24). Abundance of transcripts of palmitoylating and depalmitoylating enzymes, including 23 zDHHC-palmitoyl acyltransferases, as well as accessory proteins and proteins involved in fatty acid and fatty acyl-CoA synthesis, were investigated in the available data. HFpEF and HFrEF are plotted relative to control (normalised to 1) in the heat map with relative abundance and p-values detailed in the accompanying table produced using the data repository from Hahn et al. (2021).

altered in HF in a similar manner to that of NCX1, whereby zDHHC5 palmitoylation was significantly reduced in the pig model (Figure 5A), but modestly (albeit not significantly) increased in human HF samples (Figure 5B).

Discussion

Palmitoylation has emerged over the last decade a crucial regulatory modification for every class of protein, including several involved in cardiac excitation-contraction coupling (Chien et al., 1996; Tulloch et al., 2011; Howie et al., 2013; Gök et al., 2020; Main et al., 2022). As many of these proteins are dysregulated in diseases such as HF, palmitoylation may represent a novel mechanism to manipulate their function for therapeutic benefit (Main and Fuller, 2021). Despite this, studies investigating changes in palmitoylation in a cardiac disease setting have been limited. As such, we focussed our investigation on the most well classified cardiac zDHHC-PAT, zDHHC5, which has been implicated in A/R injury and regulates the palmitoylation of important ion transporters and accessory proteins in the heart (Tulloch et al., 2011; Hilgemann et al., 2013; Lin et al., 2013; Howie et al., 2014; Chen et al., 2020; Gök et al., 2020; Plain et al., 2020). In the present study, we provide novel evidence that zDHHC5 expression and palmitoylation are altered in cardiac disease, although this does not directly correlate with a change in the palmitoylation of its substrates NCX1 and PLM (summarised in Figure 6).

Firstly, we observed that in a LVH model of cardiac hypertrophy and remodelling, zDHHC5 expression was upregulated as early as 3 days post-onset, and this was maintained until 8 weeks post-injury (Figure 2). Because there was such an acute upregulation of zDHHC5, we investigated the impact of overexpressing zDHHC5 in cardiomyocytes to

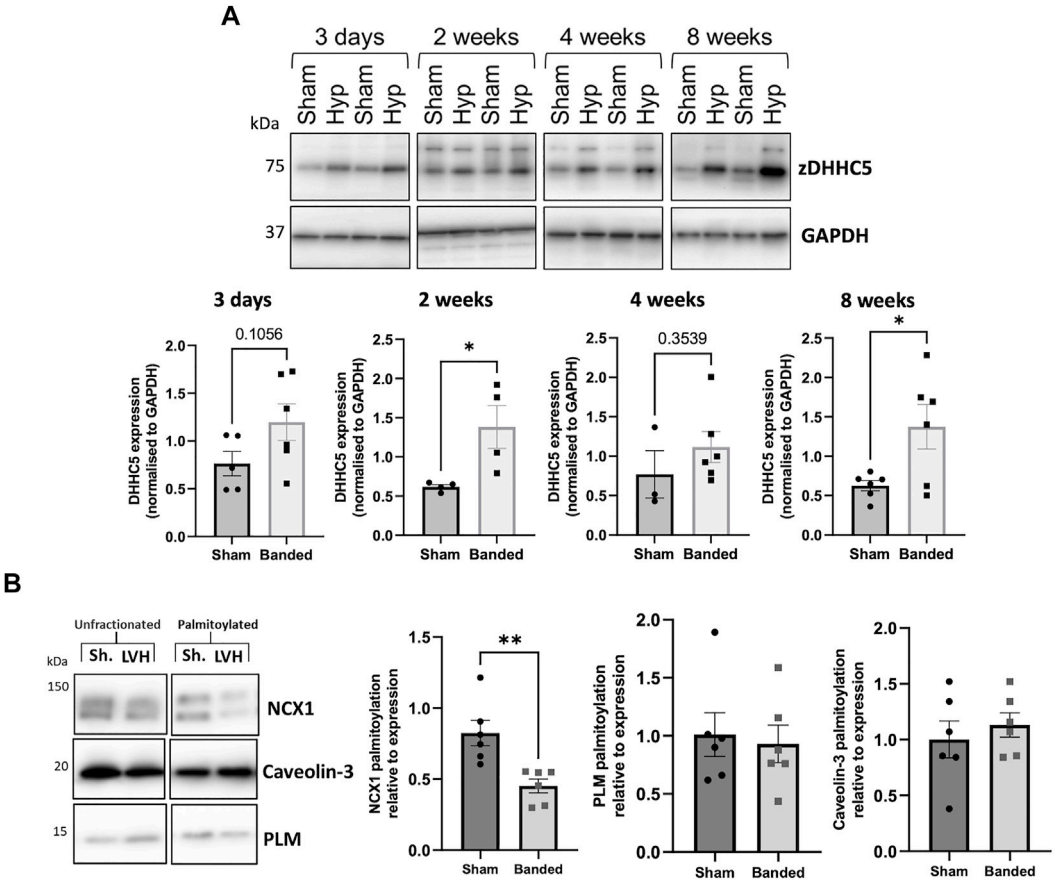

FIGURE 2
(A) Expression of zDHHC5 is increased in mice with left ventricular hypertrophy 2 weeks and 8 weeks post-onset and palmitoylation of NCX1 is reduced at 8-week. Ventricular samples from mice that developed left ventricular hypertrophy (LVH) induced by pressure overload and sham controls were taken at 3 days, 2 weeks, 4 weeks, and 8 weeks post-onset. Expression of zDHHC5 was significantly increased in hypertrophy samples compared to control at 2 weeks and 8 weeks post-onset. **(B)** Acyl-RAC of samples taken at 8-week post injury revealed palmitoylation of zDHHC5 substrate NCX1 was significantly reduced whilst palmitoylation of PLM remained unchanged. zDHHC5 expression is normalised to loading control GAPDH. Statistical comparisons made by unpaired Student s t-test. Data are mean ± S.E.M. *$p < 0.05$, **$p < 0.01$.

determine if there was a functional consequence for ventricular contractility, but this had no effect on any contractile parameters investigated (Figure 3; Supplementary Figure S3). In both LVH and virally infected cardiomyocytes, despite increased zDHHC5 expression, there was no correlated increase in substrate palmitoylation, as palmitoylation of PLM remained unchanged, whilst NCX1 palmitoylation was significantly reduced in LVH samples (Figure 3). This suggests that zDHHC5 expression levels are not rate limiting for substrate palmitoylation in ventricular muscle, and implies as-yet unidentified mechanisms control zDHHC5 activity and substrate palmitoylation in the heart. In other settings, availability of palmitoyl-CoA (Lin et al., 2013) and activity of acyl-CoA synthase enzymes (Gök et al., 2022), which may associate with zDHHC-PATs (Plain et al., 2020), have been established to be important determinants of substrate palmitoylation.

We investigated whether the changes in zDHHC5 expression were observed later in disease pathogenesis using models of ischaemic HF (rabbit and pig), as well as samples from ischaemic HF patients. In contrast to cardiac hypertrophy, zDHHC5 expression was either unchanged (rabbit), modestly reduced (pig) or significantly reduced (human) in a HF setting. However, similarly to the LVH model, this was poorly correlated with changes in substrate palmitoylation, such that palmitoylation of NCX1 was significantly reduced in the animal models of HF, but was significantly increased in human HF samples (Figure 4). Throughout this investigation we observed changes in

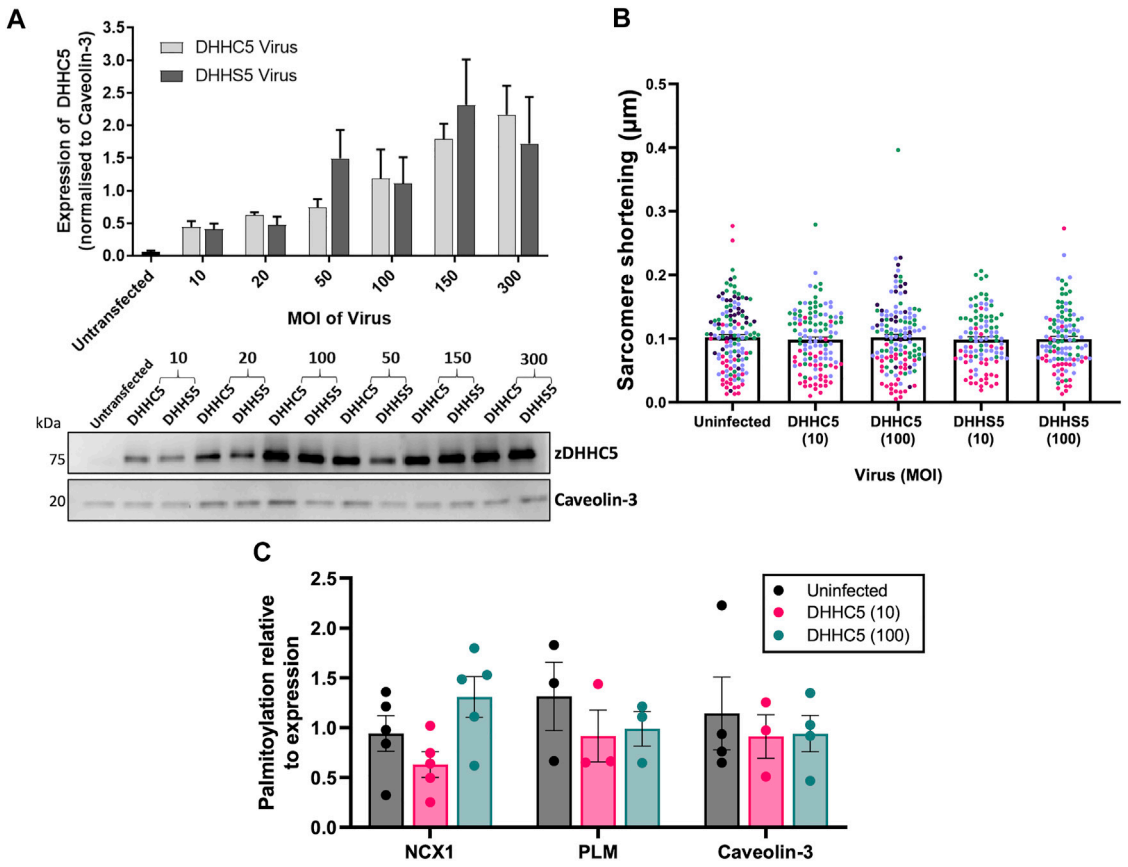

FIGURE 3
zDHHC5 overexpression does not alter parameters of rabbit ventricular cardiomyocyte contractility or lead to changes in substrate palmitoylation. **(A)** Rabbit ventricular cardiomyocytes were cultured for 18–24 h in the presence of either the HA-DHHC5 virus or a HA-DHHS5 dominant-negative virus, at an increasing range of virus particles per cell or multiplicity of infection (MOI; 10, 20, 50, 150, 300). zDHHC5 protein expression was determined *via* western blot, normalising to housekeeper protein Caveolin-3. HA-DHHC5 and HA-DHHS5 viral infection led to a dose-dependent increase in zDHHC5 expression. Data are expressed as mean ± S.E.M and is a representative image of n = 3–4 biological replicates. **(B)** Contractility recordings from cells infected with MOI of 10 and 100 were taken using CellOPTIQ®. Viral infection with either zDHHC5 or zDHHS5 at MOI 10 or 100 had no significant effect on altering the parameters of contractility including sarcomere shortening. N = 3 biological replicates for S10, C100, S100 and n = 4 biological replicates for uninfected and C100, with n = 20–51 cells per replicate. Each colour represents cells from one biological replicate. **(C)** Rabbit ventricular cardiomyocytes overexpressing HA-zDHHC5 (MOI 10 and 100) showed no significant change in NCX1 or PLM palmitoylation. Data are mean ± S.E.M analysed *via* an unpaired t-test (LVH) and a one-way ANOVA with a Dunnett's post-hoc test (overexpression) or a Sidak's post-hoc test (substrate palmitoylation). *$p < 0.05$.

zDHHC5 expression that did not consistently match changes in palmitoylation its substrates NCX1 and PLM. Indeed in the largest cohort examined (human HF and organ donors), no relationship between zDHHC5 expression levels and substrate palmitoylation levels can be detected (Supplementary Figure S4).

ZDHHC5 itself is under the control of several regulatory pathways, including palmitoylation of cysteines in its C-terminal tail which has important functional consequences for substrate recruitment and palmitoylation (Chen et al., 2020; Plain et al., 2020). In addition, its activity may be controlled by the availability of its substrate acyl-CoA, synthesised by ACSL isoforms. Analysis of zDHHC5 palmitoylation revealed that, similar to NCX1, palmitoylation was significantly reduced in the pig model and modestly increased (although not significantly) in the human heart samples (Figure 5). This may suggest there are upstream regulatory pathways driving changes in substrate palmitoylation, including that of zDHHC5. ZDHHC-PATs have been frequently reported to palmitoylate each other, and a proximity biotinylation screen identified DHHC20 as an interactor and palmitoylating enzyme of zDHHC5. Palmitoylation of the zDHHC5 C-terminal tail in response to adrenergic stimulation is required for its own stabilisation at the plasma membrane (Chen et al., 2020; Woodley and Collins, 2021). The zDHHC5 palmitoylation sites lie in an amphipathic helix containing a binding site for the Na^+/K^+ ATPase and zDHHC5 accessory protein GOLGA7, which controls its membrane localisation (Woodley and Collins, 2019; Plain et al., 2020). Increased zDHHC5 palmitoylation as observed in human HF, or reduced palmitoylation as observed in the pig model, may suggest increased or decreased activity of zDHHC5 either through a change in palmitate loading into the active site or a change in zDHHC20-mediated palmitoylation. We also do not rule out the possibility that the mismatch between zDHHC5 expression and palmitoylation of its substrates is caused changes in zDHHC5 subcellular localisation. Localisation-dependent palmitoylation of zDHHC5 substrates has previously been demonstrated following increased neuronal activity (Brigidi et al., 2015). Although we observe the virally-expressed zDHHC5 to be correctly localised to caveolar membranes in the cells surface (Supplementary Figure S1), it cannot be ruled out that altered zDHHC5 subcellular localisation in disease may change its ability to locate and palmitoylate its substrates. It should also be noted that observation of zDHHC5 expression and substrate palmitoylation in

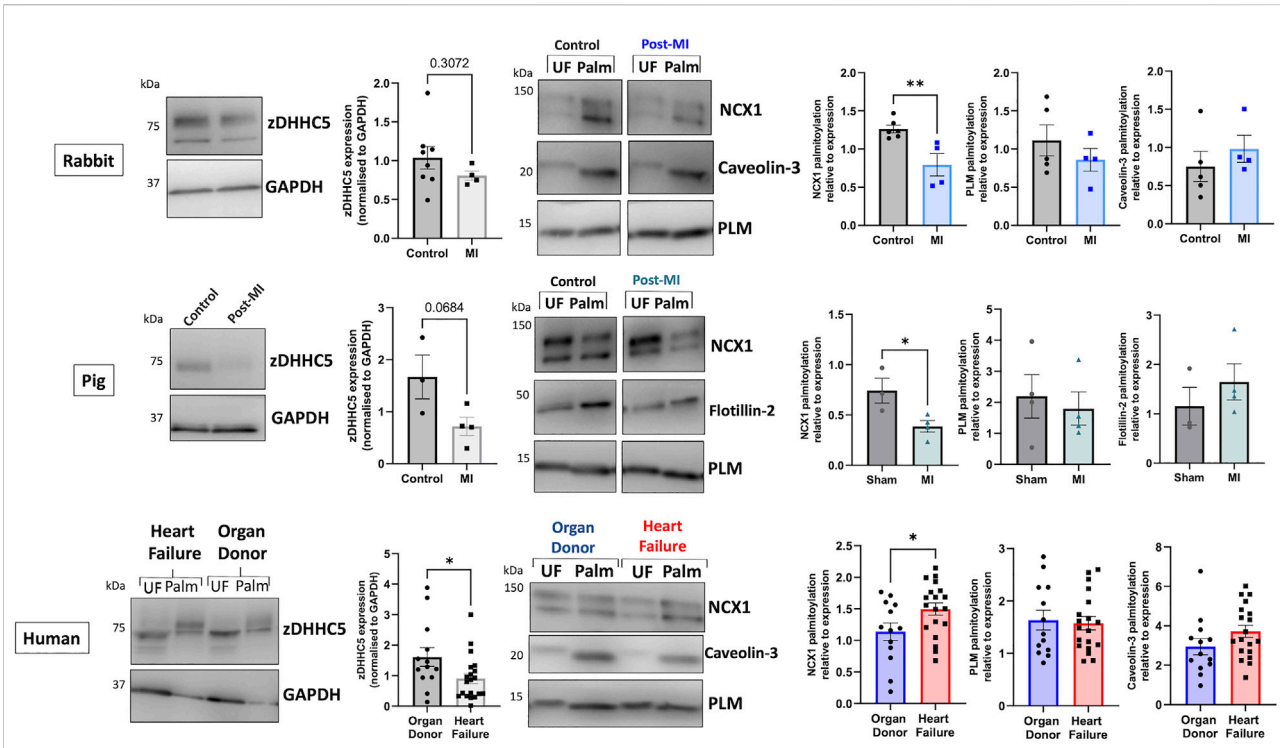

FIGURE 4
zDHHC5 expression and substrate palmitoylation in heart failure. In the rabbit model of MI-induced HF (8-week post-MI), zDHHC5 expression was unchanged whilst NCX1 palmitoylation was significantly reduced with no change in PLM or Caveolin-3 palmitoylation. In the pig model of MI-induced HF with reperfusion (3-month post-MI) zDHHC5 expression was modestly reduced ($p = 0.0684$) whilst NCX1 palmitoylation was significantly reduced with no change in PLM or Flotillin-2 palmitoylation. In samples from patients with ischaemic heart failure, zDHHC5 expression was significantly reduced compared to organ donor controls whilst NCX1 palmitoylation was significantly increased with no change in PLM or Caveolin-3 palmitoylation. zDHHC5 expression was normalised to loading control GAPDH. Data are palmitoylated fraction normalised to total protein (unfractionated, UF). Statistical comparisons made by unpaired Student's *t*-test. Data are mean ± S.E.M. $*p < 0.05$, $**p < 0.01$.

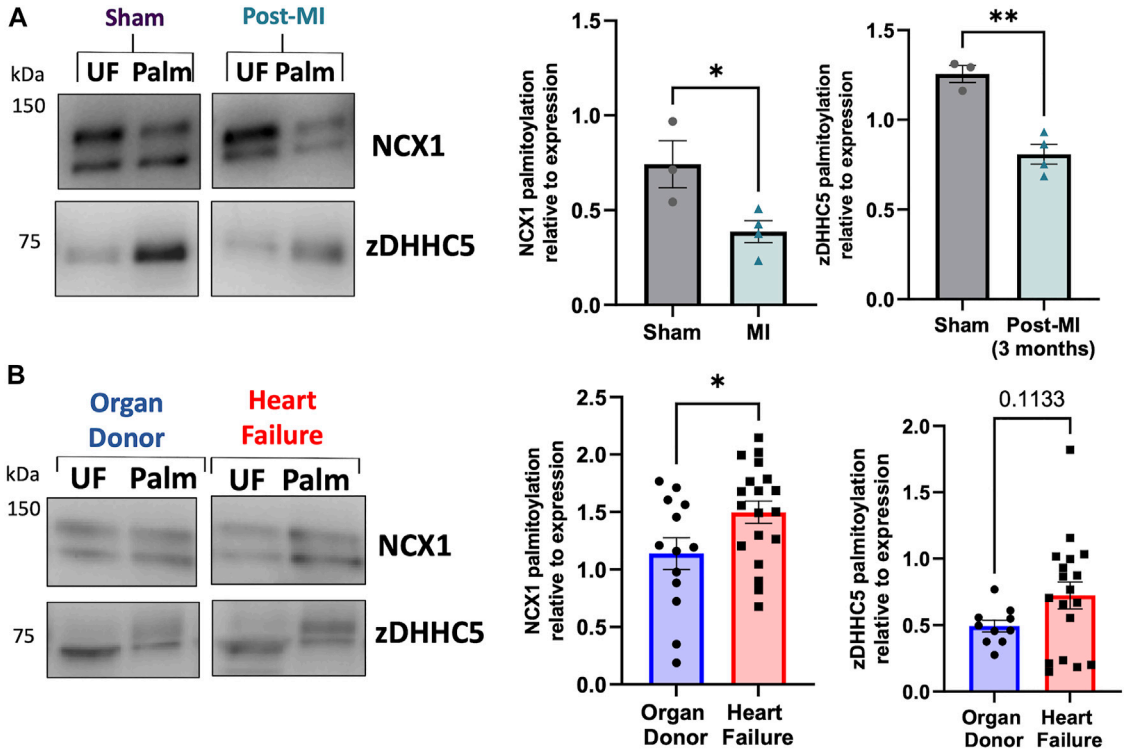

FIGURE 5
zDHHC5 palmitoylation is altered in heart failure in a similar manner to NCX1 palmitoylation. **(A)** In a pig model of MI-induced heart failure, zDHHC5 palmitoylation is significantly reduced, whilst **(B)** in human heart failure samples, zDHHC5 palmitoylation is modestly increased ($p = 0.1133$). NCX1 data taken from Figure 4 for comparison. Statistical comparisons made by unpaired Student's *t*-test. Data are mean ± S.E.M. $*p < 0.05$, $**p < 0.01$.

tissue samples (mouse, pig and human) may include a contribution of non-myocyte cells [although cardiomyocytes represent ~75% of myocardial tissue volume (Vliegen et al., 1991)].

The impact of other zDHHC5 PTMs on its activity will be important to consider in future investigations, as phosphorylation has been observed to inactivate zDHHC5 (Hao et al., 2020; Schianchi et al., 2020), while O-GlycNAcylation of zDHHC5 enhanced PLM association and palmitoylation (Plain et al., 2020; Schianchi et al., 2020). In line with our observations from hypertrophic tissue, but in contrast to the ischaemic human HF results, Miles et al. (2021) report significantly increased levels of zDHHC5 in human HF. However, the samples investigated represent a mixture of ischaemic and non-ischaemic origin (Miles et al., 2021), limiting the value of a comparison to the ischaemic samples used in our investigation. Nevertheless, given RNA-sequencing suggests levels are significantly reduced in HFpEF but not HFrEF (Hahn et al., 2021), further characterisation of zDHHC5 expression should be carried out in additional cohorts of patients.

Steady state protein palmitoylation is controlled by the balanced activities of palmitoylating and depalmitoylating enzymes. Several depalmitoylating enzymes show altered expression in both HFrEF and HFpEF, although not to the same extent as the dysregulated of zDHHC-PAT expression (Figure 1). In comparison to zDHHC-PATs, relatively little is known about the regulation of these enzymes, although APT1 was recently demonstrated to depalmitoylate NCX1 (Gök et al., 2021). However, we did not find a significant change in APT1 protein abundance in the setting of HF, so this likely does not explain the changes in substrate palmitoylation observed (Supplementary Figure S5).

Aside from information of zDHHC5 expression and palmitoylation, this study provides novel evidence that NCX1 palmitoylation is changed in cardiac disease in animal models and humans. Although NCX1 expression is often increased in the setting of LV dysfunction in HF, this does not necessarily lead to increased NCX1 activity (Hobai and O'Rourke, 2000; Quinn et al., 2003), suggesting that altered post-translational regulation of NCX1 contributes to the remodelling of its activity in HF. Increased NCX1 palmitoylation, as observed in human HF, would enhance its inactivation and reduce Ca^{2+} efflux. Whilst improving systolic function, this would contribute to diastolic impairment, of which NCX1 is a key mediator (Kass et al., 2004). Interestingly, the pattern of NCX1 palmitoylation associated with HF that we report here was recapitulated for

Sample Origin	Phenotype	zDHHC5 expression	NCX1 palmitoylation	zDHHC5 palmitoylation
Mouse	Left ventricular hypertrophy Reduced EF	↑ Significantly increased	↓ Significantly decreased	Not investigated
Rabbit	Left ventricular hypertrophy EF <45% Heart failure	— Unchanged	↓ Significantly decreased	Not investigated
Pig	Ischaemia/ reperfusion EF <45% Heart failure	↓ Modestly decreased	↓ Significantly decreased	↓ Significantly decreased
Human	Ischaemic heart failure EF <30% Co-morbidities	↓ Significantly decreased	↑ Significantly increased	↑ Modestly increased

FIGURE 6
Summary of samples investigated in this study and the changes in zDHHC5 expression and palmitoylation of NCX1 and zDHHC5. Trends or changes are in comparison to relevant controls. EF, ejection fraction.

cardiac myosin binding protein-C, again suggesting that upstream factors such as a fatty acid and fatty acyl-CoA availability may be responsible for the changes of substrate palmitoylation (Main et al., 2022).

A significant finding, but also a limitation of this study, is the lack of consistency in the changes in zDHHC5 expression and substrate palmitoylation between different animal models and human HF. This makes it challenging to draw definitive conclusion regarding the importance of palmitoylation in cardiac disease. The increased palmitoylation in the human setting may be a result of more developed decompensation compared to the animal models, or as a result of pharmacological intervention. It may also reflect a failure of the animal model to accurately reflect human pathology. Indeed, this is a major limitation of current animal models for HF research, because they rarely include study of novel therapeutic interventions in combination with current optimal clinical care, making translational potential challenging. Interestingly, whilst NCX1 palmitoylation was frequently altered, PLM palmitoylation did not change in any setting (Plain et al., 2020). However, this observation may be as a result of solely characterising palmitoylation using Acyl-RAC. Whilst this method provides a robust mechanism to detect protein palmitoylation, changes in substrate palmitoylation in singly palmitoylated proteins are most likely to be observed using this capture method, as opposed to substrates with multiple palmitoylation sites, where the substrate will still be captured even if only one site remains palmitoylated. Indeed, this may be why NCX1, with one palmitoylation site, is frequently observed to be changed whilst PLM containing two palmitoylation sites did not vary in any disease state (Tulloch et al., 2011; Reilly et al., 2015; Howie et al., 2018). Experimental approaches that measure palmitoylation site occupancy of multiply palmitoylated proteins may provide further insight into the contribution of aberrant protein palmitoylation to the pathogenesis of heart failure.

Data availability statement

The raw data supporting the conclusion of this article will be made available by the authors, without undue reservation.

Ethics statement

The studies involving human participants were reviewed and approved by the University of Kentucky's Institutional Review Board. The patients/participants provided their written informed consent to participate in this study. The animal studies were reviewed and approved by the Animal Welfare and Ethical Review Body, University of Glasgow and the Animal Welfare and Ethical Review Body, King's College London.

Author contributions

AM: Conceptualization, investigation, formal analysis, writing—original draft WF: Conceptualization, project administration, funding acquisition, supervision, writing—review and editing AB, JH, C-WK, and AR: Resources and methodology RH, FB, GS, GB, KC, and MS: Resources.

Funding

We acknowledge financial support from the British Heart Foundation: 4-year PhD studentship to AM, SP/16/3/32317 and PG/18/60/33957 to WF, RG/17/15/33106 to MS and WF, a Centre of Research Excellence award RE/18/6/34217, and NIH HL149164 and HL148785 to KC. Funding: American Heart Association TP135689, NIH1L48785, University of Kentucky Myocardial Recovery Alliance.

Acknowledgments

We acknowledge the patients and families of organ donors who donated cardiac samples.

Conflict of interest

RH was employed by Flagship Pioneering.

The remaining authors declare that the research was conducted in the absence of any commercial or financial relationships that could be construed as a potential conflict of interest.

Publisher's note

All claims expressed in this article are solely those of the authors and do not necessarily represent those of their affiliated organizations, or those of the publisher, the editors and the reviewers. Any product that may be evaluated in this article, or claim that may be made by its manufacturer, is not guaranteed or endorsed by the publisher.

Supplementary material

The Supplementary Material for this article can be found online at: https://www.frontiersin.org/articles/10.3389/fphys.2022.1023237/full#supplementary-material

References

Ambrosy, A. P., Fonarow, G. C., Butler, J., Chioncel, O., Greene, S. J., Vaduganathan, M., et al. (2014). The global Health and economic burden of hospitalizations for heart failure: Lessons learned from hospitalized heart failure registries. *J. Am. Coll. Cardiol.* 63 (12), 1123–1133. doi:10.1016/J.JACC.2013.11.053

Blair, C. A., Haynes, P., Campbell, S. G., Chung, C., Mitov, M. I., Dennis, D., et al. (2016). A protocol for collecting human cardiac tissue for research. *VAD J.* 2 (12). doi:10.13023/VAD.2016.12

Boguslavskyi, A., Pavlovic, D., Aughton, K., Clark, J. E., Howie, J., Fuller, W., et al. (2014). Cardiac hypertrophy in mice expressing unphosphorylatable phospholemman. *Cardiovasc. Res.* 104 (1), 72–82. doi:10.1093/CVR/CVU182

Brigidi, G. S., Santyr, B., Shimell, J., Jovellar, B., and Bamji, S. X. (2015). Activity-regulated trafficking of the palmitoyl-acyl transferase DHHC5. *Nat. Commun.* 6 (1), 8200–8217. doi:10.1038/ncomms9200

Chen, J. J., Marsden, A. N., Scott, C. A., Akimzhanov, A. M., and Boehning, D. (2020). DHHC5 mediates β-adrenergic signaling in cardiomyocytes by targeting gα proteins. *Biophys. J.* 118 (4), 826–835. doi:10.1016/J.BPJ.2019.08.018

Chien, A. J., Carr, K. M., Shirokov, R. E., Rios, E., and Marlene Hosey, M. (1996). Identification of palmitoylation sites within the L-type calcium channel beta2a subunit and effects on channel function. *J. Biol. Chem.* 271 (43), 26465–26468. doi:10.1074/JBC.271.43.26465

Essandoh, K., Philippe, J. M., Jenkins, P. M., and Brody, M. J. (2020). Palmitoylation: A fatty regulator of myocardial electrophysiology. *Front. Physiology* 11, 108. doi:10.3389/fphys.2020.00108

Forrester, M. T., Hess, D. T., Thompson, J. W., Hultman, R., Moseley, M. A., Stamler, J. S., et al. (2011). Site-specific analysis of protein S-acylation by resin-assisted capture. *J. Lipid Res.* 52 (2), 393–398. doi:10.1194/jlr.D011106

Fredericks, G. J., Hoffmann, F. W., Hondal, R. J., Rozovsky, S., Urschitz, J., and Hoffmann, P. R. (2017). Selenoprotein K increases efficiency of DHHC6 catalyzed protein palmitoylation by stabilizing the acyl-DHHC6 intermediate. *Antioxidants* 7 (1), 4. doi:10.3390/ANTIOX7010004

Gök, C., Main, A., Gao, X., Kerekes, Z., Plain, F., Kuo, C.-W., et al. (2021). Insights into the molecular basis of the palmitoylation and depalmitoylation of NCX1. *Cell Calcium* 97, 102408. doi:10.1016/j.ceca.2021.102408

Gök, C., Plain, F., Robertson, A. D., Howie, J., Baillie, G. S., Fraser, N. J., et al. (2020). Dynamic palmitoylation of the sodium-calcium exchanger modulates its structure, affinity for lipid-ordered domains, and inhibition by XIP. *Cell Rep.* 31, 107697. doi:10.1016/j.celrep.2020.107697

Gök, C., Robertson, A. D., and Fuller, W. (2022). Insulin-induced palmitoylation regulates the Cardiac Na+/Ca2+ exchanger NCX1. *Cell Calcium* 104, 102567. doi:10.1016/J.CECA.2022.102567

Hahn, V. S., Knutsdottir, H., Luo, X., Bedi, K., Margulies, K. B., Haldar, S. M., et al. (2021). Myocardial gene expression signatures in human heart failure with preserved ejection fraction. *Circulation* 143, 120–134. doi:10.1161/CIRCULATIONAHA.120.050498

Hao, J. W., Wang, J., Guo, H., Zhao, Y. Y., Sun, H. H., Li, Y. F., et al. (2020). CD36 facilitates fatty acid uptake by dynamic palmitoylation-regulated endocytosis. *Nat. Commun.* 11 (1), 4765. doi:10.1038/s41467-020-18565-8

Hilgemann, D. W., Fine, M., Linder, M. E., Jennings, B. C., and Lin, M.-J (2013). Massive endocytosis triggered by surface membrane palmitoylation under mitochondrial control in BHK fibroblasts. *ELife* 2013 (2), e01293. doi:10.7554/eLife.01293

Hobai, I. A., and O'Rourke, B. (2000). Enhanced Ca2+-activated Na+-Ca2+ exchange activity in canine pacing-induced heart failure. *Circ. Res.* 87 (8), 690–698. doi:10.1161/01.RES.87.8.690

Houser, S. R., Margulies, K. B., Murphy, A. M., Spinale, F. G., Francis, G. S., Prabhu, S. D., et al. (2012). Animal models of heart failure: A scientific statement from the American heart association. *Circ. Res.* 111, 131–150. doi:10.1161/RES.0B013E3182582523

Howie, J., Reilly, L., Fraser, N. J., Walker, J. M. V., Wypijewski, K. J., Ashford, M. L. J., et al. (2014). Substrate recognition by the cell surface palmitoyl transferase DHHC5. *Proc. Natl. Acad. Sci. U. S. A.* 111 (49), 17534–17539. doi:10.1073/pnas.1413627111

Howie, J., Tulloch, L. B., Shattock, M. J., and Fuller, W. (2013). Regulation of the cardiac Na(+) pump by palmitoylation of its catalytic and regulatory subunits. *Biochem. Soc. Trans.* 41 (1), 95–100. doi:10.1042/BST20120269

Howie, J., Wypijewski, K. J., Plain, F., Tulloch, L. B., Fraser, N. J., and Fuller, W. (2018). Greasing the wheels or a spanner in the works? Regulation of the cardiac sodium pump by palmitoylation. *Crit. Rev. Biochem. Mol. Biol.* 53 (2), 175–191. doi:10.1080/10409238.2018.1432560

Kass, D. A., Bronzwaer, J. G. F., and Paulus, W. J. (2004). What mechanisms underlie diastolic dysfunction in heart failure? *Circ. Res.* 94 (12), 1533–1542. doi:10.1161/01.RES.0000129254.25507.d6

Kemp, C. D., and Conte, J. v. (2012). The pathophysiology of heart failure. *Cardiovasc. Pathol.* 21 (5), 365–371. doi:10.1016/J.CARPATH.2011.11.007

Kettlewell, S., Burton, F. L., Smith, G. L., and Workman, A. J. (2013). Chronic myocardial infarction promotes atrial action potential alternans, afterdepolarizations, and fibrillation. *Cardiovasc. Res.* 99 (1), 215–224. doi:10.1093/cvr/cvt087

Ko, P. J., Woodrow, C., Dubreuil, M. M., Martin, B. R., Skouta, R., Bassik, M. C., et al. (2019). A ZDHHC5-GOLGA7 protein acyltransferase complex promotes nonapoptotic cell death. *Cell Chem. Biol.* 26 (12), 1716–1724. e9. doi:10.1016/J.CHEMBIOL.2019.09.014

Lin, M. J., Fine, M., Lu, J. Y., Hofmann, S. L., Frazier, G., and Hilgemann, D. W. (2013). Massive palmitoylation-dependent endocytosis during reoxygenation of anoxic cardiac muscle. *ELife* 2013 (2), e01295. doi:10.7554/eLife.01295

Main, A., and Fuller, W. (2021). Protein S-palmitoylation: Advances and challenges in studying a therapeutically important lipid modification. *FEBS J.* 289, 861–882. doi:10.1111/FEBS.15781

Main, A., Milburn, G. N., Balesar, R. M. N., Rankin, A. C., Smith, G. L., Campbell, K. S., et al. (2022). Cardiac myosin binding protein-C palmitoylation is associated with increased myofilament affinity, reduced myofilament Ca2+ sensitivity and is increased in ischaemic heart failure. BioRxiv. 2022.06.21.496992. doi:10.1101/2022.06.21.496992

McMurray, J., Packer, M., Desai, A., Gong, J., Lefkowitz, M., Rizkala, A., et al. (2014). Angiotensin-neprilysin inhibition versus enalapril in heart failure. *N. Engl. J. Med.* 371 (11), 993–1004. doi:10.1056/NEJMOA1409077

Miles, M. R., Seo, J., Jiang, M., Wilson, Z. T., Little, J., Hao, J., et al. (2021). Global identification of S-palmitoylated proteins and detection of palmitoylating (DHHC) enzymes in heart. *J. Mol. Cell. Cardiol.* 155, 1–9. doi:10.1016/J.YJMCC.2021.02.007

Nisbet, A. M., Camelliti, P., Walker, N. L., Burton, F. L., Cobbe, S. M., Kohl, P., et al. (2016). Prolongation of atrio-ventricular node conduction in a rabbit model of ischaemic cardiomyopathy: Role of fibrosis and connexin remodelling. *J. Mol. Cell. Cardiol.* 94, 54–64. doi:10.1016/J.YJMCC.2016.03.011

Pastore, A., and Piemonte, F. (2013). Protein glutathionylation in cardiovascular diseases. *Int. J. Mol. Sci.* 14 (10), 20845–20876. doi:10.3390/IJMS141020845

Plain, F., Howie, J., Kennedy, J., Brown, E., Shattock, M. J., Fraser, N. J., et al. (2020). Control of protein palmitoylation by regulating substrate recruitment to a zDHHC-protein acyltransferase. *Commun. Biol.* 3 (1), 411. doi:10.1038/s42003-020-01145-3

Quinn, F. R., Currie, S., Duncan, A. M., Miller, S., Sayeed, R., Cobbe, S. M., et al. (2003). Myocardial infarction causes increased expression but decreased activity of the myocardial Na+—Ca2+ exchanger in the rabbit. *J. Physiol.* 553 (1), 229–242. doi:10.1113/JPHYSIOL.2003.050716

Rame, J. E., and Dries, D. L. (2007). Heart failure and cardiac hypertrophy. *Curr. Treat. Options Cardiovasc. Med.* 9 (4), 289–301. doi:10.1007/S11936-007-0024-3

Ramila, K. C., Jong, C. J., Pastukh, V., Ito, T., Azuma, J., and Schaffer, S. W. (2015). Role of protein phosphorylation in excitation-contraction coupling in taurine deficient hearts. *Am. J. Physiol. Heart Circ. Physiol.* 308 (3), H232–H239. doi:10.1152/AJPHEART.00497.2014

Reilly, L., Howie, J., Wypijewski, K., Ashford, M. L. J., Hilgemann, D. W., and Fuller, W. (2015). Palmitoylation of the Na/Ca exchanger cytoplasmic loop controls its inactivation and internalization during stress signaling. *FASEB J.* 29 (11), 4532–4543. doi:10.1096/fj.15-276493

Rocchetti, M., Sala, L., Rizzetto, R., Irene Staszewsky, L., Alemanni, M., Zambelli, V., et al. (2014). Ranolazine prevents INaL enhancement and blunts myocardial remodelling in a model of pulmonary hypertension. *Cardiovasc. Res.* 104 (1), 37–48. doi:10.1093/CVR/CVU188

Schianchi, F., Glatz, J. F. C., Gascon, A. N., Nabben, M., Neumann, D., and Luiken, J. J. F. P. (2020). Putative role of protein palmitoylation in cardiac lipid-induced insulin resistance. *Int. J. Mol. Sci.* 21 (24), 9438. doi:10.3390/IJMS21249438

Sequeira, V., and Maack, C. (2018). Rebalancing protein phosphorylation in heart failure to prevent arrhythmias. *Eur. J. Heart Fail.* 20 (12), 1686–1689. doi:10.1002/EJHF.1315

Shah, A., Gandhi, D., Srivastava, S., Shah, K. J., and Mansukhani, R. (2017). Heart failure: A class review of pharmacotherapy. *P Trans.* 42 (7), 464–472.

Shah, K. S., Xu, H., Matsouaka, R. A., Bhatt, D. L., Heidenreich, P. A., Hernandez, A. F., et al. (2017). Heart failure with preserved, borderline, and reduced ejection fraction: 5-Year outcomes. *J. Am. Coll. Cardiol.* 70 (20), 2476–2486. doi:10.1016/J.JACC.2017.08.074

Simmonds, S. J., Cuijpers, I., Heymans, S., and Jones, E. A. V. (2020). Cellular and molecular differences between HFpEF and HFrEF: A step ahead in an improved pathological understanding. *Cells* 9 (1), E242. doi:10.3390/CELLS9010242

Tilemann, L., Lee, A., Ishikawa, K., Aguero, J., Rapti, K., Santos-Gallego, C., et al. (2013). SUMO-1 gene transfer improves cardiac function in a large-animal model of heart failure. *Sci. Transl. Med.* 5 (211), 211ra159. doi:10.1126/scitranslmed.3006487

Tulloch, L. B., Howie, J., Wypijewski, K. J., Wilson, C. R., Bernard, W. G., Shattock, M. J., et al. (2011). The inhibitory effect of phospholemman on the sodium pump requires its palmitoylation. *J. Biol. Chem.* 286 (41), 36020–36031. doi:10.1074/jbc.M111.282145

Vliegen, H. W., van der Laarse, A., Cornelisse, C. J., Eulderink, F., and vAn der Laarse, A. (1991). Myocardial changes in pressure overload-induced left ventricular hypertrophyA study on tissue composition, polyploidization and multinucleation. *Eur. Heart J.* 12 (4), 488–494. doi:10.1093/OXFORDJOURNALS.EURHEARTJ.A059928

Woodley, K. T., and Collins, M. O. (2021). Regulation and function of the palmitoyl-acyltransferase ZDHHC5. *FEBS J.* 288 (23), 6623–6634. doi:10.1111/FEBS.15709

Woodley, K. T., and Collins, M. O. (2019). S-acylated Golga7b stabilises DHHC5 at the plasma membrane to regulate cell adhesion. *EMBO Rep.* 20 (10), e47472. doi:10.15252/EMBR.201847472

Yang, W., di Vizio, D., Kirchner, M., Steen, H., and Freeman, M. R. (2010). Proteome scale characterization of human S-acylated proteins in lipid raft-enriched and non-raft membranes. *Mol. Cell. Proteomics* 9 (1), 54–70. doi:10.1074/MCP.M800448-MCP200

frontiers | Frontiers in Physiology

TYPE Review
PUBLISHED 16 November 2022
DOI 10.3389/fphys.2022.1040968

OPEN ACCESS

EDITED BY
Rebeca M. Mejias Estevez,
Sevilla University, Spain

REVIEWED BY
Niall Fraser,
University of Dundee, United Kingdom
Geert Van Den Bogaart,
University of Groningen, Netherlands

*CORRESPONDENCE
Askar M. Akimzhanov,
Askar.M.Akimzhanov@uth.tmc.edu

SPECIALTY SECTION
This article was submitted to Lipid and Fatty Acid Research, a section of the journal Frontiers in Physiology

RECEIVED 09 September 2022
ACCEPTED 02 November 2022
PUBLISHED 16 November 2022

CITATION
West SJ, Boehning D and Akimzhanov AM (2022), Regulation of T cell function by protein S-acylation. *Front. Physiol.* 13:1040968. doi: 10.3389/fphys.2022.1040968

Regulation of T cell function by protein S-acylation

Savannah J. West[1,2], Darren Boehning[3] and Askar M. Akimzhanov[1,2]*

[1]Department of Biochemistry and Molecular Biology, McGovern Medical School, University of Texas Health Science Center at Houston, Houston, TX, United States, [2]MD Anderson Cancer Center and University of Texas Health Science at Houston Graduate School, Houston, TX, United States, [3]Department of Biomedical Sciences, Cooper Medical School of Rowan University, Camden, NJ, United States

S-acylation, the reversible lipidation of free cysteine residues with long-chain fatty acids, is a highly dynamic post-translational protein modification that has recently emerged as an important regulator of the T cell function. The reversible nature of S-acylation sets this modification apart from other forms of protein lipidation and allows it to play a unique role in intracellular signal transduction. In recent years, a significant number of T cell proteins, including receptors, enzymes, ion channels, and adaptor proteins, were identified as S-acylated. It has been shown that S-acylation critically contributes to their function by regulating protein localization, stability and protein-protein interactions. Furthermore, it has been demonstrated that zDHHC protein acyltransferases, the family of enzymes mediating this modification, also play a prominent role in T cell activation and differentiation. In this review, we aim to highlight the diversity of proteins undergoing S-acylation in T cells, elucidate the mechanisms by which reversible lipidation can impact protein function, and introduce protein acyltransferases as a novel class of regulatory T cell proteins.

KEYWORDS

S-acylation, palmitoylation, protein acyltransferases, palmitoyl acyltransferases, T cell receptor, T cell signaling, DHHC enzymes

1 Introduction

Protein S-acylation is the reversible post-translational lipidation of cysteine residues *via* a labile thioester bond. It was discovered in 1979 when Schmidt and Schlesinger used thin-layer and gas-liquid chromatography to identify the post-translational addition of palmitic acid to the glycoprotein of the vesicular stomatitis virus (Schmidt and Schlesinger, 1979). Since many subsequent studies used tritiated palmitic acid or other palmitic acid analogs to monitor protein S-acylation, it is also often referred to as S-palmitoylation or, simply, palmitoylation. However, palmitate is not the only long-chain fatty acid that can reversibly modify cysteine residues. It has been found that a variety of saturated (myristate and stearate), monounsaturated (oleate), and polyunsaturated (arachidonate and eicosapentanoate) fatty acids can also modify proteins *via* the same thioester bond (Fujimoto et al., 1993; Muszbek and Laposata, 1993; Hallak et al., 1994; DeMar and Anderson, 1997; Montigny et al., 2014). Due to the

recent advances in proteomics approaches to detect protein S-acylation, the number of S-acylated proteins is rapidly growing and it has been estimated that at least 20% of the total human proteome (and more than 50% of transmembrane T cell proteins) is targeted by this modification (Morrison et al., 2015; Blanc et al., 2019).

S-acylation is a distinct form of protein lipidation since unlike other types, such as N-myristoylation or prenylation, it is reversible and the modified proteins can undergo multiple cycles of S-acylation and de-acylation (Chamberlain and Shipston, 2015). The reversible nature of the thioester bond suggests that this modification can serve as a unique signaling mechanism coordinating propagation of a signaling cascade through rapid changes in protein hydrophobicity. Indeed, we and others demonstrated the essential role of S-acylation in regulation of the critical proximal components of the T cell receptor (TCR) signaling machinery, such as Lck, Fyn, ZAP-70, LAT, and Orai1/STIM1 (further discussed below).

Although S-acylation was discovered in 1979, there have been several limitations that have hindered the progression of the field until somewhat recently, including identification of the enzymes that catalyze reactions of S-acylation and de-acylation, and the lack of efficient methods to detect protein S-acylation. It was not until 20 years after the discovery of S-acylation that the proteins facilitating this modification, protein acyltransferases, were identified in yeast. Work in *Saccharomyces cerevisiae* was critical for the field when it was uncovered that Erf2/Erf4 and Akr1 were responsible for the S-acylation of Ras2 and Yck2, respectively (Bartels et al., 1999; Lobo et al., 2002; Roth et al., 2002). These enzymes were found to have cysteine-rich domains along with a catalytic consensus sequence of Asp-His-His-Cys, giving them the name zDHHC enzymes. The discovery of zDHHC enzymes in yeast then led to studies finding them conserved in all eukaryotic organisms. Yeast have up to seven zDHHC family protein acyltransferases, while *C. elegans* and *Drosophila* are predicted to have twenty, mice have twenty-four, and humans express twenty-three zDHHC enzymes (Roth et al., 2002; Ohno et al., 2006; Bannan et al., 2008).

Another limitation the field faced was the lack of identified de-acylating enzymes. In 1993, almost twenty years after the discovery of S-acylation, Camp and Hofmann found that palmitoyl protein thioesterase 1 (PPT1) enzymatically removes the acyl group from S-acylated H-Ras (Camp and Hofmann, 1993). However, it was later shown that PPT1 primarily removes fatty acids from proteins being broken down in the lysosomal lumen, and was not localized to the cytosol where zDHHC-mediated S-acylation occurs (Verkruyse and Hofmann, 1996). Even though this enzyme contains a thioesterase signature, including a Ser-His-Asp catalytic sequence and an α/β hydrolase fold, it was not a candidate for protein de-acylation (Camp et al., 1994; Bellizzi et al., 2000), and the enzymes mediating de-acylation remained enigmatic. Then in 1998, it was found that acyl-protein thioesterase 1 (APT1), a member of the metabolic serine hydrolase superfamily, is a cytosolic enzyme and can de-acylate G_{α}s *in vivo* (Duncan and Gilman, 1998). APT1 was the first verified enzyme that reverses protein S-acylation. Following the finding of APT1, bioinformatics studies were done to search for other APTs. They led to the discovery of APT2 which de-acylates proteins such as growth associated protein 43 (GAP-43) and H-Ras (Tomatis et al., 2010; Lin and Conibear, 2015), and for several years, APT1/2 were the only enzymes known to reverse S-acylation. In 2015, Lin and Conibear, used a combination of elegant biochemical approaches to demonstrate that members of the ABHD17 family (also part of the metabolic serine hydrolase superfamily) can de-acylate N-Ras and PSD-95 proteins (Lin et al., 2015). This finding was independently confirmed by another group which showed that ABHD17 thioesterases control PSD-95 S-acylation and its synaptic function (Yokoi et al., 2016). These observations indicate that the family of de-acylating enzymes is likely much larger than originally thought and more work is expected to be done in identifying the enzymes responsible for protein de-acylation.

The final problem that delayed the S-acylation field was the lack of effective assays. Although S-acylation was discovered in 1979, it was not until the early 2000's that there were safe and efficient ways to assay protein S-acylation. Prior to this, it was mostly assayed using radioactively labeled fatty acids and autoradiography to visualize fatty acid incorporation (Schlesinger et al., 1980). This involved using radiation and exposure times that could last weeks to months. Now, we have much safer and faster assays including metabolic labeling (Hannoush and Sun, 2010), PEG-shift (Burgoyne et al., 2013), acyl-biotin exchange (Drisdel and Green, 2004), and acyl-resin assisted capture (Tewari et al., 2020). Additionally, although there is no consensus sequence to fully predict protein S-acylation, there are databases containing information on S-acylated proteins, such as SwissPalm and CSS-Palm, as well as a bioinformatics study that used machine learning algorithms to identify potential S-acylation sites (Ren et al., 2008; Blanc et al., 2019; Li et al., 2021). However, since these approaches and others, have been recently reviewed in depth (Chen et al., 2021), they will not be thoroughly discussed here.

Despite the initial obstacles which delayed the advancements of the field, it has now become clear that S-acylation is a widespread post-translational modification with a broad range of important regulatory functions. Dysfunctions of zDHHC enzymes have been shown to cause a variety of human disorders, such as Huntington disease, cystic fibrosis, schizophrenia, and several types of cancer [reviewed in (De and Sadhukhan, 2018)]. Recently, it has been found that S-acylation is required for the proper function of the immune system. For example, several key signaling T cell receptor proteins were identified as S-acylated, and this modification has been found to be critical for proper protein localization, function, and propagation of T cell receptor signaling in response

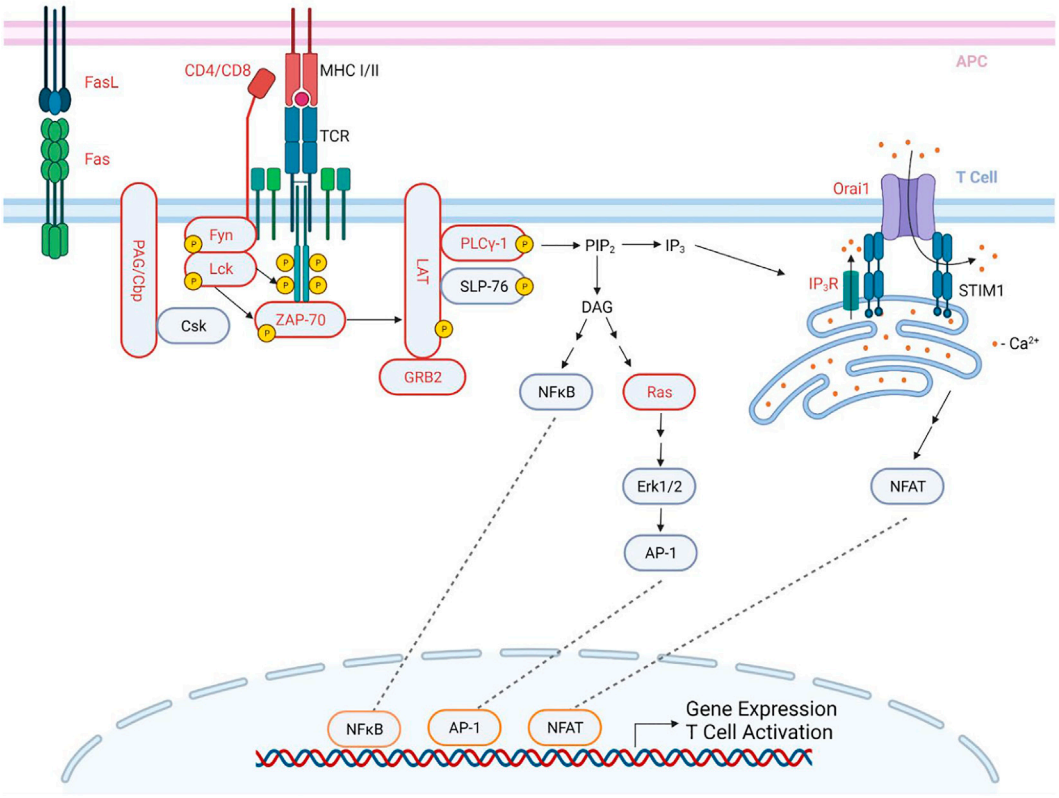

FIGURE 1
S-acylation in the proximal TCR signaling pathway. An antigen peptide, bound to an MHC of an antigen presenting cell (APC), engages and stimulates the TCR while its co-receptor (CD4/CD8) binds to the MHC, resulting in the activation of several signaling cascades, subsequently leading to T cell activation. Upon TCR stimulation, PAG/Cbp is de-phosphorylated, and disassociates from Csk, allowing for the recruitment of Lck to the TCR. Lck is then activated, and phosphorylates the ITAMs of the TCR-associated CD3 and ζ-chains. These phosphorylated ITAMs then act as a docking site for ZAP-70, which is then phosphorylated by Lck. ZAP-70 then phosphorylates and activates the scaffolding protein LAT, which is a docking site for several proteins, including SLP-76, PLC-γ1, and GRB2. These are then able to be phosphorylated and activated, many by ZAP-70. The activation of PLC-γ1 leads to the formation of IP_3 and DAG from PIP_2. IP_3 then binds to the IP_3R on the ER membrane, leading to the depletion of the ER Ca^{2+} stores. This activates STIM1, which then binds to Orai1 at ER-PM junctions, forming an activated CRAC channel, and allowing for Ca^{2+}entry into the cell (shown as red dots). This then leads to the activation of the NFAT pathway. DAG activates both the NFκB pathway and the Ras pathway. These pathways result in the activation of transcription factors, ultimately leading to gene expression and T cell activation. Proteins in red are reported to be S-acylated. APC- antigen presenting cell; TCR- T cell receptor; MHC- major histocompatibility complex; ITAMs-immunoreceptor tyrosine-based activation motifs. Created with BioRender.com.

to antigenic stimulation (Tewari et al., 2021; Fan et al., 2020; Shayahati et al., 2021). Although a lot of progress has been made in the S-acylation field in the last decade, the full extent of S-acylation in T cells is still not fully understood or appreciated. This review aims to demonstrate a broad variety of S-acylated T cell proteins, elucidate the effects of S-acylation on protein function and TCR signaling, and introduce zDHHC/APT enzymes as novel regulators of the immune system.

2 Proximal T cell signaling and the immunological synapse

T cells are activated when the TCR and its co-receptor (CD4/CD8) recognize antigen peptides presented by the major histocompatibility complex (MHC) expressed on the antigen presenting cell (APC) (Brownlie and Zamoyska, 2013) (Figure 1). Upon TCR stimulation, Lck is activated and then phosphorylates the immunoreceptor tyrosine-based activation motifs (ITAMs) of the TCR-associated CD3 and ζ-chains (Ladygina et al., 2011; Brownlie and Zamoyska, 2013; Hwang et al., 2020). ITAMs then act as a docking site for ζ-chain associated protein-70 (ZAP-70) which is subsequently phosphorylated and activated by Lck. Activated ZAP-70 then phosphorylates LAT and SLP-76, which are critical scaffolding proteins necessary for the recruitment, both direct and indirect, of downstream effectors, such as phospholipase C-γ1 (PLC-γ1), and subsequent Ca^{2+} release from the ER stores (Smith-Garvin et al., 2009; Brownlie and Zamoyska, 2013). The proper initiation of these signaling events is required for the activation of several

downstream signaling pathways, such as the NFAT, MAPK, and NF-κB pathways, which are responsible for T cell effector functions, cytokine production, cell differentiation, and cell proliferation (Ladygina et al., 2011; Brownlie and Zamoyska, 2013; Hwang et al., 2020).

These important signaling cascades are initiated at the immunological synapse (IS)—the interface between the APC and the T cell, which is highly regulated, both spatially and temporally (Bijlmakers, 2009; Dustin and Groves, 2012). Upon TCR stimulation, membrane proteins begin to reorganize into microdomains at the IS (Davis and Van Der Merwe, 2006; Ladygina et al., 2011; Dustin and Groves, 2012). These microdomains move dynamically and form concentric rings of proteins around the TCR, and the key signaling proteins are concentrated at the IS to promote T cell activation (Delon et al., 2001; Freiberg et al., 2002). A growing number of studies recognize the importance of the IS microdomains in spatial organization of pre-activated TCR signaling proteins and amplification of the specific antigenic stimuli (Burroughs et al., 2006; Seminario and Bunnell, 2008; Dustin and Depoil, 2011; Dustin and Groves, 2012; Klammt and Lillemeier, 2012). However, the mechanisms underlying antigen-induced changes in lateral movement and selective compartmentalization of the TCR signaling proteins at the IS are still not well understood.

Since lipidation is known to promote protein partitioning into the specialized liquid-ordered PM subdomains (Lucero and Robbins, 2004; Jury et al., 2007), changes in S-acylation could provide a molecular basis for protein re-organization and formation of signaling clusters at the IS upon TCR stimulation. Indeed, recent work has shown that TCR engagement leads to the S-acylation of several key T cell signaling proteins, such as ZAP-70, Lck, Orai1, and LAT, without which, these proteins do not contribute to T cell effector function (Hundt et al., 2006; Akimzhanov and Boehning, 2015; Tewari et al., 2021; Fan et al., 2020; West et al., 2022). Thus, antigen-induced protein S-acylation can be potentially explored as a novel signal transduction mechanism supporting propagation of the TCR signaling cascade at the plasma membrane.

3 S-ACYLATED T cell proteins

3.1 Receptors

3.1.1 CD4/CD8

Both CD4 and CD8 are PM-localized glycoproteins that act as TCR co-receptors by binding, respectively, to class II and class I MHC ligands, and enhancing TCR activation. In 1992, Crise and Rose discovered that CD4 is S-acylated at two cysteine residues located near the junction of the transmembrane and cytoplasmic domains (Crise and Rose, 1992; Fragoso et al., 2003). They also found that the remaining three cytoplasmic cysteines are not S-acylated. However, the effect of CD4 S-acylation on its trafficking to membrane subdomains and further signaling remains controversial. Some groups state that CD4 S-acylation is required for CD4 recruitment into plasma membrane subdomains and may help to activate tyrosine phosphorylation, however, it is not sufficient to induce TCR/protein kinase C clustering and further CD4 signaling (Fragoso et al., 2003; Balamuth et al., 2004). Other groups report that S-acylation does not affect CD4 trafficking to subdomains (Del Real et al., 2002; Popik and Alce, 2004). Unfortunately, there have not been any further studies done on the effects of CD4 S-acylation on membrane subdomain recruitment and subsequent T cell effector function. More detailed studies utilizing super resolution microscopy to investigate the effects of CD4 S-acylation on its co-localization with the TCR at PM subdomains should be done. Additionally, the impact of CD4 S-acylation on T cell activation and effector function should be determined using the acylation-deficient version of the CD4 receptor.

Similar to CD4, CD8 is also S-acylated (Arcaro et al., 2000; Arcaro et al., 2001). It has been reported that the β chain of CD8 is S-acylated on its cytoplasmic tail, however, a specific purpose for this S-acylation is not yet clear. One study reported that murine CD8β S-acylation supports its trafficking to PM subdomains and enhances downstream TCR signaling (Arcaro et al., 2000). However, another study found that S-acylation of human CD8β does not regulate PM subdomain targeting, but rather promotes more efficient CD8/Lck interaction and activation of Lck, and more constitutive association of CD8 with the TCR-CD3 complex (Dick et al., 2007). It has also been found that another CD8 chain, CD8α, is not S-acylated and does not partition into the PM subdomains, leading to CD8αα homodimers having reduced associations with Lck, and therefore, diminished TCR signaling, as compared to CD8αβ heterodimers (Gangadharan and Cheroutre, 2004; Dick et al., 2007). Thus, these observations indicate that S-acylation of CD8 could be used as a regulatory mechanism fine-tuning the TCR activation threshold through protein-protein interactions.

3.1.2 Fas receptor

Fas receptor (FasR), also referred to as CD95, is a key transmembrane receptor for facilitating apoptosis and activation induced cell death in T cells (Zhang et al., 2001; Arakaki et al., 2014). When Fas ligand (FasL) binds to FasR, FasR oligomerizes and interacts with several other proteins, forming the death-inducing signaling complex (DISC). The DISC is then internalized, leading to the activation of effector caspases and subsequent downstream apoptotic signaling (Kaufmann et al., 2012). It has been shown that in order to induce apoptotic signaling, FasR must aggregate in PM subdomains (Kischkel et al., 1995). Chakrabandhu et al. (2007) and Feig et al. (2007) demonstrated that FasR

S-acylation at Cys199 is required for its PM aggregation, and, therefore, is required for optimal apoptosis initiation. The loss of FasR S-acylation resulted in inhibited FasR internalization and suppressed activation of the downstream caspase cascade (Chakrabandhu et al., 2007; Feig et al., 2007). It has also been shown that FasL is S-acylated, as shown in a B cell lymphoma cell line (Guardiola-Serrano et al., 2010). S-acylation of FasL also enhances recruitment to PM subdomains where it can more efficiently interact with the FasR on another cell. Additionally, cells expressing acylation-deficient FasL had significantly lower levels of soluble FasL (Guardiola-Serrano et al., 2010). Overall, S-acylation of both FasR and its ligand leads to enhanced Fas-mediated apoptosis, while a loss of S-acylation in either protein impairs apoptosis (Guardiola-Serrano et al., 2010). FasR and FasL are important examples demonstrating a critical role of S-acylation in regulation of the receptor function, and its significant physiological outcomes.

3.2 Kinases

3.2.1 Lck

Lymphocyte-specific protein tyrosine kinase (Lck) is a member of the Src family of non-receptor tyrosine kinases that plays a critical role in early stages of T cell activation. Upon antigen stimulation, Lck is localized to the TCR-CD3 complex where it phosphorylates the ITAMs and, subsequently, activates recruited ZAP-70 to promote the signaling cascade (Lo et al., 2018). The kinase activity of Lck is largely controlled by phosphorylation and dephosphorylation of the tyrosine residue within the catalytic domain, and a significant fraction of Lck is constitutively activated even in quiescent T cells (Boggon and Eck, 2004; Nika et al., 2010). Interestingly, the amount of activated Lck did not change upon TCR engagement (Nika et al., 2010), indicating that dynamic regulation of Lck activity during TCR signaling is not achieved solely through its phosphorylation, but rather supported by a different mechanism.

In 1993, it was found that Lck is N-myristoylated at Gly2 and dually S-acylated at Cys3 and Cys5 (Paige et al., 1993). Although the individual impact of these cysteines is debated, it has been suggested that S-acylation of Lck, but not N-myristoylation, is required for its recruitment to the plasma membrane and propagation of TCR signaling (Yurchak and Sefton, 1995; Kabouridis et al., 1997). Using subcellular fractionation and confocal microscopy, Kabouridis, et al. (1997) demonstrated that without dual S-acylation Lck does not fully localize to the PM. Another group used total internal reflection fluorescence microscopy (TIRFM) to find that acylation-deficient Lck mutants were not detectable at the PM of Jurkat cells (Zimmermann et al., 2010). However, we have shown, using confocal microscopy, that S-acylation-deficient Lck does still localize to the Jurkat cell PM (Akimzhanov and Boehning, 2015). Despite these contrasting localization results, all of these groups concluded that Lck S-acylation is required for its proper function. Despite acylation-deficient mutants of Lck being still catalytically active (indicated by an *in vitro* assay), they failed to promote a calcium response upon TCR stimulation resulting in loss of NFAT activation, and lack of IL-2 cytokine production and CD69 surface expression, important markers of T cell activation (Kabouridis et al., 1997). Importantly, S-acylation of Lck is agonist-dependent; stimulation of either T cell or Fas receptors triggers extremely rapid (within minutes) and transient increase in S-acylation of Lck (Akimzhanov and Boehning, 2015; Fan et al., 2020; Bieerkehazhi et al., 2022). These findings suggest that activity of Lck in stimulated T cells could be regulated by S-acylation which serves as a molecular basis for dynamic spatial reorganization of pre-activated Lck molecules. Furthermore, this model implies that two classes of enzymes, zDHHC PATs and protein thioesterases, could be recognized as an essential part of the proximal TCR signaling machinery.

3.2.2 Fyn

Fyn, another member of the Src kinase family, is also involved in the early stages of T cell activation and has many of the same phosphorylation targets as Lck. Similar to Lck, Fyn is both N-myristoylated and dually S-acylated. It was found that, like Lck, N-myristoylation of the N-terminal glycine residue is a prerequisite for S-acylation at Cys3 and Cys6 (Alland et al., 1994). It is likely that N-myristoylation of Fyn increases accessibility to a Fyn-specific protein acyltransferase, allowing for the addition of two acyl chains to the protein. Although Fyn can be S-acylated at two cysteine residues, it has been shown that the majority of Fyn protein is singly S-acylated at Cys3, and lipidation of this residue is sufficient for protein localization to the PM and further partitioning into the specialized PM subdomains, such as the IS (Van 't Hof and Resh, 1997; Honda et al., 2000; Liang et al., 2001). Similar to Lck, the lack of PM-associated Fyn also results in decreased calcium fluxes and cell proliferation upon TCR activation, but is much less severe than that of S-acylation deficient Lck, probably due to a significant degree of redundancy between the two kinases (Ladygina et al., 2011). An important distinction of Fyn and Lck regulation is the requirement of N-myristoylation prior to S-acylation, illustrating a possible interplay between S-acylation and other types of protein lipidation.

3.2.3 ZAP-70

ZAP-70 is a key signaling protein of the proximal TCR pathway. Upon TCR activation, it is recruited from the cytoplasm to ITAMs where it is phosphorylated by Lck. Activated ZAP-70 is then released from ITAMs and proceeds to target its effectors, primarily membrane-bound scaffolding proteins LAT and SLP-76 (Courtney et al., 2018). Recently, our group demonstrated TCR-dependent S-acylation of ZAP-70 at a single cysteine residue, Cys564,

localized within the C-terminal part of the protein (Tewari et al., 2021). Interestingly, a homozygous mutation of this lipidation site (c.1690T>C; p. C564R) was reported to be associated with severe combined immunodeficiency in a human patient (Ren et al., 2008), indicating that impaired S-acylation of T cell proteins could be implicated in a pathogenesis of immune system disorders.

Similar to Lck, the acylation-deficient mutant of ZAP-70 was still catalytically active, however, it failed to phosphorylate its substrates resulting in disrupted TCR signaling thus preventing T cell activation (Tewari et al., 2021). Interestingly, biochemical and imaging approaches showed that loss of S-acylation did not disrupt ZAP-70 recruitment to the PM and subsequent activation by Lck (Tewari et al., 2020b). Although the reason why the acylation-deficient ZAP-70 was still unable to phosphorylate its downstream targets is not entirely clear, these observations indicate that TCR-induced S-acylation can mediate translocation of the activated ZAP-70 into spatially segregated PM subdomains containing its downstream effectors. In this scenario, PM recruitment and activation of ZAP-70 is a prerequisite for a zDHHC-mediated S-acylation that drives its subsequent migration into the LAT and SLP-76-containing lateral compartments.

3.3 Adaptor proteins

3.3.1 LAT

After phosphorylation by ZAP-70, linker for activation of T cells, LAT, acts as a docking site for several T cell signaling proteins, such as SLP-76 and phospholipase Cγ-1 (PLC-γ1). The binding of these proteins to LAT is required for their proper activation and subsequent signaling. LAT is a transmembrane protein and requires S-acylation at Cys26 and Cys29 for its localization to the PM and its interaction with the TCR (Zhang et al., 1998; Tanimura et al., 2006). Upon isolation of the IS, it was found that the TCR and S-acylated LAT form a scaffold for TCR signal transduction proteins, while acylation-deficient LAT was unable to co-localize with the TCR (Harder and Kuhn, 2000), due to its retention to the Golgi (Tanimura et al., 2006). Additionally, S-acylation of LAT and subsequent partitioning into PM subdomains is essential for efficient LAT activation, as S-acylation deficient LAT mutants were substantially less phosphorylated compared to WT LAT upon TCR stimulation in Jurkat cells (Zhang et al., 1998; Tanimura et al., 2006). S-acylation was also shown to support stability of LAT protein, as acylation-deficient LAT is more susceptible to premature degradation than WT LAT, suggesting that LAT S-acylation contributes to protein stability (Tanimura et al., 2006). Importantly, it has also been shown that impairment of LAT S-acylation in murine $CD4^+$ T cells was linked to a state of functional unresponsiveness known as T cell anergy, further supporting that S-acylation of T cell proteins has important physiological implications (Hundt et al., 2006).

3.3.2 PAG/cbp

Phosphoprotein associated with GEMs (glycosphingolipid-enriched microdomains) (PAG)/Csk-binding protein (Cbp) is another S-acylated T cell adaptor protein (Posevitz-Fejfár et al., 2008). In resting T cells, Fyn-phosphorylated PAG/Cbp recruits Csk to the PM (Yasuda et al., 2002). When bound to PAG/Cbp, Csk inhibits Src family kinases, Lck and Fyn through phosphorylation of carboxyl terminal tyrosine residues. Upon TCR stimulation, PAG/Cbp becomes dephosphorylated and dissociates from Csk. Lck and Fyn are then dephosphorylated by the protein tyrosine phosphatase CD45 and are able to be activated through phosphorylation of tyrosine residues within their respective kinase domains (Brdicka et al., 2000; Davidson et al., 2016). As a negative regulator of Lck and Fyn, PAG/Cbp plays an important role in preventing aberrant T cell activation (Hořejší, 2004).

Using radiolabeled palmitate, it was found that PAG/Cbp is S-acylated (Brdicka et al., 2000). This protein has a CxxC motif next to its transmembrane domain, making those two cysteines the most likely sites for S-acylation, however, the S-acylation site has not yet been confirmed using acylation assays. Mutating the CxxC to AxxA resulted in a presumably acylation-deficient PAG/Cbp which was used to investigate the effects of lipidation on PAG/Cbp function (Posevitz-Fejfár et al., 2008). Under normal circumstances, PAG/Cbp localizes to GEMs. While PAG/Cbp (AxxA) maintains localization to the PM, it does not localize to the GEMs. However, it is still phosphorylated by Fyn and recruits Csk to non-GEM fractions, further confirming that PAG/Cbp-Csk binding is a phosphorylation-dependent event (Kischkel et al., 1995). Although PAG/Cbp (AxxA) still binds to Csk, this mutation does affect the protein function. It was found that the AxxA mutant results in increased Lck and ZAP-70 phosphorylation, however it is not yet known if this is due to PAG/Cbp being constitutively active when localized to non-GEM domains. Lastly, Jurkat T cells over-expressing PAG/Cbp (AxxA) experienced enhanced migration in response to stromal cell-derived factor 1 (SDF-1), which is reported to preferentially signal from within GEMs (Nguyen and Taub, 2002; Posevitz-Fejfár et al., 2008). These data highlight the importance of PAG/Cbp and Csk recruitment to GEMs, and suggest that S-acylation plays an important role in this protein recruitment and further downstream signaling.

3.4 Ion channels

3.4.1 IP3R

The inositol 1,4,5-trisphosphate receptor (IP_3R) is an ER-localized Ca^{2+} channel playing a critical role in the initiation of the TCR pathway. Engagement of the TCR leads to PLC-γ1

activation and production of IP_3 which binds and activates the IP_3R channel. IP_3R-mediated depletion of the ER Ca^{2+} stores triggers store-operated Ca^{2+} entry (SOCE) and, consequently, orchestrates a variety of downstream signaling events in T cells (Hirota et al., 1998; Trebak and Kinet, 2019). Mass spectrophotometry of the IP_3R protein revealed S-acylation of two cysteines (Cys56, 849) and bioinformatic analysis predicted S-acylation of a third residue (Cys2214). Decreased S-acylation of the IP_3R resulted in reduced Ca^{2+} influx, likely due to premature lysosomal degradation and decreased protein expression, but did not affect localization to the ER (Fredericks et al., 2014). This same study found that IP_3R is S-acylated by zDHHC6 which forms a complex with selenoprotein K (SelK), further discussed below. Interestingly, prior to this discovery, this same group found that SelK KO mice have reduced T cell calcium fluxes in response to αCD3 and chemokine stimulation, as well as reduced T cell proliferation and migration, presumably due to the lack of IP_3R S-acylation (Verma et al., 2011). These data taken together suggest that S-acylation regulates the function of IP_3R through stabilizing protein expression.

3.4.2 Orai1/STIM1

SOCE is a central component of intracellular signaling pathways, including TCR responses in T cells. It is triggered upon receptor engagement and consequent depletion of ER Ca^{2+} stores thorough the IP_3R Ca^{2+} channel. In T cells, SOCE is mediated by the Ca^{2+} release-activated calcium (CRAC) channels formed primarily by STIM1 and Orai1 proteins (Feske et al., 2006; Soboloff et al., 2006; Vig et al., 2006; Zhang et al., 2006). STIM1 serves as a Ca^{2+} sensor that detects depletion of the ER stores *via* EF hands on the luminal portion of the protein. Upon store depletion, STIM1 undergoes a conformational change which allows its SOAR/CAD activation domain to bind Orai1 and gate the channel to allow Ca^{2+} entry (Kim and Muallem, 2011). Both Orai1 and STIM1 are critical for T cell immunity as evident from loss of function mutations of Orai1 or STIM1 which eliminate SOCE and result in impaired cytokine production, abrogated T cell activation, and severe combined immunodeficiency in patients (Feske et al., 2006; Gwack et al., 2008; Oh-Hora et al., 2008; Picard et al., 2009).

The critical step in activation of the CRAC channel is STIM1 translocation into large clusters ("puncta") at ER-plasma membrane junctions where it interacts with Orai1 subunits (Liou et al., 2005; Stathopulos et al., 2006; Pani et al., 2008; Stathopulos et al., 2008; Shaw et al., 2013; Yazbeck et al., 2017). In particular, the enhanced localized Ca^{2+} influx was observed at the T cell/APC contact area, indicating that in T cells Orai1/STIM1-mediated SOCE preferentially occurs within the IS (Barr et al., 2008; Lioudyno et al., 2008; Cahalan and Chandy, 2009). Using acyl-biotin exchange (ABE)-based screening, we found that both major components of the T cell CRAC channel, Orai1 and STIM1, are S-acylated proteins (West et al., 2022). We found that TCR stimulation results in rapid increase in Orai1 S-acylation at Cys143, and that modification of this residue is critical for Orai1 co-localization with STIM1, puncta formation, and SOCE (West et al., 2022). Our findings were independently confirmed by another group which showed that lack of Orai1 S-acylation also decreased NFATC1 translocation to the nucleus and led to diminished IL-2 production in Jurkat T cells (Carreras-Sureda et al., 2021). Similarly, we found that STIM1 undergoes TCR-dependent S-acylation (Kodakandla et al., 2022). Disruption of the STIM1 S-acylation site (Cys437) did not affect its ER localization, but was critical for the assembly of STIM1 into puncta with Orai1 and proper CRAC channel formation. Altogether, these data demonstrate that dynamic stimulus-dependent S-acylation of CRAC channel components is a critical regulator of Ca^{2+} signaling in T cells, and, consequently, can have significant implications for T cell function.

3.5 Other proteins

3.5.1 Ras

Ras proteins are ubiquitously expressed small GTPases critically regulating a variety of T cell processes including T cell development, differentiation, and function (Ladygina et al., 2011; Lapinski and King, 2012). Upon TCR stimulation, Ras proteins are activated by GTP exchange and promote downstream signaling cascades leading to T cell activation and proliferation (Downward et al., 1990; Ebinu et al., 2000; Genot and Cantrell, 2000; Lapinski and King, 2012). Although three Ras isoforms, H-Ras, K-Ras and N-Ras, are closely related and share conserved effector binding domains, their hypervariable C-terminal regions are subjected to different lipid modifications. All isoforms are irreversibly modified with a 15-carbon farnesyl moiety, however, only H-Ras, N-Ras and a K-Ras4B splice variant of K-Ras are S-acylated (Eisenberg et al., 2013). While farnesylation itself is not sufficient for a stable membrane association, additional single (N-Ras and K-Ras4B) or dual (H-Ras) S-acylation promotes Ras recruitment from endomembranes such as the Golgi and ER through vesicular transport, and PM association of non-acylated K-Ras4B is supported by an electrostatic interaction of its polybasic motif (Hancock et al., 1990; Rubio et al., 2010). The ability of Ras to undergo dynamic cycles of S-acylation and de-acylation plays the essential role in regulation of Ras signaling function. S-acylation increases Ras recruitment the PM, and de-acylation promotes rapid retrograde trafficking back to the Golgi, thus preventing Ras over-activation (Rocks et al., 2003). Acylation-deficient N/H-Ras mutants are retained in endomembranes and are not activated upon TCR stimulation (Rubio et al., 2010). Interestingly, non-acylated K-Ras4B is targeted to into cholesterol-independent PM subdomains that do not overlap with

H-Ras partitions (Niv et al., 2002; Prior et al., 2003), further supporting the observation that S-acylation can serve as a molecular basis for selective signaling at the PM.

3.5.2 STAT3

Signal transducer and activator of transcription 3 (STAT3) is another prime example of a protein who's function is regulated by the S-acylation/de-acylation cycle. This transcription factor is recruited to the PM upon activation of cytokine receptors where it is phosphorylated by JAK2, a member of the Janus activating kinases family. Activated STAT3 is then translocated to the nucleus where it induces transcription of its target genes, including *RORC* and *IL17A* which drive differentiation of the T helper 17 (Th17) cells (Capone and Volpe, 2020). Recently, Zhang, et al. (2020) found that STAT3 is S-acylated at Cys108. They determined that the S-acylation of STAT3 is required for the PM recruitment and activation by JAK2, however, phosphorylated STAT3 needs to be de-acylated to be translocated to the nucleus. Even though STAT3 was still able to form homodimers and was present in the nucleus, disruption of the S-acylation/de-acylation cycle of STAT3 in mouse splenocytes prevented its PM recruitment, resulting in inhibited Th17 differentiation (Zhang et al., 2020). This study reveals a unique mechanism controlling STAT3 signal transduction and indicates that S-acylation can potentially serve as a molecular switch between the classical transcriptional function of STAT3 and its non-canonical role in the cytoplasm. Since aberrant function of STAT3 is associated with a variety of human disorders, such as inflammatory diseases and cancer, this study further highlights the therapeutic potential of targeting S-acylation.

3.5.3 VAMP7

VAMP7 belongs to a ubiquitously expressed family of SNARE proteins known as mediators of the vesicular fusion. In T cells, SNAREs have been shown to be involved in TCR recycling to the IS, and it has been found that VAMP7 is particularly important for T cell activation as it is required for LAT recruitment to TCR activation sites, LAT phosphorylation, and downstream T cell signaling (Larghi et al., 2013). It has been shown that S-acylation of VAMP7 at Cys183 is required for its localization to the Golgi under resting conditions. Acylation-deficient VAMP7 instead localizes to the cytosol, presumably in vesicles, and is not properly recruited to the IS upon TCR activation (Morrison et al., 2020). Although the effects of VAMP7 mislocalization on activation of LAT were not assessed in the study, it is likely that loss of VAMP7 S-acylation has significant consequences for downstream TCR signaling.

4 zDHHC enzymes in T cells

The zDHHC family of protein acyltransferases are typically four-pass transmembrane proteins with the zDHHC (Asp-His-His-Cys) catalytic sequence and the C-terminal tail located within the cytosol. The majority of zDHHC acyltransferases were shown to be localized to the Golgi and endoplasmic reticulum (ER) membranes; others were identified as PM- and ER-localized enzymes (Gorleku et al., 2011; Abrami et al., 2017). However, localization of zDHHC enzymes was in many cases examined using proteins overexpressed in HEK293 and HeLa cell lines, therefore, further studies should be done to verify localization of endogenously expressed proteins (Ohno et al., 2006).

A 2012 study revealed the "ping-pong" enzymatic mechanism of the S-acylation reaction indicating that zDHHC enzymes employ a two-step mechanism to modify their protein substrates (Jennings and Linder, 2012). During the first step, an acyl group from acyl-CoA is first transferred to the cysteine residue within the catalytic core of the zDHHC enzyme, forming an acyl-enzyme intermediate. This is then followed by the transfer of the acyl group to a cysteine on the target protein (Figure 2) (Jennings and Linder, 2012). Consistent with the diversity of acyl chains added to substrate proteins, zDHHCs also show some level of acyl chain specificity, likely determined at the acyl-enzyme intermediate step. The first evidence of lipid substrate specificity among these enzymes was reported by Jennings and Linder (Jennings and Linder, 2012), who observed a difference in acyl-CoA preferences between zDHHC3 and zDHHC2 in a competition assay. They found that zDHHC2 is capable of transferring palmitate (C16:0) and longer fatty acids (C18:0, C20:0, C20:4) to a substrate peptide with comparable efficiency, while zDHHC3 showed strong preference for C14 and C16 fatty acids. A more recent study used chemically synthesized azide and alkyne fatty acid probes to compare the lipid substrate specificity of zDHHC3 and zDHHC7 (Greaves et al., 2017). Although these enzymes share close similarity in the primary sequence, the study showed that zDHHC7 has a greater ability to incorporate C18:0 chains compared with zDHHC3. Importantly, the preference for shorter fatty acids was linked to a single amino acid, Ile182, localized in the transmembrane domain 3 of zDHHC3 (Greaves et al., 2017). This indicates that the selectivity of zDHHCs is not decided by availability of the Acyl-CoA substrate, but likely defined at the structural level. This observation is supported by the recent insights into the structure and mechanisms of two closely related enzymes, zDHHC15 and zDHHC20, which revealed that the fatty acyl chain fits into a cavity composed of the four transmembrane helices (Rana et al., 2018a). The residues lining this cavity define its chemical properties and, consequently, the ability to accommodate fatty acyl chains of different length. The sequence analysis of the zDHHC members indicates that the cavity lining residues vary between different zDHHC enzymes indicating that the fatty acyl chain selectivity of zDHHC enzymes is likely determined at the structural level, rather than availability of Acyl-CoA species (Rana et al., 2018b). Although the biological significance of differential fatty S-acylation is still not fully understood, it is possible that

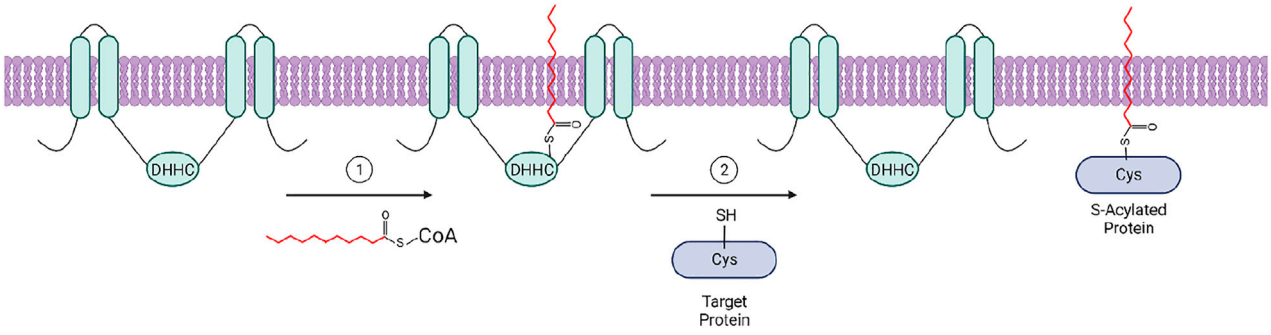

FIGURE 2
The two-step "ping pong" mechanism of zDHHC-mediated protein S-acylation: 1) The acyl group from an acyl-CoA molecule is transferred to the catalytic cysteine residue of the ZDHHC enzyme within the cytosolic loop between transmembrane domains two and three, forming an acyl-enzyme intermediate. 2) The acyl group is subsequently transferred to a free cysteine residue of a target protein, resulting in an S-acylated protein. Created with BioRender.com.

attachment of different fatty acid species can selectively drive proteins into PM domains with various degrees of membrane order. It has been shown that when cells are incubated with polyunsaturated fatty acids (PUFAs), Fyn is S-acylated with those PUFAs, resulting in decreased localization to PM subdomains and decreased MAP kinase activation (Liang et al., 2001). It is not known if this happens in a more physiologically relevant context, but does illustrate the ability of zDHHC enzymes to S-acylate proteins with fatty acids other than the often-studied palmitic acid. Thus, zDHHC protein acyltransferases could serve as enzymes controlling the threshold of T cell activation by targeting signaling proteins in and out of TCR microdomains.

The following section describes PATs that have known roles in T cell signaling. While this is not a full list of zDHHCs expressed in T cells, it does describe zDHHC enzymes known to S-acylate key T cell proteins.

4.1 DHHC6

zDHHC6, permanently localized to the ER membrane, is implicated in T cell signaling due to its ability to S-acylate and stabilize the IP_3R (Fredericks et al., 2014). In Jurkat T cells, shRNA-induced knockdown of zDHHC6 reduced S-acylation and protein expression of the IP_3R leading to decreased Ca^{2+} flux upon TCR stimulation (Fredericks et al., 2014). It was also found that in order to facilitate S-acylation of the IP_3R, zDHHC6 forms a complex with an ER-localized selenium-containing selenoprotein K (SelK), a protein previously reported to be involved in regulation of SOCE (Fredericks and Hoffmann, 2015; Fredericks et al., 2018). Similarly, SelK promotes S-acylation of CD36, the fatty acid transporter, also known to play important roles in T cell biology (Zamora et al., 2013; Wang et al., 2020; Xu et al., 2021). S-acylation of CD36 was shown to be mediated by zDHHC5, however, it is unclear whether SelK forms a complex with zDHHC5 as well. In addition to SelK, the enzymatic function of zDHHC6 can be regulated through the S-acylation of its SH3 domain by another protein acyltransferase, zDHHC16, suggesting the existence of S-acylation cascades (Fredericks et al., 2014; Abrami et al., 2017). Interestingly, S-acylation of zDHHC6 can occur at three different sites leading to potentially eight different zDHHC6 species defined by acyl site occupancy (Abrami et al., 2017), indicating that localization, stability and function of zDHHC6 can be fine-tuned through the actions of upstream protein acyltransferases and thioesterases.

4.2 zDHHC7

zDHHC7 mediates S-acylation of two proteins playing prominent roles in regulation of the T cell function: the FasR and STAT3. zDHHC7 knockdown reduced both total expression of the FasR and its PM localization preventing proper activation of Fas-induced cell death (Rossin et al., 2015). At the molecular level, zDHHC7-mediated S-acylation supports optimal cell surface expression of FasR by protecting it from premature lysosomal degradation, thus maintaining cellular sensitivity to apoptotic signals (Chakrabandhu et al., 2007; Rossin et al., 2015).

zDHHC7 is also responsible for the S-acylation of STAT3 as evidenced by a lack of STAT3 S-acylation in zDHHC7 knockout cells (Zhang et al., 2020). Furthermore, re-expression of zDHHC7 in the knockout cells resulted in a significant increase in STAT3 S-acylation that was not present when the knockout cells expressed a catalytically inactive form of zDHHC7. Since increased STAT3 activation and Th17 cell population are markers of inflammatory bowel disease (IBD) (Britton et al., 2019), the expression of *Zdhhc7* and STAT3 target genes were studied in patients with IBD. It was found that, compared to healthy individuals, patients with IBD have

increased *Zdhhc7* mRNA, pointing to a correlation between dysregulated STAT3 S-acylation and IBD (Zhang et al., 2020). To further investigate this, the authors used *Zdhhc7* knockout mice in an intestinal colitis model, and found that these mice had reduced Th17 cell differentiation and were somewhat protected from colitis. This study highlights the importance of zDHHC enzymes as potential therapeutic targets for IBD and other inflammatory diseases (Zhang et al., 2020).

4.3 zDHHC21

Our group has found that PM-localized zDHHC21 is a critical signaling protein in both human and murine T cells. In Jurkat T cells, zDHHC21 knockdown resulted in the inhibition of Fas-mediated phosphorylation of Lck, ZAP-70, and LAT, as well as the inhibition of calcium release through the IP_3R after FasL stimulation (Akimzhanov and Boehning, 2015). Stimulation of EL-4 murine T cells with cross-linked αCD3/CD28 led to an increased association of zDHHC21 with both Lck and Fyn, while zDHHC21 knockdown led to decreased Lck and Fyn S-acylation, suggesting that zDHHC21 interacts with and either directly or indirectly S-acylates Lck and Fyn (Fan et al., 2020). However, it should be noted that another group suggests that zDHHC2 is responsible for Lck S-acylation (Zeidman et al., 2011). Given that zDHHC enzymes often demonstrate a significant degree of promiscuity (Huang et al., 2009; Greaves and Chamberlain, 2011), it is possible that both zDHHC2 and zDHHC21 could play a role in Lck S-acylation. Furthermore, zDHHC21 knockdown in primary naive murine $CD4^+$ T cells resulted in decreased effector cytokine production, as well as cellular activation and differentiation (Fan et al., 2020). These results indicate a requirement of zDHHC21 for proper activation of TCR signaling proteins and T cell effector function.

The depilated mouse strain (*Zdhhc21*$^{(dep/dep)}$; dep mice) further demonstrates the importance of zDHHC21 (Mayer et al., 1093). Dep mice have a spontaneous recessive three base pair deletion in the *Zdhhc21* gene resulting in an in-frame deletion of Phe233 of zDHHC21. This mutation results in decreased enzymatic activity without significantly affecting expression levels of the enzyme (Mayer et al., 1093; Mill et al., 2009). The depilated mutation results in a loss of Fyn S-acylation, and therefore, mislocalization. Since Fyn is a key signaling protein in keratinocyte development, this affects the *epidermis* and causes disoriented, fragmented, and misshapen hair follicles and shafts, resulting in the gross phenotype of thin, short, matted, and greasy hair, giving the mouse strain the name, depilated (Mayer et al., 1093). Since zDHHC21 is expressed in several different cell types, the dep phenotype goes beyond just the *epidermis*. Dep mice also experience endothelial dysfunction and decreased endothelial inflammation after injury, indicating the functional effects of this zDHHC21 mutation (Beard et al., 2016).

Recently, we found that the dep phenotype extends to T cells as well (Bieerkehazhi et al., 2022). The deletion of F233 in zDHHC21 causes the loss of a canonical Ca^{2+}/calmodulin binding motif, which disrupts calmodulin binding to the C-terminal tail of zDHHC21 in dep $CD4^+$ T cells. This suggests that the dysfunctional nature of ΔF233 zDHHC21 is likely due to the inability of the mutated enzyme to respond to stimulation-induced Ca^{2+} release, suggesting that it is regulated by changes in cytosolic Ca^{2+} concentration and subsequent calmodulin binding. When testing to determine if ΔF233 zDHHC21 affects S-acylation of zDHHC21 substrates, we found that under resting conditions there were no differences in S-acylation of signaling proteins between $CD4^+$ T cells from WT and dep mice. However, when the cells were co-stimulated with αCD3/CD28, WT cells showed an increase in Lck, PLC-γ1, and Erk1/2 S-acylation, while dep $CD4^+$ T cells showed no changes in S-acylation. This indicates that zDHHC21 is required for TCR stimulation-induced S-acylation, but not basal S-acylation. Additionally, it was found that dep $CD4^+$ T cells had reduced phosphorylation of Lck, ZAP-70, LAT, Erk1/2, PLC-γ1, Jnk, and p38 upon TCR stimulation. Consistent with decreased PLC-γ1 phosphorylation, dep T cells also had reduced calcium release from the ER stores upon stimulation with anti-CD3. Lastly, we found that ΔF233 zDHHC21 does not affect T cell development, but it does disrupt T cell activation and differentiation into Th subtypes, as evidenced by decreased cytokine production and expression of transcription factors specific to Th1, Th2, and Th17 lineages (Bieerkehazhi et al., 2022). These data together, suggest that zDHHC21-mediated S-acylation may be one of the earliest signaling events after TCR stimulation, and demonstrate that zDHHC21-mediated S-acylation is a key part of the early TCR signal transduction cascade. Due to the changes in stimulation-induced S-acylation but not basal S-acylation observed in dep mice, ΔF233 zDHHC21 provides an opportunity to test the effects of transient agonist-induced S-acylation on cell signaling, which is not possible in conventional knockdown and knockout models.

5 Conclusion

Despite the early discovery of protein S-acylation in 1979 (Schmidt and Schlesinger, 1979), its role in the immune system remained largely unexplored. Recent development of robust biochemical techniques to detect protein S-acylation, frequently coupled with advanced proteomics approaches, resulted in a rapidly growing number of newly discovered S-acylated proteins. Among them, there is a broad variety of proteins with pivotal roles in T cell signaling, including receptors (CD4, CD8, FasR), enzymes (Lck, ZAP-70, PLC-γ1), adaptor

proteins (LAT, PAG/Cbp), calcium channels (Orai1, IP_3R), and even a transcription factor (STAT3). Given the significant impact of S-acylation on protein function, these findings indicate that S-acylation is a widespread post-translational modification playing a vital role in the T cell-mediated immune responses.

The addition of a long-chain fatty acid moiety is known to affect either protein localization to the PM, or, while at the PM, partitioning into liquid ordered, cholesterol and sphingolipid enriched PM fractions, functionally designated as PM domains or lipid rafts. These domains, including the immunological synapse in T cells, serve to confine signaling proteins and, consequently, promote specific protein-protein interactions. Although kinetics of S-acylation is not often assessed, several examples, such as kinases Lck and ZAP-70, or CRAC channel proteins, demonstrate the extremely dynamic nature of S-acylation in T cells. These observations indicate a potentially important function of S-acylation as a signal transduction mechanism mediating rapid assembly of the TCR signaling machinery at the IS in response to antigenic stimulation.

S-acylation of Lck was discovered more than two decades ago. However, until recently, enzymes that catalyze S-acylation of Lck and other T cell proteins, remained enigmatic. Although we are just beginning to understand the role of zDHHC enzymes in T cells, recent reports showing that zDHHC21 and zDHHC7 are critical for Th differentiation demonstrate that characterization of protein acyltransferases can potentiate the discovery of novel immunoregulatory pathways. These early findings provide first evidence that zDHHC enzymes can play critical functions in regulation of the adaptive immune system.

Much more work still needs to be done to further identify and characterize S-acylated T cell proteins, and define the role of zDHHC protein acyltransferases and thioesterases in regulation of T cell function. However, we hope that this review provides a sufficient insight into the importance of protein S-acylation for T cell function and demonstrates that this modification and mediating enzymes could be promising therapeutic targets in the diseases associated with altered T cell homeostasis.

Author contributions

SW, DB, and AA wrote the manuscript.

Funding

Research reported in this publication was supported by the National Institute of General Medical Sciences of the National Institutes of Health (NIH/NIGMS) under award number F31GM140644 (to SW). This work was also supported by NIH/NIGMS awards R01GM115446 (to AA) and R01GM130840 (to DB and AA).

Conflict of interest

The authors declare that the research was conducted in the absence of any commercial or financial relationships that could be construed as a potential conflict of interest.

Publisher's note

All claims expressed in this article are solely those of the authors and do not necessarily represent those of their affiliated organizations, or those of the publisher, the editors and the reviewers. Any product that may be evaluated in this article, or claim that may be made by its manufacturer, is not guaranteed or endorsed by the publisher.

References

Abrami, L., Dallavilla, T., Sandoz, P. A., Demir, M., Kunz, B., Savoglidis, G., et al. (2017). Identification and dynamics of the human ZDHHC16-ZDHHC6 palmitoylation cascade. *Elife* 6, 27826. doi:10.7554/eLife.27826

Akimzhanov, A. M., and Boehning, D. (2015). Rapid and transient palmitoylation of the tyrosine kinase Lck mediates Fas signaling. *Proc. Natl. Acad. Sci. U. S. A.* 112, 11876–11880. doi:10.1073/pnas.1509929112

Alland, L., Peseckis, S., Atherton, R., Berthiaume, L., and Resh, M. (1994). Dual myristylation and palmitylation of Src family member p59fyn affects subcellular localization. *J. Biol. Chem.* 269, 16701–16705. doi:10.1016/s0021-9258(19)89447-4

Arakaki, R., Yamada, A., Kudo, Y., Hayashi, Y., and Ishimaru, N. (2014). Mechanism of activation-induced cell death of T cells and regulation of FasL expression. *Crit. Rev. Immunol.* 34, 301–314. doi:10.1615/CRITREVIMMUNOL.2014009988

Arcaro, A., Grégoire, C., Boucheron, N., Stotz, S., Palmer, E., Malissen, B., et al. (2000). Essential role of CD8 palmitoylation in CD8 coreceptor function. *J. Immunol.* 165, 2068–2076. doi:10.4049/jimmunol.165.4.2068

Arcaro, A., Grégoire, C., Bakker, T. R., Baldi, L., Jordan, M., Goffin, L., et al. (2001). CD8beta endows CD8 with efficient coreceptor function by coupling T cell receptor/CD3 to raft-associated CD8/p56(lck) complexes. *J. Exp. Med.* 194, 1485–1495. doi:10.1084/jem.194.10.1485

Balamuth, F., Brogdon, J. L., and Bottomly, K. (2004). CD4 raft association and signaling regulate molecular clustering at the immunological synapse site. *J. Immunol.* 172, 5887–5892. doi:10.4049/jimmunol.172.10.5887

Bannan, B. A., Van Etten, J., Kohler, J. A., Tsoi, Y., Hansen, N. M., Sigmon, S., et al. (2008). The drosophila protein palmitoylome characterizing palmitoyl-thioesterases and DHHC palmitoyl-transferases. *Fly. (Austin)* 2, 198–214. doi:10.4161/fly.6621

Barr, V. A., Bernot, K. M., Srikanth, S., Gwack, Y., Balagopalan, L., Regan, C. K., et al. (2008). Dynamic movement of the calcium sensor STIM1 and the calcium channel Orai1 in activated T-cells: Puncta and distal caps. *Mol. Biol. Cell* 19, 2802–2817. doi:10.1091/mbc.E08-02-0146

Bartels, D. J., Mitchell, D. A., Dong, X., and Deschenes, R. J. (1999). Erf2, a novel gene product that affects the localization and palmitoylation of Ras2 in *Saccharomyces cerevisiae*. *Mol. Cell. Biol.* 19, 6775–6787. doi:10.1128/mcb.19.10.6775

Beard, R. S., Yang, X., Meegan, J. E., Overstreet, J. W., Yang, C. G. Y. Y., Elliott, J. A., et al. (2016). Palmitoyl acyltransferase DHHC21 mediates endothelial

dysfunction in systemic inflammatory response syndrome. *Nat. Commun.* 7, 12823. doi:10.1038/ncomms12823

Bellizzi, J., Widom, J., Kemp, C., Lu, J., Das, A., Hofmann, S., et al. (2000). The crystal structure of palmitoyl protein thioesterase 1 and the molecular basis of infantile neuronal ceroid lipofuscinosis. *Proc. Natl. Acad. Sci. U. S. A.* 97, 4573–4578. doi:10.1073/PNAS.080508097

Bieerkehazhi, S., Fan, Y., West, S. J., Tewari, R., Ko, J., Mills, T., et al. (2022). Ca2+-dependent protein acyltransferase DHHC21 controls activation of CD4+ T cells. *J. Cell Sci.* 135, jcs258186. doi:10.1242/jcs.258186

Bijlmakers, M-J. J. (2009). Protein acylation and localization in T cell signaling (Review). *Mol. Membr. Biol.* 26, 93–103. doi:10.1080/09687680802650481

Blanc, M., David, F. P. A., and van der Goot, F. G. (2019). SwissPalm 2: Protein S-palmitoylation database. *Methods Mol. Biol.* 2009, 203–214. doi:10.1007/978-1-4939-9532-5_16

Boggon, T. J., and Eck, M. J. (2004). Structure and regulation of Src family kinases. *Oncogene* 23, 7918–7927. doi:10.1038/sj.onc.1208081

Brdicka, T., Pavlistová, D., Leo, A., Bruyns, E., Korínek, V., Angelisová, P., et al. (2000). Phosphoprotein associated with glycosphingolipid-enriched microdomains (PAG), a novel ubiquitously expressed transmembrane adaptor protein, binds the protein tyrosine kinase csk and is involved in regulation of T cell activation. *J. Exp. Med.* 191, 1591–1604. doi:10.1084/JEM.191.9.1591

Britton, G., Contijoch, E., Mogno, I., Vennaro, O., Llewellyn, S., Ng, R., et al. (2019). Microbiotas from humans with inflammatory bowel disease alter the balance of gut Th17 and RORγt + regulatory T cells and exacerbate colitis in mice. *Immunity* 50, 212–224. e4. doi:10.1016/J.IMMUNI.2018.12.015

Brownlie, R. J., and Zamoyska, R. (2013). *T cell receptor signalling networks: Branched, diversified and bounded*. doi:10.1038/nri3403

Burgoyne, J. R., Oviosu, O., and Eaton, P. (2013). The PEG-switch assay: A fast semi-quantitative method to determine protein reversible cysteine oxidation. *J. Pharmacol. Toxicol. Methods* 68, 297–301. doi:10.1016/j.vascn.2013.07.001

Burroughs, N. J., Lazic, Z., and Van Der Merwe, P. A. (2006). Ligand detection and discrimination by spatial relocalization: A kinase-phosphatase segregation model of TCR activation. *Biophys. J.* 91, 1619–1629. doi:10.1529/biophysj.105.080044

Cahalan, M. D., and Chandy, K. G. (2009). The functional network of ion channels in T lymphocytes. *Immunol. Rev.* 231, 59–87. doi:10.1111/j.1600-065X.2009.00816.x

Camp, L., Verkruyse, L., Afendis, S., Slaughter, C., and Hofmann, S. (1994). Molecular cloning and expression of palmitoyl-protein thioesterase. *J. Biol. Chem.* 269, 23212–23219. doi:10.1016/s0021-9258(17)31641-1

Camp, L. A., and Hofmann, S. L. (1993). Purification and properties of a palmitoyl-protein thioesterase that cleaves palmitate from H-ras. *J. Biol. Chem.* 268, 22566–22574. doi:10.1016/S0021-9258(18)41567-0

Capone, A., and Volpe, E. (2020). Transcriptional regulators of T helper 17 cell differentiation in Health and autoimmune diseases. *Front. Immunol.* 11, 348. doi:10.3389/FIMMU.2020.00348

Carreras-Sureda, A., Abrami, L., Ji-Hee, K., Wang, W-A., Henry, C., Frieden, M., et al. (2021). S-acylation by ZDHHC20 targets ORAI1 channels to lipid rafts for efficient Ca2+ signaling by Jurkat T cell receptors at the immune synapse. *Elife* 10, 72051. doi:10.7554/eLife.72051

Chakrabandhu, K., Hérincs, Z., Huault, S., Dost, B., Peng, L., Conchonaud, F., et al. (2007). Palmitoylation is required for efficient Fas cell death signaling. *EMBO J.* 26, 209–220. doi:10.1038/sj.emboj.7601456

Chamberlain, L. H., and Shipston, M. J. (2015). The physiology of protein S-acylation. *Physiol. Rev.* 95, 341–376. doi:10.1152/physrev.00032.2014

Chen, J. J., Fan, Y., and Boehning, D. (2021). Regulation of dynamic protein S-acylation. *Front. Mol. Biosci.* 8, 65644. doi:10.3389/fmolb.2021.656440

Courtney, A. H., Lo, W. L., and Weiss, A. (2018). TCR signaling: Mechanisms of initiation and propagation. *Trends biochem. Sci.* 43, 108–123. doi:10.1016/j.tibs.2017.11.008

Crise, B., and Rose, J. K. (1992). Identification of palmitoylation sites on CD4, the human immunodeficiency virus receptor*. *J. Biol. Chem.* 267, 13593–13597. doi:10.1016/s0021-9258(18)42253-3

Davidson, D., Zhong, M-C., Pandolfi, P. P., Bolland, S., Xavier, R. J., Seed, B., et al. (2016). The csk-associated adaptor PAG inhibits effector T cell activation in cooperation with phosphatase PTPN22 and dok adaptors. *Cell Rep.* 17, 2776–2788. doi:10.1016/j.celrep.2016.11.035

Davis, S. J., and Van Der Merwe, A. (2006). The kinetic-segregation model: TCR triggering and beyond. *Nat. Immunol.* 7, 803–809. doi:10.1038/ni1369

De, I., and Sadhukhan, S. (2018). Emerging roles of DHHC-mediated protein S-palmitoylation in physiological and pathophysiological context. *Eur. J. Cell Biol.* 97, 319–338. doi:10.1016/j.ejcb.2018.03.005

Del Real, G., Jiménez-Baranda, S., Lacalle, R. A., Mira, E., Lucas, P., Gómez-Moutón, C., et al. (2002). Blocking of HIV-1 infection by targeting CD4 to nonraft membrane domains. *J. Exp. Med.* 196, 293–301. doi:10.1084/jem.20020308

Delon, J., Kaibuchi, K., and Germain, R. N. (2001). Exclusion of CD43 from the immunological synapse is mediated by phosphorylation-regulated relocation of the cytoskeletal adaptor moesin. *Immunity* 15, 691–701. doi:10.1016/S1074-7613(01)00231-X

DeMar, J. C., and Anderson, R. E. (1997). Identification and quantitation of the fatty acids composing the CoA ester pool of bovine retina, heart, and liver. *J. Biol. Chem.* 272, 31362–31368. doi:10.1074/jbc.272.50.31362

Dick, J. P., Hayday, A. C., and Bijlmakers, M. J. (2007). CD8 Raft localization is induced by its assembly into CD8alpha beta heterodimers, Not CD8alpha alpha homodimers. *J. Biol. Chem.* 282, 13884–13894. doi:10.1074/jbc.M701027200

Downward, J., Graves, J., Warne, P., Rayter, S., and Cantrell, D. (1990). Stimulation of p21ras upon T-cell activation. *Nature* 346, 719–723. doi:10.1038/346719A0

Drisdel, R. C., and Green, W. N. (2004). Labeling and quantifying sites of protein palmitoylation. *Biotechniques* 36, 276–285. doi:10.2144/04362rr02

Duncan, J. A., and Gilman, A. G. (1998). A cytoplasmic acyl-protein thioesterase that removes palmitate from G protein α subunits and p21RAS. *J. Biol. Chem.* 273, 15830–15837. doi:10.1074/JBC.273.25.15830

Dustin, M. L., and Depoil, D. (2011). New insights into the T cell synapse from single molecule techniques. *Nat. Rev. Immunol.* 11, 672–684. doi:10.1038/nri3066

Dustin, M. L., and Groves, J. T. (2012). Receptor signaling clusters in the immune synapse. *Annu. Rev. Biophys.* 41, 543–556. doi:10.1146/annurev-biophys-042910-155238

Ebinu, J. O., Stang, S. L., Teixeira, C., Bottorff, D. A., Hooton, J., Blumberg, P. M., et al. (2000). RasGRP links T-cell receptor signaling to Ras. *Blood* 95, 3199–3203. doi:10.1182/blood.v95.10.3199.010k37_3199_3203

Eisenberg, S., Laude, A. J., Beckett, A. J., Mageean, C. J., Aran, V., Hernandez-Valladares, M., et al. (2013). The role of palmitoylation in regulating Ras localization and function. *Biochem. Soc. Trans.* 41, 79–83. doi:10.1042/BST20120268

Fan, Y., Shayahati, B., Tewari, R., Boehning, D., and Akimzhanov, A. M. (2020). Regulation of T cell receptor signaling by protein acyltransferase DHHC21. *Mol. Biol. Rep.* 47, 6471–6478. doi:10.1007/s11033-020-05691-1

Feig, C., Tchikov, V., Schütze, S., and Peter, M. E. (2007). Palmitoylation of CD95 facilitates formation of SDS-stable receptor aggregates that initiate apoptosis signaling. *EMBO J.* 26, 221–231. doi:10.1038/sj.emboj.7601460

Feske, S., Gwack, Y., Prakriya, M., Srikanth, S., Puppel, S-H. H., Tanasa, B., et al. (2006). A mutation in Orai1 causes immune deficiency by abrogating CRAC channel function. *Nature* 441, 179–185. doi:10.1038/nature04702

Fragoso, R., Ren, D., Zhang, X., Su, M. W-C., Burakoff, S. J., and Jin, Y-J. (2003). Lipid raft distribution of CD4 depends on its palmitoylation and association with Lck, and evidence for CD4-induced lipid raft aggregation as an additional mechanism to enhance CD3 signaling. *J. Immunol.* 170, 913–921. doi:10.4049/jimmunol.170.2.913

Fredericks, G., and Hoffmann, P. (2015). Selenoprotein K and protein palmitoylation. *Antioxid. Redox Signal.* 23, 854–862. doi:10.1089/ARS.2015.6375

Fredericks, G. J., Hoffmann, F. K. W., Rose, A. H., Osterheld, H. J., Hess, F. M., Mercier, F., et al. (2014). Stable expression and function of the inositol 1, 4, 5-triphosphate receptor requires palmitoylation by a DHHC6/selenoprotein K complex. *Proc. Natl. Acad. Sci. U. S. A.* 111, 16478–16483. doi:10.1073/pnas.1417176111

Fredericks, G. J., Hoffmann, F. W., Hondal, R. J., Rozovsky, S., Urschitz, J., and Hoffmann, P. R. (2018). Selenoprotein K increases efficiency of DHHC6 catalyzed protein palmitoylation by stabilizing the acyl-DHHC6 intermediate. *Antioxidants* 7, E4. doi:10.3390/ANTIOX7010004

Freiberg, B. A., Kupfer, H., Maslanik, W., Delli, J., Kappler, J., Zaller, D. M., et al. (2002). Staging and resetting T cell activation in SMACs. *Nat. Immunol.* 3, 911–917. doi:10.1038/ni836

Fujimoto, T., Stroud, E., Whatley, R. E., Prescott, S. M., Muszbek, L., Laposata, M., et al. (1993). P-selectin is acylated with palmitic acid and stearic acid at cysteine 766 through a thioester linkage. *J. Biol. Chem.* 268, 11394–11400. doi:10.1016/s0021-9258(18)82137-8

Gangadharan, D., and Cheroutre, H. (2004). The CD8 isoform CD8alphaalpha is not a functional homologue of the TCR co-receptor CD8alphabeta. *Curr. Opin. Immunol.* 16, 264–270. doi:10.1016/j.coi.2004.03.015

Genot, E., and Cantrell, D. (2000). Ras regulation and function in lymphocytes. *Curr. Opin. Immunol.* 12, 289–294. doi:10.1016/S0952-7915(00)00089-3

Gorleku, O. A., Barns, A-M., Prescott, G. R., Greaves, J., and Chamberlain, L. H. (2011). Endoplasmic reticulum localization of DHHC palmitoyltransferases mediated by lysine-based sorting signals. *J. Biol. Chem.* 286, 39573–39584. doi:10.1074/jbc.M111.272369

Greaves, J., and Chamberlain, L. H. (2011). DHHC palmitoyl transferases: Substrate interactions and (patho)physiology. *Trends biochem. Sci.* 36, 245–253. doi:10.1016/j.tibs.2011.01.003

Greaves, J., Munro, K. R., Davidson, S. C., Riviere, M., Wojno, J., Smith, T. K., et al. (2017). Molecular basis of fatty acid selectivity in the zDHHC family of S-acyltransferases revealed by click chemistry. *Proc. Natl. Acad. Sci. U. S. A.* 114, E1365–E1374. doi:10.1073/pnas.1612254114

Guardiola-Serrano, F., Rossin, A., Cahuzac, N., Lückerath, K., Melzer, I., Mailfert, S., et al. (2010). Palmitoylation of human FasL modulates its cell death-inducing function. *Cell Death Dis.* 1, e88. doi:10.1038/cddis.2010.62

Gwack, Y., Srikanth, S., Oh-Hora, M., Hogan, P. G., Lamperti, E. D., Yamashita, M., et al. (2008). Hair loss and defective T- and B-cell function in mice lacking ORAI1. *Mol. Cell. Biol.* 28, 5209–5222. doi:10.1128/MCB.00360-08

Hallak, H., Brass, L. F., and Manning, D. R. (1994). Failure to myristoylate the α subunit of G(z) is correlated with an inhibition of palmitoylation and membrane attachment, but has no affect on phosphorylation by protein kinase C. *J. Biol. Chem.* 269, 4571–4576. doi:10.1016/s0021-9258(17)41815-1

Hancock, J., Paterson, H., and Marshall, C. (1990). A polybasic domain or palmitoylation is required in addition to the CAAX motif to localize p21ras to the plasma membrane. *Cell* 63, 133–139. doi:10.1016/0092-8674(90)90294-O

Hannoush, R. N., and Sun, J. (2010). The chemical toolbox for monitoring protein fatty acylation and prenylation. *Nat. Chem. Biol.* 6, 498–506. doi:10.1038/nchembio.388

Harder, T., and Kuhn, M. (2000). Selective accumulation of raft-associated membrane protein LAT in T cell receptor signaling assemblies. *J. Cell Biol.* 151, 199–208. doi:10.1083/jcb.151.2.199

Hirota, J., Baba, M., Matsumoto, M., Furuichi, T., Takatsu, K., and Mikoshiba, K. (1998). T-cell-receptor signalling in inositol 1, 4, 5-trisphosphate receptor (IP3R) type-1-deficient mice: Is IP3R type 1 essential for T-cell-receptor signalling? *Biochem. J.* 333, 615–619. doi:10.1042/bj3330615

Honda, Z., Suzuki, T., Kono, H., Okada, M., Yamamoto, T., Ra, C., et al. (2000). Sequential requirements of the N-terminal palmitoylation site and SH2 domain of Src family kinases in the initiation and progression of FcepsilonRI signaling. *Mol. Cell. Biol.* 20, 1759–1771. doi:10.1128/mcb.20.5.1759-1771.2000

Hořejší, V. (2004). Transmembrane adaptor proteins in membrane microdomains: Important regulators of immunoreceptor signaling. *Immunol. Lett.* 92, 43–49. doi:10.1016/J.IMLET.2003.10.013

Huang, K., Sanders, S., Singaraja, R., Orban, P., Cijsouw, T., Arstikaitis, P., et al. (2009). Neuronal palmitoyl acyl transferases exhibit distinct substrate specificity. *FASEB J.* 23, 2605–2615. doi:10.1096/fj.08-127399

Hundt, M., Tabata, H., Jeon, M. S., Hayashi, K., Tanaka, Y., Krishna, R., et al. (2006). Impaired activation and localization of LAT in anergic T cells as a consequence of a selective palmitoylation defect. *Immunity* 24, 513–522. doi:10.1016/j.immuni.2006.03.011

Hwang, J. R., Byeon, Y., Kim, D., and Park, S. G. (2020). Recent insights of T cell receptor-mediated signaling pathways for T cell activation and development. *Exp. Mol. Med.* 52, 750–761. doi:10.1038/s12276-020-0435-8

Jennings, B. C., and Linder, M. E. (2012). DHHC protein S-acyltransferases use similar ping-pong kinetic mechanisms but display different Acyl-CoA specificities. *J. Biol. Chem.* 287, 7236–7245. doi:10.1074/jbc.M111.337246

Jury, E. C., Flores-Borja, F., and Kabouridis, P. S. (2007). Lipid rafts in T cell signalling and disease. *Semin. Cell Dev. Biol.* 18, 608–615. doi:10.1016/j.semcdb.2007.08.002

Kabouridis, P. S., Magee, A. I., and Ley, S. C. (1997). S-acylation of LCK protein tyrosine kinase is essential for its signalling function in T lymphocytes. *EMBO J.* 16, 4983–4998. doi:10.1093/emboj/16.16.4983

Kaufmann, T., Strasser, A., and Jost, P. J. (2012). Fas death receptor signalling: Roles of bid and XIAP. *Cell Death Differ.* 19, 42–50. doi:10.1038/CDD.2011.121

Kim, J. Y., and Muallem, S. (2011). Unlocking SOAR releases STIM. *EMBO J.* 30, 1673–1675. doi:10.1038/emboj.2011.107

Kischkel, F. C., Hellbardt, S., Behrmann, I., Germer, M., Pawlita, M., Krammer, P. H., et al. (1995). *Cytotoxicity-dependent APO-1 (Fas/CD95)-associated proteins form a death-inducing signaling complex (DISC) with the receptor - PubMed.*

Klammt, C., and Lillemeier, B. F. (2012). How membrane structures control T cell signaling. *Front. Immunol.* 3, 291–299. doi:10.3389/fimmu.2012.00291

Kodakandla, G., West, S. J., Wang, Q., Tewari, R., Zhu, M. X., Akimzhanov, A. M., et al. (2022). Dynamic S-acylation of STIM1 is required for store-operated Ca2+ entry. *J. Biol. Chem.* 298 (9), 102303. doi:10.1016/j.jbc.2022.102303

Ladygina, N., Martin, B. R., and Altman, A. (2011). Dynamic palmitoylation and the role of DHHC proteins in T cell activation and anergy. *Adv. Immunol.* 109, 1–44. doi:10.1016/B978-0-12-387664-5.00001-7

Lapinski, P. E., and King, P. D. (2012). Regulation of Ras signal transduction during T cell development and activation. *Am. J. Clin. Exp. Immunol.* 1, 147–153. Available at: http://www.ncbi.nlm.nih.gov/pubmed/23205323.

Larghi, P., Williamson, D. J., Carpier, J-M., Dogniaux, S., Chemin, K., Bohineust, A., et al. (2013). VAMP7 controls T cell activation by regulating the recruitment and phosphorylation of vesicular Lat at TCR-activation sites. *Nat. Immunol.* 147 (14), 723–731. doi:10.1038/ni.2609

Li, Y., Pu, F., Wang, J., Zhou, Z., Zhang, C., He, F., et al. (2021). Machine learning methods in prediction of protein palmitoylation sites: A brief review. *Curr. Pharm. Des.* 27, 2189–2198. doi:10.2174/1381612826666201112142826

Liang, X., Nazarian, A., Erdjument-Bromage, H., Bornmann, W., Tempst, P., and Resh, M. D. (2001). Heterogeneous fatty acylation of Src family kinases with polyunsaturated fatty acids regulates raft localization and signal transduction. *J. Biol. Chem.* 276, 30987–30994. doi:10.1074/jbc.M104018200

Lin, D., and Conibear, E. (2015). Enzymatic protein depalmitoylation by acyl protein thioesterases. *Biochem. Soc. Trans.* 43, 193–198. doi:10.1042/BST20140235

Lin, D. T. S., , et al.Tse, D., Lin, S., Conibear, E., Lin, D. T. S., Conibear, E. (2015). ABHD17 proteins are novel protein depalmitoylases that regulate N-Ras palmitate turnover and subcellular localization. *Elife* 4, e11306–e11314. doi:10.7554/eLife.11306

Liou, J., Kim, M. L., Do, Heo W., Jones, J. T., Myers, J. W., Ferrell, J. E., et al. (2005). STIM is a Ca2+ sensor essential for Ca2+-store-depletion-triggered Ca2+ influx. *Curr. Biol.* 15, 1235–1241. doi:10.1016/j.cub.2005.05.055

Lioudyno, M. I., Kozak, J. A., Penna, A., Safrina, O., Zhang, S. L., Sen, D., et al. (2008). Orai1 and STIM1 move to the immunological synapse and are up-regulated during T cell activation. *Proc. Natl. Acad. Sci. U. S. A.* 105, 2011–2016. doi:10.1073/pnas.0706122105

Lo, W. L., Shah, N. H., Ahsan, N., Horkova, V., Stepanek, O., Salomon, A. R., et al. (2018). Lck promotes Zap70-dependent LAT phosphorylation by bridging Zap70 to LAT. *Nat. Immunol.* 19, 733–741. doi:10.1038/s41590-018-0131-1

Lobo, S., Greentree, W. K., Linder, M. E., and Deschenes, R. J. (2002). Identification of a ras palmitoyltransferase in *Saccharomyces cerevisiae*. *J. Biol. Chem.* 277, 41268–41273. doi:10.1074/jbc.M206573200

Lucero, H., and Robbins, P. W. (2004). Lipid rafts-protein association and the regulation of protein activity. *Arch. Biochem. Biophys.* 426, 208–224. doi:10.1016/j.abb.2004.03.020

Mayer, T. C., Kleiman, N. J., and Green, M. C. Depilated (dep), a mutant gene that affects the coat OF THE MOUSE AND ACTS IN THE EPIDERMIS. *Genetics* 84, 59–65. doi:10.1093/genetics/84.1.59

Mill, P., Lee, A. W. S., Fukata, Y., Tsutsumi, R., Fukata, M., Keighren, M., et al. (2009). Palmitoylation regulates epidermal homeostasis and hair follicle differentiation. *PLoS Genet.* 5, e1000748. doi:10.1371/journal.pgen.1000748

Montigny, C., Decottignies, P., Le Maréchal, P., Capy, P., Bublitz, M., Olesen, C., et al. (2014). S-palmitoylation and S-oleoylation of rabbit and pig sarcolipin. *J. Biol. Chem.* 289, 33850–33861. doi:10.1074/jbc.M114.590307

Morrison, E., Kuropka, B., Kliche, S., Brügger, B., Krause, E., and Freund, C. (2015). Quantitative analysis of the human T cell palmitome. *Sci. Rep.* 5, 11598. doi:10.1038/srep11598

Morrison, E., Wegner, T., Zucchetti, A. E., Álvaro-Benito, M., Zheng, A., Kliche, S., et al. (2020). Dynamic palmitoylation events following T-cell receptor signaling. *Commun. Biol.* 3, 368–369. doi:10.1038/s42003-020-1063-5

Muszbek, L., and Laposata, M. (1993). Covalent modification of proteins by arachidonate and eicosapentaenoate in platelets. *J. Biol. Chem.* 268, 18243–18248. doi:10.1016/s0021-9258(17)46836-0

Nguyen, D. H., and Taub, D. (2002). CXCR4 function requires membrane cholesterol: Implications for HIV infection. *J. Immunol.* 168, 4121–4126. doi:10.4049/JIMMUNOL.168.8.4121

Nika, K., Soldani, C., Salek, M., Paster, W., Gray, A., Etzensperger, R., et al. (2010). Constitutively active lck kinase in T cells drives antigen receptor signal transduction. *Immunity* 32, 766–777. doi:10.1016/j.immuni.2010.05.011

Niv, H., Gutman, O., Kloog, Y., and Henis, Y. I. (2002). Activated K-Ras and H-Ras display different interactions with saturable nonraft sites at the surface of live cells. *J. Cell Biol.* 157, 865–872. doi:10.1083/jcb.200202009

Oh-Hora, M., Yamashita, M., Hogan, P. G., Sharma, S., Lamperti, E., Chung, W., et al. (2008). Dual functions for the endoplasmic reticulum calcium sensors STIM1 and STIM2 in T cell activation and tolerance. *Nat. Immunol.* 9, 432–443. doi:10.1038/ni1574

Ohno, Y., Kihara, A., Sano, T., and Igarashi, Y. (2006). Intracellular localization and tissue-specific distribution of human and yeast DHHC cysteine-rich domain-containing proteins. *Biochim. Biophys. Acta* 1761, 474–483. doi:10.1016/j.bbalip.2006.03.010

Paige, L. A., Nadler, M. J. S., Harrison, M. L., Cassady, J. M., and Geahlen, R. L. (1993). Reversible palmitoylation of the protein-tyrosine kinase p56lck. *J. Biol. Chem.* 268, 8669–8674. doi:10.1016/s0021-9258(18)52927-6

Pani, B., Hwei, L. O., Liu, X., Rauser, K., Ambudkar, I. S., and Singh, B. B. (2008). Lipid rafts determine clustering of STIM1 in endoplasmic reticulum-plasma membrane junctions and regulation of store-operated Ca2+ entry (SOCE). *J. Biol. Chem.* 283, 17333–17340. doi:10.1074/jbc.M800107200

Picard, C., McCarl, C-A., Papolos, A., Khalil, S., Lüthy, K., Hivroz, C., et al. (2009). STIM1 mutation associated with a syndrome of immunodeficiency and autoimmunity. *N. Engl. J. Med.* 360, 1971–1980. doi:10.1056/NEJMoa0900082

Popik, W., and Alce, T. M. (2004). CD4 receptor localized to non-raft membrane microdomains supports HIV-1 entry. Identification of a novel raft localization marker in CD4. *J. Biol. Chem.* 279, 704–712. doi:10.1074/jbc.M306380200

Posevitz-Fejfár, A., Šmída, M., Kliche, S., Hartig, R., Schraven, B., and Lindquist, J. A. (2008). A displaced PAG enhances proximal signaling and SDF-1-induced T cell migration. *Eur. J. Immunol.* 38, 250–259. doi:10.1002/EJI.200636664

Prior, I. A., Muncke, C., Parton, R. G., and Hancock, J. F. (2003). Direct visualization of Ras proteins in spatially distinct cell surface microdomains. *J. Cell Biol.* 160, 165–170. doi:10.1083/jcb.200209091

Rana, M. S., Kumar, P., Lee, C. J., Verardi, R., Rajashankar, K. R., and Banerjee, A. (2018). Fatty acyl recognition and transfer by an integral membrane S-acyltransferase. *Science* 80, eaao6326. doi:10.1126/science.aao6326

Rana, M. S., Lee, C. J., and Banerjee, A. (2018). The molecular mechanism of DHHC protein acyltransferases. *Biochem. Soc. Trans.* 47, 157–167. doi:10.1042/BST20180429

Ren, J., Wen, L., Gao, X., Jin, C., Xue, Y., and Yao, X. (2008). CSS-palm 2.0: An updated software for palmitoylation sites prediction. *Protein Eng. Des. Sel.* 21, 639–644. doi:10.1093/protein/gzn039

Rocks, O., Peyker, A., Kahms, M., Verveer, P. J., Koerner, C., Lumbierres, M., et al. (2003). An acylation cycle regulates localization and activity of palmitoylated ras isoforms. *Palaeogeogr. Palaeoclim. Palaeoecol.* 18, 227. doi:10.1594/PANGAEA.58229

Rossin, A., Durivault, J., Chakhtoura-Feghali, T., Lounnas, N., Gagnoux-Palacios, L., and Hueber, A. O. (2015). Fas palmitoylation by the palmitoyl acyltransferase DHHC7 regulates Fas stability. *Cell Death Differ.* 22, 643–653. doi:10.1038/cdd.2014.153

Roth, A. F., Feng, Y., Chen, L., and Davis, N. G. (2002). The yeast DHHC cysteine-rich domain protein Akr1p is a palmitoyl transferase. *J. Cell Biol.* 159, 23–28. doi:10.1083/jcb.200206120

Rubio, I., Grund, S., Song, S., Biskup, C., Bandemer, S., Fricke, M., et al. (2010). TCR-induced activation of Ras proceeds at the plasma membrane and requires palmitoylation of N-Ras. *J. Immunol.* 185, 3536–3543. doi:10.4049/JIMMUNOL.1000334

Schlesinger, M. J., Magee, A. I., and Schmidt, M. F. G. (1980). Fatty acid acylation of proteins in cultured cells*. *J. Biol. Chem.* 255, 10021–10024. doi:10.1016/S0021-9258(19)70417-7

Schmidt, M. F. G., and Schlesinger, M. J. (1979). Fatty acid binding to vesicular stomatitis virus glycoprotein: A new type of post-translational modification of the viral glycoprotein. *Cell* 17, 813–819. doi:10.1016/0092-8674(79)90321-0

Seminario, M. C., and Bunnell, S. C. (2008). Signal initiation in T-cell receptor microclusters. *Immunol. Rev.* 221, 90–106. doi:10.1111/j.1600-065X.2008.00593.x

Shaw, P. J., Qu, B., Hoth, M., and Feske, S. (2013). Molecular regulation of CRAC channels and their role in lymphocyte function. *Cell. Mol. Life Sci.* 70, 2637–2656. doi:10.1007/s00018-012-1175-2

Shayahati, B., Fan, Y., West, S. J., Tewari, R., Ko, J., Mills, T., et al. (2021). Calcium-dependent protein acyltransferase DHHC21 controls activation of CD4+ T cells. *J. Cell Sci.* doi:10.1242/jcs.258186

Smith-Garvin, J. E., Koretzky, G. A., and Jordan, M. S. (2009). T cell activation. *Annu. Rev. Immunol.* 27, 591–619. doi:10.1146/annurev.immunol.021908.132706

Soboloff, J., Spassova, M. A., Tang, X. D., Hewavitharana, T., Xu, W., and Gill, D. L. (2006). Orai1 and STIM reconstitute store-operated calcium channel function. *J. Biol. Chem.* 281, 20661–20665. doi:10.1074/jbc.C600126200

Stathopulos, P. B., Li, G-Y., Plevin, M. J., Ames, J. B., and Ikura, M. (2006). Stored Ca2+ depletion-induced oligomerization of stromal interaction molecule 1 (STIM1) via the EF-SAM region: An initiation mechanism for capacitive Ca2+ entry. *J. Biol. Chem.* 281, 35855–35862. doi:10.1074/jbc.M608247200

Stathopulos, P. B., Zheng, L., Li, G-Y., Plevin, M. J., and Ikura, M. (2008). Structural and mechanistic insights into STIM1-mediated initiation of store-operated calcium entry. *Cell* 135, 110–122. doi:10.1016/j.cell.2008.08.006

Tanimura, N., Saitoh, S., Kawano, S., Kosugi, A., and Miyake, K. (2006). Palmitoylation of LAT contributes to its subcellular localization and stability. *Biochem. Biophys. Res. Commun.* 341, 1177–1183. doi:10.1016/j.bbrc.2006.01.076

Tewari, R., West, S. J., Shayahati, B., and Akimzhanov, A. M. (2020). Detection of protein S-acylation using acyl-resin assisted capture. *J. Vis. Exp.* (158). doi:10.3791/61016

Tewari, R., Shayahati, B., Fan, Y., and Akimzhanov, A. M. (2021). T cell receptor-dependent S-acylation of ZAP-70 controls activation of T cells. *J. Biol. Chem.* 296, 100311. doi:10.1016/j.jbc.2021.100311

Tomatis, V., Trenchi, A., Gomez, G., and Daniotti, J. (2010). Acyl-protein thioesterase 2 catalyzes the deacylation of peripheral membrane-associated GAP-43. *PLoS One* 5, e15045. doi:10.1371/JOURNAL.PONE.0015045

Trebak, M., and Kinet, J. P. (2019). Calcium signalling in T cells. *Nat. Rev. Immunol.* 19, 154–169. doi:10.1038/s41577-018-0110-7

Van 't Hof, W., and Resh, M. D. (1997). Rapid plasma membrane anchoring of newly synthesized p59(fyn): Selective requirement for NH2-terminal myristoylation and palmitoylation at cysteine- 3. *J. Cell Biol.* 136, 1023–1035. doi:10.1083/jcb.136.5.1023

Verkruyse, L. A., and Hofmann, S. L. (1996). Lysosomal targeting of palmitoyl-protein thioesterase. *J. Biol. Chem.* 271, 15831–15836. doi:10.1074/JBC.271.26.15831

Verma, S., Hoffmann, F. W., Kumar, M., Huang, Z., Roe, K., Nguyen-Wu, E., et al. (2011). Selenoprotein K knockout mice exhibit deficient calcium flux in immune cells and impaired immune responses. *J. Immunol.* 186, 2127–2137. doi:10.4049/jimmunol.1002878

Vig, M., Beck, A., Billingsley, J. M., Lis, A., Parvez, S., Peinelt, C., et al. (2006). CRACM1 multimers form the ion-selective pore of the CRAC channel. *Curr. Biol.* 16, 2073–2079. doi:10.1016/j.cub.2006.08.085

Wang, H., Franco, F., Tsui, Y-C., Xie, X., Trefny, M. P., Zappasodi, R., et al. (2020). CD36-mediated metabolic adaptation supports regulatory T cell survival and function in tumors. *Nat. Immunol.* 21, 298–308. doi:10.1038/s41590-019-0589-5

West, S. J., Kodakandla, G., Wang, Q., Tewari, R., Zhu, M. X., Boehning, D., et al. (2022). S-acylation of Orai1 regulates store-operated Ca2+ entry. *J. Cell Sci.* 135, jcs258579–8. doi:10.1242/jcs.258579

Xu, S., Chaudhary, O., Rodríguez-Morales, P., Sun, X., Chen, D., Zappasodi, R., et al. (2021). Uptake of oxidized lipids by the scavenger receptor CD36 promotes lipid peroxidation and dysfunction in CD8+ T cells in tumors. *Immunity* 54, 1561–1577.e7. e7. doi:10.1016/j.immuni.2021.05.003

Yasuda, K., Nagafuku, M., Shima, T., Okada, M., Yagi, T., Yamada, T., et al. (2002). Cutting edge: Fyn is essential for tyrosine phosphorylation of Csk-binding protein/phosphoprotein associated with glycolipid-enriched microdomains in lipid rafts in resting T cells. *J. Immunol.* 169, 2813–2817. doi:10.4049/JIMMUNOL.169.6.2813

Yazbeck, P., Tauseef, M., Kruse, K., Amin, M. R., Sheikh, R., Feske, S., et al. (2017). STIM1 phosphorylation at Y361 recruits Orai1 to STIM1 puncta and induces Ca 2+ entry. *Sci. Rep.* 7, 42758. doi:10.1038/srep42758

Yokoi, N., Fukata, Y., Sekiya, A., Murakami, T., Kobayashi, K., and Fukata, M. (2016). Identification of PSD-95 depalmitoylating enzymes. *J. Neurosci.* 36, 6431–6444. doi:10.1523/JNEUROSCI.0419-16.2016

Yurchak, L. K., and Sefton, B. M. (1995). Palmitoylation of either Cys-3 or Cys-5 is required for the biological activity of the Lck tyrosine protein kinase. *Mol. Cell. Biol.* 15, 6914–6922. doi:10.1128/mcb.15.12.6914

Zamora, C., Cantó, E., Nieto, J. C., Ortiz, M. A., Diaz-Torné, C., Diaz-Lopez, C., et al. (2013). Functional consequences of platelet binding to T lymphocytes in inflammation. *J. Leukoc. Biol.* 94, 521–529. doi:10.1189/jlb.0213074

Zeidman, R., Buckland, G., Cebecauer, M., Eissmann, P., Davis, D. M., and Magee, A. I. (2011). DHHC2 is a protein S-acyltransferase for Lck. *Mol. Membr. Biol.* 28, 473–486. doi:10.3109/09687688.2011.630682

Zhang, W., Trible, R. P., and Samelson, L. E. (1998). LAT palmitoylation: Its essential role in membrane microdomain targeting and tyrosine phosphorylation during T cell activation. *Immunity* 9, 239–246. doi:10.1016/S1074-7613(00)80606-8

Zhang, J., Bárdos, T., Mikecz, K., Finnegan, A., and Glant, T. T. (2001). Impaired Fas signaling pathway is involved in defective T cell apoptosis in autoimmune murine arthritis. *J. Immunol.* 166, 4981–4986. doi:10.4049/jimmunol.166.8.4981

Zhang, S. L., Yeromin, A. V., Zhang, X. H-F., Yu, Y., Safrina, O., Penna, A., et al. (2006). Genome-wide RNAi screen of Ca(2+) influx identifies genes that regulate Ca(2+) release-activated Ca(2+) channel activity. *Proc. Natl. Acad. Sci. U. S. A.* 103, 9357–9362. doi:10.1073/pnas.0603161103

Zhang, M., Zhou, L., Xu, Y., Yang, M., Xu, Y., Komaniecki, G. P., et al. (2020). A STAT3 palmitoylation cycle promotes TH17 differentiation and colitis. *Nature* 586, 434–439. doi:10.1038/s41586-020-2799-2

Zimmermann, L., Paster, W., Weghuber, J., Eckerstorfer, P., Stockinger, H., and Schütz, G. J. (2010). Direct observation and quantitative analysis of Lck exchange between plasma membrane and cytosol in living T cells. *J. Biol. Chem.* 285, 6063–6070. doi:10.1074/jbc.M109.025981

frontiers | Frontiers in Physiology

TYPE Mini Review
PUBLISHED 09 January 2023
DOI 10.3389/fphys.2022.1088840

OPEN ACCESS

EDITED BY
William Fuller,
University of Glasgow, United Kingdom

REVIEWED BY
Maria I. Bokarewa,
University of Gothenburg, Sweden

*CORRESPONDENCE
Evgeni Ponimaskin,
ponimaskin.evgeni@mh-hannover.de

SPECIALTY SECTION
This article was submitted to Lipid and Fatty Acid Research, a section of the journal Frontiers in Physiology

RECEIVED 03 November 2022
ACCEPTED 26 December 2022
PUBLISHED 09 January 2023

CITATION
Wirth A and Ponimaskin E (2023), Lipidation of small GTPase Cdc42 as regulator of its physiological and pathophysiological functions. *Front. Physiol.* 13:1088840. doi: 10.3389/fphys.2022.1088840

Lipidation of small GTPase Cdc42 as regulator of its physiological and pathophysiological functions

Alexander Wirth and Evgeni Ponimaskin*

Cellular Neurophysiology, Hannover Medical School, Hannover, Germany

The protein cell division cycle 42 (Cdc42) is a small GTPase of the Rho family regulating a plethora of physiological functions in a tissue, cell and subcellular-specific manner *via* participating in multiple signaling pathways. Since the corresponding signaling hubs are mainly organized along the cellular membranes, cytosolic proteins like Cdc42 need to be properly targeted and held at the membrane. Here, lipid modifications come into play: Cdc42 can be associated with membranes by different lipid anchors including prenylation (Cdc42-prenyl) and palmitoylation (Cdc42-palm). While Cdc42-prenyl is ubiquitously expressed, Cdc42-palm splicing variant in mainly expressed in the brain. Mechanisms underlying Cdc42 lipidation as well as its regulation are the main topic of this review. Furthermore, we will discuss the functional importance of Cdc42 lipid modifications with the focus on the role of different lipids in regulating defined Cdc42 functions. Finally, we will provide an overview of the possible implementation of Cdc42 lipidation in pathological conditions and different diseases.

KEYWORDS

Cdc42, small GTPase, palmitoylation, prenylation, lipidation

Structure and distribution of Cdc42 splicing variants

The protein cell division cycle 42 (Cdc42) was initially purified from the placental membranes during isolation of small molecular weight GTP hydrolyzing proteins (Evans et al., 1986). This protein was termed G_p (G_p = placental G protein). When later researchers investigated the interplay between cell cycle events (e.g., DNA replication) and cytosolic/membrane events (e.g., budding) in yeast *Saccharomyces cerevisiae*, they identified a mutant that was able to continue DNA synthesis and nuclear division while the emergence of buds was blocked. The responsible gene was named CDC42, in relation to another budding-involved gene, namely CDC24 (Adams et al., 1990). In the same year, Shinjo et al. isolated the cDNA clone for G_p (or G25K) and found that it has the highest degree of sequence identity (more than 80%) with the CDC42. Therefore, the corresponding human placental protein was designated Cdc42Hs. Using different probes, authors not only isolated cDNA for the Cdc42Hs, but also found a second protein with the same size but different C-terminal sequence (G_p'), concluding that these might be another reading frame within the same gene (Shinjo et al., 1990).

Today, we know that these two cDNAs refer to two alternatively spliced isoforms of Cdc42 mapping to chromosome 1p36.1 in humans (Nicole et al., 1999) and to chromosome 4 in mice (Marks and Kwiatkowski, 1996). The first isoform is also referred as G25K, Gp, Cdc42a, Cdc42-prenyl, Cdc42E7, Cdc42u or Cdc42-v1, while the second—as G_p', Cdc42-palm, Cdc42E6, Cdc42b, bCdc42, Cdc42-v2. To simplify the reading, we will mark the first isoform as Cdc42-prenyl and the second one as Cdc42-palm in the further text. The

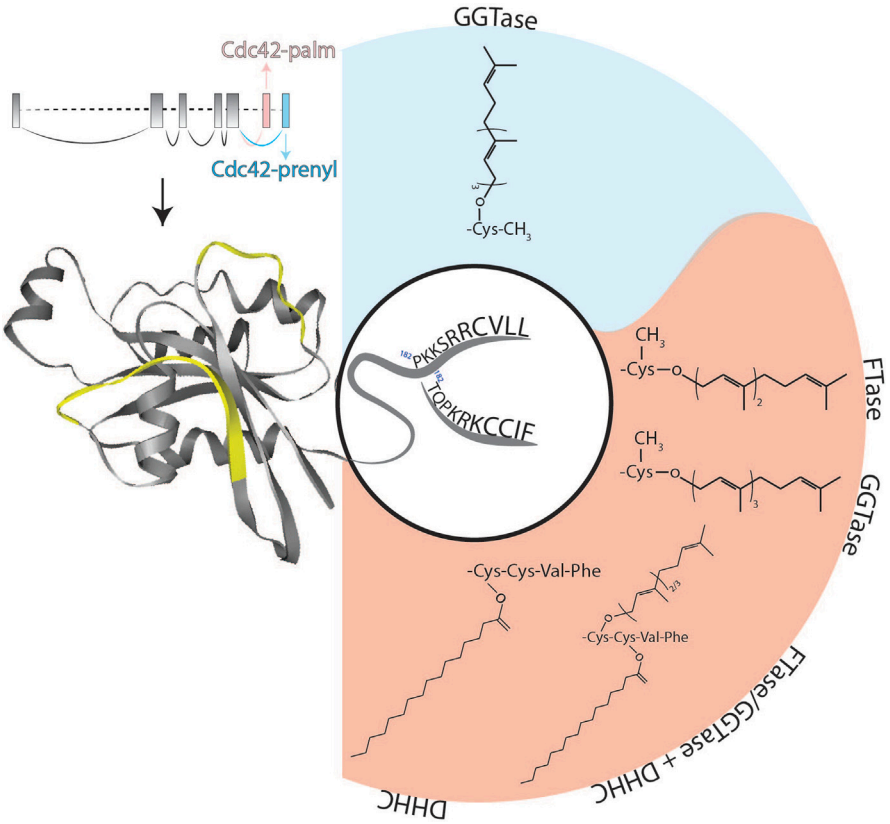

FIGURE 1
Schematic representation of the structure of Cdc42 alternatively spliced exons as well as protein and its lipid modifications. Two flexible switch regions are highlighted in yellow. The two different C-termini of Cdc42-palm (red background) and Cdc42-prenyl (blue background) isoforms together with their possible post-translational lipid modifications are shown. DHHC, palmitoyl acyl-transferase harboring a cysteine-rich domain containing a conserved DHHC (Asp-His-His-Cys) motif; FTase, farnesyltransferase; GGTase, geranylgeranyltransferase.

CDC42 gene consists of 7 exons, and the last two exons can be alternatively spliced (Figure 1; Marks and Kwiatkowski, 1996; Nicole et al., 1999; Yap et al., 2016). The common Cdc42 structure consists of five α-helices, six β-strands and two highly mobile switch regions with the switch I region resided between α1 and β2 loops, and switch II region within β3 and β4 loops (Figure 1). These regions are important for the substrate recognition and interaction together with the P-loop, which is also involved in binding a phosphate group of guanine nucleotides. Even though the structure of GTP and GDP-bound Cdc42 does not significantly differ, effector proteins are still able to bind to the activated form, inducing conformational changes within switch I and switch II loops, leading to initiation of the downstream signaling (Phillips et al., 2008).

Initial analysis performed by Marks et al. revealed that Cdc42-prenyl is broadly distributed within multiple tissues including uterus, thymus, gut, kidney and lung, whereas Cdc42-palm expression was restricted to the brain, where this isoform was expressed at relative low levels (Figure 2; Marks and Kwiatkowski, 1996). In the ensuing study, Olenik and colleagues investigated the expression of both Cdc42 isoforms in developing rat neocortices. They have shown that Cdc42-prenyl localizes to the proliferation zone, whereas Cdc42-palm was restricted to the cortical zone—a place in which neurons differentiate and settle, but do not proliferate anymore (Olenik et al., 1999). A recent study by Yap et al. shed light on the regulatory mechanisms of the alternative splicing of the CDC42 gene transcripts in developing embryonic stem cells, differentiating into glutamatergic neurons as well as into hippocampal neurons (Yap et al., 2016). They reported about a polypyrimidine tract-binding protein 1 (Ptbp)-dependent splicing switch, leading to the production of equal amounts of Cdc42-palm Cdc42-prenyl transcripts from day *in vitro* 7 onwards in neurons, but not astrocytes. A more recent study by Ciolli Mattioli and colleagues demonstrated that Cdc42-prenyl mRNA was enriched in neurites of mESC-derived and primary cortical neurons. In contrast, mRNA transcripts of Cdc42-palm isoform were predominantly localized to the cell somata (Ciolli Mattioli et al., 2019). Such compartmentalization of Cdc42-prenyl and Cdc42-palm splice variants seem to be preserved also within the peripheral nervous system. Indeed, Cdc42-prenyl mRNA has been shown to be specifically enriched in axons of sensory neurons of the dorsal root ganglion (Lee et al., 2021). In contrast, Kang and colleagues reported a dendritic localization of both isoforms in cultured hippocampal neurons (Kang et al., 2008). They also showed that GFP-tagged Cdc42-prenyl is distributed throughout the whole dendrite, including spines and shaft-like structures, whereas Cdc42-palm was restricted to dendritic spines.

Of note, our understanding of the physiological functions of both Cdc42 isoforms is still incomplete. The full deletion of Cdc42 in germline is embryonically lethal at E6.5, which points to its

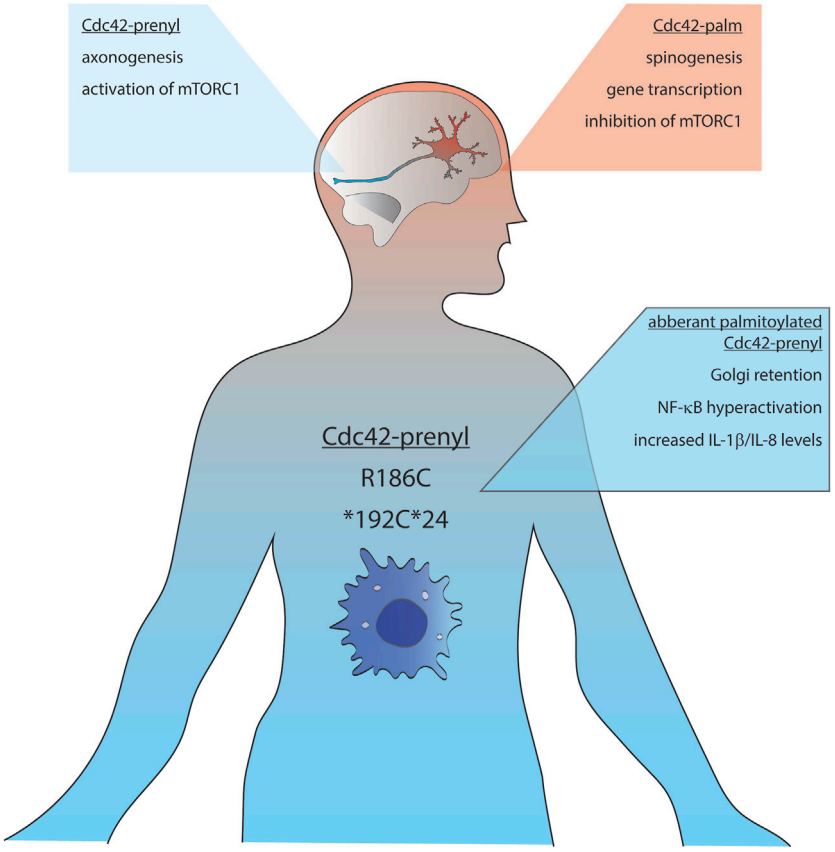

FIGURE 2
Schematic representation of the distribution and functions of Cdc42-palm (red background) and Cdc42-prenyl (blue background) isoforms. mTORC1, mammalian target of rapamycin complex 1; IL, interleukin; NF-κB, nuclear factor kappa-light-chain-enhancer of activated B cells.

biological relevance (Chen et al., 2000). A conditional deletion of Cdc42 in the developing cortex of mice at E9.5 causes mislocalization of adherens junctions due to missing cellular polarization, usually maintained by Cdc42-Par complex interaction (Cappello et al., 2006) and a telencephalon-specific knockout leads to holoprosencephaly—a incomplete bifurcation of cerebral hemispheres (Chen et al., 2006).

Cdc42 splicing variants: what is different?

At the protein level, Cdc42 isoforms differ in their C-terminal amino acid sequences: Cdc42-palm possesses a non-canonical *CCaX* motif (CCIF; in which C is cysteine, a—preferably aliphatic amino acid and X is any amino acid), whereas Cdc42-prenyl is terminated by a *CaaX*-box (CVLL) (Shinjo et al., 1990). In addition, alternative splicing of the exons 6 and 7 results in an altered polybasic region (PBR) and an exchange of lysine to arginine at position 163 (Figure 1). Whereas Cdc42-prenyl bears a di-lysine di-arginine motif separated by a serine (-KKSRR-), Cdc42-palm's PBR consists only of a lysine-arginine-lysine (-KRK-) motif (Figure 1; Marks and Kwiatkowski, 1996). The polybasic region is involved in a variety of biological processes, especially in protein-protein interaction. Moreover, PBR-motifs seem to play a crucial role for the membrane sorting, including localization at different membrane compartments (e.g., plasma membrane and endo-membranes) (reviewed in Williams, 2003).

The di-lysine motif (Lys-183 and Lys-184) within Cdc42-prenyl has been shown to be involved in interaction of Cdc42-prenyl with the γCOP subunit of the coat proteins I (COPI) complex, playing a role in regulating intracellular trafficking (Wu et al., 2000). The di-arginine motif of Cdc42-prenyl (i.e., Arg-186 and Arg-187) was shown to be responsible for its association with phosphatidylinositol 4,5-bisphosphate, which correlates with the ability of this isoform to induce oncogenic transformation (Johnson et al., 2012). In contrast, the polybasic sequence Lys-185, Arg-186, Lys-187 within Cdc42-palm (Figure 1) leads to localization of this isoform into phosphatidylinositol (3,4,5)-triphosphate microdomains (Endo and Cerione, 2022), where it can act as a tumor suppressor, at least in ovarian cancer cells (He et al., 2015). Another consequence of the alternative splicing of the CDC42 gene transcripts is the presence of a canonical nuclear localization sequence KKSR exclusively within the Cdc42-prenyl isoform (Williams, 2003).

Cdc42 prenylation

Based on sequence homology of the C-terminus of Cdc42 and Ras proteins, Johnson und Pringle predicted that Cdc42-prenyl might undergo posttranslational prenylation (Johnson and Pringle, 1990).

Protein prenylation is an irreversible post-translational modification, which is involved in the regulation of localization, functions, and protein-protein interactions of multiple small GTPases, including the Ras superfamily (Zhang and Casey, 1996). Prenylation implies covalent attachment of either a farnesyl (15 carbon atoms) or a geranylgeranyl (20 carbon atoms) isoprenoid group catalyzed by different prenyltransferases, including farnesyltransferase (FTase), geranylgeranyltransferase type I (GGTase-I), Rab geranylgeranyltransferase (GGTase-II), and geranylgeranyltransferase type III (GGTase-III) (Marchwicka et al., 2022). The isoprene derivative is linked to the cysteine residue of the C-terminal CaaX-box *via* irreversible thioether bond (Casey and Seabra, 1996). In general, prenylated proteins are further processed at the cytoplasmic face of the endoplasmic reticulum (ER) by a two-step process: 1) Trimming of the last three amino acids by Ras carboxyl CAAX endopeptidase I (RceI), and 2) methylation of the newly exposed prenylated cysteine residue by isoprenylcysteine carboxyl O-methyltransferase (Icmt) (Garcia-Mata et al., 2011). Isoprenylation of Cdc42-prenyl was experimentally confirmed by Maltese and Sheridan in cultured murine erythroleukemia (MEL) cells after radioactive labelling with [^{3}H]-mevalonate (Maltese and Sheridan, 1990). Later on, cysteine residue 188 of Cdc42-prenyl was identified as prenylation site (Ziman et al., 1993). Same authors also demonstrated redistribution of Cdc42-prenyl to cytosolic fractions in a GGTaseI mutant strain in yeast, which draws the conclusion that Cdc42-prenyl is preferentially geranylgeranylated. This finding stays also true for the human Cdc42-prenyl, which prenylation was completely blocked by the inhibition of GGTaseI (Wilson et al., 1998). Interestingly, we and others reported that also the Cdc42-palm splice variant can undergo prenylation (Nishimura and Linder, 2013; Wirth et al., 2013). Our study and experiments by Nishimura and colleagues revealed that at least a small fraction of Cdc42-palm can bypass endopeptidase cleavage and carboxymethylation, resulting in a dually lipidated Cdc42-palm. In this case, cysteine residue 188 becomes geranylgeranylated, while cysteine residue 189 undergoes palmitoylation (Nishimura and Linder, 2013).

One additional observation of our study was that Cdc42-palm can be modified by both GGTaseI and FTase with similar efficiency and thus might accepts both C15 and C20 isoprenoids (Figure 1). A possible reason for different isoprenoid prevalence of Cdc42-prenyl and Cdc42-palm can be the differences in their C-terminal amino acid sequences. Indeed, composition of the *CaaX* box has been shown to be critically involved in the determination of the nature of prenylation reaction. C-terminal *CaaX* motif of Cdc42-prenyl contains CVLL amino acids, with leucine at the last position being responsible for its preferential prenylation with GGTaseI. In contrast, FTase can accept multiple amino acids at the last position of the *CaaX* motif (Moores et al., 1991). This can be a reason, why the C-terminal tail of Cdc42-palm (CCIF) is recognized by both GGTaseI and FTase.

Cdc42 palmitoylation

Already in 1996, Marks and colleagues speculated that due to the differences in their C-terminal *CaaX*-motifs Cdc42-palm and Cdc42-prenyl can be differently lipidated (Marks and Kwiatkowski, 1996). This suggestion was experimentally confirmed only in 2008, when Kang and co-workers showed that Cdc42-palm is palmitoylated (Kang et al., 2008). The authors demonstrated palmitoylation of Cdc42-palm, both in cultured rat embryonic cortical neurons as well as in purified synaptosomal membrane fractions extracted from the whole adult rat brain. Moreover, using cultured cortical neurons as a model, they showed that palmitoylation of Cdc42-palm is a dynamic modification.

Nishimura and colleagues confirmed this finding and analyzed the lipid modification of the *CCaX*-box of Cdc42-palm in more detail. From their experiments, they concluded that Cdc42-palm gets first prenylated at cysteine residue 188 followed by palmitoylation at cysteine residue 189 (Nishimura and Linder, 2013). Nishimura and colleagues also demonstrated that upon inhibition of prenylation the palmitoylation was decreased too, suggesting that prenylation of Cys-188 might be necessary for subsequent palmitoylation of Cys-189 (Nishimura and Linder, 2013). At the same time, we studied palmitoylation of the brain-specific Cdc42-palm isoform and found that both cysteine residues, Cys-188 and Cys-189, can be palmitoylated (Wirth et al., 2013). In contrast to Nishimura's data, we demonstrated that palmitoylation of Cdc42-palm was significantly increased in the presence of a GGTase inhibitor, pointing to the ability of Cys-188 to accept the modification with palmitate (Wirth et al., 2013). Dual lipid modifications by both prenylation and palmitoylation have previously been demonstrated for Rac1 as well as for several members of the Ras protein family, including N-Ras and H-Ras (Brunsveld et al., 2009). However, in all these proteins, the cysteine residues within the *CaaX*-motif are solely prenylated, while palmitoylated cysteine residues are localized upstream of the CaaX box. Moreover, the *aaX* sequence should undergo methylation-mediated cut before the protein can be palmitoylated. Therefore, Cdc42-palm represents the unique example with cysteine residue 188 modified by either prenylation or by palmitoylation, while the palmitoylated cysteine 189 resides within the untypical CaaX box (CCIF) and should thus bypass methylation excision (Figure 1).

Our finding that Cdc42-palm can undergo dual lipidation suggests the existence of two Cdc42-palm populations in the cell. The first one could consist of Cdc42-palm prenylated at cysteine 188 and palmitoylated at cysteine 189. In the second population, both cysteine residues might be palmitoylated. A prenylated population can arise by the initial modification of cysteine 188 either by GGTaseI or FTase. This will result in increased membrane affinity and thereby facilitate palmitoylation of cysteine 189 by specific palmitoyl acyl-transferases (PATs), which reside either in the Golgi compartment or at the plasma membrane (see below). Since the CCIF sequence of Cdc42-palm represents a non-canonical CaaX motif, a part of Cdc42-palm will be not recognized by prenylating enzymes, resulting in palmitoylation of both cysteine residues (i.e., Cys-188 and Cys-189). Since prenylation and palmitoylation possess different affinity for lipid bilayers (Roy et al., 2005) and can thus target Cdc42-palm to different membrane subdomains, the dual lipidation can represent a mechanism to regulate the intracellular distribution and functions of Cdc42-palm.

More recently, we performed a detailed analysis of palmitoylation stoichiometry for Cdc42-palm isoforms by applying acyl-PEGyl exchange gel shift (APEGS) assays (Kanadome et al., 2019). Using this assay, we unexpectedly found that i) only a relatively small fraction of Cdc42-palm isoform exists in palmitoylated form, and ii) Cdc42-palm overexpressed in N1E-115 cells as well as Cdc42-palm endogenously expressed in primary rat hippocampal neurons seem to be palmitoylated only at one cysteine residue. In the same study, we identified DHHC5 as a prominent Cdc42 PAT (Wirth et al., 2022). In addition, DHHC10 and DHHC17 can also be involved in

Cdc42 palmitoylation. Interestingly, among these three Cdc42-palm specific PATs, only DHHC5 is residing at the plasma membrane (Brigidi et al., 2015). This might have an important implication for the regulation of Cdc42-palm functions at different intracellular compartments.

Although the molecular mechanisms of Cdc42-palm recognition by DHHC5 is not elucidated in detail, one possibility is the activation of DHHC5 *via* palmitoylation. Previously, it has been shown that DHHC5 could be palmitoylated at C-terminal cysteine residues outside of its catalytic core (Yang et al., 2010). This might result in conformational changes within the DHHC5 protein, leading to increased substrate specificity (Woodley and Collins, 2019). We have previously reported a reduced palmitoylation of Cdc42 in a mouse model of 22q11.2 deletion syndrome, in which DHHC8 is among the deleted genes (Moutin et al., 2017). Since overexpression of DHHC8 did not facilitate palmitoylation of Cdc42-palm (Wirth et al., 2022), DHHC8 could thus regulate enzymatic activity of DHHC5 towards Cdc42-palm *via* DHHC5 palmitoylation.

Moreover, palmitoylation of Cdc42-palm can be hierarchical organized in space and time. Indeed, Golgi-resided DHHC10 and/or DHHC17 can be responsible for the initial Cdc42 palmitoylation at Cys-188 immediately after synthesis. This will prevent prenylation and target Cdc42 to the plasma membrane. Our data revealed the increasing ratio of DHHC5 to Cdc42-palm in the brain during development, which could result in facilitation of Cdc42 palmitoylation within dendritic spines, which in turn will boost spinogenesis and spine maturation (see below).

Since palmitoylation is a dynamic and reversible process, Cdc42-palm can also undergo depalmitoylation. So far, only a few published works investigated the Cdc42 depalmitoylation. Cdc42-palm was shown to maintain asymmetric protein localization during cell division by coordinated interplay with catalytic active acyl protein thioesterase 1 (APT1) in breast cancer cells (MDA-MB-231) (Stypulkowski et al., 2018). The palmitoyl-protein thioesterases 1 (PPT1) was also found to be in favor of depalmitoylating Cdc42 (Gorenberg et al., 2022). However, the spatiotemporal palmitoylation/depalmitoylation pattern of Cdc42-palm remains elusive.

Physiological role of Cdc42 lipidation: different lipids—different functions?

Cdc42 is highly conserved from yeast to mammals and plays an important role in the regulation of a plethora of cellular processes, including phagocytosis, cell polarization, chemotaxis, cell-migration and division (Etienne-Manneville and Hall, 2002; Cerione, 2004). Cdc42 is also critically involved in the organ and tissue homeostasis and has been associated with vascularization, immune system regulation, eye and skin development as well as cardiac and pancreatic organogenesis (for review see Melendez et al., 2011). Of note, all these organs ubiquitously express the Cdc42-prenyl isoform, while Cdc42-palm—so far—represents a brain specific isoform under physiological conditions. Therefore, the best-studied organ in terms of isoform-specific functions is the brain. It might be possible, however, that Cdc42-palm was overlooked in other tissues, since the majority of investigations published before the work by Kang and co-workers (Kang et al., 2008) did not discriminate between Cdc42 isoforms. Furthermore, in many publications describing Cdc42 knockdown, authors applied shRNAs targeting non-specific sites such as exon 2, which leads to the knockdown of both isoforms. On the other hand, starting from 2008, there is growing evidence demonstrating that Cdc42 isoforms are strictly distinguished in their functions, especially in neurons. Even though the possible mechanisms responsible for functional differences between both alternatively spliced variants are far from being completely understood, there are different hypothesis explaining how the proteins, differing only in their short C-terminal sequences, might possess different functions and thereby regulate distinct signaling pathways. One of them arises by the idea that palmitoylated proteins are enriched in membrane subdomains like lipid rafts, whereas isoporenylated proteins are excluded from these microdomains (Levental et al., 2010). Indeed, protein palmitoylation represents one of the best-characterized lipid raft targeting signals (Moffett et al., 2000; Zacharias et al., 2002). Detection of numerous signaling proteins within the lipid rafts led to the assumption that these structures represent a scaffolding platform or signaling hub, which boosts signal transduction by spatially recruiting signaling components and by preventing an inappropriate cross-talk between signaling pathways. This can also be true for Cdc42 isoforms, which specific lipidation (i.e., prenylation vs. palmitoylation) might contribute to a separated/different localization of both Cdc42 isoforms along the lipid membranes, leading to different downstream interaction partners and ultimately to initiation of different signaling cascades.

An important physiological function of Cdc42 is the activation of transcription factors such as NFκB, STAT3 and SRF (Perona et al., 1997; Wu et al., 2008). In particular, SRF-mediated transcription of many immediate early genes plays a crucial role for neuronal outgrowth and differentiation (Scandaglia et al., 2015). We have previously shown a higher specificity of Cdc42-palm towards activation of SRF-pathway in comparison with Cdc42-prenyl (Wirth et al., 2013). Noteworthy, such specificity is not mediated by changes in the intrinsic Cdc42 activation between isoforms, because expression of constitutively active mutants resulted in similar activation of SRF signaling. One possible explanation therefore could be a specific localization of Cdc42-palm in lipid rafts, which will result in its sustained interaction with raft-resided downstream-effectors such as Pak1, WASP or p38 leading to specific modulation of SRF-mediated signaling. This is supported by the observation that, although the mutation of palmitoylated Cys-189 does not affect proper localization of Cdc42-palm at the plasma membrane, it significantly reduced activation of SRF pathway to the level comparable with Cdc42-prenyl isoform (Wirth et al., 2013).

Kang and colleagues also investigated the functional consequences of the different lipid modifications of Cdc42 (Kang et al., 2008). Among others, they demonstrated that a constitutively active (CA) mutant of Cdc42-palm was more effective in inducing dendritic spine formation than Cdc42-prenyl CA mutant, and that the ability of Cdc42-palm CA to induce dendritic spines was abolished either by mutating the two C-terminal cysteine residues or by chemically inhibiting the palmitoylation by 2-bromopalmitate. More importantly, the authors showed that palmitoylation of Cdc42-palm isoform is dynamically regulated by neuronal activity. Upon glutamate treatment of cortical cultures, Cdc42-palm was very rapidly (i.e., within 5 min) de-palmitoylated and dislocated from

dendritic spines. In contrast, triggering a seizure-like activity in the mouse brain by injection of kainic acid *in vivo* resulted in a significant increase of Cdc42 palmitoylation (Kang et al., 2008). Different intracellular expression patterns and, as consequence, functions of the Cdc42 splice variants were confirmed by Yap and co-authors. They found that Cdc42-palm (Cdc42E6) was critically involved in the formation of dendritic spines, whereas Cdc42-prenyl (Cdc42E7) was associated with axonogenesis (Yap et al., 2016). This observation was further confirmed by a study by Lee and colleagues, who found an enrichment of Cdc42-prenyl encoding mRNA in the axons of dorsal root ganglion neurons, where it was involved in regulating the increase in axon length. In contrast, Cdc42-palm mRNA was rather enriched in dendritic spines. Functional specificity of Cdc42 isoforms was demonstrated by the fact that global knock-down of CDC42 gene followed by rescue with Cdc42-palm was not able to facilitate an axonal outgrowth, while increased dendritic length (Lee et al., 2021).

On the other hand, our data suggest that both Cdc42 splice variants might be involved in the formation of dendritic protrusions and spines, since expression of either Cdc42-palm or Cdc42-prenyl in hippocampal neurons was able to rescue the inhibitory effect of the shRNA-mediated Cdc42 knock-down (Wirth et al., 2013). This is further supported by experiments in *Drosophila* demonstrating that fly Cdc42, which is homolog to mammalian Cdc42-prenyl, is required for multiple aspects of dendritic morphogenesis (Scott et al., 2003). The authors demonstrated that loss-of-function mutation of endogenous Cdc42 did not affect dendritic complexity but resulted in increased dendritic length accompanied by app. 50% reduction in dendritic spine density.

Detailed analysis of acylation-deficient mutants of Cdc42 revealed different roles of cysteine residues within Cdc42-palm C-terminus: If cysteine residue 188 was available as lipid acceptor, Cdc42-palm induced long dendritic protrusions only. Mutation of Cys-189 did not affect formation of long dendritic protrusions, while the number of short dendritic protrusion, which are thought to be spine precursors, was significantly reduced (Wirth et al., 2013). Together with the observation that Cdc42-palm undergoes palmitoylation in human brains, this suggests the importance of Cdc42 lipidation for the growth of new synapses as well as for activity-dependent structural and functional plasticity, including learning and long-term memory in human.

Another interesting aspect of lipid-specific regulation of Cdc42 functions is the finding that Cdc42-prenyl is essential for forming neuroprogenitor cells by activation of mTORC1 and thereby up-regulation of tissue-specific transcription factors, whereas Cdc42-palm drives the transition of neuroprogenitor cells into neurons by inhibiting mTORC1 signaling *via* activated Cdc42-associated kinase (ACK) (Endo et al., 2020). In the follow-up study, the authors identified the epidermal growth factor (EGF) receptor as an additional target of Cdc42-palm and ACK, which is down-regulated by their combined actions during neurogenesis. Thus, by down-regulating EGF receptor signaling, Cdc42-palm and ACK might determine the timing of terminal differentiation of neural progenitor cells into neurons. Mechanistically, Cdc42-palm and ACK-mediated EGF receptor degradation boost autophagy, which in turn protects neuronal progenitor from apoptosis and thus triggers their differentiation into neurons (Endo and Cerione, 2022). This idea is also in line with the accumulation of Cdc42-palm in the cortical plate, a place where neurons differentiate rather than proliferate (Olenik et al., 1999).

Can Cdc42 lipidation be involved in pathological conditions?

Many *de novo* mutations within the CDC42 gene result in heterogeneous phenotypes with highly variable symptoms including facial dysmorphism, dysregulation of growth, haematological as well as immunological and neurodevelopmental abnormalities such as Takenouchi-Kosaki syndrome (TKS) (Martinelli et al., 2018; Su and Orange, 2020). However, there is only a restricted amount of data directly demonstrating pathological contribution of the Cdc42 lipidation.

In 2019, Gernez and colleagues reported about four patients carrying CDC42 gene mutations affecting the last three to five C-terminal amino acids of Cdc42-prenyl (i.e., part responsible for lipidation). These mutations were associated with severe auto-inflammatory symptoms including anemia, cytopenia, rashes, facial dysmorphisms and are associated with increased ferritin, C-reactive protein, and interleukin IL-18 levels. In addition, patients carrying these mutations were predisposed to the development of macrophage activation syndrome and hemophagocytic lymphohistiocytosis. Of note, the novel C-terminal variants in Cdc42 all occur within or in close spatial proximity to the C-terminal di-arginine motif implicated in membrane binding and lipidation of Cdc42-prenyl. One patient had a mutation within the CDC42 coding region leading to a replacement of the stop codon by a cysteine residue, resulting in a read-through and 24 additional amino acids (*192C*24). Another patient carried the R186C mutation. The other two patients carried a C188Y mutation, which unfortunately were not further characterized in detail (Gernez et al., 2019). Therefore, we can only speculate, that mutation of cysteine 188, which is particularly important for the post-translational modification and thus the spatial organization of Cdc42, might lead to mislocalization within cells and thus aberrant signaling.

Using whole exome sequencing, Bekhouche and co-authors detected a heterozygous mutation in a patient affecting only Cdc42-prenyl, resulting in the exchange of arginine in position 186 to a cysteine residue (R186C). The main clinical characteristics of this mutation include severe neonatal dermatitis accompanied by acute episodes of hepatomegaly with cytolysis, mild facial dysmorphy, and a permanent inflammatory syndrome with occasional monocytosis (Bekhouche et al., 2020). Detailed biochemical analysis revealed that R186C mutation leads to non-physiological palmitoylation at Cys-186 (Figure 2). This results in a misbalanced regulation of Cdc42-prenyl by the GDP dissociation inhibitor, GDI1, which specifically binds to the geranylgeranylated wild-type form of Cdc42-prenyl. Due to the artificial palmitoylation upstream of the isoprenylation site, Cdc42-prenyl-GDI1-interaction was impaired and the R186C mutant was abnormally anchored in the Golgi apparatus. One consequence of such aberrant localization was decreased actin filament polymerization: the patient carrying the R186C mutation contained around 30% less F-actin than normal. Moreover, authors reported a strong NF-κB hyper-activation, which relied on the palmitoylation-dependent Golgi apparatus retention of the Cdc42-prenyl R186C mutant. This in turn resulted in increased IL-8 and IL1β levels, which can explain the pathophysiology of the disease (Bekhouche et al., 2020).

Recently, Nishitani-Isa and colleagues further analyzed molecular details of autoinflammatory pathology evoked by R186C Cdc42-prenyl mutation. Using induced-pluripotent stem cells (iPSCs)-derived myeloid and macrophages cell lines established from the patients carrying this mutation, they reported that patient-derived cells secreted larger amounts of IL-1β in response to pyrin-activating stimuli (Nishitani-Isa et al., 2022). Noteworthy, pharmacological blockade of palmitoylation released R186C mutant from the Golgi apparatus and damped the IL-1β secretion to the wild-type levels. Similar results were also obtained for another patient mutation, *192C*24. This mutant was also aberrantly palmitoylated at the newly introduced Cys-192, leading to trapping at the Golgi apparatus and over-activation of the pyrin inflammasome (Figure 2). In contrast to results obtained by Bekhouche and co-authors, Nishitani-Isa and colleagues did not obtain any changes in GTPase activity of R186C mutant or its binding affinity towards GDIs, pointing out palmitoylation-mediated aberrant localization of Cdc42-prenyl in the Golgi apparatus as main driving force for pathological activation of the pyrin inflammasome.

These combined results not only demonstrate an unexpected association between aberrant palmitoylation of Cdc42-prenyl and activation of inflammatory responses, but also suggest that this pathway might represent a novel target for treatment of autoinflammatory diseases. Moreover, results of these studies suggest that although Cdc42-prenyl is ubiquitously expressed, pathological effects of its aberrant palmitoylation seem to be related to the Cdc42-prenyl population expressed outside of the brain tissue.

Author contributions

AW: Writing—Review and Editing; EP: Conceptualization, Writing—Review and Editing.

Funding

This work was supported by the DFG Grant PO732 to EP.

Conflict of interest

The authors declare that the research was conducted in the absence of any commercial or financial relationships that could be construed as a potential conflict of interest.

Publisher's note

References

Adams, A. E., Johnson, D. I., Longnecker, R. M., Sloat, B. F., and Pringle, J. R. (1990). CDC42 and CDC43, two additional genes involved in budding and the establishment of cell polarity in the yeast *Saccharomyces cerevisiae*. *J. Cell Biol.* 111, 131–142. doi:10.1083/jcb.111.1.131

Bekhouche, B., Tourville, A., Ravichandran, Y., Tacine, R., Abrami, L., Dussiot, M., et al. (2020). A toxic palmitoylation of Cdc42 enhances NF-κB signaling and drives a severe autoinflammatory syndrome. *J. Allergy Clin. Immunol.* 146, 1201–1204. doi:10.1016/j.jaci.2020.03.020

Brigidi, G. S., Santyr, B., Shimell, J., Jovellar, B., and Bamji, S. X. (2015). Activity-regulated trafficking of the palmitoyl-acyl transferase DHHC5. *Nat. Commun.* 6, 8200. doi:10.1038/ncomms9200

Brunsveld, L., Waldmann, H., and Huster, D. (2009). Membrane binding of lipidated Ras peptides and proteins — the structural point of view. *Biochim. Biophys. Acta BBA - Biomembr.* 1788, 273–288. doi:10.1016/j.bbamem.2008.08.006

Cappello, S., Attardo, A., Wu, X., Iwasato, T., Itohara, S., Wilsch-Bräuninger, M., et al. (2006). The Rho-GTPase cdc42 regulates neural progenitor fate at the apical surface. *Nat. Neurosci.* 9, 1099–1107. doi:10.1038/nn1744

Casey, P. J., and Seabra, M. C. (1996). Protein prenyltransferases. *J. Biol. Chem.* 271, 5289–5292. doi:10.1074/jbc.271.10.5289

Cerione, R. A. (2004). Cdc42: New roads to travel. *Trends Cell Biol.* 14, 127–132. doi:10.1016/j.tcb.2004.01.008

Chen, F., Ma, L., Parrini, M. C., Mao, X., Lopez, M., Wu, C., et al. (2000). Cdc42 is required for PIP2-induced actin polymerization and early development but not for cell viability. *Curr. Biol.* 10, 758–765. doi:10.1016/S0960-9822(00)00571-6

Chen, L., Liao, G., Yang, L., Campbell, K., Nakafuku, M., Kuan, C.-Y., et al. (2006). Cdc42 deficiency causes Sonic hedgehog-independent holoprosencephaly. *Proc. Natl. Acad. Sci.* 103, 16520–16525. doi:10.1073/pnas.0603533103

Ciolli Mattioli, C., Rom, A., Franke, V., Imami, K., Arrey, G., Terne, M., et al. (2019). Alternative 3′ UTRs direct localization of functionally diverse protein isoforms in neuronal compartments. *Nucleic Acids Res.* 47, 2560–2573. doi:10.1093/nar/gky1270

Endo, M., and Cerione, R. A. (2022). The brain-specific splice variant of the CDC42 GTPase works together with the kinase ACK to down-regulate the EGF receptor in promoting neurogenesis. *J. Biol. Chem.* 298, 102564. doi:10.1016/j.jbc.2022.102564

Endo, M., Druso, J. E., and Cerione, R. A. (2020). The two splice variant forms of Cdc42 exert distinct and essential functions in neurogenesis. *J. Biol. Chem.* 295, 4498–4512. doi:10.1074/jbc.RA119.011837

Etienne-Manneville, S., and Hall, A. (2002). Rho GTPases in cell biology. *Nature* 420, 629–635. doi:10.1038/nature01148

Evans, T., Brown, M. L., Fraser, E. D., and Northup, J. K. (1986). Purification of the major GTP-binding proteins from human placental membranes. *J. Biol. Chem.* 261, 7052–7059. doi:10.1016/S0021-9258(19)62720-1

Garcia-Mata, R., Boulter, E., and Burridge, K. (2011). The "invisible hand": Regulation of RHO GTPases by RHOGDIs. *Nat. Rev. Mol. Cell Biol.* 12, 493–504. doi:10.1038/nrm3153

Gernez, Y., de Jesus, A. A., Alsaleem, H., Macaubas, C., Roy, A., Lovell, D., et al. (2019). Severe autoinflammation in 4 patients with C-terminal variants in cell division control protein 42 homolog (CDC42) successfully treated with IL-1β inhibition. *J. Allergy Clin. Immunol.* 144, 1122–1125. e6. doi:10.1016/j.jaci.2019.06.017

Gorenberg, E. L., Tieze, S. M., Yücel, B., Zhao, H. R., Chou, V., Wirak, G. S., et al. (2022). Identification of substrates of palmitoyl protein thioesterase 1 highlights roles of depalmitoylation in disulfide bond formation and synaptic function. *PLOS Biol.* 20, e3001590. doi:10.1371/journal.pbio.3001590

He, X., Yuan, C., and Yang, J. (2015). Regulation and functional significance of CDC42 alternative splicing in ovarian cancer. *Oncotarget* 6, 29651–29663. doi:10.18632/oncotarget.4865

Johnson, D. I., and Pringle, J. R. (1990). Molecular characterization of CDC42, a *Saccharomyces cerevisiae* gene involved in the development of cell polarity. *J. Cell Biol.* 111, 143–152. doi:10.1083/jcb.111.1.143

Johnson, J. L., Erickson, J. W., and Cerione, R. A. (2012). C-Terminal di-arginine motif of Cdc42 protein is essential for binding to phosphatidylinositol 4, 5-Bisphosphate-containing membranes and inducing cellular transformation. *J. Biol. Chem.* 287, 5764–5774. doi:10.1074/jbc.M111.336487

Kanadome, T., Yokoi, N., Fukata, Y., and Fukata, M. (2019). "Systematic screening of depalmitoylating enzymes and evaluation of their activities by the acyl-PEGyl exchange gel-shift (APEGS) assay," in Protein lipidation: Methods and protocols *methods in molecular biology*. Editor M. E. Linder (New York, NY: Springer), 83–98. doi:10.1007/978-1-4939-9532-5_7

Kang, R., Wan, J., Arstikaitis, P., Takahashi, H., Huang, K., Bailey, A. O., et al. (2008). Neural palmitoyl-proteomics reveals dynamic synaptic palmitoylation. *Nature* 456, 904–909. doi:10.1038/nature07605

Lee, S. J., Zdradzinski, M. D., Sahoo, P. K., Kar, A. N., Patel, P., Kawaguchi, R., et al. (2021). Selective axonal translation of the mRNA isoform encoding prenylated Cdc42 supports axon growth. *J. Cell Sci.* 134, jcs251967. doi:10.1242/jcs.251967

Levental, I., Grzybek, M., and Simons, K. (2010). Greasing their way: Lipid modifications determine protein association with membrane rafts. *Biochemistry* 49, 6305–6316. doi:10.1021/bi100882y

Maltese, W. A., and Sheridan, K. M. (1990). Isoprenoid modification of G25K (Gp), a low molecular mass GTP-binding protein distinct from p21ras. *J. Biol. Chem.* 265, 17883–17890. doi:10.1016/s0021-9258(18)38246-2

Marchwicka, A., Kamińska, D., Monirialamdari, M., Błażewska, K. M., and Gendaszewska-Darmach, E. (2022). Protein prenyltransferases and their inhibitors: Structural and functional characterization. *Int. J. Mol. Sci.* 23, 5424. doi:10.3390/ijms23105424

Marks, P. W., and Kwiatkowski, D. J. (1996). Genomic organization and chromosomal location of MurineCdc42. *Genomics* 38, 13–18. doi:10.1006/geno.1996.0586

Martinelli, S., Krumbach, O. H. F., Pantaleoni, F., Coppola, S., Amin, E., Pannone, L., et al. (2018). Functional dysregulation of CDC42 causes diverse developmental phenotypes. *Am. J. Hum. Genet.* 102, 309–320. doi:10.1016/j.ajhg.2017.12.015

Melendez, J., Grogg, M., and Zheng, Y. (2011). Signaling role of Cdc42 in regulating mammalian Physiology. *J. Biol. Chem.* 286, 2375–2381. doi:10.1074/jbc.R110.200329

Moffett, S., Brown, D. A., and Linder, M. E. (2000). Lipid-dependent targeting of G proteins into rafts. *J. Biol. Chem.* 275, 2191–2198. doi:10.1074/jbc.275.3.2191

Moores, S. L., Schaber, M. D., Mosser, S. D., Rands, E., O'Hara, M. B., Garsky, V. M., et al. (1991). Sequence dependence of protein isoprenylation. *J. Biol. Chem.* 266, 14603–14610. doi:10.1016/s0021-9258(18)98729-6

Moutin, E., Nikonenko, I., Stefanelli, T., Wirth, A., Ponimaskin, E., De Roo, M., et al. (2017). Palmitoylation of cdc42 promotes spine stabilization and rescues spine density deficit in a mouse model of 22q11.2 deletion syndrome. *Cereb. Cortex N. Y. N.* 27, 3618–3629. doi:10.1093/cercor/bhw183

Nicole, S., White, P. S., Topaloglu, H., Beigthon, P., Salih, M., Hentati, F., et al. (1999). The human CDC42 gene: Genomic organization, evidence for the existence of a putative pseudogene and exclusion as a SJS1 candidate gene. *Hum. Genet.* 105, 98–103. doi:10.1007/s004399900065

Nishimura, A., and Linder, M. E. (2013). Identification of a novel prenyl and palmitoyl modification at the CaaX motif of Cdc42 that regulates RhoGDI binding. *Mol. Cell. Biol.* 33, 1417–1429. doi:10.1128/MCB.01398-12

Nishitani-Isa, M., Mukai, K., Honda, Y., Nihira, H., Tanaka, T., Shibata, H., et al. (2022). Trapping of CDC42 C-terminal variants in the Golgi drives pyrin inflammasome hyperactivation. *J. Exp. Med.* 219, e20211889. doi:10.1084/jem.20211889

Olenik, C., Aktories, K., and Meyer, D. K. (1999). Differential expression of the small GTP-binding proteins RhoA, RhoB, Cdc42u and Cdc42b in developing rat neocortex. *Mol. Brain Res.* 70, 9–17. doi:10.1016/S0169-328X(99)00121-7

Perona, R., Montaner, S., Saniger, L., Sánchez-Pérez, I., Bravo, R., and Lacal, J. C. (1997). Activation of the nuclear factor-kappaB by Rho, CDC42, and Rac-1 proteins. *Genes Dev.* 11, 463–475. doi:10.1101/gad.11.4.463

Phillips, M. J., Calero, G., Chan, B., Ramachandran, S., and Cerione, R. A. (2008). Effector proteins exert an important influence on the signaling-active state of the small GTPase Cdc42. *J. Biol. Chem.* 283, 14153–14164. doi:10.1074/jbc.M706271200

Roy, S., Plowman, S., Rotblat, B., Prior, I. A., Muncke, C., Grainger, S., et al. (2005). Individual palmitoyl residues serve distinct roles in H-ras trafficking, microlocalization, and signaling. *Mol. Cell. Biol.* 25, 6722–6733. doi:10.1128/MCB.25.15.6722-6733.2005

Scandaglia, M., Benito, E., Morenilla-Palao, C., Fiorenza, A., del Blanco, B., Coca, Y., et al. (2015). Fine-tuned SRF activity controls asymmetrical neuronal outgrowth: Implications for cortical migration, neural tissue lamination and circuit assembly. *Sci. Rep.* 5, 17470. doi:10.1038/srep17470

Scott, E. K., Reuter, J. E., and Luo, L. (2003). Small GTPase Cdc42 is required for multiple aspects of dendritic morphogenesis. *J. Neurosci.* 23, 3118–3123. doi:10.1523/JNEUROSCI.23-08-03118.2003

Shinjo, K., Koland, J. G., Hart, M. J., Narasimhan, V., Johnson, D. I., Evans, T., et al. (1990). Molecular cloning of the gene for the human placental GTP-binding protein Gp (G25K): Identification of this GTP-binding protein as the human homolog of the yeast cell-division-cycle protein CDC42. *Proc. Natl. Acad. Sci.* 87, 9853–9857. doi:10.1073/pnas.87.24.9853

Stypulkowski, E., Asangani, I. A., and Witze, E. S. (2018). The depalmitoylase APT1 directs the asymmetric partitioning of Notch and Wnt signaling during cell division. *Sci. Signal.* 11, eaam8705. doi:10.1126/scisignal.aam8705

Su, H. C., and Orange, J. S. (2020). The growing spectrum of human diseases caused by InheritedCDC42 mutations. *J. Clin. Immunol.* 40, 551–553. doi:10.1007/s10875-020-00785-8

Williams, C. L. (2003). The polybasic region of ras and Rho family small GTPases: A regulator of protein interactions and membrane association and a site of nuclear localization signal sequences. *Cell. Signal.* 15, 1071–1080. doi:10.1016/S0898-6568(03)00098-6

Wilson, A. L., Erdman, R. A., Castellano, F., and Maltese, W. A. (1998). Prenylation of Rab8 GTPase by type I and type II geranylgeranyl transferases. *Biochem. J.* 333, 497–504. doi:10.1042/bj3330497

Wirth, A., Chen-Wacker, C., Wu, Y.-W., Gorinski, N., Filippov, M. A., Pandey, G., et al. (2013). Dual lipidation of the brain-specific Cdc42 isoform regulates its functional properties. *Biochem. J.* 456, 311–322. doi:10.1042/BJ20130788

Wirth, A., Labus, J., Galil, D. A., Schill, Y., Schmidt, S., Bunke, T., et al. (2022). Palmitoylation of the small GTPase Cdc42 by DHHC5 modulates spine formation and gene transcription. *J. Biol. Chem.* 298, 102048. doi:10.1016/j.jbc.2022.102048

Woodley, K. T., and Collins, M. O. (2019). S-acylated Golga7b stabilises DHHC5 at the plasma membrane to regulate cell adhesion. *EMBO Rep.* 20, e47472. doi:10.15252/embr.201847472

Wu, F., Chen, Y., Li, Y., Ju, J., Wang, Z., and Yan, D. (2008). RNA-interference-mediated Cdc42 silencing down-regulates phosphorylation of STAT3 and suppresses growth in human bladder-cancer cells. *Biotechnol. Appl. Biochem.* 49, 121–128. doi:10.1042/BA20070107

Wu, W. J., Erickson, J. W., Lin, R., and Cerione, R. A. (2000). The γ-subunit of the coatomer complex binds Cdc42 to mediate transformation. *Nature* 405, 800–804. doi:10.1038/35015585

Yang, W., Di Vizio, D., Kirchner, M., Steen, H., and Freeman, M. R. (2010). Proteome scale characterization of human S-acylated proteins in lipid raft-enriched and non-raft membranes. *Mol. Cell. Proteomics MCP* 9, 54–70. doi:10.1074/mcp.M800448-MCP200

Yap, K., Xiao, Y., Friedman, B. A., Je, H. S., and Makeyev, E. V. (2016). Polarizing the neuron through sustained Co-expression of alternatively spliced isoforms. *Cell Rep.* 15, 1316–1328. doi:10.1016/j.celrep.2016.04.012

Zacharias, D. A., Violin, J. D., Newton, A. C., and Tsien, R. Y. (2002). Partitioning of lipid-modified monomeric GFPs into membrane microdomains of live cells. *Science* 296, 913–916. doi:10.1126/science.1068539

Zhang, F. L., and Casey, P. J. (1996). Protein prenylation: Molecular mechanisms and functional consequences. *Annu. Rev. Biochem.* 65, 241–269. doi:10.1146/annurev.bi.65.070196.001325

Ziman, M., Preuss, D., Mulholland, J., O'Brien, J. M., Botstein, D., and Johnson, D. I. (1993). Subcellular localization of Cdc42p, a *Saccharomyces cerevisiae* GTP-binding protein involved in the control of cell polarity. *Mol. Biol. Cell* 4, 1307–1316. doi:10.1091/mbc.4.12.1307

frontiers | Frontiers in Physiology

TYPE Original Research
PUBLISHED 13 January 2023
DOI 10.3389/fphys.2023.1086112

OPEN ACCESS

EDITED BY
Rebeca M. Mejias Estevez,
Sevilla University, Spain

REVIEWED BY
Javier Valdez Taubas,
CONICET Center for Research in Biological Chemistry, Argentina
Evgeni Ponimaskin,
Hannover Medical School, Germany

*CORRESPONDENCE
Michael R. Hayden,
mrh@cmmt.ubc.ca

†These authors have contributed equally to this work and share senior authorship

‡PRESENT ADDRESS
Shaun S. Sanders,
Department of Molecular and Cellular Biology, University of Guelph, Guelph, ON, Canada
Dale D. O. Martin,
Department of Biology, University of Waterloo, Waterloo, ON, Canada

SPECIALTY SECTION
This article was submitted to Lipid and Fatty Acid Research, a section of the journal
Frontiers in Physiology

RECEIVED 01 November 2022
ACCEPTED 02 January 2023
PUBLISHED 13 January 2023

CITATION
Lemarié FL, Sanders SS, Nguyen Y, Martin DDO and Hayden MR (2023), Full-length huntingtin is palmitoylated at multiple sites and post-translationally myristoylated following caspase-cleavage. *Front. Physiol.* 14:1086112.
doi: 10.3389/fphys.2023.1086112

Full-length huntingtin is palmitoylated at multiple sites and post-translationally myristoylated following caspase-cleavage

Fanny L. Lemarié, Shaun S. Sanders‡, Yen Nguyen, Dale D. O. Martin†‡ and Michael R. Hayden*†

Centre for Molecular Medicine and Therapeutics, BC Children's Hospital Research Institute, University of British Columbia, Vancouver, BC, Canada

Introduction: Huntington disease is an autosomal dominant neurodegenerative disorder which is caused by a CAG repeat expansion in the HTT gene that codes for an elongated polyglutamine tract in the huntingtin (HTT) protein. Huntingtin is subjected to multiple post-translational modifications which regulate its cellular functions and degradation. We have previously identified a palmitoylation site at cysteine 214 (C214), catalyzed by the enzymes ZDHHC17 and ZDHHC13. Reduced palmitoylation level of mutant huntingtin is linked to toxicity and loss of function. Moreover, we have described N-terminal myristoylation by the N-myristoyltransferases of a short fragment of huntingtin (HTT553-586) at glycine 553 (G553) following proteolysis at aspartate 552 (D552).

Results: Here, we show that huntingtin is palmitoylated at numerous cysteines: C105, C433, C3134 and C3144. In addition, we confirm that full-length huntingtin is cleaved at D552 and post-translationally myristoylated at G553. Importantly, blocking caspase cleavage at the critical and pathogenic aspartate 586 (D586) significantly increases posttranslational myristoylation of huntingtin. In turn, myristoylation of huntingtin promotes the co-interaction between C-terminal and N-terminal huntingtin fragments, which is also protective.

Discussion: This suggests that the protective effect of inhibiting caspase-cleavage at D586 may be mediated through post-translational myristoylation of huntingtin at G553.

KEYWORDS

huntingtin, HTT, huntington disease, fatty acylation, myristoylation and palmitoylation, post-translational modification (PTM)

1 Introduction

Huntington disease (HD) is an autosomal dominant neurodegenerative disorder characterized clinically by behavioral changes and a progressive deterioration of motor function and cognitive ability that ultimately leads to death (Ghosh and Tabrizi, 2018). The genetic cause of HD is a CAG trinucleotide repeat expansion (>35 repeats) in the huntingtin gene (*HTT*) resulting in an abnormally long polyglutamine (polyQ) stretch near the N-terminal region of the huntingtin (HTT) protein. Wild-type HTT is a 3,144 amino acid long scaffold protein that plays a critical role in brain development, neuronal health and connectivity (Harjes and Wanker, 2003; Reiner et al., 2003; McKinstry et al., 2014; Dragatsis et al., 2018; Mehler et al., 2019; Burrus et al., 2020). Through interactions with its numerous protein partners, HTT is

involved in many cellular processes, including endocytosis, vesicle/organelle transport and recycling, autophagy, and DNA transcription (Ochaba et al., 2014; Saudou and Humbert, 2016; Maiuri et al., 2017).

The wild-type HTT protein undergoes a large variety of post-translational modifications (PTMs) including phosphorylation (Humbert et al., 2002; Warby et al., 2005; Schilling et al., 2006; Aiken et al., 2009; Watkin et al., 2014), ubiquitination (Kalchman et al., 1996), SUMOylation (Steffan et al., 2004), acetylation (Jeong et al., 2009), proteolysis (Graham et al., 2006) and fatty acylation (Yanai et al., 2006; Martin et al., 2014). The role of the identified PTMs has mainly been studied in relation to the toxicity and aggregation of mutant HTT, but their effects on wild-type HTT functions remain elusive.

PTMs likely regulate different aspects of wild-type HTT scaffolding function, including subcellular localization and protein-protein interactions (Ehrnhoefer et al., 2011). Many PTMs of HTT are altered in the presence of the polyQ expansion, impacting mutant HTT clearance and aggregation which, in turn, modulate mutant HTT toxicity (Atwal et al., 2007; 2011; Caron et al., 2013; Kratter et al., 2016; Cariulo et al., 2017; Lontay et al., 2020).

S-palmitoylation of proteins refers to the reversible addition of long-chain fatty acids, commonly the 16-carbon palmitic acid, onto a cysteine residue *via* a thioester bond (Martin B. R et al., 2011). This PTM increases the hydrophobicity of proteins and plays a key role in protein trafficking, stability, membrane association and protein-protein interactions (Fukata and Fukata, 2010). We have initially described the palmitoylation of HTT at cysteine 214 (C214) by ZDHHC17 and 13 (also known as HIP14 and HIP14L) (Yanai et al., 2006). Mutant HTT is less palmitoylated compared to wild-type HTT in multiple experimental models of HD (Yanai et al., 2006; Lemarié et al., 2021). Transient expression of mutant HTT carrying a palmitoylation-resistant mutation (C214 to serine, C214S) in immortalized cell lines and primary neurons leads to increased mutant HTT aggregation and nuclear inclusion formation, cell death, and susceptibility to excitotoxicity (Yanai et al., 2006). Importantly, modulating palmitoylation by inhibiting depalmitoylating acyl-protein thioesterases (APTs) is protective in HD cells (immortalized cell lines, primary neurons, iPSC-derived neurons) and in the $Hdh^{CAG140/+}$ knock-in mouse model (Lemarié et al., 2021; Virlogeux et al., 2021).

N-myristoylation corresponds to the irreversible addition of the 14-carbon myristic acid *via* a covalent amide bond to the N-terminal glycine residue of proteins, catalyzed by two N-myristoyltransferases (NMTs) (Martin D. D. O et al., 2011; Giglione and Meinnel, 2022). Myristoylation occurs either co-translationally, following the removal of the initiator methionine residue, or post-translationally, when a previously internal glycine residue becomes exposed by proteolytic cleavage (Martin D. D. O et al., 2011). We previously identified the post-translational myristoylation of a short fragment of huntingtin ($HTT_{553-586}$) at glycine 553 (G553), following caspase-3 cleavage of HTT_{1-588}-YFP at aspartate 552 (D552) (Martin et al., 2012; Martin et al., 2014). Overexpressed myristoylated $HTT_{553-586}$ fragment robustly induced autophagy, which is defective in HD (Martinez-Vicente et al., 2010; Ochaba et al., 2014). In addition, while studying a novel caspase-cleavage site in HTT_{1-588}, we noted that blocking proteolysis of wild-type and mutant huntingtin at the pathogenic site D586 promoted the generation of post-translationally myristoylated HTT (Martin et al., 2018a). In turn, we recently found that the protective effect of preventing mutant HTT proteolysis at amino acid 586 by caspases 6 and 8 in the YAC128 mouse model (C6R mouse line) makes mutant HTT a better substrate for autophagy while also promoting global autophagy (Ehrnhoefer et al., 2018). Conversely, transient expression of wild-type HTT_{1-588} carrying a human mutation that blocks myristoylation (G553E) was toxic and induced apoptosis in HD striatal-like cells ($ST Hdh^{111}$) suggesting that post-translational myristoylation is protective in HD (Martin et al., 2018b). Finally, HTT proteolysis at multiple sites is toxic, while proteolysis at one site is not, which promotes the interaction of N- and C-terminal HTT fragments (El-Daher et al., 2015). This led us to propose a PTM crosstalk model in which impairing D586 cleavage promotes D552 cleavage and post-translational myristoylation of HTT at G553 (Graham et al., 2006; Wong et al., 2015; Ehrnhoefer et al., 2018).

The study of HTT PTMs has mostly been restricted to the N-terminal region of HTT (1–600 amino acid region), and little is known about the modifications located in the remaining protein (600–3,144 amino acids). With advances in the detection of palmitoylation, it has become apparent that there are likely additional palmitoylation sites within HTT, as the mutation of the C214 residue (C214S) reduces but does not abrogate HTT palmitoylation. Here, we investigate and identify the existence of additional palmitoylation sites within the full-length HTT protein and further characterize post-translational myristoylation in the context of full-length HTT.

2 Materials and methods

2.1 Materials

2.1.1 Reagents and chemicals

Table 1 lists the reagents and chemicals used for this study along with the application, manufacturer and catalogue number or bibliographic reference.

2.1.2 Antibodies

Table 2 displays the list of antibodies used for this study along with the application, concentrations and experimental conditions.

2.1.3 Plasmids

15Q-HTT_{1-548}(C105S): gBlock® gene fragment coding for 15Q-HTT carrying the C105S mutation and including EcoRI and PspXI restriction sites were designed and ordered from IDT. The gBlock® gene fragment and the pCI-neo 15Q-HTT_{1-548} construct [15Q 1955; NM_002111; (Wellington et al., 1998)] were digested with EcoRI and PspXI restriction enzymes, gel-purified using the QIAquick gel extraction kit and ligated using Quick Ligation Kit followed by transformation of MAX Efficiency Stbl2 competent cells (Figure 1C). 15Q-HTT_{1-548}(C433S): gBlock® gene fragment coding for carrying the C433S mutation and the flanking PshAI and EcoRV restriction sites were designed and ordered from IDT. The gBlock® gene fragment and the pCI-neo 15Q-HTT_{1-548} construct were digested with PshAI and EcoRV restriction enzymes, gel-purified and ligated (Figure 1C). 15Q-HTT_{1-548}(C105/214/433S): The 15Q-HTT_{1-548}(C214S), (C105S) and (C433S) plasmids were digested with PspXI, PshAI, EcoRV and EcoRI restriction enzymes to isolate on agarose gel and purify fragments and open vector containing each CS mutations that were then ligated (Figure 1C). 15Q-HTT_{1-1212}(C1027/1028S): gBlock® gene fragment coding for an HTT fragment carrying the

10.3389/fphys.2023.1086112

TABLE 1 List of reagents and chemicals used.

	Reagent	Manufacturer	#Catalogue or PMID
Cloning	Agarose	Invitrogen	#16500
	gBlock gene fragment	Integrated DNA tech	–
	MAX Efficiency Stbl2 Competent Cells	Invitrogen	#10268019
	mCherry-23/100Q-HTT$_{1-3144}$-EGFP WT, TEV552, TEV586	–	PMID: 26165689
	pCI-neo 15Q-HTT$_{1-548}$	In-house	PMID: 15603740
	pCI-neo 15Q-HTT$_{1-1212}$	In-house	PMID: 18992820
	15Q-HTT$_{1-3144}$	In-house	PMID: 10770929
	QIAquick Gel Extraction Kit	Qiagen	#28706
	Quick Ligation Kit	New England Biolabs	#M2200
	Restriction Enzymes (EcoRI, PspXI, PshAI, EcoRV, PciI, XbaI)	New England Biolabs	-
	Subcloning Efficiency DH5α Competent Cells	Invitrogen	#18265017
Cell Culture Reagents	Dimethyl sulfoxide (DMSO)	Millipore-Sigma	#D2650
	Fetal Bovine Serum (FBS), qualified, Canada	Gibco	#12483020
	GlutaMAX Supplement	Gibco	#35050061
	Nunc EasYFlask Cell Culture 75 cm^2	Thermo Fisher Scientific	#156472
	Penicillin-Streptomycin (10,000 U/mL)	Gibco	#15140122
	Pepstatin A Protease Inhibitor	Thermo Fisher Scientific	#78436
	Phosphate-Buffered Saline (PBS) (10X)	Gibco	#70011044
	Phenylmethylsulfonyl fluoride (PMSF) protease inhibitor	Thermo Fisher Scientific	#36978
	Sodium pyruvate (100 mM)	Gibco	#11360070
	Trypsin-EDTA (0.25%), phenol red	Gibco	#25200056
	X-tremeGENE 9 DNA Reagent	Roche	#6365809001
Fatty Acylation Assays	Biotin Azide	Invitrogen	#B10184
	Caspase inhibitor I (Z-VAD (OMe)-FMK)	Calbiochem	#627610
	Charcoal-stripped FBS	Gibco	#12676029
	Click Tag Myristic Acid Alkyne (13-tetradecynoic acid)	Cayman Chemical	#13267
	Click Tag Palmitic Acid Alkyne	Cayman Chemical	#13266
	Cycloheximide (CHX)	Millipore-Sigma	#C7698
	Dulbecco's Modified Eagle (DMEM)	Gibco	#11960044
	Dynabeads Protein G	Invitrogen	#10003D
	EZ-Link BMCC-Biotin	Thermo Fisher Scientific	#21900
	Fatty acid free Bovine Serum Albumin (BSA)	Millipore-Sigma	#A6003
	Hydroxylamine hydrochloride (HA)	Millipore-Sigma	#255580
	N-ethylmaleimide (NEM)	Sigma-Aldrich	#E3876
	Re-blot Plus Strong Solution (10X)	Millipore-Sigma	#2504
	Sodium Dodecyl Sulfate (SDS)	Thermo Fisher Scientific	#BP166-500
	Staurosporine (STS) solution	Millipore-Sigma	#S6942
	Triton X-100	Roche	#T9284
	Tris (benzyltriazolylmethyl)amine (TBTA)	Millipore-Sigma	#678937

(Continued on following page)

TABLE 1 (*Continued*) List of reagents and chemicals used.

	Reagent	Manufacturer	#Catalogue or PMID
	Tris-carboxyethylphosphine (TCEP)	Millipore-Sigma	#C4706
Western Blot Analysis	Amersham Hybond P WB membranes, PVDF	Cytiva	#10600023
	Amersham Protran WB membranes, nitrocellulose	Cytiva	#GE10600020
	Complete Protease Inhibitor Cocktail	Roche	#11836145001
	Complete EDTA-free protease inhibitors	Roche	#04693132001
	Dithiothreitol (DTT)	Millipore-Sigma	#3483–12–3
	Gel Cassettes, mini, 1.5 mm	Thermo Fisher Scientific	#NC2015
	Invitrogen UltraPure TEMED	Thermo Fisher Scientific	#15524010
	Methanol	Thermo Fisher Scientific	#A412P4
	NuPAGE LDS Sample Buffer (4X)	Thermo Fisher Scientific	#NP0007
	NuPAGE Transfer Buffer (20X)	Invitrogen	#NP00061
	NuPAGE Novex 3%–8% Tris-Acetate gels	Thermo Fisher Scientific	#EA0375
	PROTEAN II xi Cell system	Bio-Rad	#1651804
	Protein Assay Reagent A	Bio-Rad	#5000113
	Protein Assay Reagent B	Bio-Rad	#5000114
	Tween 20	Thermo Fisher Scientific	#BP337-500
	2% Bis Solution	Bio-Rad	#1610142
	30% Acrylamide/Bis Solution, 29:1	Bio-Rad	#1610156
	40% Acrylamide Solution	Bio-Rad	#1610140

C1027S and C1028S mutations and including PciI and XbaI restriction sites were designed and ordered from IDT. The gBlock® fragment and the pCI-neo 15Q-HTT$_{1\text{-}1212}$ construct [15Q 3949; NM_002111; (Warby et al., 2009)] were digested with PciI and XbaI restriction enzymes, purified and ligated, followed by transformation of MAX Efficiency Stbl2 competent cells (Figure 1C). 15Q-HTT$_{1\text{-}3144}$(C3134S) and (C3144S): The plasmids were generated using PCR based site directed mutagenesis using primers carrying the C3134S or C3144S mutations followed by ligation at the SalI sites in full-length HTT (15Q-HTT) (Wellington et al., 2000) (Figure 1C). C-term HTT$_{553\text{-}3144}$-EGFP WT, G553A and mCherry-23Q and 100Q-HTT$_{1\text{-}3144}$-EGFP WT, G553A, TEV586 and TEV552: Dr. Saudou kindly shared the mCherry-23Q and 100Q-HTT$_{1\text{-}3144}$-EGFP with and without caspase cleavage sites at D552 and D586 replaced with Tobacco Etch virus (TEV) proteolytic sites (El-Daher et al., 2015). The G553A myristoylation-resistant mutation was introduced in the mCherry-23Q and 100Q-HTT$_{1\text{-}3144}$-EGFP WT by TOP Gene Technologies (Quebec, Canada). The HTT$_{553\text{-}3144}$-EGFP WT and G553A constructs were generated by TOP Gene Technologies, by excising the mCherry-23Q and 100Q-HTT$_{1\text{-}552}$ fragments from the mCherry-23Q and 100Q-HTT$_{1\text{-}3144}$-EGFP WT and G553A plasmids, and by introducing a N-terminal methionine (Figures 4A, C; Figure 5A). All the constructs were verified by DNA sequencing (CMMT facility).

2.1.4 Experimental models (cell lines)

HeLa, HEK293 and COS-7 cells were grown at 37°C using in Dulbecco's Modified Eagle Medium (DMEM) supplemented with 10% fetal bovine serum (FBS), 1 mM sodium pyruvate, 2 mM GlutaMAX and 10 units/mL of penicillin and 10 µg/mL of streptomycin. Cells were grown in 75 cm^2 flasks at 37°C and 5% CO_2, and were split using a 0.25% trypsin-EDTA solution (1:10 dilution) when cells were ~90% confluent by microscopy.

2.2 Methods

2.2.1 Plasmid transfection

Cells were seeded in 6-well or 10-cm plates overnight at 37°C and 5% CO_2. The next day, cells were transfected with cDNA constructs encoding for 15Q-HTT$_{1\text{-}548}$, HTT$_{1\text{-}1212}$ and full-length HTT$_{1\text{-}3144}$, mCherry-23Q or 100Q-HTT$_{1\text{-}3144}$-EGFP and HTT$_{553\text{-}3144}$-EGFP using X-tremeGENE 9 DNA transfection reagent (ratio 3:1 or 6:1, reagent (µL): DNA (µg)) or calcium phosphate transfection (Graham and van der Eb, 1973). Cells were treated or harvested 18–48 h post-transfection.

2.2.2 Palmitoylation assays

2.2.2.1 Bio-orthogonal labeling assay using alkyne-palmitate (click chemistry)

To measure the dynamic palmitoylation level of HTT, cells transiently transfected with HTT constructs for 18 h were incubated for 1 h in DMEM supplemented with 5% charcoal-stripped FBS, to deprive the cells of lipids. Cells were subsequently metabolically labeled with 100 µM alkyne-palmitate in fatty acid-free bovine serum albumin (BSA) for 6 h. Cells were lifted from plates in

TABLE 2 List of antibodies used and application.

Target (Clone)	Species	Type	Supplier	Catalogue / AB registry reference	Application	Dilution	Volume[a]
HTT	Mouse	Monoclonal	Sigma-Aldrich	MAB2166	WB	1:1,000	–
(1HU-4C8)				AB_2123255	IP	–	2 µL
HTT	Rabbit	Monoclonal	Cell Signaling Technology	5656	WB	1:1,000	–
(D7F7)				AB_10827977			
HTT	Rabbit	Polyclonal	in-house	Kalchman et al. (1996)	IP	–	2 µL
(BKP1/HD46)					WB	1:400	–
HTT	Rabbit	Polyclonal	Sigma-Aldrich	H7540	WB	1:1,000	–
				AB_1840946	IP	–	2 µL
mCherry	Rabbit	Polyclonal	Abcam	ab167453	WB	1:1,000	–
Streptavidin	–	Conjugated to AF-680	Invitrogen	S-32358	WB	1:5,000	–
GFP	Goat	Polyclonal	Eusera	EU4	IP	–	0.75 µL
GFP	Rabbit	Polyclonal	Eusera	EU2	WB	1:5,000	–
					IP	–	0.75 µL
Goat IgG	–	–	Thermo Fisher Scientific	02–6202	IP	–	0.75 µL
Mouse IgM (µ chain specific)	Goat	–	Rockland Immuno-chemicals	92,632,210	WB (secondary)	1:5,000	–
Rabbit IgG	Goat	–		926–32211	WB (secondary)	1:5,000	–

[a]Volume of antibodies used for 20 µL of Dynabeads and 200 µg–2 mg proteins.

phosphate-buffered saline (PBS) using cell scrapers, pelleted by centrifugation (500 × *g*, 5 min, +4°C) and subsequently lysed in EDTA-free RIPA buffer (150 mM $NaCl_2$, 50 mM HEPES pH 7.4, 1% Igepal CA-630, 0.5% sodium deoxycholate, 0.1% sodium dodecyl sulfate (SDS) in water, EDTA-free cOmplete protease inhibitors) for 10 min on ice, 5 min at 4°C on rotator and were centrifuged (16,000 × *g*, 10 min, +4°C). Protein concentrations were assessed using the DC protein assay. HTT was immunoprecipitated from cell lysates by overnight incubation with Dynabeads Protein G and appropriate antibodies (Table 2). Bio-orthogonal click chemistry of alkyne-palmitate with biotin azide was performed on cell lysates, as previously described (Yap et al., 2010; Liao et al., 2021). The immunoprecipitated proteins were adjusted to 1% SDS and incubated with 100 mM tris (benzyltriazolylmethyl)amine (TBTA), 1 mM $CuSO_4$, 1 mM tris-carboxyethylphosphine (TCEP) and 100 mM biotin azide (PEG4 carboxamide-6-Azidohexanyl biotin) at 37°C in darkness for 30 min. Total HTT and palmitoylated HTT were detected by western blot analysis.

2.2.2.2 Acyl-biotin exchange assay on immunoprecipitated proteins (IP-ABE)

The IP-ABE assay was performed as previously described to measure the global palmitoylation level of HTT (Drisdel and Green, 2004; Huang et al., 2009). Briefly, cells transiently expressing HTT constructs for 48 h were lifted from plates in PBS using cell scrapers and then pelleted by centrifugation (500 × *g*, 5 min, +4°C). Subsequently, cell pellets were lysed on ice in lysis buffer (150 mM NaCl, 50 mM tris, 5 mM EDTA, 0.1% SDS, 1% Triton X-100, pH 7.4) containing 100 mM N-ethylmaleimide (NEM). Homogenates were sonicated to shear DNA, and the insoluble material was removed by centrifugation (20,000 × *g*, 15 min, +4°C). Protein concentrations in lysates were assessed by DC protein assay. HTT was immunoprecipitated from cell lysates by overnight incubation with Dynabeads Protein G and appropriate antibodies (Table 2). Beads were then washed and split into two and treated with neutral pH hydroxylamine in lysis buffer (HAM+) or just lysis buffer (HAM-) for 2 h. Following HAM treatment, beads were washed and treated with 2.5 µM EZ-Link BMCC-Biotin in pH 6.2 lysis buffer for 1 h at 4°C. At the end of the BMCC-Biotin treatment, beads were washed and then heated for 10 min at 70°C with NuPAGE LDS sample buffer and 100 mM dithiothreitol (DTT) to elute proteins. Total HTT and palmitoylated HTT were detected by western blot analysis.

2.2.3 Myristoylation assay (bio-orthogonal labeling assay using alkyne-myristate)

Myristoylation of HTT was detected as previously described (Yap et al., 2010; Martin et al., 2012; Martin et al., 2014; Martin et al., 2018b; Liao et al., 2021). HEK293 cells were transiently transfected with the $HTT_{553-3144}$-EGFP WT and G553A plasmids using the calcium phosphate transfection protocol. The following day, the cells were

starved of lipids in DMEM supplemented with 5% charcoal-stripped FBS for 30 min, and then treated with 100 µM alkyne-myristate in fatty acid-free BSA for 4 h. HeLa cells were transiently transfected with mCherry-23Q and 100Q-HTT$_{1-3144}$-EGFP WT, G553A, TEV552 and TEV586 plasmids using X-tremeGENE 9 as per the manufacturer's directions. HeLa cells transfected for 40 h were washed in PBS and starved in DMEM supplemented with 5% charcoal-stripped FBS for 30 min. HeLa cells were then incubated with 100 µM alkyne-myristate in fatty acid-free BSA for 30 min, prior to the addition of 1 µM staurosporine (STS) to promote caspase activity, and cycloheximide (CHX) at 5 µg/mL to inhibit protein synthesis for 4 h. HEK293 and HeLa cells were lysed in modified EDTA-free RIPA buffer (50 mM HEPES pH 7.4, 0.5% sodium deoxycholate, 150 mM NaCl, 1% Igepal, 0.1% SDS, 2 mM $MgCl_2$) supplemented with PMSF, pepstatin A and caspase inhibitor I (Z-VAD-FMK). Proteins were immunoprecipitated from cell lysates by overnight incubation with Protein G Dynabeads and goat anti-GFP antibodies, and subsequently subjected to click chemistry, as previously described in the section 'Bio-orthogonal labeling assay using alkyne-palmitate'. Sample denaturation was conducted in NuPAGE LDS sample buffer and 100 mM DTT for 10 min at 70°C. Total HTT and myristoylated HTT were detected by western blot analysis.

2.2.4 Co-immunoprecipitation (Co-IP)

HeLa cells were seeded in 6-well plates and transfected with the mCherry-23Q-HTT$_{1-3144}$-EGFP WT, TEV552, TEV586 or G553A using X-tremeGENE 9 Transfection reagent for 46 h, and treated for 2 h with 5 µM STS and 5 µg/mL cycloheximide (STS/CHX). Cells were then lysed in SDP lysis buffer (50 mM tris pH 8.0, 150 mM NaCl, 1% Igepal, 10 mM NaF, 40 mM β-glycerophosphate) supplemented with fresh protease inhibitors (cOmplete protease inhibitor cocktail, 1 mM sodium orthovanadate, 1 µM pepstatin A, and 5 µM Z-VAD-FMK), homogenized using an Eppendorf homogenizer, rotated at 4°C for 20 min and centrifuged (16,000 × *g*, 12 min, +4°C). Protein concentrations in the supernatants were assessed by DC assay. Lysates were pre-cleared with 10 µL Dynabeads Protein G for 30 min at 4°C. Full-length and C-terminal HTT-EGFP were immunoprecipitated from lysates by overnight incubation with Dynabeads Protein G and goat anti-GFP antibodies. Proteins were eluted from beads and denatured in NuPAGE LDS sample buffer with 100 mM DTT for 15 min at 70°C. Immunoblots for N-terminal HTT fragments were conducted with HTT [MAB2166/1HU-4C8, amino acid ~443–457 (Cong et al., 2005)], or mCherry antibodies. Immunoblots for full-length and C-terminal HTT fragments were conducted with rabbit anti-GFP antibodies.

2.2.5 Western blot analysis

For the palmitoylation assays, denatured protein samples were run on NuPAGE 3%–8% tris-acetate gradient protein gels in tris-acetate SDS running buffer (50 mM tricine, 50 mM tris base, 0.1% SDS, pH 8.24). Proteins were transferred to 0.45 µm nitrocellulose membranes, in NuPAGE transfer buffer supplemented with 5% methanol. For the myristoylation assay, the lysates from HEK293 cells expressing C-terminal HTT$_{553-3144}$-EGFP were run on tris-glycine gels (7%) in SDS-tris-glycine running buffer (25 mM tris base, 190 mM glycine, 3.5 mM SDS). Lysates from HeLa cells expressing mCherry-HTT-EGFP were run on 10% low bis acrylamide (1:200 bis-acrylamide:acrylamide) gels (without β-mercaptoethanol) in SDS-tris-glycine running buffer (Carroll et al., 2011; Caron et al., 2021). Proteins were transferred to 0.45 µm PVDF membranes, in NuPAGE transfer buffer supplemented with 5% methanol. For the co-immunoprecipitation assay, denatured HeLa lysates were run on large tris-glycine gels (10%) in SDS-tris-glycine running buffer using the Bio-Rad PROTEAN II xi Cell system. Proteins were transferred to 0.45 µm nitrocellulose membranes, in NuPAGE transfer buffer supplemented with 5% methanol.

PVDF and nitrocellulose membranes were blocked in 3%–5% BSA in tris-buffered saline (TBS) supplemented with 0.1%–0.5% Tween-20 (T). Primary antibody dilutions in 3%–5% BSA TBST were applied to the immunoblots at room temperature for 1-2 h or overnight at 4°C (Table 2). Membranes were washed in PBST or TBST (4 × 5 min, room temperature). The appropriate secondary antibodies and Alexa Fluor 680 conjugated streptavidin were then applied in 3%–5% BSA TBST for 1-2 h at room temperature. Membranes were washed in TBST (4 × 5 min, room temperature) and imaged using the LI-COR Odyssey Infrared Imaging System (LI-COR Biosciences). To perform membrane stripping, PVDF membranes were washed with PBS, submerged in Re-blot plus strong solution and incubated at 55°C for 30 min with intermittent agitation. The membranes were washed twice in TBST (2 × 10 min, room temperature), blocked for 1 h in 3% BSA in TBST, and re-probed with primary and secondary antibodies. Densitometry was quantified using the LI-COR Image Studio Lite software and median signal intensity following background subtraction was used for analysis. Acylation was analyzed as a ratio of myristoylation or palmitoylation signal (streptavidin) to total immunoprecipitated protein signal and normalized to the control. All the uncropped immunoblots are displayed in Supplementary Figures S1–S10.

2.2.6 Statistical analysis

GraphPad Prism 9 (9.4.1) was used for all statistical analyses and graph preparation. Figures were generated in Adobe Illustrator 2020. All data are presented as mean ± SEM. Biological replicates (n) are displayed on each graph, or indicated in the captions. Student's *t*-test or 1, 2, or 3-way ANOVA statistical tests with post-hoc analysis (Sidak, Tukey, Bonferroni) were used for all experiments.

3 Results

3.1 Identification of new palmitoylation sites of huntingtin within its N-terminal region

We have previously shown that HTT is palmitoylated at cysteine 214 (C214), using radioactive labeling techniques (Yanai et al., 2006). With recent advances in the detection of palmitoylation it has become apparent that there are likely additional palmitoylation sites within HTT, as the C214S mutation only reduces HTT palmitoylation levels by 30%–40% (*unpublished data*; displayed in Figures 2, 3). To identify these potential palmitoylation sites, the HTT amino acid sequence was run through the CSS-Palm 3.0 prediction program to determine which cysteines are predicted to be palmitoylated (Figure 1A) (Zhou et al., 2006). Cysteine residues with a prediction score higher than 1.2 were prioritized for testing as potential palmitoylation sites (3144, 1028, 3134, 1027 and 433). We also included the cysteine 105 as it is localized in the N-terminal 548 amino acid fragment, which contains the interaction domain of HTT with ZDHHC17 and 13 (Sanders et al., 2014) (Figure 1B).

In order to reduce the number of potential sites detected, we first sought to identify new palmitoylated residues within the N-terminal

10.3389/fphys.2023.1086112

A CSS-Palm 3.0 palmitoylation site prediction of full-length Huntingtin

Position	Peptide	Score
3144	NVHKVTTC*******	3.2
1028	RALTFGCCEALCLLS	2.1
214	YLVNLLPCLTRTSKR	1.9
3134	PYHRLLTCLRNVHKV	1.5
1027	TRALTFGCCEALCLL	1.4
433	IAGGGSSCSPVLSRK	1.2
105	KKDRVNHCLTICENI	1.1
2362	PKYITAACEMVAEMV	1.1
825	KDESSVTCKLACTAV	1.1
1032	FGCCEALCLLSTAFP	1.1
1313	EPMMATVCVQQLLKT	1.1
840	RNCVMSLCSSSYSEL	1.1
2307	TEFVTHACSLIYCVH	1
2283	DLQAGLDCCCLALQL	0.6
1597	FILVLQQCHKENEDK	0.4
1154	LLKVINICAHVLDDV	0.3
2150	NLSLLAPCLSLGMSE	0.3
638	LLKNMSHCRQPSDSS	0.3
2015	RMVDILACRRVEMLL	0.3
280	AGSAVSICQHSRRTQ	0.3
1710	FSPYLISCTVINRLR	0.3
2312	HACSLIYCVHFILEA	0.2
829	SVTCKLACTAVRNCV	0.2
517	DSVDLASCDLTSSAT	0.2
1302	ILGYLKSCFSREPMM	0.2
944	VPKLFYKCDQGQADP	0.2
2528	AGNPAVSCLEQQPRN	0.2

B Potential new palmitoylation sites of huntingtin

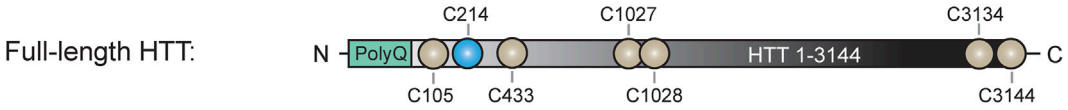

C Cysteine to serine mutant constructs

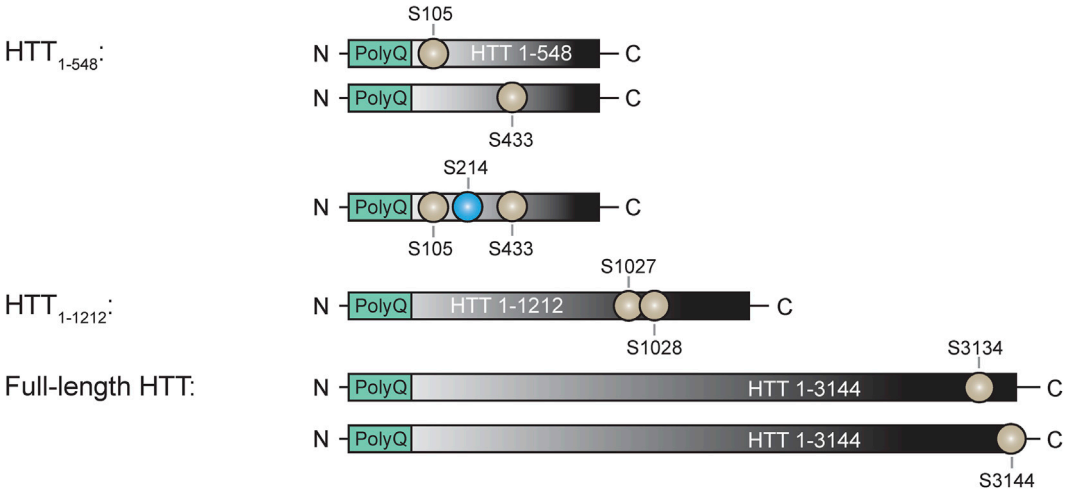

FIGURE 1
Potential new palmitoylation sites of huntingtin. **(A)** CSS-Palm 3.0 palmitoylation site prediction of full-length HTT, **(B)** palmitoylation site of HTT (in blue: C214) and potential new palmitoylation sites investigated in this study (in light grey: C105, C433, C1027, C1028, C3134 and C3144), **(C)** cysteine-to-serine mutant DNA constructs generated to investigate the potential new palmitoylation sites of huntingtin. Point mutations were introduced in N-terminal HTT_{1-548}, HTT_{1-1212} or full-length HTT_{1-3144} at C105, C214, C433, C105/214/433, C1027/C1028, C3134 and C3144.

548 amino acid fragment (Figure 1C and Figure 2; uncropped blots displayed in Supplementary Figures S1–S4). The palmitoylation level of 15Q-HTT_{1-548} WT, carrying a cysteine-to-serine mutation at C214 (C214S), C105 (C105S) or C433 (C433S) was measured in COS-7 cells using the IP-ABE assay (Figure 2A). The palmitoylation level of HTT C214S was significantly decreased compared to the WT control (by

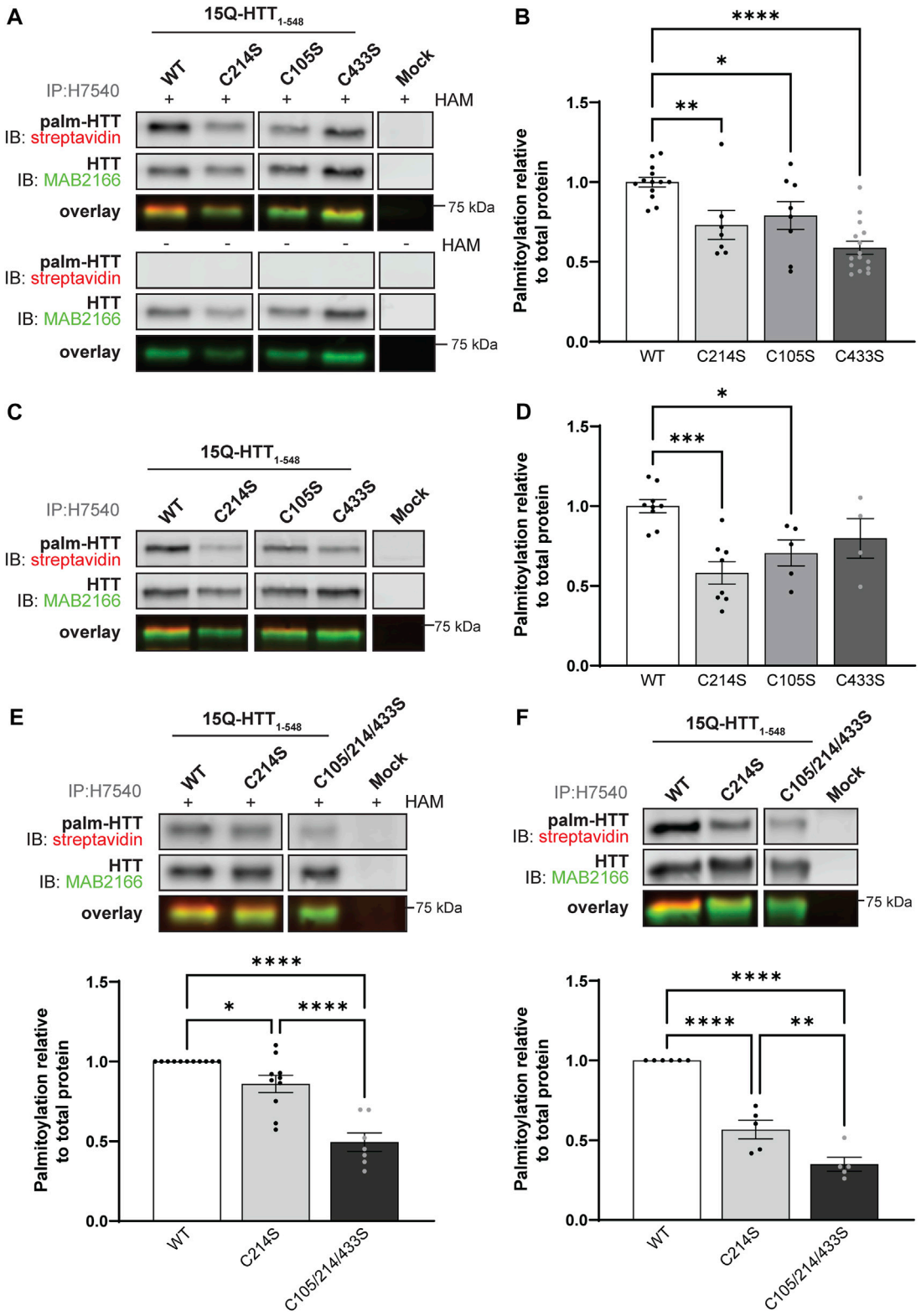

FIGURE 2
Huntingtin is palmitoylated at cysteines 105 and 433. **(A)** COS-7 cells transiently expressing 15Q-HTT$_{1-548}$ WT or carrying cysteine-to-serine mutations at residues 214 (C214S), 105 (C105S) or 433 (C433S) were harvested 48 h post-transfection, and subjected to the IP-ABE assay. Mock transfections were included to determine baseline background levels. Proteins were immunoprecipitated from lysates using N-terminal HTT antibodies (H7540). Palmitoylated HTT labeled with biotin was detected by western blot analysis using streptavidin, and total HTT with MAB2166 antibodies. The palmitoylation signal (palm-HTT, HAM+) and the negative control treatment (palm-HTT, HAM-) are shown in the top panels, the total HTT protein immunoprecipitated are presented in the corresponding middle panels, and the overlay of the two are displayed in the bottom panels. The western blot images are composites of different lanes from the same image (Supplementary Figure S1), **(B)** HTT palmitoylation level was calculated as the ratio of palmitoylation over total HTT protein signal, and expressed relative to 15Q-HTT$_{1-548}$ WT (n = 7–15), **(C)** COS-7 cells transiently expressing 15Q-HTT$_{1-548}$ WT or C214S, C105S and C443S were labeled with

(*Continued*)

FIGURE 2 (Continued)
alkyne-palmitate for 6 h, and harvested 48 h post-transfection. Proteins were immunoprecipitated from lysates with H7540 antibodies, and bio-orthogonally labeled with azido-biotin by click chemistry. Palmitoylated HTT_{1-548} (top panel) labeled with biotin was detected with streptavidin, and total HTT (corresponding middle panel) was detected with HTT antibodies (MAB2166). The overlay of the two is displayed in the bottom panel. The western blot images are composites of different lanes from the same image (Supplementary Figure S2) **(D)** HTT palmitoylation level was calculated as the ratio of palmitoylated HTT over total HTT protein signal, and expressed relative to 15Q-HTT_{1-548} WT (n = 5–7) **(E)** Palmitoylation of 15Q-HTT_{1-548} WT, C214S, C105/214/433S expressed in COS-7 cells was measured as described in **(A, B)**, by IP-ABE assay (n = 7–11) **(F)** Palmitoylation of 15Q-HTT_{1-548} WT, C214S, C105/214/433S expressed in COS-7 cells was measured as described in **(C, D)**, by bio-orthogonal labeling following metabolic labeling with alkyne-palmitate (n = 5–6). The western blot images are composites of different lanes from the same image (Supplementary Figures S3, S4). *Statistical analysis*: **(B)** 1-way ANOVA: C to S mutations, ****$p < .0001$. Tukey's multiple comparisons test: WT vs. C214S, **$p = .0084$; WT vs. C105S, *$p = .040$; WT vs. C433S, ****$p < .0001$. **(D)** 1-way ANOVA: C to S mutations, ***$p = .0009$. Tukey's multiple comparisons test: WT vs. C214S, ***$p = .0003$; WT vs. C105S, *$p = .024$; WT vs. C433S, $p = .23$. **(E)** 1-way ANOVA: C to S mutations, ****$p < .0001$. Tukey's multiple comparisons test: WT vs. C214S, *$p = .044$; WT vs. C105/214/433S, ****$p < .0001$; C214S vs. C105/214/433S, ****$p < .0001$. (**F**) 1-way ANOVA: C to S mutations, ****$p < .0001$. Tukey's multiple comparisons test: WT vs. C214S, ****$p < .0001$; WT vs. C105/214/433S, ****$p < .0001$; C214S vs. C105/214/433S, **$p = .0058$.

30%; 1-way ANOVA: $p < .0001$; Tukey's test: WT vs. C214S, $p = .0084$), but not abrogated (Figure 2B). Palmitoylation levels of 15Q-HTT carrying the C105S or C433S mutations were significantly lower than the WT control, by 20% and 40%, respectively (Tukey's test: WT vs. C105S, $p = .040$; WT vs. C433S, $p < .0001$). This result supports that C214 is not the only palmitoylated residue of HTT, and that C105 and C433 are two palmitoylation sites within the huntingtin protein.

The dynamic palmitoylation level of 15Q-HTT_{1-548} WT, C214S, C105S and C433S was also measured in COS-7 cells by bio-orthogonal labeling following metabolic labeling with alkyne-palmitate (Figure 2C). As expected, the HTT C214S palmitoylation level was significantly reduced compared to the WT control (by 40%; 1-way ANOVA: $p = .0009$; Tukey's test: WT vs. C214S, $p = .0003$) (Figure 2D). The palmitoylation level of 15Q-HTT C105S was significantly decreased compared to the WT control (by 30%; Tukey's test: WT vs. C105S, $p = .024$). The data support that the residue C105 of the HTT protein is dynamically palmitoylated, similar to C214. While the palmitoylation level of 15Q-HTT C433S was lower than that of the WT control (20%), this decrease did not reach statistical significance due to a higher variability of the data (Tukey's test: WT vs. C433S, $p = .23$). This result could be indicative of a slower palmitoylation turnover of HTT at C433.

The palmitoylation levels of 15Q-HTT_{1-548} WT, C214S or carrying three cysteine-to-serine mutations at C105, 214 and 433 (C105/214/433S) were measured in COS-7 cells using the IP-ABE (Figure 2E) and the bio-orthogonal assays (Figure 2F). The palmitoylation level of 15Q-HTT C105/214/433S was significantly reduced compared to 15Q-HTT WT (by 50%; Tukey's test: $p < .0001$) and 15Q-HTT C214S (by 40%; Tukey's test: $p < .0001$) when measured with the IP-ABE assay (Figure 2E). The dynamic palmitoylation level of 15Q-HTT C105/214/433S was also significantly decreased compared to 15Q-HTT WT (by 65%; Tukey's test: $p < .0001$) and 15Q-HTT C214S (by 40%; Tukey's test: $p < .0001$) when measured by bio-orthogonal labeling assay (Figure 2F). Our data show an additive effect of the cysteine residues C214, C105 and C433 on the global and dynamic palmitoylation levels of HTT. Altogether, these results support that the cysteines 105 and 433 of HTT are palmitoylated.

3.2 Identification of new palmitoylation sites of huntingtin within its C-terminal region

Next, we investigated the existence of potential new palmitoylated residues within HTT at C1027 and C1028 by using a longer fragment of HTT, 15Q-HTT_{1-1212} (Figure 1C and Figure 3; uncropped blots displayed in Supplementary Figure S5). The global palmitoylation level of 15Q-HTT_{1-1212} WT, or carrying two cysteine-to-serine mutations at C1027 and C1028 (C1027/1028S) was measured in COS-7 cells using the IP-ABE assay (Figure 3A). The palmitoylation level of 15Q-HTT C1027/1028S was not significantly modified compared to the WT control (Figure 3B; *t*-test: $p = .11$). The dynamic palmitoylation level of 15Q-HTT_{1-1212} WT or C1027/1028S was also measured in COS-7 cells by bio-orthogonal labeling assay following metabolic labeling with alkyne-palmitate (Figure 3C). The palmitoylation level of 15Q-HTT C1027/1028S was significantly increased compared to the WT control (Figure 3D; *t*-test: $p = .0058$). The higher palmitoylation turnover measured with the bio-orthogonal labeling assay, without any change of the total palmitoylation level with the ABE assay, could be explained by an increased palmitoylation dynamism at other HTT residues when C1027 and C1028 are mutated. This could be the consequence of conformational, location or protein-protein interaction changes in HTT C1027/1028S that would allow more efficient palmitoylation at other sites. Altogether, the data generated with these two palmitoylation assays support that the C1027 and C1028 residues are not palmitoylated.

Finally, we sought to identify new sites of palmitoylation using full-length HTT (Figure 1C). The palmitoylation level of full-length HTT WT, carrying a cysteine-to-serine mutation at C214, C3134 or C3144 was measured in HeLa cells by bio-orthogonal labeling assay following metabolic labeling with alkyne-palmitate (Figure 3E; uncropped blots displayed in Supplementary Figure S6). The palmitoylation level of HTT C214S was significantly decreased compared to the WT control (by 25%; 1-way ANOVA: $p = .0024$; Bonferroni's test: WT vs. C214S, $p = .0090$) (Figure 3F). Palmitoylation levels of 15Q-HTT carrying the C3134S and C3144S were reduced compared to the WT control, by 25% and 30%, respectively (Bonferroni's test: WT vs. C3134S, $p = .0073$; WT vs. C3144S, $p = .0031$). Therefore, these results suggest that cysteines 3134 and 3144 of HTT are dynamically palmitoylated. The palmitoylation level of full-length HTT WT, C214S, C3134S and C3144S could not be reliably detected using the IP-ABE assay in this experimental model, for unknown reasons (data not shown).

3.3 Full-length huntingtin is cleaved at D552 and post-translationally myristoylated at G553

We previously demonstrated that a truncated version of HTT (HTT_{1-588}-YFP) undergoes post-translational myristoylation at the newly exposed glycine 553 (G553) following caspase cleavage at D552 (Martin et al., 2014). To determine if longer C-terminal fragments of

10.3389/fphys.2023.1086112

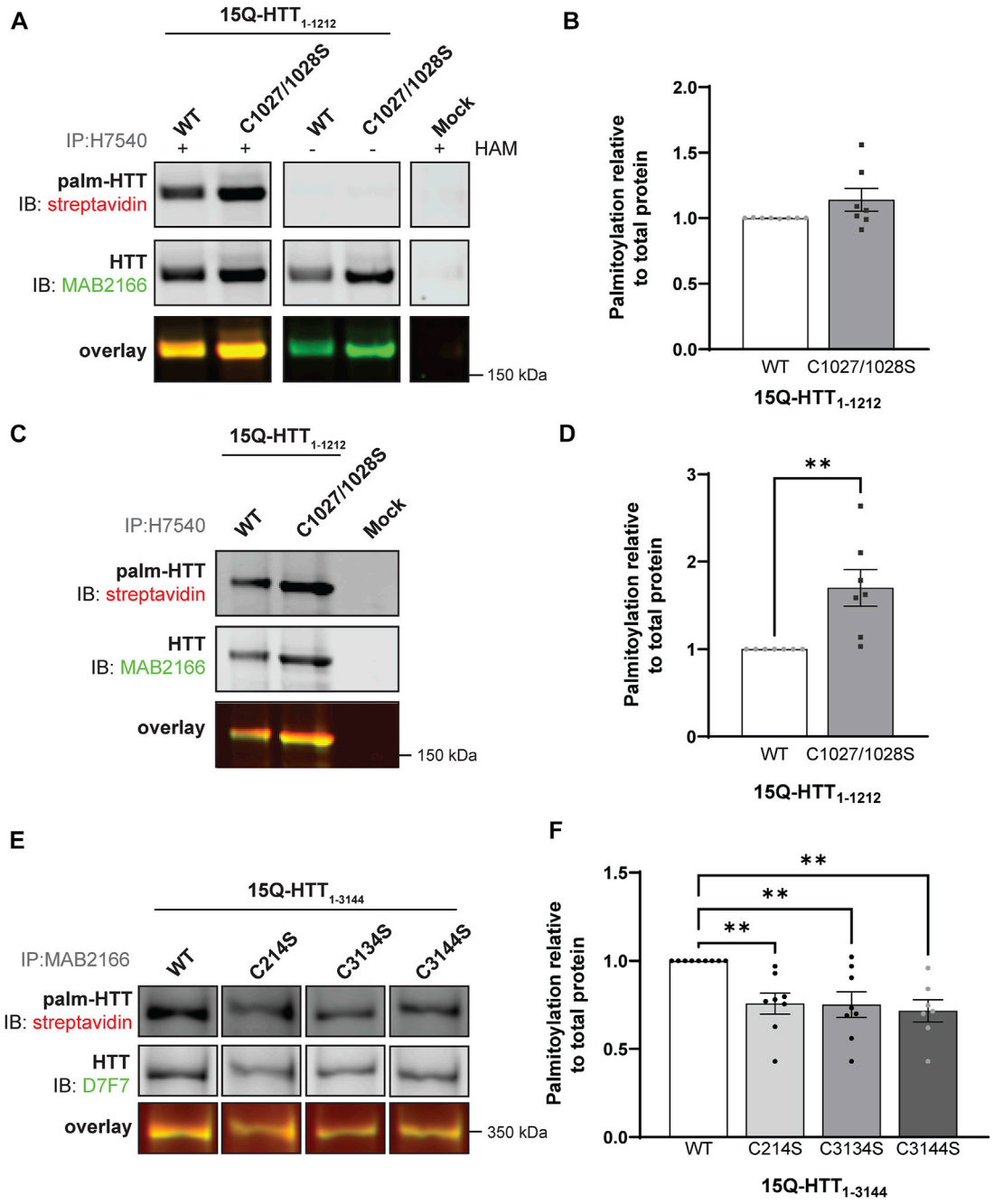

FIGURE 3
Huntingtin is palmitoylated at cysteines 3134 and 3144. **(A)** COS-7 cells transiently expressing 15Q-HTT_{1-1212} WT or carrying two cysteine-to-serine mutations at residues 1027 and 1028 (C1027/1028S) were harvested 48 h post-transfection, and subjected to the IP-ABE assay. Proteins were immunoprecipitated from lysates using N-terminal HTT antibodies (H7540). Palmitoylated HTT labeled with biotin was detected by western blot analysis using streptavidin, and total HTT with MAB2166 antibodies. The palmitoylation signal (palm-HTT, HAM+) and the negative control treatment (HAM-) are shown in the top panels, the total HTT protein immunoprecipitated is presented in the corresponding middle panels, and the overlay of the two is displayed in the bottom panels. Uncropped blots are displayed in Supplementary Figure S5, **(B)** HTT palmitoylation level was calculated as the ratio of palmitoylated HTT over total HTT protein signal, and represented relative to 15Q-HTT_{1-1212} WT (n = 7), **(C)** COS-7 cells transiently expressing 15Q-HTT_{1-1212} WT or C1027/1028S were labeled with alkyne-palmitate for 6 h, and harvested 48 h post-transfection. Proteins were immunoprecipitated from lysates with H7540 antibodies, and bio-orthogonally labeled with azido-biotin by click chemistry. Palmitoylated HTT_{1-1212} (top panel) labeled with biotin was detected with streptavidin, and total HTT (corresponding middle panels) was detected with HTT antibodies (MAB2166). The overlay of the two is displayed in the bottom panels. Uncropped blots are displayed in Supplementary Figure S5, **(D)** HTT palmitoylation level was calculated as the ratio of palmitoylated HTT over total HTT protein signal, and represented relative to 15Q-HTT_{1-1212} WT (n = 7), **(E)** HeLa cells transiently expressing 15Q-HTT_{1-3144} WT, C214S, C3134S and C3144S were labeled with alkyne-palmitate for 6 h, and harvested 48 h post-transfection. Proteins were immunoprecipitated from lysates with HTT (MAB2166) antibodies, and bio-orthogonally labeled with azido-biotin by click chemistry. Palmitoylated HTT_{1-3144} (top panel) labeled with biotin was detected with streptavidin, and total HTT (corresponding middle panels) was detected with HTT antibodies (D7F7). The overlay of the two is displayed in the bottom panels. The western blot images are composites of different lanes from the same image (Supplementary Figure S6), **(F)** HTT palmitoylation level was calculated as the ratio of palmitoylated HTT over total HTT protein signal, and represented relative to 15Q-HTT_{1-3144} WT (n = 7–8). *Statistical analysis*: **(B)** Unpaired *t*-test: $p = .11$. **(C)** Unpaired *t*-test: $^{**}p = .0058$. **(F)** 1-way ANOVA: C to S mutations, $^{**}p = .0024$. Bonferroni's multiple comparisons test: WT vs. C214S, $^{**}p = .0090$; WT vs. C3134S, $^{**}p = .0073$; WT vs. C3144S, $^{**}p = .0031$.

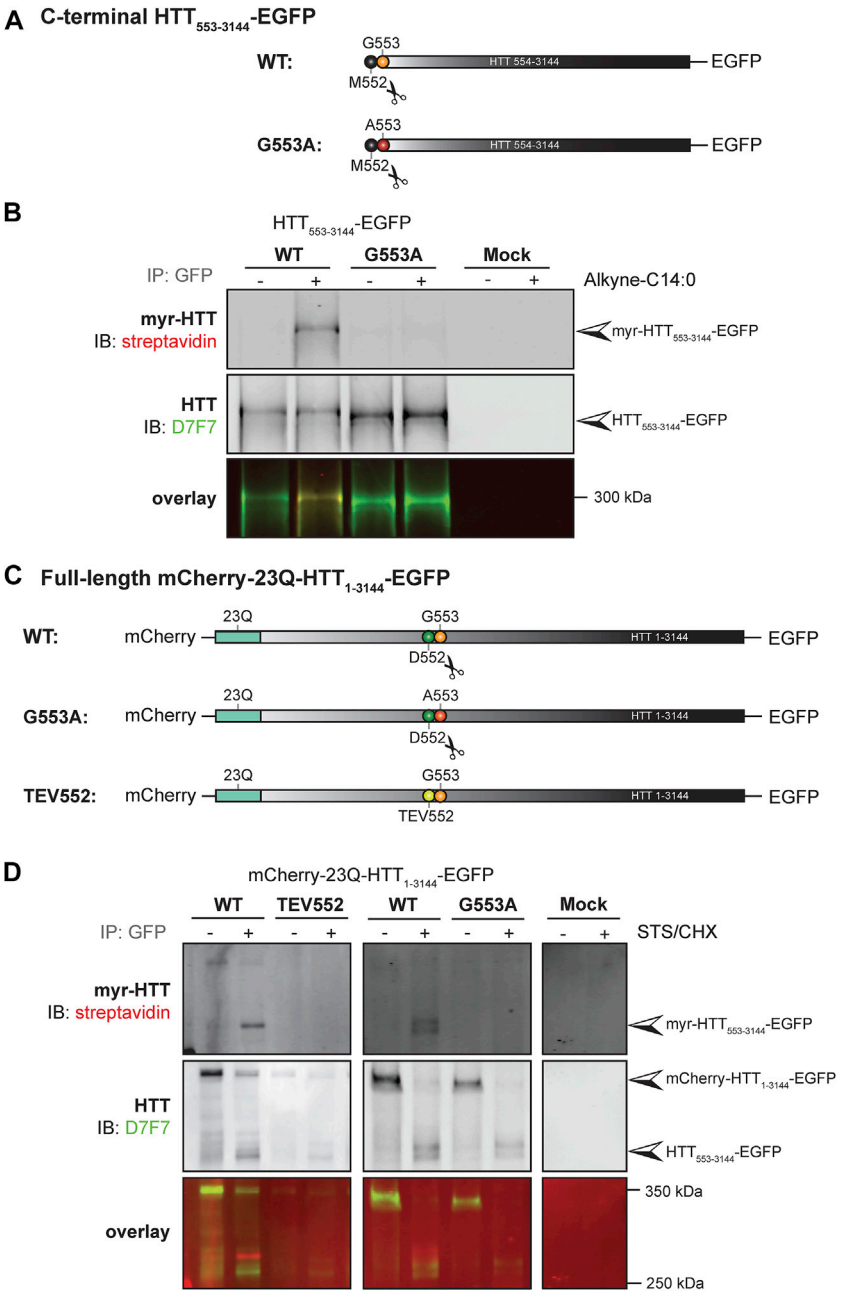

FIGURE 4
C-terminal $HTT_{553-3144}$ is co- and post-translationally myristoylated at G553 in C-terminal $HTT_{553-3144}$ and full-length HTT_{1-3144}, respectively. **(A)** Schematic representation of the C-terminal $HTT_{553-3144}$-EGFP constructs WT or carrying a glycine 5s53 to alanine (G553A). The scissors symbol indicates the cleavage of the N-terminal methionine M552, **(B)** HEK293 cells transfected with C-terminal $HTT_{553-3144}$-EGFP WT or G553A mutation were labeled with DMSO or 100 µM alkyne-myristate for 4 h, **(C)** schematic representation of the full-length mCherry-23Q-HTT_{1-3144}-EGFP constructs WT, G553A or with the D552 caspase cleavage site replaced with a Tobacco Etch Virus proteolytic site (TEV552). The scissors symbol indicates the D552 cleavage site, **(D)** HeLa cells were transfected with mCherry-23Q-HTT_{1-3144}-EGFP constructs WT, G553A, or TEV552. Cells were labeled with 100 µM alkyne-myristate for 30 min, and then treated for 4 h with 1 µM staurosporine (STS) and 5 µg/mL cycloheximide (CHX) to induce proteolysis and inhibit protein synthesis, respectively. For both **(B, D)**, HTT fragments were immunoprecipitated from cell lysates using goat anti-GFP antibodies. The myristate analog was covalently linked to biotin azide through click chemistry. Myristoylated $HTT_{553-3144}$-EGFP orthogonally labeled with biotin was detected with streptavidin and total HTT was detected with HTT antibodies (D7F7). Arrowheads indicate myristoylated HTT (myr-$HTT_{553-3144}$-EGFP), total C-terminal HTT ($HTT_{553-3144}$-EGFP) and full-length HTT (mCherry-HTT_{1-3144}-EGFP). $HTT_{553-3144}$-GFP myristoylation signal is not detected when the glycine 553 is mutated to alanine (G553A), or when the D552 cleavage site is blocked (TEV552). The images displayed in **(B, D)** are representative of three repetitions of each experiment. The western blot images in B are composites of different lanes from the same image for WT, G553A and mock, and a different image for WT and TEV552 as these constructs were expressed in independent experiments.

HTT can be myristoylated and detected *in vitro*, we first used a simplified experimental model allowing us to study HTT co-translational myristoylation, without inducing toxicity and proteolysis at D552 (Figures 4A, B; uncropped blots displayed in Supplementary Figure S7). Co-translational myristoylation of C-terminal $HTT_{553-3144}$ was measured in HEK293 cells transiently

expressing $HTT_{553-3144}$-EGFP WT or carrying the G553A mutation and metabolically labeled with alkyne-myristate (Alkyne-C14:0) or DMSO (as a negative control) followed by click chemistry (Figure 4B). Myristoylation was detected in the WT form, but the G553A mutation entirely abrogates HTT myristoylation. The molecular weight of C-terminal $HTT_{553-3144}$ G553A was slightly lower than that of C-terminal $HTT_{553-3144}$ WT, which is consistent with what we observed previously with $HTT_{553-588}$-YFP (Martin et al., 2014; Martin et al., 2018a; Martin et al., 2018b).

Our objective was then to fully characterize the post-translational myristoylation of full-length HTT (Figures 4C, D; uncropped blots displayed in Supplementary Figures S8). Myristoylation of C-terminal $HTT_{533-3144}$ in HeLa cells exogenously expressing mCherry-23Q-HTT_{1-3144}-EGFP WT, with the D552 caspase cleavage sites replaced with TEV proteolytic site (TEV552) or G553A, in the presence or absence of staurosporine (STS) which promotes caspase activity (Belmokhtar et al., 2001), was measured by bio-orthogonal labeling following metabolic labeling with alkyne-myristate (Figure 4D). The full-length mCherry-23Q-HTT_{1-3144}-EGFP (indicated by the top arrowhead in the middle panel) was not orthogonally labeled with biotin, as expected (Martin et al., 2014). Myristoylated $HTT_{553-3144}$ signal was detected when cells expressing the full-length HTT WT plasmid were treated with STS (myr-$HTT_{553-3144}$-EGFP, indicated by an arrowhead in the top panel). A weaker signal was also detected in the absence of STS treatment, likely due to basal caspase activity, suggesting this is a constitutive PTM. Myristoylated $HTT_{553-3144}$ was not detected when the D552 cleavage site of full-length HTT was replaced with a TEV proteolytic site nor in the presence of the G553A mutation. Altogether, the data confirms myristoylation of C-terminal $HTT_{553-3144}$ at G553 after cleavage at D552 and shows for the first time that C-terminal HTT fragments longer than $HTT_{553-558}$ undergo post-translational myristoylation, suggesting it occurs in endogenous HTT.

3.4 Huntingtin myristoylation increases when proteolytic cleavage of full-length huntingtin at D586 is impaired

Similar to palmitoylation, we have previously shown that a truncated version of HTT (HTT_{1-588}-YFP) was less myristoylated in the presence of the HD mutation (Martin et al., 2014). Therefore, reduced myristoylation of huntingtin may be associated with increased toxicity of mutant HTT. Furthermore, we showed that blocking proteolysis of HTT_{1-588}-YFP at D586 increases myristoylation at G553 (Martin et al., 2018b). Altogether, our data suggest that the protective effect of blocking proteolysis at D586 observed *in vitro* and *in vivo* (Graham et al., 2006; Graham et al., 2011; Wong et al., 2015) may be mediated, at least in part, through increased myristoylation at G553. Our aims were to assess the impact of the expanded polyQ tract and of D586 cleavage of full-length HTT on the myristoylation level of $HTT_{553-3144}$.

Post-translational myristoylation of HTT was assessed in HeLa cells exogenously expressing full-length mCherry-23Q or 100Q-HTT_{1-3144}-EGFP WT or with the D586 caspase cleavage sites replaced with TEV proteolytic sites (TEV586) in the presence or absence of STS to promote proteolysis, using the bio-orthogonal labeling assay (Figures 5A, B; uncropped blots displayed in Supplementary Figure S9). Again, post-translationally myristoylated C-terminal $HTT_{533-3144}$ was detected in all conditions, but significantly increased in the presence of STS, supporting that this PTM is constitutive, after basal caspase activity (Figure 5B). Post-translational myristoylation of C-terminal $HTT_{553-3144}$ was significantly reduced by 30% in mutant 100Q-HTT_{1-3144} compared to the wild-type control (23Q-HTT_{1-3144}) in the presence or absence of STS (Figure 5C; 2-way ANOVA: HD mutation, $p = .0011$). Post-translational myristoylation of C-terminal $HTT_{533-3144}$ was significantly increased when D586 cleavage of full-length 23Q and 100Q-HTT_{1-3144} was impaired (TEV586) compared to fully-cleavable 23Q and 100Q-HTT_{1-3144} WT (Figure 5D; 3-way ANOVA: WT vs. TEV586, $p < .0001$). The presence of the HD mutation did not significantly alter the myristoylation level of 100Q-HTT_{1-3144} TEV586, compared to 23Q-HTT_{1-3144} TEV586 (Figure 5B; 2-way ANOVA: HD mutation, $p = .79$). These results confirm that blocking full-length HTT cleavage at D586 promotes $HTT_{533-3144}$ myristoylation at G553, and normalizes the effect of the HD mutation on $HTT_{533-3144}$ myristoylation.

3.5 Huntingtin post-translational myristoylation promotes the co-interaction between C-terminal and N-terminal HTT fragments

It has previously been shown that C-terminal domains of HTT can interact with N-terminal HTT after proteolysis at single sites (Ochaba et al., 2014; El-Daher et al., 2015). In addition, C-terminal HTT alone appears to be toxic, particularly when HTT is processed at multiple sites, which decreases the interaction between the N- and C-termini (El-Daher et al., 2015). Our next goal was to investigate the impact of HTT myristoylation on the binding affinity between N-terminal and C-terminal HTT fragments, as we hypothesized that myristoylated fragments of HTT induce autophagy by impacting HTT protein-protein interaction.

The co-interaction between C- and N-terminal HTT was investigated in HeLa cells transiently expressing mCherry-23Q-HTT_{1-3144}-EGFP WT, TEV586, TEV552 or G553A, after treatment with STS to induce proteolysis, by co-immunoprecipitation (Figure 6; uncropped blots displayed in Supplementary Figure S10). Full-length mCherry-23Q-HTT_{1-3144}-EGFP (black arrowheads) and C-terminal HTT-EGFP fragments (grey arrowhead) generated by proteolysis were immunoprecipitated from lysates using GFP antibodies, and N-terminal HTT fragments co-immunoprecipitated were detected by western blot analysis using mCherry and N-terminal HTT antibodies (Figure 6A). Two main N-terminal HTT fragments with a molecular weight of ~82 (red arrowheads) and 90 kDa (green arrowheads) detected by both mCherry and MAB2166 (amino acid ~443–457) antibodies were co-immunoprecipitated with C-terminal fragments and full-length mCherry-HTT_{1-3144}-EGFP. Additionally, co-immunoprecipitated N-terminal fragments with a molecular weight of 85, 100 and 115 kDa were detected at a lower level. This data confirm the interaction between N- and C-terminal HTT previously described (Palidwor et al., 2009; Ochaba et al., 2014; El-Daher et al., 2015). The amount of co-immunoprecipitated N-terminal HTT fragments (tagged with mCherry) with a molecular weight of between 75 and 100 kDa normalized to the level of full-length and C-terminal HTT (tagged with GFP) in non-treated or STS-treated cells is displayed in Figure 6B. Impairing post-translational myristoylation of full-length HTT_{1-3144} at G553 significantly reduced the co-interaction between the N-terminal fragments with full-length and C-terminal HTT compared to HTT WT and TEV586 in the STS-treated cells (2-way ANOVA, PTM mutation, $p = .0076$; Tukey's post-test, WT vs. G553A, $p = .017$; TEV586 vs. G553A, $p = .0038$). Blocking proteolysis of full-length HTT at D552, which also blocks post-translational myristoylation, also significantly reduced C-

10.3389/fphys.2023.1086112

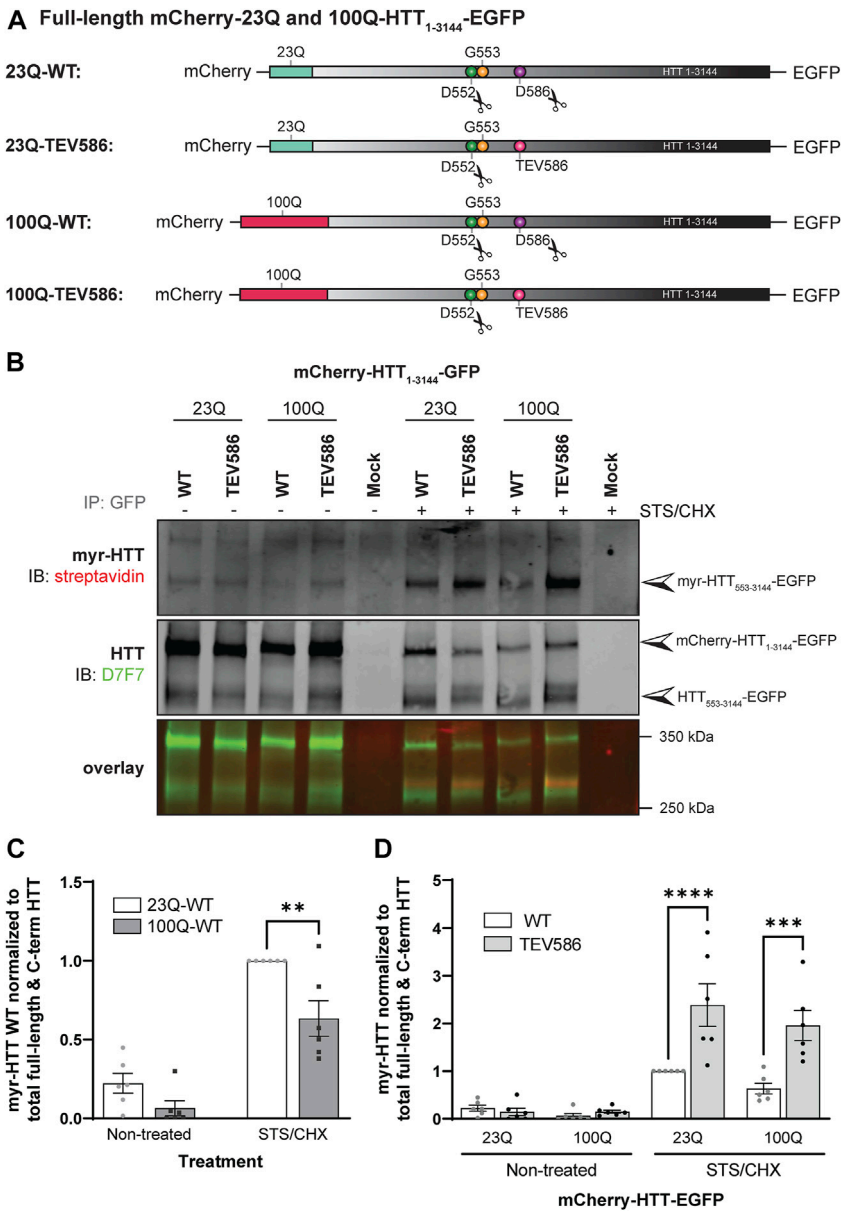

FIGURE 5
Myristoylation of C-terminal $HTT_{553-3144}$ is reduced in the presence of the HD mutation, and increased when proteolytic cleavage of full-length huntingtin at D586 is impaired. **(A)** Schematic representation of the full-length mCherry-23Q and 100Q-HTT_{1-3144}-EGFP constructs WT, or with the D586 caspase cleavage site replaced with a Tobacco Etch Virus proteolytic site (TEV586). The scissor symbols indicate the D552 and D586 cleavage sites, **(B)** HeLa cells were transfected with mCherry-23Q and mCherry-100Q-HTT_{1-3144}-EGFP constructs WT or TEV586. Cells were metabolically labeled with 100 µM alkyne-myristate for 30 min in the absence or presence of 1 µM staurosporine and 5 µg/mL cycloheximide (STS/CHX) for 4 h to promote proteolysis and inhibit protein synthesis, respectively. Full-length and C-terminal HTT fragments were immunoprecipitated from cell lysates using goat anti-GFP antibodies. The myristate analog was covalently linked to biotin azide through click chemistry. Myristoylated $HTT_{553-3144}$-EGFP orthogonally labeled with biotin was detected with streptavidin and total HTT was detected with HTT antibodies (D7F7). Arrowheads indicate myristoylated HTT (myr-$HTT_{553-3144}$-EGFP) in the top panel, total C-terminal HTT ($HTT_{553-3144}$-EGFP) and full-length HTT (mCherry-HTT_{1-3144}-EGFP) in the middle panel, **(C)** myristoylation of HTT is reduced in the presence of the HD mutation. Myristoylation levels of HTT were quantified as the ratio of myristoylated HTT (myr-$HTT_{553-3144}$-EGFP) normalized to the sum of full-length HTT (mCherry-HTT_{1-3144}-EGFP) and C-terminal HTT fragments ($HTT_{553-3144}$-EGFP), and expressed relatively to myristoylation of 23Q-HTT WT in cells treated with STS (n = 6), **(D)** Myristoylation of HTT is significantly increased when D586 cleavage of full-length HTT is impaired. Myristoylation of HTT was quantified as the ratio of myristoylated HTT normalized to the sum of full-length HTT and C-terminal HTT fragments, and expressed relatively to myristoylation of 23Q-HTT WT in cells treated with STS (n = 6). *Statistical analysis*: **(C)** 2-way ANOVA: interaction, p = .15; STS/CHX treatment, ****p < .0001; HD mutation, **p = .0011. Sidak's multiple comparison test, **p = .0025. **(D)** 3-way ANOVA: WT vs. TEV586, ****p < .0001; Non-treated vs. STS/CHX, ****p < .0001; 23Q vs. 100Q, p = .10. Sidak's multiple comparison test (WT vs. TEV586), ****p < .0001, ***p < .0001.2-way ANOVA (TEV586 constructs only): interaction, p = .44; Non-treated vs. STS/CHX, ***p < .0001; 23Q vs. 100Q, p = .79.

an N-terminal fragment co-interaction compared to HTT TEV586, in STS-treated cells (Tukey's post-test, TEV586 vs. TEV552, p = .033; t-test: WT vs. TEV552, p = .0056). This result suggests that post-translational myristoylation of HTT promotes the interaction between N-terminal and C-terminal HTT fragments in this model, which could contribute to the protective effect of blocking proteolysis at D586 in HD.

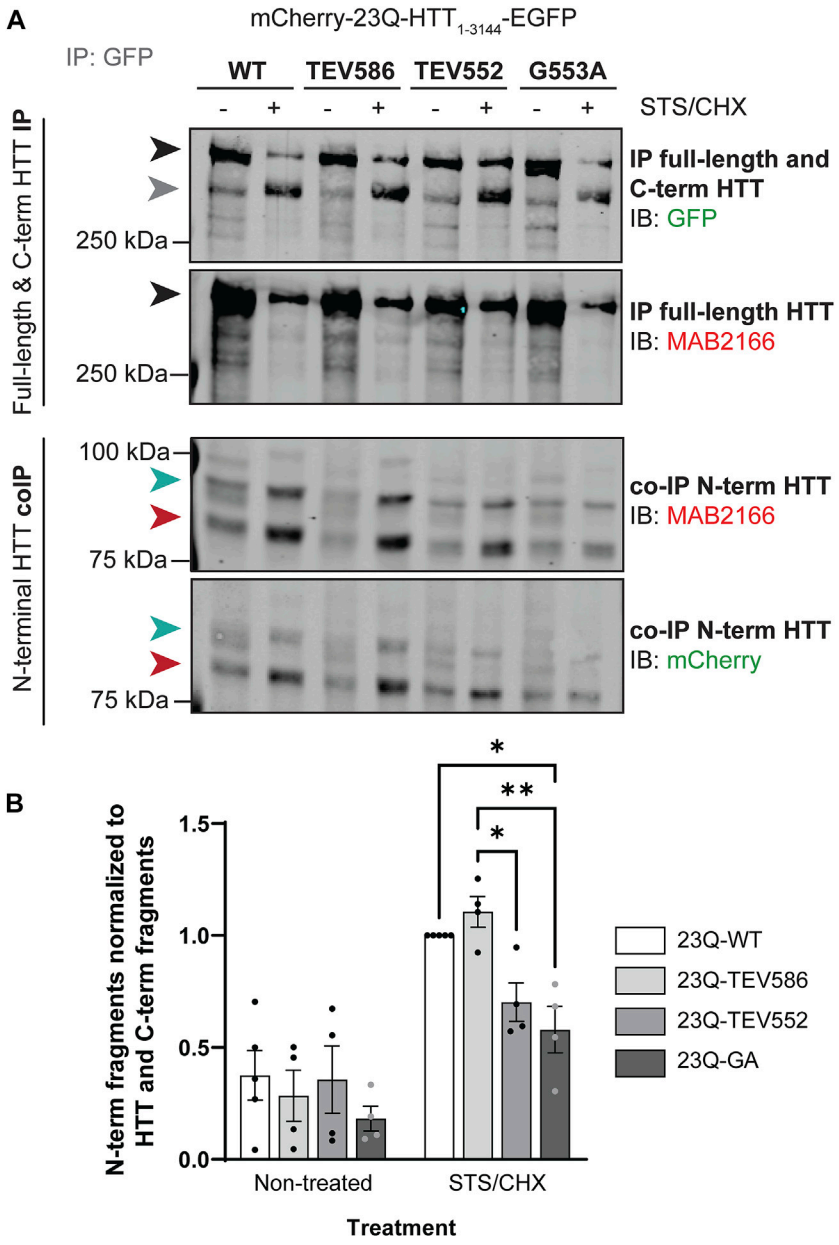

FIGURE 6
Blocking post-translational myristoylation in full-length wild-type HTT reduced the interaction between the N- and C-terminal fragments. **(A)** HeLa cells transiently expressing mCherry-23Q-HTT$_{1-3144}$-EGFP WT, TEV586, TEV552 or G553A for 46 h were treated for 2 h with 5 μM STS and 5 μg/mL cycloheximide (STS/CHX) to induce proteolysis and inhibit protein synthesis, respectively. HTT-EGFP was immunoprecipitated from lysates with goat anti-GFP antibodies. Immunoblots were conducted with mouse anti-HTT (MAB2166; amino acid 443–457) and rabbit anti-GFP antibodies. Then, the membranes were stripped and re-probed with rabbit anti-mCherry antibodies. Full-length mCherry-23Q-HTT$_{1-3144}$-EGFP, detected with GFP or MAB2166 antibodies, is indicated by a black arrowhead. C-terminal HTT-EGFP fragments, detected with GFP antibodies, are indicated by a grey arrowhead. The green and red arrowheads indicate the two main N-terminal mCherry-23Q-HTT fragments co-immunoprecipitated and detected by both mCherry and MAB2166 antibodies, with an apparent molecular weight of ~82 and 90 kDa, respectively, **(B)** interaction between N-terminal HTT fragments with full-length and C-terminal HTT was quantified as the ratio of the co-immunoprecipitated N-terminal HTT fragments detected with mCherry antibodies with molecular weights between 75 and 100 kDa normalized to the sum of immunoprecipitated full-length HTT and all C-terminal HTT fragments detected with GFP antibodies, and expressed relatively to 23Q-HTT WT in cells treated with STS (n = 4). *Statistical analysis*: 2-way ANOVA: interaction, p = .076; STS/CHX treatment, ****p < .0001; PTM mutation, **p = .0076. Tukey's multiple comparisons test: 23Q-WT vs. 23Q-G553A, *p = .017; 23Q-TEV586 vs. 23Q-TEV552, *p = .033; 23Q-TEV586 vs. 23Q-G553A, **p = .0038.

4 Discussion

Proper cellular localization of proteins is crucial to their function and is particularly important in neurons that require proteins to traffic long distances along axons and complex dendrites. Mislocalization of neuronal proteins can lead to proteostasis deficiencies and toxicity. Consequently, altered palmitoylation and myristoylation have been implicated in many psychiatric and neurodegenerative disorders (Sanders et al., 2015; Cho

and Park, 2016; Pinner et al., 2016; Philippe and Jenkins, 2019; Seo et al., 2022). While targeting acyltransferase enzymes and their substrate proteins could be a promising approach to treat neurological disorders, there are still many unanswered questions that need to be addressed regarding the role of fatty acylation on protein trafficking and targeting to specific neuronal locations, or more generally on brain health and functions (Ji and Skup, 2021; Petropavlovskiy et al., 2021).

We have shown that the palmitoylation level of HTT and many synaptic proteins are reduced in HD (Yanai et al., 2006; Lemarié et al., 2021). Modulating palmitoylation by inhibiting depalmitoylating APTs is protective in HD cells (immortalized cell lines, primary neurons, iPSC-derived neurons) and in the *Hdh*$^{CAG140/+}$ knock-in mouse model (Lemarié et al., 2021; Virlogeux et al., 2021). However, the biological functions of HTT fatty acylation and the role that loss of HTT fatty acylation plays on disease progression are still not fully elucidated.

Only one site of palmitoylation was previously identified at C214 using radioactive labeling techniques (Yanai et al., 2006). With recent advances in the detection of palmitoylation, it has become apparent that there are likely additional palmitoylation sites within HTT. The exhaustive identification of fatty palmitoylation sites within HTT is essential to allow us to identify the specific sites that mediate protection in HD in the presence of depalmitoylation inhibitors.

Here, we investigated the existence of additional palmitoylation sites within the full-length HTT protein, by transiently expressing HTT carrying cysteine-to-serine mutations at sites predicted to be palmitoylated (CSS-Palm 3.0 prediction program; Figure 1) and by measuring HTT palmitoylation levels using the IP-ABE and bio-orthogonal labeling assays (Figures 2 and 3). Within the N-terminal region of HTT, our data support that C105 and C433 of HTT are palmitoylated (Figures 2A-D). This conclusion is supported by high throughput screening by resin-assisted capture of S-acylated proteins (acyl-RAC) followed by LC-MS/MS that identified these two residues as S-palmitoylation and S-nitrosylation (addition of nitric oxide (NO)) sites (Ni et al., 2016). The residues C109, C152, C204 and C280 were considered as palmitoylated in the Ni *et al.* study 2016. However, only C280 appeared in the CSS-Palm 3.0 prediction list with a low score (Figure 1A), and was therefore not investigated by low throughput palmitoylation assay. We observed an additive effect of the mutations of C105, C214 and C433 on HTT_{1-548} palmitoylation level, although HTT palmitoylation was still not entirely abrogated (Figures 2E, F). Blocking palmitoylation at C105, C214 and C433 may be compensated by palmitoylation at alternate sites in close proximity (C109 for C105 and C204 for C214) a phenomenon that has been observed for other proteins, including the voltage-gated sodium channel Nav1.6 (Pan et al., 2020).

In the middle region of the HTT protein, the cysteine residues 1027 and 1028 have a high palmitoylation prediction score according to the CSS-Palm 3.0 program (Figure 1A). Both residues were mutated to serine in case these adjacent cysteines were interchangeably palmitoylated. The double cysteine-to-serine mutations C1027/1028S did not significantly alter HTT_{1-1212} palmitoylation level using the IP-ABE assay (Figures 3A, B), but surprisingly increased HTT dynamic palmitoylation level when measured with the bio-orthogonal labeling assay (Figures 3C, D). This unexpected increase in palmitoylation turnover measured with the bio-orthogonal labeling assay, without any change of the global palmitoylation level with the ABE assay, could be due to an indirect effect of the C1027/1028 residue mutation which may impact HTT conformation, localization, or protein-protein interaction, and in doing so could promote palmitoylation of a nearby residue, such as C944 which was predicted to be palmitoylated (Ni et al., 2016). Alternatively, the significant increase in palmitoylation observed with the bio-orthogonal labeling assay may be indicative of transacylation (or catalytic cysteine palmitoyl relay (CCPR)) of HTT and these sites may serve as recipients of palmitate from other sites on HTT, similar to mitochondrial HMG-CoA synthase (Kostiuk et al., 2010). However, these two cysteines were not identified as palmitoylation sites in the acyl-RAC high throughput performed in the Ni et al., 2016 study. Therefore, they are unlikely to be new sites of palmitoylation, but this highlights an important issue when trying to identify new sites of palmitoylation.

In the C-terminal region of HTT, C3134 and C3144 were investigated as potential new palmitoylation sites. Palmitoylation of full-length 15Q-HTT C3134S and C3144S was decreased compared to the WT control to the same extent than the C214S mutation, suggesting that cysteines 3134 and 3144 of HTT are dynamically palmitoylated (Figures 3E, F). Of note, when expressing full-length HTT, our method also measures endogenous HTT palmitoylation. This suggests that the effect of blocking palmitoylation of exogenous HTT at these sites may be greater than what we measured.

To summarize, we have identified multiple new palmitoylation sites of huntingtin at C105, C433, C3134 and C3144. It will be important to confirm the palmitoylation of these residues by mass spectrometry. Investigating the effects of these palmitoylation sites on wild-type and mutant HTT localization, clearance, aggregation or protein trafficking will be necessary to further decipher the biological functions of HTT palmitoylation. Additionally, because proteins that contain multiple palmitoylation sites can be modified at different intracellular locations by various PATs (Tian et al., 2010; Kang et al., 2019), it will be relevant to assess if additional enzymes, aside from ZDHHC17 and 13, are involved in the palmitoylation of these residues.

Myristoylation has been shown to be essential for the function of many proteins and is required for cell survival (Martin D. D. O et al., 2011; Thinon et al., 2016). Previously, using truncated forms of HTT, we showed that HTT is post-translationally myristoylated at G553 following caspase-cleavage (Martin et al., 2014). Like HTT palmitoylation, post-translational myristoylation of HTT_{1-588} is significantly decreased in the presence of the polyQ expansion (Martin et al., 2014). We also found that the myristoylated $HTT_{553-585}$ fragment induces the formation of autophagosomes, and thereby plays a role in the initiation of autophagy, a process altered in HD (Martinez-Vicente and Cuervo, 2007; Krainc, 2010; Martinez-Vicente et al., 2010; Ochaba et al., 2014; Menzies et al., 2015; Ehrnhoefer et al., 2018). Furthermore, our data show that blocking proteolysis of HTT_{1-588} at D586 increases myristoylation at G553 (Martin et al., 2018b). This suggests that the protective effect of blocking proteolysis at D586 (Graham et al., 2006; Graham et al., 2011; Wong et al., 2015) may be mediated, at least partially, through increased myristoylation at G553. This potential crosstalk between D586 cleavage and G553 myristoylation could explain the rescue of autophagy dysregulation in the C6R mouse model (YAC128 line carrying a mutation preventing proteolysis at D586) compared to the YAC128 mouse line (Ehrnhoefer et al., 2018). Developing tools to characterize post-translational myristoylation in full-length HTT is now essential to confirm our findings.

For the first time, co- and post-translational myristoylation of C-terminal $HTT_{533-3144}$ was detected in human cells exogenously expressing $HTT_{533-3144}$-EGFP WT (Figure 4B), mCherry-23Q-HTT_{1-3144}-EGFP WT (Figure 4D) and mCherry-23Q and 100Q-HTT_{1-3144}-EGFP WT and D586 proteolysis-resistant (TEV586) (Figure 5B), in the presence or absence of STS to induce proteolysis. Myristoylation of HTT in the absence of stressors suggests that HTT is likely constitutively post-

translationally myristoylated endogenously. The presence of the G553A or the D552 proteolysis-resistant (TEV552) mutations entirely abrogated the myristoylation of $HTT_{533-3144}$. Consistent with shorter N-terminal fragments of HTT, myristoylation of $HTT_{533-3144}$ was reduced in the presence of the HD mutation (Figure 5C). In contrast, post-translational myristoylation of C-terminal $HTT_{553-3144}$-EGFP was significantly increased when the cleavage of full-length HTT at D586 was impaired (TEV586) (Figure 5D). This result confirms our hypothesis that blocking HTT cleavage at D586 promotes HTT myristoylation at G553, and supports the PTM crosstalk we proposed in Ehrnhoefer et al., 2018 study.

A role for HTT in the regulation of autophagy has been described (Steffan, 2010; Ochaba et al., 2014; Rui et al., 2015; Ashkenazi et al., 2017a; Ashkenazi et al., 2017b), with both the HTT N- and C-termini playing different but inter-dependent roles in autophagy (Ochaba et al., 2014). This process may be promoted by the interaction of the two halves after proteolysis (Palidwor et al., 2009; El-Daher et al., 2015). C-terminal HTT alone appears to be toxic, particularly when HTT is processed at multiple sites (D586, D513 and D167), which decreases the interaction between the N- and C-termini (El-Daher et al., 2015). C-terminal HTT toxicity involves inactivation of dynamin 1 at ER membrane and ER dilatation and stress (El-Daher et al., 2015). Impairing myristoylation of wild-type 23Q-HTT_{1-3144} significantly decreased the interaction of two N-terminal HTT fragments (~82 and 90 kDa) with C-terminal $HTT_{553-3144}$ compared to the WT control and the TEV586 (Figure 6).

This result suggests that myristoylation of HTT promotes the interaction between C-terminal $HTT_{553-3144}$ and N-terminal HTT fragments. Thus, the protective effect of blocking cleavage of full-length HTT at D586 may be mediated through promoting proteolysis at D552 and post-translational myristoylation of HTT, thereby maintaining the interaction between the toxic N- and C-termini. These N- and C-terminal fragments can then potentially be directed to the autophagosome for degradation. Altogether, the data support our hypothesis that targeting myristoylation could be beneficial in the context of HD. It would be relevant to modulate myristoylation levels of HTT to assess the impact on N- and C-terminal fragments co-interaction and clearance. Inhibitors of NMTs, which impair protein myristoylation, have been developed to treat cancer cells (Thinon et al., 2016; Beauchamp et al., 2020; Sangha et al., 2022) and various parasitic protozoa (Khalil et al., 2019). However, the irreversible nature of myristoylation makes it a more challenging target compared to palmitoylation, specifically if the goal is to promote its levels.

Our study reveals new palmitoylation sites of HTT and new insights into the regulation of HTT by myristoylation. Myristoylation often regulates protein anchoring to the membrane via second signals such as palmitoylation (Resh, 2016; Seo et al., 2022), and we can hypothesize that acylation cascades may impact wild-type HTT functions and mutant HTT toxicity. Moreover, some of the new palmitoylation sites identified in this study are located in clusters of PTMs of HTT that modulate mutant HTT functional or toxic properties (Arbez et al., 2017), and could therefore impact key PTMs of HTT. Determining the physiological relevance of these new palmitoylation sites, and the interplay between different PTMs of HTT will help develop new therapeutic strategies to treat HD.

Data availability statement

The raw data supporting the conclusion of this article will be made available by the authors, without undue reservation.

Author contributions

FL, SS, DM, and MRH conceived of and helped design the study. FL, SS, and YN carried out experiments. FL and DM summarized the data, performed analysis, and drafted the manuscript. FL, DM, SS and MRH revised the final manuscript. All authors contributed to the article and approved the submitted version.

Funding

This study was supported by a CIHR Foundation grant (FDN-154278) and a CHDI Foundation grant to MRH. FL was supported by a Canadian Institutes of Health Research (CIHR) Postdoctoral Fellowship (MFE-164631) and by the James Family foundation.

Acknowledgments

The authors would like to thank Mark Wang, Xiaofan Qu and Qingwen Xia for their technical support, Amirah Ali, Nicholas Caron, Hailey Findlay-Black, Mandi Schmidt, Jennifer Collins, and Stephanie Bortnick for their support on the project. The authors also thank the CIHR, as well as the CHDI and James Family foundations for their financial support.

Conflict of interest

The authors declare that the research was conducted in the absence of any commercial or financial relationships that could be construed as a potential conflict of interest.

Publisher's note

Supplementary material

The Supplementary Material for this article can be found online at: https://www.frontiersin.org/articles/10.3389/fphys.2023.1086112/full#supplementary-material

SUPPLEMENTARY FIGURE S1
Uncropped blots used for Figure 2A displaying total (MAB2166/green channel) and palmitoylated HTT (Streptavidin/red channel) measured by IP-ABE assay in COS-7 cells transiently expressing 15Q-HTT1-548 WT, C214S, C105S or C433S.

SUPPLEMENTARY FIGURE S2
Uncropped blots used for Figure 2C displaying total (MAB2166/green channel) and palmitoylated HTT (Streptavidin/red channel) measured by bio-orthogonal labeling assay in COS-7 cells transiently expressing 15Q-HTT1-548 WT, C214S, C105S or C433S.

SUPPLEMENTARY FIGURE S3
Uncropped blots used for Figure 2E displaying total (MAB2166/green channel) and palmitoylated HTT (Streptavidin/red channel) measured by IP-ABE assay in COS-7 cells transiently expressing 15Q-HTT1-548 WT, C214S or C105/214/433S.

SUPPLEMENTARY FIGURE S4
Uncropped blots used for Figure 2F displaying total (MAB2166/green channel) and palmitoylated HTT (Streptavidin/red channel) measured by bio-orthogonal labeling assay in COS-7 cells transiently expressing 15Q-HTT1-548 WT, C214S or C105/214/433S.

SUPPLEMENTARY FIGURE S5
Uncropped blots used for Figure 3A and 3C displaying total (MAB2166/green channel) and palmitoylated HTT (Streptavidin/red channel) measured by IP-ABE or bio-orthogonal labeling assays in COS-7 cells transiently expressing 15Q-HTT1-1212 WT or C1027/1028S.

SUPPLEMENTARY FIGURE S6
Uncropped blots used for Figure 3E displaying total (D7F7/green channel) and palmitoylated HTT (Streptavidin/red channel) measured by bio-orthogonal labeling assay in HeLa cells transiently expressing 15Q-HTT1-3144 WT, C214S, C3134S or C3144S.

SUPPLEMENTARY FIGURE S7
Uncropped blots used for Figure 4B displaying total (D7F7/green channel) and myristoylated HTT (Streptavidin/red channel) measured by bio-orthogonal labeling assay in HEK293 cells transfected with C-terminal HTT553-3144-EGFP WT or G553A.

SUPPLEMENTARY FIGURE S8
Uncropped blots used for Figure 4D displaying total (D7F7/green channel) and myristoylated HTT (Streptavidin/red channel) measured by bio-orthogonal labeling assay in HeLa cells transfected with mCherry-23Q-HTT1-3144-EGFP constructs WT, G553A, or TEV552.

SUPPLEMENTARY FIGURE S9
Uncropped blots used for Figure 5B displaying total (D7F7/green channel) and myristoylated HTT (Streptavidin/red channel) measured by bio-orthogonal assay in HeLa cells were transfected with mCherry-23Q and mCherry-100Q-HTT1-3144-EGFP constructs WT or TEV586.

SUPPLEMENTARY FIGURE S10
Uncropped blots used for Figure 6A displaying immunoprecipitated full length and C-term HTT (GFP/green channel; MAB2166/red channel) and co-immunoprecipitated N terminal HTT (MAB166/red channel; mCherry/green channel) in HeLa cells transiently expressing mCherry-23Q-HTT1-3144-EGFP WT, TEV586, TEV552 or G553A.

References

Aiken, C. T., Steffan, J. S., Guerrero, C. M., Khashwji, H., Lukacsovich, T., Simmons, D., et al. (2009). Phosphorylation of threonine 3: Implications for huntingtin aggregation and neurotoxicity. *J. Biol. Chem.* 284, 29427–29436. doi:10.1074/jbc.M109.013193

Arbez, N., Ratovitski, T., Roby, E., Chighladze, E., Stewart, J. C., Ren, M., et al. (2017). Post-translational modifications clustering within proteolytic domains decrease mutant huntingtin toxicity. *J. Biol. Chem.* 292, 19238–19249. doi:10.1074/jbc.M117.782300

Ashkenazi, A., Bento, C. F., Ricketts, T., Vicinanza, M., Siddiqi, F., Pavel, M., et al. (2017a). Polyglutamine tracts regulate autophagy. *Autophagy* 13, 1613–1614. doi:10.1080/15548627.2017.1336278

Ashkenazi, A., Bento, C. F., Ricketts, T., Vicinanza, M., Siddiqi, F., Pavel, M., et al. (2017b). Polyglutamine tracts regulate beclin 1-dependent autophagy. *Nature* 545, 108–111. doi:10.1038/nature22078

Atwal, R. S., Desmond, C. R., Caron, N., Maiuri, T., Xia, J., Sipione, S., et al. (2011). Kinase inhibitors modulate huntingtin cell localization and toxicity. *Nat. Chem. Biol.* 7, 453–460. doi:10.1038/nchembio.582

Atwal, R. S., Xia, J., Pinchev, D., Taylor, J., Epand, R. M., and Truant, R. (2007). Huntingtin has a membrane association signal that can modulate huntingtin aggregation, nuclear entry and toxicity. *Hum. Mol. Genet.* 16, 2600–2615. doi:10.1093/hmg/ddm217

Beauchamp, E., Yap, M. C., Iyer, A., Perinpanayagam, M. A., Gamma, J. M., Vincent, K. M., et al. (2020). Targeting N-myristoylation for therapy of B-cell lymphomas. *Nat. Commun.* 11, 5348. doi:10.1038/s41467-020-18998-1

Belmokhtar, C. A., Hillion, J., and Ségal-Bendirdjian, E. (2001). Staurosporine induces apoptosis through both caspase-dependent and caspase-independent mechanisms. *Oncogene* 20, 3354–3362. doi:10.1038/sj.onc.1204436

Burrus, C. J., McKinstry, S. U., Kim, N., Ozlu, M. I., Santoki, A. V., Fang, F. Y., et al. (2020). Striatal projection neurons require huntingtin for synaptic connectivity and survival. *Cell Rep.* 30, 642–657. doi:10.1016/j.celrep.2019.12.069

Cariulo, C., Azzollini, L., Verani, M., Martufi, P., Boggio, R., Chiki, A., et al. (2017). Phosphorylation of huntingtin at residue T3 is decreased in Huntington's disease and modulates mutant huntingtin protein conformation. *PNAS* 114, E10809–E10818. doi:10.1073/pnas.1705372114

Caron, N. S., Anderson, C., Black, H. F., Sanders, S. S., Lemarié, F. L., Doty, C. N., et al. (2021). Reliable resolution of full-length huntingtin alleles by quantitative immunoblotting. *J. Huntingt. Dis.* 10, 355–365. doi:10.3233/JHD-200463

Caron, N. S., Desmond, C. R., Xia, J., and Truant, R. (2013). Polyglutamine domain flexibility mediates the proximity between flanking sequences in huntingtin. *Proc. Natl. Acad. Sci. U. S. A.* 110, 14610–14615. doi:10.1073/pnas.1301342110

Carroll, J. B., Warby, S. C., Southwell, A. L., Doty, C. N., Greenlee, S., Skotte, N., et al. (2011). Potent and selective antisense oligonucleotides targeting single-nucleotide polymorphisms in the Huntington disease gene/allele-specific silencing of mutant huntingtin. *Mol. Ther.* 19, 2178–2185. doi:10.1038/mt.2011.201

Cho, E., and Park, M. (2016). Palmitoylation in Alzheimer's disease and other neurodegenerative diseases. *Pharmacol. Res.* 111, 133–151. doi:10.1016/j.phrs.2016.06.008

Cong, S.-Y., Pepers, B. A., Roos, R. A. C., Van Ommen, G.-J. B., and Dorsman, J. C. (2005). Epitope mapping of monoclonal antibody 4C8 recognizing the protein huntingtin. *Hybrid. (Larchmt)* 24, 231–235. doi:10.1089/hyb.2005.24.231

Dragatsis, I., Dietrich, P., Ren, H., Deng, Y. P., Del Mar, N., Wang, H. B., et al. (2018). Effect of early embryonic deletion of huntingtin from pyramidal neurons on the development and long-term survival of neurons in cerebral cortex and striatum. *Neurobiol. Dis.* 111, 102–117. doi:10.1016/j.nbd.2017.12.015

Drisdel, R. C., and Green, W. N. (2004). Labeling and quantifying sites of protein palmitoylation. *BioTechniques* 36, 276–285. doi:10.2144/04362RR02

Ehrnhoefer, D. E., Martin, D. D. O., Schmidt, M. E., Qiu, X., Ladha, S., Caron, N. S., et al. (2018). Preventing mutant huntingtin proteolysis and intermittent fasting promote autophagy in models of Huntington disease. *Acta Neuropathol. Commun.* 6, 16. doi:10.1186/s40478-018-0518-0

Ehrnhoefer, D. E., Sutton, L., and Hayden, M. R. (2011). Small changes, big impact: Posttranslational modifications and function of huntingtin in Huntington disease. *Neuroscientist* 17, 475–492. doi:10.1177/1073858410390378

El-Daher, M.-T., Hangen, E., Bruyère, J., Poizat, G., Al-Ramahi, I., Pardo, R., et al. (2015). Huntingtin proteolysis releases non-polyQ fragments that cause toxicity through dynamin 1 dysregulation. *EMBO J.* 34, 2255–2271. doi:10.15252/embj.201490808

Fukata, Y., and Fukata, M. (2010). Protein palmitoylation in neuronal development and synaptic plasticity. *Nat. Rev. Neurosci.* 11, 161–175. doi:10.1038/nrn2788

Ghosh, R., and Tabrizi, S. J. (2018). Clinical features of huntington's disease. *Adv. Exp. Med. Biol.* 1049, 1–28. doi:10.1007/978-3-319-71779-1_1

Giglione, C., and Meinnel, T. (2022). Mapping the myristoylome through a complete understanding of protein myristoylation biochemistry. *Prog. Lipid Res.* 85, 101139. doi:10.1016/j.plipres.2021.101139

Graham, F. L., and van der Eb, A. J. (1973). A new technique for the assay of infectivity of human adenovirus 5 DNA. *Virology* 52, 456–467. doi:10.1016/0042-6822(73)90341-3

Graham, R. K., Deng, Y., Slow, E. J., Haigh, B., Bissada, N., Lu, G., et al. (2006). Cleavage at the caspase-6 site is required for neuronal dysfunction and degeneration due to mutant huntingtin. *Cell* 125, 1179–1191. doi:10.1016/j.cell.2006.04.026

Graham, R. K., Ehrnhoefer, D. E., and Hayden, M. R. (2011). Caspase-6 and neurodegeneration. *Trends Neurosci.* 34, 646–656. doi:10.1016/j.tins.2011.09.001

Harjes, P., and Wanker, E. E. (2003). The hunt for huntingtin function: Interaction partners tell many different stories. *Trends Biochem. Sci.* 28, 425–433. doi:10.1016/S0968-0004(03)00168-3

Huang, K., Sanders, S., Singaraja, R., Orban, P., Cijsouw, T., Arstikaitis, P., et al. (2009). Neuronal palmitoyl acyl transferases exhibit distinct substrate specificity. *FASEB J.* 23, 2605–2615. doi:10.1096/fj.08-127399

Humbert, S., Bryson, E. A., Cordelières, F. P., Connors, N. C., Datta, S. R., Finkbeiner, S., et al. (2002). The IGF-1/Akt pathway is neuroprotective in Huntington's disease and involves Huntingtin phosphorylation by Akt. *Dev. Cell* 2, 831–837. doi:10.1016/s1534-5807(02)00188-0

Jeong, H., Then, F., Melia, T. J., Mazzulli, J. R., Cui, L., Savas, J. N., et al. (2009). Acetylation targets mutant huntingtin to autophagosomes for degradation. *Cell* 137, 60–72. doi:10.1016/j.cell.2009.03.018

Ji, B., and Skup, M. (2021). Roles of palmitoylation in structural long-term synaptic plasticity. *Mol. Brain* 14, 8–27. doi:10.1186/s13041-020-00717-y

Kalchman, M. A., Graham, R. K., Xia, G., Koide, H. B., Hodgson, J. G., Graham, K. C., et al. (1996). Huntingtin is ubiquitinated and interacts with a specific ubiquitin-conjugating enzyme. *J. Biol. Chem.* 271, 19385–19394. doi:10.1074/jbc.271.32.19385

Kang, R., Wang, L., Sanders, S. S., Zuo, K., Hayden, M. R., and Raymond, L. A. (2019). Altered regulation of striatal neuronal N-Methyl-D-Aspartate receptor trafficking by palmitoylation in Huntington disease mouse model. *Front. Synaptic Neurosci.* 11. doi:10.3389/fnsyn.2019.00003

Khalil, R., Ashraf, S., Khalid, A., and Ul-Haq, Z. (2019). Exploring novel N-myristoyltransferase inhibitors: A molecular dynamics simulation approach. *ACS Omega* 4, 13658–13670. doi:10.1021/acsomega.9b00843

Kostiuk, M. A., Keller, B. O., and Berthiaume, L. G. (2010). Palmitoylation of ketogenic enzyme HMGCS2 enhances its interaction with PPARalpha and transcription at the Hmgcs2 PPRE. *FASEB J.* 24, 1914–1924. doi:10.1096/fj.09-149765

Krainc, D. (2010). Clearance of mutant proteins as a therapeutic target in neurodegenerative diseases. *Arch. Neurol.* 67, 388–392. doi:10.1001/archneurol.2010.40

Kratter, I. H., Zahed, H., Lau, A., Tsvetkov, A. S., Daub, A. C., Weiberth, K. F., et al. (2016). Serine 421 regulates mutant huntingtin toxicity and clearance in mice. *J. Clin. Invest.* 126, 3585–3597. doi:10.1172/JCI80339

Lemarié, F. L., Caron, N. S., Sanders, S. S., Schmidt, M. E., Nguyen, Y. T. N., Ko, S., et al. (2021). Rescue of aberrant huntingtin palmitoylation ameliorates mutant huntingtin-induced toxicity. *Neurobiol. Dis.* 158, 105479. doi:10.1016/j.nbd.2021.105479

Liao, L. M. Q., Gray, R. A. V., and Martin, D. D. O. (2021). Optimized incorporation of alkynyl fatty acid analogs for the detection of fatty acylated proteins using click chemistry. *JoVE J. Vis. Exp.*, e62107. doi:10.3791/62107

Lontay, B., Kiss, A., Virág, L., and Tar, K. (2020). How do post-translational modifications influence the pathomechanistic landscape of huntington's disease? A comprehensive review. *Int. J. Mol. Sci.* 21, 4282. doi:10.3390/ijms21124282

Maiuri, T., Mocle, A. J., Hung, C. L., Xia, J., van Roon-Mom, W. M. C., and Truant, R. (2017). Huntingtin is a scaffolding protein in the ATM oxidative DNA damage response complex. *Hum. Mol. Genet.* 26, 395–406. doi:10.1093/hmg/ddw395

Martin, B. R., Wang, C., Adibekian, A., Tully, S. E., and Cravatt, B. F. (2011). Global profiling of dynamic protein palmitoylation. *Nat. Methods* 9, 84–89. doi:10.1038/nmeth.1769

Martin, D. D. O., Ahpin, C. Y., Heit, R. J., Perinpanayagam, M. A., Yap, M. C., Veldhoen, R. A., et al. (2012). Tandem reporter assay for myristoylated proteins post-translationally (TRAMPP) identifies novel substrates for post-translational myristoylation: PKCε, a case study. *FASEB J.* 26, 13–28. doi:10.1096/fj.11-182360

Martin, D. D. O., Beauchamp, E., and Berthiaume, L. G. (2011). Post-translational myristoylation: Fat matters in cellular life and death. *Biochimie* 93, 18–31. doi:10.1016/j.biochi.2010.10.018

Martin, D. D. O., Heit, R. J., Yap, M. C., Davidson, M. W., Hayden, M. R., and Berthiaume, L. G. (2014). Identification of a post-translationally myristoylated autophagy-inducing domain released by caspase cleavage of huntingtin. *Hum. Mol. Genet.* 23, 3166–3179. doi:10.1093/hmg/ddu027

Martin, D. D. O., Schmidt, M. E., Nguyen, Y. T., Lazic, N., and Hayden, M. R. (2018a). Identification of a novel caspase cleavage site in huntingtin that regulates mutant huntingtin clearance. *FASEB J.* 33, 3190–3197. doi:10.1096/fj.201701510RRR

Martin, D. D. O., Kay, C., Collins, J. A., Nguyen, Y. T., Slama, R. A., and Hayden, M. R. (2018b). A human huntingtin SNP alters post-translational modification and pathogenic proteolysis of the protein causing Huntington disease. *Sci. Rep.* 8, 8096. doi:10.1038/s41598-018-25903-w

Martinez-Vicente, M., and Cuervo, A. M. (2007). Autophagy and neurodegeneration: When the cleaning crew goes on strike. *Lancet Neurology* 6, 352–361. doi:10.1016/S1474-4422(07)70076-5

Martinez-Vicente, M., Talloczy, Z., Wong, E., Tang, G., Koga, H., Kaushik, S., et al. (2010). Cargo recognition failure is responsible for inefficient autophagy in Huntington's disease. *Nat. Neurosci.* 13, 567–576. doi:10.1038/nn.2528

McKinstry, S. U., Karadeniz, Y. B., Worthington, A. K., Hayrapetyan, V. Y., Ozlu, M. I., Serafin-Molina, K., et al. (2014). Huntingtin is required for normal excitatory synapse development in cortical and striatal circuits. *J. Neurosci.* 34, 9455–9472. doi:10.1523/JNEUROSCI.4699-13.2014

Mehler, M. F., Petronglo, J. R., Arteaga-Bracho, E. E., Gulinello, M. E., Winchester, M. L., Pichamoorthy, N., et al. (2019). Loss-of-Huntingtin in medial and lateral ganglionic lineages differentially disrupts regional interneuron and projection neuron subtypes and promotes huntington's disease-associated behavioral, cellular, and pathological hallmarks. *J. Neurosci.* 39, 1892–1909. doi:10.1523/JNEUROSCI.2443-18.2018

Menzies, F. M., Fleming, A., and Rubinsztein, D. C. (2015). Compromised autophagy and neurodegenerative diseases. *Nat. Rev. Neurosci.* 16, 345–357. doi:10.1038/nrn3961

Ni, C.-L., Seth, D., Fonseca, F. V., Wang, L., Xiao, T. S., Gruber, P., et al. (2016). Polyglutamine tract expansion increases S-nitrosylation of huntingtin and ataxin-1. *PLOS ONE* 11, e0163359. doi:10.1371/journal.pone.0163359

Ochaba, J., Lukacsovich, T., Csikos, G., Zheng, S., Margulis, J., Salazar, L., et al. (2014). Potential function for the Huntingtin protein as a scaffold for selective autophagy. *Proc. Natl. Acad. Sci. U.S.A.* 111, 16889–16894. doi:10.1073/pnas.1420103111

Palidwor, G. A., Shcherbinin, S., Huska, M. R., Rasko, T., Stelzl, U., Arumughan, A., et al. (2009). Detection of alpha-rod protein repeats using a neural network and application to huntingtin. *PLOS Comput. Biol.* 5, e1000304. doi:10.1371/journal.pcbi.1000304

Pan, Y., Xiao, Y., Pei, Z., and Cummins, T. R. (2020). S-Palmitoylation of the sodium channel Nav1.6 regulates its activity and neuronal excitability. *J. Biol. Chem.* 295, 6151–6164. doi:10.1074/jbc.RA119.012423

Petropavlovskiy, A. A., Kogut, J. A., Leekha, A., Townsend, C. A., and Sanders, S. S. (2021). A sticky situation: Regulation and function of protein palmitoylation with a spotlight on the axon and axon initial segment. *Neuronal Signal* 5, NS20210005. doi:10.1042/NS20210005

Philippe, J. M., and Jenkins, P. M. (2019). Spatial organization of palmitoyl acyl transferases governs substrate localization and function. *Mol. Membr. Biol.* 35, 60–75. doi:10.1080/09687688.2019.1710274

Pinner, A. L., Tucholski, J., Haroutunian, V., McCullumsmith, R. E., and Meador-Woodruff, J. H. (2016). Decreased protein S-palmitoylation in dorsolateral prefrontal cortex in schizophrenia. *Schizophrenia Res.* 177, 78–87. doi:10.1016/j.schres.2016.01.054

Reiner, A., Dragatsis, I., Zeitlin, S., and Goldowitz, D. (2003). Wild-type huntingtin plays a role in brain development and neuronal survival. *Mol. Neurobiol.* 28, 259–276. doi:10.1385/MN:28:3:259

Resh, M. D. (2016). Fatty acylation of proteins: The long and the short of it. *Prog. Lipid Res.* 63, 120–131. doi:10.1016/j.plipres.2016.05.002

Rui, Y.-N., Xu, Z., Patel, B., Chen, Z., Chen, D., Tito, A., et al. (2015). Huntingtin functions as a scaffold for selective macroautophagy. *Nat. Cell Biol.* 17, 262–275. doi:10.1038/ncb3101

Sanders, S. S., Martin, D. D. O., Butland, S. L., Lavallée-Adam, M., Calzolari, D., Kay, C., et al. (2015). Curation of the mammalian palmitoylome indicates a pivotal role for palmitoylation in diseases and disorders of the nervous System and cancers. *PLOS Comput. Biol.* 11, e1004405. doi:10.1371/journal.pcbi.1004405

Sanders, S. S., Mui, K. K. N., Sutton, L. M., and Hayden, M. R. (2014). Identification of binding sites in huntingtin for the huntingtin interacting proteins HIP14 and HIP14L. *PLOS ONE* 9, e90669. doi:10.1371/journal.pone.0090669

Sangha, R., Davies, N. M., Namdar, A., Chu, M., Spratlin, J., Beauchamp, E., et al. (2022). Novel, first-in-human, oral PCLX-001 treatment in a patient with relapsed diffuse large B-cell lymphoma. *Curr. Oncol.* 29, 1939–1946. doi:10.3390/curroncol29030158

Saudou, F., and Humbert, S. (2016). The biology of huntingtin. *Neuron* 89, 910–926. doi:10.1016/j.neuron.2016.02.003

Schilling, B., Gafni, J., Torcassi, C., Cong, X., Row, R. H., LaFevre-Bernt, M. A., et al. (2006). Huntingtin phosphorylation sites mapped by mass spectrometry. Modulation of cleavage and toxicity. *J. Biol. Chem.* 281, 23686–23697. doi:10.1074/jbc.M513507200

Seo, J., Hwang, H., Choi, Y., Jung, S., Hong, J.-H., Yoon, B.-J., et al. (2022). Myristoylation-dependent palmitoylation of cyclin Y modulates long-term potentiation and spatial learning. *Prog. Neurobiol.* 218, 102349. doi:10.1016/j.pneurobio.2022.102349

Steffan, J. S., Agrawal, N., Pallos, J., Rockabrand, E., Trotman, L. C., Slepko, N., et al. (2004). SUMO modification of Huntingtin and Huntington's disease pathology. *Science* 304, 100–104. doi:10.1126/science.1092194

Steffan, J. S. (2010). Does Huntingtin play a role in selective macroautophagy? *Cell Cycle* 9, 3401–3413. doi:10.4161/cc.9.17.12718

Thinon, E., Morales-Sanfrutos, J., Mann, D. J., and Tate, E. W. (2016). N-myristoyltransferase inhibition induces ER-stress, cell cycle arrest, and apoptosis in cancer cells. *ACS Chem. Biol.* 11, 2165–2176. doi:10.1021/acschembio.6b00371

Tian, L., McClafferty, H., Jeffries, O., and Shipston, M. J. (2010). Multiple palmitoyltransferases are required for palmitoylation-dependent regulation of large conductance calcium- and voltage-activated potassium channels. *J. Biol. Chem.* 285, 23954–23962. doi:10.1074/jbc.M110.137802

Virlogeux, A., Scaramuzzino, C., Lenoir, S., Carpentier, R., Louessard, M., Genoux, A., et al. (2021). Increasing brain palmitoylation rescues behavior and neuropathology in Huntington disease mice. *Sci. Adv.* 7, eabb0799. doi:10.1126/sciadv.abb0799

Warby, S. C., Chan, E. Y., Metzler, M., Gan, L., Singaraja, R. R., Crocker, S. F., et al. (2005). Huntingtin phosphorylation on serine 421 is significantly reduced in the striatum and by polyglutamine expansion *in vivo*. *Hum. Mol. Genet.* 14, 1569–1577. doi:10.1093/hmg/ddi165

Warby, S. C., Doty, C. N., Graham, R. K., Shively, J., Singaraja, R. R., and Hayden, M. R. (2009). Phosphorylation of huntingtin reduces the accumulation of its nuclear fragments. *Mol. Cell. Neurosci.* 40, 121–127. doi:10.1016/j.mcn.2008.09.007

Watkin, E. E., Arbez, N., Waldron-Roby, E., O'Meally, R., Ratovitski, T., Cole, R. N., et al. (2014). Phosphorylation of mutant huntingtin at serine 116 modulates neuronal toxicity. *PLoS One* 9, e88284. doi:10.1371/journal.pone.0088284

Wellington, C. L., Ellerby, L. M., Hackam, A. S., Margolis, R. L., Trifiro, M. A., Singaraja, R., et al. (1998). Caspase cleavage of gene products associated with triplet expansion disorders generates truncated fragments containing the polyglutamine tract. *J. Biol. Chem.* 273, 9158–9167. doi:10.1074/jbc.273.15.9158

Wellington, C. L., Singaraja, R., Ellerby, L., Savill, J., Roy, S., Leavitt, B., et al. (2000). Inhibiting caspase cleavage of huntingtin reduces toxicity and aggregate formation in neuronal and nonneuronal cells. *J. Biol. Chem.* 275, 19831–19838. doi:10.1074/jbc.M001475200

Wong, B. K. Y., Ehrnhoefer, D. E., Graham, R. K., Martin, D. D. O., Ladha, S., Uribe, V., et al. (2015). Partial rescue of some features of Huntington Disease in the genetic absence of caspase-6 in YAC128 mice. *Neurobiol. Dis.* 76, 24–36. doi:10.1016/j.nbd.2014.12.030

Yanai, A., Huang, K., Kang, R., Singaraja, R. R., Arstikaitis, P., Gan, L., et al. (2006). Palmitoylation of huntingtin by HIP14 is essential for its trafficking and function. *Nat. Neurosci.* 9, 824–831. doi:10.1038/nn1702

Yap, M. C., Kostiuk, M. A., Martin, D. D. O., Perinpanayagam, M. A., Hak, P. G., Siddam, A., et al. (2010). Rapid and selective detection of fatty acylated proteins using omega-alkynyl-fatty acids and click chemistry. *J. Lipid Res.* 51, 1566–1580. doi:10.1194/jlr.D002790

Zhou, F., Xue, Y., Yao, X., and Xu, Y. (2006). CSS-palm: Palmitoylation site prediction with a clustering and scoring strategy (CSS). *Bioinformatics* 22, 894–896. doi:10.1093/bioinformatics/btl013

Glossary

Acyl-RAC acyl-resin-assisted capture
APT acyl-protein thioesterase
BSA bovine serum albumin
C6R caspase-6 resistant
CCPR catalytic cysteine palmitoyl relay
CHX cycloheximide
DTT dithiothreitol
DMEM Dulbecco's modified Eagle medium
EGFP enhanced green fluorescent protein
ER endoplasmic reticulum
FBS fetal bovine serum
HIP14 huntingtin interacting protein 14
HIP14L huntingtin interacting protein 14-like
HTT huntingtin
HD Huntington disease
HAM hydroxylamine
IB immunoblot
IP immunoprecipitation
IP-ABE acyl-biotin exchange assay on immunoprecipitated proteins
NEM N-ethylmaleimide
NMT N-myristoyltransferase
NO nitric oxide
PMSF phenylmethylsulfonyl fluoride
PBS phosphate-buffered saline
PolyQ polyglutamine
PTM post-translational modification
SDS sodium dodecyl sulfate
STS staurosporine
TEV Tobacco Etch virus
TBTA tris (benzyltriazolylmethyl)amine
TCEP tris-carboxyethylphosphine
WT wild-type
ZDHHC17 Zinc finger DHHC-type palmitoyltransferase 17
ZDHHC13 Zinc finger DHHC-type palmitoyltransferase 13

frontiers | Frontiers in Physiology

TYPE Original Research
PUBLISHED 24 January 2023
DOI 10.3389/fphys.2023.1110550

OPEN ACCESS

EDITED BY
Rebeca M. Mejias Estevez,
Sevilla University, Spain

REVIEWED BY
William Fuller,
University of Glasgow, United Kingdom
Shaun S. Sanders,
University of Guelph, Canada

*CORRESPONDENCE
Shernaz X. Bamji,
shernaz.bamji@ubc.ca

SPECIALTY SECTION
This article was submitted to Lipid and Fatty Acid Research, a section of the journal Frontiers in Physiology

RECEIVED 28 November 2022
ACCEPTED 09 January 2023
PUBLISHED 24 January 2023

CITATION
Wild AR, Hogg PW, Flibotte S, Kochhar S, Hollman RB, Haas K and Bamji SX (2023), CellPalmSeq: A curated RNAseq database of palmitoylating and de-palmitoylating enzyme expression in human cell types and laboratory cell lines.
Front. Physiol. 14:1110550.
doi: 10.3389/fphys.2023.1110550

CellPalmSeq: A curated RNAseq database of palmitoylating and de-palmitoylating enzyme expression in human cell types and laboratory cell lines

Angela R. Wild[1], Peter W. Hogg[1], Stephane Flibotte[2], Shruti Kochhar[1], Rocio B. Hollman[1], Kurt Haas[1] and Shernaz X. Bamji[1]*

[1]Bamji Lab, Department of Cellular and Physiological Sciences, Life Sciences Institute and Djavad Mowafaghian Centre for Brain Health, Vancouver, BC, Canada, [2]Life Sciences Institute Bioinformatics Facility, University of British Columbia, Vancouver, BC, Canada

The reversible lipid modification protein S-palmitoylation can dynamically modify the localization, diffusion, function, conformation and physical interactions of substrate proteins. Dysregulated S-palmitoylation is associated with a multitude of human diseases including brain and metabolic disorders, viral infection and cancer. However, the diverse expression patterns of the genes that regulate palmitoylation in the broad range of human cell types are currently unexplored, and their expression in commonly used cell lines that are the workhorse of basic and preclinical research are often overlooked when studying palmitoylation dependent processes. We therefore created CellPalmSeq (https://cellpalmseq.med.ubc.ca), a curated RNAseq database and interactive webtool for visualization of the expression patterns of the genes that regulate palmitoylation across human single cell types, bulk tissue, cancer cell lines and commonly used laboratory non-human cell lines. This resource will allow exploration of these expression patterns, revealing important insights into cellular physiology and disease, and will aid with cell line selection and the interpretation of results when studying important cellular processes that depend on protein S-palmitoylation.

KEYWORDS

palmitoylation, ZDHHC, depalmitoylating enzyme, cancer, cell line, human, RNAseq, expression

1 Introduction

Protein *S*-palmitoylation is a reversible post-translational modification, in which the 16-carbon fatty acid, palmitate, is attached to a thiol group of specific cysteine residues *via* a labile thioester bond. As the most common form of *S*-acylation, this modification has profound influence over protein function and cellular signaling in the brain (Globa and Bamji, 2017; Matt et al., 2019; Ji and Skup, 2021), immune system (Lin, 2021; Zhang et al., 2021) and cardiovascular system (Essandoh et al., 2020). Furthermore, dysregulated *S*-palmitoylation is also associated with metabolic disorders (Qu et al., 2021), brain disorders (Zaręba-Kozioł et al., 2018) and viral infection (e.g., SARS-CoV-2) (Abdulrahman et al., 2021; Wu et al., 2021; Li et al., 2022). In recent years, considerable evidence has accumulated that *S*-palmitoylation of oncogenes can play a critical role in cancer progression, with the palmitoylating and

depalmitoylating enzymes being investigated as drug targets to modify tumor growth (Ko and Dixon, 2018). *S*-palmitoylation is mediated by a family of 24 human ZDHHC enzymes that differ structurally but share a consensus 'DHHC' catalytic motif (Malgapo and Linder, 2021; Puthenveetil et al., 2022). These enzymes can associate with several known ZDHHC accessory proteins that regulate their function and stability (Salaun et al., 2020). Furthermore, depalmitoylation is mediated by a growing number of acyl-protein thioesterase enzymes, which are still in the process of being fully characterized (Won, Cheung See Kit and Martin, 2018). However, the precise distribution of these enzymes within the broad range of cell types and tissues in the human body has not been characterized, and is often overlooked when using model systems to study biological and pathological processes that are regulated by *S*-palmitoylation.

Cell lines are the workhorse of many laboratories and are often used for basic and clinical research in place of primary cell culture. In addition to being cost effective, easy to use, and generating relatively reproducible data, cells lines also bypass the need for ethical approval that is associated with human and non-human animal tissue. Furthermore, human cancer cell lines that share many transcriptomic similarities with primary tumors (Barretina et al., 2012), are the primary preclinical model systems for the investigation of cancer biology and testing the efficacy of anticancer drugs (Gonzalez-Nicolini and Fussenegger, 2005).

In addition to the numerous cancer cell lines that are central to cancer research, alternative animal cell lines are used across a huge variety of research disciplines, in fields as diverse as primary research, vaccine production, study of gene function, protein production and drug toxicity research (Allen et al., 2008; Khan, 2013; Genzel, 2015) (Allen et al., 2008; Khan, 2013; Genzel, 2015). However, the influence of the background transcriptome of a given cell line is not always taken into account when utilizing these models to study cellular processes.

The recent publication of numerous large scale RNAseq studies has enabled the transcriptional profiling of a large variety of tissues, including from human samples, animal model systems and immortalized cell lines. Importantly, this wealth of expression data is publicly available through web resources such as the Gene Expression Omnibus (GEO) and other purpose designed web resources. However, there are often barriers to easy access of this data, particularly when web resources for data viewing are not available.

A recent study from our lab collated and analyzed publicly available RNAseq data revealing considerable heterogeneity in the expression patterns of the genes that regulate *S*-palmitoylation in the mouse brain, and demonstrated how these expression patterns can be used to better understand the etiology of diseases that are related to dysregulated *S*-palmitoylation, and to predict and validate enzyme-substrate interactions (Wild et al., 2022). However, a resource for non-brain RNAseq data in human tissues and commonly used cell lines is currently lacking. We have therefore applied a similar approach to RNAseq data curation and visualization for genes that regulate *S*-palmitoylation, this time assessing their expression patterns in human bulk and single-cell RNAseq datasets, in addition to human and non-human cell lines that are a mainstay of basic biological and preclinical research. To create an accessible resource for visualizing the expression of the *S*-palmitoylationg and depalmitoylating enzymes across a vast number of cell lines, we curated data from several large scale RNAseq databases that cover hundreds of human cancer cell lines, and also curated GEO expression data from several of the most commonly used non-human and human laboratory cell lines. We then created a webtool (CellPalmSeq; https://cellpalmseq.med.ubc.ca) to allow easy interrogation of this multi-study data using simple interactive heatmaps.

2 Results

2.1 Creation of CellPalmSeq, an interactive database and webtool for visualization of the expression patterns of the genes that regulate *S*-palmitoylation

In recent years, numerous RNAseq studies of varying scales have characterized the transcriptomes of human tissues and hundreds of commonly used cell lines. However, this data is often difficult to access and visualize, with no single resource existing with transcriptomic data from a large number of non-human cell lines. Furthermore, datasets from individual studies are challenging for non-bioinformaticians to access, and available webtools often do not allow comparison of the expression of multiple genes at once. We therefore created "CellPalmSeq", an interactive resource for visualization of expression data for the genes that regulate *S*-palmitoylation, curated from multi-study RNAseq datasets from non-diseased human tissues, human cancer cell lines and commonly used non-human laboratory cell lines. We processed data for the 24 ZDHHC enzymes (*ZDHHC1-ZDHHC24*, plus *ZDHHC11B* and omitting *ZDHHC10* which is not included in the ZDHHC genes), the known ZDHHC accessory proteins (*GOLGA7*, *GOLGA7B* and *SELENEOK*; Salaun et al., 2020) and the depalmitoylating enzymes that have been well characterized and/or are inhibited by the depalmitoylating enzyme blockers (HDFP) and Palmostatin B (*LYPLA1, LYPLA2, PPT1, ABHD4, ABHD6, ABHD10, ABHD12, ABHD13, ABHD16A, ABHD17A, ABHD17B, ABHD17C;* Lin et al., 2017). To compare across datasets, we present all datasets in the same expression units and reanalyzed from the raw reads where needed. All data are freely available for download on CellPalmSeq, so that users can replot data in their preferred format. We then utilized this resource to study the expression patterns of this gene family in order to highlight the importance of accounting for their expression when studying cellular signaling in different cell types, tissues, and cellular model systems.

2.2 Expression of the genes that regulate *S*-palmitoylation in human single cell types

We first curated single-cell RNAseq data from the Human Protein Atlas, which analyzed collated data from 26 studies of cells from non-diseased human tissues and organs, identifying 76 broad single-cell types, divided into 15 cell type clusters (https://www.proteinatlas.org/; Karlsson et al., 2021). Single-cell RNAseq data reveal the gene expression profile of a particular cell type, as opposed to bulk tissue which is composed of multiple cell types. We downloaded expression data (normalized transcripts per million; nTPM) for the genes that regulate *S*-palmitoylation from this dataset and plotted heatmaps of ZDHHC expression. We found initially that a small number of the ZDHHC genes were expressed considerably higher

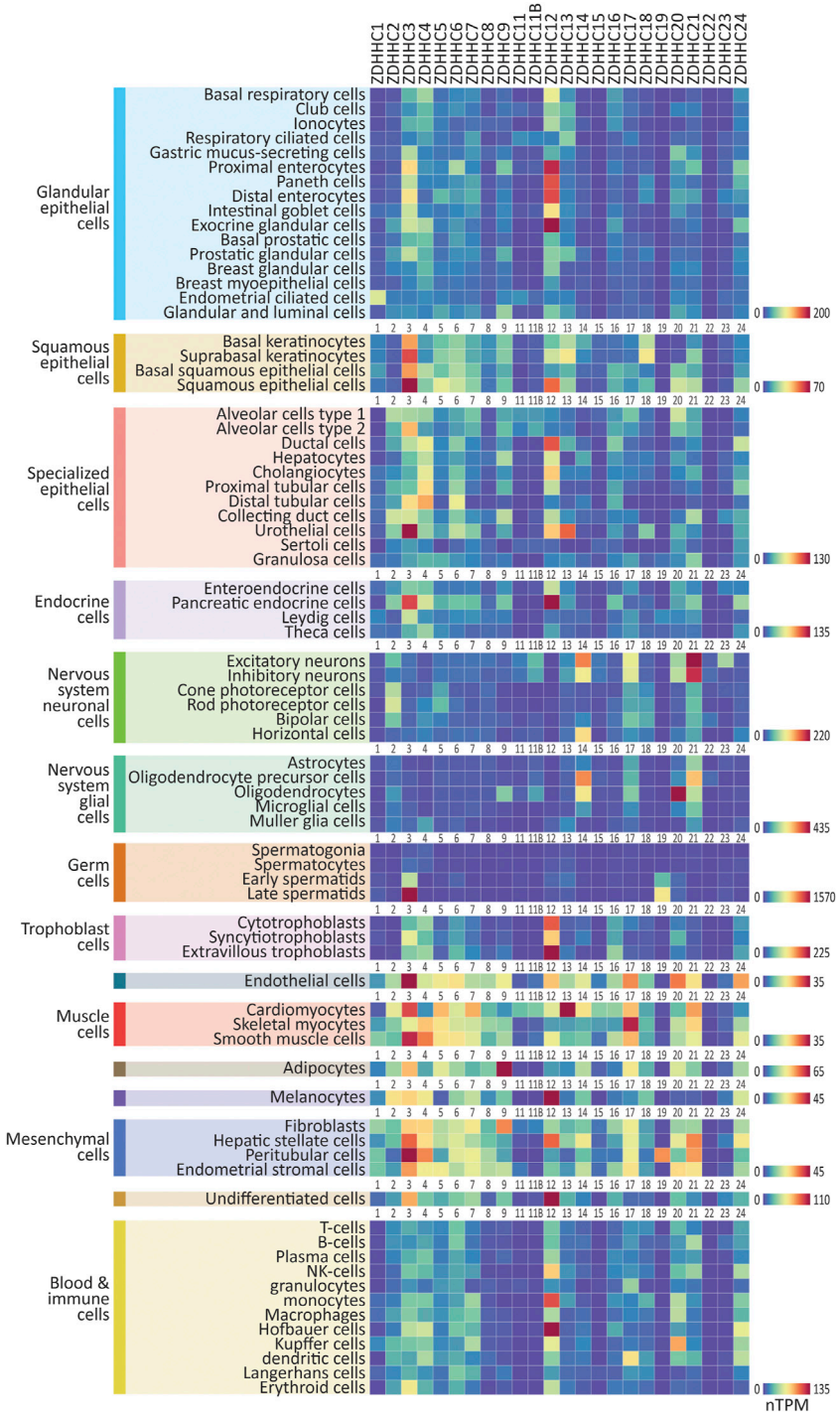

FIGURE 1
Expression patterns of the ZDHHC enzymes in major human cell types. Heatmaps showing human single-cell RNAseq expression data for the ZDHHC enzymes, downloaded from the Human Protein Atlas. 76 major cell types were identified within 15 cell type clusters. Heatmaps are grouped according to cell type cluster to view relative expression. Heatmap units: TPM. All data available for download on CellPalmSeq.

than others, making visual comparison between the majority of genes difficult within a single heatmap (notably *ZDHHC3* and *ZDHHC19* in late spermatids, see CellPalmSeq for interactive heatmaps). Therefore, we plotted individual heatmaps of ZDHHC expression *within each cell-type cluster*, with heatmaps scaled separately for each cell type cluster (Figure 1). Overall, when looking at expression by cell type cluster, we observed highly heterogeneous expression, in line with specific functions of the various components of the *S*-palmitoylation machinery in different cellular contexts. Certain cell type clusters showed a preference for a very select group of ZDHHC enzymes, whereas others expressed a broader range of ZDHHC enzymes. On average, *ZDHHC3* was the highest expressing ZDHHC enzyme across

10.3389/fphys.2023.1110550

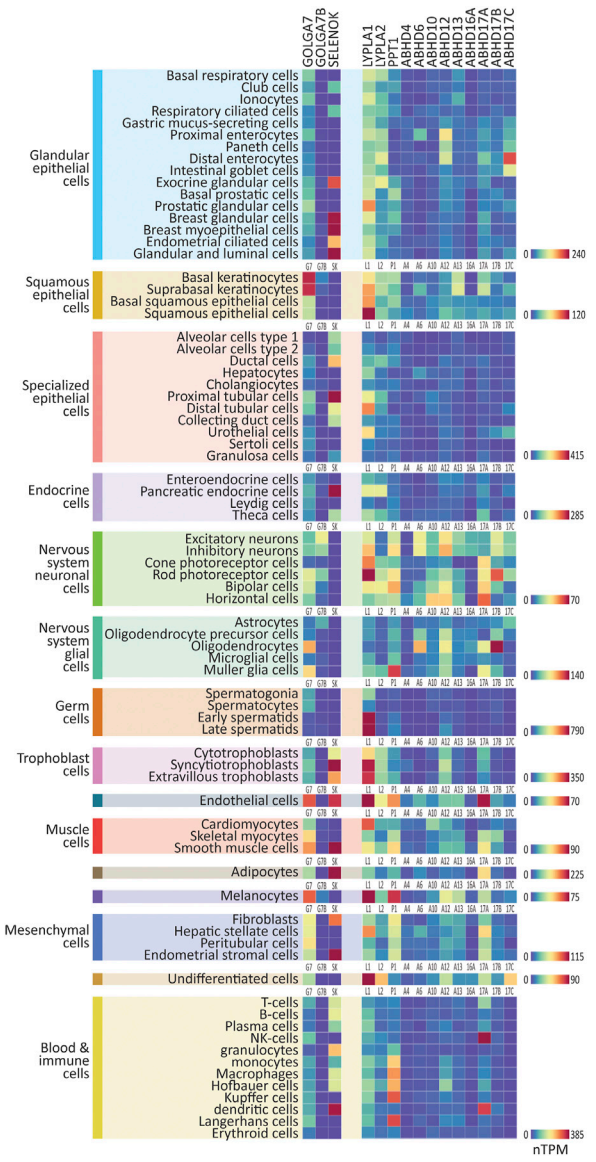

FIGURE 2
Expression patterns of the ZDHHC accessory proteins and depalmitoylating enzymes in major human cell types. Heatmaps showing human single-cell RNAseq expression data for the ZDHHC accessory proteins and depalmitoylating enzymes, downloaded from the Human Protein Atlas. 76 major cell types were identified within 15 cell type clusters. Heatmaps are grouped according to cell type cluster to view relative expression. Heatmap units: Transcripts per million (TPM). All data available for download on CellPalmSeq.

all cell types, followed by *ZDHHC12*, *ZDHHC21,* and *ZDHHC4*. For the ZDHHC accessory proteins (Figure 2), *GOLGA7* was broadly expressed within the majority of cell type clusters, whereas *SELENOK* expression was highly heterogeneous. For the depalmitoylating enzymes (Figure 2), *LYPLA1* had the highest expression on average and was expressed highly in a number of cell types such as squamous epithelial cells, cardiomyocytes, and hepatic stellate cells, while *PPT1* was the depalmitoylating enzyme with the highest expression in immune cells. Interactive heatmaps for this (and all other) data are available on CellPalmSeq to plot expression data according to user preferences.

Next, to visualize the relative expression of each individual ZDHHC enzyme *across all cell types*, we plotted z-scores for each ZDHHC enzyme, calculated from expression values across all cell types examined (Supplementary Figure S1). A positive or negative z-score indicates enriched or depleted expression, respectively, in a given cell type. Several ZDHHCs were highly enriched in certain cell types, for example, ZDHHC19 in late spermatids and ZDHHC16 in extravillous trophoblasts. Depalmitoylating enzymes showed similarly enriched expression, including *ABHD17A* in NK cells, and *ABHD17B* in oligodendrocytes (Supplementary Figure S2). For the accessory proteins, *GOLGA7B* was highly enriched in cells of the nervous system, particularly neuronal cells, mirroring previous findings of enrichment of *Golga7b* in mouse neuronal cells (Supplementary Figure S2; Wild et al., 2022).

In addition to the single-cell RNAseq data presented here, bulk RNAseq data of the major human tissues curated from the Human Protein Atlas are also available on the CellPalmSeq website.

Together, these expression patterns give insight into the specialized roles that certain palmitoylating and depalmitoylating enzymes are likely to have in different cell types within the human body, and can be used to make predictions about potential substrate interactions between this machinery and cell type enriched substrates (Wild et al., 2022). Furthermore, these patterns of enrichment will aid in the understanding of potential off target effects of drugs developed to modify the *S*-palmitoylation machinery, in non-target tissues.

2.3 Expression of the genes that regulate *S*-palmitoylation in human cancer cell lines

Cancer cell lines are heavily utilized as preclinical model systems for cancer research (Barretina et al., 2012), and have been critical for the discovery of many fundamental processes in cell biology, such as the characterization of the signaling machinery engaged by T-cell receptors using tumor derived Jurkat cells (Abraham and Weiss, 2004). Importantly, *S*-palmitoylation is known to play a role in the activation of oncogenic signaling networks, and the enzymes that regulate *S*-palmitoylation are known to be dysregulated in a number of cancers (Yeste-Velasco et al., 2015; Anderson and Ragan, 2016; Fhu and Ali, 2021). We next investigated two large scale cancer RNAseq compendia, the Cancer Cell Line Encyclopedia (CCLE; 1406 cell lines; Barretina et al., 2012; Ghandi et al., 2019) and Cell Model Passports (CMP; 442 cell lines; Garcia-Alonso et al., 2017; Picco et al., 2019), that measured gene expression across several hundred cancer cell lines. Expression data (transcripts per million; TPM) were again downloaded for the genes that regulate *S*-palmitoylation and are available for interactive plotting on CellPalmSeq. To provide an overview of differential enrichment of these genes, we averaged expression according to the primary disease tissue (or cancer type) from which the cell lines were isolated, and plotted heatmaps that revealed highly heterogeneous expression of the genes that regulate *S*-palmitoylation across cancer cell lines for both the CCLE (Figure 3A) and CMP datasets (Supplementary Figure S3). The heatmap columns were ranked by descending averages to determine which genes had the broadest expression across cancer cell lines. For the ZDHHC enzymes, *ZDHHC4, ZDHHC5, ZDHHC6, ZDHHC7, ZDHHC12, ZDHHC16, and ZDHHC20* were the highest expressing ZDHHC enzymes across cell lines in both datasets, although their ranked expression differed in each set. This is likely

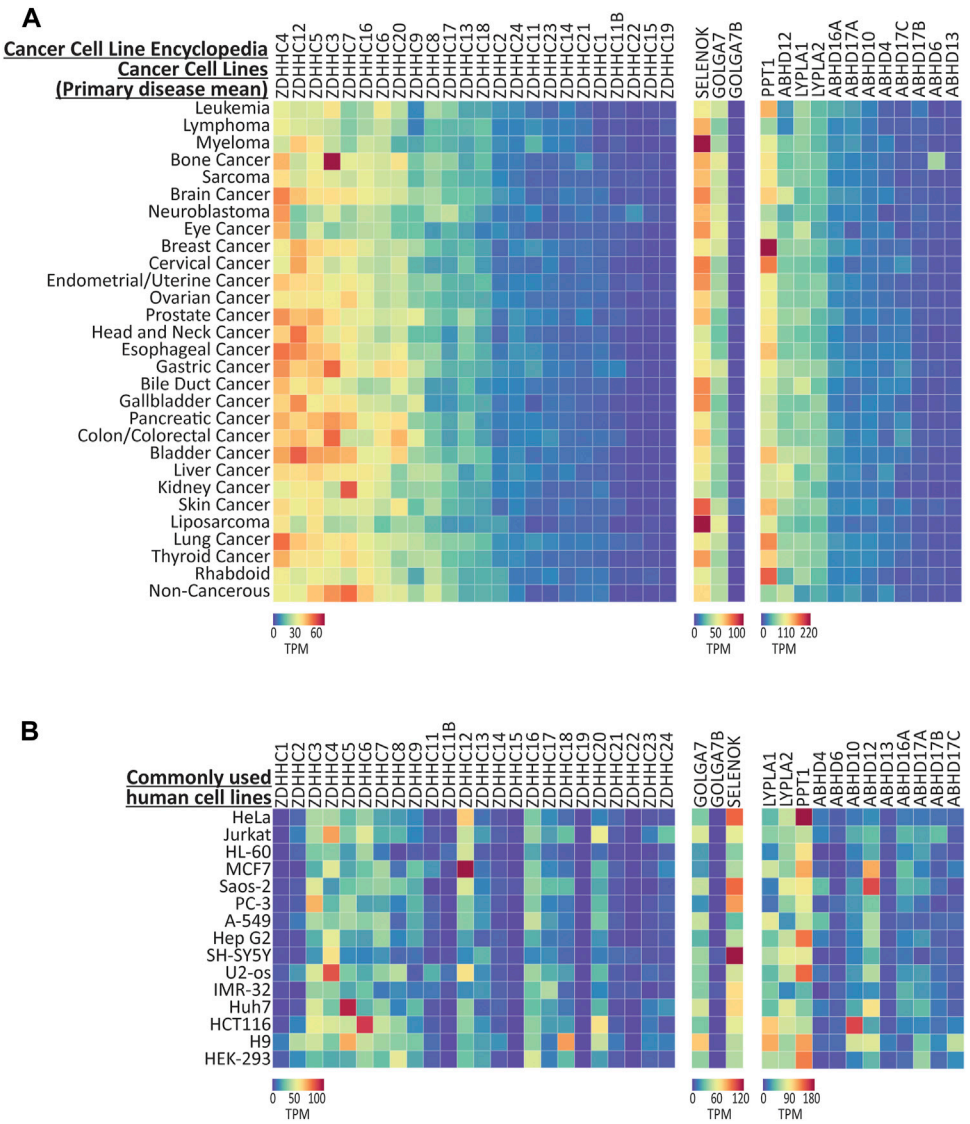

FIGURE 3
Expression of the genes that regulate palmitoylation from CCLE cancer cell lines. **(A)** Heatmap showing RNAseq expression data for the genes that regulate *S*-palmitoylation, downloaded from CCLE and averaged according to 'Primary Disease'. Data are included from 1406 cell lines, averaged into 30 primary disease types. **(B)** Expression data for selected human cell lines that are commonly used for basic research. All data were extracted from the CCLE dataset, except the H9 cell line which was found only in the CMP dataset, and HEK-293 that was found in the HPA cell line dataset. Heatmap units: Transcripts per million (TPM). All data available for download on CellPalmSeq.

due to differences in the number of unique cell lines selected for testing, as only 161 out of 442 cell lines from the CMP dataset were also tested in the CCLE panel. Conversely, expression of *ZDHHC15* and *ZDHHC19* was very low in the majority of cell lines in both studies. Some patterns of expression were consistent across the two datasets (Figure 3A; Supplementary Figure S3A), including high expression of *ZDHHC3* and *ABHD6* in bone cancer derived cell lines, particularly those derived from Ewing's sarcoma tumors. *ZDHHC7* was elevated in kidney cancer cell lines in both datasets, and *PPT1* was highly expressed in cell lines from breast cancer tumors. Conversely, *ZDHHC9* expression was markedly lowest in cell lines derived from leukemia and lymphoma tissues in both datasets. Because human cancer cell lines often share many transcriptomic similarities with primary tumors (Barretina et al., 2012), this resource to examine the expression patterns of the genes that regulate *S*-palmitoylation across cancer cell lines and cancer types may enable hypothesis generation regarding how *S*-palmitoylation is regulated in certain cancers.

We next plotted the expression data for *S*-palmitoylation associated genes across several of the most commonly used human cell lines (Figure 3B). Although these cell lines have been used extensively for cancer research, many have been utilized outside of this field for fundamental research into cell biology and drug discovery (Supplementary Table S1). Furthermore, the HEK-293 human cells are included as they are commonly used in basic research, although this cell line was derived embryonic kidney cells transformed with adenovirus, and not from tumor tissue (Graham et al., 1977). Heterogeneous expression of the palmitoylating enzymes, their

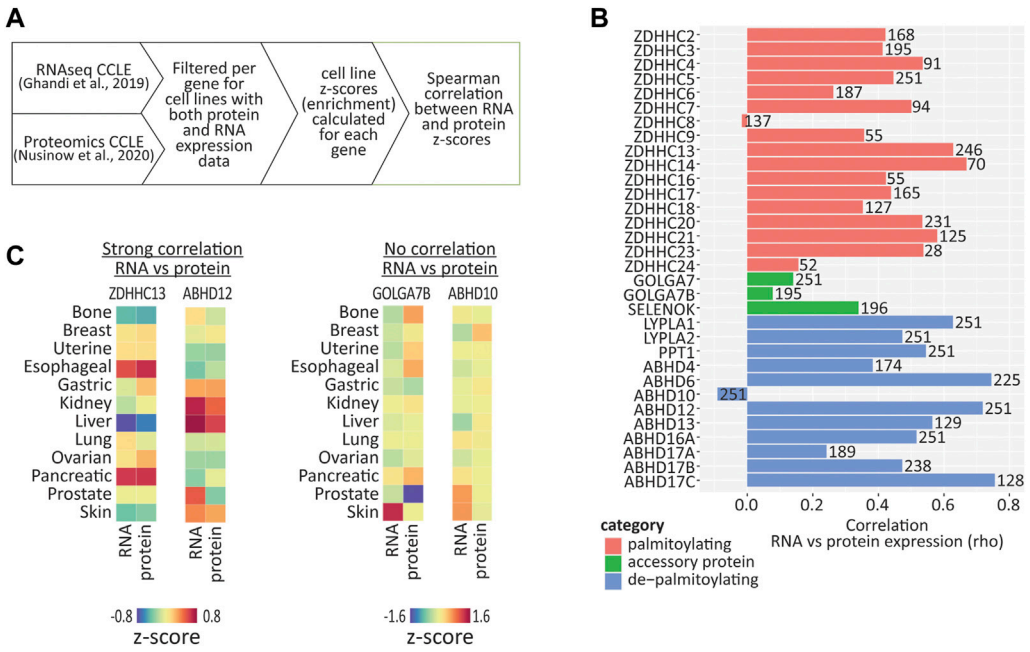

FIGURE 4
Correlation between RNA and protein expression using cancer cell line data. **(A)** Diagram illustrating how expression values were converted to z-scores and then correlation values calculated, using CCLE RNAseq and proteomic data. **(B)** Graph of Spearman correlation values calculated from expression z-scores across available CCLE cell lines, for RNA vs. protein. Number on each bar represents the number of cell lines (in which both RNA and protein were detected) used for each correlation calculation. **(C)** Heatmap showing enrichments of both RNA and protein across cancer type clusters for selected palmitoylating and depalmitoylating enzymes. Heatmap units: z-score.

accessory proteins and the depalmitoylating enzymes was again observed across these cell lines, highlighting the importance of considering the expression of this family of enzymes when choosing cell lines as model systems for research on processes that are regulated by *S*-palmitoylation.

2.4 Correlation of RNA and protein expression for genes that regulate *S*-palmitoylation in human cancer cell lines

Although RNA expression patterns are a useful tool to predict the protein expression in a given cell type, the correlation between RNA and protein expression can be poor, due to post-translational protein processing and degradation (Vogel and Marcotte, 2012). To determine which of the *S*-palmitoylation associated genes have RNA expression patterns that are maintained at the protein level in human cancer cell lines, we compared RNA (Ghandi et al., 2019) and protein (mass spectrometry proteomics; Nusinow et al., 2020) expression data, both generated by the CCLE study (Figure 4A). We found 251 cell lines that were present in both datasets, however, not all of our proteins of interest were detected across all cell lines. We therefore only performed correlations on cell lines that had values for both RNA and protein for a given gene, and converted the expression values into z-scores across these cell lines in order to perform a comparison of cell line enrichments (Supplementary Table S2). In addition, several genes were not detected at all at the protein level, including *ZDHHC1, ZDHHC11, ZDHHC11B, ZDHHC12, ZDHHC19* and *ZDHHC22*. We found that 21 out of the 33 genes examined showed a moderate or strong positive correlation ($R > 0.4$; $p < 0.001$) between RNA and protein z-scores (Figure 4B), indicating that RNA expression patterns are predictive of protein abundance for the majority of *S*-palmitoylation associated genes. There were however several notable examples of very poor correlation, including *ZDHHC8*, *GOLGA7B* and *ABHD10*.

Closer examination of examples of genes with high correlations between RNA and protein revealed that certain genes were either enriched or depleted within certain cancer cell line clusters (Figure 4C). For example, ZDHHC13 RNA and protein were highly enriched in esophageal and pancreatic cancer cell lines, and depleted in liver cancer cell lines, while ABHD12 was enriched in kidney and liver cancer cell lines. Conversely, GOLGA7B and ABHD10 showed very poor correlation, indicating that caution should be taken if attempting to infer expression patterns of these genes from RNA expression patterns alone.

2.5 Expression of the genes that regulate *S*-palmitoylation in commonly used non-human cell lines

Numerous non-human cell lines are widely utilized in basic and pre-clinical research and have been used for the study of basic cell biology, drug toxicity, gene therapy and vaccine production (Verma et al., 2020). However, to our knowledge no single resource exists that has performed a multi-cell line RNAseq study on the most commonly

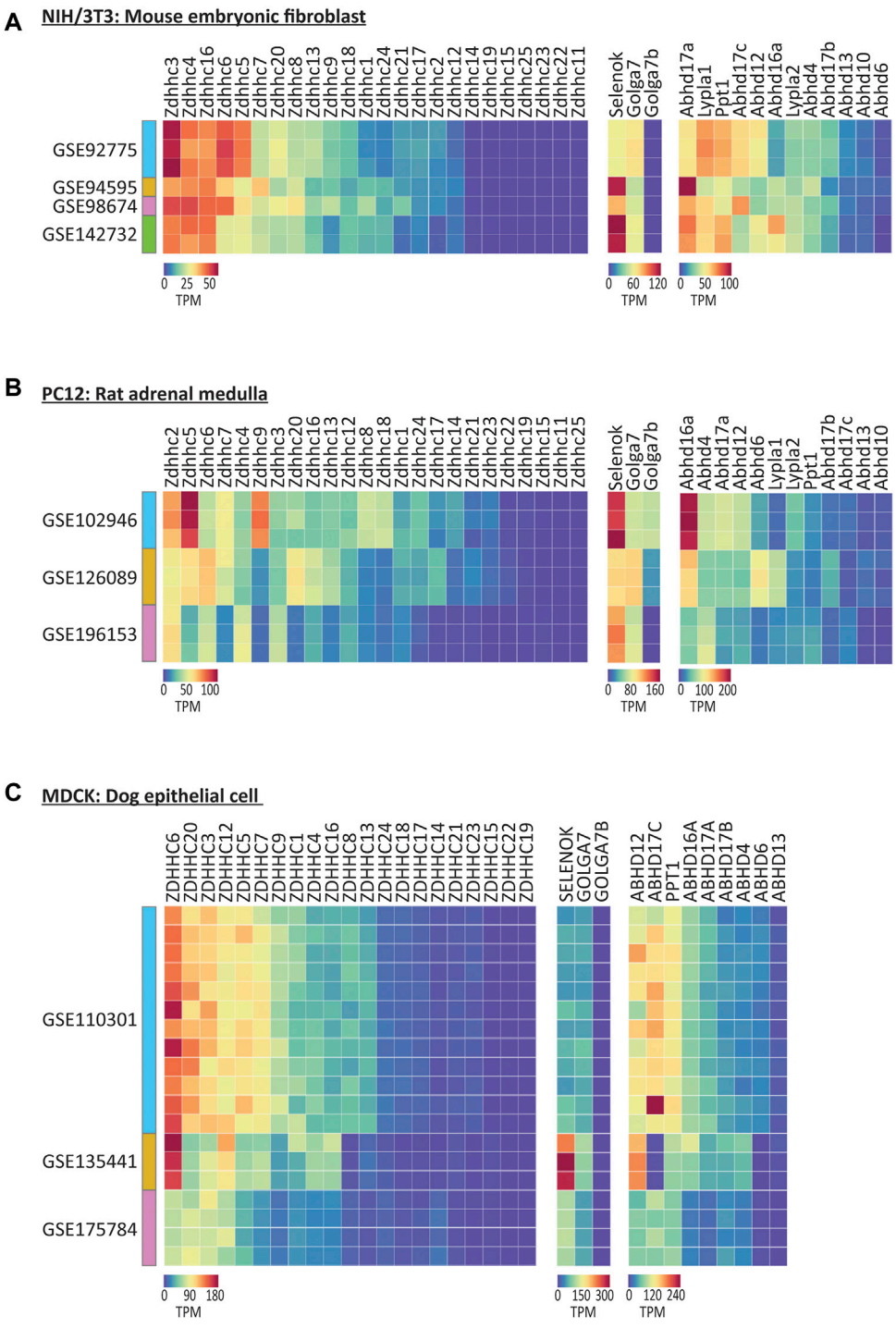

FIGURE 5
Expression of the genes that regulate S-palmitoylation in selected commonly used non-human cell lines. **(A)** Heatmap of RNAseq expression data for the genes that regulate *S*-palmitoylation in control/untreated samples from mouse NIH/3T3 cell line, downloaded from selected datasets on GEO (labelled with GEO accession numbers). *N* = 1–3 control samples per dataset. Units = Transcripts per million (TPM). **(B)** As A but for Rat PC12 cell line samples. *N* = 3 samples per cell dataset. **(C)** As A but for dog MDCK cell line samples. *N* = 3–12 samples per dataset.

used non-human cell lines. We therefore turned to the Gene Expression Omnibus (GEO; https://www.ncbi.nlm.nih.gov/geo/), a database repository of high throughput gene expression data, to manually curate available RNAseq data for the several of the most commonly used cell lines including: NIH/3T3, PC12, MDCK, BHK21, CHO, VeroE6, and Calu3 (Supplementary Table S3). We curated studies according to the following criteria: i) datasets were associated with a peer reviewed publication; ii) control samples had been tested with minimal manipulation and iii) the source of the cell line used was well defined or the cell line had been authenticated by short tandem repeat (STR) profiling. We then reanalyzed control samples from these curated datasets from the raw reads using the same analysis pipeline.

The predicted ensembl (https://ensembl.org) gene set for each species was used to extract the *S*-palmitoylation genes but as expected, not all genes we previously analyzed in human are identified in each species, therefore only those identified are included. All of these datasets are available for interactive visualization and download on CellPalmSeq.

We began with the mouse NIH/3T3 cell line, which is one of the most commonly used embryonic fibroblast lines with 8,826 citations on PubMed.gov. We found that expression patterns for the genes that regulate *S*-palmitoylation were very similar across four independent studies, particularly for the ZDHHC enzymes, despite the cell lines originating from three independent sources (Figure 5A; Supplementary Table S3). *Zdhhc3*, *Zdhhc4* and *Zdhhc16* were the highest expressing ZDHHCs across studies, while numerous ZDHHCs were not detected at all. *Abhd17a*, *Lypla1*, and *Ppt1* were the highest expressing depalmitoylating enzymes, and of the accessory proteins, all were detected except *Golga7b*.

The expression patterns were markedly different in PC12 cells derived from rat adrenal medulla, that share many common features with neuronal cells (Figure 5B; Westerink and Ewing, 2008). Notably, *Zdhhc2* and *Zdhhc5* were on average the highest expressing ZDHHCs across three studies analyzed. Overall, less cross study similarity was observed, highlighting the potential transcriptional heterogeneity in this cell line when derived from different sources. Unlike NIH/3T3 cells, *Golga7b* expression was detected in two of the three studies of PC12 cells, consistent with the neuronal expression for this accessory protein (Wild et al., 2022).

Analysis of MDCK cells derived from canine epithelial cells (Dukes et al., 2011), which have been used in broad applications in biological research and vaccine production, and have been cited over 11,000 times on PubMed, revealed again differences in the highest expressing enzymes, this time with *ZDHHC6* and *ZDHHC20* having the highest expression on average of the ZDHHCs and *ABHD12* being the highest expressing depalmitoylating enzyme (Figure 5C).

Finally, we analyzed several of the most commonly used cell lines for SARS-CoV-2 research, as *S*-palmitoylation of the SARS-CoV-2 spike protein is essential for viral membrane fusion and infectivity (Wu et al., 2021). We collated data for VeroE6 from African Green Monkey and Calu-3, which is a human derived cancer cell line. These cell lines are often selected for SARS-CoV-2 research due to their expression of the ACE-2 receptor, which is required for SARS-CoV-2 entry into the cell (Kumar et al., 2021). We plotted the average of VeroE6 and Calu-3 datasets collated from GEO, along with data from several human cell lines that have been used to identify the palmitoylating enzymes for SARS-CoV-2 spike protein (Supplementary Figure S4; Mesquita et al., 2021; Puthenveetil et al., 2021; Ramadan et al., 2022). We found that expression of the putative ZDHHC enzymes that palmitoylate the SARS-CoV-2 spike protein (*ZDHHC3*, *ZDHHC5*, *ZDHHC8*, *ZDHHC9* and *ZDHHC20*; red bars Supplementary Figure S4) differed across the cell lines, which could alter *S*-palmitoylation of the spike protein, and in turn viral infectivity. Overall, these results reveal how understanding the composition of the *S*-palmitoylation related machinery in a cell line might aid with cell line selection, the design of experiments and the interpretation of results, when using cell lines to study important biological processes that depend on protein *S*-palmitoylation.

3 Discussion

3.1 Heterogeneous expression of the genes that regulate *S*-palmitoylation across human cell types

Protein *S*-palmitoylation is a dynamic regulator of numerous signaling pathways that are critical for normal cell function (Main and Fuller, 2022). It is estimated that over 10% of proteins in the human proteome are *S*-palmitoylation substrates (Blanc et al., 2015), therefore the majority of cellular signaling pathways are likely to be regulated by this post translational modification. The list of *S*-palmitoylated proteins that are known to be critically involved in human diseases is expanding (Fraser, 2019), and therefore understanding the unique makeup of the *S*-palmitoylation machinery in a given cell type is essential when studying processes that are regulated by *S*-palmitoylation.

Recent advances in RNAseq technologies have enabled the detailed characterization of cellular transcriptomes at a reduced monetary cost, with increased sequencing depth and single cell resolution. This has been accompanied by an increase in the number of studies performed on human tissue, and an appreciation for the importance of open data that can be accessed by the research community in order to reveal novel insights into human physiology and disease. Here, we capitalized on these advances by using open data to investigate the expression patterns of the genes that regulate *S*-palmitoylation in human single cell types, tissues and cancer cell lines, and created an interactive resource to give other researchers easy access to this data.

When examining the distribution of the genes that regulate *S*-palmitoylation in the various cell types from isolated human tissues, we observed that many cell types express a unique compliment of palmitoylating and depalmitoylating enzymes. Because members of this family of proteins are targeted to different subcellular organelles (Globa and Bamji, 2017), and this subcellular targeting can influence the localization and trafficking of substrates (Solis et al., 2022), differential expression of these enzymes and accessory proteins will have a profound influence on substrate function in different cellular contexts. For example, the ZDHHC5 accessory protein GOLGA7B, which is known to regulate ZDHHC5 cell membrane localization, was expressed in neuronal cells, but not detected in cardiomyoctyes. Because ZDHHC5 is known to have an important role in both of these cell types (Woodley and Collins, 2021), this differential expression of GOLGA7B could alter the function of ZDHHC5 in these different cellular contexts.

Drugs that target the ZDHHC palmitoylating enzymes are a potential avenue to treat disorders that are associated with dysregulated *S*-palmitoylation (Fraser, 2019). Efforts are currently underway to develop drugs that selectively target individual ZDHHC enzymes (Salaun et al., 2022). However, a large number of proteins can be *S*-palmitoylated by more than one ZDHHC enzyme, resulting in functional redundancy within this enzyme family that may reduce the therapeutic potential of selective inhibition of individual ZDHHCs. Examination of the relative expression of functionally related ZDHHC enzymes within a given cell type using CellPalmSeq will therefore facilitate predictions of the therapeutic efficacy of selective ZDHHC inhibitors. Furthermore, this data will enable researchers and clinicians to identify ZDHHCs with enriched expression in target cell types and tissues, and better predict off-target effects of selective inhibitors in non-diseased tissues.

3.2 Expression patterns of the genes that regulate *S*-palmitoylation in cancer cell lines may give insight into cancer pathologies

The role of *S*-palmitoylation in cancer pathology is now well established (Anderson and Ragan, 2016; Lin et al., 2017; Ko and Dixon, 2018; Lobo, 2019). A recent study identified 299 cancer driving genes (Bailey et al., 2018), of which 78 are substrates for *S*-palmitoylation (Ko and Dixon, 2018). Furthermore, altered expression of almost all of the 24 ZDHHC enzymes is associated with positive or negative prognosis in various cancers (Ko and Dixon, 2018). Interestingly, several of the expression patterns of the genes that regulate *S*-palmitoylation that we found here in certain cancer cell lines have also been previously reported in the literature. For example, we observed elevated expression of *ABHD6* in cell lines with a bone cancer origin, particularly those from Ewing's sarcoma cell lines. High expression of *ABHD6* in Ewing's sarcoma cell lines were found previously (Max et al., 2009), while another study found a carcinogenic role for ABHD6 in metastatic seeding of murine pancreatic ductal adenocarcinoma cells *in vivo* (Grüner et al., 2016). Although ABHD6 has an important function in degrading the endocannabinoid 2-arachidonoylglycerol, the role of ABHD6 as a depalmitoylating enzyme has not yet been studied, despite being potently inhibited by depalmitoylating enzyme inhibitors HDFP and PalmB (Lin et al., 2017). We also observed across studies highly elevated expression of *ZDHHC7* in kidney cancer cell lines and *PPT1* in breast cancer cell lines, opening potential avenues for research into the role of these enzymes in these cancers. Extensive RNAseq datasets are now available that have characterized gene expression in patient isolated tumors. Investigation of the expression patterns of the genes that regulate *S*-palmitoylation from these data will further expand any insight into the role of this family of proteins within certain cancer types.

While RNAseq expression patterns are useful for the prediction of protein abundance in certain cell types, RNA and protein expression do not often correlate well due to post translational protein processing (Vogel and Marcotte, 2012). Furthermore, the sensitivity of proteomic assays currently lags behind that of RNA sequencing, as unlike RNA, protein cannot be amplified to enhance detection. Here we took advantage of the availability of both RNAseq and proteomic datasets covering a large number of cancer cell lines, which allowed us to perform an in-depth study of the correlation between RNA and protein expression for the majority of the genes that regulate *S*-palmitoylation. Although we observed moderate or strong positive correlation for the majority of genes tested, there are notable exceptions including ZDHHC8, ZDHHC24, GOLGA7, GOLGA7B, and ABHD10 which correlated poorly. Particular caution is therefore advised when inferring protein abundance from RNA expression for these proteins, which may be subject to more extensive post transcriptional regulation.

3.3 Consideration of the expression of the genes that regulate *S*-palmitoylation when using cellular model systems to study biology and disease

We have used examples of non-human cell lines and the cell lines that are most commonly used for SARS-CoV-2 research to demonstrate that heterogeneity in ZDHHC expression should be taken into account when choosing cell lines for research and interpreting results, particularly when studying *S*-palmitoylation dependent processes. For example, when selecting cell lines for SARS-CoV-2 research, we show that the expression of the putative ZDHHC palmitoylating enzymes for the spike protein differed across cell lines that are commonly used for this research. In addition, consideration of the similarities in expression profiles between laboratory cell lines and the endogenous cell types being studied will also be beneficial. For studies on SARS-CoV-2 infection, which predominantly affects respiratory ciliated cells (Hou et al., 2020; Robinot et al., 2021), the single-cell expression profile for this cell type detailed in Figure 1, combined with the expression profiles of the popular cell lines used for SARS-CoV-2 research in Supplementary Figure S4, can guide the selection of the most suitable cell line.

Finally, we found that certain cell lines were more consistent in their expression of the ZDHHC enzymes, when derived from multiple sources, and researchers are recommended to sequence their own cell lines for most accurate assessment of gene expression. When available, we believe that the large panel screens of multiple cell lines that use systematic and standardized culture and RNAseq protocols (such as CCLE and CMP) are the most reliable resource for assessing relative trends in expression profiles of these genes.

CellPalmSeq will be an invaluable resource that will enable researchers and clinicians to easily interrogate the expression patterns of the *S*-palmitoylation machinery in the human body and cell line model systems, and therefore will facilitate research into the role of *S*-palmitoylation in cellular biology and disease.

4 Materials and methods

4.1 Data processing for CellPalmSeq

For Human Protein Atlas, normalized single-cell RNAseq data collated from 26 datasets (www.proteinatlas.org/download/rna_single_cell_type.tsv.zip) were directly downloaded from (www.proteinatlas.org/about/download) and data were extracted (nTPM) for the genes that regulate *S*-palmitoylation.

For Cancer Cell Line Encylclopedia (CCLE), RNAseq data were downloaded from https://depmap.org/portal/download/ (file CCLE_expression.csv version 22Q2) and averaged by cell lineage and primary disease. Proteomic data were downloaded from https://gygi.hms.harvard.edu/publications/ccle.html (file Supplementary Table S2_Protein_Quant_Normalized.xlsx). Correlations between RNAseq and proteomic data were performed with R using the Spearman method.

For Cell Model Passports (CMP), data were downloaded from https://cellmodelpassports.sanger.ac.uk/downloads (file rnaseq_all_20220624.zip) and averaged by tissue and cancer type.

For datasets downloaded from the GEO, the reference transcriptome of each species for which cell lines were analyzed from raw sequencing reads was acquired from https://ensembl.org. The RNAseq reads were downloaded from the Gene Expression Omnibus (https://www.ncbi.nlm.nih.gov/geo/), the series accession numbers and individual sample numbers are listed in Supplementary Table S3. For each sample, RNAseq expression values (TPM) at the gene level were obtained using kallisto (Bray

et al., 2016) with the appropriate reference transcriptome by summing the TPM values of individual isoforms.

4.2 Heatmap creation for CellPalmSeq

All plots for the CellPalmSeq database were generated using curated RNA sequencing datasets. Python 3 and Javascript scripts were used with the plotting library Bokeh to generate the interactive heatmaps to display and compare these datasets on the CellPalmSeq website (Bokeh Development Team, 2018).

4.3 Data presentation

Heatmaps within the manuscript were plotted in Displayr (https://www.displayr.com). Bar charts were plotted in GraphPad Prism 9.2.0 (San Diego, CA, and United States).

Data availability statement

Publicly available datasets were analyzed in this study. This data can be found here: https://cellpalmseq.med.ubc.ca.

Author contributions

AW, SB contributed to conception and design of the study. AW, RH curated data. SF curated and analyzed data. PH created code for the website. AW, SK built the website. AW wrote the first draft of the manuscript. All authors contributed to manuscript revision, read, and approved the submitted version.

Funding

AW, RH, SK, and SB were funded by Canadian Health Services Research Foundation (F18-00650 CIHR Foundation Grant). PH, KH were funded by Canadian Institutes of Health Research (FDN-148468 Foundation Grant). This work was supported by resources made available through the Dynamic Brain Circuits cluster and the NeuroImaging and NeuroComputation Centre at the UBC Djavad Mowafaghian Centre for Brain Health (RRID SCR_019086).

Conflict of interest

The authors declare that the research was conducted in the absence of any commercial or financial relationships that could be construed as a potential conflict of interest.

Publisher's note

Supplementary material

The Supplementary Material for this article can be found online at: https://www.frontiersin.org/articles/10.3389/fphys.2023.1110550/full#supplementary-material

References

Abdulrahman, D. A., Meng, X., and Veit, M. (2021). S-acylation of proteins of coronavirus and influenza virus: Conservation of acylation sites in animal viruses and dhhc acyltransferases in their animal reservoirs. *Pathogens* 10 (6), 669. doi:10.3390/pathogens10060669

Abraham, R. T., and Weiss, A. (2004). Jurkat T cells and development of the T-cell receptor signalling paradigm. *Nat. Rev. Immunol.* 4, 301–308. doi:10.1038/nri1330

Allen, D. D., Caviedes, R., Cardenas, A. M., Shimahara, T., Segura-Aguilar, J., and Caviedes, P. A. (2008). Cell lines as *in vitro* models for drug screening and toxicity studies. *Taylor Francis* 31 (8), 757–768. doi:10.1080/03639040500216246

Anderson, A. M., and Ragan, M. A. (2016). Palmitoylation: A protein S-acylation with implications for breast cancer. *NPJ Breast Cancer* 2 (1), 16028. doi:10.1038/npjbcancer.2016.28

Bailey, M. H., Tokheim, C., Porta-Pardo, E., Sengupta, S., Bertrand, D., Weerasinghe, A., et al. (2018). Comprehensive characterization of cancer driver genes and mutations. *Cell* 173 (2), 371–385. e18. doi:10.1016/j.cell.2018.02.060

Barretina, J., Giordano, C., Nicolas, S., Kavitha, V., Adam, A. M., Sungjoon, K., et al. (2012). The Cancer Cell Line Encyclopedia enables predictive modelling of anticancer drug sensitivity. *Nature* 483 (7391), 603–607. doi:10.1038/nature11003

Blanc, M., David, F., Abrami, L., Migliozzi, D., Armand, F., Burgi, J., et al. (2015). SwissPalm: Protein palmitoylation database. *F1000Res.* 4, 261. doi:10.12688/f1000research.6464.1

Bray, N. L., Pimentel, H., Melsted, P., and Pachter, L. (2016). Near-optimal probabilistic RNA-seq quantification. *Nat. Biotechnol.* 34 (5), 525–527. doi:10.1038/nbt.3519

Dukes, J. D., Whitley, P., and Chalmers, A. D. (2011). The MDCK variety pack: Choosing the right strain. *BMC Cell Biol.* 12 (1), 43. doi:10.1186/1471-2121-12-43/TABLES/2

Essandoh, K., Philippe, J. M., Jenkins, P. M., and Brody, M. J. (2020). Palmitoylation: A fatty regulator of myocardial electrophysiology. *Front. Physiology* 11, 108. doi:10.3389/fphys.2020.00108

Fhu, C. W., and Ali, A. (2021). Protein lipidation by palmitoylation and myristoylation in cancer. *Front. Cell Dev. Biol.* 9, 673647. doi:10.3389/FCELL.2021.673647

Fraser, N. J. (2019) Therapeutic targeting of protein S-acylation for the treatment of disease. doi:10.1042/BST20190707

Garcia-Alonso, L., Iorio, F., Matchan, A., Fonseca, N., Jaaks, P., Peat, G., et al. (2017). Transcription factor activities enhance markers of drug sensitivity in cancer. *Cancer Res.* 78 (3), 769–780. doi:10.1158/0008-5472.CAN-17-1679

Genzel, Y. (2015). Designing cell lines for viral vaccine production: Where do we stand? *Biotechnol. J.* 10 (5), 728–740. doi:10.1002/BIOT.201400388

Ghandi, M., Huang, F. W., Jané-Valbuena, J., Kryukov, G. V., Lo, C. C., and McDonald, E. R. (2019). Next-generation characterization of the cancer cell line Encyclopedia. *Nature* 569 (7757), 503–508. doi:10.1038/s41586-019-1186-3

Globa, A. K., and Bamji, S. X. (2017). Protein palmitoylation in the development and plasticity of neuronal connections. *Curr. Opin. Neurobiol.* 45, 210–220. doi:10.1016/j.conb.2017.02.016

Gonzalez-Nicolini, V., and Fussenegger, M. (2005). *In vitro* assays for anticancer drug discovery - a novel approach based on engineered mammalian cell lines. *Anti-Cancer Drugs* 16, 223–228. doi:10.1097/00001813-200503000-00001

Graham, F. L., Smiley, J., Russell, W. C., and NaiRn, R. (1977). Characteristics of a human cell line transformed by DNA from human adenovirus type 5. *J. General Virology* 36 (1), 59–74. doi:10.1099/0022-1317-36-1-59

Grüner, B. M., Schulze, C. J., Yang, D., Ogasawara, D., Dix, M. M., Rogers, Z. N., et al. (2016). An *in vivo* multiplexed small-molecule screening platform. *Nat. Methods* 13 (10), 883–889. doi:10.1038/nmeth.3992

Hou, Y. J., Okuda, K., Edwards, C. E., Martinez, D. R., Asakura, T., Dinnon, K. H., et al. (2020). SARS-CoV-2 reverse genetics reveals a variable infection gradient in the respiratory tract. *Cell* 182 (2), 429–446. doi:10.1016/j.cell.2020.05.042

Ji, B., and Skup, M. (2021). Roles of palmitoylation in structural long-term synaptic plasticity. *Mol. Brain* 14 (1), 1–27. doi:10.1186/s13041-020-00717-y

Karlsson, M., Zhang, C., Mear, L., Zhong, W., Digre, A., Katona, B., et al. (2021). A single–cell type transcriptomics map of human tissues. *Sci. Adv.* 7 (31), eabh2169. doi:10.1126/sciadv.abh2169

Khan, K. H. (2013). Gene expression in mammalian cells and its applications. *Adv. Pharm. Bull.* 3 (2), 257–263. doi:10.5681/apb.2013.042

Ko, P., and Dixon, S. J. (2018). Protein palmitoylation and cancer. *EMBO Rep.* 19 (10), e46666. doi:10.15252/EMBR.201846666

Kumar, S., Sarma, P., Kaur, H., Prajapat, M., Bhattacharyya, A., Avti, P., et al. (2021). Clinically relevant cell culture models and their significance in isolation, pathogenesis, vaccine development, repurposing and screening of new drugs for SARS-CoV-2: A systematic review. *Tissue Cell* 70, 101497. doi:10.1016/J.TICE.2021.101497

Li, X., Shen, L., Xu, Z., Liu, W., and Xu, J. (2022). Protein palmitoylation modification during viral infection and detection methods of palmitoylated proteins. *Front. Cell. Infect. Microbiol.* 12, 821596. doi:10.3389/fcimb.2022.821596

Lin, D. T. S., Davis, N. G., and Conibear, E. (2017). Targeting the Ras palmitoylation/depalmitoylation cycle in cancer. *Biochem. Soc. Trans.* 45 (4), 913–921. doi:10.1042/BST20160303

Lin, H. (2021). Protein cysteine palmitoylation in immunity and inflammation. *FEBS J.* 288, 7043–7059. doi:10.1111/febs.15728

Lobo, S. (2019). "Protein palmitoylation in cancer," in *Unravelling cancer signaling pathways: A multidisciplinary approach* (Springer Singapore), 57–87. doi:10.1007/978-981-32-9816-3_3/TABLES/1

Main, A., and Fuller, W. (2022). Protein S-palmitoylation: Advances and challenges in studying a therapeutically important lipid modification. *FEBS J.* 289 (4), 861–882. doi:10.1111/FEBS.15781

Malgapo, M. I. P., and Linder, M. E. (2021). Substrate recruitment by zDHHC protein acyltransferases. *Open Biol.* 11 (4), 210026. doi:10.1098/rsob.210026

Matt, L., Karam, K., Dhrubajyoti, C., and Johannes, W. H. (2019). Role of palmitoylation of postsynaptic proteins in promoting synaptic plasticity. *Front. Mol. Neurosci.* 12, 8. doi:10.3389/fnmol.2019.00008

Max, D., Manuela, H., Ines, V., and Martin, S. S. (2009). High expression of the evolutionarily conserved α/β hydrolase domain containing 6 (ABHD6) in Ewing tumors. *Cancer Sci.* 100 (12), 2383–2389. doi:10.1111/J.1349-7006.2009.01347.X

Mesquita, F. S., Abrami, L., Sergeeva, O., Turelli, P., Qing, E., Kunz, B., et al. (2021). S-acylation controls SARS-CoV-2 membrane lipid organization and enhances infectivity. *Dev. Cell* 56 (20), 2790–2807. e8. doi:10.1016/j.devcel.2021.09.016

Nusinow, D. P., John, S., Mahmoud, G., Christopher, M. R., Robert McDonald, E., Marian, K., et al. (2020). Quantitative proteomics of the cancer cell line Encyclopedia. *Cell* 180 (2), 387–402. e16. doi:10.1016/J.CELL.2019.12.023

Picco, G., Elisabeth, D. C., Luz Garcia, A., Fiona, M. B., Emanuel, G., Graham, B., et al. (2019). Functional linkage of gene fusions to cancer cell fitness assessed by pharmacological and CRISPR-Cas9 screening. *Nat. Commun.* 10 (1), 2198. doi:10.1038/s41467-019-09940-1

Puthenveetil, R., Gómez-Navarro, N., and Banerjee, A. (2022). Access and utilization of long chain fatty acyl-CoA by zDHHC protein acyltransferases. *Curr. Opin. Struct. Biol.* 77, 102463. doi:10.1016/J.SBI.2022.102463

Puthenveetil, R., Lun, C. M., Murphy, R. E., Healy, L. B., Vilmen, G., Christenson, E. T., et al. (2021). S-acylation of SARS-CoV-2 spike protein: Mechanistic dissection, *in vitro* reconstitution and role in viral infectivity. *J. Biol. Chem.* 279 (4), 101112. doi:10.1016/j.jbc.2021.101112

Qu, M., Zhou, X., Wang, X., and Li, H. (2021). Lipid-induced s-palmitoylation as a vital regulator of cell signaling and disease development. *Int. J. Biol. Sci.* 17, 4223–4237. doi:10.7150/ijbs.64046

Ramadan, A. A., Mayilsamy, K., McGill, A. R., Ghosh, A., Giulianotti, M. A., Donow, H. M., et al. (2022). Identification of SARS-CoV-2 spike palmitoylation inhibitors that results in release of attenuated virus with reduced infectivity. *Viruses* 14 (3), 531. doi:10.3390/v14030531

Robinot, R., Hubert, M., de Melo, G. D., Lazarini, F., Bruel, T., Smith, N., et al. (2021). SARS-CoV-2 infection induces the dedifferentiation of multiciliated cells and impairs mucociliary clearance. *Nat. Commun.* 12 (1), 4354. doi:10.1038/s41467-021-24521-x

Salaun, C., Takizawa, H., Galindo, A., Munro, K. R., McLellan, J., and Sugimoto, I. (2022). Development of a novel high-throughput screen for the identification of new inhibitors of protein S-acylation. *J. Biol. Chem.* 298 (10), 102469. doi:10.1016/J.JBC.2022.102469

Salaun, C., Locatelli, C., Zmuda, F., Cabrera Gonzalez, J., and Chamberlain, L. H. (2020). Accessory proteins of the zDHHC family of S-acylation enzymes. *J. Cell Sci.* 133 (22), jcs251819. doi:10.1242/jcs.251819

Solis, G. P., Arghavan, K., Laurence, A., Jana, V., Cecilia, A., Gisou van der Goot, F., et al. (2022). Local and substrate-specific S-palmitoylation determines subcellular localization of Gαo. *Nat. Commun.* 13 (1), 1–21. doi:10.1038/s41467-022-29685-8

Verma, A., Verma, M., and Singh, A. (2020). "Animal tissue culture principles and applications," in *Animal biotechnology: Models in discovery and translation*, 269–293. doi:10.1016/B978-0-12-811710-1.00012-4

Vogel, C., and Marcotte, E. M. (2012). Insights into the regulation of protein abundance from proteomic and transcriptomic analyses. *Nat. Rev. Genet.* 13 (4), 227–232. doi:10.1038/nrg3185

Westerink, R. H. S., and Ewing, A. G. (2008). The PC12 cell as model for neurosecretion. *Acta Physiol.* 192, 273–285. doi:10.1111/j.1748-1716.2007.01805.x

Wild, A. R., Hogg, P. W., Flibotte, S., Nasseri, G. G., Hollman, R. B., Abazari, D., et al. (2022). Exploring the expression patterns of palmitoylating and de-palmitoylating enzymes in the mouse brain using the curated RNA-seq database BrainPalmSeq. *eLife* 11, e75804. doi:10.7554/ELIFE.75804

Won, S. J., Cheung See Kit, M., and Martin, B. R. (2018). Protein depalmitoylases. *Crit. Rev. Biochem. Mol. Biol.* 53 (1), 83–98. doi:10.1080/10409238.2017.1409191

Woodley, K. T., and Collins, M. O. (2021). Regulation and function of the palmitoyl-acyltransferase ZDHHC5. *FEBS J.* 288 (23), 6623–6634. doi:10.1111/FEBS.15709

Wu, Z., Zhang, Z., Wang, X., Zhang, J., Ren, C., Li, Y., et al. (2021). Palmitoylation of SARS-CoV-2 S protein is essential for viral infectivity. *Signal Transduct. Target. Ther.* 6, 231. doi:10.1038/s41392-021-00651-y

Yeste-Velasco, M., Linder, M. E., and Lu, Y. J. (2015). Protein S-palmitoylation and cancer. *Biochimica Biophysica Acta - Rev. Cancer* 1856 (1), 107–120. doi:10.1016/j.bbcan.2015.06.004

Zaręba-Kozioł, M., Figiel, I., Bartkowiak-Kaczmarek, A., and Wlodarczyk, J. (2018). Insights into protein S-palmitoylation in synaptic plasticity and neurological disorders: Potential and limitations of methods for detection and analysis. *Front. Mol. Neurosci.* 11, 175. doi:10.3389/fnmol.2018.00175

Zhang, Y., Qin, Z., Sun, W., Chu, F., and Zhou, F. (2021). Function of protein S-palmitoylation in immunity and immune-related diseases. *Front. Immunol.* 12, 661202. doi:10.3389/fimmu.2021.661202

frontiers | Frontiers in Physiology

TYPE Methods
PUBLISHED 21 February 2023
DOI 10.3389/fphys.2023.1063247

OPEN ACCESS

EDITED BY
Rebeca M. Mejias Estevez,
Sevilla University, Spain

REVIEWED BY
Stefano Brigidi,
The University of Utah, United States
Luke Chamberlain,
University of Strathclyde, United Kingdom

*CORRESPONDENCE
Eric Witze,
ewitze@upenn.edu

SPECIALTY SECTION
This article was submitted to Lipid and Fatty Acid Research, a section of the journal Frontiers in Physiology

RECEIVED 06 October 2022
ACCEPTED 06 February 2023
PUBLISHED 21 February 2023

CITATION
Schek N, Lee J-Y, Burslem GM and Witze E (2023), Chemical probe mediated visualization of protein S-palmitoylation in patient tissue samples.
Front. Physiol. 14:1063247.
doi: 10.3389/fphys.2023.1063247

Chemical probe mediated visualization of protein S-palmitoylation in patient tissue samples

Nancy Schek[1,2], Jia-Ying Lee[1,2], George M. Burslem[1,2,3] and Eric Witze[1,2,4]*

[1]Department of Cancer Biology, Philadelphia, PA, United States, [2]Perelman School of Medicine, University of Pennsylvania, Philadelphia, PA, United States, [3]Department of Biochemistry and Biophysics, Philadelphia, PA, United States, [4]Abramson Family Cancer Research Institute, Philadelphia, PA, United States

While protein palmitoylation has been studied for decades, our understanding of its clinical importance is minimal compared to other post translational modifications. As a result of the inherent challenges preventing the production of antibodies to palmitoylated epitopes we are unable to correlate levels of protein palmitoylation in biopsied tissues at a meaningful resolution. The most common method for detecting palmitoylated proteins without metabolic labelling is through chemical labeling of palmitoylated cysteines with the acyl-biotinyl exchange (ABE) assay. We have adapted the ABE assay to detect protein palmitoylation in formalin fixed paraffin embedded (FFPE) tissue sections. The assay is sufficient to detect subcellular regions of cells with increased labeling which indicates areas enriched in palmitoylated proteins. To visualize specific palmitoylated proteins in both cultured cells and in FFPE preserved tissue arrays we have integrated the ABE assay with a proximity ligation assay (ABE-PLA). Our findings demonstrate for the first time that FFPE preserved tissues can be labelled with unique chemical probes to detect either areas enriched in palmitoylated proteins or the localization of specific palmitoylated proteins using our ABE-PLA methodology.

KEYWORDS

palmitoylation, cancer, signaling, chemical probe, EGFR

Introduction

Chemical probes enable detection of the chemical reactivity of proteins and enable activity-based proteomics screens to identify reactive proteins in cell lysates and potential drug binding sites on proteins (Bak et al., 2019), (Adam et al., 2002). However, methods to determine the spatial localization of the reactive form of the protein in intact cells under specific environmental conditions and more importantly in patient tissue samples are still lacking (Lu and Fang, 2020). An essential application for chemical probe labeling is in detecting protein modifications that are not recognized by conventional antibody-based methods and require chemical labeling of the modified residue. For example, S-palmitoylation is a common protein modification, but its physiological and disease importance is still poorly understood since it is difficult to directly measure protein palmitoylation in disease tissues. While an antibody to palmitoylated postsynaptic scaffold protein PSD-95 has been reported, the hydrophobic properties of palmitate have

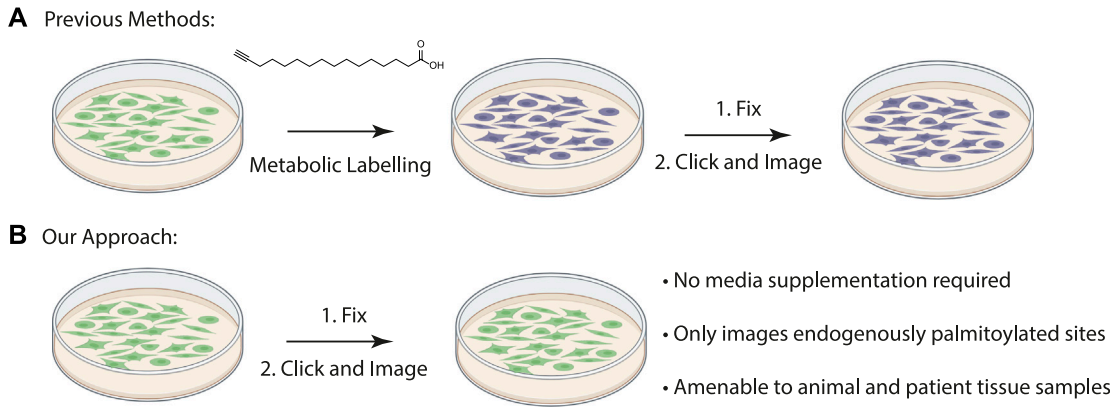

FIGURE 1
(A) Schematic of previously described procedure for visualizing palmitoylated proteins by metabolic labeling of cultured cells with palmitic acid alkyne. **(B)** New method to visualize palmitoylated proteins without metabolic labeling.

hindered production of antibodies which are typically used to correlate PTMs like phosphorylation and acetylation with disease state in patient samples thus new chemical biology approaches are required (Fukata et al., 2013; Main and Fuller, 2022).

Duolink proximity ligation assay generates a fluorescent signal when the two antibodies are within 40 nM from each other (Fredriksson et al., 2002). Previously proximity ligation assays have been used to visualize specific palmitoylated proteins in cells by metabolically labeling cultured cells with palmitic acid alkyne followed by Cu(II) mediated azide alkyne cycloaddition (CuAAC) Oregon green-azide (Figure 1A) (Rostovtsev et al., 2002; Tornøe et al., 2002; Gao and Hannoush, 2016). Protein specific antibodies are used to label the target protein and Oregon Green is detected with anti-Oregon Green antibodies. This method allowed for the first time the visualization of subcellular localization of the O-palmitoylated proteins hedgehog and Wnt as well as S-palmitoylated Ras, but its use is limited to cultured cells that can be metabolically labelled (Gao and Hannoush, 2016). Visualizing palmitoylated proteins in patient samples requires methods free of metabolic label detection that have yet to be described.

The acyl-biotinyl exchange (ABE) assay is a method for detecting palmitoylated proteins in cell lysates which uses cysteine reactive probes to label palmitoylated cysteine residues (Drisdel and Green, 2004). The free cysteine thiols are blocked with n-ethylmaleimide (NEM) after which palmitate is removed with hydroxylamine and the revealed free cysteine residues are labeled with a thiol reactive agent such as iodoacetamide-biotin or biotin-HPDP (N-[6-(biotinamido) hexyl]-3'-(2′-pyridyldithio) propionamide) (Figure 1B). The advantage to this method is that unlike metabolic labeling with click-based probes the ABE is amenable to detecting proteins in formalin-fixed, paraffin-embedded (FFPE) patient samples. An assay for measuring palmitoylation of specific proteins in patient samples will allow direct correlations between palmitoylation levels of specific proteins and disease state. As a first step we asked if chemical probes react with target proteins in FFPE prepared tissue samples allowing us to detect S-palmitoylated proteins. We sought to extend this method to the chemical labeling of specific proteins through the integration of the ABE assay with a proximity ligation assay (PLA) in FFPE tissue samples and thus demonstrate for the first time that chemical imaging of PTMs is possible in fixed tissues.

Results and discussion

Fluorescent imaging of ABE labeled palmitoylated proteins in FFPE samples

In the ABE assay free cysteine thiols are blocked with N-ethylmaleimide (NEM) to prevent non-specific labeling of unpalmitoylated cysteines with the cysteine reactive probe. We anticipated that the main challenge in labeling FFPE tissues is saturating the free thiols with NEM in the highly crosslinked fixed tissues to reduce non-specific background labeling and therefore carefully optimized a procedure for efficient ABE in fixed tissues.

We reasoned that for the ABE assay to detect palmitoylation of unidentified proteins in FFPE samples we would need to identify cells enriched in palmitoylated proteins. Using FFPE mouse lung serial sections as a model system, we prepared them as for standard immunohistochemistry. Sections were treated with xylene to solubilize and remove all paraffin, followed by washes in ethanol to remove the xylene, and then in decreasing concentrations of ethanol for rehydration. In order to remove protein crosslinks formed by formaldehyde treatment, which can mask antibody-binding epitopes, sections were heated to 100°C (Kim et al., 2016). Immediately following this antigen retrieval step, slides were blocked with buffer containing NEM in 150 mM NaCl, 50 mM HEPES pH 7.4, 5 mM EDTA (ABE buffer), and 0.2% Triton X-100. After washing with ABE buffer, slides were incubated with 1.5 M solution of hydroxylamine in ABE buffer and as a negative control a slide containing an adjacent serial tissue section was incubated in the same buffer without hydroxylamine. Slides were washed followed by incubation in buffer containing biotin-HPDP (N-[6-(biotinamido) hexyl]-3'-(2′-pyridyldithio)

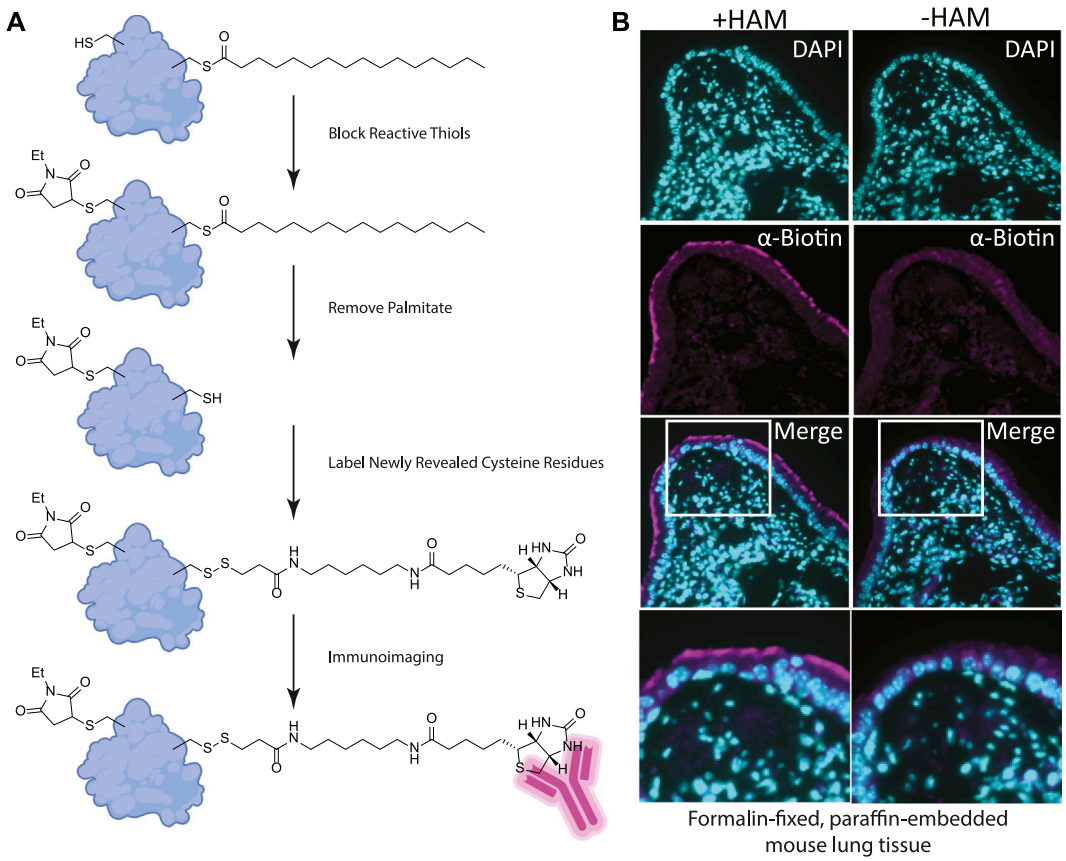

FIGURE 2
(A) Label free method for detecting palmitoylated proteins to be used on FFPE prepared tissues. 1) NEM treatment blocks free thiol groups on all proteins. 2, 3) Hydroxylamine (HAM) treatment removes palmitate and biotin-HPDP reacts with the revealed thiol. As a negative control HAM is omitted, but biotin-HPDP is still added. 4) The biotin is recognized with an anti-biotin antibody and detected with a fluorescently conjugated secondary antibody. **(B)** FFPE tissue sections of mouse lung airway. The hydroxylamine treated (+HAM) samples reveal anti-biotin antibody labelling at the apical surface of the airway cells (magenta). In an adjacent section of the same sample where hydroxylamine (HAM-) has been omitted the labeling is absent. DNA is stained with DAPI (cyan).

propionamide). The slides were blocked in 5% bovine serum albumin (BSA) dissolved in tris buffered saline with 0.5% Tween 20 (TBST) followed by an overnight incubation with anti-biotin antibody (Figures 1B, 2A). After incubation with fluorescently tagged secondary antibody slides were mounted and imaged by widefield fluorescence microscopy.

Building on our previous studies examining the function of palmitoylated EGFR in lung adenocarcinoma, we chose to use FFPE mouse lung sections to develop the assay (Kharbanda et al., 2020). Gratifyingly, using our optimized procedure, we observed a distinct subcellular labelling pattern in the airway of the lungs with the anti-biotin antibody restricted to the apical surface of the airway epithelial cells (Figure 2B). This labeling was absent in the -hydroxylamine control, validating our method was labeling only palmitoylated (thioester) proteins that are enriched at the apical surface of the airway cells. The results of this *in situ* labeling method are consistent with the important role protein palmitoylation plays in establishing or maintaining polarized structures in cells. Ciliated cells line the airway and a dual-lipidation signal consisting of myristoylation followed by palmitoylation functions as a cilia protein targeting signal (Kumeta et al., 2018). Whilst this demonstrates the chemical probe-based imaging of cysteine palmitoylation in FFPE tissue for the first time, it lacks protein level specificity which is crucial for understanding PTMs. To address this liability, we next asked if this method could be adapted to detect specific proteins that react with the cysteine reactive probe *via* proximity ligation assays.

ABE-PLA assay in cultured cells

The proximity ligation assay (PLA) generates a signal when the antibody to the labelled cysteine is within 40 nm of the binding site of the protein specific antibody. With the success in detecting protein palmitoylation in FFPE tissues with the ABE assay we sought to integrate the ABE assay with the PLA to detect specific palmitoylated proteins without the need for metabolic labelling, which is impossible in human tissues. Our lab has previously found that the epidermal growth factor receptor (EGFR) is palmitoylated in multiple cancer cell lines and blocking EGFR palmitoylation blocks Kras driven lung tumor growth in animal models (Runkle et al., 2016; Kharbanda et al., 2020). We showed previously that EGF

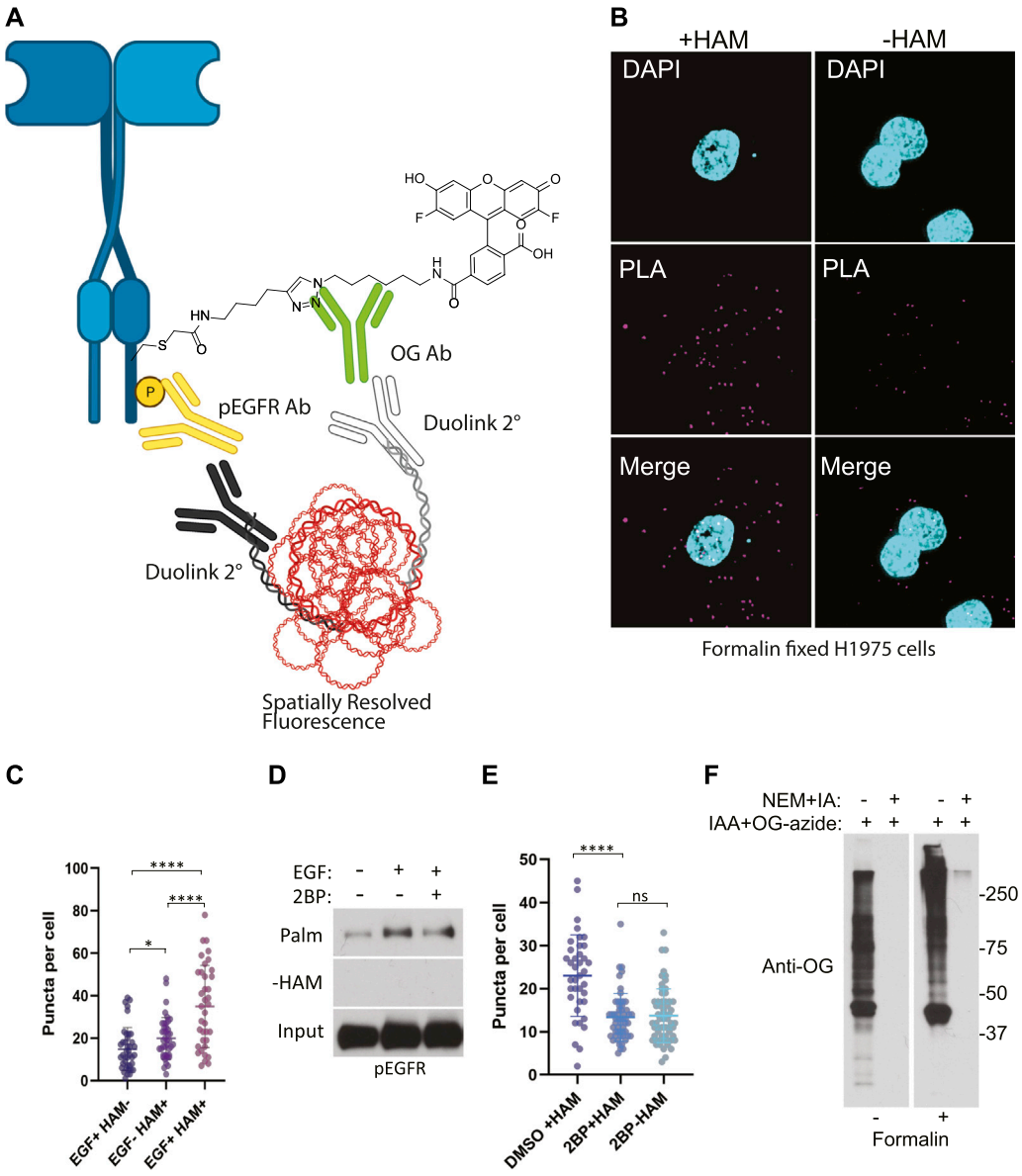

FIGURE 3
(A) Schematic of the ABE-PLA showing method for detecting palmitoylated EGFR in formalin fixed cells processed with the ABE protocol and palmitate was replaced with Oregon green-iodoacetamide. Following the ABE, the proximity ligation assay was performed using primary antibodies to EGFR-phosphoTyrosine1068 and the Oregon Green (OG) label. Samples were incubated with species specific secondary PLA antibodies followed by annealing to single stranded circular DNA which is then amplified with DNA polymerase. The amplified DNA is detected with fluorescently tagged complimentary oligonucleotides and is visualized as fluorescent puncta. **(B)** Formalin fixed H1975 lung cancer cells processed with the ABE-PLA. PLA signal is detected in cells treated with hydroxylamine (+HAM). Omitting hydroxylamine reduces the number of puncta in the negative control (-HAM) DAPI is shown in cyan and PLA signal in magenta. **(C)** Puncta per cell were quantified in all conditions (Unpaired Student's *T*-test: EGF + HAM-vs. EGF + HAM+ ****$p < 0.0001$; EGF + HAM + vs. EGF- HAM+ ****$p < 0.0001$; EGF + HAM-vs EGF-HAM+ *$p < 0.05$). Total Number of Cells = 119. **(D)** Standard ABE assay of H1975 cells treated with 100 nM 2-bromopalmitate followed by 100 ng/mL EGF stimulation. **(E)** Quantitation of ABE-PLA puncta of cells with or without 2-bromopalmitate with and without EGF stimulation. [Unpaired Student's *T*-test: DMSO + HAM + vs. 2BP + HAM+ ****$p < 0.0001$; 2BP + HAM + vs. 2BP + HAM-not significant (ns)]. Total Number of Cells = 153. **(F)** Validation of efficient cysteine blocking and labelling of formalin fixed cells *in vitro*.

stimulation increases palmitoylation of phosphorylated EGFR (Runkle et al., 2016). We therefore sought to visualize palmitoylated phosphorylated EGFR in H1975 lung cancer cell lines which harbor activating mutations in EGFR.

We stimulated H1975 cells with EGF for 5 min to increase EGFR auto-phosphorylation compared to non-treated controls. Cells were then fixed in formalin containing NEM and permeabilized with ABE buffer containing 0.2% Triton X-100 and NEM to quench reactive cysteines as before. Coverslips were washed in 0.2% Triton X-100 ABE buffer and incubated in the same buffer containing iodoacetamide which we found during extensive optimization was necessary to block free cysteine residues and reduce non-

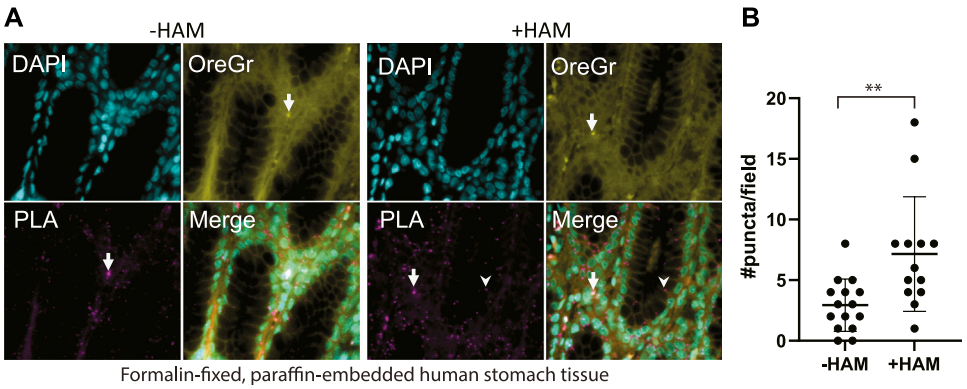

FIGURE 4
(A) Multi-organ tissue arrays were treated with the ABE-PLA. DNA was labelled with DAPI (cyan). Cytosolic staining of cells demarcating the cell boundary is visible in the Oregon Green channel (Yellow). Hydroxylamine treatment increases the number of magenta PLA puncta (arrowhead) compared to the -hydroxylamine control in the epithelia of the stomach tissue samples. **(B)** Quantification of the number of puncta per field in two sample cores. Puncta that are both magenta and yellow (arrow) were not counted. Error bars are standard deviation. (Unpaired Student's *T*-test ***p*-value = 0.0045).

specific cysteine labeling. Coverslips were washed and incubated with or without HAM followed by incubation with the cysteine reactive label. Initial samples were prepared using biotin-HPDP however, labelling with biotin resulted in high background which could be due to presence of endogenous biotin. Subsequently, we switched to using iodoacetamide-alkyne followed by Cu(II) mediated azide alkyne cycloaddition (CuAAC) with Oregon Green-azide to label the HAM unmasked reactive cysteine residues. Coverslips were then incubated with antibodies to Oregon Green and to phospho-EGFR (Y1068). Finally, the proximity ligation assay (Duolink) was performed by the addition of oligo labelled secondary antibodies followed by a polymerase and fluorescently labelled complementary oligos, and coverslips were mounted and imaged (Figure 3A). The PLA puncta were present in multiple focal planes and therefore a z-series of images were captured allowing quantification of puncta throughout the cell. This results in fluorescent puncta which are significantly more numerous in cells stimulated with EGF and appear in a HAM dependent fashion, thus indicating that they result specifically from EGFR bearing both palmitoylation and phosphorylation PTMs (Figures 3B, C).

While the omission of hydroxylamine significantly decreased the number of puncta compared to the hydroxylamine treated sample, we further confirmed that the puncta are representative of palmitoylated EGFR by treating cells with the palmitoylation inhibitor 2-bromopalmitate (2BP). Using the conventional ABE assay, we detect an increase in palmitoylated EGFR phosphorylated on tyrosine 1068 upon EGF treatment (Figure 3D). Treatment of the cells with 100 nM 2BP decreased palmitoylated EGFR compared to DMSO control but is still higher than -HAM control. Using the ABE-PLA assay, treatment of cells with 2BP reduced the number of puncta compared to cells treated with the vehicle control (Figure 3E). Omitting hydroxylamine did not reduce the number of puncta below cells treated with 2BP (Figure 3E).

Finally, we asked if the puncta present in the -HAM control were the result of incomplete blocking of thiols due to chemical fixation. Cultured cells were fixed with formalin containing NEM, followed by blocking cysteine residues with NEM and IA in ABE buffer while attached to the tissue culture plate. The cells were then washed and treated with iodoacetamide alkyne which was then conjugated to Oregon Green-azide. The cells were then harvested, and lysate was analyzed by SDS-PAGE followed by immunoblotting with anti-Oregon Green antibodies. We found that treating cells with formalin resulted in a very minor increase in background in the NEM/IA treated condition compared to cells that were not formalin fixed (Figure 3F). We concluded that the background PLA puncta were not likely caused by residual free thiols. The background in the fixed cells could be the result of non-specific binding of the labeling agents that may require additional blocking strategies to further reduce the background.

Having developed a novel chemical probe-based imaging approach (ABE-PLA) for palmitoylation, we sought to apply it to the imaging of disease relevant human samples.

ABE-PLA in FFPE tissue arrays

We applied our optimized ABE-PLA approach to tissue arrays of multiple human tissue types. In the tissue sections we observed two distinct types of PLA positive puncta. Both types of puncta were present in the HAM treated, as well as the untreated negative control. One type was characterized by magenta PLA probe puncta that appeared in the absence of Oregon Green puncta (Figure 4A, arrowhead). The second type had equally high levels of Oregon Green and magenta PLA probe signal (Figure 4A, arrow). We reasoned that if the signal was the amplified product of the PLA, then the PLA signal should be markedly stronger than any non-specific Oregon Green labeling. We therefore only scored a magenta punctum to be PLA positive if the Oregon Green did not form a

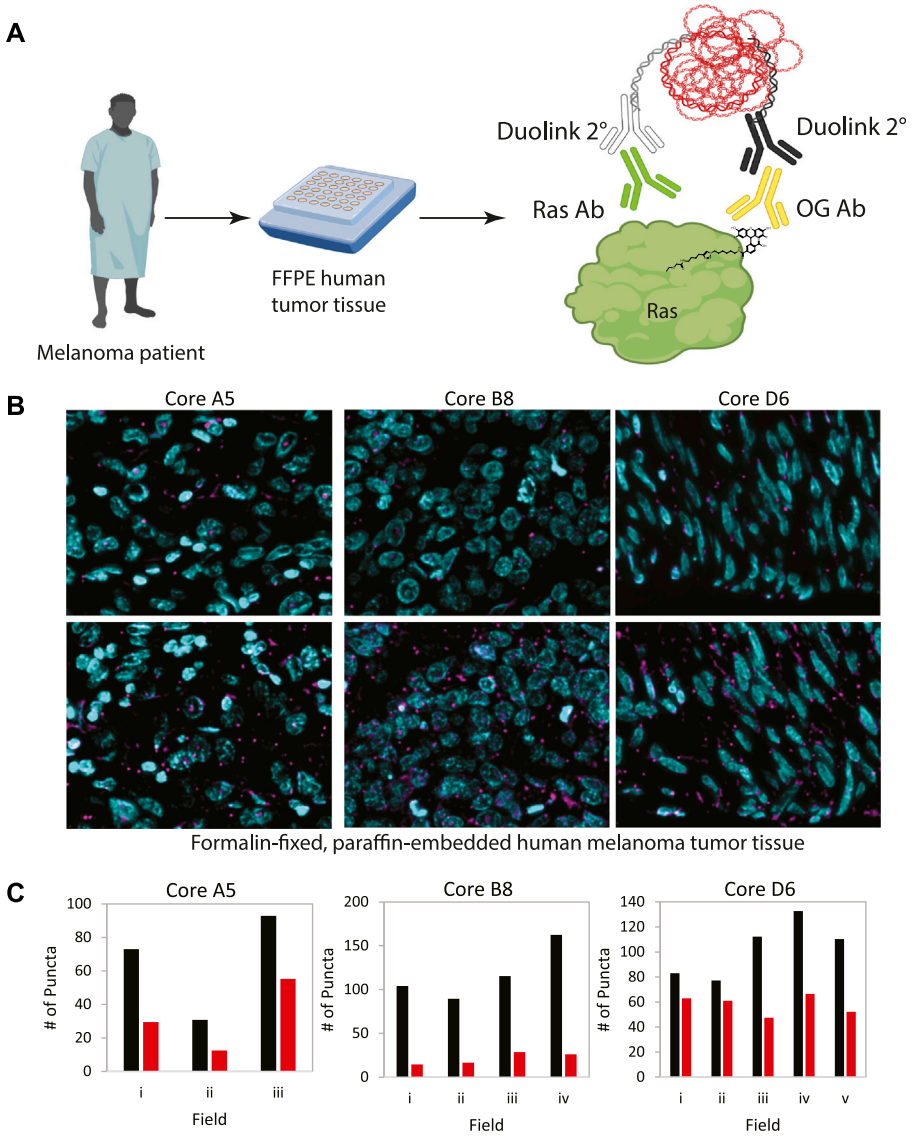

FIGURE 5
(A) Workflow for analysis of patient tumor samples on a tissue array. **(B)** Melanoma tissue arrays were treated with the ABE-PLA. Three different samples are shown. **(C)** The number of PLA puncta (magenta) per field were counted in the -HAM control slide and the +HAM treated slide. Variation in background signal (-HAM, Red bars) between samples and between fields within a sample are shown compared to the ABE generated signal (+HAM, Black bars). Statistical significance of the difference between−HAM and + HAM samples: A5 p-value = 0.049, B8 p-value = 0.006, D6 p-value = 0.015; Paired Student's T-test.

punctum at the same site. In stomach tissues we observed clear PLA specific puncta that increase in the HAM treated sample (Figure 4B).

In order to demonstrate the generalizability of this approach to visualize other palmitoylated proteins using the ABE-PLA, we next examined the localization of palmitoylated Ras in human patient melanoma arrays (Figure 5A). While only a small fraction of EGFR is palmitoylated, HRas and Nras rapidly cycle between palmitoylated and unpalmitoylated states which shuttles Ras between the plasma membrane and Golgi apparatus (Dudler and Gelb, 1996; Rocks et al., 2005). Nras is particularly relevant to melanoma as Nras mutations are found in 15%–20% of melanoma tumors (Curtin et al., 2005; Jakob et al., 2012). We therefore examined Ras palmitoylation in melanoma tumor arrays using a pan-Ras antibody. The array of strictly melanoma samples allowed comparison between multiple tumor samples with varying levels of ABE-PLA puncta formation (Figure 5B). Quantifying the number of puncta in 3–5 different fields in each tumor core provides insight into variations in background signal in the -HAM control relative to the +HAM treated samples (Figure 5C). We found there were different levels of background between samples as well as within the same sample. For example, sample B8 had very low background (less than 25 puncta/field) relative to the high levels produced by HAM treatment (100–150 puncta/field). In contrast, the background for sample A5 ranged from 30–50 puncta/field, with HAM treated samples generally having 2-fold more puncta than the background.

Finally, in core D6 two -HAM fields had about 60 puncta per field with the corresponding fields in the +HAM sample showing only a modest increase (75–80 puncta/field) over the negative control, whereas other fields had similar background levels but much higher puncta in the +HAM condition (120–140 puncta per field). The variability in background between samples could be caused by differences in the quality of individual tissue samples and how samples were handled prior to array preparation.

Overall, these results provide a tantalizing glimpse of the potential for using the ABE-PLA assay as a diagnostic tool or as a biomarker for palmitoylation inhibitors *in vivo* in future, highlighting the power of chemical imaging approaches.

Conclusion

These are the first reported methods for detecting S-palmitoylated proteins in FFPE tissue samples. Moreover, specific protein targets can also be detected by performing PLA after the ABE assay. Using this strategy, we were able to detect palmitoylated phospho-EGFR in multiple tissue types and palmitoylated Ras in human melanoma samples. This approach could not only provide important biological insights but also represents a conceptual advance in chemical proteomics and PTM specific imaging. The applications of using chemical probes in tissue arrays go far beyond detecting specific palmitoylated proteins. One can envision myriad applications from drug target engagement studies in clinical trials to unbiased screening of chemical probes across tissues to identify tissue specific liabilities.

Our previous studies found that EGF stimulation increased EGFR palmitoylation and that palmitoylated EGFR was also phosphorylated on tyrosine 1068 (Runkle et al., 2016). Detection of palmitoylated EGFR by the conventional ABE assay required cells from a 60 mm dish (approximately 1×10^6 cells) (Fredriksson et al., 2002; Runkle et al., 2016). The ABE-PLA assay can detect EGFR palmitoylation in single cells and detects the increase in dually palmitoylated-phosphorylated EGFR in response to EGF stimulation. Further work is needed to establish the range limits of the assay in detecting palmitoylation before it can be used to correlate palmitoylation of specific proteins with disease state or outcome. Our future work will focus on extending this approach to additional post-translational modifications with additional chemistries and multiplexing multiple PTMs within the same tissue arrays.

Materials and methods

Cell culture and drug treatment

NCI-H1975 cells (ATCC) were maintained in RPMI media supplemented with 10% FBS. Cells were treated with 2-bromopalmitate (100 nM) overnight for approximately 15 h.

ABE on cultured cells

NCI-H1975 cells were serum starved in serum free media for 2 h followed by EGF (100 ng/mL) stimulation for 5 min. Cells were processed using the ABE assay as described previously (Runkle et al., 2016).

ABE on FFPE mouse tissues

Formalin fixed paraffin embedded mouse tissue samples were sectioned at 4-µm thickness and deparaffinized in xylene and rehydrated with a series of ethanol washes. Antigen retrieval was performed using edetic acid buffer (Electron Microscopy Sciences #62706–11). Immediately after antigen retrieval, samples were incubated in in NEM buffer (50 mM NEM, 150 mM NaCl, 50 mM Hepes pH 7.4, and 10 mM EDTA, and 0.2%Triton X-100) at room temperature, in the dark, for 30 min. The arrays were then washed and re-incubated in fresh NEM buffer overnight at 4°C. Samples were washed in ABE buffer (150 mM NaCl, 50 mM Hepes pH 7.4, and 10 mM EDTA, and 0.2%Triton X-100), then incubated at room temperature for 2 h in the same buffer, with or without 0.7 M hydroxylamine. After washing in ABE buffer, samples were incubated with ABE buffer with added biotin-HPDP (10 µM) for 1 h at room temperature. Samples were then washed in TBST buffer (50 mM Tris HCl pH 7.4, 150 mM NaCl, 0.05% Tween) and then blocked with 5% BSA dissolved in TBST for 1 h at room temperature. Samples were stained by overnight incubation at 4°C with antibodies against biotin (1:1000; abcam), followed by detection with Alexa 488 nm and Alexa 594 nm conjugated secondary antibodies (1:1000; Life Technologies). Coverslips were mounted and DNA staining done using Fluoro-Gel II (EMS #17985–50).

ABE-PLA on cultured cells

NCI-H1975 cells were grown on 18 mm cover glasses in a 12-well tissue culture plate for 24 h followed by incubation in serum free RPMI media for 80 min, stimulated with EGF (100 ng/mL) for 5 min, then fixed in 10% neutral buffered formalin (Fisher Scientific 23–245-685) containing 50 mM NEM for 30 min at room temperature. After washing in Dulbecco's phosphate-buffered saline (DPBS), cells were permeabilized in NEM buffer for 30 min at room temperature. Samples were washed in ABE buffer followed by incubation in 4 mM iodoacetamide in ABE buffer for 30 min in the dark at room temperature. After washing, this treatment was repeated with fresh iodoacetamide buffer overnight at 4°C. Samples were washed with ABE buffer, then treated with 0.7 M hydroxylamine as described above for 1 h, then washed once with ABE buffer followed by three washes with DPBS. Next, the samples were incubated in a solution of 10 µM iodoacetamide-alkyne in DPBS for 1 h at room temperature in the dark, followed by washing in DPBS. Cells were then treated with a click reaction mix containing 25 µM OG 488 Azide (Click Chemistry Tools #1264–1), 1 mM CuSO4, and 1 mM tris(2-carboxyethyl) phosphine (TCEP) in DPBS for 45–60 min at room temperature in the dark. After washing in DPBS, proteins were blocked with Duolink blocking solution for 1 hour at 37°C. Incubation with primary antibodies specific for phosphorylated EGFR (Y1068) (Novus Biologicals #MAB3570) and for fluorescein/OG 488 (Life Technologies A-889) was done overnight at 4°C. The Duolink assay was performed as per manufacturer's protocol with the exception that the amplification time was shortened from 100 min to 60 min.

ABE-PLA on tissue arrays

Human tissue arrays were purchased from US Biomax, Inc. Slides were heated at 60°C for 4 min, then deparaffinized and rehydrated as described above. Antigen retrieval was performed using citrate buffer (Electron Microscopy Sciences #62706–13). Immediately after antigen retrieval, the tissue array was washed with ABE buffer and then incubated in NEM buffer at 37°C for 30 min. Next, samples were washed three times in ABE buffer, followed by incubation in ABE buffer with added iodoacetamide (4 mM) overnight in the dark at room temperature. The arrays were washed and then re-incubated with fresh ABE buffer containing 4 mM iodoacetamide for 30 min. The samples were washed three times in ABE buffer followed by 1 hour incubation with ABE buffer containing hydroxylamine (0.7 M) as described above. The samples were washed one time in ABE buffer and the 1-h hydroxylamine step was repeated. The arrays were then washed once in ABE buffer followed by three washes in DPBS. The samples were incubated with DPBS containing 10 μM iodoacetamide-alkyne, followed by incubation with click reaction mix as described above, then blocked in 5% BSA in TBST. The remaining steps were as previously described for ABE-PLA on cultured cells. Ras was detected in melanoma tissues using a pan-Ras monoclonal antibody (Invitrogen #PIMA1012X).

Microscopy

The samples were imaged using a Leica DMI600B widefield epifluorescent microscope. Images were captured using a Hamamatsu Orca-R2 digital camera. A z-series of focal planes were captured and deconvolved using Leica LAS X 3D-deconvolution software.

Statistics

Statistical analyses were performed using Prism software (GraphPad Prism 9). Experiments are reported as mean ± sd as noted in the legends. Data were analyzed using a 2-tailed Student's *t*-test for comparison between 2 data sets. A *p*-value of less than 0.05 was considered statistically significant.

Data availability statement

The raw data supporting the conclusion of this article will be made available by the authors, without undue reservation.

Author contributions

EW planned all experiments, interpreted results and prepared the manuscript. NS carried out all experiments and interpreted results. GB planned experiments, helped trouble shoot, prepared figures and prepared the manuscript.

Funding

This project is funded, in part, under a grant with the Pennsylvania Department of Health. The Department specifically disclaims responsibility for any analyses, interpretations or conclusion. J-YL was funded by the training grant T32CA115299.

Conflict of interest

The authors declare that the research was conducted in the absence of any commercial or financial relationships that could be construed as a potential conflict of interest.

Publisher's note

References

Adam, G. C., Sorensen, E. J., and Cravatt, B. F. (2002). Chemical strategies for functional proteomics. *Mol. Cell. Proteomics* 1 (10), 781–790. doi:10.1074/mcp.R200006-MCP200

Bak, D. W., Bechtel, T. J., Falco, J. A., and Weerapana, E. (2019). Cysteine reactivity across the sub-cellular universe. *Curr. Opin. Chem. Biol.* 48, 96–105. doi:10.1016/j.cbpa.2018.11.002

Curtin, J. A., Fridlyand, J., Kageshita, T., Patel, H. N., Busam, K. J., Kutzner, H., et al. (2005). Distinct sets of genetic alterations in melanoma. *N. Engl. J. Med.* 353 (20), 2135–2147. doi:10.1056/NEJMoa050092

Drisdel, R. C., and Green, W. N. (2004). Labeling and quantifying sites of protein palmitoylation. *BioTechniques* 36 (2), 276–285. doi:10.2144/04362RR02

Dudler, T., and Gelb, M. H. (1996). Palmitoylation of ha-ras facilitates membrane binding, activation of downstream effectors, and meiotic maturation in Xenopus oocytes (*). *J. Biol. Chem.* 271 (19), 11541–11547. doi:10.1074/jbc.271.19.11541

Fredriksson, S., Gullberg, M., Jarvius, J., Olsson, C., Pietras, K., Gústafsdóttir, S. M., et al. (2002). Protein detection using proximity-dependent DNA ligation assays. *Nat. Biotechnol.* 20 (5), 473–477. doi:10.1038/nbt0502-473

Fukata, Y., Dimitrov, A., Boncompain, G., Vielemeyer, O., Perez, F., and Fukata, M. (2013). Local palmitoylation cycles define activity-regulated postsynaptic subdomains. *J. Cell Biol.* 202 (1), 145–161. doi:10.1083/jcb.201302071

Gao, X., and Hannoush, R. N. (2016). Visualizing Wnt palmitoylation in single cells. *Methods Mol. Biol. Clifton N. J.* 1481, 1–9. doi:10.1007/978-1-4939-6393-5_1

Jakob, J. A., Bassett, R. L., Ng, C. S., Curry, J. L., Joseph, R. W., Alvarado, G. C., et al. (2012). NRAS mutation status is an independent prognostic factor in metastatic melanoma. *Cancer* 118 (16), 4014–4023. doi:10.1002/cncr.26724

Kharbanda, A., Walter, D. M., Gudiel, A. A., Schek, N., Feldser, D. M., and Witze, E. S. (2020). Blocking EGFR palmitoylation suppresses PI3K signaling and mutant KRAS lung tumorigenesis. *Sci. Signal.* 13 (621), eaax2364. doi:10.1126/scisignal.aax2364

Kim, S.-W., Roh, J., and Park, C.-S. (2016). Immunohistochemistry for pathologists: Protocols, pitfalls, and tips. *J. Pathol. Transl. Med.* 50 (6), 411–418. doi:10.4132/jptm.2016.08.08

Kumeta, M., Panina, Y., Yamazaki, H., Takeyasu, K., and Yoshimura, S. H. (2018). N-terminal dual lipidation-coupled molecular targeting into the primary cilium. *Genes cells.* 23 (8), 715–723. doi:10.1111/gtc.12603

Lu, H., and Fang, C. (2020). Methodology for detecting protein palmitoylation. *Adv. Exp. Med. Biol.* 1248, 425–430. doi:10.1007/978-981-15-3266-5_17

Main, A., and Fuller, W. (2022). Protein S-palmitoylation: Advances and challenges in studying a therapeutically important Lipid modification. *FEBS J.* 289 (4), 861–882. doi:10.1111/febs.15781

Rocks, O., Peyker, A., Kahms, M., Verveer, P. J., Koerner, C., Lumbierres, M., et al. (2005). An acylation cycle regulates localization and activity of palmitoylated Ras isoforms. *Science* 307 (5716), 1746–1752. doi:10.1126/science.1105654

Rostovtsev, V. V., Green, L. G., Fokin, V. V., and Sharpless, K. B. (2002). A stepwise huisgen cycloaddition process: Copper(I)-Catalyzed regioselective "ligation" of azides and terminal alkynes. *Angew. Chem. Int. Ed. Engl.* 41 (14), 2596–2599. doi:10.1002/1521-3773(20020715)41:14<2596:AID-ANIE2596>3.0.CO;2-4

Runkle, K. B., Kharbanda, A., Stypulkowski, E., Cao, X.-J., Wang, W., Garcia, B. A., et al. (2016). Inhibition of DHHC20-mediated EGFR palmitoylation creates a dependence on EGFR signaling. *Mol. Cell* 62 (3), 385–396. doi:10.1016/j.molcel.2016.04.003

Tornøe, C. W., Christensen, C., and Meldal, M. (2002). Peptidotriazoles on solid phase: [1,2,3]-Triazoles by regiospecific copper(I)-Catalyzed 1,3-dipolar cycloadditions of terminal alkynes to azides. *J. Org. Chem.* 67 (9), 3057–3064. doi:10.1021/jo011148j

frontiers | Frontiers in Physiology

TYPE Original Research
PUBLISHED 23 March 2023
DOI 10.3389/fphys.2023.1167094

OPEN ACCESS

EDITED BY
William Fuller,
University of Glasgow, United Kingdom

REVIEWED BY
Mark Oliver Collins,
The University of Sheffield,
United Kingdom
Jennifer Greaves,
Coventry University, United Kingdom

*CORRESPONDENCE
Toshimitsu Kawate,
toshi.kawate@cornell.edu
Maurine E. Linder,
mel237@cornell.edu

SPECIALTY SECTION
This article was submitted to Lipid and Fatty Acid Research, a section of the journal Frontiers in Physiology

RECEIVED 15 February 2023
ACCEPTED 13 March 2023
PUBLISHED 23 March 2023

CITATION
Nguyen PL, Greentree WK, Kawate T and Linder ME (2023), GCP16 stabilizes the DHHC9 subfamily of protein acyltransferases through a conserved C-terminal cysteine motif.
Front. Physiol. 14:1167094.
doi: 10.3389/fphys.2023.1167094

GCP16 stabilizes the DHHC9 subfamily of protein acyltransferases through a conserved C-terminal cysteine motif

Phillip L. Nguyen, Wendy K. Greentree, Toshimitsu Kawate* and Maurine E. Linder*

Department of Molecular Medicine, Cornell University, Ithaca, NY, United States

Protein *S*-acylation is a reversible lipid post-translational modification that allows dynamic regulation of processes such as protein stability, membrane association, and localization. Palmitoyltransferase ZDHHC9 (DHHC9) is one of the 23 human DHHC acyltransferases that catalyze protein *S*-acylation. Dysregulation of DHHC9 is associated with X-linked intellectual disability and increased epilepsy risk. Interestingly, activation of DHHC9 requires an accessory protein—GCP16. However, the exact role of GCP16 and the prevalence of a requirement for accessory proteins among other DHHC proteins remain unclear. Here, we report that one role of GCP16 is to stabilize DHHC9 by preventing its aggregation through formation of a protein complex. Using a combination of size-exclusion chromatography and palmitoyl acyltransferase assays, we demonstrate that only properly folded DHHC9-GCP16 complex is enzymatically active *in vitro*. Additionally, the ZDHHC9 mutations linked to X-linked intellectual disability result in reduced protein stability and DHHC9-GCP16 complex formation. Notably, we discovered that the C-terminal cysteine motif (CCM) that is conserved among the DHHC9 subfamily (DHHC14, -18, -5, and -8) is required for DHHC9 and GCP16 complex formation and activity *in vitro*. Co-expression of GCP16 with DHHCs containing the CCM improves DHHC protein stability. Like DHHC9, DHHC14 and DHHC18 require GCP16 for their enzymatic activity. Furthermore, GOLGA7B, an accessory protein with 75% sequence identity to GCP16, improves protein stability of DHHC5 and DHHC8, but not the other members of the DHHC9 subfamily, suggesting selectivity in accessory protein interactions. Our study supports a broader role for GCP16 and GOLGA7B in the function of human DHHCs.

KEYWORDS

post-translational modification (PTM), protein acylation, protein stability, protein complex, membrane protein, Golga7b, GOLGA7

Introduction

Cells utilize a wide array of protein post-translational modifications to extend the chemical properties of the 20 standard amino acids, dramatically expanding the ways in which proteins regulate cellular processes. In eukaryotes, protein *S*-acylation is the process in which long-chain fatty acids (with palmitate being the most prevalent) are added to proteins at cysteine residues *via* a labile thioester linkage. While the fundamental chemical effect of *S*-acylation is a local increase in protein hydrophobicity, the reversible nature of *S*-acylation can result in a range of consequences such as dynamic changes in protein stability, membrane affinity and binding, and protein trafficking and localization (Chamberlain and Shipston, 2015).

DHHC protein acyltransferases (PATs) are the enzymes responsible for catalyzing the addition of long-chain fatty acids to substrate proteins (Gottlieb and Linder, 2017). Members of the DHHC family are conserved throughout eukaryotic evolution, with 5-7 members in yeast and as many as 23 members in humans (Mitchell et al., 2006; Zhang et al., 2013). Furthermore, dysregulation of DHHC proteins is associated with a myriad of diseases that include cancers and neurodegenerative disorders (Young et al., 2012; Yeste-Velasco et al., 2015). DHHC proteins are aptly named for the conserved Asp-His-His-Cys motif required for their PAT activity, which is embedded in a cysteine-rich domain (CRD) involved in zinc ion binding (Gonzalez Montoro et al., 2013; Gottlieb et al., 2015; Rana et al., 2018). Additionally, all DHHC proteins are multipass transmembrane proteins, with subfamily diversity stemming from varied membrane topologies, sequence divergence in the amino- and carboxy-terminal regions, and protein partner requirements (Lobo et al., 2002; Swarthout et al., 2005; Salaun et al., 2020). It is generally accepted that DHHC proteins utilize a two-step ping-pong mechanism (Mitchell et al., 2010; Jennings and Linder, 2012). First, the DHHC protein uses acyl-CoA as an acyl group donor to form an acyl-enzyme intermediate; then, the acyl group is transferred from the DHHC cysteine to the target cysteine on the protein substrate. While this mechanism is thought to be shared by all DHHCs, a majority of mechanistic and structural insight has been determined from studies on one subfamily of DHHCs that include DHHC2, 3, and 20 (Jennings and Linder, 2012; Gottlieb et al., 2015; Rana et al., 2018). Thus, this leaves many other DHHC proteins underrepresented, and potentially subfamily-specific insights are yet to be discovered.

In humans, DHHC9 was the first DHHC protein discovered to require an accessory protein—GCP16 (also known as GOLGA7)—for its enzymatic function, based on sequence homology with the yeast Ras PAT Erf2-Erf4 (Swarthout et al., 2005). DHHC9 colocalizes with and requires GCP16 for its enzymatic activity (Swarthout et al., 2005). GCP16 is a small peripheral membrane protein that is itself palmitoylated, and it associates with proteins involved in vesicular transport at the Golgi (Ohta et al., 2003). However, it is unclear what the exact role of GCP16 is in DHHC9 protein regulation, how GCP16 supports DHHC PAT activity, and to what extent GCP16 or a related protein GOLGA7B function within the DHHC protein family. Furthermore, loss of function mutations in ZDHHC9 result in X-linked intellectual disability (XLID), with affected individuals displaying neurodevelopmental delay, seizures, and facial dysmorphism (Raymond et al., 2007; Baker et al., 2015; Han et al., 2017; Schirwani et al., 2018). Despite the strong clinical relevance, the molecular basis for how ZDHHC9 mutations affect DHHC9 protein function and regulation is incompletely understood. In this study, we sought to better understand the role of GCP16 in the DHHC9-GCP16 PAT complex, and we investigated the stability of the DHHC9 disease mutants. We also assessed whether the accessory proteins GCP16 and GOLG7B associate more widely with members of the DHHC protein family.

Materials and methods

Construction of expression plasmids

Amino acid sequences were obtained from the UniProt database for the following human proteins: DHHC9 (Q9Y397), DHHC14 (Q8IZN3), DHHC18 (Q9NUE0), DHHC5 (Q8VDZ4), DHHC8 (Q9ULC8), DHHC3 (Q9NYG2), DHHC20 (Q5W0Z9), and GCP16 (Q7F5G4). Genes were synthesized based on protein sequences (GenScript, Piscataway, NJ). The plasmid encoding GOLGA7B was obtained from the Harvard Medical School Plasmid repository. All DHHC genes used were PCR amplified to exclude the start methionine and to include flanking BamHI/XhoI sites. Similarly, GOLGA7 and GOLGA7B were amplified to exclude the start methionine and to include AgeI/NotI sites. All genes were subcloned *via* standard molecular biology techniques into their respective expression vectors. Any mutations were generated *via* quick change PCR.

For FSEC, we used a dual mammalian expression vector modified from the pIRES-EGFP RK6 vector provided by M. Mayer, National Institutes of Health, Bethesda, MD. The vector encoded a start methionine followed by mNeonGreen (A0A1S4NYF2), a BamHI/XhoI insertion site, an EMCV internal ribosomal entry site (IRES), an AgeI/NotI insertion site, and a stop codon. DHHC genes were incorporated using BamHI/XhoI, and GOLGA7 or GOLGA7B genes were incorporated using AgeI/NotI.

For protein purification, genes were subcloned into a modified pFastBac baculovirus expression vector (Thermo Fisher Scientific, Waltham, MA). DHHC9, DHHC9 TM (C283S, C284S, and C288S), and GCP16 were encoded to express a C-terminal strep-tag. DHHC14 and DHHC18 were encoded to express an N-terminal strep-tag.

Fluorescence-detection size-exclusion chromatography

Human embryonic kidney (HEK) cells were maintained in DMEM medium (Thermo Fisher Scientific) supplemented with 10% fetal bovine serum (Atlanta Biologicals, Flowery Branch, GA), and 10 μg/ml gentamicin (Thermo Fisher Scientific) per manufacturer's instructions. For FSEC experiments, cells were transfected at 80–95% confluency with 2.5 μg of expression plasmid using jetPRIME transfection reagent per the manufacturer's instructions. Cells were grown at 37°C for 48 h.

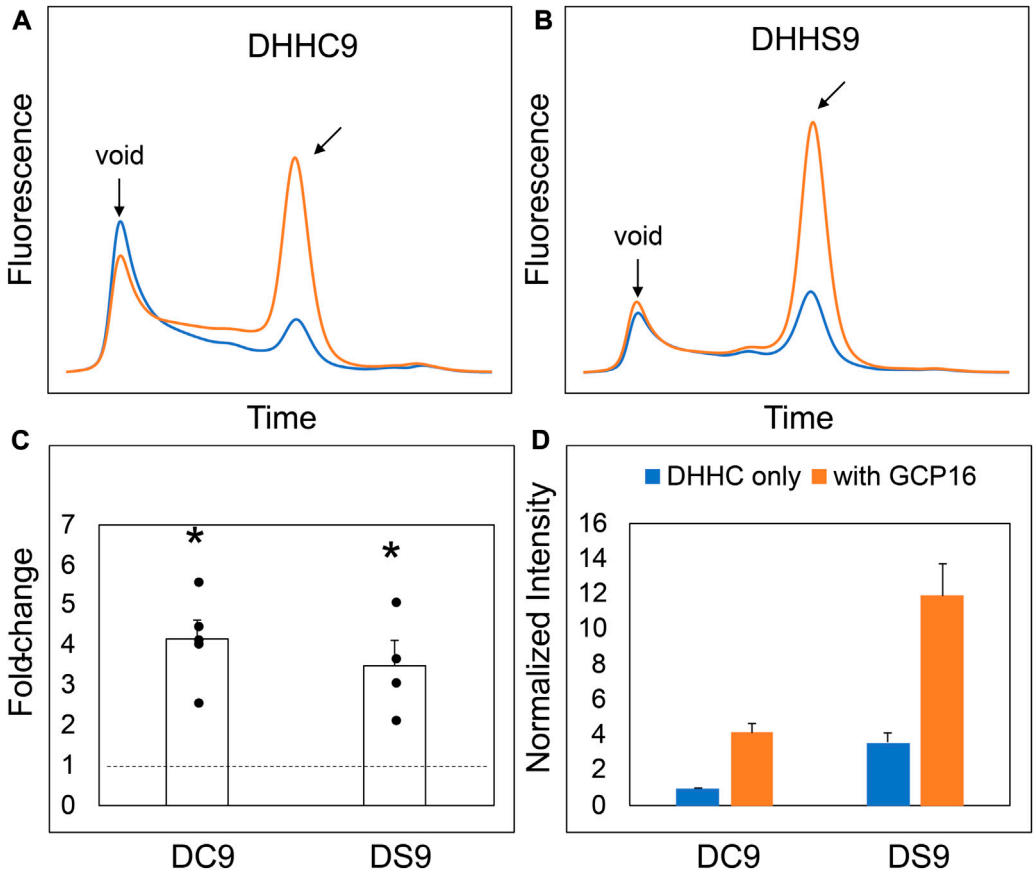

FIGURE 1
DHHC9 is Stabilized by Co-expression with GCP16 Independent of the Catalytic Cysteine. FSEC profiles of **(A)** DHHC9 and **(B)** DHHS9. HEK cells were transfected with vector to express the indicated constructs without or with GCP16 co-expression shown with blue and orange traces, respectively. Cells were solubilized in a DDM-containing buffer, and the cleared lysate was analyzed *via* SEC detected by fluorescence at excitation and emission wavelengths of 480 nm and 508 nm, respectively. Arrows indicate the void retention time and the approximate retention time corresponding to the size of DHHC9. Bar charts showing **(C)** average fold-change and **(D)** normalized max intensity upon GCP16 co-expression for the indicated constructs at n ≥ 4 experiments. Normalization was done as described in the experimental procedures. The dashed line indicates a fold-change of 1. Error bars represent the standard error of the mean. Asterisks indicate a significance for *p*-value <0.05 determined by two-tailed *t*-test against the null hypothesis.

TABLE 1 DHHC9 Constructs. Table denoting the generated constructs (left) and amino acid changes (right).

Construct	Description
DHHC9 (full-length)	
DHHC9 N2	Δ2-19
DHHC9 C1	Δ301-364
DHHC9 C2	Δ278-364
DHHC9 N2C1	Δ2-19, Δ301-364
DHHC9 N2C1.1	Δ2-19, Δ295-364
DHHC N2C29 N2C1.2	Δ2-19, Δ289-364
DHHC9 N2C1.3	Δ2-19, Δ282-364
DHHC9	Δ2-19, Δ278-364

The media was aspirated, cells were suspended and washed in 2 ml of cold PBS, and samples were lysed in 150 μL of lysis buffer (1x PBS, 1% n-Dodecyl-β-D-Maltopyranoside (DDM), 1x Roche protease inhibitor) for 30 min at 4 °C with rotation. Whole-cell lysates were cleared by centrifugation in an Eppendorf FA-45–24-11 rotor at 21,000 x g for 10 min at 4°C. The supernatant was further cleared by ultracentrifugation in a TLA 100.3 rotor at 265,000 x g for 20 min. An aliquot (50 μL) was applied onto a Superdex 200 Increase 10/300 GL column pre-equilibrated with running buffer (1x PBS, 0.5 mM DDM). The eluate from the SEC column was passed through a fluorometer set to excitation, 480nm, and emission, 508 nm.

For quantitation, peak intensities in arbitrary fluorescence units were obtained at the expected DHHC peak for every profile. For DHHC9 constructs, values were normalized to either DHHC9 or DHHC9 N2C1, depending on the set of constructs tested for that given day. Data sets across different days were then normalized to DHHC9 globally. For experiments that included other DHHCs, i.e., DHHC14, 18, 5, 8, 3, and 20, raw intensity values were used without normalization. For statistical analysis, we used two-tailed t-tests assuming unequal variances against the null-hypothesis that GCP16/GOLGA7B co-expression has no significant effect on DHHC protein signal.

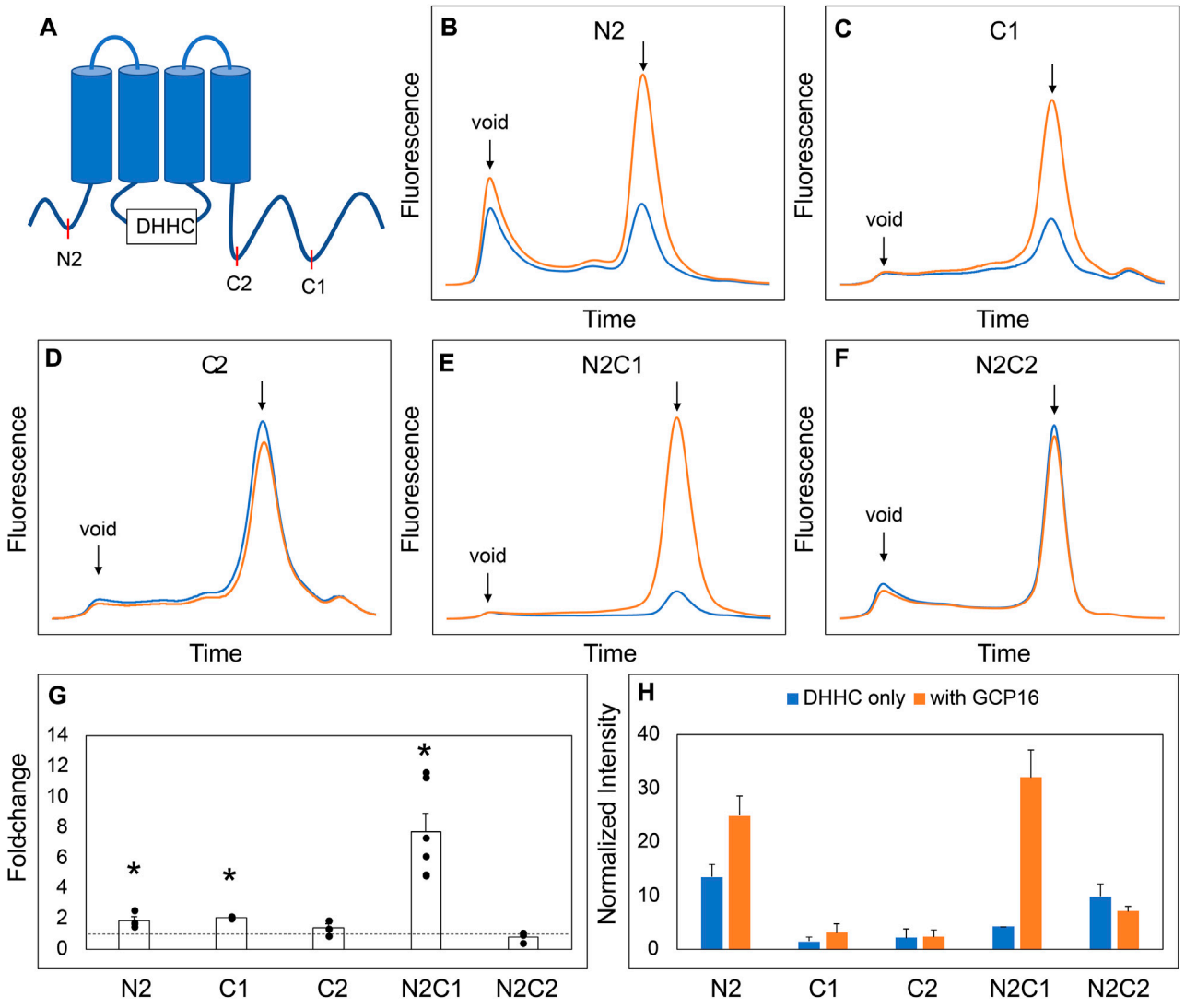

FIGURE 2
A Conserved Region in the DHHC9 CTD is Required for GCP16-mediated Stabilization. **(A)** Cartoon depicting the tested DHHC9 truncations. **(B–F)** FSEC profiles for the indicated constructs. HEK cells were transfected with DHHC9 without (blue) or with GCP16 (orange). Cells were solubilized in a DDM-containing buffer, and the cleared lysate was analyzed by FSEC. Bar charts showing **(G)** average fold-change and **(H)** normalized max intensity upon GCP16 co-expression for the indicated constructs at n ≥ 3 experiments. Error bars represent the standard error of the mean. Asterisks indicate a significance for *p*-value <0.05 determined by two-tailed *t*-test against the null hypothesis.

Expression and purification of DHHC proteins and DHHC-GCP16 complexes

All constructs were expressed using the Invitrogen Bac-to-Bac® baculovirus-insect cell expression system. Sf9 cells (1–2L) were infected at 2.5—4.0 × 10^6 cells/mL with P2 virus (107–108 PFU/ml, 30 ml/L). Cells were incubated at 27°C for 24 h and moved to 18 °C for an additional 48 h. All purification steps were done on ice or with 4°C buffer unless stated otherwise. Cells were harvested by centrifugation at 2,040 x g and washed with 200 ml of PBS. Cells were solubilized in buffer A (PBS, 15% glycerol, 0.5 mM TCEP, 0.5ug/mL leupeptin, 2ug/mL aprotinin, 0.5ug/mL pepstatin A, and 0.5 mM phenylmethylsulfonyl fluoride) containing 1% DDM w/v at a ratio of 250 mg DDM/g of cells. Solubilization was performed at 4 °C with stirring for 1 hour. Large debris were removed by centrifugation at 12,000 x g. The supernatant was further clarified by ultracentrifugation at 185,000 x g for 45 min to remove remaining insolubilized material. To the supernatant, 2 ml of equilibrated StrepTactin Sepharose High Performance resin (GE Healthcare, Marlborough, MA) was incubated with stirring for 1-h. The resin was collected by centrifugation and transferred to a gravity column (Bio-Rad). The resin was washed with 10 resin bed volumes of wash buffer (buffer A with 0.5 mM DDM) and eluted with elution buffer (buffer A with 2.5 mM desthiobiotin, 0.5 mM DDM). Protein was concentrated using Amicon ultra concentrators. Size exclusion chromatography was done using a Superdex 200 (GE Healthcare) in SEC buffer (150 mM NaCl, 20 mM HEPES pH 7.4, 0.5 mM TCEP, 15% glycerol, 0.5 mM DDM).

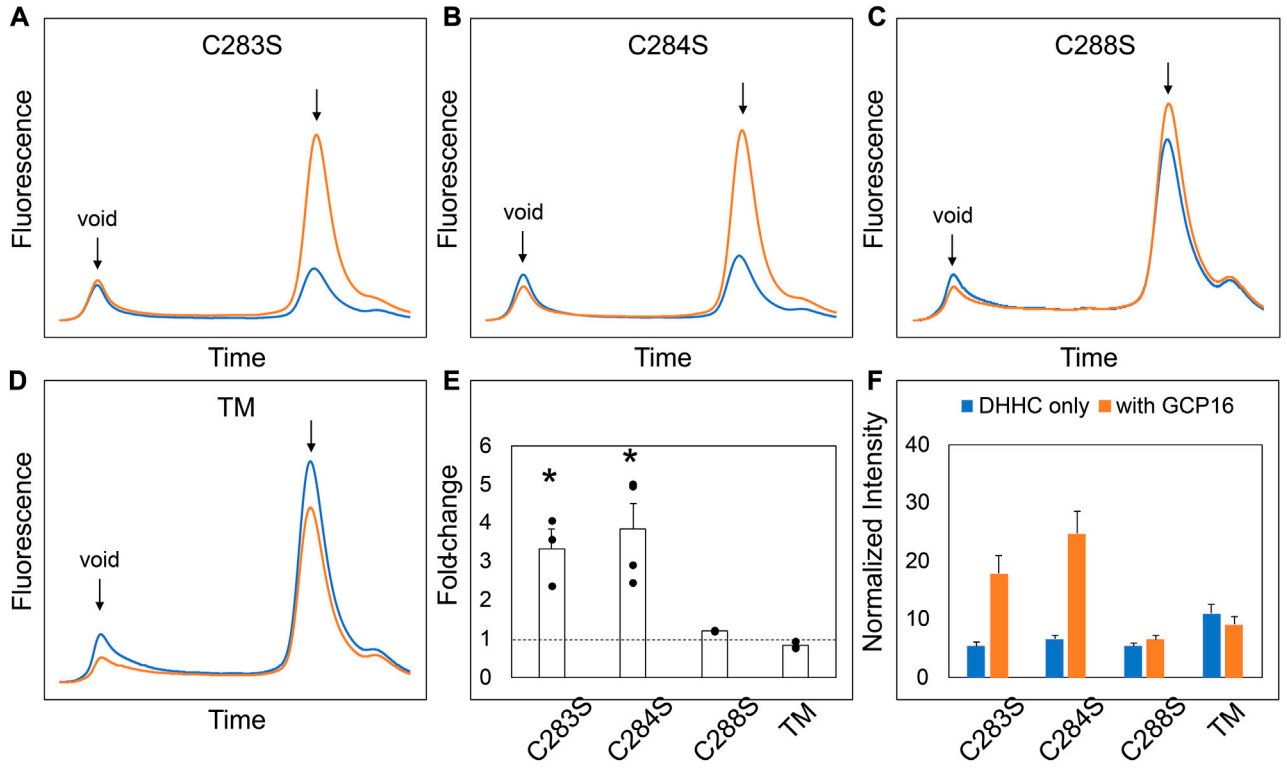

FIGURE 3
Cysteines in the DHHC9 CTD are required for GCP16-mediated Stabilization. **(A–C)** FSEC profiles for the indicated cysteine to serine mutation and **(D)** the triple mutation (TM) in the DHHS9 N2C1 parent construct. HEK cells were transfected with DHHC9 without (blue) or with GCP16 (orange). Cells were solubilized in DDM-containing buffer, and the cleared lysate was analyzed *via* FSEC. Bar charts showing **(E)** average fold-change and **(F)** normalized max intensity upon GCP16 co-expression for the indicated constructs at n ≥ 3 experiments. The dashed line indicates a fold-change of 1. Error bars represent the standard error of the mean. Asterisks indicate a significance for *p*-value <0.05 determined by two-tailed *t*-test against the null hypothesis.

PAT assays

PAT assays were performed immediately following purification and SEC as described previously (Swarthout et al., 2005). Protein concentrations were determined by NanoDrop (Thermo Scientific) using predicted extinction coefficients. Enzyme was diluted to 250 nM in enzyme dilution buffer (50 mM MES pH 6.4, 100 mM NaCl, 10% glycerol, 0.05% DDM, 0.5 mM TCEP). H-Ras (80 μM, purified from insect cells infected with recombinant Baculovirus) was diluted to 10 μM in enzyme dilution buffer. For a 50 μL reaction, the final concentration was 50 nM enzyme, 2 μM H-Ras, 1 μM [^{3}H]-palm-CoA. Each reaction was incubated at room temperature for 10 min. Reactions were quenched in SDS loading dye containing 25 mM TCEP. Samples were split and run on two SDS-PAGE gels in parallel. For fluorography, one gel was exposed to a solution of 1M sodium salicylate, 15% methanol, dried under vacuum for 2 h, and exposed to film for 4–15 days. For liquid scintillation spectroscopy, the gel was stained with Coomassie, H-Ras bands were extracted, and a section of gel around the expected DHHC protein size was extracted. Extracted gel pieces were dissolved in 500 μL Soluene overnight at 37°C. Ultima Gold scintillation fluid (5 ml) was added, and disintegrations per minute (DPM) was measured using a scintillation counter after allowing for stabilization for 8–24 h. For each experiment, we used DHHC20 as a positive control and H-Ras without enzyme to account for non-enzymatic acylation. Background DPM was subtracted from each sample before converting counts to picomoles based on the specific activity of palmitoyl-CoA.

Results

GCP16 stabilizes DHHC9 through a conserved C-terminal cysteine motif

Our initial attempts to express and purify DHHC9 from Sf9 cells were met with low protein yield, reduced purity, and extensive protein aggregation. This was consistent with a previous report that DHHC9 purified without GCP16 resulted in an increased fraction of DHHC9 protein being proteolyzed (Swarthout et al., 2005). Thus, we reasoned that one function of GCP16 is to stabilize DHHC9 and prevent misfolding or aggregation. We used fluorescence-detection size-exclusion chromatography (FSEC) to examine the effect of GCP16 on DHHC9 protein stability in cell lysates (Kawate and Gouaux, 2006). DHHC9 fused with N-terminal mNeonGreen was expressed in HEK293 cells with or without GCP16. We chose to fuse the fluorescent protein to the DHHC9 N-terminus to minimize perturbing its C-terminus, based on previous reports that N-terminal modifications to Erf2 had no effect on its stability and that the C-terminus of DHHC proteins are generally thought

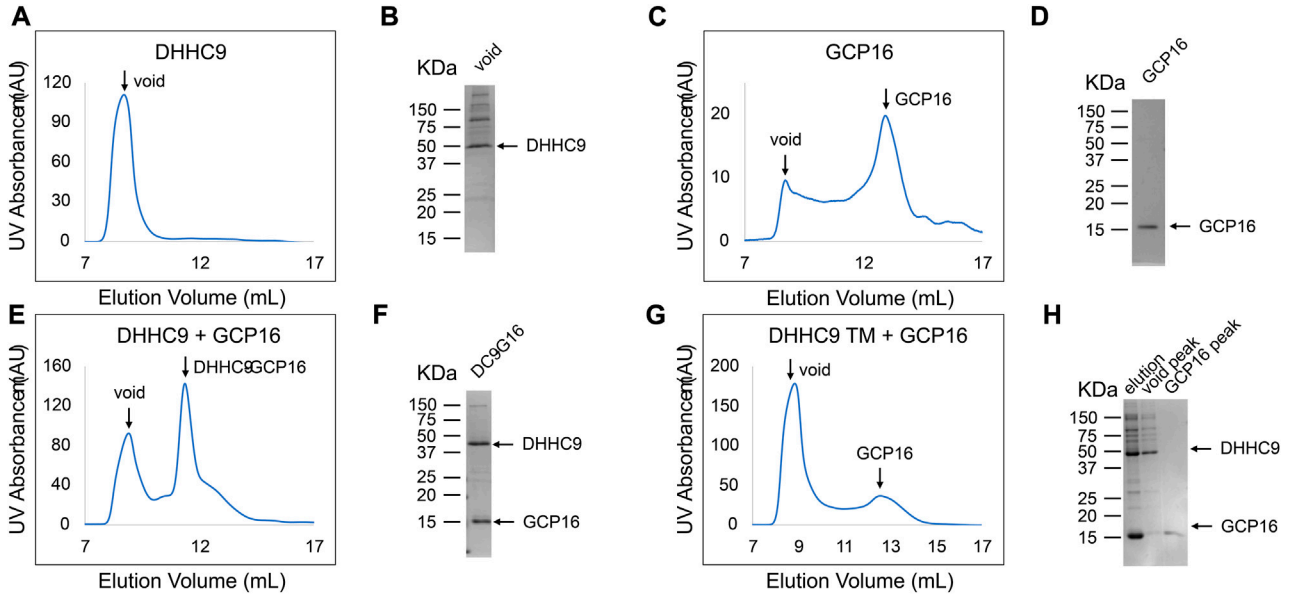

FIGURE 4
DHHC9 CTD Cysteines are Required for Complex Formation with GCP16. Sf9 cells were infected with recombinant baculovirus encoding the indicated variations of the following: DHHC9-strep, DHHC9 with the conserved triple cysteines mutated to serine (DHHC9 TM), or GCP16-strep. Protein was purified *via* strep-affinity purification and SEC as in the experimental procedures. SEC profiles and SDS-PAGE Coomassie analyses for **(A,B)** DHHC9 **(C,D)** GCP16, **(E,F)** the DHHC9-GCP16 complex, and DHHC9-TM co-purified with GCP16 **(G,H)**. Arrows in the SEC profiles correspond to the labeled lanes for the corresponding SDS-PAGE.

to mediate protein-protein interactions (Mitchell et al., 2012; Malgapo and Linder, 2021). Cells were solubilized in a dodecylmaltoside (DDM)-containing buffer, and cleared lysates were applied to a gel-filtration column coupled to a fluorometer to monitor fluorescence (Figure 1). DHHC9 expressed alone showed a prominent void peak characteristic of high-molecular weight protein aggregate and only a minor peak at the expected retention time for a well-folded, monomeric protein (Figure 1A blue trace). By contrast, DHHC9 co-expressed with GCP16 showed improved monodispersity and a 4-fold increase in magnitude (Figure 1A orange trace, C, D). To determine if the GCP16-mediated stabilizing effect is dependent on the catalytic cysteine, we performed the same assay using DHHS9, in which the catalytic cysteine was mutated to serine. Compared to DHHS9 alone, DHHS9 co-expressed with GCP16 showed an almost identical improvement in monodispersity and expression as DHHC9 (Figures 1B–D). These data suggest that DHHC9 is stabilized by GCP16 co-expression, and this effect is not dependent on DHHC9 catalytic activity.

Next, we asked which regions and amino acid residues of DHHC9 are required for the GCP16-mediated stabilizing effect. We used evolutionary conservation to generate combinatorial N- and C-terminal deletions of DHHC9 (Table 1; Supplementary Figure S1) and assessed the effect of GCP16 co-expression for each construct by FSEC (Figure 2). For DHHC9 with N-terminal truncation N2, C-terminal truncation C1, or both, GCP16 co-expression improved protein behavior, similar to the full-length construct (Figures 2B,C,E,G,H). However, for DHHC9 constructs containing truncation C2, GCP16 co-expression showed no significant difference when compared to DHHC9 alone (Figures 2D,F). We observed that some individual truncations alter total levels of DHHC9 detected (Figure 2H). For example, constructs N2 and N2C1 improved DHHC9 protein stability in the absence of GCP16, possibly by removing disordered/aggregation-prone regions of DHHC9 (Figures 2B,E,G,H). Nonetheless, the addition of GCP16 further increased the stabilizing-effect in constructs that included truncation C1. Thus, DHHC9 residues between truncation C1 and C2 are required for GCP16-mediated stabilization.

We next sought to determine the exact residues between DHHC9 C1 and C2 that are required for GCP16-mediated stabilization. We made finer truncations between regions C1 and C2 in the N2C1 background and assayed for the effect of GCP16 co-expression using FSEC (Supplementary Figure S2). Much like the parent construct, truncations C1.1 and C1.2 showed an increase in expression and monodispersity with GCP16 co-expression (Supplementary Figures S2B, S2C, S2E, S2F). However, truncation C1.3 displayed no significant difference whether GCP16 was co-expressed or not (Supplementary Figure S2D, S2E, S2F). Between truncations C1.2 and C1.3, we identified a conserved sequence "CCXXXC" at residues 283–288, which we refer to as the C-terminal cysteine motif (CCM). Given that cysteines may play a role in protein-protein interactions, we tested whether mutation of these CCM cysteines would abolish the stabilizing effect. We generated serine mutants at each individual cysteine in the CCM using the DHHS9 N2C1 background and assessed the effect of GCP16 co-expression on DHHC9 protein (Figure 3). DHHS9 NC21 was used as the parent construct because it gave a more consistent FSEC signal in the absence of GCP16 than that of full-length DHHC9. Mutations C283S and C284S showed a diminished but statistically significant improvement in protein

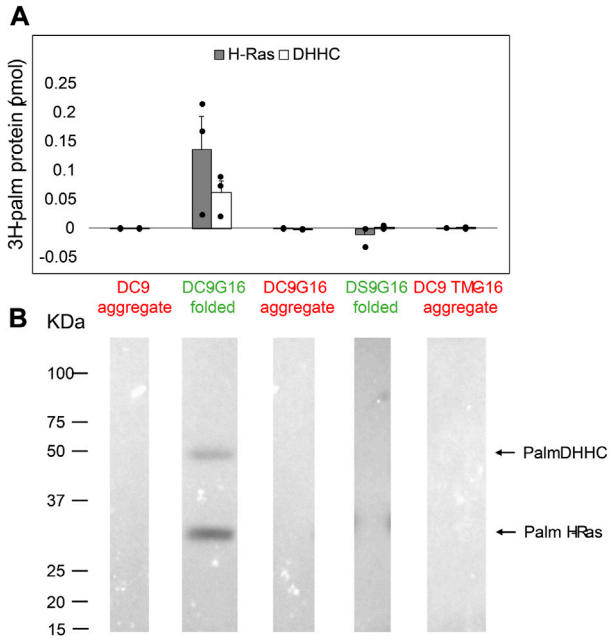

FIGURE 5
DHHC9 Requires Proper Protein Folding for H-Ras Activity. DHHC9 constructs were purified and classified into aggregated (red) or folded (green) states based on their respective SEC profiles. Purified DHHC9 was assayed for activity using H-Ras and [^{3}H]-palmitoyl CoA. Radiolabeled protein was quantified *via* liquid scintillation spectroscopy **(A)** and detected *via* fluorography **(B)**. The *Y*-axis represents picomoles of ^{3}H-labeled protein after subtracting background radiation. Grey bars represent the quantity of labeled H-Ras, and white bars represent the quantity of labeled DHHC protein. Error bars represent the standard error of the mean for n ≥ 2 independent protein preparations. Arrows indicate bands corresponding to radiolabeled DHHC9 and H-Ras.

expression when co-expressed with GCP16 (Figures 3A,B,E,F). Interestingly, C288S or the triple mutations at all three cysteines (TM) showed no effect of GCP16 co-expression on DHHC9 protein quality (Figures 3C–F). Taken together, these data show that DHHC9 protein expression and monodispersity is significantly improved by GCP16 co-expression, and this stabilization effect requires a conserved DHHC9 C-terminal cysteine motif, with cysteine 288 being the most critical.

DHHC9 CCM is required for complex formation with GCP16

While FSEC is an efficient way to probe whether GCP16 expression influences DHHC9 stability, it cannot address whether the two proteins are interacting. To determine if DHHC9 and GCP16 form a complex, we co-expressed these two proteins in Sf9 insect cells, affinity purified, and assessed whether they co-elute in SEC (Figure 4). Across multiple experiments, affinity-purified DHHC9 in the absence of GCP16 consistently eluted at the void volume (Figure 4A). This and the observation that the protein remains impure after tandem affinity chromatography and SEC (Figure 4B), suggested that purified DHHC9 primarily exists as a high molecular weight protein aggregate. GCP16 alone eluted around ~13ml, which was consistent with its molecular size with detergent micelle (Figures 4C, D). When DHHC9 and GCP16 were co-expressed, both proteins co-eluted at a volume of ~11 ml (Figures 4E, F) with a monodispersed peak, supporting that DHHC9-GCP16 exists as a folded complex.

Next, we tested whether the CCM of DHHC9 is required for complex formation with GCP16. We co-purified DHHC9 TM with GCP16 and analyzed the SEC profile. We confirmed by SDS-PAGE that both DHHC9 TM and GCP16 were present in the elution from affinity purification (Figure 4H lane 1). However, the SEC profile exhibited two distinct peaks at the void volume and at ~13 ml (Figure 4G), paralleling what was seen for DHHC9 and GCP16 when purified separately. Furthermore, SDS-PAGE analysis showed enrichment for DHHC9-strep in the fraction corresponding to the void peak and GCP16-strep in the fraction at ~13 ml (Figure 4H lane 2–3). Together, these experiments support that DHHC9 and GCP16 form a complex when co-expressed and co-purified. Furthermore, mutation of the conserved DHHC9 C-terminal cysteines prevents complex formation under these conditions of detergent solubilization.

DHHC9 enzymatic activity for H-Ras correlates with protein folding

Protein *S*-acylation by DHHC proteins occurs *via* a two-step mechanism (Mitchell et al., 2010; Jennings and Linder, 2012). The DHHC protein uses acyl-CoA to form an acyl-enzyme intermediate; then, upon substrate binding, the acyl group is transferred to the target cysteine on the protein substrate. We previously demonstrated that GCP16 increases the equilibrium levels of both autoacylated DHHC9 and its substrate H-Ras *in vitro* (Swarthout et al., 2005). However, it remains unclear whether GCP16 directly affects catalysis, or whether GCP16 simply increases the amount of folded and active DHHC9. Therefore, we purified DHHC9 with or without GCP16 and classified whether the protein was folded or aggregated based on SEC profiles. Immediately following purification and SEC, we assayed PAT activity using H-Ras and [^{3}H]-Palmitoyl-CoA. The folded DHHC9-GCP16 complex exhibited radiolabeling for both H-Ras and autoacylated DHHC9 (Figure 5 lane 2). The observed activity was attributed to the catalytic activity of DHHC9, as catalytically inactive DHHS9 protein failed to show any PAT activity (Figure 5 lane 4). In contrast, the aggregated DHHC9-GCP16 did not exhibit detectable PAT activity (Figure 5 lane 3). Likewise, aggregated DHHC9 purified in the absence of GCP16 exhibited no detectable activity (Figure 5 lane 1). Similarly, DHHC9 TM was unable to form a complex with GCP16 and resulted in only aggregated protein. This aggregated DHHC9 TM exhibited no detectable activity for H-Ras (Figure 5 lane 5). Taken together, these experiments suggest that DHHC9 requires GCP16 for its enzymatic activity. DHHC9 co-purified with GCP16 results in enrichment of a folded DHHC9 state, which is enzymatically active. However, when GCP16 is absent or when DHHC9 is unable to form a complex with GCP16 (as is the case with DHHC9 TM), essentially all DHHC9 protein is aggregated and exhibits no detectable PAT activity for H-Ras.

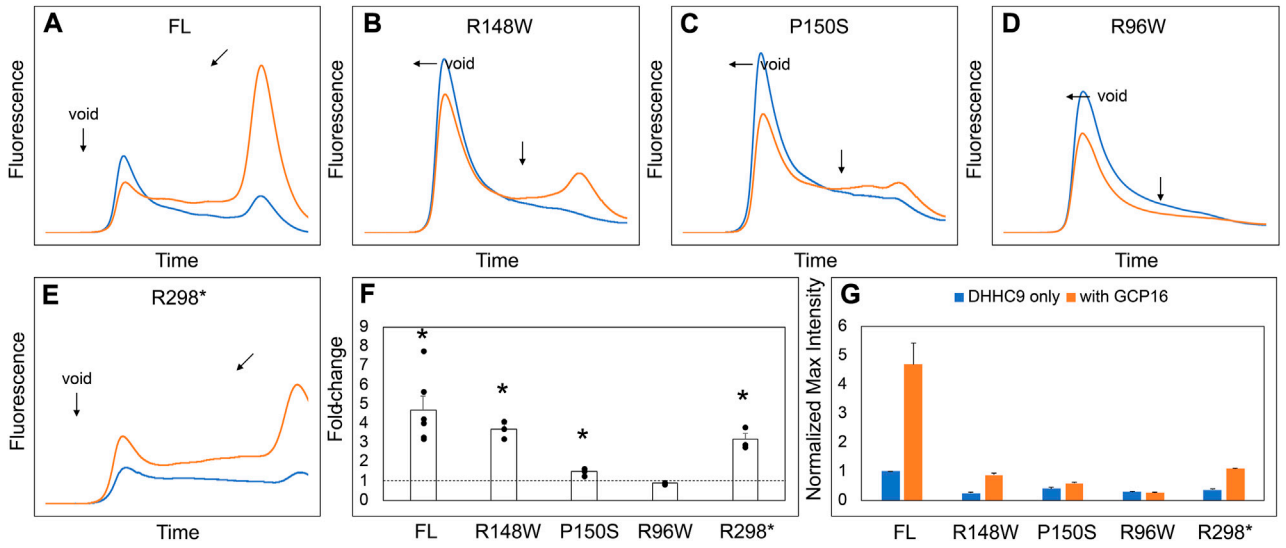

FIGURE 6
DHHC9 Disease Mutations Exhibit Reduced Protein Stability. **(A–E)** FSEC profiles for full-length DHHC9 (FL), the indicated point mutations, and DHHC9 truncation at R298 (R298*). HEK cells were transfected with vector to express DHHC9 without (blue) and with GCP16 (orange). Bar charts showing **(F)** average fold-change and **(G)** normalized max intensity upon GCP16 co-expression for the indicated constructs at n ≥ 3 experiments. Max intensities were normalized to DHHC9 FL as described in the experimental procedures. The dashed line indicates a fold-change of 1. Error bars represent the standard error of the mean. Asterisks indicate a significance for *p*-value <0.05 determined by two-tailed *t*-test against the null hypothesis.

DHHC9 disease mutations result in reduced protein stability

DHHC9 protein pathogenic variants include missense mutations R148W, P150S, and R96W, and a non-sense mutation terminating at R298 (Schirwani et al., 2018). An earlier study reported that DHHC9 (R148W) and DHHC9 (P150S) possessed reduced steady state levels of autopalmitoylated DHHC9 (Mitchell et al., 2014). Given the importance of GCP16 in stabilizing DHHC9 protein folding with a corresponding effect on enzyme activity, we asked how the missense and non-sense mutations affected complex formation with GCP16. Compared to wildtype DHHC9, DHHC9 with R148W, P150S, R96W, or R298X mutations exhibited a greater extent of protein aggregation and reduced monodispersity as monitored by FSEC (Figures 6A–E, blue traces, F). Co-expression with GCP16 resulted in improved protein behavior compared to the respective DHHC9 constructs alone for all the mutants except R96W, although with a diminished effect compared to wildtype (Figures 6A–E, orange traces, F). These results suggest the DHHC9 mutations associated with XLID result in decreased protein stability and reflect reduced formation of a DHHC9-GCP16 complex.

GCP16 and GOLGA7B stabilize DHHCs in a subtype-specific manner

Our experiments suggest that the CCM in DHHC9 plays an important role in complex formation with GCP16. This motif is present in other DHHCs closely related to DHHC9, namely, DHHC14, 18, 5, and 8, but it is not present in distantly related DHHCs, such as DHHC3 and DHHC20 (Figure 7A). DHHC9 was the first human DHHC to be identified to require a protein partner for its activation, based on its homology to yeast Erf2-Erf4 (Swarthout et al., 2005). Recent studies suggest that GCP16 and GOLGA7B, a protein with ~75% amino acid sequence identity to GCP16, function as accessory proteins for additional members of the DHHC protein family. Woodley and Collins reported that DHHC5 interacts with GOLGA7B, facilitating DHHC5 localization at the plasma membrane and enabling its interactions with components of desmosomes to regulate cell adhesion (Woodley and Collins, 2019). Ko et al. identified ZDHHC5 and GOLGA7 (GCP16) in a screen for genes involved in an unconventional non-apoptotic cell death pathway triggered by the synthetic small molecule oxime, CIL56 (Ko et al., 2019). They went on to show that DHHC5 and GCP16 form a mutually stabilizing protein complex localized at the plasma membrane. Complex formation is dependent upon C-terminal cysteines in the conserved CCM motif, consistent with our results for DHHC9-GCP16 complex formation. To determine the potential of other DHHC proteins to form complexes with GCP16 and/or GOLGA7B, we tested whether co-expression of GCP16 or GOLGA7B affects the protein behavior of a set of DHHC proteins using FSEC. Like DHHC9, all DHHCs containing the CCM exhibited improved protein expression and monodispersity when co-expressed with GCP16 (Figures 7B–E,H,I). However, representative DHHCs without the CCM showed no significant difference whether GCP16 was co-expressed (Figures 7F–I). This supports that the GCP16-mediated stabilization is specific to certain DHHCs that possess the CCM. Interestingly, DHHC protein co-expression with GOLGA7B showed a similar, but distinct, result (Figure 8). While GOLGA7B co-expression significantly improved DHHC5 and DHHC8 protein (Figures 8D,E,H,I), it had no significant stabilizing effect on DHHC9, 14, 18, 3, and 20

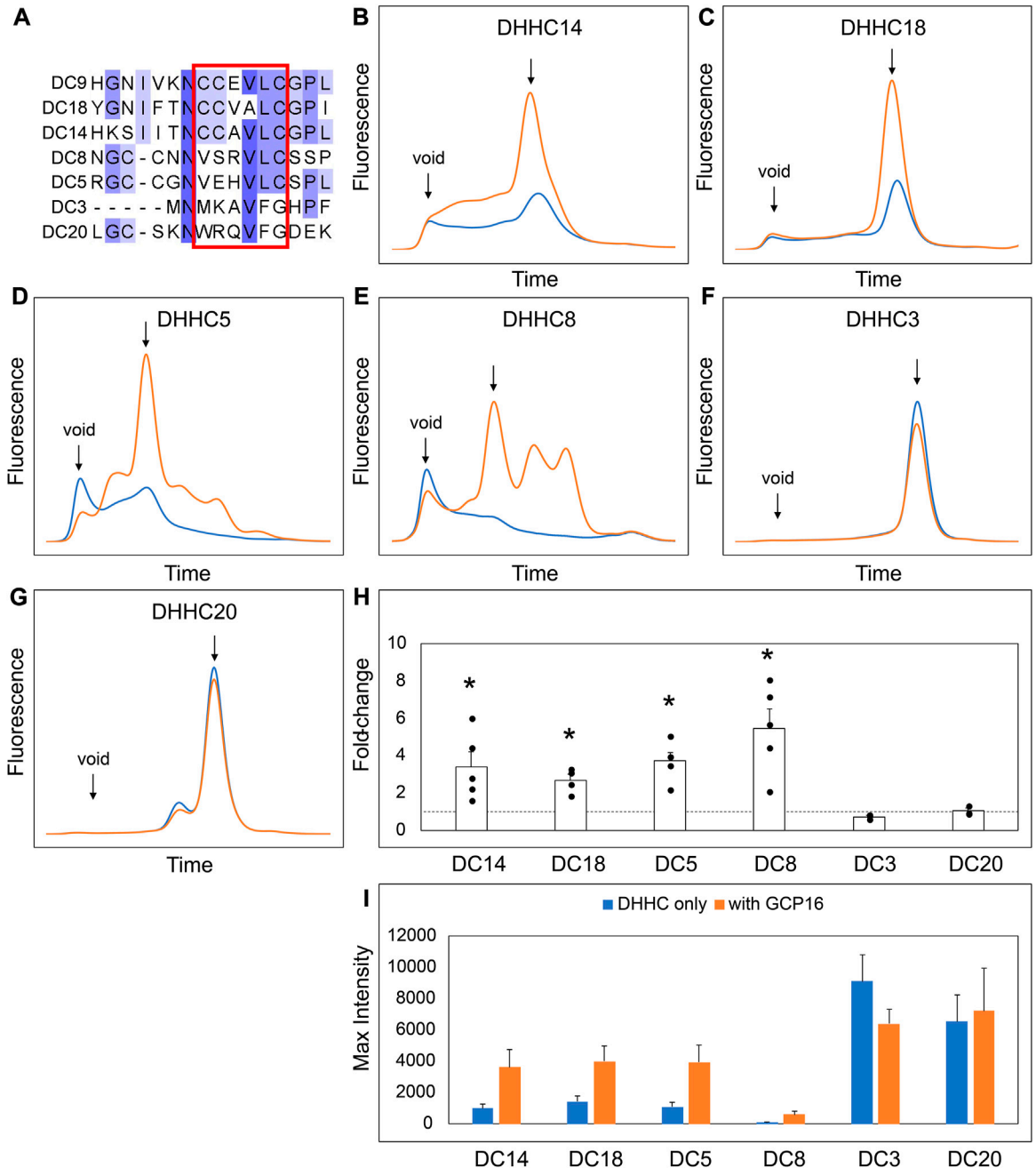

FIGURE 7
GCP16 Co-expression Stabilizes DHHC Proteins with the Conserved C-terminal Cysteine Motif. **(A)** Amino acid sequence alignment of select DHHC proteins at the conserved CTD cysteine motif. The conserved cysteine motif is boxed in red. **(B–G)** FSEC analysis of crude HEK lystates for the indicated constructs without (blue) or with GCP16 (orange). Bar charts showing **(H)** fold-change upon and **(I)** average max intensity for the indicated constructs upon GCP16 co-expression at n ≥ 3 experiments. Error bars represent the standard error of the mean. Asterisks indicate a significance for *p*-value <0.05 determined by two-tailed *t*-test against the null hypothesis.

(Figures 8A–C, F-I). Taken together, our FSEC experiments suggest GCP16 and GOLGA7B stabilize DHHC proteins in a subtype-specific manner.

To better understand the effect of GCP16 on the DHHC9 subfamily, we purified DHHC14 and DHHC18 and assessed the relationship between protein folding and PAT activity (Figure 9). As was the case with DHHC9, DHHC14 purified without GCP16 resulted in nearly complete protein aggregation (Figures 9A,B) and exhibited no detectable PAT activity (Figure 9E lane 1). On the other hand, DHHC14 co-purified with GCP16 was monodisperse (Figures 9C,D) and the folded complex in the included volume exhibited enzymatic activity for H-Ras and DHHC14 autoacylation (Figure 9E lane 3). Surprisingly, the DHHC14-GCP16 aggregate detected in the

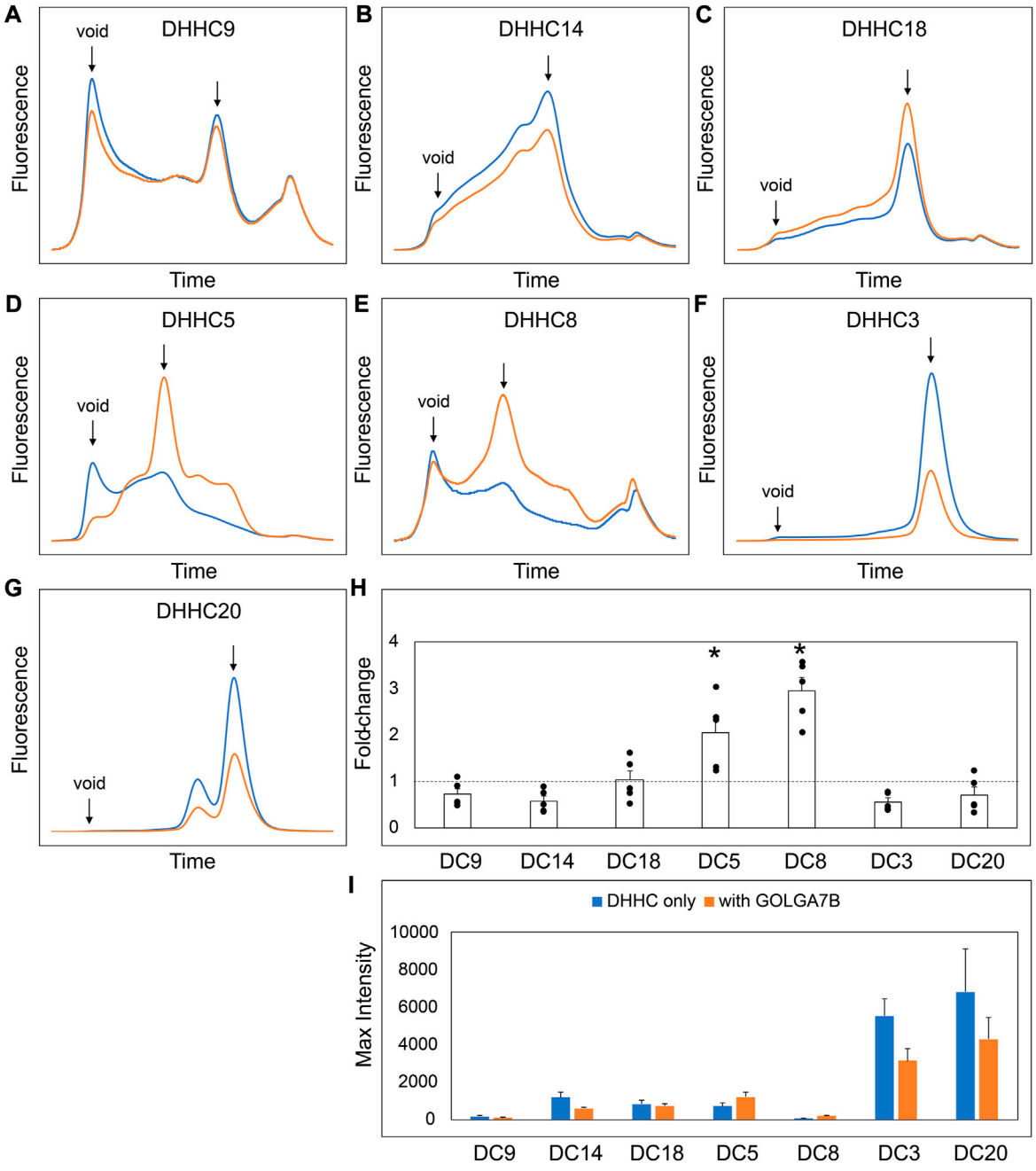

FIGURE 8
GOLGA7B Co-expression Stabilizes DHHC Proteins. **(A–G)** FSEC profiles for the indicated constructs. HEK cells were transfected with DHHC without (blue) or with GOLGA7B (orange). Bar charts showing **(H)** fold-change upon and **(I)** average max intensity for the indicated constructs upon GOLGA7B co-expression at n = 5 experiments. Error bars represent the standard error of the mean. Asterisks indicate a significant increase with GOLGA7B for *p*-value <0.05 determined by two-tailed *t*-test against the null hypothesis.

void volume exhibited PAT activity, albeit reduced relative to the folded complex (Figure 9E lane 2). Similarly, DHHC18 purified by itself was aggregated and enzymatically inactive (Figures 9F,G,J lane 1). Like DHHC14-GCP16, the DHHC18-GCP16 complex purified as two species with the folded complex having more activity than that found in the aggregate (Figures 9H–J lane 2). These results suggest that the stabilizing effect of GCP16 spans the DHHC9 subfamily.

Discussion

In this study, we sought to understand the function of GCP16 in the DHHC9-GCP16 complex. We found that co-expression of GCP16 with DHHC9 improved DHHC9 protein levels and homogeneity. Through truncations, mutagenesis, and FSEC screening, we identified a conserved C-terminal cysteine motif in DHHC9 that is required for the GCP16-mediated stabilization effect. We used the SEC profiles of purified

10.3389/fphys.2023.1167094

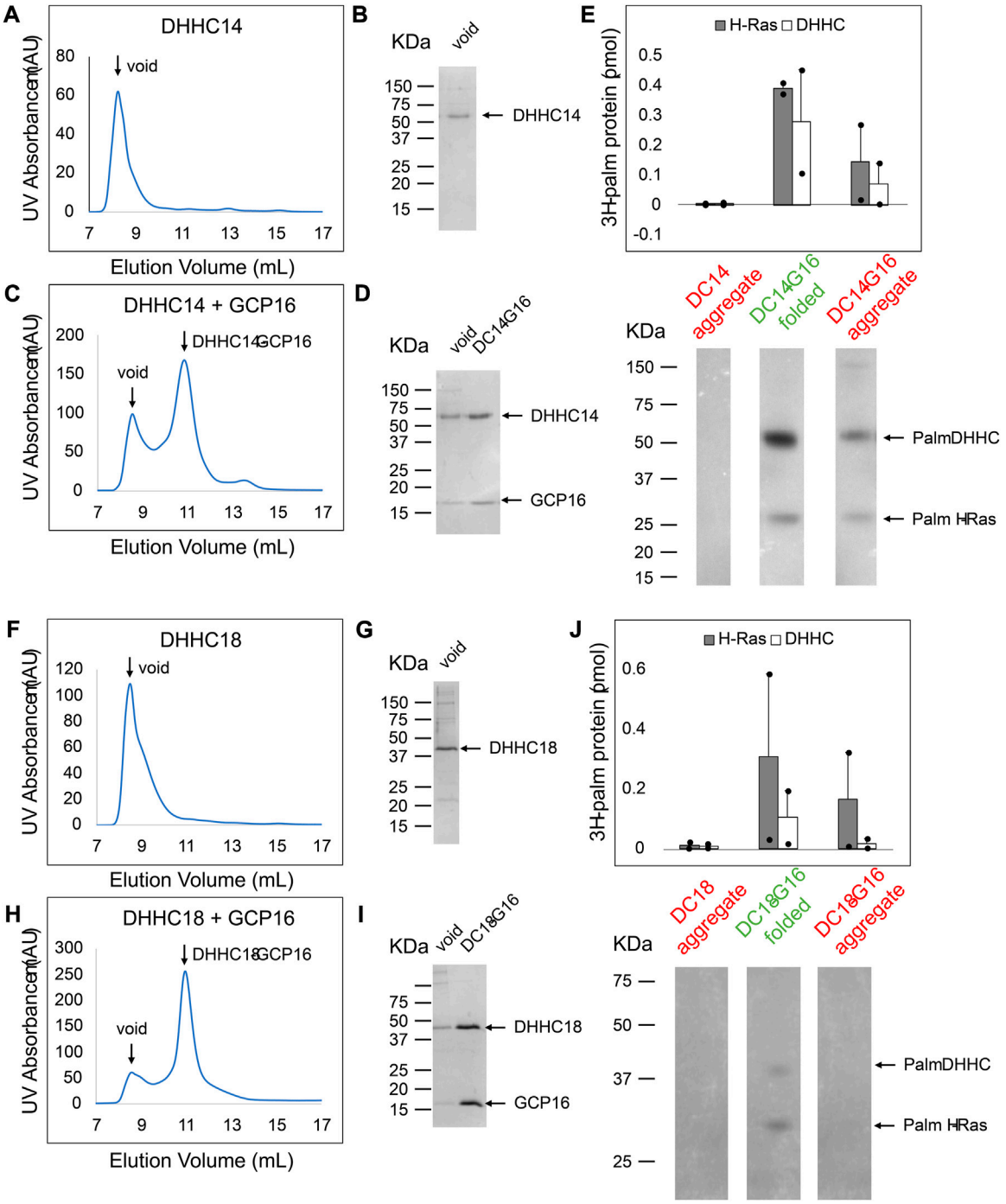

FIGURE 9
DHHC14 and DHHC18 Each Forms a Complex with GCP16 to Confer PAT Activity. Sf9 cells were infected with recombinant baculovirus encoding strep-tagged DHHC alone or DHHC + GCP16. Protein was purified *via* strep-affinity purification and SEC. SEC profiles and SDS-PAGE Coomassie for **(A,B)** DHHC14 **(C,D)** the DHHC14 co-purified with GCP16, **(F,G)** DHHC18, and **(H,I)** DHHC18 co-purified with GCP16 are shown. Arrows in the SEC profiles correspond to the labeled lanes for the corresponding SDS-PAGE analysis. **(E,J)** Purified DHHC14/DHHC18 was classified into aggregated (red) or folded (green) states based on the SEC profile. DHHC14/DHHC18 was assayed for activity using H-Ras and [^{3}H]palmitoyl CoA. Radiolabeled protein was quantified *via* liquid scintillation spectroscopy and detected *via* fluorography. The *y*-axis represents picomoles of ^{3}H-labeled protein after subtracting background radiation. Gray bars represent the quantity of labeled H-Ras, and white bars represent the quantity of labeled DHHC protein. Error bars represent the standard error of the mean for n = 2 independent protein preparations. Arrows indicate bands corresponding to radiolabeled DHHC and H-Ras.

proteins to show the CCM is required for formation of the DHHC9-GCP16 complex. Without GCP16, purified DHHC9 aggregates, and only folded DHHC9-GCP16 complex formation is enzymatically active for H-Ras *in vitro*. Furthermore, we showed that disease mutations associated with XLID result in decreased protein stability and diminished DHHC9-GCP16 complex formation.

DHHC9 and GCP16 were discovered based on homology to yeast palmitoyltransferase Erf2-Erf4 (Lobo et al., 2002; Swarthout et al., 2005). DHHC9 and GCP16 share 31% and 17% sequence identity with Erf2 and Erf4, respectively. While the exact sequence identity between the pair is limited, they possess functional similarities. For example, both form heteromeric DHHC protein complexes and are putative Ras PATs in their respective organisms (Lobo et al., 2002; Swarthout et al., 2005). Furthermore, DHHC9-GCP16 can substitute for loss of Erf2 in *S. cerevisiae* (Mitchell et al., 2014). Mitchell et al. showed, in the absence of Erf4, Erf2 steady-state protein levels and its half-life are significantly lowered and that one function of Erf4 is to stabilize Erf2 by impeding its ERAD-mediated degradation (Mitchell et al., 2012). Similarly, our data support that one role for GCP16 is to provide local stability for DHHC9, suggesting this function for the partner protein may be evolutionarily conserved. However, the role of the accessory protein may extend beyond DHHC protein stabilization. For example in yeast, stabilization of Erf2 does not suppress loss of Erf4 *in vivo*, and Erf2 exhibits distinct enzyme kinetics with and without Erf4 *in vitro* (Mitchell et al., 2012). Specifically, the absence of Erf4 does not abolish Erf2 autopalmitoylation, suggesting that residues of Erf4 do not participate directly in this step. However, the absence of Erf4 does increase the rate of hydrolysis of the thioester on the acyl-enzyme intermediate, causing Erf2 to undergo a futile cycle of autopalmitoylation and hydrolysis. Erf4 is required for Erf2 to transfer the palmitoyl group to the protein substrate, with the exact mechanism remaining unclear (Mitchell et al., 2012).

Earlier proteomics studies identified the C-terminal CCX7-13C*(S/T) sequence among DHHC proteins where cysteines centered around the "GCxxN" motif were palmitoylated, and these cysteines in DHHC5 and DHHC8 were palmitoylated *in vivo* (Yang et al., 2010; Collins et al., 2017). Subsequently, Ko et al. showed DHHC5 and GCP16 are mutually stabilizing and that DHHC5-GCP16 complex formation, as assessed by immunoprecipitation, is dependent on the DHHC5 C-terminal cysteines (Ko et al., 2019). The catalytically active DHHC5-GCP16 complex is required for non-apoptotic cell death induced by the synthetic oxime-containing small molecule caspase-independent lethal 56 (CIL56) (Ko et al., 2019). DHHC5 has also been shown to interact with the GCP16 relative, GOLGA7B. Palmitoylation of the DHHC5 C-terminal cysteines controls its interaction with and its ability to palmitoylate GOLGA7B, which in turn regulates DHHC5 internalization and turnover and its protein interactome (Woodley and Collins, 2019). Howie et al. observed that the DHHC5 C-terminus between N218-T334, which includes the CCM, is required for palmitoylation of the Na-pump accessory protein phospholemman (PLM) (Howie et al., 2014). Interestingly, PLM does not bind directly to this region of DHHC5, but rather it associates with DHHC5 through an intermediate, the Na-pump α subunit, which does bind directly to DHHC5 N218-T334 (Plain et al., 2020). Nonetheless, the DHHC5 region containing the CCM is specifically required for palmitoylation of its substrates PLM and Flotillin-2, while other substrates such as PSD-5 and GRIP1 require the PSD-95/Discs-large/ZO-1 homology (PDZ) binding motif (Howie et al., 2014). The CCM we identified in the DHHC9 subfamily overlaps with the end of the previously described CCX7-13C*(S/T) sequence. Taken together, we reason that the CCM cysteines are likely to be palmitoylated and mediate accessory protein interaction either directly or indirectly by exposing a GCP16/GOLGA7B binding site. Interaction with the accessory protein provides protein stability, and it expands the DHHC protein interactome, which may be a mechanism of substrate recruitment and regulation. How subtype preferences for GCP16/GOLGA7B are governed is to be resolved, though it seems likely to involve additional protein domain coordination.

While this manuscript was in revision, a preprint deposited in bioRxiv reported the cryo-EM structures of human DHHC9-GCP16 and yeast Ef2-Erf4 (Yang et al., 2022). Several of their findings are consistent with our results. We found that the CCM motif and in particular, Cys 288, is essential for DHHC9 activity and stability. Yang et al. identified palmitate on Cys288 and showed that its mutation resulted in the loss of catalytic activity (Yang et al., 2022). Within the DHHC9-GCP16 structure, the palmitate attached to Cys288 in the DHHC9 α3 helix inserts adjacent to transmembrane domains 2 and 3 and the α2' helix of GCP16, thereby promoting membrane association of the DHHC9 α3 helix and adding stability to the DHHC9-GCP16 complex. Noting the conservation of the CCM in DHHC14 and DHHC18, Yang et al. also reported that DHHC14 and DHHC18 formed catalytically active complexes with GCP16 that palmitoylated HRAS and NRAS, corroborating the results reported herein.

Our study demonstrates that a subgroup of the larger DHHC protein family that includes DHHC9, 14, 18, 5, and 8 all require accessory proteins for their stability *in vitro*. Whereas GCP16 potentiated all subfamily members, GOLGA7B potentiated only DHHC5 and DHHC8. Using purified components, we establish that both DHHC14 and DHHC18 when complexed with GCP16 can function as Ras palmitoyltransferases. Our research supports a broader role for GCP16 and GOLGA7B in the function of human DHHC proteins.

Data availability statement

The original contributions presented in the study are included in the article/Supplementary Materials, further inquiries can be directed to the corresponding authors.

Author contributions

PN and WG performed experiments. TK and ML designed the project. PN wrote the first draft and all authors contributed to manuscript preparation.

Funding

This study was supported by the National Institutes of Health NS101390 (TK and ML), GM114379 (TK) and GM121540 (ML).

Acknowledgments

We thank the members of the Kawate and Linder labs for discussion.

Conflict of interest

The authors declare that the research was conducted in the absence of any commercial or financial relationships that could be construed as a potential conflict of interest.

Publisher's note

All claims expressed in this article are solely those of the authors and do not necessarily represent those of their affiliated organizations, or those of the publisher, the editors and the reviewers. Any product that may be evaluated in this article, or claim that may be made by its manufacturer, is not guaranteed or endorsed by the publisher.

Supplementary material

The Supplementary Material for this article can be found online at: https://www.frontiersin.org/articles/10.3389/fphys.2023.1167094/full#supplementary-material

References

Baker, K., Astle, D. E., Scerif, G., Barnes, J., Smith, J., Moffat, G., et al. (2015). Epilepsy, cognitive deficits and neuroanatomy in males with ZDHHC9 mutations. *Ann. Clin. Transl. Neurol.* 2, 559–569. doi:10.1002/acn3.196

Chamberlain, L. H., and Shipston, M. J. (2015). The physiology of protein S-acylation. *Physiol. Rev.* 95, 341–376. doi:10.1152/physrev.00032.2014

Collins, M. O., Woodley, K. T., and Choudhary, J. S. (2017). Global, site-specific analysis of neuronal protein S-acylation. *Sci. Rep.* 7, 4683. doi:10.1038/s41598-017-04580-1

Gonzalez Montoro, A., Quiroga, R., and Valdez Taubas, J. (2013). Zinc co-ordination by the DHHC cysteine-rich domain of the palmitoyltransferase Swf1. *Biochem. J.* 454, 427–435. doi:10.1042/BJ20121693

Gottlieb, C. D., and Linder, M. E. (2017). Structure and function of DHHC protein S-acyltransferases. *Biochem. Soc. Trans.* 45, 923–928. doi:10.1042/BST20160304

Gottlieb, C. D., Zhang, S., and Linder, M. E. (2015). The cysteine-rich domain of the DHHC3 palmitoyltransferase is palmitoylated and contains tightly bound zinc. *J. Biol. Chem.* 290, 29259–29269. doi:10.1074/jbc.M115.691147

Han, J. Y., Lee, I. G., Shin, S., Kim, M., Jang, J. H., and Park, J. (2017). The first patient with sporadic X-linked intellectual disability with de novo ZDHHC9 mutation identified by targeted next-generation sequencing. *Eur. J. Med. Genet.* 60, 499–503. doi:10.1016/j.ejmg.2017.07.002

Howie, J., Reilly, L., Fraser, N. J., Vlachaki Walker, J. M., Wypijewski, K. J., Ashford, M. L., et al. (2014). Substrate recognition by the cell surface palmitoyl transferase DHHC5. *Proc. Natl. Acad. Sci. U. S. A.* 111, 17534–17539. doi:10.1073/pnas.1413627111

Jennings, B. C., and Linder, M. E. (2012). DHHC protein S-acyltransferases use similar ping-pong kinetic mechanisms but display different acyl-CoA specificities. *J. Biol. Chem.* 287, 7236–7245. doi:10.1074/jbc.M111.337246

Kawate, T., and Gouaux, E. (2006). Fluorescence-detection size-exclusion chromatography for precrystallization screening of integral membrane proteins. *Structure* 14, 673–681. doi:10.1016/j.str.2006.01.013

Ko, P. J., Woodrow, C., Dubreuil, M. M., Martin, B. R., Skouta, R., Bassik, M. C., et al. (2019). A ZDHHC5-GOLGA7 protein acyltransferase complex promotes nonapoptotic cell death. *Cell Chem. Biol.* 26, 1716–1724 e9. doi:10.1016/j.chembiol.2019.09.014

Lobo, S., Greentree, W. K., Linder, M. E., and Deschenes, R. J. (2002). Identification of a Ras palmitoyltransferase in *Saccharomyces cerevisiae*. *J. Biol. Chem.* 277, 41268–41273. doi:10.1074/jbc.M206573200

Malgapo, M. I. P., and Linder, M. E. (2021). Substrate recruitment by zDHHC protein acyltransferases. *Open Biol.* 11, 210026. doi:10.1098/rsob.210026

Mitchell, D. A., Hamel, L. D., Ishizuka, K., Mitchell, G., Schaefer, L. M., and Deschenes, R. J. (2012). The Erf4 subunit of the yeast Ras palmitoyl acyltransferase is required for stability of the Acyl-Erf2 intermediate and palmitoyl transfer to a Ras2 substrate. *J. Biol. Chem.* 287, 34337–34348. doi:10.1074/jbc.M112.379297

Mitchell, D. A., Hamel, L. D., Reddy, K. D., Farh, L., Rettew, L. M., Sanchez, P. R., et al. (2014). Mutations in the X-linked intellectual disability gene, zDHHC9, alter autopalmitoylation activity by distinct mechanisms. *J. Biol. Chem.* 289, 18582–18592. doi:10.1074/jbc.M114.567420

Mitchell, D. A., Mitchell, G., Ling, Y., Budde, C., and Deschenes, R. J. (2010). Mutational analysis of *Saccharomyces cerevisiae* Erf2 reveals a two-step reaction mechanism for protein palmitoylation by DHHC enzymes. *J. Biol. Chem.* 285, 38104–38114. doi:10.1074/jbc.M110.169102

Mitchell, D. A., Vasudevan, A., Linder, M. E., and Deschenes, R. J. (2006). Protein palmitoylation by a family of DHHC protein S-acyltransferases. *J. lipid Res.* 47, 1118–1127. doi:10.1194/jlr.R600007-JLR200

Ohta, E., Misumi, Y., Sohda, M., Fujiwara, T., Yano, A., and Ikehara, Y. (2003). Identification and characterization of GCP16, a novel acylated Golgi protein that interacts with GCP170. *J. Biol. Chem.* 278, 51957–51967. doi:10.1074/jbc.M310014200

Plain, F., Howie, J., Kennedy, J., Brown, E., Shattock, M. J., Fraser, N. J., et al. (2020). Control of protein palmitoylation by regulating substrate recruitment to a zDHHC-protein acyltransferase. *Commun. Biol.* 3, 411. doi:10.1038/s42003-020-01145-3

Rana, M. S., Kumar, P., Lee, C. J., Verardi, R., Rajashankar, K. R., and Banerjee, A. (2018). Fatty acyl recognition and transfer by an integral membrane S-acyltransferase. *Science* 359, eaao6326. doi:10.1126/science.aao6326

Raymond, F. L., Tarpey, P. S., Edkins, S., Tofts, C., O'Meara, S., Teague, J., et al. (2007). Mutations in ZDHHC9, which encodes a palmitoyltransferase of NRAS and HRAS, cause X-linked mental retardation associated with a Marfanoid habitus. *Am. J. Hum. Genet.* 80, 982–987. doi:10.1086/513609

Salaun, C., Locatelli, C., Zmuda, F., Cabrera Gonzalez, J., and Chamberlain, L. H. (2020). Accessory proteins of the zDHHC family of S-acylation enzymes. *J. Cell Sci.* 133, jcs251819. doi:10.1242/jcs.251819

Schirwani, S., Wakeling, E., Smith, K., Study, D. D. D., and Balasubramanian, M. (2018). Expanding the molecular basis and phenotypic spectrum of ZDHHC9-associated X-linked intellectual disability. *Am. J. Med. Genet. A* 176, 1238–1244. doi:10.1002/ajmg.a.38683

Swarthout, J. T., Lobo, S., Farh, L., Croke, M. R., Greentree, W. K., Deschenes, R. J., et al. (2005). DHHC9 and GCP16 constitute a human protein fatty acyltransferase with specificity for H- and N-Ras. *J. Biol. Chem.* 280, 31141–31148. doi:10.1074/jbc.M504113200

Woodley, K. T., and Collins, M. O. (2019). S-acylated Golga7b stabilises DHHC5 at the plasma membrane to regulate cell adhesion. *EMBO Rep.* 20, e47472. doi:10.15252/embr.201847472

Yang, A., Liu, S., Zhang, Y., Chen, J., Feng, S., Wu, J., et al. (2022). Regulation of RAS palmitoyltransferases by accessory proteins and palmitoylation. *bioRxiv*.

Yang, W., Di Vizio, D., Kirchner, M., Steen, H., and Freeman, M. R. (2010). Proteome scale characterization of human S-acylated proteins in lipid raft-enriched and non-raft membranes. *Mol. Cell Proteomics* 9, 54–70. doi:10.1074/mcp.m800448-mcp200

Yeste-Velasco, M., Linder, M. E., and Lu, Y. J. (2015). Protein S-palmitoylation and cancer. *Biochim. Biophys. Acta* 1856, 107–120. doi:10.1016/j.bbcan.2015.06.004

Young, F. B., Butland, S. L., Sanders, S. S., Sutton, L. M., and Hayden, M. R. (2012). Putting proteins in their place: Palmitoylation in huntington disease and other neuropsychiatric diseases. *Prog. Neurobiol.* 97, 220–238. doi:10.1016/j.pneurobio.2011.11.002

Zhang, M. M., Wu, P. Y., Kelly, F. D., Nurse, P., and Hang, H. C. (2013). Quantitative control of protein S-palmitoylation regulates meiotic entry in fission yeast. *PLoS Biol.* 11, e1001597. doi:10.1371/journal.pbio.1001597

frontiers | Frontiers in Physiology

TYPE Original Research
PUBLISHED 30 March 2023
DOI 10.3389/fphys.2023.959660

OPEN ACCESS

EDITED BY
William Fuller,
University of Glasgow, United Kingdom

REVIEWED BY
Gareth Thomas,
Temple University, United States
Rebeca M. Mejias Estevez,
Sevilla University, Spain

*CORRESPONDENCE
Paul M. Jenkins,
pjenkins@umich.edu

SPECIALTY SECTION
This article was submitted to Lipid and Fatty Acid Research, a section of the journal Frontiers in Physiology

RECEIVED 01 June 2022
ACCEPTED 21 March 2023
PUBLISHED 30 March 2023

CITATION
Gupta JP and Jenkins PM (2023), Ankyrin-B is lipid-modified by *S*-palmitoylation to promote dendritic membrane scaffolding of voltage-gated sodium channel $Na_V1.2$ in neurons.
Front. Physiol. 14:959660.
doi: 10.3389/fphys.2023.959660

Ankyrin-B is lipid-modified by *S*-palmitoylation to promote dendritic membrane scaffolding of voltage-gated sodium channel $Na_V1.2$ in neurons

Julie P. Gupta[1] and Paul M. Jenkins[1,2]*

[1]Department of Pharmacology, University of Michigan Medical School, Ann Arbor, MI, United States, [2]Department of Psychiatry, University of Michigan Medical School, Ann Arbor, MI, United States

Neuronal ankyrin-B is an intracellular scaffolding protein that plays multiple roles in the axon. By contrast, relatively little is known about the function of ankyrin-B in dendrites, where ankyrin-B is also localized in mature neurons. Recently, we showed that ankyrin-B acts as a scaffold for the voltage-gated sodium channel, $Na_V1.2$, in dendrites of neocortical pyramidal neurons. How ankyrin-B is itself targeted to the dendritic membrane is not well understood. Here, we report that ankyrin-B is lipid-modified by S-palmitoylation to promote dendritic localization of $Na_V1.2$. We identify the palmitoyl acyl transferase zDHHC17 as a key mediator of ankyrin-B palmitoylation in heterologous cells and in neurons. Additionally, we find that zDHHC17 regulates ankyrin-B protein levels independently of its S-acylation function through a conserved binding mechanism between the ANK repeat domain of zDHHC17 and the zDHHC ankyrin-repeat binding motif of ankyrin-B. We subsequently identify five cysteines in the N-terminal ankyrin repeat domain of ankyrin-B that are necessary for ankyrin-B palmitoylation. Mutation of these five cysteines to alanines not only abolishes ankyrin-B palmitoylation, but also prevents ankyrin-B from scaffolding $Na_V1.2$ at dendritic membranes of neurons due to ankyrin-B's inability to localize properly at dendrites. Thus, we show palmitoylation is critical for localization and function of ankyrin-B at dendrites. Strikingly, loss of ankyrin-B palmitoylation does not affect ankyrin-B-mediated axonal cargo transport of synaptic vesicle synaptotagmin-1 in neurons. This is the first demonstration of S-palmitoylation of ankyrin-B as an underlying mechanism required for ankyrin-B localization and function in scaffolding $Na_V1.2$ at dendrites.

KEYWORDS

Ankyrin-B, post-translational modification, S-palmitoylation, zDHHC enzymes, localization, scaffolding, dendrites, axons

Abbreviations: A, Alanine; AIS, Axon Initial Segment; ASD, Autism Spectrum Disorder; A5B, AAAAA-ankyrin-B-GFP; BFP, Blue Fluorescent Protein; C, Cysteine; DIV, Days *in Vitro*; GFP, Green Fluorescent Protein; HA, Hydroxylamine; HEK, Human Embryonic Kidney; IB, Immunoblotting; LCMS/MS, Liquid Chromatography tandem Mass Spectrometry; MMTS, S-methyl thiomethanesulfonate; PAT, Palmitoyl Acyl Transferase; RAC, Resin Assisted Capture; RT, Room temperature; Syt1, Synaptotagmin-1; VGSC, Voltage-Gated Sodium Channel; WT, Wild-type; zDABM, zDHHC ankyrin-repeat binding motif.

1 Introduction

The ankyrin family of scaffolding proteins target and anchor membrane, cytoskeletal, and cytoplasmic proteins at specialized membrane domains to establish and maintain cell polarity and function in many vertebrate tissues (Bennett and Lorenzo, 2013). One member of the ankyrin family, ankyrin-B, encoded by the *ANK2* gene, localizes ion channels, transporters, structural proteins, as well as signaling molecules to specialized membranes in the heart, skeletal muscle, adipocytes, and brain. In neurons, multiple axonal roles have been shown for ankyrin-B, including axonal cargo transport, scaffolding of cell adhesion molecules to repress axonal branching, and proper positioning of ankyrin-G at the axon initial segment (AIS) (Galiano et al., 2012; Lorenzo et al., 2014; Yang et al., 2019). By contrast, the role of ankyrin-B at dendritic membranes had been relatively understudied until recently, when ankyrin-B was shown to serve as an essential scaffold for voltage-gated sodium channels, $Na_V1.2$, at dendrites to promote dendritic excitability and synaptic plasticity in neocortical pyramidal neurons (Nelson et al., 2022). Heterozygous loss of *Ank2* causes dramatic impairments in dendritic excitability and synaptic plasticity, and phenocopies effects of heterozygous loss of *Scn2a*, which encodes $Na_V1.2$, suggesting ankyrin-B is critical for $Na_V1.2$-mediated dendritic function (Spratt et al., 2019; Nelson et al., 2022).

ANK2 is amongst the top genes linked to autism spectrum disorder (ASD) (Satterstrom et al., 2020). R2608fs, an ASD-associated variant in exon 37 of *ANK2*, which encodes the 440-kDa isoform of ankyrin-B, induces a frameshift that disrupts axonal scaffolding of the cell adhesion molecule L1CAM, causing alterations in axonal connectivity and behavior reminiscent of the deficits in communicative and social behaviors observed in human ASD patients (Yang et al., 2019). *SCN2A*, which encodes $Na_V1.2$, is also a high-risk gene for ASD (Sanders et al., 2015; Ben-Shalom et al., 2017; Sanders et al., 2018). $Na_V1.2$ and ankyrin-B interacting to promote dendritic excitability provides strong rationale that deficits in dendritic excitability may be a common point of convergence in ASD etiology. Although it is clear that $Na_V1.2$ relies on ankyrin-B to properly target to dendritic membranes in neurons, how ankyrin-B itself reaches the dendritic membrane is unknown. Understanding how ankyrin-B targets to the dendritic membrane to mediate the localization and function of $Na_V1.2$ may shed light onto ASD pathophysiology.

Another member of the ankyrin family, ankyrin-G, relies on the posttranslational modification, *S*-palmitoylation, for normal localization and function (He et al., 2012). *S*-palmitoylation is the covalent addition of a 16-carbon fatty acid to cysteine residues of proteins through the formation of a labile thioester bond, and is catalyzed by a family of 23 enzymes known as palmitoyl acyl transferases (zDHHC PATs) (Fukata and Fukata, 2010). Ankyrin-G is *S*-palmitoylated at a single cysteine in its N-terminal ankyrin repeat domain, Cys70 (He et al., 2012). Mutation of Cys70 to alanine (C70A) renders ankyrin-G palmitoylation-dead and subsequently incapable of functioning in epithelial cell membrane biogenesis or in scaffolding neuronal proteins at the axon initial segment (He et al., 2012; He et al., 2014; Tseng et al., 2015). Ankyrin-G is palmitoylated by two functionally redundant zDHHC PATs, zDHHC5 and zDHHC8. Taken together, these data demonstrate that ankyrin-G *S*-palmitoylation is required for ankyrin-G localization and function at the lateral membrane of epithelial cells as well as at the neuronal AIS. Whether ankyrin-B is also palmitoylated as a mechanism to regulate its plasma membrane localization and scaffolding of $Na_V1.2$ at dendrites remains unclear.

Here, we asked if ankyrin-B is *S*-palmitoylated and whether palmitoylation could regulate ankyrin-B localization and function in neurons. We find that ankyrin-B is indeed palmitoylated in whole mouse brain and in neurons, identifying zDHHC17 as a key mediator of ankyrin-B palmitoylation in heterologous cells and in neurons. We also demonstrate that zDHHC17 regulates ankyrin-B protein levels in a palmitoylation-independent manner through a conserved binding mechanism between the ANK repeat of zDHHC17 and the zDHHC ankyrin-repeat binding motif (zDABM) of ankyrin-B. We identify five cysteines as possible ankyrin-B palmitoylation sites. Mutation of these five cysteines in the N-terminal ANK repeat domain of ankyrin-B renders ankyrin-B palmitoylation-dead. While ankyrin-B palmitoylation does not regulate its ability to mediate axonal cargo function, ankyrin-B palmitoylation is required to target $Na_V1.2$ to dendrites in neocortical pyramidal neurons. These data provide evidence for two pools of ankyrin-B in neurons, one palmitoylation-dependent pool at dendrites, and one palmitoylation-independent pool in vesicles at the axon. This work highlights novel mechanisms regulating ankyrin-B localization and function in neurons that may provide insights into *ANK2*-associated ASD.

2 Materials and methods

2.1 Antibodies

The antibodies used for western blotting in this study were chicken anti-GFP antibody (Abcam, 1:2000), rabbit anti-Flotillin-1 antibody (Cell Signaling Technologies, 1:1000), rabbit/mouse anti-HA antibody (Cell Signaling Technologies, 1:1000), and rabbit anti-ankyrin-B C-terminus (custom-made in-house, 1:1000). The specificity of the anti-ankyrin-B antibody has been shown previously by western blotting (Lorenzo et al., 2014). LiCor fluorescent secondary antibodies were used: IRDye 800CW donkey anti-rabbit and anti-chicken (for anti-ankyrin-B, anti-HA, anti-Flotillin-1) and IRDye 680RD donkey anti-mouse (for anti-HA) were diluted 1:10,000. The antibodies used for immunofluorescence studies were mouse anti-FLAG M2 (Millipore Sigma, 1:1000), chicken anti-GFP antibody (Abcam, 1:1000), and sheep anti-ankyrin-B C-terminus (custom-made, in-house, 1:1000). Alexa Fluor 488, 568, or 647 secondary antibodies (Fisher scientific) were used at 1:250.

2.2 Expression vectors

The panel (1–24) of mouse zDHHC cDNA constructs subcloned in a pEF-BOS HA backbone were kindly gifted to us by Dr. Masaki Fukata (National Institute of Physiological Sciences, Okazaki, Japan; (Fukata et al., 2004)). The zDHHA17 mutant generated by site-directed mutagenesis was kindly gifted to us by Dr. Luke Chamberlain (University of Strathclyde); (Locatelli et al., 2020)).

The N100A zDHHC/A17 mutants were generated by our laboratory by site-directed mutagenesis using primers designed by Agilent QuickChange II XL primer design software and using QuickChange II XL site-directed mutagenesis kit (Agilent Technologies), and confirmed by DNA sequencing through Eurofins Genomics (Louisville, KY). Human ankyrin-B-GFP containing the small 220kD splice variant of ankyrin-B in a pEGFP-N1 vector was previously described (Lorenzo et al., 2014). All point mutations generated using the ankyrin-B-GFP cDNA construct were made using site-directed mutagenesis (QuickChange II XL, Agilent Technologies) and confirmed by DNA sequencing through Eurofins Genomics (Louisville, KY). Syt1-tdTomato was generously donated by Drs. Ronald Holz and Arun Anantharam (University of Michigan Medical School, Ann Arbor, MI). CAG-Cre-2A-BFP and CAG-BFP in a pLenti6-V5-DEST viral vector were previously used and described (Tseng et al., 2015). Note: TagBFP (referred to as BFP throughout) is a DsRed derivative that shares virtually no sequence homology with GFP, and thus is not recognized by anti-GFP antibodies.

2.3 Animals

Wild type C57Bl/6J (Jackson Laboratories), floxed Zdhhc17 (on an FVB background (Sanders et al., 2016)), and floxed *Ank2* mice (previously described (Chang et al., 2014)) were housed in the Unit for Laboratory Animal Medicine at the University of Michigan. All procedures involving animals were performed in accordance with National Institutes of Health guidelines with approval by the Institutional Animal Care and Use Committee (IACUC) of the University of Michigan.

2.4 Cell culture and transfections

HEK293T cells (gifted to us by Dr. Gareth Thomas, Temple University) were grown in Dulbecco's modified Eagle's high glucose medium with 10% fetal bovine serum, 1% penicillin/streptomycin, and 1% GlutaMax (ThermoFisher) at 37°C, 5% CO_2. For Acyl-RAC experiments, HEK293T cells were plated in 10 cm dishes at 80–90% confluency the day before transfection and transfected 16 h later with 4 μg total DNA (2 μg of each plasmid) using Lipofectamine 3,000 (Invitrogen) according to the manufacturer's instructions.

2.5 Neuronal cultures, transfections, and viral transductions

Cortical neurons were dissociated from P0 floxed *Zdhhc17* mouse pups and cultures were prepared as previous described (Nelson et al., 2018). At DIV2, neocortical cultures were transduced with β-galactosidase control adenovirus or Cre recombinase adenovirus, which are previously described (Davis et al., 2015; Brody et al., 2016; Brody et al., 2018). Cells were transduced in half of their original media for 6 h before replacing with the remaining half of their original media and half of fresh, new media. Neurons were left to incubate for 10 days before being processed for RT-PCR or Acyl-RAC analysis.

Hippocampal neurons were dissociated from P0 *Ank2*$^{flox/flox}$ mouse pups and cultures were prepared as previously described (Nelson et al., 2018). For the axonal cargo transport imaging experiments, DIV3 hippocampal neurons were transfected with 1 μg of either CAG-BFP or CAG-Cre-2A-BFP cDNA in combination with 500 ng of the other plasmids (Synaptotagmin-1-tdTomato, WT ankyrin-B-GFP, AAAAA-ankyrin-B-GFP) using Lipofectamine 2000. Briefly, 1 μg or 1.5 μg of cDNA constructs were added to 200 μL of Neurobasal-A medium (Gibco) in an Eppendorf tube. In another tube, 3 μL or 4.5 μL, respectively, of Lipofectamine 2000 were added to 200 μL of Neurobasal-A medium. The two tubes were incubated separately in the hood for 5 min before merging, mixing well, and incubating for 20 more minutes. The neuronal growth media on the neurons was collected and saved at 37°C. The transfection mix was then added dropwise to the appropriate dishes of DIV3 neurons and incubated at 37°C for 1 h. The transfection mix was aspirated, cells were washed once with Neurobasal-A medium, and the original growth media was added back onto the neurons. Cells were maintained in culture for 48 h before live imaging.

For the dendritic ankyrin-B function and localization experiments, neocortical neurons were dissociated from P0 floxed *Ank2* mouse pups and cultures were prepared as previously described (Nelson et al., 2018). DIV2 neurons were transfected with 0.5 μg of each plasmid using Lipofectamine 2000 as described in the above paragraph. Axons were identified both by morphology (as axons are much longer and thinner than dendrites) and by a relative lack of ankyrin-B staining in the proximal axon (Galiano et al., 2012). Residual $Na_V1.2$-3x FLAG staining in the proximal axon was confirmed to be localized to the AIS by colocalization with the AIS scaffolding protein, ankyrin-G (Nelson et al., 2022).

2.6 qRT-PCR

RNA was isolated from cultured hippocampal neurons in 6-well dishes (Thermo Fisher) using the RNeasy Mini Kit (QIAGEN). cDNA was prepared using the SuperScript IV First-Strand Synthesis Kit (Invitrogen). Quantitative RT-PCR on the mouse Zdhhc17 gene using primers spanning exons 1 and 2 (5′-ACCCGGAGGAAATCA AACCACAGA-3′ and 5′-TACATCGTAACCCGCTTCCACCAA-3′) and Sso/Advanced Universal SYBR green supermix (Fisher Scientific) was performed on CFX96 Real Time System (C1000 Touch Thermal Cycler, BioRad) under default conditions. Each sample was run in triplicates. Expression levels for mRNA were normalized to β-actin (5′- CATTGCTGACAGGATGCAGAAGG-3′ and 5′-TGCTGGAAGGTGGACAGTGAGG-3′).

2.7 Acyl Resin Assisted Capture (Acyl-RAC)

Approximately 24 h post-transfection, transfected HEK293T cells were lysed in "blocking buffer" containing 100 mM HEPES, 1 mM EDTA, 2.5% SDS, and 4% MMTS (Sigma), adjusted to pH 7.5 and sonicated. Samples were left to simultaneously heat and shake overnight at 40°C and 850 rpm in a Thermal Mixer II (Fisher Scientific). Samples were precipitated with cold acetone (incubated in ice) to remove residual MMTS

(previously described (Bouza et al., 2020)) and pellet was re-dissolved in 500 µL of "binding buffer" containing 100 mM HEPES, 1 mM EDTA, and 1% SDS, pH adjusted to 7.5, in Thermal Mixer II at 40°C and 850 rpm overnight. Protein samples were spun down in standard benchtop centrifuge at maximal speed for 5 min to pellet out any non-dissolved protein. Supernatant was then split into three 1.5 mL Eppendorf tubes, one containing 40 µL of unmanipulated starting material, one containing 200 µL of sample for hydroxylamine treatment ("+HA"), and one containing 200 µL of sample for NaCl treatment ("-HA"). 40 µL (1:1) of 5x SDS-PAGE buffer (5% wt/vol SDS, 25% wt/vol sucrose, 50 mM Tris pH 8, 5 mM EDTA, and bromophenol blue) supplemented with 100 mM DTT (Gold Biotechology) was added to the unmanipulated starting material and placed at 65°C for 10 min. 50 µL of 1:1 slurry of pre-activated thiopropyl-Sepharose 6b beads (GE, discontinued) were added to the "+HA" and "-HA" samples (previously described (Bouza et al., 2020)). 40 µL of freshly prepared 2 M hydroxylamine (HA) (Sigma), adjusted to pH 7.5, were added only to the "+HA" designated sample. 40 µL of 2 M NaCl were added to the "-HA" designated sample. Samples treated with HA and beads were left to incubate while rotating at room temperature for 2.5 h before being spun down at 5,000 x g for 1 min and washed 3x with "binding buffer", each time discarding the supernatant and recovering the beads. 40 µL of 5x SDS-PAGE/DTT buffer were used to elute palmitoylated proteins off of the beads and heated for 10 min at 65°C. Samples were analyzed by western blotting.

For assessing palmitoylation of proteins from brain tissue or from cultured hippocampal neurons, after overnight MMTS block, samples were transferred to a Slide-A-Lyzer Dialysis Cassette (10,000 MWCO) (Thermo Scientific) for overnight buffer exchange with "binding buffer". Buffer exchanged samples were recovered from the dialysis cassette and the assay continued as described in the previous paragraph.

2.8 Mass spectrometry (LC-MS/MS)

After subjecting lysates to the Acyl-RAC assay and ensuring sufficient pulldown by western blotting (Supplementary Figure S3A), the sample was submitted to the University of Michigan Mass Spectrometry-Based Proteomics Resource Facility (Department of Pathology). There, the thiopropyl sepharose beads (washed without SDS for optimal mass spectrometry analysis) were re-suspended in 50 µL of 8M urea/0.1M ammonium bicarbonate buffer (pH~8). Cysteines (including those holding the previously palmitoylated proteins to the beads) were reduced by adding 50 µL of 10 mM DTT and incubating at 45°C for 30 min. Samples were cooled to room temperature and cysteines were alkylated using 65 mM 2-Chloroacetamide in the dark for 30 min at room temperature. Upon diluting the urea to a final concentration of <1 M, samples were incubated with 1 µg sequencing grade, modified trypsin at 37°C overnight. Digestion was stopped by acidification and peptides were desalted using SepPak C18 cartridges using manufacturer's protocol (Waters). Samples were completely dried using vacufuge. To perform the mass spectrometry, trypsinized peptides were dissolved in 9 µL of 0.1% formic acid/2% acetonitrile solution. Two µls of the resulting peptide solution were resolved on a nano-capillary reverse phase column (Acclaim PepMap C18, 2 micron, 50 cm, ThermoScientific) using a 0.1% formic acid/acetonitrile gradient at 300 nL/min over a period of 180 min. Eluent was directly introduced into Orbitrap Fusion Tribrid mass spectrometer (Thermo Scientific, San Jose CA) using an EasySpray source. MS1 scans were acquired at 60K resolution (AGC target = $3x10^6$; max IT = 50 ms). Data-dependent collision-induced dissociation MS/MS spectra were acquired on 20 most abundant ions following each MS1 scan (NCE ~28%; AGC target $1x10^5$; max IT 45 m). Proteins were identified by searching the data against Uniprot protein database using Proteome Discoverer (v2.4, Thermo Scientific). Search parameters included MS1 mass tolerance of 10 ppm and fragment tolerance of 0.2 Da. Two missed cleavages were allowed; carbamidomethylation of cysteines (+57.021 Da), oxidation of methionine (+15.995 Da), deamidation of asparagine and glutamine (+0.984 Da), and palmitoylation (+238.23 Da) were all considered variable modifications. False discovery rate (FDR) was determined using Percolator and proteins/peptides with an FDR of ≤1% (high confidence) were retained for further analysis.

2.9 Western blotting

Protein lysates, following Acyl-RAC or otherwise, were separated by 3.5–17.5% gradient bis-acrylamide gel in 1x Tris buffer, pH 7.4 (40 mM Tris, 20 mM NaOAc, and 2 mM NaEDTA) and 0.2% SDS at 175 V for ~4–5 h. Transfer to a nitrocellulose membrane was performed overnight at 300 mAmps, 4°C in 0.5x Tris buffer and 0.01% SDS. Once transferred, membranes were blocked with 5% Bovine Serum Albumin (BSA) in 1x TBS and rotated overnight at 4°C with primary antibodies diluted at appropriate dilution factor in blocking buffer (5% BSA, 0.1% tween in TBS). Membranes were then washed 3x for 10 min each with 1x TBS-T (TBS with 0.1% tween) and incubated for 1 h with LiCor fluorescent antibodies in blocking buffer. Membranes were washed 3x for 10 min each in 1x TBS-T before imaging on LiCor Odyssey Clx Imager. Immunoreactive signals were quantified using ImageJ.

2.10 Live imaging of hippocampal neurons and image analyses

Live microscopy of neuronal cultures was performed 48 h following neuronal transfections using a Zeiss LSM 880 with a 63X NA1.4 Oil/DIC Plan-Apochromat objective with excitation achieved using 405, 488, and 561 nm lasers in fast Airyscan mode. A humidified and temperature-controlled chamber was used to maintain the transfected hippocampal cultures at 37°C and 5% CO_2 in warm Physiological Saline Solution (130 mM NaCl, 4 mM KCl, 1.5 mM $CaCl_2$, 1 mM $MgCl_2$, 5 mM Glucose, 10 mM HEPES, adjusted to pH 7.4, and filter sterilized). Time-lapse images captured transfected hippocampal neurons in the mid-axon so as to avoid the axon initial segment at a rate of 200 m intervals in fast Airyscan mode. Images were Airyscan-processed using the Zeiss image analysis software (Zen Blue). Kymographs were then generated from each time-lapse image using the KymoToolBox

plugin in ImageJ (National Institutes of Health, Schindelin et al. (2012)), as previously described (Zala et al., 2013). Briefly, the axon was outlined and traced, from which a kymograph calibrated in space (*x*-axis in micrometers) and time (*y*-axis in seconds) was generated. Individual particle movement/trajectory was traced along the kymograph, which the KymoToolBox plugin analyzed in terms of directionality (red for retrograde, green for anterograde, and blue for stationary), directional velocities (μm/seconds), and directional run length for each traced particle.

2.11 Fluorescence labeling of cortical neurons and image acquisition

Dissociated cortical neurons at DIV21 (transfected DIV2) were fixed for 15 min at room temperature with 4% paraformaldehyde, followed by permeabilization with 0.2% triton in PBS for 10 min at room temperature, and further blocked with blocking buffer (5% BSA, 0.2% Tween 20 in PBS) for 1 hour. Primary antibodies were diluted in blocking buffer and incubated at 4°C overnight. The next day, cells were washed three times for 10 min with washing buffer (0.2% Tween 20 in PBS) before incubating the cells with secondary antibodies (1:250) diluted in blocking buffer for 1 h at room temperature. Cells were washed three times for 10 min with washing buffer and mounted with Prolong Gold. Multi-color imaging was performed as previously described using a Zeiss 880 confocal microscope (Jenkins et al., 2015). All images were processed in Adobe Photoshop CS6 and quantified using GraphPad Prism 9.

2.12 Statistical analysis

Statistical analyses for Acyl-RAC experiments were performed with n ≥ 3 for each experiment (N100A) zDHHC/A17: $n = 4$, Zdhhc17/Cre neurons, $n = 4$, C60A: $n = 7$, 120 kDa ankyrin-B: n = 3, for AAAAA: n = 5). For the Zdhhc17$^{f/f}$ neuron Acyl-RAC, the C60A ankyrin-B Acyl-RAC, and the 120-kDa ankyrin-B Acyl-RAC experiments, a two-tailed student's t-test (unpaired) was performed. Data are represented as mean ± SEM. For the Acyl-RACs that included multiple comparisons ((N100A) zDHHC/A17 and AAAAA-ankyrin-B), a one-way ANOVA with multiple comparisons and Tukey's post-hoc test was performed. For the cargo transport experiment, four independent experiments were performed. Statistical significance for axonal velocity and run length of Syt1 particles, which included 4-8 axons per condition (n = 88–154 particles per condition), was determined with one-way ANOVA with Tukey's post-hoc test. To determine statistical significance for percentage of stationary, reversing, or motile Syt1-tdTomato-positive or ankyrin-B-GFP-positive particles, a two-way ANOVA with multiple comparisons and Tukey's post-hoc test was performed. Statistical significance for axonal velocity and run length of ankyrin-B particles, which included 3-7 axons per condition (n = 38–76 particles per condition), was determined with a two-tailed student's t-test (unpaired). All cargo transport data are represented as mean ± SEM. The $Na_V1.2$-3x FLAG microcopy experiment had an n of 7–14 neurons/condition and was performed in three independent replicates. Mean fluorescence intensity of dendritic FLAG signal and mean fluorescence intensity of AIS FLAG signal were analyzed using one-way ANOVA with multiple comparisons and Tukey's post-hoc test. Data are represented as mean ± SEM.

3 Results

3.1 Ankyrin-B is S-palmitoylated in whole mouse brain and in neurons

The homologous family member of ankyrin-B, ankyrin-G, is *S*-palmitoylated to drive ankyrin-G localization and function in epithelial cells and in neurons (He et al., 2012). Ankyrin-G and ankyrin-B share significant homology across their shared domains, with 74% homology shared in their N-terminal ankyrin repeat domain, where ankyrin-G's palmitoylated cysteine resides (Mohler et al., 2002). Given such high homology, we asked whether ankyrin-B is also *S*-palmitoylated and if so, whether *S*-palmitoylation regulates ankyrin-B's diverse functions in neurons. We used the Acyl Resin Assisted Capture (Acyl-RAC) assay to assess steady-state palmitoylation of ankyrin-B (previously described (Bouza et al., 2020)). To validate this assay in our laboratory, we confirmed previous results demonstrating ankyrin-G is *S*-palmitoylated (He et al., 2012; Tseng et al., 2015). Using C57Bl/6J adult mouse whole-brain lysates subjected to Acyl-RAC, we observed that all three neuronal isoforms of ankyrin-G, 190-, 270-, and 480-kDa ankyrin-G, are *S*-palmitoylated, as demonstrated by hydroxylamine-dependent binding of endogenous ankyrin-G to sepharose beads ("+HA" lane) (Figures 1A,B). We also observed that the 220-kDa and 440-kDa isoforms of ankyrin-B are *S*-palmitoylated in whole mouse brain, as evidenced by the presence of hydroxylamine-dependent ankyrin-B signal (Figures 1A,C). Given our interest in understanding whether palmitoylation regulates the diverse functions of ankyrin-B in neurons, we asked whether ankyrin-B is also palmitoylated in cultured hippocampal neurons from C57Bl/6J mice. Cultured hippocampal neurons represent a rational model from which to test ankyrin-B palmitoylation given that the axonal cargo transport function of ankyrin-B was previously established in hippocampal neurons (Lorenzo et al., 2014). Indeed, we observed palmitoylation of both 220- and 440-kDa isoforms of ankyrin-B in cultured hippocampal neurons by Acyl-RAC, as shown by the hydroxylamine-dependent ankyrin-B signal (Figure 1D). Taken together, these data provide the first evidence that ankyrin-B is *S*-palmitoylated in whole mouse brain and in cultured neurons, implicating palmitoylation as a potential mechanism underlying ankyrin-B localization and function in neurons.

3.2 Ankyrin-B expression and S-palmitoylation are increased by the palmitoyl acyltransferase zDHHC17 in heterologous cells

Multiple studies have shown that the palmitoyl acyltransferase (PAT) zDHHC17 binds tightly to its substrates in order to palmitoylate them (Lemonidis et al., 2014; Verardi et al., 2017).

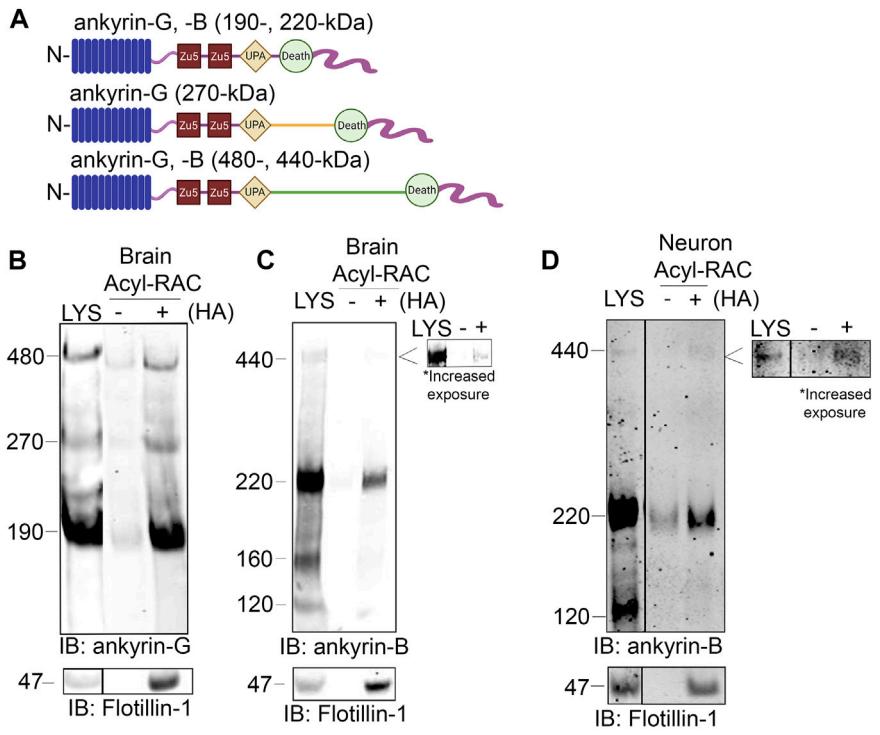

FIGURE 1
Ankyrin-B is *S*-palmitoylated in whole mouse brain and in cultured neurons. **(A)**. Schematic of neuronal ankyrin-G and ankyrin-B, which share highly homologous domains: the N-terminal ankyrin repeat domain (blue), two ZU5 spectrin binding domains (red), a UPA domain (yellow), a death domain (light green), and a highly divergent unstructured C-terminal regulatory domain (pink). The giant isoforms (480-kDa ankyrin-G and 440-kDa ankyrin-B) have a large single exon (orange and dark green) inserted between their respective UPA and death domains. **(B)**. Whole brains from C57Bl/6J mice were processed for the Acyl-RAC assay to detect *S*-palmitoylation. *S*-palmitoylation of all neuronal isoforms of ankyrin-G (190-, 270-, and 480-kDa) is detected in whole brain from C57Bl/6J mice using an antibody against endogenous ankyrin-G, as demonstrated by the anti-ankyrin-G signal in the '+HA' lane, compared to the minimal background signal in the negative control '-HA' lane. Flotillin-1 is used as a positive control for the Acyl-RAC assay (N = 3). **(C)**. *S*-palmitoylation of the known neuronal isoforms of ankyrin-B (220- and 440-kDa) is detected by Acyl-RAC in whole brain from C57Bl/6J mice using an antibody against endogenous ankyrin-B (N = 3). **(D)**. DIV17 cultured hippocampal neurons from C57Bl/6J mice were subjected to the Acyl-RAC assay. *S*-palmitoylation of the 220-kDa and 440-kDa isoforms of ankyrin-B is detected in cultured hippocampal neurons using an antibody against endogenous ankyrin-B (N = 3). All conditions shown are run on the same blot; black line delineates spliced portion of the gel containing a condition not relevant to this figure. IB, immunoblotting.

The N-terminal ANK repeat (AR) domain of zDHHC17 recognizes a conserved zDHHC AR-binding motif (zDABM), (VIAP) (VIT) XXQP (where X is any amino acid) in its substrates (Lemonidis et al., 2014; Lemonidis et al., 2015; Verardi et al., 2017). Interestingly, a previous study identified the zDABM domain in the ankyrin family, including in ankyrin-B, using a peptide array screening approach (Figure 2A) (Lemonidis et al., 2017). This finding provided rationale for investigating the role of zDHHC17 in ankyrin-B palmitoylation. We subjected lysates from HEK293T cells transiently transfected with HA-tagged zDHHC17 and ankyrin-B-GFP to Acyl-RAC and found that zDHHC17 significantly enhanced both the palmitoylation and protein levels of ankyrin-B-GFP, compared to ankyrin-B-GFP in the absence of any exogenous PATs (Figures 2B–E). The presence of GFP signal in the negative control "-HA" lane is likely due to incomplete blocking of all free cysteines in ankyrin-B-GFP, presumably due to the GFP tag, which has numerous cysteines embedded in stable secondary structure that our lysis conditions may not disrupt completely. However, our quantification accounts for this background signal by subtracting any signal in the "-HA" lane from the "+HA" signal. To ensure that the increase in palmitoylation and expression levels of ankyrin-B-GFP seen with zDHHC17 were PAT-specific and not a function of overexpression, we screened the zDHHC library consisting of all 23 PATs (Supplementary Figure S1A–D). Using Acyl-RAC, we observed most zDHHC PATs did not enhance the palmitoylation nor the expression levels of ankyrin-B-GFP, compared to ankyrin-B-GFP alone, suggesting that the assay is able to detect PAT-dependent differences in palmitoylation and protein expression. Consistent with our results from Figure 3.2, our PAT screen revealed zDHHC17 was the only exogenous PAT able to significantly enhance the palmitoylation of ankyrin-B, compared to ankyrin-B alone (Supplementary Figure S1A, B). zDHHC17 was also the only PAT that significantly increased ankyrin-B protein expression, compared to ankyrin-B alone (Supplementary Figure S1C, D). To test whether the increase in ankyrin-B-GFP protein levels seen in the presence of zDHHC17 was dependent on palmitoylation, we transiently transfected ankyrin-B-GFP with a catalytically-dead version of HA-tagged zDHHC17 (zDHHA17) in HEK293T cells and subjected the lysates to Acyl-RAC. zDHHA17 retains its recognition site for substrates (ANK repeat domain) but loses its enzymatic activity as the cysteine of the catalytic DHHC motif (C467) is mutated to alanine (Locatelli et al., 2020). We observed

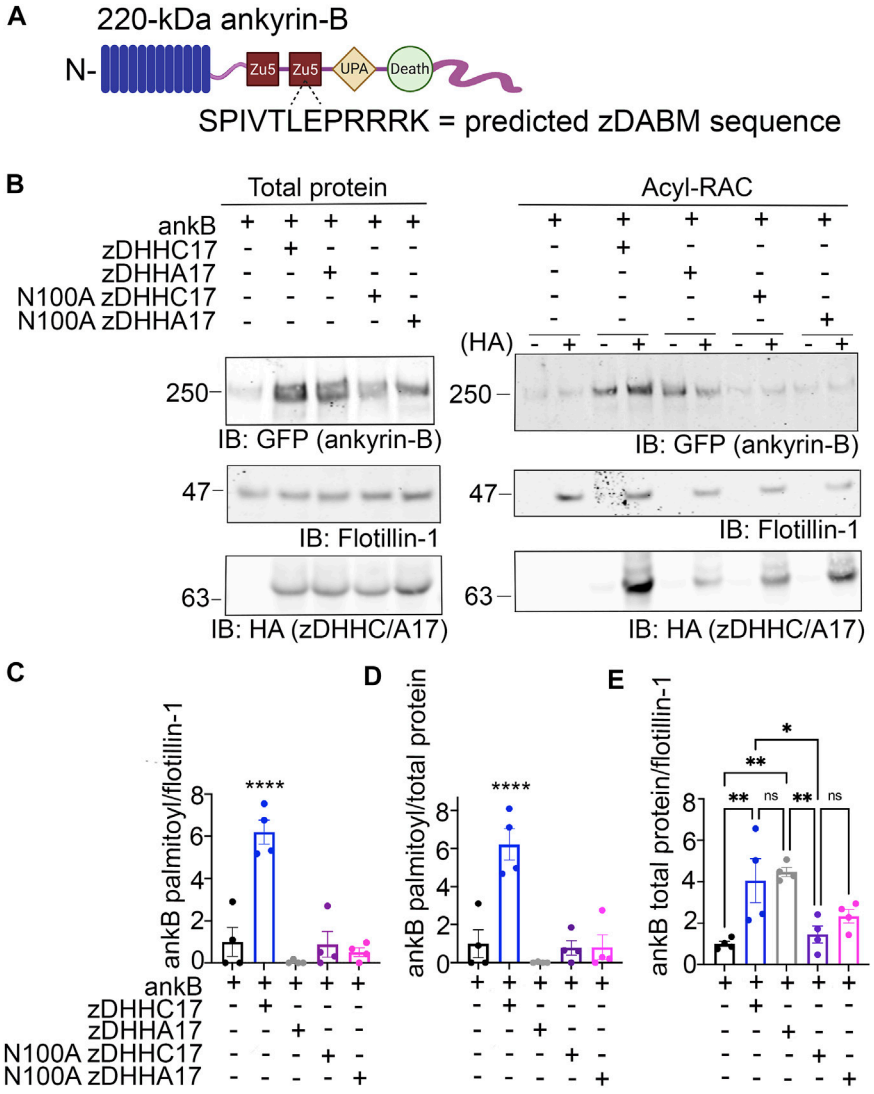

FIGURE 2
zDHHC17 recognizes the zDABM domain of ankyrin-B to regulate ankyrin-B protein expression and palmitoylation in HEK293T cells. **(A)**. Schematic of ankyrin-B with the predicted zDHHC ANK repeat binding motif sequence (zDHHC17 recognition site, predicted from (Lemonidis et al., 2017)) located in the second ZU5 domain. **(B)**. Representative western blot showing total protein levels of ankyrin-B-GFP (*left*) and palmitoylation levels of ankyrin-B-GFP (*right*) from lysates of HEK293T cells transiently transfected with WT ankyrin-B-GFP alone or together with WT zDHHC17, enzymatically-dead zDHHA17, N100A zDHHC17, or N100A zDHHA17 subjected to the Acyl-RAC assay. Ankyrin-B-GFP protein and palmitoylation levels are detected with an antibody against GFP. Palmitoylation of ankyrin-B-GFP is strongly detected in a hydroxylamine-dependent manner ('+HA' lane), compared to the background signal in the negative control '-HA' lane. Co-expression of zDHHC17 increases both the protein levels (*left*) and palmitoylation levels (*right*) of ankyrin-B-GFP, compared to ankyrin-B expressed alone. WT ankyrin-B-GFP with zDHHA17, N100A zDHH17, or N100A zDHHA17 is not palmitoylated, compared to when ankyrin-B-GFP is co-expressed with zDHHC17. Ankyrin-B-GFP protein levels are unaffected by co-expression of zDHHA17, but are drastically reduced with co-expression of N100A zDHHC17 or N100A zDHHA17. **(C)**. Quantified *S*-palmitoylation levels of ankyrin-B-GFP from N = 4 independent replicates per condition from **(A)**. ****$p < 0.0001$ relative to ankyrin-B alone; one-way ANOVA with Tukey's *post-hoc* test. For each condition, the palmitoylation signal was calculated by subtracting the −HA lane signal from that of the +HA lane and normalized to the flotillin-1 signal from the *+HA* lane, and normalized again to the average of ankyrin-B alone signal to get the relative fold change in ankyrin-B-GFP palmitoylation. **(D)**. Quantified ankyrin-B-GFP *S*-palmitoylation levels normalized to total ankyrin-B protein levels for each condition, relative to ankyrin-B alone palmitoylation levels. Data from N = 4 independent replicates per condition from **(A)**. ****$p < 0.0001$ relative to ankyrin-B alone; one-way ANOVA with Tukey's *post-hoc* test. **(E)**. Quantified ankyrin-B-GFP protein levels normalized to total flotillin-1 levels, relative to ankyrin-B alone protein levels. Data from N = 4 independent replicates per condition from **(A)**. **$p < 0.01$, *$p < 0.05$; one-way ANOVA with Tukey's *post-hoc* test.

that palmitoylation of ankyrin-B-GFP was completely abolished in the presence of enzymatically-dead zDHHA17, as compared to that with WT zDHHC17 (Figures 2B–D). In fact, there was no significant difference in ankyrin-B-GFP palmitoylation between ankyrin-B-GFP alone and ankyrin-B-GFP co-expressed with zDHHA17 (Figures 2B–D). Thus, the increase in ankyrin-B-GFP palmitoylation observed upon co-expression of WT zDHHC17 is indeed driven by the catalytic activity of zDHHC17. Notably, however, ankyrin-B-GFP levels were still increased by zDHHA17, similar to what we observed with WT zDHHC17 (Figures 2B,E).

These results suggest that the observed increase in ankyrin-B-GFP protein levels in the presence of zDHHC17 is not

palmitoylation-dependent and may instead be due to recognition of ankyrin-B-GFP by zDHHC17. To test whether the enhancement in ankyrin-B protein levels are dependent on zDHHC17 recognition, we co-expressed a version of zDHHC17 whose substrate binding site is abolished, the HA-tagged N100A zDHHC17. N100A zDHHC17 is a well-characterized ANK repeat mutant that fails to recognize zDABM-containing substrates (Verardi et al., 2017; Niu et al., 2020). Notably, ankyrin-B-GFP protein levels were reduced approximately three fold in the presence of N100A zDHHC17 compared to that with WT or zDHHA17 (Figures 2B, E), suggesting that zDHHC17 recognition of ankyrin-B regulates ankyrin-B protein expression in heterologous cells. Surprisingly, ankyrin-B protein stability was unchanged in the presence of WT or N100A zDHHC17, compared to ankyrin-B alone by cycloheximide chase assay, suggesting that zDHHC17 is not regulating ankyrin-B expression by conferring stability in heterologous cells (Supplementary Figure S2A, BA). Future studies will need to investigate the mechanisms underlying zDHHC17-dependent increases in ankyrin-B protein expression in heterologous cells. Given that zDHHC17 often requires direct interaction with its substrates to palmitoylate them (Lemonidis et al., 2017), we hypothesized that the N100A mutation in zDHHC17 would also prevent palmitoylation. As predicted, loss of zDHHC17-ankyrin-B recognition induced by the N100A mutation in zDHHC17 or zDHHA17 results in drastically reduced palmitoylation levels compared to that with WT zDHHC17 (Figures 2B–D). These results are consistent with the canonical zDHHC17 AR-substrate zDABM binding paradigm necessary for palmitoylation and confirms the findings of the peptide array screen that showed ankyrin-B has a zDABM domain (Lemonidis et al., 2017).

3.3 zDHHC17 is required to palmitoylate endogenous ankyrin-B in cultured hippocampal neurons

Our findings using overexpression in heterologous cells suggest that zDHHC17 is a strong candidate for ankyrin-B palmitoylation. To address whether zDHHC17 palmitoylates endogenous ankyrin-B, we used cultured hippocampal neurons from floxed *Zdhhc17* mice (Sanders et al., 2016) that were transduced with either a β-galactosidase control adenovirus or a Cre-recombinase adenovirus before lysates were either subjected to RT-PCR analysis to probe for extent of *Zdhhc17* deletion or the Acyl-RAC assay to probe for effects on ankyrin-B palmitoylation. RT-PCR analysis revealed a 95% reduction of *Zdhhc17* mRNA levels 10 days post-transduction of Cre adenovirus in floxed *Zdhhc17* hippocampal neurons, compared to neurons treated with β-galactose control adenovirus (Figure 3A). Acyl-RAC revealed an 80% loss of ankyrin-B palmitoylation in Cre-treated floxed *Zdhhc17* hippocampal neurons, compared to that with the control virus (Figures 3B–D). Results from Figure 3.2 demonstrating that zDHHC17 recognizing ankyrin-B is sufficient to increase protein levels led us to hypothesize that loss of endogenous zDHHC17 would reduce endogenous ankyrin-B protein levels. However, there was no significant difference in ankyrin-B protein levels between the Cre virus-treated and the control virus-treated neurons (Figure 3E), suggesting that neurons may utilize mechanisms independent of zDHHC17 to regulate ankyrin-B protein levels, unlike in heterologous cells. Taken together, these data demonstrate zDHHC17 is a major regulator of ankyrin-B palmitoylation in neurons.

3.4 Ankyrin-B is S-palmitoylated at multiple cysteines in its N-terminal ankyrin repeat domain

The palmitoylation sites within ankyrin-B are unknown. Ankyrin-B's homologous family member, ankyrin-G, is *S*-palmitoylated at a single cysteine in its N-terminal ankyrin repeat domain, Cys70 (He et al., 2012). Cys70 is conserved among all three human ankyrin members and vertebrate ankyrins (He et al., 2012), with ankyrin-B possessing a homologous cysteine at Cys60 (Figure 4A). Given the conservation of this amino acid, we hypothesized that Cys60 in ankyrin-B is the principal palmitoylated cysteine. Using site-directed mutagenesis, we engineered a cDNA construct in which Cys60 in ankyrin-B was converted to an alanine (C60A ankyrin-B-GFP). The C60A ankyrin-B-GFP mutant construct was transiently transfected with HA-tagged zDHHC17 into HEK293T cells, and lysates were subjected to Acyl-RAC to test the mutant's effects on ankyrin-B palmitoylation. The C60A ankyrin-B mutant led to a 60% reduction in ankyrin-B palmitoylation, compared to WT ankyrin-B, despite efficient expression of C60A ankyrin-B-GFP (Figures 4B, C). These data suggest that there are additional palmitoylated cysteine sites in ankyrin-B beyond Cys60.

Ankyrin-B has 26 cysteines, seven of which are harbored in the N-terminal ankyrin repeat domain, a domain necessary for ankyrins to interact with their membrane-associated partners (Figure 4A) (Bennett and Lorenzo, 2013). To narrow down on additional palmitoylation sites in ankyrin-B, we asked whether the N-terminal ankyrin repeat domain of ankyrin-B was required for palmitoylation. Acyl-RAC on lysates from HEK293T cells transiently transfected with a truncated version of ankyrin-B which completely lacks the ankyrin repeat domain (120-kDa ankyrin-B-GFP) as well as zDHHC17 demonstrated an almost complete reduction of ankyrin-B-GFP palmitoylation, compared to WT ankyrin-B-GFP, despite efficient expression of 120-kDa ankyrin-B-GFP (Figures 4D, E). These data suggest that additional palmitoylation sites of ankyrin-B are either located within the ankyrin repeat domain itself or that the ankyrin repeat domain is required for interaction with zDHHC17 and subsequent palmitoylation.

To determine if the additional palmitoylation sites are within the ankyrin-B ankyrin repeat domain, we employed mass spectrometry to identify peptides with *S*-palmitoylated cysteine sites in ankyrin-B. Lysates from HEK293T cells transfected with ankyrin-B-GFP and zDHHC17-HA were processed for the Acyl-RAC assay, digested, and analyzed by nano Liquid Chromatography tandem Mass Spectrometry (LC-MS/MS). With this approach, we identified five ankyrin-B peptides containing Cys60, Cys305, Cys347, Cys375, and Cys406 (Figure 4A (bolded), Supplementary Figure S3A). We did not detect peptides containing Cys482 and Cys736, likely indicating that these cysteines were not palmitoylated

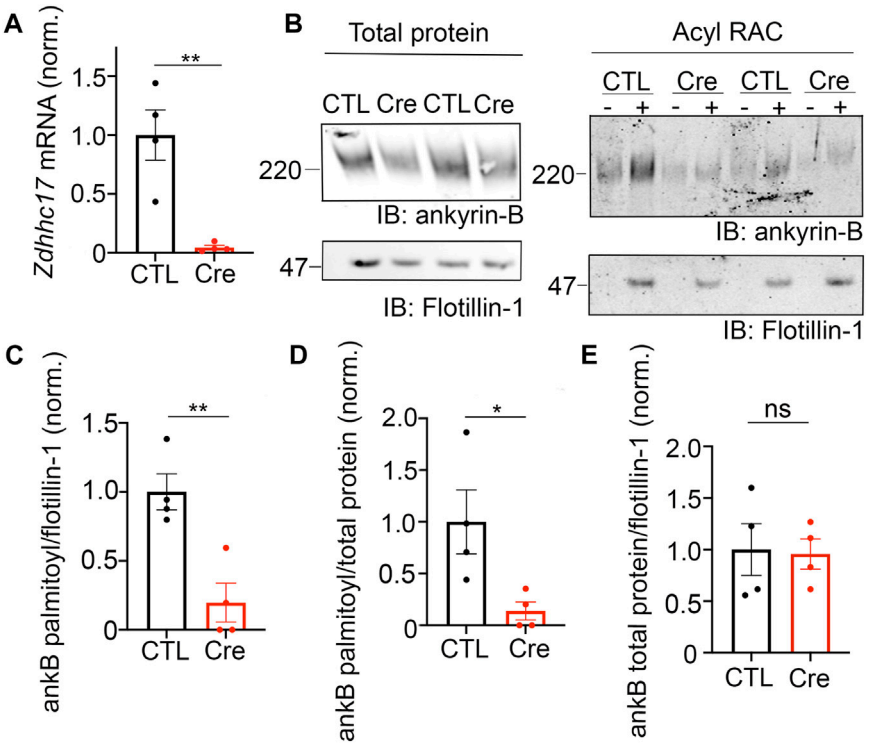

FIGURE 3
zDHHC17 is a critical regulator of endogenous ankyrin-B palmitoylation in cultured hippocampal neurons from. **(A)**. *Zdhhc17* mRNA levels in cultured hippocampal neurons from *Zdhhc17* mice transduced with either a β-galactose control adenovirus or Cre-recombinase adenovirus for 10 days prior to sample collection for RT-PCR analysis (n = 4). *Zdhhc17* mRNA was decreased by ~95% in the Cre-recombinase condition compared to control. $^{**}p < 0.01$; Student's *t-test* (unpaired). **(B)**. Representative western blot showing total protein levels of endogenous ankyrin-B (*left*) and palmitoylation levels of endogenous ankyrin-B (*right*) from lysates of floxed *Zdhhc17* hippocampal neurons transduced with either a β-galactose control adenovirus or Cre-recombinase adenovirus for 10 days before Acyl-RAC processing (N = 4). Both protein (*left*) and palmitoylation (*right*) levels of endogenous ankyrin-B are immunoblotted with an antibody against ankyrin-B for all conditions. Palmitoylation of ankyrin-B is strongly detected in a hydroxylamine dependent manner ('+HA' lane) from cultures infected with the control virus, but is greatly reduced in cultures infected with the Cre virus, as demonstrated by the lower ankyrin-B signal intensity in the '+HA' lane. **(C)**. Quantified endogenous ankyrin-B *S*-palmitoylation normalized to flotillin-1 levels from the Acyl-RAC fractions and further normalized to control virus. Data from N = 4 independent replicates per condition from **(A)**. $^{**}p < 0.01$; Student's *t-test* (unpaired). **(D)**. Quantified endogenous ankyrin-B *S*-palmitoylation normalized to total ankyrin-B protein levels for each condition, and further normalized to control virus. Data from N = 4 independent replicates per condition from **(A)**. $^{**}p < 0.05$; Student's *t-test* (unpaired). **(E)**. Quantified endogenous ankyrin-B levels normalized to total flotillin-1 levels for each condition, and further normalized to control virus. Data from N = 4 independent replicates per condition from **(A)**. not significant (ns); Student's *t-test* (unpaired).

(Supplementary Figure S3A). To confirm that Cys482 and Cys736 were not palmitoylation sites in ankyrin-B, we engineered cDNA constructs containing a cysteine-to-alanine mutation at C482A and another at C736A in ankyrin-B-GFP. C482A ankyrin-B-GFP and C736A ankyrin-B-GFP were individually expressed with zDHHC17-HA in HEK293T cells and processed for the Acyl-RAC assay to test their individual effects on ankyrin-B palmitoylation. Indeed, co-expression of zDHHC17-HA and either C482A ankyrin-B-GFP or C736A ankyrin-B-GFP did not affect ankyrin-B palmitoylation, compared to WT ankyrin-B (Supplementary Figure S3B, C).

To further investigate the functional role of the remaining four candidate palmitoylation sites in ankyrin-B identified in the mass spectrometry study (C305, C347, C375, C406) (Figure 4A), we constructed a mutant version of ankyrin-B with the five cysteine residues, Cys60 included, substituted to alanine residues using site-directed mutagenesis. This mutant GFP-tagged ankyrin-B construct is referred to as AAAAA-ankyrin-B-GFP (or A5B), and when co-expressed with zDHHC17, demonstrated virtually no ability to be palmitoylated compared to WT ankyrin-B-GFP, despite efficient expression of this mutant (Figures 4F, G). This is shown by the loss of hydroxylamine-dependent GFP signal in the presence of AAAAA-ankyrin-B-GFP, compared to WT and C60A ankyrin-B-GFP. These data demonstrate that ankyrin-B is palmitoylated at multiple cysteine sites harbored in its N-terminal ankyrin-repeat domain. Furthermore, the palmitoylation-dead ankyrin-B mutant, AAAAA-ankyrin-B-GFP, represents a novel tool for investigating the functional consequences of ankyrin-B palmitoylation on downstream ankyrin-B localization and function.

3.5 S-palmitoylation does not regulate ankyrin-B-mediated axonal cargo transport in hippocampal neurons

Deletion of *Ank2*, which encodes ankyrin-B, leads to impaired organelle transport in axons of cultured hippocampal neurons (Lorenzo et al., 2014). Here, we asked whether palmitoylation

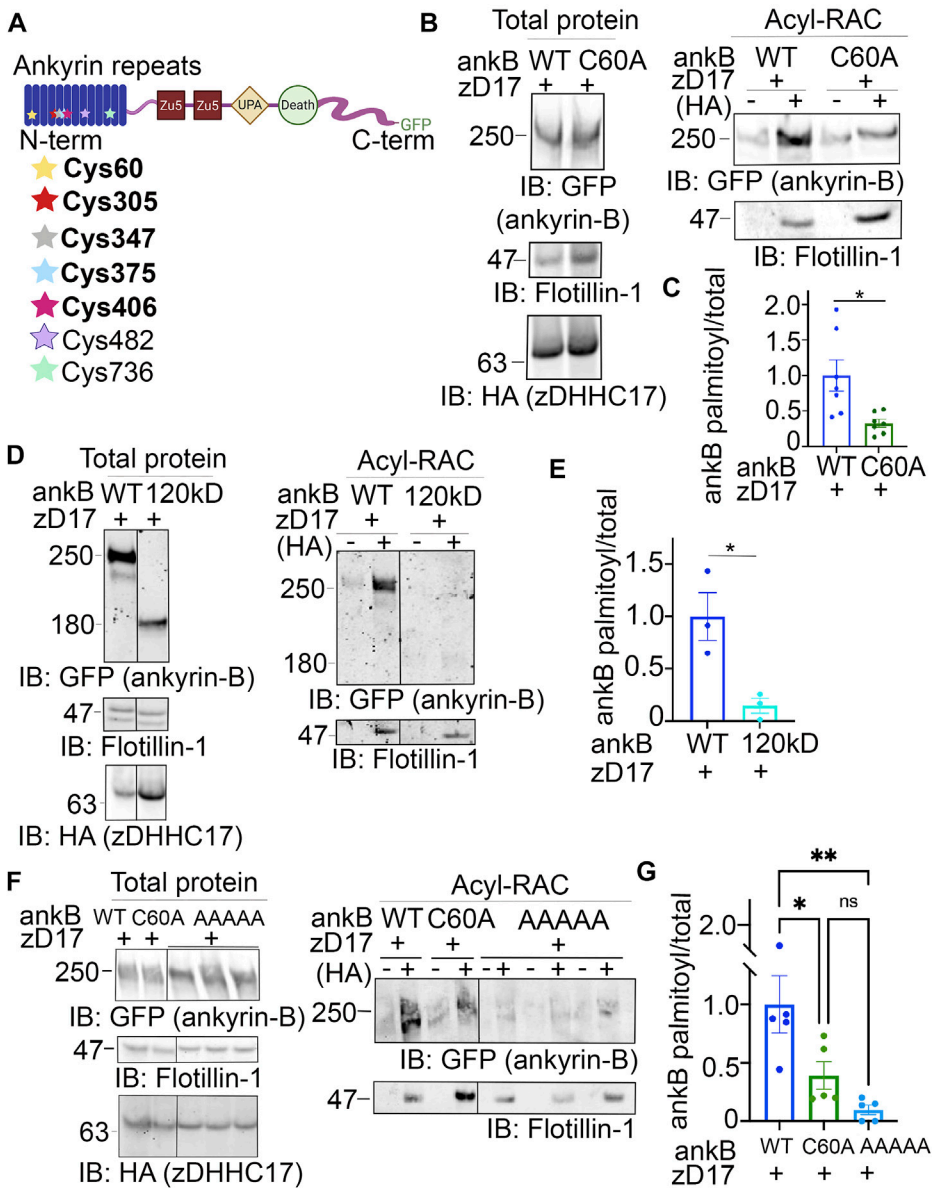

FIGURE 4
Identification of ankyrin-B *S*-palmitoylated cysteine sites. **(A)**. Schematic of the domains in ankyrin-B and the cysteine residues harbored in the N-terminal ankyrin repeat domain, which are candidate palmitoylation sites. Bolded cysteine residues are the cysteine residues that were substituted to alanine to generate the palmitoylation-dead ankyrin-B mutant. **(B)**. Representative western blot showing total protein levels of ankyrin-B-GFP (*left*) and palmitoylation levels of ankyrin-B-GFP (*right*) from lysates of HEK293T cells transiently co-transfected with WT ankyrin-B-GFP or C60A ankyrin-B-GFP and zDHHC17 processed for the Acyl-RAC assay (N = 7). *S*-palmitoylation of C60A ankyrin-B-GFP is greatly reduced, as evidenced by the lower GFP signal in the '+HA' lane compared to that of the WT ankyrin-B-GFP. **(C)**. Quantified ankyrin-B-GFP *S*-palmitoylation levels normalized to total ankyrin-B protein levels for each condition, relative to palmitoylation levels of WT ankyrin-B-GFP co-expressed with zDHHC17. Data from N = 7 independent replicates per condition from **(A)**. $*p = 0.0119$; Student's *t-test* (unpaired). **(D)**. Representative western blot showing total protein levels of ankyrin-B-GFP (*left*) and palmitoylation levels of ankyrin-B-GFP (*right*) from lysates of HEK293T cells transiently co-transfected with WT ankyrin-B-GFP or 120-kDa ankyrin-B-GFP and zDHHC17 processed for the Acyl-RAC assay (N = 3). All conditions shown are run on the same blot; black line delineates spliced portion of the gel containing a condition not relevant to this figure. *S*-palmitoylation of 120-kDa ankyrin-B-GFP is not detected using an antibody against GFP, as shown by the absence of anti-GFP signal in the '+HA' lane, compared to that when WT ankyrin-B-GFP is co-expressed with zDHHC17. **(E)**. Quantified ankyrin-B-GFP *S*-palmitoylation levels normalized to total ankyrin-B protein levels for each condition, relative to palmitoylation levels of WT ankyrin-B-GFP co-expressed with zDHHC17. Data from N = 3 independent replicates per condition from **(D)**. $*p = 0.0241$; Student's *t-test* (unpaired). **(F)**. Representative western blot showing total protein levels of ankyrin-B-GFP (*left*) and palmitoylation levels of ankyrin-B-GFP (*right*) from lysates of HEK293T cells transiently co-transfected with WT ankyrin-B-GFP, C60A ankyrin-B-GFP, or AAAAA-ankyrin-B-GFP and zDHHC17 processed for the Acyl-RAC assay (N = 5). All conditions shown are run on the same blot; black line delineates spliced portion of the gel containing a condition not relevant to this figure. Compared to WT ankyrin-B-GFP and C60A ankyrin-B-GFP, *S*-palmitoylation of AAAAA-ankyrin-B-GFP is almost completely abolished. **(G)**. Quantified ankyrin-B-GFP *S*-palmitoylation levels normalized to total ankyrin-B protein levels for each condition, relative to palmitoylation levels of WT ankyrin-B-GFP co-expressed with zDHHC17. Data from N = 5 independent replicates per condition from **(F)**. $**p < 0.01$, $*p < 0.05$; one-way ANOVA with Tukey's *post-hoc* test.

could regulate the axonal transport function of ankyrin-B. To study the effects of the palmitoylation-dead form of ankyrin-B on an ankyrin-B-null background, we used cultured hippocampal neurons from floxed *Ank2* mice to knock out ankyrin-B with transfection of Cre recombinase and simultaneously rescued with either wild-type (WT) 220-kDa ankyrin-B-GFP or palmitoylation-dead AAAAA-ankyrin-B-GFP (A5B) cDNA. Transfection of Cre-recombinase and rescue cDNA at 2 days *in vitro* (DIV) and imaging by time-lapse video microscopy 48 h later allowed for observation of optimal motility of synaptic vesicle protein tdTomato-tagged synaptotagmin-1 (Syt1-tdTomato) along the axon in real time. Syt1-tdTomato moved bidirectionally along the axon with high processivity in control neurons only transfected with Syt1-tdTomato (Figure 5A, B; Supplementary Movie S1), as observed previously (Lorenzo et al., 2014). In neurons transfected with Syt1-tdTomato and Cre recombinase-2A-BFP to knock out ankyrin-B, we observed an increased percentage of stationary or trapped synaptic vesicles in axonal swellings along the axons (Figure 5B). Additionally, the Syt1-tdTomato vesicles that still retained motility in the Cre-knockout condition exhibited slower velocities and traveled shorter distances bidirectionally along the axons, compared to controls (Figure 5A, B; Supplementary Movie S2), which recapitulated the organelle transport deficits observed in the *AnkB*$^{-/-}$ mice (Lorenzo et al., 2014). The retrograde velocity deficits of Syt1-tdTomato particles observed upon deletion of ankyrin-B (Cre-2A-BFP) were partially rescued with addition of WT 220-kDa ankyrin-B-GFP or palmitoylation-dead AAAAA-ankyrin-B-GFP, whereas neither WT nor AAAAA-ankyrin-B-GFP rescued the anterograde velocity deficits of Syt1 particles induced by deletion of ankyrin-B (Figure 5A, B; Supplementary Movie S3 ,4). The retrograde run length deficits of Syt1-tdTomato particles in the absence of ankyrin-B (Cre-2A-BFP) were fully rescued with addition of WT ankyrin-B-GFP or palmitoylation-dead AAAAA-ankyrin-B-GFP, whereas neither WT or AAAAA-ankyrin-B-GFP rescued anterograde run length deficits of Syt1 particles induced by deletion of ankyrin-B (Figures 5A, B). Longer expression times may be necessary to observe rescue of anterograde velocity or run length deficits with WT ankyrin-B-GFP. Addition of WT or AAAAA-ankyrin-B-GFP also rescued the increase in Syt1-tdTomato stationary particles induced by deletion of ankyrin-B (Cre-2A-BFP) (Figure 5B). Furthermore, we did not observe any significant differences in the speed, distance, or relative mobility of WT (left) or palmitoylation-dead AAAAA-ankyrin-B-GFP (right) particles (Figures 5C, D; Supplementary Movie S5, 6). Taken together, these results suggest palmitoylation-dead ankyrin-B is capable of mediating axonal cargo transport of Syt1 similar to WT ankyrin-B. Thus, ankyrin-B-mediated cargo transport of synaptic vesicles, like Syt1, is not dependent on ankyrin-B palmitoylation.

3.6 S-palmitoylation is required for ankyrin-B-mediated scaffolding of $Na_V1.2$ at the dendritic membranes of neocortical pyramidal neurons

Given the lack of effect in axonal transport, we asked whether palmitoylation of ankyrin-B could serve other functions. Recently, we showed that ankyrin-B scaffolds the voltage-gated sodium channel $Na_V1.2$ at the dendritic membrane to promote dendritic excitability and synaptic function (Nelson et al., 2022). Here, we asked whether palmitoylation was required for ankyrin-B to scaffold $Na_{V\text{dendritic localization due to ankyrin}}1.2$ at the dendritic membrane. Given that the dendritic deficits observed upon heterozygous loss of ankyrin-B *in vivo* were observed in the prefrontal layer 5b of mouse cortex and loss of $Na_V1.2$ dendritic localization due to ankyrin-B deletion were observed in neocortical neuron cultures (Nelson et al., 2022), we investigated the role of ankyrin-B palmitoylation for $Na_V1.2$ scaffolding in neocortical cultures. To validate that $Na_V1.2$ localized properly at the AIS, where it is canonically scaffolded by ankyrin-G, as well as at dendritic membranes, we transfected DIV2 floxed *Ank2* neocortical neurons with $Na_V1.2$-3x FLAG, fixed at DIV21 (when the $Na_V1.2$ AIS-to-dendrite shift has occurred (Spratt et al., 2019)), and stained with antibodies against FLAG and ankyrin-B. We observed intense $Na_V1.2$-3x FLAG staining at the AIS, consistent with $Na_V1.2$'s role at the AIS in mature neurons (referenced by the white star in Figure 6A), and $Na_V1.2$-3x FLAG staining at dendritic membranes, as evidenced by the "railroad track" footprint that overlaps with endogenous ankyrin-B staining (Figures 6A, B top row). To validate that deletion of ankyrin-B in neocortical neurons results in loss of $Na_V1.2$-3x FLAG dendritic localization (Nelson et al., 2022), we transfected DIV2 floxed *Ank2* neocortical neurons with $Na_V1.2$-3x FLAG and Cre-2A-BFP to knockout ankyrin-B. As expected, we observed nearly complete reduction in $Na_V1.2$-3x FLAG dendritic immunostaining upon loss of ankyrin-B (Figures 6A–C). Remaining $Na_V1.2$-3x FLAG immunoreactivity has been shown to be localized to the AIS, as indicated by ankyrin-G staining and relative lack of ankyrin-B staining, as described previously (Nelson et al., 2022). $Na_V1.2$-3x FLAG immunostaining at the AIS remained unchanged, consistent with ankyrin-G-dependent localization of $Na_V1.2$-3x FLAG at the AIS (Figures 6A, B, D) (Jenkins et al., 2015). While rescue of Cre-mediated deletion of ankyrin-B with WT ankyrin-B-GFP resulted in the re-appearance of membrane-associated $Na_V1.2$-3x FLAG immunostaining specifically at the dendrites, as evidenced by the "railroad track-like" FLAG staining (Figures 6A–C), addition of palmitoylation-dead AAAAA-ankyrin-B-GFP did not rescue loss of $Na_V1.2$-3x FLAG immunostaining at the dendrites in *Ank2* neocortical neurons (Figures 6A–C). These data suggest that ankyrin-B palmitoylation is required for proper dendritic localization of $Na_V1.2$ in neocortical pyramidal neurons.

3.7 Palmitoylation-dead AAAAA-ankyrin-B cannot properly localize to dendritic membranes of neocortical pyramidal neurons

We reasoned that the inability of palmitoylation-dead ankyrin-B to function in scaffolding $Na_V1.2$ at dendritic membranes may be because palmitoylation-dead ankyrin-B is unable to properly target to dendritic membranes itself. To investigate whether dendritic localization of ankyrin-B is altered when ankyrin-B is unable to be palmitoylated, we first validated proper dendritic membrane localization of ankyrin-B as observed previously (Figures 6A,B)

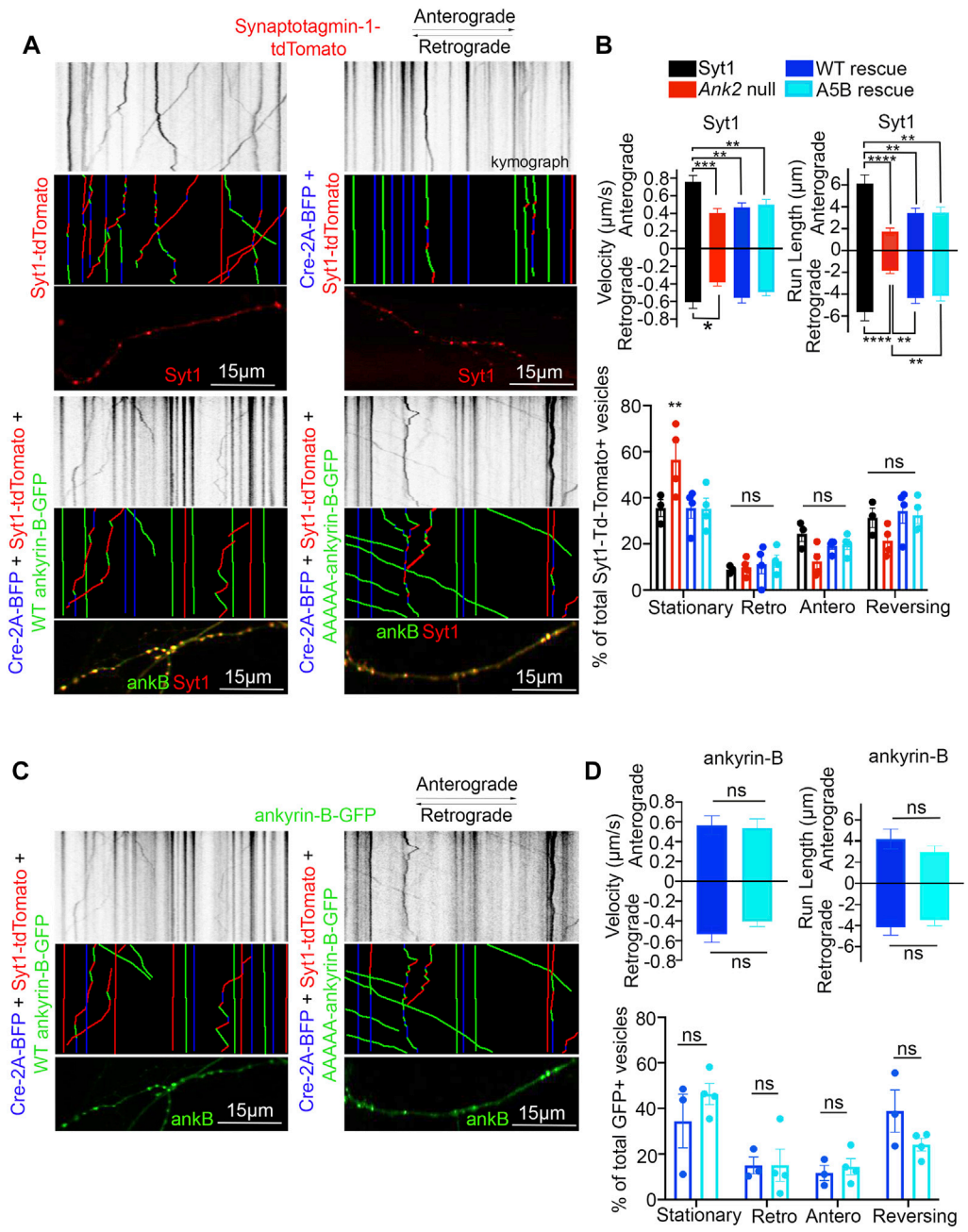

FIGURE 5
Loss of ankyrin-B palmitoylation does not affect axonal cargo transport of synaptic vesicle protein Synaptotagmin-1 (Syt1). **(A)** (Top) Representative kymographs of tdTomato-tagged Syt1 particle movement along DIV4 axons of floxed *Ank2* hippocampal neurons in the absence or presence of Cre-2A-BFP to knock-out ankyrin-B and WT or palmitoylation-dead AAAAA-ankyrin-B-GFP as rescue plasmids. (Middle) Corresponding color-coded trajectories for tdTomato-positive particles demonstrating static vesicles (blue), anterograde-moving particles (green), and retrograde-moving particles (red). (Bottom) Puncta distribution of Syt1-tdTomato vesicles along axons (region of axon used to generate kymographs). **(B)**. Axonal velocity and run length for Syt1 particles. Data shown is from one representative experiment out of 4 independent repeats. N = four to eight axons per condition (n = 88–154 particles per condition). Data represent means ± SEM. $^{**}p < 0.01$, $^{***}p < 0.001$, $^{****}p < 0.0001$. For velocity and run lengths analyses, one-way ANOVA with Tukey's *post-hoc* test were performed. For % motility analysis, two-way ANOVA with multiple comparisons and Tukey's *post-hoc* was performed. **(C)**. (Top) Representative kymographs of GFP-tagged ankyrin-B particle movement along DIV4 axons of floxed *Ank2* hippocampal neurons in the absence or presence of Cre-2A-BFP to knock-out ankyrin-B and WT or palmitoylation-dead AAAAA-ankyrin-B-GFP as rescue plasmids. (Middle) Corresponding color-coded trajectories for GFP-positive particles demonstrating static vesicles (blue), anterograde-moving particles (green), and retrograde-moving particles (red). (Bottom) Puncta distribution of WT or AAAAA-ankyrin-B-GFP vesicles along axons (region of axon used to generate kymographs). **(D)**. Axonal velocity and run length for ankyrin-B particles. Data shown is from one representative experiment out of 4 independent repeats. N = 3-7 axons per condition (n = 38–76 particles per condition). Data represent means ± SEM. not significant (ns). For velocity and run lengths analyses, Student's *t-tests* were performed. For % motility analysis, two-way ANOVA with multiple comparisons and Tukey's *post-hoc* was performed.

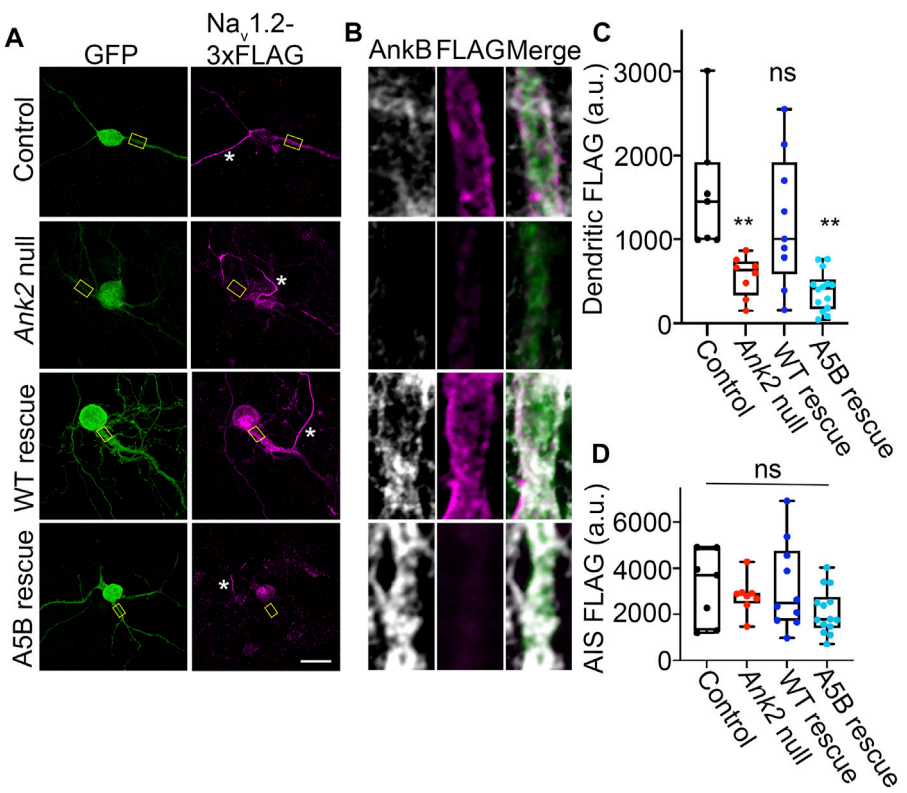

FIGURE 6
Loss of ankyrin-B palmitoylation prevents Na$_V$1.2 from localizing properly at dendritic membranes of cultured neocortical neurons. **(A)**. Representative collapsed *Z*-stacks of DIV21 cultured floxed *Ank2* cortical neurons transfected at DIV2 with Na$_V$1.2-3x FLAG (Control) (*Top*), Cre-2A-BFP and Na$_V$1.2-3x FLAG to generate total ankyrin-B-null neurons (*Second from top*), or Cre-2A-BFP, Na$_V$1.2-3x FLAG, and indicated GFP rescue constructs (*Bottom*). Stars denote axon initial segment. Scale bars 20 μm. Neurons stained with anti-GFP shown in green, anti-FLAG shown in magenta, and anti-ankyrin-B shown in greyscale. **(B)**. Zoomed-in single-stack images of selected dendritic compartment from *A* (denoted by yellow square). Anti-FLAG is shown in magenta, and anti-ankyrin-B is shown in far red. AAAAA-ankyrin-B-cannot rescue the loss of dendritic membrane localization of Na$_V$1.2-3x FLAG induced by Cre-mediated deletion of ankyrin-B, compared to WT ankyrin-B-GFP. **(C)**. Quantification of mean fluorescence intensity of dendritic Na$_V$1.2-3x FLAG from *A,B*. $^{**}p < 0.01$ relative to Control; one-way ANOVA with Tukey's *post-hoc* test, N = 7–14 for each group across three independent replicates. **(D)**. Quantification of mean fluorescence intensity of AIS Na$_V$1.2-3x FLAG from *A,B*. There is no change in AIS Na$_V$1.2-3x FLAG localization for any of the conditions. NS (not significant) by one-way ANOVA with Tukey's *post-hoc* test, N = 7–14 for each group across three independent replicates.

(Nelson et al., 2022). As expected, we observed ankyrin-B membrane localization at the dendritic plasma membrane, as evidenced by the "railroad-track" like appearance of ankyrin-B immunostaining in BFP-transfected control neurons (Figures 7, B). We confirmed the efficiency of our knockout by verifying that dendritic membrane ankyrin-B localization was significantly reduced in *Ank2*$^{flox/flox}$ neurons transfected with Cre-2A-BFP (*Ank2* null) compared to BFP-transfected (wild-type) control neurons (Figures 7, B). Rescue of Cre-mediated loss of ankyrin-B with WT 220-kDa ankyrin-B-GFP resulted in the re-appearance of membrane-associated ankyrin-B-GFP staining at the dendrite, as shown by the two green GFP peaks flanking the soluble BFP peak in the plot profile (Figures 7C, D). Strikingly, rescue of Cre-mediated loss of ankyrin-B with palmitoylation-dead AAAAA-ankyrin-B-GFP resulted in loss of membrane-association of ankyrin-B, as demonstrated by the lack of "railroad-track" like appearance of AAAAA-ankyrin-B-GFP and as shown by the overlapping green GFP and blue soluble BFP peaks (Figures 7C, D). These data suggest palmitoylation-dead ankyrin-B is not able to associate with dendritic membranes and is instead mainly distributed in the dendrite cytoplasm. This phenotype is consistent with the fate of palmitoylation-dead neuronal ankyrin-G, C70A ankyrin-G, which is unable to associate specifically with the AIS membrane and instead distributes in a non-polarized fashion throughout the cytoplasm, rendering it non-functional and thus incapable of clustering binding partners such as neurofascin (Tseng et al., 2015). These data highlight that palmitoylation is required for ankyrin-B dendritic targeting, which is critical for ankyrin-B function in scaffolding Na$_V$1.2 in neocortical pyramidal neurons.

4 Discussion

Ankyrin-B's functions as a membrane organizer at the axon have been well-characterized. At the axon, ankyrin-B links the dynein/dynactin motor complex to organelles to promote fast axonal cargo transport, scaffolds the cell adhesion molecule L1CAM at the distal axon to repress axonal branching, and assembles a distal axonal cytoskeleton with βII-spectrin and αII-spectrin that restricts ankyrin-G positioning at the AIS (Galiano et al., 2012; Lorenzo et al., 2014; Yang et al., 2019). Recently,

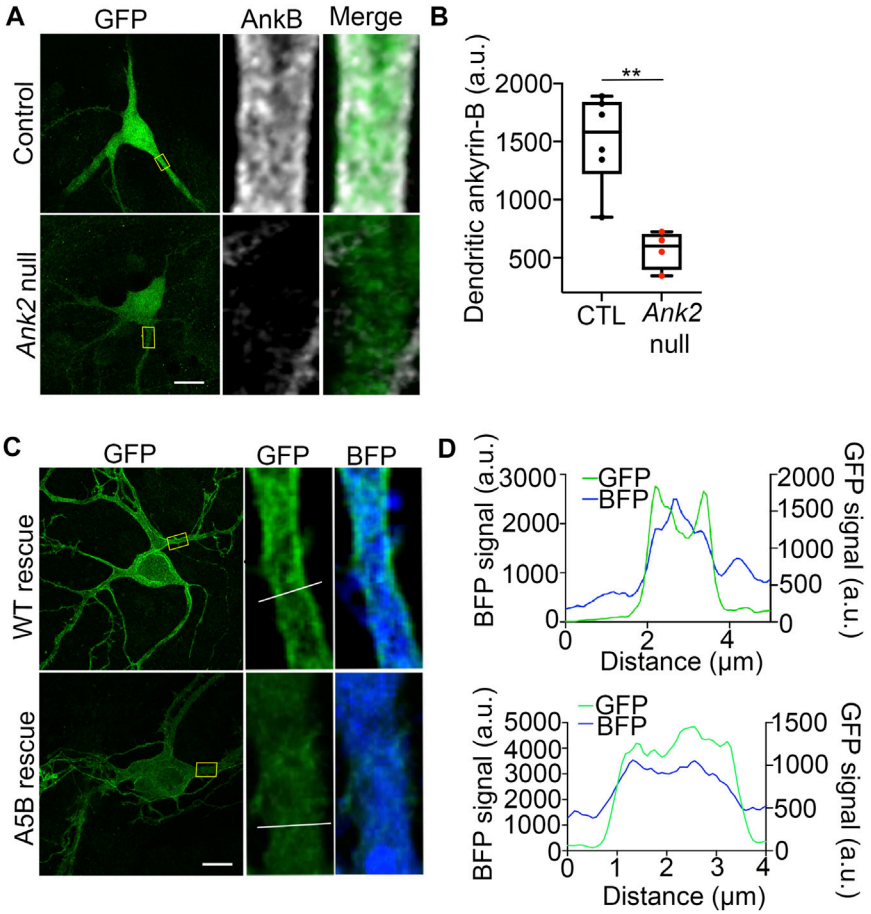

FIGURE 7
Palmitoylation-dead ankyrin-B is unable to target to dendritic membranes in neocortical pyramidal neurons. **(A)**. Representative collapsed *Z*-stack (*left*) and zoomed-in single stack images (*right*) of DIV21 cultured floxed *Ank2* cortical neurons transfected at DIV2 with soluble GFP and BFP (*top*) or soluble GFP and Cre-2A-BFP (*bottom*) to knock-out ankyrin-B. Boxes denote zoomed-in section of the dendrite. Scale bars 20 μm. Neurons stained with anti-GFP shown in green and anti-ankyrin-B shown in far red. Note: residual ankyrin-B immunoreactivity is due to nearby untransfected floxed *Ank2* neurons, which are Cre -negative, and thus still express ankyrin-B. **(B)**. Quantification of mean fluorescence intensity of dendritic ankyrin-B from **(A)**. P**<0.01 relative to Control; student's *t-test* (unpaired), N = 4-6 neurons for each group across three independent replicates. **(C)**. Representative collapsed *Z*-stack (*left*) and zoomed-in single stack images (*right*) of DIV21 cultured floxed *Ank2* cortical neurons transfected at DIV2 both transfected with Cre-2A-BFP to knock-out ankyrin-B and either rescued with WT ankyrin-B-GFP (*top*) palmitoylation-dead AAAAA-ankyrin-B-GFP (*bottom*) to assess dendritic membrane localization of ankyrin-B. Yellow boxes denote zoomed-in section of the dendrite. White line denotes region of interest across the dendrite used to generate plot profiles outlining membrane *versus* cytoplasmic ankyrin-B-GFP staining. Scale bars 20 μm. Neurons stained with anti-GFP shown in green. Blue fluorescence comes from the BFP downstream of the 2A peptide, which fills the cell as soluble BFP. **(D)**. Plot profile outlining membrane *versus* cytoplasmic GFP (ankyrin-B) (green) and BFP (blue) staining across dendrite (region of interest denoted by white line on zoomed-in single stack). What appears as plasma-membrane localization of ankyrin-B at dendrites is demonstrated by the two green peaks flanking the soluble BFP peak. The two green peaks in plot profile representing membrane-localized ankyrin-B are present in WT ankyrin-B-GFP rescue, but not in the palmitoylation-dead ankyrin-B-GFP rescue. N = 3 independent replicates.

ankyrin-B, itself highly enriched in dendrites, was revealed to localize the voltage-gated sodium channel $Na_V1.2$ to dendritic membranes to facilitate dendritic excitability (Nelson et al., 2022). Thus, ankyrin-B plays important roles in ensuring neuronal connectivity, polarization, and excitability. Dysfunction in *ANK2* is highly implicated in ASD, yet it remains unclear how *ANK2*, independently or by converging with the high-risk ASD gene *SCN2A* or other ASD-associated genes, contributes to ASD etiology.

Given the strong association between *SCN2A* and *ANK2* in ASD, and the importance of ankyrin-B-mediated scaffolding of $Na_V1.2$ at dendrites for proper dendritic and synaptic function, it is important to understand how ankyrin-B targets to the dendritic membrane to allow for $Na_V1.2$ localization. Previous studies showed other members of the ankyrin family, like ankyrin-R and ankyrin-G, are *S*-palmitoylated and that ankyrin-G palmitoylation was required for proper ankyrin-G localization and function in polarized epithelial cells and in neurons (Staufenbiel, 1987; He et al., 2012; He et al., 2014; Tseng et al., 2015). Here, we extend those findings to show for the first time that ankyrin-B is also *S*-palmitoylated, and relies on palmitoylation for proper localization and function at dendritic membranes in neurons. We also show ankyrin-B palmitoylation does not affect ankyrin-B-mediated axonal cargo transport.

Importantly, this work highlights that ankyrin-B utilizes distinct palmitoylation mechanisms compared to ankyrin-G, which is palmitoylated by functionally redundant zDHHC5 and

zDHHC8 at a single cysteine residue, Cys70 (He et al., 2012; He et al., 2014). We show that ankyrin-B is capable of being palmitoylated by zDHHC17 in heterologous cells and further validated those findings by demonstrating zDHHC17 is a critical mediator of endogenous ankyrin-B palmitoylation in neurons. This is consistent with previous palmitoylproteomic studies that have identified ankyrin-B as being palmitoylated in brain (Pinner et al., 2016; Zaręba-Kozioł et al., 2021; Gorenberg et al., 2022); however, no follow-up functional experiments were performed in these studies. In heterologous cells, we observed zDHHC17 recognizes the zDABM domain of ankyrin-B to regulate both ankyrin-B expression levels and ankyrin-B palmitoylation. A previous study demonstrated the ANK domain of zDHHC17 recognizes a specific zDABM signature ((VIAP) (VIT)XXQP (where X is any amino acid)) in its substrate proteins in order to palmitoylate them (Lemonidis et al., 2014; Lemonidis et al., 2015; Lemonidis et al., 2017). Notably, the interaction between the ANK domain of zDHHC17 and the zDABM domain of ankyrin-B observed in this study was previously predicted by a peptide screen that identified the presence of the zDABM protein motif in ankyrins, suggesting our results are consistent with the conserved mechanism zDHHC17 utilizes to recognize and bind its substrates (Lemonidis et al., 2017). In line with the aforementioned study, we observed that the ability of ankyrin-B to recognize zDHHC17 is required for ankyrin-B palmitoylation, as demonstrated by the loss of ankyrin-B palmitoylation when the substrate binding site of zDHHC17 is ablated with the N100A mutation. Strikingly, loss of zDHHC17-ankyrin-B recognition also drastically reduced ankyrin-B protein levels. Although the enzymatic activity of zDHHC17 was required to regulate ankyrin-B palmitoylation, it was not sufficient to affect ankyrin-B expression levels. These data imply the observed zDHHC17-mediated increase in ankyrin-B protein expression is independent of palmitoylation, even though both protein expression and palmitoylation rely on recognition of ankyrin-B by zDHHC17.

The C60A and AAAAA-ankyrin-B-GFP mutants generated in this study to identify ankyrin-B palmitoylation sites also validated our findings that ankyrin-B protein expression was independent of ankyrin-B palmitoylation. While ankyrin-B palmitoylation was reduced by co-expression of either C60A or AAAAA-ankyrin-B-GFP with zDHHC17, protein expression of these mutant ankyrin-B plasmids was unchanged compared to WT ankyrin-B-GFP (Figures 4B,C,F,G). We reasoned this was likely because the zDABM in C60A and AAAAA-ankyrin-B-GFP remained intact, such that zDHHC17 is still capable of recognizing mutant ankyrin-B and thereby maintaining its expression. Our cycloheximide chase assays demonstrated that zDHHC17 does not stabilize ankyrin-B in our heterologous cell system with the experimental timepoints used for this assay. Thus, other potential palmitoylation-independent functions of zDHHC17 will need to be investigated to understand how zDHHC17 modulates ankyrin-B expression in heterologous cells.

Multiple studies have discussed the possibility of palmitoylation-independent functions of zDHHC17. Only half of the total number of proteins known to interact with zDHHC17 through their zDABM domain are known zDHHC17 substrates, suggesting that a major pool of zDHHC17 interactors rely on zDHHC17 for palmitoylation-independent functions (Lemonidis et al., 2015). Furthermore, the zDHHC17 orthologue zDHHC13 also has an ANK repeat domain capable of recognizing zDABM domains in proteins, but is not capable of palmitoylating them (Lemonidis et al., 2014). The zDABM domain of peripheral membrane protein SNAP25 is capable of interacting with the ANK repeat domains of both zDHHC13 and zDHHC17, but is only capable of being palmitoylated by zDHHC17 and not zDHHC13 in heterologous cells (Lemonidis et al., 2014). These data suggest that although zDHHC17-zDABM binding is usually associated with palmitoylation, it can also serve additional substrate recruitment functions independent of zDHHC17 catalytic activity. The biological implications of ANK repeat-zDABM binding outside of zDHHC catalytic activity are only beginning to be uncovered. zDHHC17, by way of its ANK repeat domain, has been hypothesized to act as a hub for protein interaction networks. zDHHC17 is capable of forming large protein complexes by interacting with proteins involved in neurotransmission, neuronal development, trafficking, signal transduction, and transcriptional regulation, many of which have not been identified as palmitoylated substrates or zDHHC17-specific substrates (Butland et al., 2014). However, the functional implications of these interactions are currently unknown. zDHHC17 interacts with c-Jun N terminus kinase (JNK) to activate JNK and promote neuronal cell death in response to pathophysiological triggers like ischemic stroke (Yang and Cynader, 2011). zDHHC17 has been shown to promote the TrkA-tubulin complex, which regulates signal transmission in axon growth (Shi et al., 2015). Thus, our work is consistent with the ability of zDHHC17 to modulate substrates independently of its catalytic zDHHC domain, though this work is the first evidence to our knowledge that zDHHC17-zDABM binding directly regulates protein expression of a substrate in heterologous cells. However, what regulation of ankyrin-B protein levels by zDHHC17 means biologically and in what physiological context this finding is relevant will need to be further investigated. Consistent with our results in heterologous cells, we observed that a 95% reduction in *Zdhhc17* mRNA in hippocampal neurons resulted in drastic loss of endogenous ankyrin-B palmitoylation. However, ankyrin-B protein levels remained unchanged in the absence of *Zdhhc17* mRNA, suggesting that neurons may have other means of regulating ankyrin-B protein levels independent of zDHHC17. In light of recent work demonstrating zDHHC17 is localized to the somatic Golgi (Singaraja et al., 2002; Ohno et al., 2006; Niu et al., 2020), ankyrin-B, which is highly localized to dendrites of mature neurons (Nelson et al., 2022), may not depend on zDHHC17 for maintenance of its protein pool out in the dendrites.

Functional studies with the palmitoylation-dead AAAAA-ankyrin-B-GFP demonstrated that palmitoylation regulates distinct functions of ankyrin-B. Palmitoylation of ankyrin-B was required for ankyrin-B to scaffold $Na_V1.2$ at dendritic membranes of neonatal cortical pyramidal cells, but was not required for ankyrin-B to mediate axonal cargo transport of synaptotagmin-1. These data suggest there may be two pools of 220-kDa ankyrin-B in neurons, one palmitoylation-dependent pool at the dendrites that promotes $Na_V1.2$ targeting and one palmitoylation-independent pool at the distal axon that promotes cargo transport. Consistent with the hypothesis that some palmitoylated substrates are locally palmitoylated (Philippe and Jenkins, 2019), somatic Golgi zDHHC17 may be conveniently located to palmitoylate the pool

of 220-kDa ankyrin-B destined for dendrites at the soma before ankyrin-B is forward trafficked into dendrites, where it subsequently scaffolds $Na_V1.2$. By contrast, zDHHC17 is specifically excluded from the axon in dorsal root ganglion neurons (Niu et al., 2020), which may explain why palmitoylation did not contribute to the axonal cargo function of 220-kDa ankyrin-B at the axon: 220-kDa ankyrin-B may simply not be palmitoylated at the axon due to the absence of zDHHC17 there. Interestingly, the pool of 220-kDa ankyrin-B that mediates cargo transport is targeted to vesicles and palmitoylation-independent, while the pool of 220-kDa ankyrin-B that scaffolds $Na_V1.2$ channels at dendrites is plasma-membrane-associated and palmitoylation-dependent. Palmitoylation of the homologous ankyrin-G also drives ankyrin-G targeting at plasma membrane domains of epithelial cells and neurons (He et al., 2012; He et al., 2014). It may be that ankyrin palmitoylation defines the precise localization of plasma-membrane-associated pools of ankyrins, such as AIS-localized ankyrin-G and dendritic ankyrin-B, but other mechanisms, posttranslational or otherwise, may drive the specific targeting of intracellular membrane pools of ankyrins, such as vesicular ankyrin-B, at the axon. If this is the case, then 440-kDa ankyrin-B, which is targeted to the axonal plasma membrane of neurons to scaffold the cell adhesion molecule L1CAM and repress axonal branching (Yang et al., 2019), may rely on palmitoylation for its axonal membrane targeting as well. Our observation that 440-kDa ankyrin-B is palmitoylated both in the brain and in neurons in Figure 1 is consistent with this hypothesis.

Despite the high homology shared between the ankyrin repeat domains of ankyrin-G and ankyrin-B, which harbor their respective palmitoylated cysteine sites, this study revealed non-conserved palmitoylation mechanisms between ankyrin family members. While ankyrin-G is palmitoylated by zDHHC5 and zDHHC8 at one cysteine site Cys70 (He et al., 2012; He et al., 2014), our study demonstrated that ankyrin-B is palmitoylated by zDHHC17 at multiple cysteine sites. This raises important questions about the biological implications of such distinct palmitoylation mechanisms, and may provide insight into the long-standing question about how two highly homologous proteins like ankyrin-G and ankyrin-B target to distinct membrane sites and function in a non-overlapping manner. Studies have shown that divergent domains within ankyrins can confer specificity for ankyrin-B or ankyrin-G localization and function in various cell types (Mohler et al., 2002; He et al., 2013), though this has not yet been investigated in neurons. The highly divergent C-terminal domain confers specificity for ankyrin-B function at membranes of the sarcoplasmic reticulum (SR) in neonatal cardiomyocytes (Mohler et al., 2002). Additionally, the highly divergent short linker peptide between the ankyrin repeat domain and the $ZU5_2$-UPA module inhibits ankyrin-B binding to plasma membrane domains and drives intracellular membrane localization of ankyrin-B in epithelial cells (He et al., 2013). Given that no consensus has been reached on which domain(s) determine specificity for ankyrin-G or ankyrin-B localization, this work has brought forward the importance of considering palmitoylation as a potential mechanism underlying the distinct localization and functions of ankyrin-B and ankyrin-G.

In light of the recent discoveries highlighting ankyrin-B's role in scaffolding $Na_V1.2$ at dendrites to promote dendritic function (Nelson et al., 2022), it will be of interest to investigate the role of ankyrin-B palmitoylation for dendritic excitability and synaptic plasticity, especially as efforts to understand the convergent roles of ankyrin-B and $Na_V1.2$ in the etiology of ASD continue. Our findings regarding the dendritic pool of ankyrin-B being palmitoylation-dependent and the vesicular pool of ankyrin-B at the distal axon being palmitoylation-independent highlights an opportunity to leverage palmitoylation as a drug target to specifically modulate the dendritic pool of ankyrin-B without affecting the vesicular pool of ankyrin-B at the axon, should the dendritic pool of ankyrin-B be implicated in ASD pathophysiology. It will also be important to investigate the role of $Na_V1.2$ palmitoylation to understand how this may affect the formation and maintenance of the ankyrin-B/$Na_V1.2$ complex at dendritic membranes.

Data availability statement

The original contributions presented in the study are included in the article/Supplementary Material. Further inquiries can be directed to the corresponding author.

Ethics statement

The animal study was reviewed and approved by the Institutional Animal Care and Use Committee, University of Michigan.

Author contributions

Conceptualization and methodology: JG and PJ; Investigation, formal analysis, and writing (original draft): JG, Writing (review and editing): JG and PJ; Funding: JG and PJ; Supervision and resources: PJ.

Funding

This work was supported by a Pharmacological Sciences Training Program T32 grant (T32GM007767), the Charles W. Edmunds Fellowship, and the Rackham Predoctoral Fellowship to JG, and Simon's Foundation for Autism Research Initiative (SFARI) pilot grant 675594 and NIH R01MH126960 to PJ.

Acknowledgments

We are grateful to members of the PJ lab, as well as Drs. L. Isom and K. Bender for comments and feedback. The authors thank Dr. William Fuller (University of Glasgow) for gifting us with functionalized thiopropyl beads, as well as Dr. Matthew Brody (University of Michigan) for providing feedback and guidance on this manuscript. The authors acknowledge support from Dr. Venkatesha Basrur with the University of Michigan Mass Spectrometry-Based Proteomics Resource Facility in the UM Department of Pathology.

Conflict of interest

The authors declare that the research was conducted in the absence of any commercial or financial relationships that could be construed as a potential conflict of interest.

Publisher's note

All claims expressed in this article are solely those of the authors and do not necessarily represent those of their affiliated organizations, or those of the publisher, the editors and the reviewers. Any product that may be evaluated in this article, or claim that may be made by its manufacturer, is not guaranteed or endorsed by the publisher.

Supplementary material

The Supplementary Material for this article can be found online at: https://www.frontiersin.org/articles/10.3389/fphys.2023.959660/full#supplementary-material

References

Ben-Shalom, R., Keeshen, C. M., Berrios, K. N., An, J. Y., Sanders, S. J., and Bender, K. J. (2017). Opposing effects on NaV1.2 function underlie differences between SCN2A variants observed in individuals with autism spectrum disorder or infantile seizures. *Biol. Psychiatry* 82 (3), 224–232. doi:10.1016/j.biopsych.2017.01.009

Bennett, V., and Lorenzo, D. N. (2013). Spectrin- and ankyrin-based membrane domains and the evolution of vertebrates. *Curr. Top. Membr.* 72, 1–37. doi:10.1016/B978-0-12-417027-8.00001-5

Bouza, A. A., Philippe, J. M., Edokobi, N., Pinsky, A. M., Offord, J., Calhoun, J. D., et al. (2020). Sodium channel β1 subunits are post-translationally modified by tyrosine phosphorylation, *S*-palmitoylation, and regulated intramembrane proteolysis. *J. Biol. Chem.* 295 (30), 10380–10393. doi:10.1074/jbc.RA120.013978

Brody, M. J., Schips, T. G., Vanhoutte, D., Kanisicak, O., Karch, J., Maliken, B. D., et al. (2016). Dissection of thrombospondin-4 domains involved in intracellular adaptive endoplasmic reticulum stress-responsive signaling. *Mol. Cell. Biol.* 36 (1), 2–12. doi:10.1128/MCB.00607-15

Brody, M. J., Vanhoutte, D., Schips, T. G., Boyer, J. G., Bakshi, C. V., Sargent, M. A., et al. (2018). Defective flux of thrombospondin-4 through the secretory pathway impairs cardiomyocyte membrane stability and causes cardiomyopathy. *Mol. Cell. Biol.* 38 (14), e00114-18. doi:10.1128/MCB.00114-18

Butland, S. L., Sanders, S. S., Schmidt, M. E., Riechers, S. P., Lin, D. T., Martin, D. D., et al. (2014). The palmitoyl acyltransferase HIP14 shares a high proportion of interactors with huntingtin: Implications for a role in the pathogenesis of huntington's disease. *Hum. Mol. Genet.* 23 (15), 4142–4160. doi:10.1093/hmg/ddu137

Chang, K. J., Zollinger, D. R., Susuki, K., Sherman, D. L., Makara, M. A., Brophy, P. J., et al. (2014). Glial ankyrins facilitate paranodal axoglial junction assembly. *Nat. Neurosci.* 17 (12), 1673–1681. doi:10.1038/nn.3858

Davis, J., Salomonis, N., Ghearing, N., Lin, S. C., Kwong, J. Q., Mohan, A., et al. (2015). MBNL1-mediated regulation of differentiation RNAs promotes myofibroblast transformation and the fibrotic response. *Nat. Commun.* 6, 10084. doi:10.1038/ncomms10084

Fukata, M., Fukata, Y., Adesnik, H., Nicoll, R. A., and Bredt, D. S. (2004). Identification of PSD-95 palmitoylating enzymes. *Neuron* 44 (6), 987–996. doi:10.1016/j.neuron.2004.12.005

Fukata, Y., and Fukata, M. (2010). Protein palmitoylation in neuronal development and synaptic plasticity. *Nat. Rev. Neurosci.* 11 (3), 161–175. doi:10.1038/nrn2788

Galiano, M. R., Jha, S., Ho, T. S., Zhang, C., Ogawa, Y., Chang, K. J., et al. (2012). A distal axonal cytoskeleton forms an intra-axonal boundary that controls axon initial segment assembly. *Cell.* 149 (5), 1125–1139. doi:10.1016/j.cell.2012.03.039

Gorenberg, E. L., Massaro Tieze, S., Yücel, B., Zhao, H. R., Chou, V., Wirak, G. S., et al. (2022). Identification of substrates of palmitoyl protein thioesterase 1 highlights roles of depalmitoylation in disulfide bond formation and synaptic function. *PLoS Biol.* 20 (3), e3001590. doi:10.1371/journal.pbio.3001590

He, M., Abdi, K. M., and Bennett, V. (2014). Ankyrin-G palmitoylation and βII-spectrin binding to phosphoinositide lipids drive lateral membrane assembly. *J. Cell. Biol.* 206 (2), 273–288. doi:10.1083/jcb.201401016

He, M., Jenkins, P., and Bennett, V. (2012). Cysteine 70 of ankyrin-G is S-palmitoylated and is required for function of ankyrin-G in membrane domain assembly. *J. Biol. Chem.* 287 (52), 43995–44005. doi:10.1074/jbc.M112.417501

He, M., Tseng, W. C., and Bennett, V. (2013). A single divergent exon inhibits ankyrin-B association with the plasma membrane. *J. Biol. Chem.* 288 (21), 14769–14779. doi:10.1074/jbc.M113.465328

Jenkins, P. M., Kim, N., Jones, S. L., Tseng, W. C., Svitkina, T. M., Yin, H. H., et al. (2015). Giant ankyrin-G: A critical innovation in vertebrate evolution of fast and integrated neuronal signaling. *Proc. Natl. Acad. Sci. U. S. A.* 112 (4), 957–964. doi:10.1073/pnas.1416544112

Lemonidis, K., Gorleku, O. A., Sanchez-Perez, M. C., Grefen, C., and Chamberlain, L. H. (2014). The Golgi S-acylation machinery comprises zDHHC enzymes with major differences in substrate affinity and S-acylation activity. *Mol. Biol. Cell.* 25 (24), 3870–3883. doi:10.1091/mbc.E14-06-1169

Lemonidis, K., MacLeod, R., Baillie, G. S., and Chamberlain, L. H. (2017). Peptide array-based screening reveals a large number of proteins interacting with the ankyrin-repeat domain of the zDHHC17 S-acyltransferase. *J. Biol. Chem.* 292 (42), 17190–17202. doi:10.1074/jbc.M117.799650

Lemonidis, K., Sanchez-Perez, M. C., and Chamberlain, L. H. (2015). Identification of a novel sequence motif recognized by the ankyrin repeat domain of zDHHC17/13 S-acyltransferases. *J. Biol. Chem.* 290 (36), 21939–21950. doi:10.1074/jbc.M115.657668

Locatelli, C., Lemonidis, K., Salaun, C., Tomkinson, N. C. O., and Chamberlain, L. H. (2020). Identification of key features required for efficient S-acylation and plasma membrane targeting of sprouty-2. *J. Cell. Sci.* 133 (21), jcs249664. doi:10.1242/jcs.249664

Lorenzo, D. N., Badea, A., Davis, J., Hostettler, J., He, J., Zhong, G., et al. (2014). A PIK3C3-ankyrin-B-dynactin pathway promotes axonal growth and multiorganelle transport. *J. Cell. Biol.* 207 (6), 735–752. doi:10.1083/jcb.201407063

Mohler, P. J., Gramolini, A. O., and Bennett, V. (2002). The ankyrin-B C-terminal domain determines activity of ankyrin-B/G chimeras in rescue of abnormal inositol 1,4,5-trisphosphate and ryanodine receptor distribution in ankyrin-B (-/-) neonatal cardiomyocytes. *J. Biol. Chem.* 277 (12), 10599–10607. doi:10.1074/jbc.M110958200

Nelson, A. D., Caballero-Floran, R. N., Rodriguez Diaz, J. C., Hull, J. M., Yuan, Y., Li, J., et al. (2018). Ankyrin-G regulates forebrain connectivity and network synchronization via interaction with GABARAP. *Mol. Psychiatry* 25, 2800–2817. doi:10.1038/s41380-018-0308-x

Nelson, A. D., Catalfio, A. M., Gupta, J. M., Min, L., Caballero-Floran, R. N., Dean, K. P., et al. (2022). Physical and functional convergence of the autism risk genes Scn2a and Ank2 in neocortical pyramidal cell dendrites. bioRxiv, 2022.2005.2031.494205. doi:10.1101/2022.05.31.494205

Niu, J., Sanders, S. S., Jeong, H. K., Holland, S. M., Sun, Y., Collura, K. M., et al. (2020). Coupled control of distal axon integrity and somal responses to axonal damage by the palmitoyl acyltransferase ZDHHC17. *Cell. Rep.* 33 (7), 108365. doi:10.1016/j.celrep.2020.108365

Ohno, Y., Kihara, A., Sano, T., and Igarashi, Y. (2006). Intracellular localization and tissue-specific distribution of human and yeast DHHC cysteine-rich domain-containing proteins. *Biochim. Biophys. Acta* 1761 (4), 474–483. doi:10.1016/j.bbalip.2006.03.010

Philippe, J. M., and Jenkins, P. M. (2019). Spatial organization of palmitoyl acyl transferases governs substrate localization and function. *Mol. Membr. Biol.* 35 (1), 60–75. doi:10.1080/09687688.2019.1710274

Pinner, A. L., Tucholski, J., Haroutunian, V., McCullumsmith, R. E., and Meador-Woodruff, J. H. (2016). Decreased protein S-palmitoylation in dorsolateral prefrontal cortex in schizophrenia. *Schizophr. Res.* 177 (1-3), 78–87. doi:10.1016/j.schres.2016.01.054

Sanders, S. J., Campbell, A. J., Cottrell, J. R., Moller, R. S., Wagner, F. F., Auldridge, A. L., et al. (2018). Progress in understanding and treating SCN2A-mediated disorders. *Trends Neurosci.* 41 (7), 442–456. doi:10.1016/j.tins.2018.03.011

Sanders, S. J., He, X., Willsey, A. J., Ercan-Sencicek, A. G., Samocha, K. E., Cicek, A. E., et al. (2015). Insights into autism spectrum disorder genomic architecture and biology from 71 risk loci. *Neuron* 87 (6), 1215–1233. doi:10.1016/j.neuron.2015.09.016

Sanders, S. S., Parsons, M. P., Mui, K. K., Southwell, A. L., Franciosi, S., Cheung, D., et al. (2016). Sudden death due to paralysis and synaptic and behavioral deficits when

Hip14/Zdhhc17 is deleted in adult mice. *BMC Biol.* 14 (1), 108. doi:10.1186/s12915-016-0333-7

Satterstrom, F. K., Kosmicki, J. A., Wang, J., Breen, M. S., De Rubeis, S., An, J. Y., et al. (2020). Large-scale exome sequencing study implicates both developmental and functional changes in the neurobiology of autism. *Cell.* 180 (3), 568–584.e23. doi:10.1016/j.cell.2019.12.036

Schindelin, J., Arganda-Carreras, I., Frise, E., Kaynig, V., Longair, M., Pietzsch, T., et al. (2012). Fiji: An open-source platform for biological-image analysis. *Nat. Methods* 9 (7), 676–682. doi:10.1038/nmeth.2019

Shi, W., Wang, F., Gao, M., Yang, Y., Du, Z., Wang, C., et al. (2015). ZDHHC17 promotes axon outgrowth by regulating TrkA-tubulin complex formation. *Mol. Cell. Neurosci.* 68, 194–202. doi:10.1016/j.mcn.2015.07.005

Singaraja, R. R., Hadano, S., Metzler, M., Givan, S., Wellington, C. L., Warby, S., et al. (2002). HIP14, a novel ankyrin domain-containing protein, links huntingtin to intracellular trafficking and endocytosis. *Hum. Mol. Genet.* 11 (23), 2815–2828. doi:10.1093/hmg/11.23.2815

Spratt, P. W. E., Ben-Shalom, R., Keeshen, C. M., Burke, K. J., Jr., Clarkson, R. L., Sanders, S. J., et al. (2019). The autism-associated gene Scn2a contributes to dendritic excitability and synaptic function in the prefrontal cortex. *Neuron* 103 (4), 673–685. e5. doi:10.1016/j.neuron.2019.05.037

Staufenbiel, M. (1987). Ankyrin-bound fatty acid turns over rapidly at the erythrocyte plasma membrane. *Mol. Cell. Biol.* 7 (8), 2981–2984. doi:10.1128/mcb.7.8.2981-2984.1987

Tseng, W. C., Jenkins, P. M., Tanaka, M., Mooney, R., and Bennett, V. (2015). Giant ankyrin-G stabilizes somatodendritic GABAergic synapses through opposing endocytosis of GABAA receptors. *Proc. Natl. Acad. Sci. U. S. A.* 112 (4), 1214–1219. doi:10.1073/pnas.1417989112

Verardi, R., Kim, J. S., Ghirlando, R., and Banerjee, A. (2017). Structural basis for substrate recognition by the ankyrin repeat domain of human DHHC17 palmitoyltransferase. *Structure* 25 (9), 1337–1347. e6. doi:10.1016/j.str.2017.06.018

Yang, G., and Cynader, M. S. (2011). Palmitoyl acyltransferase zD17 mediates neuronal responses in acute ischemic brain injury by regulating JNK activation in a signaling module. *J. Neurosci.* 31 (33), 11980–11991. doi:10.1523/JNEUROSCI.2510-11.2011

Yang, R., Walder-Christensen, K. K., Kim, N., Wu, D., Lorenzo, D. N., Badea, A., et al. (2019). ANK2 autism mutation targeting giant ankyrin-B promotes axon branching and ectopic connectivity. *Proc. Natl. Acad. Sci. U. S. A.* 116 (30), 15262–15271. doi:10.1073/pnas.1904348116

Zala, D., Hinckelmann, M. V., Yu, H., Lyra da Cunha, M. M., Liot, G., Cordelieres, F. P., et al. (2013). Vesicular glycolysis provides on-board energy for fast axonal transport. *Cell.* 152 (3), 479–491. doi:10.1016/j.cell.2012.12.029

Zaręba-Kozioł, M., Bartkowiak-Kaczmarek, A., Roszkowska, M., Bijata, K., Figiel, I., Halder, A. K., et al. (2021). S-palmitoylation of synaptic proteins as a novel mechanism underlying sex-dependent differences in neuronal plasticity. *Int. J. Mol. Sci.* 22 (12), 6253. doi:10.3390/ijms22126253

frontiers | Frontiers in Physiology

TYPE Original Research
PUBLISHED 13 April 2023
DOI 10.3389/fphys.2023.1163339

OPEN ACCESS

EDITED BY
Vincenza Cifarelli,
Saint Louis University, United States

REVIEWED BY
Jyot Antani,
Yale University, United States
Shaun S. Sanders,
University of Guelph, Canada

*CORRESPONDENCE
Jules C. Hancox,
jules.hancox@bristol.ac.uk
William Fuller,
will.fuller@glasgow.ac.uk

SPECIALTY SECTION
This article was submitted to Lipid and Fatty Acid Research, a section of the journal Frontiers in Physiology

RECEIVED 10 February 2023
ACCEPTED 31 March 2023
PUBLISHED 13 April 2023

CITATION
Congreve SD, Main A, Butler AS, Gao X, Brown E, Du C, Choisy SC, Cheng H, Hancox JC and Fuller W (2023), Palmitoylation regulates the magnitude of HCN4-mediated currents in mammalian cells.
Front. Physiol. 14:1163339.
doi: 10.3389/fphys.2023.1163339

Palmitoylation regulates the magnitude of HCN4-mediated currents in mammalian cells

Samitha Dilini Congreve[1,2], Alice Main[1], Andrew S. Butler[2], Xing Gao[1], Elaine Brown[1], Chunyun Du[2], Stephanié C. Choisy[2], Hongwei Cheng[2], Jules C. Hancox[2]* and William Fuller[1]*

[1]School of Cardiovascular & Metabolic Health, University of Glasgow, Glasgow, United Kingdom, [2]School of Physiology, Pharmacology and Neuroscience, University of Bristol, Bristol, United Kingdom

The sinoatrial node (SAN) and subsidiary pacemakers in the cardiac conduction system generate spontaneous electrical activity which is indispensable for electrical and therefore contractile function of the heart. The hyperpolarisation-activated cyclic nucleotide-gated channel HCN4 is responsible for genesis of the pacemaker "funny" current during diastolic depolarisation. S-palmitoylation, the reversible conjugation of the fatty acid palmitate to protein cysteine sulfhydryls, regulates the activity of key cardiac Na^+ and Ca^{2+} handling proteins, influencing their membrane microdomain localisation and function. We investigated HCN4 palmitoylation and its functional consequences in engineered human embryonic kidney 293T cells as well as endogenous HCN4 in neonatal rat ventricular myocytes. HCN4 was palmitoylated in all experimental systems investigated. We mapped the HCN4 palmitoylation sites to a pair of cysteines in the HCN4 intracellular amino terminus. A double cysteine-to-alanine mutation CC93A/179AA of full length HCN4 caused a ~67% reduction in palmitoylation in comparison to wild type HCN4. We used whole-cell patch clamp to evaluate HCN4 current (I_{HCN4}) in stably transfected 293T cells. Removal of the two N-terminal palmitoylation sites did not significantly alter half maximal activation voltage of I_{HCN4} or the activation slope factor. I_{HCN4} was significantly larger in cells expressing wild type compared to non-palmitoylated HCN4 across a range of voltages. Phylogenetic analysis revealed that although cysteine 93 is widely conserved across all classes of HCN4 vertebrate orthologs, conservation of cysteine 179 is restricted to placental mammals. Collectively, we provide evidence for functional regulation of HCN4 *via* palmitoylation of its amino terminus in vertebrates. We suggest that by recruiting the amino terminus to the bilayer, palmitoylation enhances the magnitude of HCN4-mediated currents, but does not significantly affect the kinetics.

KEYWORDS

sinoatrial node, funny current, acylation, heart rate, ion channel, palmitoylation

Introduction

The intrinsic automaticity of the sinoatrial node (SAN) is fundamental for pacemaking in mammalian hearts. In cells of the SAN (and elsewhere in the cardiac conduction system) slow depolarisation during diastole is the basis of this automaticity, distinguishing these specialised cells from the working myocardium (Choudhury et al., 2015). Multiple

electrogenic processes contribute to this diastolic depolarisation. Surface membrane ion currents ("membrane clock") and the rhythmic oscillation of local calcium release ("calcium clock") work interdependently and are believed to form a coupled-clock system that drives pacemaker automaticity and its regulation on a beat-to-beat basis (DiFrancesco, 2010; Lakatta et al., 2010).

The hyperpolarisation-activated cyclic nucleotide-gated channel HCN4 is a key component of the membrane clock. HCN4 is the predominant HCN isoform expressed in the sinoatrial node (Bucchi et al., 2012), contributing 75%–90% of the sinoatrial "funny" current (I_f) during diastolic depolarisation (Stieber et al., 2003; Baruscotti et al., 2011). This native cardiac I_f current carried by HCN4 was christened "funny" when it was first identified because of its "funny" (unusual) property of being activated by hyperpolarisation (Brown et al., 1979; DiFrancesco, 2019). HCN channels are tetrameric, with each subunit consisting of 6 transmembrane (TM) domains, with the voltage sensor in TM4, a re-entrant loop between TM5 and 6 forming the channel pore and cytosolic amino and carboxyl termini (Saponaro et al., 2021). Unique properties of HCN channels such as the depolarising mixed (Na^+ and K^+) inward current on membrane hyperpolarisation over the diastolic range of voltages, facilitate the channel's contribution to the early diastolic depolarisation (DiFrancesco, 2010). In addition, a cyclic nucleotide binding site in the carboxyl terminus enables direct activation of HCN channels by cAMP binding without the classic effector kinase (Baruscotti et al., 2005). Loss of function mutations of HCN4 are associated with sinus node dysfunction (Verkerk and Wilders, 2015). Tamoxifen-induced HCN4 knockout in the adult murine heart produces profound bradycardia and also atrioventricular (AV) block, indicating roles for HCN4 not just in the SAN but also in the AV node (Baruscotti et al., 2011). Ivabradine, the first clinically approved drug that selectively inhibits the funny current in the SAN, is used therapeutically to slow the heart rate specifically in the settings of heart failure and chronic stable angina (DiFrancesco and Camm, 2004).

Regulation of ion channels *via* post translational modifications is an integral component of the complex sinoatrial pacemaking network (Tsutsui et al., 2018). For example, phosphorylation of key calcium handling proteins that constitute the calcium clock accelerates diastolic depolarisation and increases heart rate (Lakatta et al., 2010). S-palmitoylation is a form of lipidation that involves the covalent addition of a 16-carbon palmitate to a thiol group of a cysteine residue in a protein (Linder and Deschenes, 2007). Palmitoylation is uniquely reversible amongst protein lipid modifications. A zDHHC-motif containing family of integral membrane palmitoyl acyl transferase (zDHHC-PATs) palmitoylates proteins (Rana et al., 2018), and this reaction is reversed by thioesterases (Won, 2018). Hence palmitoylation facilitates the dynamic regulation of both soluble and integral membrane proteins (Guan and Fierke, 2011; Main and Fuller, 2022).

In recent years, palmitoylation has emerged as an important post translational modification regulating many physiological and pathophysiological processes in the heart (Essandoh et al., 2020; Main et al., 2022; Main and Fuller, 2022). Essential cardiac sodium (Reilly et al., 2015; Pei et al., 2016; Gok et al., 2020; Gok et al., 2022) and calcium (Kuo et al., 2023) handling proteins are dynamically palmitoylated, influencing their membrane microdomain localisation and function. Palmitoylation regulates the activities of several proteins known to be central to SAN pacemaking, including NCX1 (Reilly et al., 2015; Gok et al., 2020) and Ca(v)1.2,[25] and all isoforms of HCN channels except HCN3 are palmitoylated (Itoh et al., 2016). However, functional regulation of HCN4 channels by palmitoylation has not yet been established. The present *in-vitro* study was undertaken to characterise palmitoylation of HCN4 channels and to establish its functional consequences. The findings demonstrate that HCN4 is primarily palmitoylated at its N-terminus at cysteine 93 and 179. Mutations of both cysteines significantly reduced palmitoylation of HCN4 and altered the magnitude but not activation kinetics of macroscopic HCN4 current.

Methods

Ethics statement

This study utilized cardiac tissue from rat and rabbits. All protocols involving animals were approved by the University of Glasgow or University of Bristol Animal Welfare and Ethics Review Board. Rodent cardiac tissues were collected post-mortem after sacrificing animals using a method designated Schedule 1 by the Animals (Scientific Procedures) Act 1986. Rabbit hearts were excised following humane killing in accordance with UK Home Office legislation.

Mutagenesis and cloning

Cysteine-to-alanine substitution reactions were performed using Q5-site directed mutagenesis kit (New England Biolabs). The primers for the mutagenesis reactions were designed using the manufacturer's online primer design tool.

The InFusion cloning system was used to subclone full length HCN4. The amino (1-266) terminus and the carboxyl (518-1203) terminus were amplified from the human full length HCN4 in pcDNA 3 and inserted into pEYFP-C1 (Clontech) to express as fusions to the YFP C-terminus. Full-length HCN4 was amplified and inserted in pcDNA5/FRT/TO (Invitrogen).

Cells and tissue

Cell lines stably expressing tetracycline-inducible wild type and mutant HCN4 channels were generated using the Flp-In™ T-Rex™ System. All transient transfections of plasmid DNA were carried out in a 6 or 12 multi-well plate seeded with a high cell density using Invitrogen Lipofectamine 2000 as instructed by the manufacturer. The cells were harvested 18–24 h following transfection.

Neonatal rat whole hearts were obtained from male and female Sprague Dawley rats aged 1–4 days old. Briefly, animals were euthanised with a lethal dose of Euthatal before severing the femoral artery. Hearts were quickly excised and placed into a solution of ice-cold excision buffer (100 mM NaCl, 20 mM HEPES, 0.8 mM NaH_2PO_4, 5.3mM KCl, 0.4 mM $MgSO_4$, 5 mM glucose; pH 7.4). Excess blood and tissue were removed from hearts using a sterile scalpel. For analysis of atrial tissue only, the atria were identified and separated from the ventricular tissue.

SAN tissue was obtained from adult male New Zealand White rabbits. The heart was rapidly excised and cleared of blood. The SAN region in the right atrium was identified in relation to known landmarks (the crista terminalis, superior vena cava, interatrial septum and inferior vena cava (Denyer and Brown, 1990; Brioschi et al., 2009), and tissue encompassing the entire SAN region was excised and snap-frozen for subsequent determination of HCN4 palmitoylation.

Palmitoylation assays

Palmitoylated proteins were purified using resin-assisted capture of acylated proteins (acyl-RAC) (Forrester et al., 2011). Briefly, cells were lysed in blocking buffer (2.5% SDS, 1 mM EDTA, 100 mM HEPES, 1% v/v MMTS pH 7.5) and incubated at 40°C for 4 h to alkylate free cysteines. Proteins were precipitated with 3 volumes of ice-cold acetone to remove excess unreacted MMTS, protein pellets extensively washed with 70% acetone, dried, and redissolved in binding buffer (1% SDS, 1 mM EDTA, 100 mM HEPES pH 7.5). Palmitoylated proteins were captured by agitating for 2.5 h with thiopropyl sepharose beads in the presence of 250 mM neutral hydroxylamine sulphate. In some reactions hydroxylamine was replaced with sodium chloride as a negative control. After capture, beads were extensively washed with binding buffer, and palmitoylated proteins eluted in SDS PAGE loading buffer supplemented with 100 mM DTT.

Intact cardiac tissue was homogenised using ceramic beads (BeadBug) in blocking buffer for 4 h at 40°C. Any unhomogenised tissue was discarded before the precipitation step.

Western blotting

This investigation used antibodies raised to HCN4 (1:5000-1:10000 dilution Alomone labs #APC-052), caveolin-3 (1:2000 dilution, BD Biosciences 610420), flotillin-2 (1:2000 dilution, BD Bioscences 610383), GFP (1:5000 dilution, Abcam ab6556) and Na^+/K^+ ATPase α1 subunit (1:100 dilution, Developmental Studies Hybridoma Bank clone α6F). Secondary antibodies were anti-rabbit conjugated to HRP (Jackson ImmunoResearch, 111-035-144, raised in goat) and anti-mouse conjugated to HRP (Jackson ImmunoResearch, 315-035-003, raised in rabbit).

Images of western immunoblots were acquired using a BioRad Chemidoc XRS imaging system and analysed using QuantityOne (BioRad) and ImageLab (BioRad) software.

Preparation of surface membrane proteins

Surface membrane proteins were biotinylated by incubating cells in 1 mg/mL sulfo-NHS-SS-biotin in PBS for 30min at 37°C. Cells were lysed in 1% Triton X-100, 0.1% SDS in PBS supplemented with protease inhibitor cocktail. Biotinylated proteins were captured using streptavidin sepharose (Tulloch et al., 2011). Only surface membrane proteins, not intracellular proteins, are captured using this experimental design (Gao et al., 2022).

Whole cell patch clamp

Stably transfected Flp-In™ 293 T-REx cells (Thermo) were plated on 10 mm glass coverslips in a 35 mm culture dish and HCN4 expression induced with tetracycline (1 μg/mL) for at least 24 h prior to being used for electrophysiology recordings. Whole cell patch clamp recordings employed an internal solution comprised of (in mmol/L): 130 KCl, 1 $MgCl_2$, 5 EGTA, 5 MgATP and 10 HEPES (titrated to pH 7.2 with KOH) and extracellular Tyrode solution comprised of (in mmol/L): 140 NaCl, 4 KCl, 2.5 $CaCl_2$, 1 $MgCl_2$, 10 glucose, and 5 HEPES (titrated to pH 7.4 with NaOH). Patch pipettes (A-M Systems Inc., USA, Schott #8250) were pulled on a dual stage glass micropipette puller (Narishige PC-10) and heat-polished (Narishige, MF 83) to obtain a final resistance of 2–3 MΩ. The cells on coverslips were transferred to a bath chamber mounted on the stage of an inverted microscope and continually superfused with Tyrode solution preheated to 37°C. Whole cell patch clamp recordings of I_{HCN4} were made using: 1) an Axopatch 1D amplifier (Axon Instruments) and a CV-4 headstage, with a Digidata 1200B or 1440A A-D interface (Molecular Devices) and Clampex software 10.7 (Molecular Devices); or 2) an Axopatch 200B amplifier (Axon instruments), digitization using an ITC-18 computer interface (Instrutech corporation) and HEKA Pulse software. Series resistance was compensated by 70%–75% (typically 2.5–7.5 MΩ). The I_{HCN4} currents recorded were filtered at 1–2 kHz and digitized at 10 kHz. Data acquired were analysed primarily using Clampfit 10.7 (Molecular Devices), Microsoft Excel 2204, and OriginPro 2021b. Cells with leak current of more than 100 pA at the −40 mV holding potential were not included in the analysis.

Sequence alignments

Sequences were acquired from the National Centre for Biotechnology Information (NCBI) GenBank (accessed June 2020). Only HCN4 ortholog sequences with the complete whole channel sequence were selected and partial sequences generating an incomplete transcript were not included in the phylogenetic analysis. To minimise misalignment in the analysis, the full-length sequences were trimmed to amino acids 1 to 300 which included the full N-terminus and the start of the S1 domain which exhibits high sequence identity within the sequences used. Sequence alignments of the trimmed sequences and phylogenetic trees were generated using Clustal omega. Sequences that displayed little homology were removed from the alignment.

Statistical analysis

Statistical analysis was performed using GraphPad Prism software. All quantitative data are presented as mean ± standard error of the mean (SEM). The statistical significance difference between the experimental groups were analysed using one-way analysis of variance (ANOVA) with Tukey's *post hoc* multiple comparison tests. A Welch's ANOVA was used to compare experimental groups with unequal standard deviations. Differences between experimental groups with p-values < 0.05 were considered

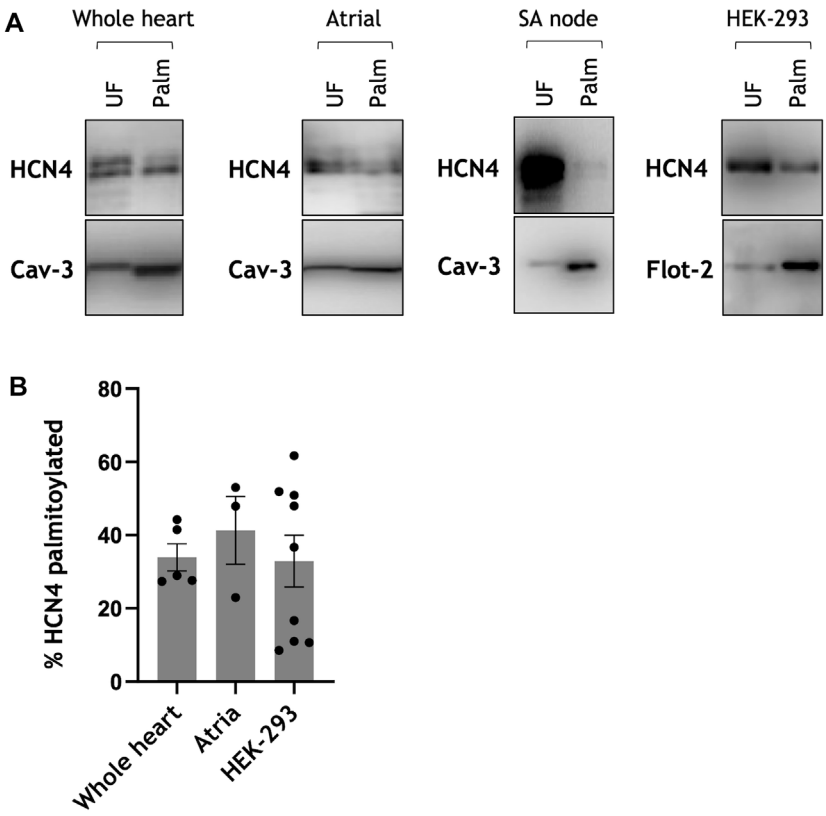

FIGURE 1
HCN4 palmitoylation in cardiac tissue and transfected cells. **(A)** Palmitoylation of HCN4 assessed using acyl-RAC from isolated rat neonatal whole heart, rat neonatal atria, rabbit sinoatrial node and following transient transfection of HEK-293 cells. The constitutively palmitoylated proteins caveolin-3 (Cav-3) and flotillin-2 (Flot-2) were used as a marker of assay efficiency. Full length HCN4 was detected with anti-HCN4 antibody. **(B)** Palmitoylation stoichiometry of endogenous HCN4 in rat neonatal cardiac tissue (whole heart, atria) and transiently transfected cells relative to caveolin-3 and flotillin-2, respectively. Compared to caveolin-3 the fraction of HCN4 palmitoylated is ~33 ± 4% in rat neonatal whole heart (n = 5) and ~41 ± 9% in rat neonatal atria (n = 3). Compared to flotillin-2 the fraction of HCN4 palmitoylated in HEK-293 cells is ~33 ± 7% (n = 9). Each spot in the bar chart represents a measurement made from an independent population of cells. UF: Unfractionated cell lysate; Palm: palmitoylated protein.

statistically significant and accordingly denoted by * $p < 0.05$, ** $p < 0.01$, *** $p < 0.001$ and **** $p < 0.0001$.

Results

HCN4 is palmitoylated in multiple experimental model systems

We investigated palmitoylation of HCN4 using resin-assisted capture of acylated proteins (acyl-RAC), which purifies acylated proteins (but not those interacting with them) under strongly denaturing conditions. All assays were analysed by immunoblotting for HCN4 and a constitutively palmitoylated protein: caveolin-3 from muscle, and flotillin-2 from cultured cells (Figure 1A). HCN4 was palmitoylated in all systems investigated (whole neonatal rat hearts, neonatal rat atria, rabbit sinoatrial node, HEK-293 cells transiently transfected with HCN4). We estimated the fraction of HCN4 that is palmitoylated by comparing its enrichment in the acyl-RAC assay with the enrichment of the constitutively palmitoylated control proteins. Consistently 33%–40% of HCN4 was captured in these assays (Figure 1B), suggesting that two different populations of HCN4 are present in cardiac tissue: approximately one third of total HCN4 is palmitoylated and approximately two thirds is not palmitoylated.

HCN4 palmitoylation sites are located in the protein's amino terminus

We next set out to identify the palmitoylated cysteines in HCN4. Human HCN4 has seven intracellular cysteine residues: two in the amino terminus before the first transmembrane domain and five in the carboxyl tail after the sixth transmembrane domain (Figure 2A). In order to determine which region(s) of HCN4 contained the palmitoylation site(s) we fused the HCN4 amino terminus (1-266) or carboxyl terminus (518-1203) to YFP, expressed fusion proteins in HEK-293 cells and measured their palmitoylation by acyl-RAC (Figure 2B). Palmitoylation of the carboxyl terminal fusion protein was essentially undetectable, but a proportion of the amino terminal fusion protein was palmitoylated, suggesting one or both of the amino terminal cysteines are palmitoylated. We mutated one (C93A, C179A) or both (CC93/179AA) cysteines in the YFP fusion protein and assessed the palmitoylation status of the fusion proteins using acyl-RAC.

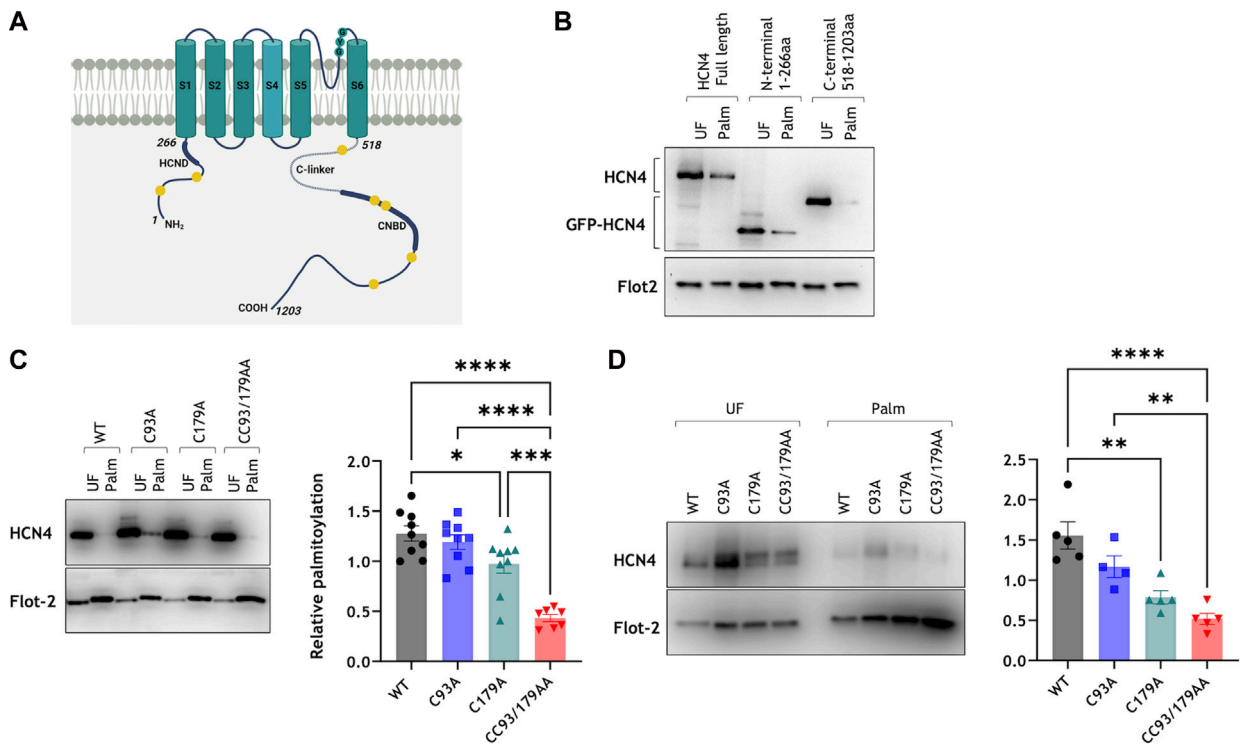

FIGURE 2
Palmitoylation site mapping in HCN4. **(A)** HCN4 schematic indicating the positions of the HCN domain (HCND) in the intracellular amino terminus, the C-linker and cyclic nucleotide binding domain (CNBD) in the intracellular carboxyl terminus, and all intracellular cysteines (yellow circles) in the amino (C93, C179) and carboxyl (C586, C662, C679, C755, C887) termini. **(B)** Palmitoylation of full length HCN4, YFP-N-terminus (1-266) and YFP-C-terminus (518-1203) in transiently transfected HEK-293 cells was assessed by acyl-RAC. Full length HCN4 was detected with anti-HCN4 antibody and the YFP fused N-/C- terminal fragments were detected with anti-GFP antibody. Flotillin-2 enrichment (Flot 2) confirms the efficiency of the acyl-RAC assay. UF, Unfractionated cell lysate; Palm: Palmitoylated proteins; representative figure of $n = 8$. **(C)** Site-directed mutagenesis on the YFP-fused N-terminus reveals cysteine 93 and 179 as palmitoylation sites. **(D)** Palmitoylation of stably expressed wild type and mutant HCN4 confirm cysteine 179 as the primary palmitoylation site of HCN4. * $p < 0.05$, ** $p < 0.01$, *** $p < 0.001$ and **** $p < 0.0001$, one way ANOVA followed by Tukey's *post hoc* test. All groups are not significantly different from each other except where indicated.

Mutagenesis of C93 did not reduce the amount of YFP-tagged amino terminus captured by acyl-RAC, but mutagenesis of C179 did (Figure 2C). The modest reduction in the amount of C179A captured by acyl-RAC was significantly further reduced by mutagenesis of C93. The acyl-RAC assay captures proteins regardless of the number of palmitoylation sites occupied, and consequently does not differentiate between singly and doubly palmitoylated proteins. When a protein has one 'dominant' palmitoylation site and one 'secondary' palmitoylation site, if the secondary palmitoylation site is mutated then acyl-RAC still captures the protein *via* the dominant site. It is only when the dominant site has already been removed that the impact of mutating the secondary site can be seen. We conclude from these experiments that both cysteines in the fusion protein between YFP and the HCN4 amino terminus are palmitoylated, and that C179 may be the principal palmitoylation site.

To confirm the identity of the HCN4 palmitoylation sites in the full-length protein we generated 293T cells stably expressing tetracycline inducible wild type (WT), C93A, C179A and CC93/179AA HCN4. This system enables consistent expression levels in all cells investigated so is, in principle, considerably superior to transient transfection. Mutagenesis of C179 caused the greatest reduction in the amount of HCN4 captured using acyl-RAC, and mutagenesis of both amino terminal cysteines further reduced the amount of palmitoylated HCN4 (Figure 2D). A small amount (10% ± 2% of total HCN4) of CC93/179AA HCN4 was purified by acyl-RAC, so we do not rule out residual palmitoylation of cysteines in the HCN4 C terminus. However, since the most quantitatively significant palmitoylation occurred in the HCN4 N terminus, in subsequent experiments we focussed on identifying the functional consequences of palmitoylation in this region of HCN4.

Palmitoylation does not influence cell surface delivery of HCN4

Palmitoylation can regulate both anterograde transport of proteins through the secretory pathway to the plasma membrane (Ernst et al., 2018), and the rate of internalisation of proteins from the plasma membrane (Tulloch et al., 2011). We first investigated steady state expression of HCN4 at the surface membrane using membrane-impermeable biotinylation reagents. The quantity of HCN4 present at the cell surface was not different between cells expressing WT, C93A, C179A or CC93/179AA HCN4 (Figure 3A). Next, we assessed the rate of degradation of surface-localised HCN4 using pulse chase

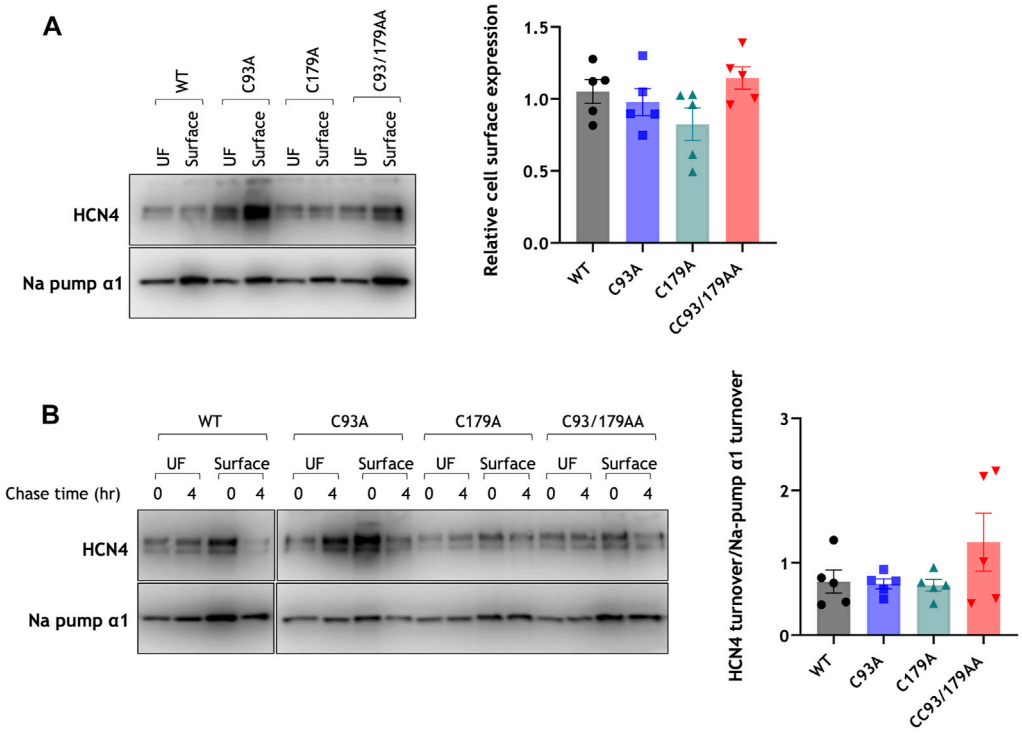

FIGURE 3
Palmitoylation and HCN4 trafficking. **(A)** Surface membrane proteins were prepared from stably transfected 293T cells using membrane-impermeable biotinylation reagents and immunoblotted alongside their corresponding unfractionated cell lysate. The plasma membrane associated housekeeper Na^+/K^+ ATPase α1 subunit (Na pump α1) was used as a marker of assay efficiency. The bar chart presents quantification of biotinylated HCN4 and Na^+/K^+ ATPase α1 subunit relative to its total expression and normalised to the daily experimental average. WT, wild type; UF, unfractionated cell lysate; n = 5. **(B)** Surface membrane HCN4 (surface) purified at 0 h and 4 h after biotinylation of surface membrane proteins were immunoblotted alongside their unfractionated cell lysate (UF). The plasma membrane associated housekeeper Na^+/K^+ ATPase α1 subunit (Na pump α1) was used as a marker of assay efficiency. HCN4 turnover was normalised to the turnover of housekeeper Na^+/K^+ ATPase α1 subunit. WT, wild type; UF, unfractionated cell lysate; n = 5. No groups are significantly different from each other.

experiments. Surface membrane proteins were biotinylated and either prepared immediately or after a 4 h 'chase' (Figure 3B). We compared the fraction of biotinylated HCN4 remaining after the 4 h chase with the fraction of the housekeeping protein Na^+/K^+ ATPase α1 subunit in the same samples (Figure 3B). The relative rate of degradation of HCN4 was not different between the different cell lines, leading to a conclusion that palmitoylation does not influence trafficking or degradation of HCN4.

Palmitoylation modifies the magnitude but not the activation properties of HCN4-mediated currents

We used whole-cell patch clamping to evaluate HCN4 current (I_{HCN4}) in stably transfected 293T cells in which HCN4 expression was induced with tetracycline. Endogenous HCN4 is not expressed in HEK293 cells, but this expression system is well-validated to interrogate I_{HCN4} (Varghese et al., 2006). Representative currents and current voltage relationships are presented in Figure 4, and analysis of these currents is presented in Figure 5. In cells expressing WT HCN4, hyperpolarising voltage steps for 2 s from a holding potential of −40 mV (protocol shown in Figure 4A) resulted in a brief instantaneous current followed by a progressively developing sigmoidal time-dependent current characteristic of I_{HCN4}. Depolarising to 5 mV for 0.5 s following the hyperpolarising test pulse elicited outward tail currents which inactivated in a voltage-dependent manner. These WT currents are similar to those reported in prior studies of HCN4 expressed in HEK cells (Milanesi et al., 2006; Nof et al., 2007; Schweizer et al., 2010; Liao et al., 2012). The peak amplitude of the current elicited by each of the hyperpolarising test pulses was measured and normalised to the corresponding whole cell capacitance and data pooled across cells (Figure 4F). The amplitude of currents conducted by WT HCN4 was significantly larger than that of palmitoylation site mutants in the voltage range −90 mV to −120 mV. The normalised whole cell conductance (G/Gmax) values were plotted against their corresponding test voltage and the resulting data fitted with a standard Boltzmann function in order to establish the voltage dependence of activation of WT and mutant HCN4 (Figure 5A). There was no significant difference in the half maximal activation voltage ($V_{0.5}$) between the WT and mutant channels (Figure 5B: −90.2 ± 1.1 mV for C93A, −90.1 ± 2.0 mV for C179A, −90.4 ± 1.6 mV for CC93/179AA vs. −90.4 ± 2.5 mV for WT). Similarly, there were no significant changes in the slope factor

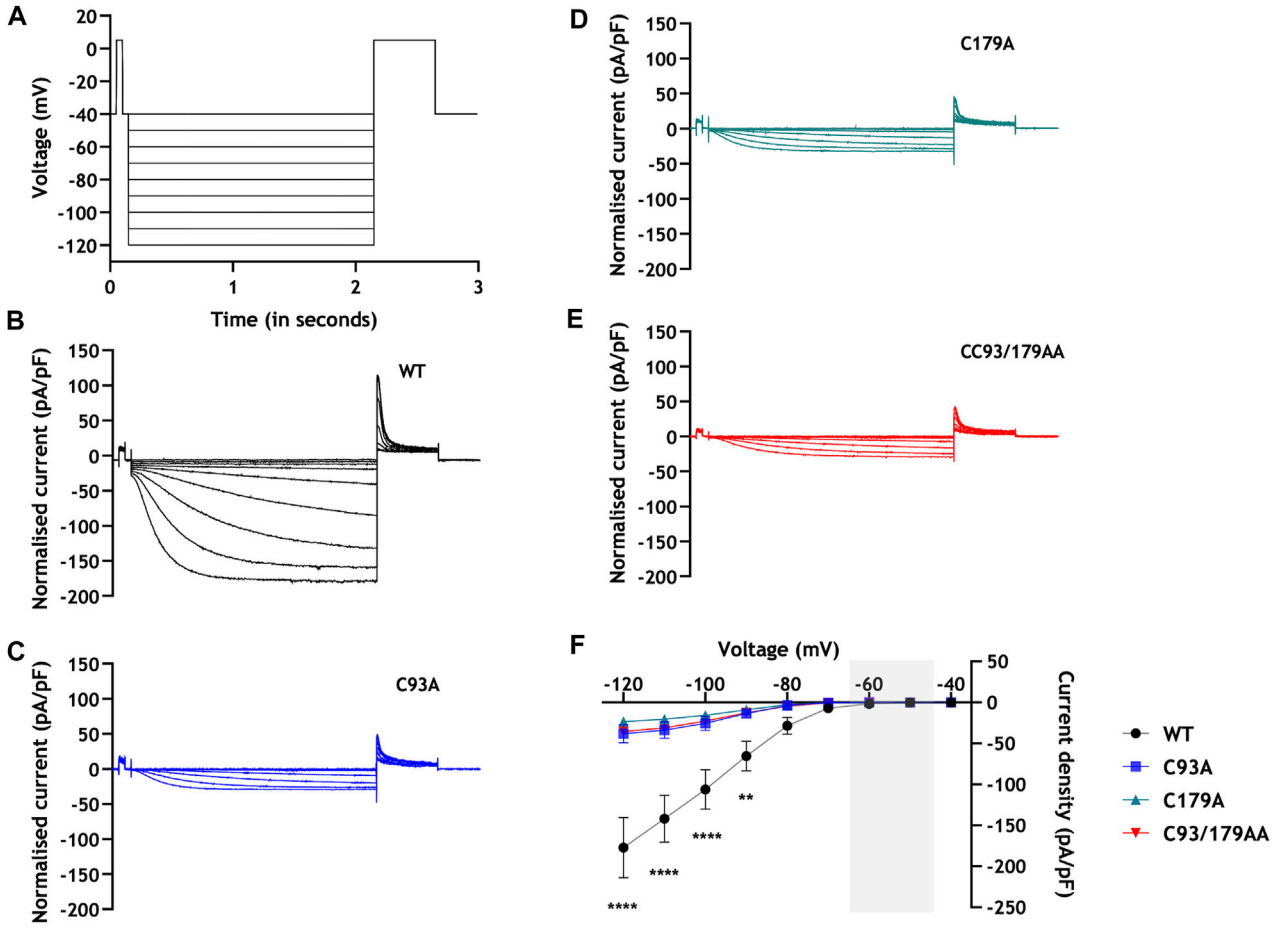

FIGURE 4
Palmitoylation and HCN4 currents: current-voltage relationships. **(A)** Voltage protocol. Two second hyperpolarising voltage steps were made from a holding potential of −40 mV. B-E: Representative families of currents from cells stably expressing WT **(B)**, C93A **(C)**, C179A **(D)** and CC93/179AA **(E)** HCN4. **(F)** The average steady-state current-voltage relationship from 293T cells stably expressing WT (black), C93A (blue), C179A (green) and CC93/179AA (red) HCN4. The sinoatrial diastolic depolarisation voltage range is highlighted in grey. **, $p < 0.01$; ****, $p < 0.0001$ (two-way ANOVA followed by Tukey's *post hoc* comparison); n = 8-13.

for the activation relation between the WT and the mutant HCN4 channels (Figure 5C: 7.1 ± 0.5 mV for WT, 6.0 ± 0.3 mV for C93A, 6.4 ± 0.5 mV for C179A, 6.0 ± 0.2 mV for CC93/179AA). The time dependence of I_{HCN4} activation was quantified by measuring the time to half-maximal current over a range of the test potentials from −90 mV to −120 mV, for each cell. There was no difference between the activation time-course of WT and mutant channels (Figure 5D). We therefore conclude that palmitoylation significantly influences I_{HCN4} magnitude but not activation gating.

Conservation of HCN4 palmitoylation sites

We investigated conservation of the HCN4 palmitoylation sites between species. A cysteine analogous to human C93 is present in all vertebrate HCN4 homologues but is absent from all invertebrates. In contrast, C179 is absent from invertebrates, fish, amphibia and reptiles but is conserved in mammals and possibly birds (Figure 6). These observations suggest that HCN4 regulation by palmitoylation is an adaptation specific for vertebrates and endotherms.

Discussion

This study set out to investigate the functional impact of HCN4 palmitoylation. We identify two cysteines in the HCN4 amino terminus that are palmitoylated in mammalian cells. Mutation of one or both cysteines significantly reduces HCN4 palmitoylation and profoundly reduces the magnitude of HCN4-mediated currents. We therefore conclude that palmitoylation is a potent positive regulator of I_{HCN4}. Given the importance of the funny current for diastolic depolarisation, HCN4 palmitoylation has the potential to exert a powerful influence on heart rate.

Palmitoylation and I_{HCN4}

The results of prior experiments on HCN1 and HCN2 channels have suggested that amino terminal interactions are important for HCN subunit assembly (Proenza et al., 2002). Combined deletion of the amino and carboxyl termini of HCN4 has been reported to result in a ~10 mV hyperpolarizing shift in voltage dependence of current

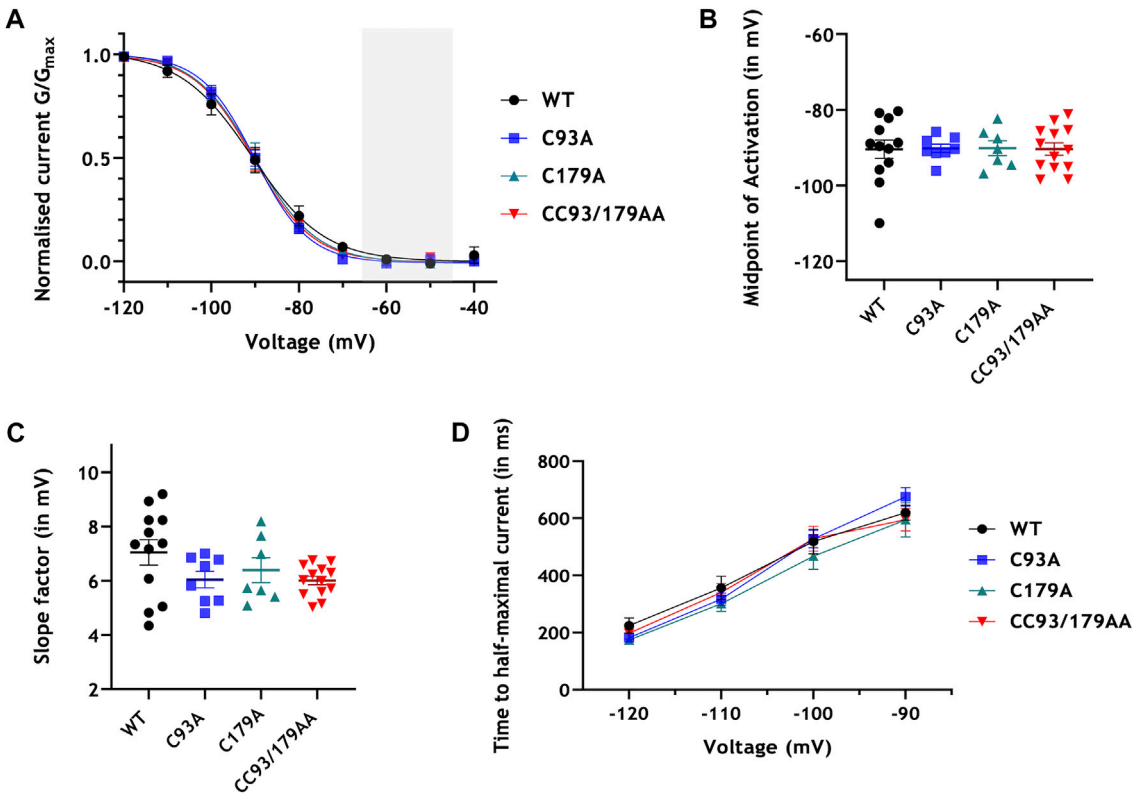

FIGURE 5
Palmitoylation and HCN4 currents: analysis. **(A)** Whole cell channel conductance (G) was normalised to the maximum conductance (G_{max}) of each cell and fitted with a Boltzmann function. The sinoatrial diastolic depolarisation voltage range is highlighted in grey. **(B)** Half-maximal activation potentials ($V_{0.5}$) obtained from the Boltzmann fits of the activation curves for each cell. **(C)** Slope factor (k) obtained from the Boltzmann fits of the activation curves for each cell. **(D)** Time to half-maximal activation at voltages −90 mV to −120 mV. No groups are significantly different from each other; *n* = 8-13.

activation and to slow activation timecourse (Ishii et al., 2001). Comparison of brain and heart HCN4 variants with distinct amino termini, together with mutagenesis studies have also demonstrated a role for the amino terminus in HCN4 channel activation (Liu and Aldrich, 2011). Our results showed no significant difference in the activation parameters investigated between WT and unpalmitoylatable HCN4, but found a profound effect on the magnitude of I_{HCN4}. Similar results to those shown here for inducible HCN4 expression (Figures 4, 5) were seen in additional experiments (data not shown) using transient transfection. Macroscopic current magnitudes through any voltage sensitive channel are determined by the number of channels present at the cell surface (*N*), the single channel conductance (*G*), and the channel open probability (*Po*). We found no obvious influence of palmitoylation in the HCN4 amino terminus on steady state abundance of HCN4 protein at the cell surface membrane. We hence rule out any significant influence of palmitoylation on *N*. Since the HCN4 amino terminus is relatively far from the channel's pore (Saponaro et al., 2021), it seems unlikely that palmitoylation produces a profound alteration in *G*. We therefore propose that HCN4 *Po* is regulated by palmitoylation. There is precedent for the single channel properties and *Po* of HCN4 to be regulated by the presence of an accessory subunit (Brandt et al., 2009). It is also well-established that HCN4 gating is not adequately described by a second-order Hodgkin-Huxley model (DiFrancesco et al., 1986; Hoppe et al., 1998). Five closed and five open states have been proposed (Altomare et al., 2001), and experimental recordings of single channel events are consistent with the existence of numerous open and closed states (Michels et al., 2005). Clearly there is considerable scope for post-translational events to control the lifetime of one or more state and consequently regulate HCN4 *Po*. However, we do not rule out the possibility that 'silent' channels in the plasma membrane are recruited by palmitoylation. Co-operative gating of individual HCN2 channels has also been described (Dekker and Yellen, 2006). If co-operativity were enhanced by HCN4 palmitoylation this would manifest as increased *Po* and larger currents. Future experiments measuring single channel activity in WT and unpalmitoylated HCN4 mutants are required to distinguish these possibilities. Experiments to determine how cAMP regulates palmitoylated and non-palmitoylated HCN4 are also a high future priority. Although cAMP binds to the channel's carboxyl terminus we do not rule out the possibility that it differentially regulates channels based on the palmitoylation status of their amino terminus.

The typical consequence of protein palmitoylation is for the palmitoylated region of a protein to be anchored to the membrane (Main and Fuller, 2022). In the case of HCN4 our results are consistent with 'pinning' of the channel's amino terminus to the membrane leading to enhanced *Po*. This implies either that in the unpalmitoylated state the HCN4 amino terminus (which is predicted to be highly disordered) negatively regulates channel activity or that in the palmitoylated state the amino terminus is a channel facilitator.

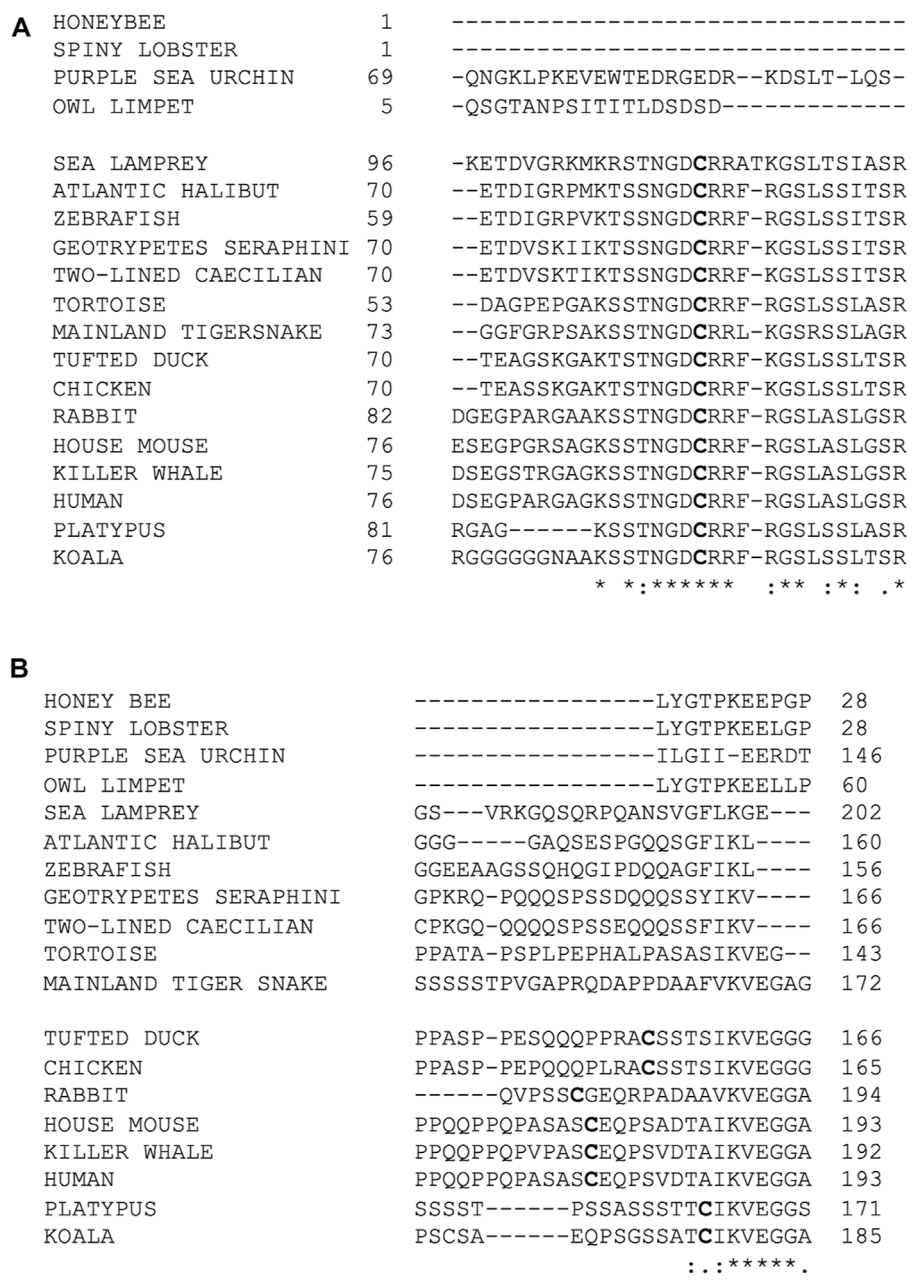

FIGURE 6
Conservation of palmitoylation sites amongst HCN4 homologues. **(A)** Conservation of cysteine 93. Alignment was generated using Clustal Omega. Palmitoylation site C93 and analogous cysteines are highlighted in bold. C93 is conserved in all vertebrates. The sequence surrounding C93 includes the cassette *SSTNGDCRRFKGSLSSLTSR* which is uniquely conserved amongst the vertebrates. **(B)** Conservation of cysteine 179. Alignment was generated using Clustal Omega. Palmitoylation site C179 and analogous cysteines are highlighted in bold. C179 is conserved in mammals and birds only."*" below an amino acid indicates 100% conservation between isoforms; ":" indicates amino acids of highly similar properties; "." indicates amino acids of weakly similar properties.

AlphaFold predicts the amino terminus of HCN4 to be extensively disordered, and no secondary structure was observed in this region of the protein in a recent HCN4 cryoEM structure (Saponaro et al., 2021). We acknowledge the possibility that cysteine to alanine mutagenesis of the HCN4 amino terminus may alter HCN4 behaviour independent of changes in palmitoylation. However, given the lack of structure in this region of the protein we suggest that the conservative substitutions introduced in this investigation are unlikely to significantly impact HCN4 folding.

Palmitoylation and HCN4 oligomerisation

We observe a substantial functional impact of palmitoylation on I_{HCN4} when only ~33% of HCN4 is palmitoylated. Mature

HCN4 channels are tetrameric (Saponaro et al., 2021). If palmitoylation has no influence on how monomers assemble to form this tetramer, then the probability of a tetramer assembling from entirely non-palmitoylated HCN4 is 0.67^4: approximately 0.2. Hence, we predict approximately 80% of HCN4 tetramers will contain one or more palmitoylated subunits. The oligomerisation of individual subunits offers an elegantly efficient way to achieve substantial functional differences even at a relatively low overall palmitoylation stoichiometry. If palmitoylation doesn't influence oligomerisation then mature HCN4 formed from a single palmitoylated subunit would be the most common form, but a significant proportion formed from two palmitoylated protomers would also exist. Future experiments using gain of function approaches to enhance HCN4 palmitoylation [for example, (Li et al., 2020)] will need to address whether there are functional differences between mature HCN4 formed from single or multiple palmitoylated monomers.

Palmitoylation and the regulation of other HCN channels

Although the present study is the first detailed study of sites and consequences of palmitoylation of HCN4, palmitoylation of HCN1, 2 and 4 has been described by others (Itoh et al., 2016). Multiple cysteines in the HCN2 amino terminus are palmitoylated, but no functional effect was observed when these sites were mutated. However, this earlier investigation relied on biochemical measurements of palmitoylation only in HEK cells but functional experiments only in *Xenopus* oocytes, and did not present evidence that HCN2 is palmitoylated in oocytes (Itoh et al., 2016). The lack of conservation of the human HCN4 palmitoylation sites in amphibians means it is doubtful whether oocytes possess the necessary enzymatic machinery to palmitoylate HCN channels. In addition, the membrane properties of an oocyte at room temperature are very different to a mammalian cell at 37°C. Since palmitoylation typically alters the relationship between an integral membrane protein and the phospholipid bilayer in which it resides, the usefulness of the oocyte system to evaluate the functional impact of palmitoylation is questionable. We suggest that the possibility that palmitoylation regulates important functional properties of other HCN channels in mammalian expression systems is one worthy of further pursuit.

Palmitoylation sites in HCN4

In our experiments, mutagenesis of the HCN4 amino terminal cysteines significantly reduced, but did not abolish its palmitoylation. We consider the small amount of residual CC93/179AA HCN4 captured in our palmitoylation assays to be largely 'background', but we do not rule out the possibility of a low level of palmitoylation in the channel's C terminus. The HCN4 CryoEM structure does not resolve large regions of the amino (1-214) and carboxyl (716-1023) termini. Those cysteines in the C terminus that are resolved (C586, C662, C679) are not positioned near membrane, making them unlikely palmitoylation sites [juxtamembrane cysteines are typically palmitoylated because the active site of the palmitoylating enzymes lies at the membrane/cytosol interface (Rana et al., 2018)]. We cannot rule out palmitoylation of C755 or C887.

Conclusion and future directions

The data in this study collectively indicate that native HCN4 protein in cardiac tissue is palmitoylated and reveal the importance of palmitoylation sites in the amino terminus of HCN4 channels. Further work, likely including measurements at the single channel level, is required to elucidate the mechanism(s) by which the loss of palmitoylation reduces I_{HCN4} magnitude. The differences in I_{HCN4} amplitudes observed here were significant at relatively negative membrane voltages. In order to determine the consequences of the loss of HCN4 amino terminal palmitoylation on the channel activity over diastolic depolarization voltages and function of the intact SAN, the future use of appropriately genetically modified mice is now warranted. This would allow effects of HCN4 modification by palmitoylation to be ascertained for the intact native SAN in the absence of whole cell dialysis. The present study provides a strong foundation from which such work can be undertaken.

Data availability statement

The raw data supporting the conclusion of this article will be made available, upon request, without undue qualification.

Ethics statement

Protocols involving animal use were reviewed and approved by University of Glasgow & University of Bristol Animal Welfare and Ethics Review Board.

Author contributions

Conceptualisation, supervision, writing—original draft: WF, JH; investigation, writing—review and editing: SC, AM, AB, XG, CD, SC, and HC; resources: EB.

Funding

This work was funded by the British Heart Foundation (FS/17/14/32773, FS/17/60/33474, PG/14/42/30886, PG/14/21/30673 and PG/19/26/34302).

Acknowledgments

The authors thank Dr. Yihong Zhang for helpful discussion.

Conflict of interest

The authors declare that the research was conducted in the absence of any commercial or financial relationships that could be construed as a potential conflict of interest.

Publisher's note

References

Altomare, C., Bucchi, A., Camatini, E., Baruscotti, M., Viscomi, C., Moroni, A., et al. (2001). Integrated allosteric model of voltage gating of HCN channels. *J. Gen. Physiol.* 117, 519–532. doi:10.1085/jgp.117.6.519

Baruscotti, M., Bucchi, A., and Difrancesco, D. (2005). Physiology and pharmacology of the cardiac pacemaker ("funny") current. *Pharmacol. Ther.* 107, 59–79. doi:10.1016/j.pharmthera.2005.01.005

Baruscotti, M., Bucchi, A., Viscomi, C., Mandelli, G., Consalez, G., Gnecchi-Rusconi, T., et al. (2011). Deep bradycardia and heart block caused by inducible cardiac-specific knockout of the pacemaker channel gene *Hcn4*. *Proc. Natl. Acad. Sci. U. S. A.* 108, 1705–1710. doi:10.1073/pnas.1010122108

Brandt, M. C., Endres-Becker, J., Zagidullin, N., Motloch, L. J., Er, F., Rottlaender, D., et al. (2009). Effects of KCNE2 on HCN isoforms: Distinct modulation of membrane expression and single channel properties. *Am. J. Physiol. Heart Circ. Physiol.* 297, H355–H363. doi:10.1152/ajpheart.00154.2009

Brioschi, C., Micheloni, S., Tellez, J. O., Pisoni, G., Longhi, R., Moroni, P., et al. (2009). Distribution of the pacemaker HCN4 channel mRNA and protein in the rabbit sinoatrial node. *J. Mol. Cell Cardiol.* 47, 221–227. doi:10.1016/j.yjmcc.2009.04.009

Brown, H. F., DiFrancesco, D., and Noble, S. J. (1979). How does adrenaline accelerate the heart? *Nature* 280, 235–236. doi:10.1038/280235a0

Bucchi, A., Barbuti, A., Difrancesco, D., and Baruscotti, M. (2012). Funny current and cardiac rhythm: Insights from HCN knockout and transgenic mouse models. *Front. Physiol.* 3, 240. doi:10.3389/fphys.2012.00240

Choudhury, M., Boyett, M. R., and Morris, G. M. (2015). Biology of the sinus node and its disease. *Arrhythm. Electrophysiol. Rev.* 4, 28–34. doi:10.15420/aer.2015.4.1.28

Dekker, J. P., and Yellen, G. (2006). Cooperative gating between single HCN pacemaker channels. *J. Gen. Physiol.* 128, 561–567. doi:10.1085/jgp.200609599

Denyer, J. C., and Brown, H. F. (1990). Rabbit sino-atrial node cells: Isolation and electrophysiological properties. *J. Physiol.* 428, 405–424. doi:10.1113/jphysiol.1990.sp018219

DiFrancesco, D. (2019). A brief history of pacemaking. *Front. Physiol.* 10, 1599. doi:10.3389/fphys.2019.01599

DiFrancesco, D., and Camm, J. A. (2004). Heart rate lowering by specific and selective (i_f) current inhibition with ivabradine: A new therapeutic perspective in cardiovascular disease. *Drugs* 64, 1757–1765. doi:10.2165/00003495-200464160-00003

DiFrancesco, D., Ferroni, A., Mazzanti, M., and Tromba, C. (1986). Properties of the hyperpolarizing-activated current (i_f) in cells isolated from the rabbit sino-atrial node. *J. Physiol.* 377, 61–88. doi:10.1113/jphysiol.1986.sp016177

DiFrancesco, D. (2010). The role of the funny current in pacemaker activity. *Circ. Res.* 106, 434–446. doi:10.1161/CIRCRESAHA.109.208041

Ernst, A. M., Syed, S. A., Zaki, O., Bottanelli, F., Zheng, H., Hacke, M., et al. (2018). S-palmitoylation sorts membrane cargo for anterograde transport in the golgi. *Dev. Cell* 47, 479–493.e7. doi:10.1016/j.devcel.2018.10.024

Essandoh, K., Philippe, J. M., Jenkins, P. M., and Brody, M. J. (2020). Palmitoylation: A fatty regulator of myocardial electrophysiology. *Front. Physiol.* 11, 108. doi:10.3389/fphys.2020.00108

Forrester, M. T., Hess, D. T., Thompson, J. W., Hultman, R., Moseley, M. A., Stamler, J. S., et al. (2011). Site-specific analysis of protein S-acylation by resin-assisted capture. *J. Lipid Res.* 52, 393–398. doi:10.1194/jlr.D011106

Gao, X., Kuo, C. W., Main, A., Brown, E., Rios, F. J., Camargo, L. L., et al. (2022). Palmitoylation regulates cellular distribution of and transmembrane Ca flux through TrpM7. *Cell Calcium* 106, 102639. doi:10.1016/j.ceca.2022.102639

Gok, C., Plain, F., Robertson, A. D., Howie, J., Baillie, G. S., Fraser, N. J., et al. (2020). Dynamic palmitoylation of the sodium-calcium exchanger modulates its structure, affinity for lipid-ordered domains, and inhibition by XIP. *Cell Rep.* 31, 107697. doi:10.1016/j.celrep.2020.107697

Gok, C., Robertson, A. D., and Fuller, W. (2022). Insulin-induced palmitoylation regulates the Cardiac Na^+/Ca^{2+} exchanger NCX1. *Cell Calcium* 104, 102567. doi:10.1016/j.ceca.2022.102567

Guan, X., and Fierke, C. A. (2011). Understanding protein palmitoylation: Biological significance and enzymology. *Sci. China Chem.* 54, 1888–1897. doi:10.1007/s11426-011-4428-2

Hoppe, U. C., Jansen, E., Sudkamp, M., and Beuckelmann, D. J. (1998). Hyperpolarization-activated inward current in ventricular myocytes from normal and failing human hearts. *Circulation* 97, 55–65. doi:10.1161/01.cir.97.1.55

Ishii, T. M., Takano, M., and Ohmori, H. (2001). Determinants of activation kinetics in mammalian hyperpolarization-activated cation channels. *J. Physiol.* 537, 93–100. doi:10.1111/j.1469-7793.2001.0093k.x

Itoh, M., Ishihara, K., Nakashima, N., and Takano, M. (2016). The hyperpolarization-activated cyclic nucleotide-gated (HCN) channels contain multiple S-palmitoylation sites. *J. Physiol. Sci.* 66, 241–248. doi:10.1007/s12576-015-0420-5

Kuo, C. S., Dobi, S., Gok, C., Da Silva Costa, A., Main, A., Robertson-Gray, O., et al. (2023). Palmitoylation of the pore-forming subunit of Ca(v)1.2 controls channel voltage sensitivity and calcium transients in cardiac myocytes. *Proc. Natl. Acad. Sci. U. S. A.* 120, e2207887120. doi:10.1073/pnas.2207887120

Lakatta, E. G., Maltsev, V. A., and Vinogradova, T. M. (2010). A coupled SYSTEM of intracellular Ca^{2+} clocks and surface membrane voltage clocks controls the timekeeping mechanism of the heart's pacemaker. *Circ. Res.* 106, 659–673. doi:10.1161/CIRCRESAHA.109.206078

Li, Y., Wang, S., Chen, Y., Li, M., Dong, X., Hang, H. C., et al. (2020). Site-specific chemical fatty-acylation for gain-of-function analysis of protein S-palmitoylation in live cells. *Chem. Commun. (Camb)* 56, 13880–13883. doi:10.1039/d0cc06073a

Liao, Z., Lockhead, D., St Clair, J. R., Larson, E. D., Wilson, C. E., and Proenza, C. (2012). Cellular context and multiple channel domains determine cAMP sensitivity of HCN4 channels: Ligand-independent relief of autoinhibition in HCN4. *J. Gen. Physiol.* 140, 557–566. doi:10.1085/jgp.201210858

Linder, M. E., and Deschenes, R. J. (2007). Palmitoylation: Policing protein stability and traffic. *Nat. Rev. Mol. Cell Biol.* 8, 74–84. doi:10.1038/nrm2084

Liu, H., and Aldrich, R. W. (2011). Tissue-specific N terminus of the HCN4 channel affects channel activation. *J. Biol. Chem.* 286, 14209–14214. doi:10.1074/jbc.M110.215640

Main, A., Boguslavskyi, A., Howie, J., Kuo, C. W., Rankin, A., Burton, F. L., et al. (2022). Dynamic but discordant alterations in zDHHC5 expression and palmitoylation of its substrates in cardiac pathologies. *Front. Physiol.* 13, 1023237. doi:10.3389/fphys.2022.1023237

Main, A., and Fuller, W. (2022). Protein S-palmitoylation: Advances and challenges in studying a therapeutically important lipid modification. *FEBS J.* 289, 861–882. doi:10.1111/febs.15781

Michels, G., Er, F., Khan, I., Sudkamp, M., Herzig, S., and Hoppe, U. C. (2005). Single-channel properties support a potential contribution of hyperpolarization-activated cyclic nucleotide-gated channels and if to cardiac arrhythmias. *Circulation* 111, 399–404. doi:10.1161/01.CIR.0000153799.65783.3A

Milanesi, R., Baruscotti, M., Gnecchi-Ruscone, T., and DiFrancesco, D. (2006). Familial sinus bradycardia associated with a mutation in the cardiac pacemaker channel. *N. Engl. J. Med.* 354, 151–157. doi:10.1056/NEJMoa052475

Nof, E., Luria, D., Brass, D., Marek, D., Lahat, H., Reznik-Wolf, H., et al. (2007). Point mutation in the HCN4 cardiac ion channel pore affecting synthesis, trafficking, and functional expression is associated with familial asymptomatic sinus bradycardia. *Circulation* 116, 463–470. doi:10.1161/CIRCULATIONAHA.107.706887

Pei, Z., Xiao, Y., Meng, J., Hudmon, A., and Cummins, T. R. (2016). Cardiac sodium channel palmitoylation regulates channel availability and myocyte excitability with implications for arrhythmia generation. *Nat. Commun.* 7, 12035. doi:10.1038/ncomms12035

Proenza, C., Tran, N., Angoli, D., Zahynacz, K., Balcar, P., and Accili, E. A. (2002). Different roles for the cyclic nucleotide binding domain and amino terminus in assembly and expression of hyperpolarization-activated, cyclic nucleotide-gated channels. *J. Biol. Chem.* 277, 29634–29642. doi:10.1074/jbc.M200504200

Rana, M. S., Kumar, P., Lee, C. J., Verardi, R., Rajashankar, K. R., and Banerjee, A. (2018). Fatty acyl recognition and transfer by an integral membrane S-acyltransferase. *Science* 359, eaao6326. doi:10.1126/science.aao6326

Reilly, L., Howie, J., Wypijewski, K., Ashford, M. L., Hilgemann, D. W., and Fuller, W. (2015). Palmitoylation of the Na/Ca exchanger cytoplasmic loop controls its inactivation and internalization during stress signaling. *FASEB J.* 29, 4532–4543. doi:10.1096/fj.15-276493

Saponaro, A., Bauer, D., Giese, M. H., Swuec, P., Porro, A., Gasparri, F., et al. (2021). Gating movements and ion permeation in HCN4 pacemaker channels. *Mol. Cell* 81, 2929–2943.e6. doi:10.1016/j.molcel.2021.05.033

Schweizer, P. A., Duhme, N., Thomas, D., Becker, R., Zehelein, J., Draguhn, A., et al. (2010). cAMP sensitivity of HCN pacemaker channels determines basal heart rate but is not critical for autonomic rate control. *Circ. Arrhythm. Electrophysiol.* 3, 542–552. doi:10.1161/CIRCEP.110.949768

Stieber, J., Herrmann, S., Feil, S., Loster, J., Feil, R., Biel, M., et al. (2003). The hyperpolarization-activated channel HCN4 is required for the generation of pacemaker action potentials in the embryonic heart. *Proc. Natl. Acad. Sci. U. S. A.* 100, 15235–15240. doi:10.1073/pnas.2434235100

Tsutsui, K., Monfredi, O. J., Sirenko-Tagirova, S. G., Maltseva, L. A., Bychkov, R., Kim, M. S., et al. (2018). A coupled-clock system drives the automaticity of human sinoatrial nodal pacemaker cells. *Sci. Signal* 11, eaap7608. doi:10.1126/scisignal.aap7608

Tulloch, L. B., Howie, J., Wypijewski, K. J., Wilson, C. R., Bernard, W. G., Shattock, M. J., et al. (2011). The inhibitory effect of phospholemman on the sodium pump requires its palmitoylation. *J. Biol. Chem.* 286, 36020–36031. doi:10.1074/jbc.M111.282145

Varghese, A., Tenbroek, E. M., Coles, J., Jr., and Sigg, D. C. (2006). Endogenous channels in HEK cells and potential roles in HCN ionic current measurements. *Prog. Biophys. Mol. Biol.* 90, 26–37. doi:10.1016/j.pbiomolbio.2005.05.002

Verkerk, A. O., and Wilders, R. (2015). Pacemaker activity of the human sinoatrial node: An update on the effects of mutations in HCN4 on the hyperpolarization-activated current. *Int. J. Mol. Sci.* 16, 3071–3094. doi:10.3390/ijms16023071

Won, S. J. (2018). Protein depalmitoylases. *Crit. Rev. Biochem. Mol. Biol.* 53, 83–98. doi:10.1080/10409238.2017.1409191

frontiers | Frontiers in Physiology

TYPE Review
PUBLISHED 04 May 2023
DOI 10.3389/fphys.2023.1167873

OPEN ACCESS

EDITED BY
William Fuller,
University of Glasgow, United Kingdom

REVIEWED BY
Thomas Lanyon-Hogg,
University of Oxford, United Kingdom
Peng Wang,
Chinese Academy of Tropical Agricultural Sciences, China
Jing-Xiang Wu,
Chinese Academy of Medical Sciences and Peking Union Medical College, China

*CORRESPONDENCE
James L. Hougland,
hougland@syr.edu

RECEIVED 16 February 2023
ACCEPTED 19 April 2023
PUBLISHED 04 May 2023

CITATION
Pierce MR and Hougland JL (2023), A rising tide lifts all MBOATs: recent progress in structural and functional understanding of membrane bound *O*-acyltransferases.
Front. Physiol. 14:1167873.
doi: 10.3389/fphys.2023.1167873

A rising tide lifts all MBOATs: recent progress in structural and functional understanding of membrane bound *O*-acyltransferases

Mariah R. Pierce[1] and James L. Hougland[1,2,3]*

[1]Department of Chemistry, Syracuse University, Syracuse, NY, United States, [2]Department of Biology, Syracuse University, Syracuse, NY, United States, [3]BioInspired Syracuse, Syracuse University, Syracuse, NY, United States

Acylation modifications play a central role in biological and physiological processes. Across a range of biomolecules from phospholipids to triglycerides to proteins, introduction of a hydrophobic acyl chain can dramatically alter the biological function and cellular localization of these substrates. Amongst the enzymes catalyzing these modifications, the membrane bound *O*-acyltransferase (MBOAT) family occupies an intriguing position as the combined substrate selectivities of the various family members span all three classes of these biomolecules. MBOAT-dependent substrates are linked to a wide range of health conditions including metabolic disease, cancer, and neurodegenerative disease. Like many integral membrane proteins, these enzymes have presented challenges to investigation due to their intractability to solubilization and purification. However, over the last several years new solubilization approaches coupled with computational modeling, crystallography, and cryoelectron microscopy have brought an explosion of structural information for multiple MBOAT family members. These studies enable comparison of MBOAT structure and function across members catalyzing modifications of all three substrate classes, revealing both conserved features amongst all MBOATs and distinct architectural features that correlate with different acylation substrates ranging from lipids to proteins. We discuss the methods that led to this renaissance of MBOAT structural investigations, our new understanding of MBOAT structure and implications for catalytic function, and the potential impact of these studies for development of new therapeutics targeting MBOAT-dependent physiological processes.

KEYWORDS

membrane-bound *O*-acyltransferase, cryoelectron microscopy, acylation, MBOAT fold, computational structure prediction, ghrelin, Wnt, Hedgehog

1 Introduction

1.1 Membrane bound *O*-acyltransferase family—history and background

The membrane bound *O*-acyltransferase (MBOAT) family comprises a group of enzymes characterized by multiple transmembrane domains and a conserved histidine residue. The first family member reported in the literature was acyl-coenzyme A: cholesterol acyltransferase, also known as sterol *O*-acyltransferase (ACAT1/SOAT1) (Mukherjee and Alfin-Slater, 1958; Goodman et al., 1964). ACAT1/SOAT1 is responsible for the acylation of the alcohol on cholesterol to form cholesterol esters. ACAT1/SOAT1 was first extracted from rat liver homogenates and was later identified as a membrane bound enzyme (Mukherjee and Alfin-Slater, 1958; Goodman et al., 1964). Identification of the gene encoding ACAT1/SOAT1, the *ACAT/SOAT* gene, led to discovery of the homologous ACAT2/SOAT2 (Chang et al., 1993; Yang et al., 1996; Yu et al., 1996; Cases et al., 1998a; Anderson et al., 1998; Oelkers et al., 1998). In addition to ACAT2/SOAT2, a related enzyme diacylglycerol *O*-acyltransferase 1 (DGAT1) was identified by sequence similarity to ACAT1/SOAT1 (Cases et al., 1998b). This enzyme performs similar acylation modifications on a distinct substrate diacylglycerol with involvement in triglyceride biosynthesis. Further sequence analysis led to yet another enzyme, Porcupine (PORCN) (Hofmann, 2000). PORCN is an acyltransferase in the Wnt signaling pathway, where it acylates the secreted signaling protein Wnt in contrast to the lipid and cholesterol substrates for ACAT1/SOAT1 and DGAT1. In 2000, Hofmann identified PORCN as an additional acyltransferase and named this enzyme family the membrane bound *O*-acyltransferases (MBOAT) (Hofmann, 2000).

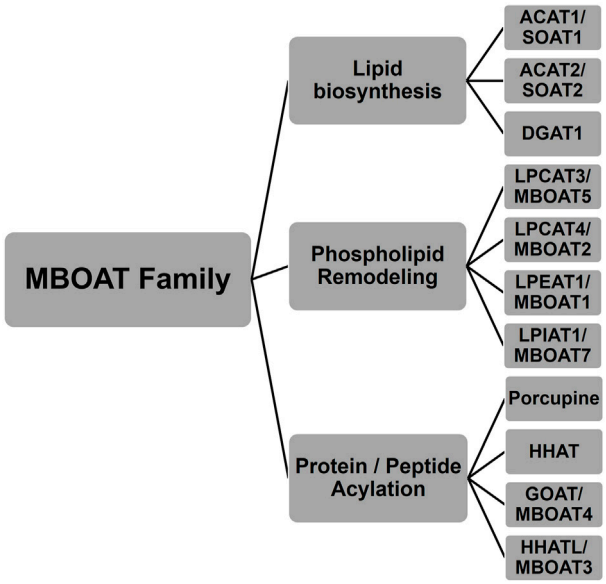

FIGURE 1
Membrane bound *O*-acyltransferase (MBOAT) family of enzymes. These integral membrane enzymes acylate cholesterol, diacylglycerol, phospholipids, peptides, and proteins.

1.2 MBOAT family: acylation substrates lead to subfamily classifications

The MBOAT family of enzymes can be classified by the biochemical reaction each enzyme performs (Figure 1). MBOAT enzymes were first classified as enzymes that perform lipid biosynthesis. This group includes the ACAT/SOAT enzymes and DGAT1 that acylates cholesterol and triglycerides. Another group of MBOATs are lysophospholipid acyltransferases responsible for acylating phospholipids. The last group is responsible for acylating proteins and peptides. Below we describe the known mammalian MBOATs and their major roles in the cell. In section c we will describe their roles in signaling and disease.

1.2.1 Lipid Biosynthesis

As noted above, ACAT1/SOAT1 is responsible for the acylation of cholesterol to cholesterol ester. Cholesterol esters provide a storage option to prevent cholesterol build-up in cell membranes. Consequently, ACAT1/SOAT1 is expressed in multiple cell types in the body. Chang and co-workers expressed and purified ACAT1/SOAT1 with full biological activity in 1998 (Chang et al., 1998). ACAT1/SOAT1 is a homotetrameric enzyme with 9 transmembrane domains per monomer, with this multimeric nature posing difficulties for enzyme studies (Yu et al., 1999). Two conserved amino acids, His460 and Asn421, have been implicated in its acylation activity (Guo et al., 2007). ACAT1/SOAT1 will bind sterols and steroids and contains multiple binding sites for these substrates.

ACAT2/SOAT2 is mainly found in the small intestine and liver (Anderson et al., 1998). Its expression and cloning was also reported in 1998 (Cases et al., 1998a). The predominant theory for the existence of both enzymes is that ACAT1/SOAT1 acts to maintain cholesterol levels throughout the body whereas ACAT2/SOAT2 is coupled to lipoprotein particle assembly and secretion (Joyce et al., 2000). Further analysis of acylation by these enzymes has been pursued using the structure publication that will be described below.

While ACAT/SOAT modifies cholesterol, acyl-CoA: diacylglycerol acyltransferase (DGAT) acylates precursors to create triglycerides. Triglycerides are used for energy storage and membrane lipid formation. While triglycerides are important for normal physiological behavior, an excess of these glycerol triesters can lead to disease states such as obesity (Birch et al., 2010; Lee et al., 2010). In 1956, it was reported that DGAT used fatty acyl-CoAs as acyl donors (Weiss and Kennedy, 1956), and the connection to the ACAT enzymes at the sequence level came in 1998 (Weiss et al., 1960; Cases et al., 1998b). Knockout of both DGAT1 and DGAT2 in mice lead to reduced triacylglyceride levels (Smith et al., 2000; Stone et al., 2004). DGAT1 prefers monosaturated substrates where DGAT2 did not show a saturation preference but a chain length preference. DGAT2 prefers shorter chain acyl-CoAs and short/medium chain fatty acyl moieties (Cases et al., 2001; Lardizabal et al., 2001). DGAT2 is more efficient at triacylglycerol (TAG) acylation, while DGAT1 has the potential to acylate multiple substrates (Ross, 1982; Batten et al., 2004; Yen et al., 2005). This is further believed to be true as their topologies are drastically different with DGAT1 containing multiple transmembrane

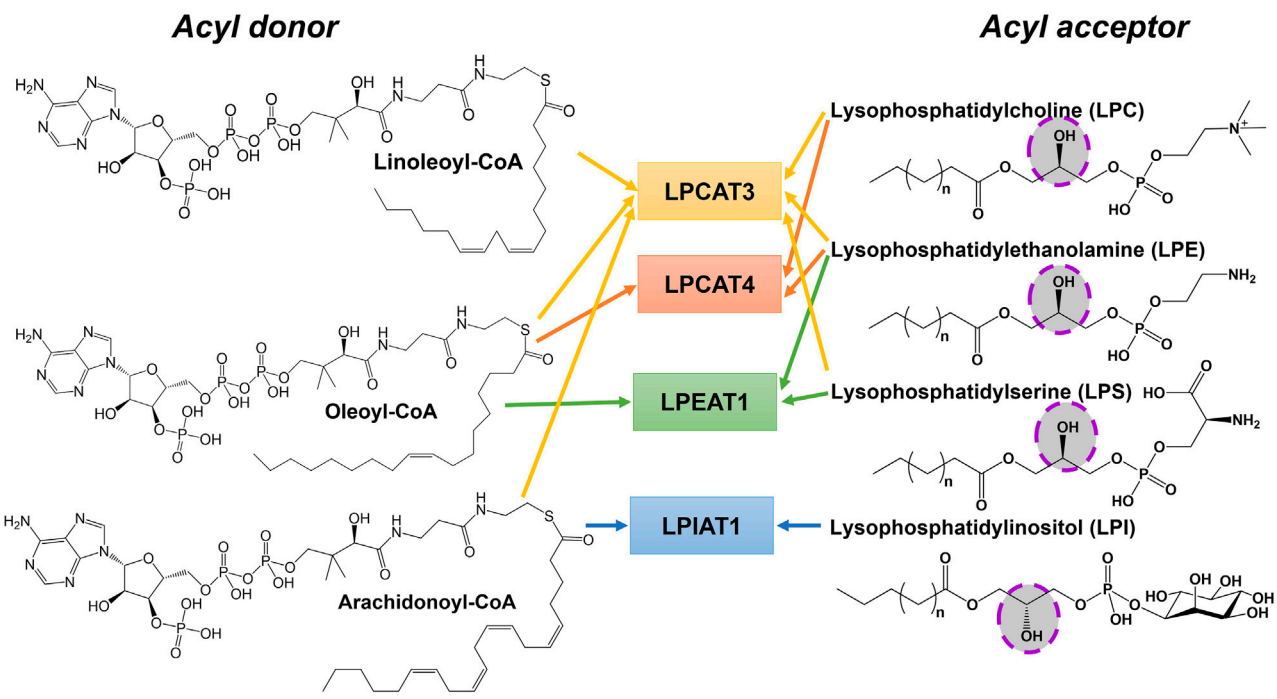

FIGURE 2
Phospholipid remodeling MBOAT enzymes have multiple substrates and utilize multiple acyl-CoAs as acyl donors. Phospholipid remodeling enzymes can acylate various substrates using a range of acyl donors. This figure shows a subset of these potential enzyme-acyl acceptor–acyl donor combinations for acyl donors bearing unsaturated fatty acids. The hydroxyl group that becomes acylated in the acyl acceptor substrate is highlighted.

domains and DGAT2 with significantly fewer domains (Cases et al., 2001; Cheng et al., 2001; Lardizabal et al., 2001; Weselake et al., 2006). For more detailed discussion of DGAT1 and DGAT2 activity, expression, and topology, the authors direct to the following excellent reviews on these topics by Yen et al., in 2008 and most recently by Chen et al., in 2022 (Yen et al., 2008; Chen et al., 2022).

1.2.2 Lysophospholipid acyltransferases

MBOAT family members also play key roles in phospholipid synthesis and recycling (Figure 2). Phosphatidylcholine (PC), phosphatidylethanolamine (PE), and phosphatidylserine (PS) are the major phospholipids in membranes and surfactants in mammals. PC acyl chain remodeling is performed by lysophosphatidylcholine acyltransferases (LPCATs). Only LPCAT3 and LPCAT4 acylate lyso-PC with unsaturated acyl chains at the *sn-2* hydroxyl, with both of these enzymes annotated as MBOAT family members (Hofmann, 2000; Hishikawa et al., 2008). LPCAT3/MBOAT5 has seven transmembrane domains and the conserved His and Asn residues that typify MBOAT family members. LPCAT3/MBOAT5 favors unsaturated fatty acyl-CoAs such as oleoyl-CoA, linoleoyl-CoA, and arachidonyl-CoA as acyl donors and 1-myristoyl-lyso-PC and 1-palmitoyl-lyso-PC as acyl acceptors/acylation substrates (Zhao et al., 2008; Jain et al., 2009). LPCAT4/MBOAT2 and LPEAT1/MBOAT1 both prefer oleoyl-CoA as their acyl donor and catalyze reactions with lyso-PC, lyso-PE, and lyso-PS (Hishikawa et al., 2008). The last lysophospholipid acyltransferase amongst the MBOATs is lysophosphatidylinositol acyltransferase 1 (LPIAT1). LPIAT1/MBOAT7 adds an arachidonic acid or an eicosapentaenoic acid onto lyso-PI (Caddeo et al., 2019; Caddeo et al., 2021). LPIAT1 catalyzes the transfer of an acyl chain to lyso-PI and mutations to its conserved Asn321 and His356 resulted in a loss of acyltransferase activity like most other MBOAT family members (Caddeo et al., 2021). LPIAT1 prefers polyunsaturated fatty acids as opposed to saturated or unsaturated fatty acids (Caddeo et al., 2021). LPIAT1 has a predicted six transmembrane domains and is an integral membrane enzyme tightly bound to endosomes (Caddeo et al., 2019).

1.2.3 Acylation of proteins/peptides

There are three MBOATs that catalyze the acylation of proteins or peptides, PORCN, Hedgehog acyltransferase (HHAT), and ghrelin *O*-acyltransferase (GOAT/MBOAT4) (Figure 3). PORCN, identified as the first protein acylating MBOAT, acylates the signaling protein Wnt with a palmitoleate (C16:1) group (Zhai et al., 2004; Rios-Esteves et al., 2014). This modification occurs at a conserved serine and is required for receptor (Frizzled) binding and signaling (Takada et al., 2006; Janda et al., 2012). HHAT catalyzes the acylation of Hedgehog proteins (Sonic, Indian, and Desert) which bind and signal through the Patched receptor(Kong et al., 2019). HHAT palmitoylates (C16:0) the N-terminal cysteine on SHH (Pepinsky et al., 1998). GOAT octanoylates ghrelin on the third serine, and like HHAT/hedgehog and PORCN/Wnt this acylation modification is required for ghrelin binding and signaling through its receptor GHS-R1a (Kojima et al., 1999; Abizaid and Hougland, 2020).

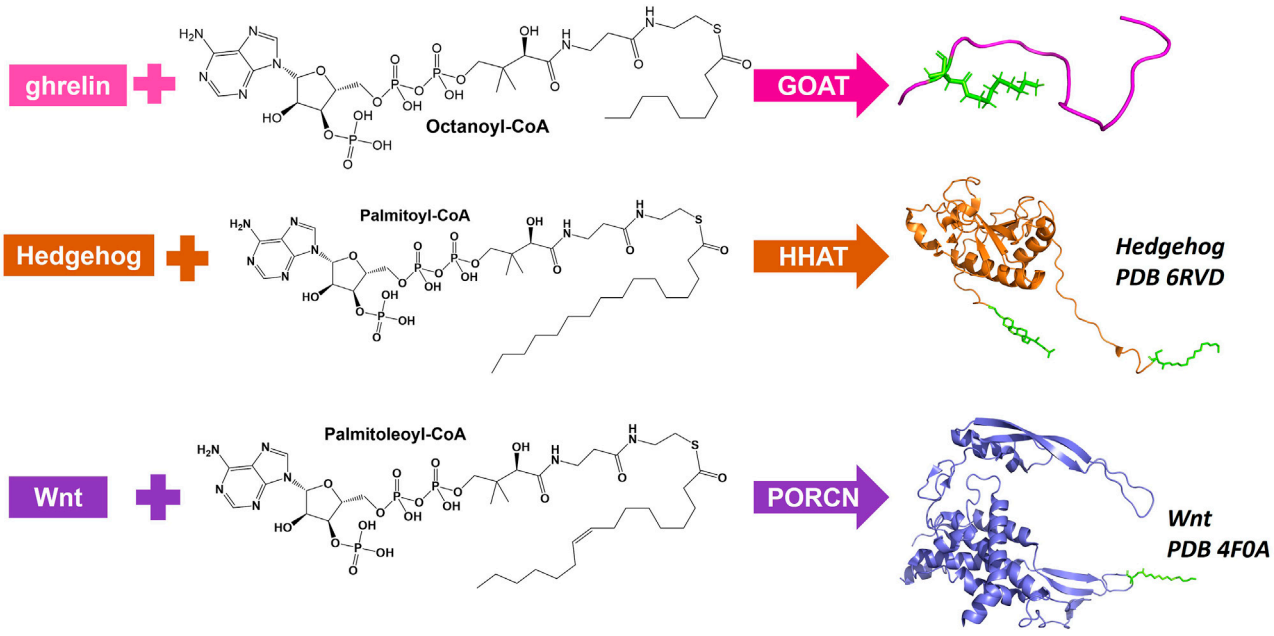

FIGURE 3
Protein and peptide acylating MBOATs. GOAT acylates the peptide hormone ghrelin and prefers octanoyl-CoA as the acyl donor. Hedgehog (PBD: 6RVD) first gets modified with a cholesterol moiety (green) then gets acylated by HHAT with a preference for palmitoyl-CoA. Wnt (PDB: 4F0A) is acylated by PORCN using palmitoleoyl-CoA.

1.3 Importance of MBOATs in signaling and disease

1.3.1 ACAT/SOAT

Multiple studies show ACAT/SOAT to be an important enzyme to facilitate improvement in human health and disease. For example, inhibition of ACAT1/SOAT1 was shown to lower the level of neurological disease in an Alzheimer's mouse model (Hutter-Paier et al., 2004; Bhattacharyya and Kovacs, 2010; Bryleva et al., 2010). It has been shown that by inhibiting ACAT1/SOAT1 cholesterol can be re-directed to repair other organelles (Hutter-Paier et al., 2004; Bhattacharyya and Kovacs, 2010; Bryleva et al., 2010). By way of modulating T-cell cholesterol metabolism, ACAT1/SOAT1 has been shown to facilitate cancer treatment (Yang et al., 2016). ACAT2/SOAT2 is only active in the hepatocytes and intestinal cells, and when ACAT2/SOAT2 is not functioning normally it can cause reduced assembly and secretion of low-density lipoprotein (LDL). This eliminates hypercholesterolemia and atherosclerosis (Buhman et al., 2000; Willner et al., 2003; Rudel et al., 2005; Ohshiro et al., 2015). Related to those diseases, a buildup of cholesterol and lipids in circulation can lead to heart attacks. Inhibiting ACAT2/SOAT2 has been suggested to be especially helpful in preventing these cardiovascular risks (Goldstein and Brown, 2009).

1.3.2 DGAT1

DGAT1 is expressed in multiple tissues throughout the body. It has a major role in dietary fat absorption and protecting the body by preventing fatty acid (FA)-induced toxicity (Yen et al., 2008). Unesterified FAs promotes endoplasmic reticulum (ER) stress leading insulin resistance and impaired (Chitraju et al., 2017). DGAT1 performs the last step in TAG biosynthesis in the Kennedy and monoacylglycerol (MG) pathways, and without DGAT1 there was a severe loss in dietary fat absorption (Buhman et al., 2002). Inhibition of DGAT1 would prevent the absorption of TAG into the body, leading to reduced lipid storage in the body (Smith et al., 2000; Chen et al., 2002). Consequently, DGAT is a target for prevention of obesity, glucose metabolism, and insulin secretion.

1.3.3 LPCAT3/MBOAT5

LPCAT3/MBOAT5 catalyzes a polyunsaturated acyl moiety (18:2 and 20:4) onto lyso-PC, lyso-PE, and lyso-PS (Hishikawa et al., 2008). This changes the composition of the cell membrane, and the function of the proteins in the surrounding area. LPCAT3 is a key component of the Kennedy pathway and the Lands' Cycle (Kennedy and Weiss, 1956; Lands, 1958; Lands, 2000). LPCAT3 is primarily expressed in liver and is a key regulator of in phospholipid and triglyceride metabolism (Zhao et al., 2008). Of the four LPCATs, LPCAT3 is the major isoform in metabolic issues and has been proposed as a drug target for atherosclerosis and hyperlipidemia (Wang and Tontonoz, 2019; Liu et al., 2020). However, this approach has the potential for off target effects on cholesterol biosynthesis and fat accumulation (Rong et al., 2015; Wang et al., 2018). LPCAT3 has been implicated in obesity induced skeletal myopathy, with mice overexpressing LPCAT3 exhibiting worse skeletal myopathy when fed a high-fat diet then those mice fed a normal diet. LPCAT3 is consequently a therapeutic target for treatment of obesity induced skeletal myopathy (Zhang et al.,

2012). LPCAT3 also plays a role in diabetes. Mice overexpressing LPCAT3 showed improved postprandial hyperglycemia and glucose tolerance (Ferrara et al., 2021). However, in skeletal muscle the opposite is observed with overexpression of LPCAT3 in skeletal muscle leading to glucose intolerance (Labonté et al., 2006). For more detailed discussion of recent progress in understanding LPCAT3's role in cancer and diseases, the authors direct your attention to a recent review by Shao et al. (Shao et al., 2022).

1.3.4 LPCAT4/MBOAT2

Like LPCAT3, LPCAT4 is also a key component of the Kennedy pathway and Lands' Cycle (Kennedy and Weiss, 1956; Lands, 1958; Lands, 2000). LPCAT4 is also referred to acyl-CoA:lyso-PE (LPEAT2) due to its lyso-PE activity, but following the publication by Hishikawa and co-workers it is now only called LPCAT4 (Hishikawa et al., 2008). LPCAT4 is responsible for acylating lyso- PC and lyso- PE that make up the cell membrane (Hishikawa et al., 2008). LPCAT4 is expressed in the brain, testis, epididymis, and ovary (Cao et al., 2008; Hishikawa et al., 2008). LPCAT4's expression is upregulated in colorectal cancer cells. The ratio of PC to Lyso-PC has been implicated as a biomarker for colorectal cancer, indicating LPCAT4 as a key factor for improving standard of care for colorectal cancer (Kurabe et al., 2013). LPCAT4 is known to regulate chondrogenic differentiation in skeletal development (Tabe et al., 2017). Suppressing LPCAT4 activity has recently been implicated to slow down pancreatic tumor progression (Zhou et al., 2021; Li et al., 2022; Xie et al., 2022).

1.3.5 LPEAT1/MBOAT1

Lysophosphatidylethanolamine acyltransferase 1 (LPEAT1) acylates lyso-PE and lyso-PS with oleoyl-CoA (18:1) (Hishikawa et al., 2008). LPEAT1 is also a contributor to the Lands Cycle and Kennedy pathway (Kennedy and Weiss, 1956; Lands, 1958; Lands, 2000). The gene for LPEAT1 is located in chromosome 6 and when it is disrupted leads to brachydactyly-syndactyly syndrome (Dauwerse et al., 2007). Tabe et al. found that when LPEAT1 expression is knocked down, the growth of neurites decreased leading the authors to conclude that LPEAT is implicated in neurite outgrowth and function (Tabe et al., 2016). An exome screen in infertile Chinese male patients revealed two mtations in *MBOAT1,* the gene that encodes LPEAT1. This mutation, Thr257Met, impedes the translation of *MBOAT1* and leads to a lower expression of LPEAT1 (Wan et al., 2022). Similar evidence of infertility related to low LPEAT1 expression has been reported in *Drosophila* (Steinhauer et al., 2009).These authors are excited to see more developments from those labs studying LPEAT1.

1.3.6 LPIAT1/MBOAT7

LPIAT1 is also one of the many acyltransferases in the Lands cycle (Lands, 1958; Lands, 2000). In a global study of patients with neurodevelopmental disorders, a significant number of patients had biallelic or pathogenic variants in LPIAT1 or MBOAT7 (Johansen et al., 2016). LPIAT1 was also shown to be required for correct brain development in mice (Lee et al., 2012; Anderson et al., 2013). Loss of lyso-PI acylation due to LPIAT1/MBOAT7 depletion resulted in a large increase in triglycerides in hepatocytes (Tanaka et al., 2021). Recently it has been suggested that LPIAT1 is a major contributor to liver disease, with a loss-of-function variant near *MBOAT7* gene associated with various liver diseases such as metabolic-associated fatty liver disease, nonalcoholic fatty liver disease, and alcohol-associated liver disease (Varadharajan et al., 2022).

1.3.7 HHAT

Hedgehog signaling ligands were first discovered in *Drosophila* patterning (Nüsslein-Volhard and Wieschaus, 1980). Hedgehog acyltransferase (HHAT) catalyzes the lipidation of Hedgehog proteins (Buglino and Resh, 2008). This lipidation is essential to maintain Hedgehog signaling. Mutations to Hedgehog signaling proteins can cause congenital diseases and holoprosencephaly (Roessler et al., 1997; Briscoe and Thérond, 2013). Abnormal signaling of this pathway in involved in various malignancies including pancreatic, breast, and lung cancer (Konitsiotis et al., 2014; Wu et al., 2017; Chahal et al., 2018). The acylation activity of HHAT has been directly linked to pancreatic dual adenocarcinoma (Petrova et al., 2015). Hedgehog proteins are specific substrates for HHAT and this specificity makes HHAT a favorable pharmaceutical target. Abnormal Hedgehog signaling can be blocked by HHAT inhibitors. Multiple inhibitors have been designed to inhibit HHAT acylation activity, with photochemical probes utilized to identify the small molecule inhibitor binding site within HHAT (Lanyon-Hogg et al., 2015a; Lanyon-Hogg et al., 2015b; Lanyon-Hogg et al., 2016; Rodgers et al., 2016; Lanyon-Hogg et al., 2019; Lanyon-Hogg et al., 2021). One such example is RU-SKI 43 which was able to inhibit HHAT function *in vitro* and in cells with an IC_{50} of 850 nM (Petrova et al., 2013). A subsequent study demonstrated off-target cytotoxicity from RU-SKI 43 in cell studies and showed that a related compound RU-SKI 201 specifically inhibits HHAT acylation activity within cells with potencies in the range of 730–870 nM in independent assays (Rodgers et al., 2016).

1.3.8 PORCN

For Wnt to be trafficked from the ER to the Golgi and bind to its subsequent receptor Frizzled, it must undergo palmitoleoylation by PORCN (Takada et al., 2006; Galli et al., 2016). This chemical modification is required for proper Wnt signaling. Consequently, PORCN has been implicated as an important target for inhibition in the Wnt pathway (Chen et al., 2009; Dodge et al., 2012). Wnt signaling is implicated in several cancers and orphan diseases. Inhibition of PORCN was shown to prevent the growth of mammary tumors in mice with little toxicity to the mouse (Proffitt et al., 2013). Another PORCN inhibitor, LGK974, was found to prevent Wnt signaling in murine and rat mechanistic breast cancer models and human head and neck cell model (HN30) (Liu et al., 2013). PORCN inhibitors LGK974, ETC-159, CGX1321, and RXC004 have reached Phase I clinical trials as treatment for various cancers (Shah et al., 2021). In addition to developmental cancers, Wnt signaling is also implicated in focal dermal hypoplasia (FDH). Specifically, this disease is characterized by mutations to PORCN itself that impact Wnt acylation and subsequent biological activity (Wang et al., 2007; Barrott et al., 2011).

1.3.9 GOAT

GOAT is a key enzyme in the ghrelin signaling pathway. Ghrelin signaling was first linked to growth hormone secretion and appetite regulation (Müller et al., 2015). In addition it has implications in glucose metabolism, energy homeostasis, and organismal response to starvation

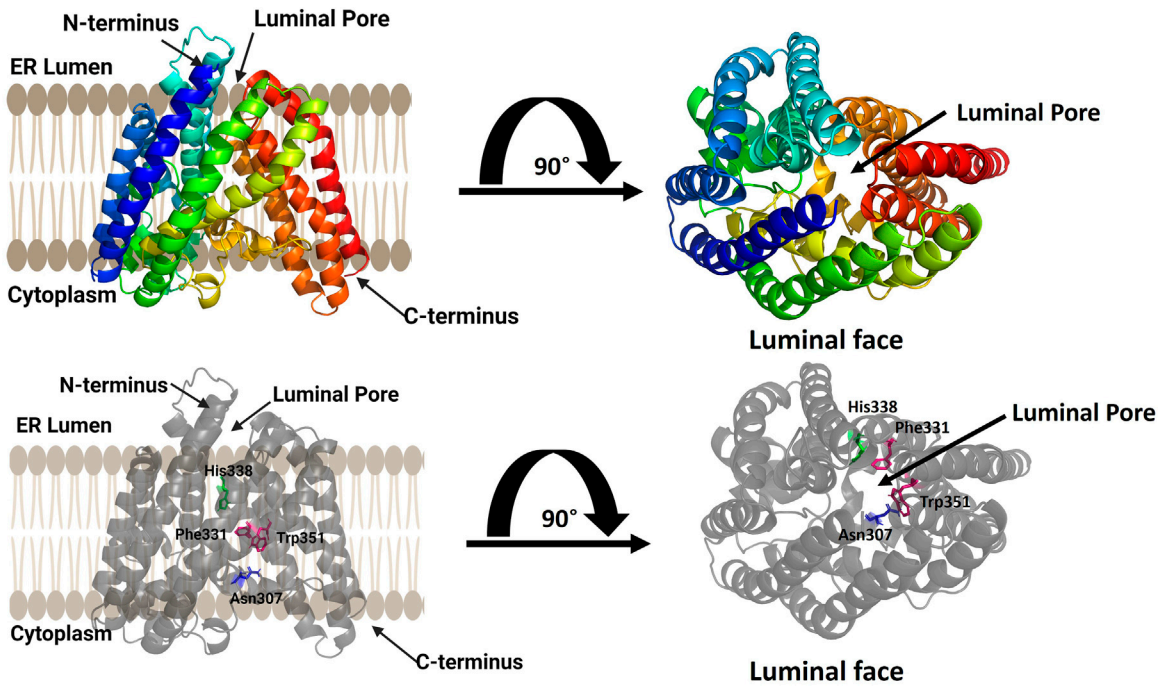

FIGURE 4
Computational model of ghrelin O-acyltransferase (GOAT). GOAT has 11 transmembrane helices and a transmembrane catalytic channel containing amino acids required for activity such as His 338 (green) and Asn 307 (blue) and residues implicated in acyl donor selectivity such as Trp351 and Phe331 (purple). The luminal pore for ghrelin binding and the catalytic channel can be seen in the top view from the luminal face of the membrane (right). Figure created using Biorender.

(Egido et al., 2002; Reimer et al., 2003; Zhao et al., 2010a; Zhao et al., 2010b; Tong et al., 2010; Goldstein et al., 2011; Heppner et al., 2012; Li et al., 2012; Yada et al., 2014; Gagnon et al., 2015). Less obviously ghrelin signaling has also been implicated in cardio-protection, protection against muscle atrophy, and bone metabolism (Nass et al., 2008; Müller et al., 2015; Pearson et al., 2019; Tokudome and Kangawa, 2019; Agosti et al., 2020; Wu et al., 2020). Most recently ghrelin acylation and signaling has been linked to addictive behavior and alcoholism (Zallar et al., 2017; Farokhnia et al., 2019; Farokhnia et al., 2020; Farokhnia et al., 2021). Several classes of GOAT inhibitors that have been developed. The first are peptide-based drugs that mimic the product and/or substrate of GOAT. These molecules tend to be potent inhibitors, but have received little pharmaceutical interest due to their likely limited oral bioavailability (Iyer et al., 2020; Moose et al., 2020). Amongst small-molecule GOAT inhibitors, LY3073084 is in clinical trials for treatment of several metabolism-related disorders and BI 1356225 has been investigated in Phase 1 trials for treatment of obesity (Bianzano et al., 2023). Several more small molecule GOAT inhibitors have been reported, some with picomolar IC_{50}, but these have yet to reach clinical trials (Moose et al., 2020).

2 Modeling MBOAT structure using computational methods

Like many integral membrane proteins, MBOATs have proven to be challenging to solubilize and purify for functional and structural studies. While recent work has accomplished significant advances in experimental structural determination of MBOAT family members, several MBOAT structural models were created using computational methods. These computational models proved useful for interpreting and designing biochemical studies of these enzymes, and comparison to more recently released structures of MBOAT family members demonstrated the power of computational methods to generate reasonable models for MBOATs.

2.1 GOAT

GOAT was computationally modeled using coevolutionary contact analysis combined with atomistic molecular dynamics (Figure 4) (Campaña et al., 2019). Coevolutionary contacts analysis relies on the hypothesis that amino acids that contact each other within a folded protein will co-evolve to maintain their interaction to create the most energetically favorable fold (Marks et al., 2012; Ovchinnikov et al., 2017). Using multiple sequence alignments to identify probable coevolutionary contacts, Campana and co-workers developed a set of distance constraints for computationally modeling human GOAT using standard protein folding approaches (Campaña et al., 2019). An array of 30,000 potential structures were created and evaluated for agreement with coevolutionary contact and topological constraints, leading to a best-fit structural model. This model was then embedded in a virtual lipid membrane and energy minimized by molecular dynamics (Campaña et al., 2019).

The structural model of human GOAT oriented the N-terminus within the ER lumen and the C-terminus in the cytoplasm and contained 11 transmembrane, consistent with a previously published topology of mouse GOAT (Taylor et al., 2013). Surprisingly, the GOAT model contains a channel through the core the enzyme connecting the lumen to the cytoplasm. This channel contains the conserved catalytically essential His338 residue, and extensive mutagenesis confirmed the functional requirement of this channel (Campaña et al., 2019). This channel and the core transmembrane helices surrounding it form what is now considered the MBOAT central core fold as denoted by Ma and co-workers (Ma et al., 2018).

The acyl donor octanoyl-CoA was docked into the GOAT model, illustrating the coenzyme A binding site on the cytosolic exposed face of the enzyme. The acyl donor chain penetrates into the core of GOAT and makes a turn to position it favorably for interactions with His338 and Asn307 (Campaña et al., 2019). Upon alanine mutagenesis of two aromatic residues contacting the distal end of the octanoyl chain, Trp351 and Phe331, GOAT lost the substrate preference for octanoyl-CoA and preferred longer-chain fatty acid chains as acyl donors (Campaña et al., 2019). This GOAT model and associated biochemical studies illustrated the structural basis for the unique octanoyl acyl chain selectivity exhibited by this enzyme in modifying ghrelin (Kojima et al., 1999; Darling et al., 2015), and is particularly important as there are no reported crystal or cryo-EM structures of GOAT.

2.2 HHAT

An HHAT homology model was published in 2021 by Lanyon-Hogg and co-workers. The published crystal structure of DltB and two published topology models for HHAT proved sufficient to support construction of this homology model (Konitsiotis et al., 2015; Matevossian and Resh, 2015; Ma et al., 2018). This model contained the protein/peptide MBOAT central core containing the catalytically essential His379 and Asp339 residues (Lanyon-Hogg et al., 2021). In addition, residues Pro212, Val213, and His215 involved in binding an HHAT inhibitor, (+)-6 IMP-1575, also located in this central core. The model has 10 integral membrane helices, with the N-terminus in the cytosol and the C-terminus in the luminal (Lanyon-Hogg et al., 2021). The overall shape of the HHAT model is consistent with the tent-like structure of the other protein/peptide acylating MBOATs. This model tends to be overlooked as experimental structures of HHAT were also published in 2021 as described below.

2.3 PORCN

Two computationally-derived structural models for PORCN were published in 2021. One model by Galli and co-workers was developed using homology modeling coupled with partial permeabilization studies and N-linked glycosylation analysis to establish the PORCN membrane topology (Galli et al., 2021). In this study, six different algorithms were applied to predict the PORCN membrane topology which yielded a range of 8–11 transmembrane domains. To experimentally determine the PORCN topology, introduction of antibody epitopes and N-linked glycosylation sites were used to identify if those epitopes/sites were exposed to the luminal space or the cytosol. Guided by these combined analyses, a homology model was developed consisting of nine transmembrane domains and two reentrant loops with the N-terminus facing the lumen and C-terminus in the cytosol. This model contains a funnel on the luminal side of the structure leading to a transmembrane tunnel, with the conserved His341 residue located in the center of the funnel (Galli et al., 2021).

A second PORCN computational model was created using homology modeling guided by the published MBOAT structures available at the time (Yu et al., 2021). Yu and co-workers used multiple sequence analysis algorithms and MODELLER to create their homology model for PORCN, which has ten transmembrane domains and both the N-terminus and C-terminus located in the cytoplasm. This model also contains a transmembrane tunnel with the conserved His341 residue and depicts binding sites for both the acyl donor and Wnt substrates. Several PORCN inhibitors were also docked into the homology model, with these inhibitors binding into the enzyme active site. These two PORCN structural models provided important context for understanding how this enzyme binds its substrates and catalyzes Wnt acylation, and served as points for comparison for the experimentally determined structure of PORCN released the following year, as described below (Liu et al., 2022).

3 Experimentally determined MBOAT structures

3.1 DltB

In 2018, Ma and co-workers published the crystallographic structure of bacterial *D*-alanyltransferase DltB, the first such structure of an MBOAT family member (Ma et al., 2018). DltB is essential for the D-alanylation of cell wall teichoic acids, using an acyl carrier protein DltC as the acyl donor (Ma et al., 2018). The structure of this bacterial MBOAT homolog facilitated homology modeling of PORCN and provided a valuable reference to validate features of the computational GOAT structural model (Campaña et al., 2019; Galli et al., 2021; Yu et al., 2021). DltB was expressed in bacteria and solubilized with n-decyl-β-D-maltopyranoside, with samples for crystallization solubilized in n-decyl-nonyl-β-D-glucopyranoside (Ma et al., 2018). The DltB structure contains 17 helices and both the N-terminus and C-terminus are on the same side of the membrane. Of the 17 helical domains, 11 are transmembrane domains that form a ring-shaped cone with a conserved MBOAT structural core and a transmembrane channel with a funnel on the extracellular interface. At the time of publication, the DltB structure was described as a funnel with a fold dissimilar to any available structures. As described below, subsequent structures of additional MBOATs have revealed that DltB contains most of the conserved features of this enzyme family.

3.2 hACAT/hSOAT

2020 brought the MBOAT community the first structures of mammalian MBOATs, with two ACAT1/SOAT1 structures and two DGAT1 structures published in the same issue of Nature

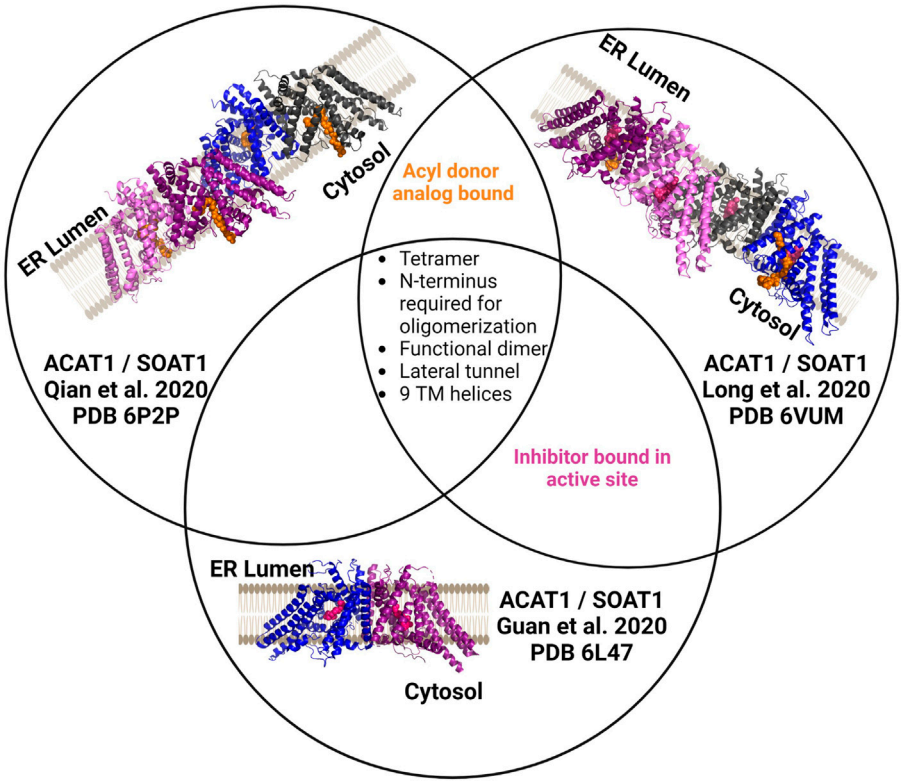

FIGURE 5
Independently determined structures of ACAT1/SOAT1 reveal common characteristics. All three published ACAT1/SOAT1 structures are consistent in identifying a multimeric complex, with at least two structures of the three also containing bound acyl donor and/or an inhibitor bound in the catalytic core of the enzyme. Different colors denote each monomeric unit within the dimeric or tetrameric complexes. Bound inhibitors are shown in purple, and acyl donor analogs are in orange. Figure created using Biorender.

followed shortly by a third ACAT1/SOAT1 (Guan et al., 2020; Long et al., 2020; Qian et al., 2020; Sui et al., 2020; Wang et al., 2020).

3.2.1 ACAT1/SOAT1

ACAT1/SOAT1 was purified as a tetrameric protein or dimer of dimers in the three published structures (Figure 5) (Guan et al., 2020; Long et al., 2020; Qian et al., 2020). The four monomers in the ACAT1/SOAT1 complex provide sufficient size and mass to allow cryo-EM analysis of the enzyme complex alone. Each ACAT1/SOAT1 monomer contains nine transmembrane helices, where the N-terminus "hugs" or folds into the other N-terminii of the other monomers forming the tetrameric complex (Guan et al., 2020; Long et al., 2020; Qian et al., 2020). The tetramer, dimer, and monomer were tested for catalytic activity and it was found that only the monomer lacked ACAT1/SOAT1 acylation activity consistent with the dimer forming the catalytically active unit (Guan et al., 2020; Qian et al., 2020).

In the structures by Long et al. and Qian et al., several amino acids (His425, Tyr433, Lys445, Ser456) interact with acyl-CoA and were annotated to either form the cytosolic interface or a cytosolic tunnel where the acyl donor binds (Long et al., 2020; Qian et al., 2020). However, Guan and co-workers did not identify an oleoyl-CoA binding site as the other structures described. These authors hypothesize that the inhibitor CI-976 bound in their preparation leads to an ACAT1/SOAT1 conformation that does not effectively bind the acyl-CoA donor.

In addition to the residues noted above in the acyl donor binding site, Asn 421 was also shown to be required for ACAT1/SOAT1 acylation activity (Long et al., 2020; Qian et al., 2020). These residues all reside in the catalytic core and have contacts with acyl-CoA. The structures also reveal two cholesterol binding sites, with one serving as the substrate binding site for this cholesterol acyltransferase and the other proposed to serve an allosteric role (Long et al., 2020). Qian et al. and Guan et al. suggest evidence of not only a CoA substrate tunnel, but a transmembrane channel that is hypothesized to bind cholesterol (Guan et al., 2020; Qian et al., 2020). This channel converges with the acyl-CoA donor binding site/tunnel at the conserved His460 residues within the enzyme core. Mutations along this tunnel were detrimental to activity, consistent with the proposed role for this feature in acylation catalysis (Qian et al., 2020).

3.2.2 ACAT2/SOAT2

ACAT2/SOAT2 was purified as a dimer of dimers with each monomer containing nine transmembrane helices with only a RMSD of 0.8Å between ACAT1/SOAT1 and ACAT2/SOAT2 (Figure 6) (Long et al., 2021). ACAT2/SOAT2 also contains the conserved acyl-CoA binding pocket and the hydrophobic core for

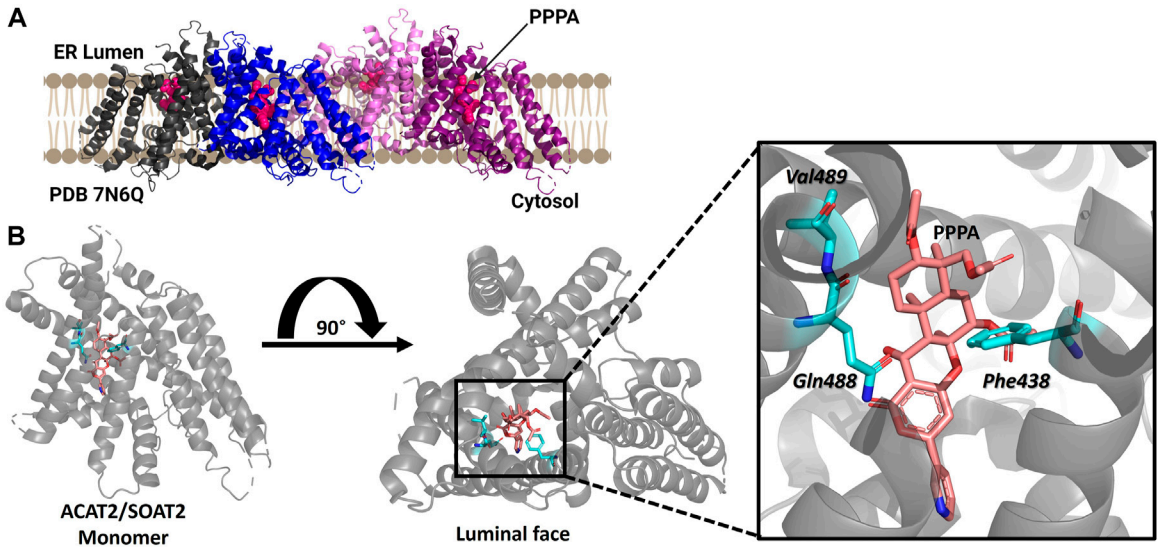

FIGURE 6
Structure of ACAT2/SOAT2 bound to the PPPA inhibitor. **(A)** ACAT2/SOAT2 forms a tetramer, but only requires dimer formation for acylation activity. Monomers are shown in gray, blue, pink, and purple, and the PPPA inhibitor in each monomer is hot pink. **(B)** One molecule of PPPA binds per monomer of ACAT2/SOAT2, contacting residues Val489, Gln488, and Phe438. PDB ID: 7N6Q. Figure created using Biorender.

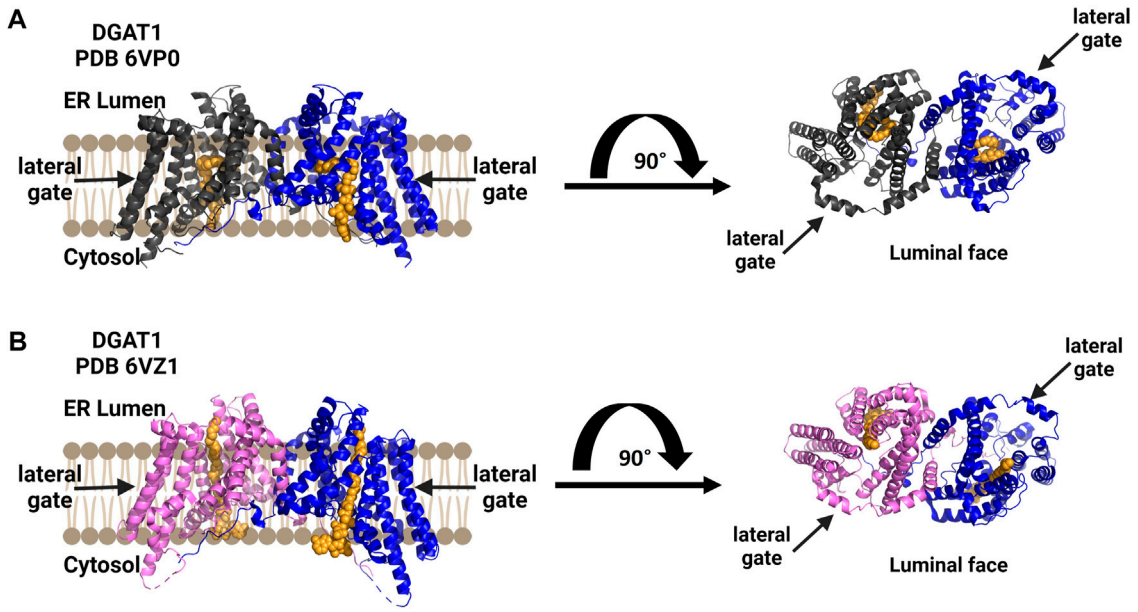

FIGURE 7
DGAT1 is a dimeric enzyme with a central cavity and a lateral gate. Independent structures confirm the formation of functional dimers (blue and dark gray), with a lateral gate for substrate access denoted by black arrows on each structure's top view from the luminal face (right). Both structures contain a non-hydrolyzable CoA analog in orange. **(A)** Structure by Wang and co-workers (PDB ID 6VP0). **(B)** Structure by Sui and co-workers (PDB ID 6VZ1). Figure created using Biorender.

cholesterol esterification observed in ACAT1/SOAT1 (Guan et al., 2020; Long et al., 2020; Qian et al., 2020; Long et al., 2021; Long et al., 2022). The cholesterol tunnel described for ACAT1/SOAT1 is also present in ACAT2/SOAT2 and has access to the proposed catalytic histidine His434 (Long et al., 2021). ACAT2/SOAT2 also contained an additional cholesterol binding site each monomer separate from the cholesterol present in the substrate binding site within the catalytic core. In both ACAT1/SOAT1 and ACAT2/SOAT2 the

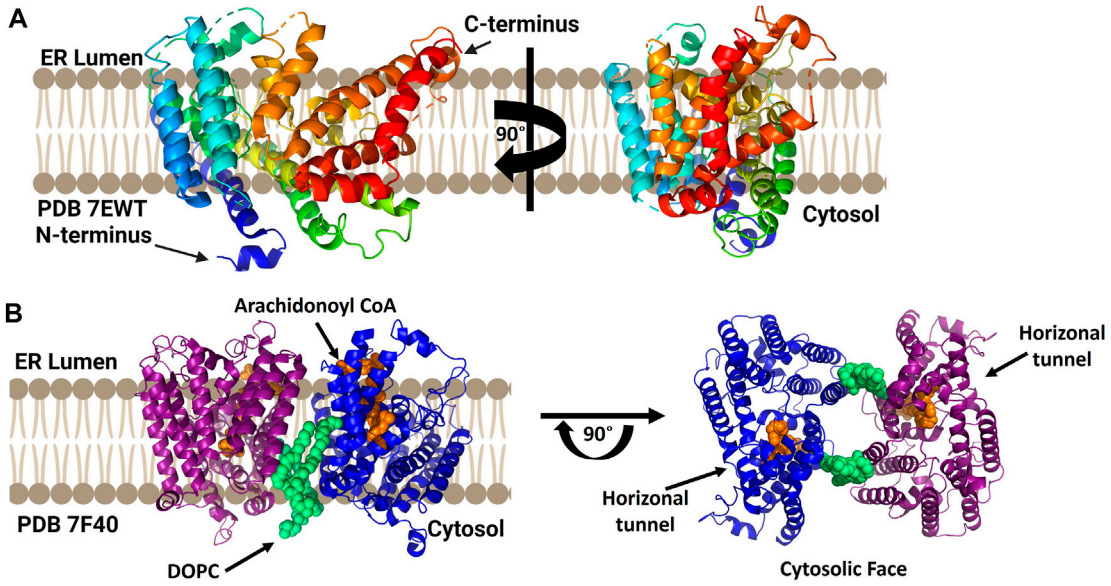

FIGURE 8
cLPCAT3 structural analysis reveals a condition-dependent dimerization state. **(A)** X-ray crystal structure of cLPCAT3 (PDB ID 7EWT) solved without substrates bound. For comparison to the dimer structure from cryoelectron microscopy, the rotated image on the right is presented in the same orientation as the right (blue) subunit of the dimer in left side of panel **(B)** Dimeric structure of cLPCAT3 solved by cryoelectron microscopy (PDB ID 7F40) with arachidonoyl CoA (orange) and 1,2-dioleoyl-sn-glycero-3-phosphocholine (DOPC, lime green) bound to each monomer. Arrows on the cytosolic top view indicate the lateral/horizontal tunnel for acyl acceptor entry. Figure created using Biorender.

second cholesterol binding site is proposed to be allosteric and mutation of both of cholesterol binding sites reduce acylation activity (Long et al., 2020; Long et al., 2021).

3.3 hDGAT1

Human diacylglycerol acyltransferase I (hDGAT1) was resolved as a dimer and structurally analyzed by cryo-EM (Figure 7) (Sui et al., 2020; Wang et al., 2020). In the study by Sui and co-workers, the amphipol PMAL-C8 was used to maintain a homogenous oligomer structure for structure determination (Sui et al., 2020). hDGAT1 has nine transmembrane domains with the N-terminus facing the cytosol and the C-terminus facing the lumen (Sui et al., 2020; Wang et al., 2020). The hDGAT1 dimer is formed through hydrogen-bonding and interactions with phospholipids present between monomers. DGAT1 has a large central core and a lateral gate that is open to the membrane. Its substrate diacylglycerol (DAG) can enter the membrane from the lumen or the cytosol. The conserved histidine His415 is also present in the large central core where the lateral gate connects to the active site (Sui et al., 2020; Wang et al., 2020) Oleoly-CoA binds within the central core, but the acyl binding site is long enough to accommodate longer chain fatty acids (Sui et al., 2020). Similar to the cholesterol acyltransferases, DGAT1 has a channel connecting to the lipid membrane and Sui and co-workers identified a diacylglycerol in this channel that co-purified with the enzyme. Wang et al. also found a similar lateral gateway, but could not resolve the density present in this chamber (Wang et al., 2020). DGAT has a bend in the lateral gateway that is proposed to select lipid substrates over rigid like structures like cholesterol (Sui et al., 2020). For a more detailed comparison of these structures, the authors direct attention to a recent review of DGAT enzymes (Chen et al., 2022).

3.4 cLPCAT3

While a mammalian lysophosphatidylcholine acyltransferase structure remains to be reported, Zhang and co-workers reported the crystal structure of chicken lysophophatidylcholine acyltransferase 3 (LPCAT3) (Figure 8). To obtain this structure, LPCAT3 was solubilized in undecyl maltoside and two residues at the enzyme C-terminus were removed to improve homogeneity and stability resulting structures at 3.4 Å resolution (Zhang et al., 2021). LPCAT3 has an overall bell shape comprising 11 transmembrane domains and 6 short helices, with the transmembrane domains surrounding a central cavity (Zhang et al., 2021). Similar to ACAT1/SOAT1 and DGAT1, LPCAT3 also contains a lateral tunnel connecting the central cavity to the surrounding membrane. To characterize the substrate binding pockets in LPCAT3, cryo-EM was utilized as substrate-bound crystals were not obtained. When purified in LMNG for cryo-EM analysis, cLPCAT3 was oligomeric. The cryo-EM structure was solved in the presence of both enzyme substrates, the arachidonoyl-CoA (araCoA) acyl donor and 1-dodecanoyl-sn-glyero-3-phosphocholine (12:0-LPC) in a dimeric state (Zhang et al., 2021). The cLPCAT3/araCoA structure had an araCoA in the central cavity with the acyl chain downstream of the unsaturation "kink" entering a side pocket. This acyl chain conformation leaves the horizonal tunnel available for the LPCAT3 acyl acceptor, resulting in araCoA lining up with the conserved His388 residue and acyl acceptor within the enzyme core (Zhang et al., 2021). Cross-linking

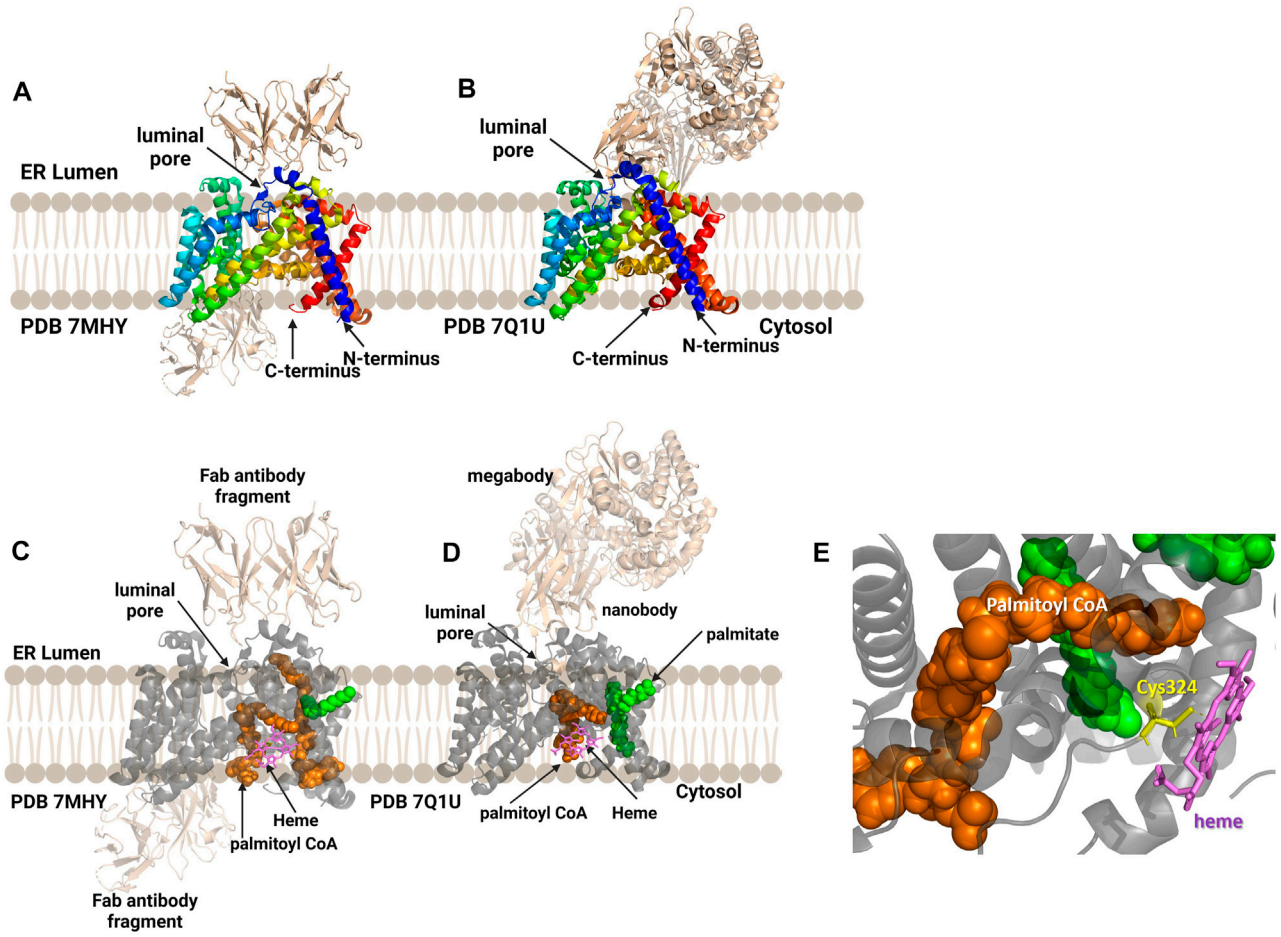

FIGURE 9
Antibody-based complexes enabled cryoelectron microscopy determination of HHAT structure, revealing substrate binding sites, inhibitor binding, and an unanticipated heme cofactor. **(A)** Cryo-EM structure of HHAT by Jiang and co-workers (PDB ID 7MHY) shows the overall structure of the enzyme complexed to antibodies on both the cytoplasmic and luminal interfaces. **(B)** Binding to a designed megabody partner enabled the cryo-EM structure of HHAT by Coupland and co-workers (PDB ID 7Q1U). **(C, D)** Both groups report the presence of a heme (violet) in their structures; antibodies/megabody shown in beige, palmitoyl-CoA in orange, and palmitic acid in green. **(E)** Heme binding site in PDB ID 7Q1U showing heme iron coordination by Cys324. Figure created using Biorender.

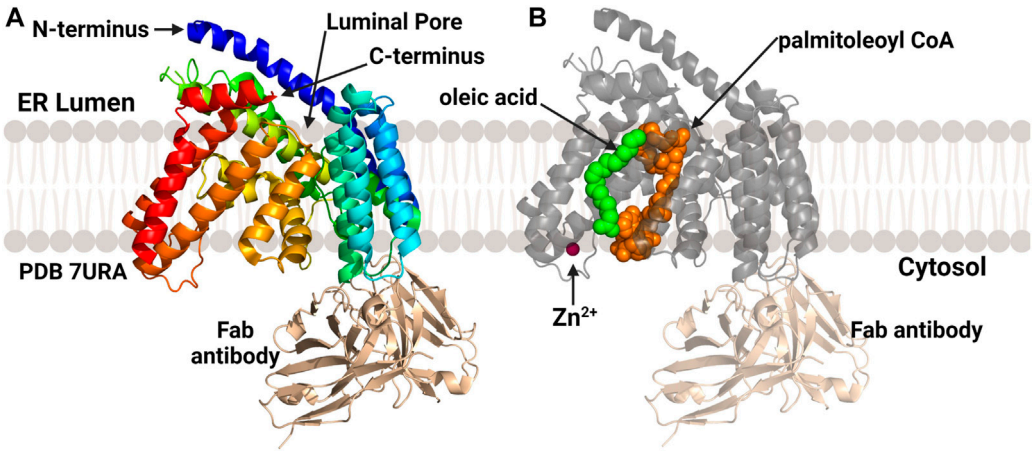

FIGURE 10
Structures of PORCN bound to substrates. **(A)** Overall structure of PORCN with 11 transmembrane domains and both the N-terminus and C-terminus in the ER lumen. **(B)** PORCN in complex with palmitoyl-CoA (orange) (PDB ID 7URA), showing the bound zinc ion (magenta) and palmitic acid (green). The antibody structural chaperone is shown in wheat. Figure created using Biorender.

TABLE 1 MBOAT structures from computational and experimental studies.

MBOAT	Year Reported	Monomer/Multimer	PDB ID(s)	Reference
Computational Modeling				
GOAT	2019	Monomer	n/a	Campaña et al. (2019)
PORCN	2020	Monomer	n/a	Galli et al. (2021)
PORCN	2020	Monomer	n/a	Yu et al. (2021)
X-ray crystallography				
DltB	2018	Monomer	6BUG, 6BUH, 6BUI	Ma et al. (2018)
LPCAT3	2021	Monomer	7EWT	Zhang et al. (2021)
Cryoelectron microscopy				
ACAT1/SOAT1	2020	Tetramer	6VUM	Long et al. (2020)
ACAT1/SOAT1	2020	Tetramer	6P2J, 6P2P	Qian et al. (2020)
ACAT1/SOAT1	2020	Tetramer	6L47, 6L48	Guan et al. (2020)
DGAT1	2020	Dimer	6VYI, 6VZ1	Sui et al. (2020)
DGAT1	2020	Dimer	6VP0	Wang et al. (2020)
ACAT2/SOAT2	2021	Tetramer	7N6R, 7N6Q	Long et al. (2021)
LPCAT3	2021	Dimer	7F3X, 7F40	Zhang et al. (2021)
HHAT	2021	Monomer	7Q1U, 7Q6Z	Coupland et al. (2021)
HHAT	2021	Monomer	7MHY	Jiang et al. (2021)
HHAT	2022	Monomer	7URF	Liu et al. (2022)
PORCN	2022	Monomer	7URA, 7URC, 7URD,7URE	Liu et al. (2022)

studies support the biological relevance of cLPCAT3 dimerization, but the specific function of monomer-monomer interaction remains to be understood (Zhang et al., 2021). Looking towards the catalytic mechanism for lysophospholipid acylation, the authors suggest a mechanism for acyl transfer wherein the acyl donor and acyl acceptor are bound simultaneously within the enzyme core. The carbonyl carbon of the acyl donor is activated by Asn352 in a manner reminiscent of oxyanion hole interactions in serine proteases, while the sn-2 hydroxyl of the acyl receiver is activated by His388 acting as a general base. Acylation proceeds by attack of the activated sn-2 hydroxyl group on the activate thioester of the acyl donor and resolves with transfer of the acyl chain to the acceptor (Zhang et al., 2021).

3.5 hHHAT

Human hedgehog acyltransferase (hHHAT) is a monomeric enzyme whose size is insufficient to support cryo-EM analysis of the enzyme alone, leading two research groups to employ antibody-derived binding partners to increase the enzyme-complex size sufficiently to allow structure determination (Figure 9) (Coupland et al., 2021; Jiang et al., 2021). The HHAT structures reveal 12 transmembrane helices connected by intervening alpha helical and loop regions forming the now-canonical "MBOAT fold". This aligns the conserved His379 residue with the conserved residues in the structures of other MBOAT family members (Coupland et al., 2021; Jiang et al., 2021). Jiang and co-workers modeled a palmitoyl-CoA acyl donor into the central cavity of the enzyme. The central cavity connects to the cytosolic face of the ER membrane (Jiang et al., 2021). Coupland et al. also resolved a non-hydrolyzable palm-CoA analog bound within the central tunnel which would span from the cytosolic to luminal sides of the ER membrane. This places the palmitoyl-CoA close to the conserved His379 and catalytically required Asp339 residues (Coupland et al., 2021). Surprisingly, both structures revealed a heme coordinated to Cys324, with subsequent mutagenesis and functional studies indicating this heme is required for enzyme stability (Coupland et al., 2021; Jiang et al., 2021). Jiang and co-workers suggest a one-step mechanism where Asp339 activates the N-terminal cysteine of Hedgehog for nucleophilic attack on the thioester carbonyl atom of the acyl donor, with the Oxford group supporting further studies before defining a mechanism (Coupland et al., 2021; Jiang et al., 2021). The HHAT structure was solved with the IMP1575 inhibitor bound by three labs (Coupland et al., 2021; Jiang et al., 2021; Liu et al., 2022). IMP1575 is the most potent reported HHAT inhibitor (Lanyon-Hogg et al., 2021). This structure depicted a directed binding interaction to the catalytic His379 and creates a conformational change within the enzyme. This conformational change rearranges Asp339, Asn443, and Trp335. Trp335 rotates into the binding pocket, and this residue is responsible for preventing water penetration into the enzyme core without palmitoyl-CoA bound (Coupland et al., 2021).

3.6 hPORCN

In 2022 the structure of PORCN, the acyltransferase responsible for Wnt acylation (Figure 10), was published by Lie and co-workers (Liu et al., 2022). Similar to HHAT, PORCN was purified as a monomer

which required antibody-derived binding partners to reach the mass/size range compatible with cryo-EM methods. Consistent with the computational models described above, PORCN was determined to contain 11 transmembrane helical domains with 6 intervening alpha helices and 2 beta strands. The Wnt substrate binding site on the luminal face of the enzyme is composed of portions of TMs 1, 2, 5, and 7. The catalytic core and central domain of PORCN containing the conserved His336 residue are consistent with other protein/peptide acylating MBOAT. A co-structure with palmitoleoyl-CoA showed this core also binds the acyl donor substrate in a cavity made by TM7 and TM10. A zinc ion found coordinated to four residues (Cys370, Cys376, Cys380, and His382) consistent with previous studies of PORCN, although the role of zinc in PORCN structure and function remains to be defined (Lee et al., 2019; Liu et al., 2022). In addition to the palmitoleoyl-CoA co-structure, one additional co-structure was solved with a PORCN inhibitor LGK974 bound (Liu et al., 2013). This co-structure found that Ser332 of PORCN interacts with the carbonyl oxygen of LGK974 and is consistent with the acyl-CoA competitive nature of this inhibitor (Liu et al., 2022).

4 Conclusion and lessons learned from MBOAT structures

For more than two decades, the MBOAT enzyme family has posed intriguing challenges across the fields of enzymology, structural biology, lipid synthesis and remodeling, and cellular signaling by acylated proteins (Hofmann, 2000). The recent explosion in MBOAT structures and structural models spanning all three classes of acylation substrates has dramatically advanced our understanding of these integral membrane enzymes (Table 1). These structures have revealed family-wide shared characteristics, illustrated distinct properties of enzymes depending on their acyl acceptor substrates, and brought into clearer focus questions regarding their acylation mechanisms and the potential for inhibitor creation towards therapeutic application. Between experimental structural studies, structure modeling using the approaches described in this review, and application of AI-based folding prediction approaches such as AlphaFold (Jumper et al., 2021; Binder et al., 2022), the prospects for continuing the rapid advancement in our understanding of the MBOAT enzyme family are incredibly promising.

Comparison of all reported MBOAT structures supports the establishment of a "MBOAT core" fold, with a cone shaped bundle of transmembrane domains surrounding a conserved core region. This core region, comprising helices and domains annotated as cytoplasmic loops in topological studies, contains an open channel or cavity within which sits the conserved histidine residues that is a hallmark of MBOAT family members. This central catalytic channel also connects to an acyl donor binding site exposed to the cytoplasmic space. We note that, except for the bacterial MBOAT DltB, all other MBOATS utilize acyl-coenzyme A as their acyl donor substrates. These enzymes feature catalytic cores that lie within the plane of their surrounding membranes, presenting an elegant answer to early questions in the MBOAT field of whether their active sites would lie on the cytoplasmic or luminal/extracellular faces of these acyltransferases.

Within the MBOAT family, structural and mechanistic distinctions are most notable between the protein-modifying members (GOAT, HHAT, and PORCN) and the small molecule/lipid modifying enzymes. The protein-modifying members are active as monomers, which corresponds with their experimentally solved structures. In contrast, the small molecule/lipid acylation MBOATs function as dimers or higher oligomers consistent with the tetramers or dimer of dimers in the experimentally determined structures. Focusing on the location of the acyl acceptor entry site and nature of the catalytic channel, the protein-modifying family members all contain channels that completely span the membrane with acyl acceptors (ghrelin, Hedgehog, and Wnt) entering the enzyme through a luminal pore and acyl donors binding from the cytoplasmic interface. This catalytic topology matches what would be expected for modification of proteins transiting the secretion pathway through the ER lumen. The channel in the protein/peptide MBOATs structures explains how substrates on opposites sides of the membrane interact to effect substrate acylation, a long-outstanding question in the MBOAT community. Rather than entry from the lumen, acyl acceptors for the small molecule/lipid modifying family members enter through a "lateral gate" into the central channel/core that presumably allows these hydrophobic substrates to transit from the membrane bilayer into the enzyme active site for acylation. Several of the small molecule/lipid modifying MBOATs also contain secondary binding sites for cholesterol and lipids, although the functional importance of these sites remains to be conclusively demonstrated. Perhaps the most surprising finding amongst the MBOAT structures is the heme binding site within HHAT that impacts enzyme stability. It is hypothesized the heme binding is essential to stabilize enzyme structure, rather than participating directly in the enzyme catalysis of substrate acylation.

Moving forward with this newfound bounty of MBOAT structural data, our studies should focus on a comprehensive mechanistic understanding of acyl transfer by MBOATs and development of potent and specific MBOAT inhibitors. For example, on the mechanistic front it remains unresolved whether these enzymes use a one-step direct transfer mechanism with the acyl chain moving directly to acyl acceptor or a two-step transfer mechanism involving an acyl-enzyme intermediate. Given the structural and topological distinctions between the protein- and small molecule/lipid-modifying MBOAT family members, it will be interesting to determine whether these distinct enzyme subclasses also exhibit mechanistic differences. Combination of current and future structural information with mechanistic insights will guide the creation of the next-generation of MBOAT inhibitors, which are needed to explore and exploit the therapeutic potential of these enzymes for treating a range of human diseases.

Author contributions

MP and JH wrote the manuscript.

Funding

This work was supported by the National Institutes of Health (grant GM134102 to JH) and Syracuse University.

Acknowledgments

The authors gratefully acknowledge countless discussions with colleagues within the protein lipidation community regarding MBOAT acylation. In particular, we also wish to thank those many groups cited in this review whose years-long efforts have led to our current renaissance in MBOAT structural biology.

Conflict of interest

The authors declare that the research was conducted in the absence of any commercial or financial relationships that could be construed as a potential conflict of interest.

Publisher's note

References

Abizaid, A., and Hougland, J. L. (2020). Ghrelin signaling: Goat and ghs-r1a take A leap in complexity. *Trends Endocrinol. Metab.* 31, 107–117.

Agosti, E., De Feudis, M., Angelino, E., Belli, R., Alves Teixeira, M., Zaggia, I., et al. (2020). Both ghrelin deletion and unacylated ghrelin overexpression preserve muscles in aging mice. *Aging (Albany Ny)* 12, 13939–13957.

Anderson, K. E., Kielkowska, A., Durrant, T. N., Juvin, V., Clark, J., Stephens, L. R., et al. (2013). Lysophosphatidylinositol-Acyltransferase-1 (Lpiat1) is required to maintain physiological levels of ptdins and ptdinsp(2) in the mouse. *Plos One* 8, E58425. doi:10.1371/journal.pone.0058425

Anderson, R. A., Joyce, C., Davis, M., Reagan, J. W., Clark, M., Shelness, G. S., et al. (1998). Identification of A form of acyl-coa:cholesterol acyltransferase specific to liver and intestine in nonhuman primates. *J. Biol. Chem.* 273, 26747–26754. doi:10.1074/jbc.273.41.26747

Barrott, J. J., Cash, G. M., Smith, A. P., Barrow, J. R., and Murtaugh, L. C. (2011). Deletion of mouse porcn blocks Wnt ligand secretion and reveals an ectodermal etiology of human focal dermal hypoplasia/goltz syndrome. *Proc. Natl. Acad. Sci. U. S. A.* 108, 12752–12757. doi:10.1073/pnas.1006437108

Batten, M. L., Imanishi, Y., Maeda, T., Tu, D. C., Moise, A. R., Bronson, D., et al. (2004). Lecithin-retinol acyltransferase is essential for accumulation of all-trans-retinyl esters in the eye and in the liver. *J. Biol. Chem.* 279, 10422–10432. doi:10.1074/jbc.M312410200

Bhattacharyya, R., and Kovacs, D. M. (2010). Acat inhibition and amyloid beta reduction. *Biochim. Biophys. Acta* 1801, 960–965. doi:10.1016/j.bbalip.2010.04.003

Bianzano, S., Henrich, A., Herich, L., Kalsch, B., Sarubbi, D., Seitz, F., et al. (2023). Efficacy and safety of the ghrelin-O-acyltransferase inhibitor Bi 1356225 in overweight/obesity: Data from two Phase I, randomised, placebo-controlled studies. *Metabolism* 143, 155550. doi:10.1016/j.metabol.2023.155550

Binder, J. L., Berendzen, J., Stevens, A. O., He, Y., Wang, J., Dokholyan, N. V., et al. (2022). Alphafold illuminates half of the dark human proteins. *Curr. Opin. Struct. Biol.* 74, 102372. doi:10.1016/j.sbi.2022.102372

Birch, A. M., Buckett, L. K., and Turnbull, A. V. (2010). Dgat1 inhibitors as anti-obesity and anti-diabetic agents. *Curr. Opin. Drug Discov. Devel* 13, 489–496.

Briscoe, J., and Thérond, P. P. (2013). The mechanisms of hedgehog signalling and its roles in development and disease. *Nat. Rev. Mol. Cell Biol.* 14, 416–429. doi:10.1038/nrm3598

Bryleva, E. Y., Rogers, M. A., Chang, C. C., Buen, F., Harris, B. T., Rousselet, E., et al. (2010). Acat1 gene ablation increases 24(S)-Hydroxycholesterol content in the brain and ameliorates amyloid pathology in mice with ad. *Proc. Natl. Acad. Sci. U. S. A.* 107, 3081–3086. doi:10.1073/pnas.0913828107

Buglino, J. A., and Resh, M. D. (). Hhat is A palmitoylacyltransferase with specificity for N-palmitoylation of sonic hedgehog. *J. Of Biol. Chem.* 283, 22076–22088. doi:10.1074/jbc.M803901200

Buhman, K. K., Accad, M., Novak, S., Choi, R. S., Wong, J. S., Hamilton, R. L., et al. (2000). Resistance to diet-induced hypercholesterolemia and gallstone formation in acat2-deficient mice. *Nat. Med.* 6, 1341–1347. doi:10.1038/82153

Buhman, K. K., Smith, S. J., Stone, S. J., Repa, J. J., Wong, J. S., Knapp, F. F., Jr., et al. (2002). Dgat1 is not essential for intestinal triacylglycerol absorption or chylomicron synthesis. *J. Of Biol. Chem.* 277, 25474–25479. doi:10.1074/jbc.M202013200

Caddeo, A., Hedfalk, K., Romeo, S., and Pingitore, P. (2021). Lpiat1/Mboat7 contains A catalytic dyad transferring polyunsaturated fatty acids to lysophosphatidylinositol. *Biochimica Biophysica Acta (Bba) - Mol. And Cell Biol. Of Lipids* 1866, 158891. doi:10.1016/j.bbalip.2021.158891

Caddeo, A., Jamialahmadi, O., Solinas, G., Pujia, A., Mancina, R. M., Pingitore, P., et al. (2019). Mboat7 is anchored to endomembranes by six transmembrane domains. *J. Of Struct. Biol.* 206, 349–360. doi:10.1016/j.jsb.2019.04.006

Campaña, M. B., Irudayanathan, F. J., Davis, T. R., Mcgovern-Gooch, K. R., Loftus, R., Ashkar, M., et al. (2019). The ghrelin O-acyltransferase structure reveals A catalytic channel for transmembrane hormone acylation. *J. Of Biol. Chem.* 294, 14166–14174. doi:10.1074/jbc.AC119.009749

Cao, J., Shan, D., Revett, T., Li, D., Wu, L., Liu, W., et al. (2008). Molecular identification of a novel mammalian brain isoform of acyl-CoA:lysophospholipid acyltransferase with prominent ethanolamine lysophospholipid acylating activity, LPEAT2. *J. Of Biol. Chem.* 283, 19049–19057. doi:10.1074/jbc.M800364200

Cases, S., Novak, S., Zheng, Y.-W., Myers, H. M., Lear, S. R., Sande, E., et al. (1998a). Acat-2, A second mammalian acyl-coa:cholesterol acyltransferase: Its cloning, expression, and characterization. *J. Of Biol. Chem.* 273, 26755–26764. doi:10.1074/jbc.273.41.26755

Cases, S., Smith, S. J., Zheng, Y. W., Myers, H. M., Lear, S. R., Sande, E., et al. (1998b). Identification of A gene encoding an acyl coa:diacylglycerol acyltransferase, A key enzyme in triacylglycerol synthesis. *Proc. Natl. Acad. Sci. U. S. A.* 95, 13018–13023. doi:10.1073/pnas.95.22.13018

Cases, S., Stone, S. J., Zhou, P., Yen, E., Tow, B., Lardizabal, K. D., et al. (2001). Cloning of Dgat2, A second mammalian diacylglycerol acyltransferase, and related family members. *J. Biol. Chem.* 276, 38870–38876. doi:10.1074/jbc.M106219200

Chahal, K. K., Parle, M., and Abagyan, R. (2018). Hedgehog pathway and smoothened inhibitors in cancer therapies. *Anti-Cancer Drugs* 29, 387–401. doi:10.1097/CAD.0000000000000609

Chang, C. C., Huh, H. Y., Cadigan, K. M., and Chang, T. Y. (1993). Molecular cloning and functional expression of human acyl-coenzyme A:cholesterol acyltransferase cdna in mutant Chinese hamster ovary cells. *J. Of Biol. Chem.* 268, 20747–20755. doi:10.1016/s0021-9258(19)36846-2

Chang, C. C., Lee, C. Y., Chang, E. T., Cruz, J. C., Levesque, M. C., and Chang, T. Y. (1998). Recombinant acyl-coa:cholesterol acyltransferase-1 (Acat-1) purified to essential homogeneity utilizes cholesterol in mixed micelles or in vesicles in A highly cooperative manner. *J. Biol. Chem.* 273, 35132–35141. doi:10.1074/jbc.273.52.35132

Chen, B., Dodge, M. E., Tang, W., Lu, J., Ma, Z., Fan, C. W., et al. (2009). Small molecule-mediated disruption of wnt-dependent signaling in tissue regeneration and cancer. *Nat. Chem. Biol.* 5, 100–107. doi:10.1038/nchembio.137

Chen, G., Harwood, J. L., Lemieux, M. J., Stone, S. J., and Weselake, R. J. (2022). Acyl-Coa:Diacylglycerol acyltransferase: Properties, physiological roles, metabolic engineering and intentional control. *Prog. Lipid Res.* 88, 101181. doi:10.1016/j.plipres.2022.101181

Chen, H. C., Smith, S. J., Ladha, Z., Jensen, D. R., Ferreira, L. D., Pulawa, L. K., et al. (2002). Increased insulin and leptin sensitivity in mice lacking acyl coa:diacylglycerol acyltransferase 1. *J. Clin. Invest.* 109, 1049–1055. doi:10.1172/JCI14672

Cheng, D., Meegalla, R. L., He, B., Cromley, D. A., Billheimer, J. T., and Young, P. R. (2001). Human acyl-coa:diacylglycerol acyltransferase is A tetrameric protein. *Biochem. J.* 359, 707–714. doi:10.1042/0264-6021:3590707

Chitraju, C., Mejhert, N., Haas, J. T., Diaz-Ramirez, L. G., Grueter, C. A., Imbriglio, J. E., et al. (2017). Triglyceride synthesis by Dgat1 protects adipocytes from lipid-induced Er stress during lipolysis. *Cell Metab.* 26, 407–418. E3. doi:10.1016/j.cmet.2017.07.012

Coupland, C. E., Andrei, S. A., Ansell, T. B., Carrique, L., Kumar, P., Sefer, L., et al. (2021). Structure, mechanism, and inhibition of hedgehog acyltransferase. *Mol. Cell* 81, 5025–5038.e10. E10. doi:10.1016/j.molcel.2021.11.018

Darling, J. E., Zhao, F., Loftus, R. J., Patton, L. M., Gibbs, R. A., and Hougland, J. L. (2015). Structure–activity analysis of human ghrelin O-acyltransferase reveals chemical determinants of ghrelin selectivity and acyl group recognition. *Biochemistry* 54, 1100–1110. doi:10.1021/bi5010359

Dauwerse, J. G., De Vries, B. B. A., Wouters, C. H., Bakker, E., Rappold, G., Mortier, G. R., et al. (2007). A T(4;6)(Q12;P23) translocation disrupts A membrane-associated O-acetyl transferase gene (Mboat1) in A patient with A novel brachydactyly–syndactyly syndrome. *Eur. J. Of Hum. Genet.* 15, 743–751. doi:10.1038/sj.ejhg.5201833

Dodge, M. E., Moon, J., Tuladhar, R., Lu, J., Jacob, L. S., Zhang, L. S., et al. (2012). Diverse chemical scaffolds support direct inhibition of the membrane-bound O-acyltransferase porcupine. *J. Biol. Chem.* 287, 23246–23254. doi:10.1074/jbc.M112.372029

Egido, E. M., Rodriguez-Gallardo, J., Silvestre, R. A., and Marco, J. (2002). Inhibitory effect of ghrelin on insulin and pancreatic somatostatin secretion. *Eur. J. Endocrinol.* 146, 241–244. doi:10.1530/eje.0.1460241

Farokhnia, M., Abshire, K. M., Hammer, A., Deschaine, S. L., Saravanakumar, A., Cobbina, E., et al. (2021). Neuroendocrine response to exogenous ghrelin administration, combined with alcohol, in heavy-drinking individuals: Findings from A randomized, double-blind, placebo-controlled human laboratory study. *Int. J. Neuropsychopharmacol.* 24, 464–476. doi:10.1093/ijnp/pyab004

Farokhnia, M., Faulkner, M. L., Piacentino, D., Lee, M. R., and Leggio, L. (2019). Ghrelin: From A gut hormone to A potential therapeutic target for alcohol use disorder. *Physiol. Behav.* 204, 49–57. doi:10.1016/j.physbeh.2019.02.008

Farokhnia, M., Portelli, J., Lee, M. R., Mcdiarmid, G. R., Munjal, V., Abshire, K. M., et al. (2020). Effects of exogenous ghrelin administration and ghrelin receptor blockade, in combination with alcohol, on peripheral inflammatory markers in heavy-drinking individuals: Results from two human laboratory studies. *Brain Res.* 1740, 146851. doi:10.1016/j.brainres.2020.146851

Ferrara, P. J., Rong, X., Maschek, J. A., Verkerke, A. R., Siripoksup, P., Song, H., et al. (2021). Lysophospholipid acylation modulates plasma membrane lipid organization and insulin sensitivity in skeletal muscle. *J. Clin. Invest.* 131, e135963. doi:10.1172/JCI135963

Gagnon, J., Baggio, L. L., Drucker, D. J., and Brubaker, P. L. (2015). Ghrelin is A novel regulator of glp-1 secretion. *Diabetes* 64, 1513–1521. doi:10.2337/db14-1176

Galli, L. M., Anderson, M. O., Gabriel Fraley, J., Sanchez, L., Bueno, R., Hernandez, D. N., et al. (2021). Determination of the membrane topology of porcn, an O-acyl transferase that modifies Wnt signalling proteins. *Open Biol.* 11, 200400. doi:10.1098/rsob.200400

Galli, L. M., Zebarjadi, N., Li, L., Lingappa, V. R., and Burrus, L. W. (2016). Divergent effects of porcupine and wntless on Wnt1 trafficking, secretion, and signaling. *Exp. Cell Res.* 347, 171–183. doi:10.1016/j.yexcr.2016.07.028

Goldstein, J. L., and Brown, M. S. (2009). The ldl receptor. *Arterioscler Thromb Vasc Biol.* 29, 431–438. doi:10.1161/ATVBAHA.108.179564

Goldstein, J. L., Zhao, T. J., Li, R. L., Sherbet, D. P., Liang, G., and Brown, M. S. (2011). Surviving starvation: Essential role of the ghrelin-growth hormone Axis. *Cold Spring Harb. Symp. Quant. Biol.* 76, 121–127. doi:10.1101/sqb.2011.76.010447

Goodman, D. S., Deykin, D., and Shiratori, T. (1964). The Formation of cholesterol esters with rat liver enzymes. *J. Biol. Chem.* 239, 1335–1345. doi:10.1016/s0021-9258(18)91319-0

Guan, C., Niu, Y., Chen, S.-C., Kang, Y., Wu, J.-X., Nishi, K., et al. (2020). Structural insights into the inhibition mechanism of human sterol O-acyltransferase 1 By A competitive inhibitor. *Nat. Commun.* 11, 2478. doi:10.1038/s41467-020-16288-4

Guo, Z.-Y., Chang, C. C. Y., and Chang, T.-Y. (2007). Functionality of the seventh and eighth transmembrane domains of acyl-coenzyme A:cholesterol acyltransferase 1. *Biochemistry* 46, 10063–10071. doi:10.1021/bi7011367

Heppner, K. M., Müller, T. D., Tong, J., and Tschöp, M. H. (2012). "Chapter fifteen - ghrelin in the control of energy, lipid, and glucose metabolism," in *Methods in enzymology*. Editors M. Kojima and K. Kangawa (Academic Press).

Hishikawa, D., Shindou, H., Kobayashi, S., Nakanishi, H., Taguchi, R., and Shimizu, T. (2008). Discovery of A lysophospholipid acyltransferase family essential for membrane asymmetry and diversity. *Proc. Of Natl. Acad. Of Sci.* 105, 2830–2835. doi:10.1073/pnas.0712245105

Hofmann, K. (2000). A superfamily of membrane-bound O-acyltransferases with implications for Wnt signaling. *Trends Biochem. Sci.* 25, 111–112. doi:10.1016/s0968-0004(99)01539-x

Hutter-Paier, B., Huttunen, H. J., Puglielli, L., Eckman, C. B., Kim, D. Y., Hofmeister, A., et al. (2004). The acat inhibitor cp-113,818 markedly reduces amyloid pathology in A mouse model of alzheimer's disease. *Neuron* 44, 227–238. doi:10.1016/j.neuron.2004.08.043

Iyer, M. R., Wood, C. M., and Kunos, G. (2020). Recent progress in the discovery of ghrelin O-acyltransferase (goat) inhibitors. *Rsc Med. Chem.* 11, 1136–1144. doi:10.1039/d0md00210k

Jain, S., Zhang, X., Khandelwal, P. J., Saunders, A. J., Cummings, B. S., and Oelkers, P. (2009). Characterization of human lysophospholipid acyltransferase 3. *J. Of Lipid Res.* 50, 1563–1570. doi:10.1194/jlr.M800398-JLR200

Janda, C. Y., Waghray, D., Levin, A. M., Thomas, C., and Garcia, K. C. (2012). Structural basis of Wnt recognition by frizzled. *Science* 337, 59–64. doi:10.1126/science.1222879

Jiang, Y., Benz, T. L., and Long, S. B. (2021). Substrate and product complexes reveal mechanisms of hedgehog acylation by hhat. *Science* 372, 1215–1219. doi:10.1126/science.abg4998

Johansen, A., Rosti, R. O., Musaev, D., Sticca, E., Harripaul, R., Zaki, M., et al. (2016). Mutations in Mboat7, encoding lysophosphatidylinositol acyltransferase I, lead to intellectual disability accompanied by epilepsy and autistic features. *Am. J. Hum. Genet.* 99, 912–916. doi:10.1016/j.ajhg.2016.07.019

Joyce, C. W., Shelness, G. S., Davis, M. A., Lee, R. G., Skinner, K., Anderson, R. A., et al. (2000). Acat1 and Acat2 membrane topology segregates A serine residue essential for activity to opposite sides of the endoplasmic reticulum membrane. *Mol. Biol. Of Cell* 11, 3675–3687. doi:10.1091/mbc.11.11.3675

Jumper, J., Evans, R., Pritzel, A., Green, T., Figurnov, M., Ronneberger, O., et al. (2021). Highly accurate protein structure prediction with alphafold. *Nature* 596, 583–589. doi:10.1038/s41586-021-03819-2

Kennedy, E. P., and Weiss, S. B. (1956). The function of cytidine coenzymes in the biosynthesis of phospholipides. *J. Biol. Chem.* 222, 193–214. doi:10.1016/s0021-9258(19)50785-2

Kojima, M., Hosoda, H., Date, Y., Nakazato, M., Matsuo, H., and Kangawa, K. (1999). Ghrelin is A growth-hormone-releasing acylated peptide from stomach. *Nature* 402, 656–660. doi:10.1038/45230

Kong, J. H., Siebold, C., and Rohatgi, R. (2019). *Biochemical mechanisms of vertebrate hedgehog signaling*. Development, 146.dev166892. doi:10.1242/dev.166892

Konitsiotis, A. D., Chang, S. C., Jovanović, B., Ciepla, P., Masumoto, N., Palmer, C. P., et al. (2014). Attenuation of hedgehog acyltransferase-catalyzed sonic hedgehog palmitoylation causes reduced signaling, proliferation and invasiveness of human carcinoma cells. *Plos One* 9, E89899. doi:10.1371/journal.pone.0089899

Konitsiotis, A. D., Jovanović, B., Ciepla, P., Spitaler, M., Lanyon-Hogg, T., Tate, E. W., et al. (2015). Topological analysis of hedgehog acyltransferase, A multipalmitoylated transmembrane protein. *J. Biol. Chem.* 290, 3293–3307. doi:10.1074/jbc.M114.614578

Kurabe, N., Hayasaka, T., Ogawa, M., Masaki, N., Ide, Y., Waki, M., et al. (2013). Accumulated phosphatidylcholine (16:0/16:1) in human colorectal cancer; possible involvement of Lpcat4. *Cancer Sci.* 104, 1295–1302. doi:10.1111/cas.12221

Labonté, E. D., Kirby, R. J., Schildmeyer, N. M., Cannon, A. M., Huggins, K. W., and Hui, D. Y. (2006). Group 1b phospholipase A2-mediated lysophospholipid absorption directly contributes to postprandial hyperglycemia. *Diabetes* 55, 935–941. doi:10.2337/diabetes.55.04.06.db05-1286

Lands, W. E. (1958). Metabolism of glycerolipides; A comparison of lecithin and triglyceride synthesis. *J. Biol. Chem.* 231, 883–888. doi:10.1016/s0021-9258(18)70453-5

Lands, W. E. (2000). Stories about acyl chains. *Biochim. Biophys. Acta* 1483, 1–14. doi:10.1016/s1388-1981(99)00177-8

Lanyon-Hogg, T., Masumoto, N., Bodakh, G., Konitsiotis, A. D., Thinon, E., Rodgers, U. R., et al. (2015a). Click chemistry armed enzyme-linked immunosorbent assay to measure palmitoylation by hedgehog acyltransferase. *Anal. Biochem.* 490, 66–72. doi:10.1016/j.ab.2015.08.025

Lanyon-Hogg, T., Masumoto, N., Bodakh, G., Konitsiotis, A. D., Thinon, E., Rodgers, U. R., et al. (2016). Synthesis and characterisation of 5-acyl-6,7-dihydrothieno[3,2-C] pyridine inhibitors of hedgehog acyltransferase. *Data Brief* 7, 257–281. doi:10.1016/j.dib.2016.02.012

Lanyon-Hogg, T., Ritzefeld, M., Masumoto, N., Magee, A. I., Rzepa, H. S., and Tate, E. W. (2015b). Modulation of amide bond rotamers in 5-acyl-6,7-dihydrothieno[3,2-C] pyridines. *J. Of Org. Chem.* 80, 4370–4377. doi:10.1021/acs.joc.5b00205

Lanyon-Hogg, T., Ritzefeld, M., Sefer, L., Bickel, J. K., Rudolf, A. F., Panyain, N., et al. (2019). Acylation-coupled lipophilic induction of polarisation (Acyl-Clip): A universal assay for lipid transferase and hydrolase enzymes. *Chem. Sci.* 10, 8995–9000. doi:10.1039/c9sc01785b

Lanyon-Hogg, T., Ritzefeld, M., Zhang, L., Andrei, S. A., Pogranyi, B., Mondal, M., et al. (2021). Photochemical probe identification of A small-molecule inhibitor binding site in hedgehog acyltransferase (hhat). *Angew. Chem. Int. Ed. Engl.* 60, 13542–13547. doi:10.1002/anie.202014457

Lardizabal, K. D., Mai, J. T., Wagner, N. W., Wyrick, A., Voelker, T., and Hawkins, D. J. (2001). Dgat2 is A new diacylglycerol acyltransferase gene family: Purification, cloning, and expression in insect cells of two polypeptides from mortierella ramanniana with diacylglycerol acyltransferase activity. *J. Biol. Chem.* 276, 38862–38869. doi:10.1074/jbc.M106168200

Lee, B., Fast, A. M., Zhu, J., Cheng, J. X., and Buhman, K. K. (2010). Intestine-specific expression of acyl coa:diacylglycerol acyltransferase 1 reverses resistance to diet-induced hepatic steatosis and obesity in Dgat1-/- mice. *J. Lipid Res.* 51, 1770–1780. doi:10.1194/jlr.M002311

Lee, C. J., Rana, M. S., Bae, C., Li, Y., and Banerjee, A. (2019). *In vitro* reconstitution of Wnt acylation reveals structural determinants of substrate recognition by the acyltransferase human porcupine. *J. Biol. Chem.* 294, 231–245. doi:10.1074/jbc.RA118.005746

Lee, H. C., Inoue, T., Sasaki, J., Kubo, T., Matsuda, S., Nakasaki, Y., et al. (2012). Lpiat1 regulates arachidonic acid content in phosphatidylinositol and is required for cortical lamination in mice. *Mol. Biol. Cell* 23, 4689–4700. doi:10.1091/mbc.E12-09-0673

Li, R. L., Sherbet, D. P., Elsbernd, B. L., Goldstein, J. L., Brown, M. S., and Zhao, T. J. (2012). Profound hypoglycemia in starved, ghrelin-deficient mice is caused by decreased gluconeogenesis and reversed by lactate or fatty acids. *J. Biol. Chem.* 287, 17942–17950. doi:10.1074/jbc.M112.358051

Li, Z., Zhuang, H., Chen, X., Zhang, Y., Ma, Z., Wang, S., et al. (2022). Identification of Mboat2 as an unfavorable biomarker correlated with kras activation and reduced Cd8(+) T-cell infiltration in pancreatic cancer. *J. Oncol.* 2022, 4269733. doi:10.1155/2022/4269733

Liu, J., Pan, S., Hsieh, M. H., Ng, N., Sun, F., Wang, T., et al. (2013). Targeting wnt-driven cancer through the inhibition of porcupine by Lgk974. *Proc. Natl. Acad. Sci. U. S. A.* 110, 20224–20229. doi:10.1073/pnas.1314239110

Liu, N., Sun, Q., Xu, H., Yu, X., Chen, W., Wei, H., et al. (2020). Hyperuricemia induces lipid disturbances mediated by Lpcat3 upregulation in the liver. *Faseb J.* 34, 13474–13493. doi:10.1096/fj.202000950R

Liu, Y., Qi, X., Donnelly, L., Elghobashi-Meinhardt, N., Long, T., Zhou, R. W., et al. (2022). Mechanisms and inhibition of porcupine-mediated Wnt acylation. *Nature* 607, 816–822. doi:10.1038/s41586-022-04952-2

Long, T., Debler, E. W., and Li, X. (2022). Structural enzymology of cholesterol biosynthesis and storage. *Curr. Opin. Struct. Biol.* 74, 102369. doi:10.1016/j.sbi.2022.102369

Long, T., Liu, Y., and Li, X. (2021). Molecular structures of human Acat2 disclose mechanism for selective inhibition. *Structure* 29, 1410–1418.E4. doi:10.1016/j.str.2021.07.009

Long, T., Sun, Y., Hassan, A., Qi, X., and Li, X. (2020). Structure of nevanimibe-bound tetrameric human Acat1. *Nature* 581, 339–343. doi:10.1038/s41586-020-2295-8

Ma, D., Wang, Z., Merrikh, C. N., Lang, K. S., Lu, P., Li, X., et al. (2018). Crystal structure of A membrane-bound O-acyltransferase. *Nature* 562, 286–290. doi:10.1038/s41586-018-0568-2

Marks, D. S., Hopf, T. A., and Sander, C. (2012). Protein structure prediction from sequence variation. *Nat. Biotechnol.* 30, 1072–1080. doi:10.1038/nbt.2419

Matevossian, A., and Resh, M. D. (2015). Membrane topology of hedgehog acyltransferase. *J. Biol. Chem.* 290, 2235–2243. doi:10.1074/jbc.M114.625764

Moose, J. E., Leets, K. A., Mate, N. A., Chisholm, J. D., and Hougland, J. L. (2020). An overview of ghrelin O-acyltransferase inhibitors: A literature and patent review for 2010-2019. *Expert Opin. Ther. Pat.* 30, 581–593. doi:10.1080/13543776.2020.1776263

Mukherjee, S., and Alfin-Slater, R. B. (1958). The effect of the nature of dietary fat on synthesis of cholesterol from acetate-1-C14 in rat liver slices. *Archives Of Biochem. And Biophysics* 73, 359–365. doi:10.1016/0003-9861(58)90281-9

Müller, T. D., Nogueiras, R., Andermann, M. L., Andrews, Z. B., Anker, S. D., Argente, J., et al. (2015). *Ghrelin. Mol. Metab.* 4, 437–460. doi:10.1016/j.molmet.2015.03.005

Nass, R., Pezzoli, S. S., Oliveri, M. C., Patrie, J. T., Harrell, F. E., Jr., Clasey, J. L., et al. (2008). Effects of an oral ghrelin mimetic on body composition and clinical outcomes in healthy older adults: A randomized trial. *Ann. Intern Med.* 149, 601–611. doi:10.7326/0003-4819-149-9-200811040-00003

Nüsslein-Volhard, C., and Wieschaus, E. (1980). Mutations affecting segment number and polarity in Drosophila. *Nature* 287, 795–801. doi:10.1038/287795a0

Oelkers, P., Behari, A., Cromley, D., Billheimer, J. T., and Sturley, S. L. (1998). Characterization of two human genes encoding acyl coenzyme A:cholesterol acyltransferase-related enzymes. *J. Biol. Chem.* 273, 26765–26771. doi:10.1074/jbc.273.41.26765

Ohshiro, T., Ohtawa, M., Nagamitsu, T., Matsuda, D., Yagyu, H., Davis, M. A., et al. (2015). New pyripyropene A derivatives, highly soat2-selective inhibitors, improve hypercholesterolemia and atherosclerosis in atherogenic mouse models. *J. Pharmacol. Exp. Ther.* 355, 299–307. doi:10.1124/jpet.115.227348

Ovchinnikov, S., Park, H., Varghese, N., Huang, P.-S., Pavlopoulos, G. A., Kim, D. E., et al. (2017). Protein structure determination using metagenome sequence data. *Science* 355, 294–298. doi:10.1126/science.aah4043

Pearson, J. T., Shirai, M., Sukumaran, V., Du, C. K., Tsuchimochi, H., Sonobe, T., et al. (2019). Ghrelin and vascular protection. *Vasc. Biol.* 1, H97-H102–H102. doi:10.1530/VB-19-0024

Pepinsky, R. B., Zeng, C., Wen, D., Rayhorn, P., Baker, D. P., Williams, K. P., et al. (1998). Identification of A palmitic acid-modified form of human sonic hedgehog. *J. Biol. Chem.* 273, 14037–14045. doi:10.1074/jbc.273.22.14037

Petrova, E., Matevossian, A., and Resh, M. D. (2015). Hedgehog acyltransferase as A target in pancreatic ductal adenocarcinoma. *Oncogene* 34, 263–268. doi:10.1038/onc.2013.575

Petrova, E., Rios-Esteves, J., Ouerfelli, O., Glickman, J. F., and Resh, M. D. (2013). Inhibitors of hedgehog acyltransferase block sonic hedgehog signaling. *Nat. Chem. Biol.* 9, 247–249. doi:10.1038/nchembio.1184

Proffitt, K. D., Madan, B., Ke, Z., Pendharkar, V., Ding, L., Lee, M. A., et al. (2013). Pharmacological inhibition of the Wnt acyltransferase porcn prevents growth of wnt-driven mammary cancer. *Cancer Res.* 73, 502–507. doi:10.1158/0008-5472.CAN-12-2258

Qian, H., Zhao, X., Yan, R., Yao, X., Gao, S., Sun, X., et al. (2020). Structural basis for catalysis and substrate specificity of human Acat1. *Nature* 581, 333–338. doi:10.1038/s41586-020-2290-0

Reimer, M. K., Pacini, G., and Ahrén, B. (2003). Dose-dependent inhibition by ghrelin of insulin secretion in the mouse. *Endocrinology* 144, 916–921. doi:10.1210/en.2002-220819

Rios-Esteves, J., Haugen, B., and Resh, M. D. (2014). Identification of key residues and regions important for porcupine-mediated Wnt acylation. *J. Biol. Chem.* 289, 17009–17019. doi:10.1074/jbc.M114.561209

Rodgers, U. R., Lanyon-Hogg, T., Masumoto, N., Ritzefeld, M., Burke, R., Blagg, J., et al. (2016). Characterization of hedgehog acyltransferase inhibitors identifies A small molecule probe for hedgehog signaling by cancer cells. *Acs Chem. Biol.* 11, 3256–3262. doi:10.1021/acschembio.6b00896

Roessler, E., Belloni, E., Gaudenz, K., Vargas, F., Scherer, S. W., Tsui, L.-C., et al. (1997). Mutations in the C-terminal domain of sonic hedgehog cause holoprosencephaly. *Hum. Mol. Genet.* 6, 1847–1853. doi:10.1093/hmg/6.11.1847

Rong, X., Wang, B., Dunham, M. M., Hedde, P. N., Wong, J. S., Gratton, E., et al. (2015). Lpcat3-Dependent production of arachidonoyl phospholipids is A key determinant of triglyceride secretion. *Elife* 4, E06557. doi:10.7554/eLife.06557

Ross, A. C. (1982). Retinol esterification by rat liver microsomes. Evidence for A fatty acyl coenzyme A: Retinol acyltransferase. *J. Biol. Chem.* 257, 2453–2459. doi:10.1016/s0021-9258(18)34945-7

Rudel, L. L., Lee, R. G., and Parini, P. (2005). Acat2 is A target for treatment of coronary heart disease associated with hypercholesterolemia. *Arteriosclerosis, Thrombosis, And Vasc. Biol.* 25, 1112–1118. doi:10.1161/01.ATV.0000166548.65753.1e

Shah, K., Panchal, S., and Patel, B. (2021). Porcupine inhibitors: Novel and emerging anti-cancer therapeutics targeting the Wnt signaling pathway. *Pharmacol. Res.* 167, 105532. doi:10.1016/j.phrs.2021.105532

Shao, G., Qian, Y., Lu, L., Liu, Y., Wu, T., Ji, G., et al. (2022). Research progress in the role and mechanism of Lpcat3 in metabolic related diseases and cancer. *J. Cancer* 13, 2430–2439. doi:10.7150/jca.71619

Smith, S. J., Cases, S., Jensen, D. R., Chen, H. C., Sande, E., Tow, B., et al. (2000). Obesity resistance and multiple mechanisms of triglyceride synthesis in mice lacking dgat. *Nat. Genet.* 25, 87–90. doi:10.1038/75651

Steinhauer, J., Gijón, M. A., Riekhof, W. R., Voelker, D. R., Murphy, R. C., and Treisman, J. E. (2009). Drosophila lysophospholipid acyltransferases are specifically required for germ cell development. *Mol. Biol. Cell* 20, 5224–5235. doi:10.1091/mbc.e09-05-0382

Stone, S. J., Myers, H. M., Watkins, S. M., Brown, B. E., Feingold, K. R., Elias, P. M., et al. (2004). Lipopenia and skin barrier abnormalities in dgat2-deficient mice. *J. Biol. Chem.* 279, 11767–11776. doi:10.1074/jbc.M311000200

Sui, X., Wang, K., Gluchowski, N. L., Elliott, S. D., Liao, M., Walther, T. C., et al. (2020). Structure and catalytic mechanism of A human triacylglycerol-synthesis enzyme. *Nature* 581, 323–328. doi:10.1038/s41586-020-2289-6

Tabe, S., Hikiji, H., Ariyoshi, W., Hashidate-Yoshida, T., Shindou, H., Okinaga, T., et al. (2016). Lysophosphatidylethanolamine acyltransferase 1/membrane-bound O-acyltransferase 1 regulates morphology and function of P19c6 cell-derived neurons. *Faseb J.* 30, 2591–2601. doi:10.1096/fj.201500097R

Tabe, S., Hikiji, H., Ariyoshi, W., Hashidate-Yoshida, T., Shindou, H., Shimizu, T., et al. (2017). Lysophosphatidylcholine acyltransferase 4 is involved in chondrogenic differentiation of Atdc5 cells. *Sci. Rep.* 7, 16701. doi:10.1038/s41598-017-16902-4

Takada, R., Satomi, Y., Kurata, T., Ueno, N., Norioka, S., Kondoh, H., et al. (2006). Monounsaturated fatty acid modification of Wnt protein: Its role in Wnt secretion. *Dev. Cell* 11, 791–801. doi:10.1016/j.devcel.2006.10.003

Tanaka, Y., Shimanaka, Y., Caddeo, A., Kubo, T., Mao, Y., Kubota, T., et al. (2021). Lpiat1/Mboat7 depletion increases triglyceride synthesis fueled by high phosphatidylinositol turnover. *Gut* 70, 180–193. doi:10.1136/gutjnl-2020-320646

Taylor, M. S., Ruch, T. R., Hsiao, P.-Y., Hwang, Y., Zhang, P., Dai, L., et al. (2013). Architectural organization of the metabolic regulatory enzyme ghrelin O-acyltransferase. *J. Of Biol. Chem.* 288, 32211–32228. doi:10.1074/jbc.M113.510313

Tokudome, T., and Kangawa, K. (2019). Physiological significance of ghrelin in the cardiovascular system. *Proc. Jpn. Acad. Ser. B Phys. Biol. Sci.* 95, 459–467. doi:10.2183/pjab.95.032

Tong, J., Prigeon, R. L., Davis, H. W., Bidlingmaier, M., Kahn, S. E., Cummings, D. E., et al. (2010). Ghrelin suppresses glucose-stimulated insulin secretion and deteriorates glucose tolerance in healthy humans. *Diabetes* 59, 2145–2151. doi:10.2337/db10-0504

Varadharajan, V., Massey, W. J., and Brown, J. M. (2022). Membrane-bound O-acyltransferase 7 (Mboat7)-Driven phosphatidylinositol remodeling in advanced liver disease. *J. Lipid Res.* 63, 100234. doi:10.1016/j.jlr.2022.100234

Wan, Y. Y., Guo, L., Yao, Y., Shi, X. Y., Jiang, H., Xu, B., et al. (2022). Mboat1 homozygous missense variant causes nonobstructive azoospermia. *Asian J. Androl.* 24, 186–190. doi:10.4103/aja202160

Wang, B., Rong, X., Palladino, E. N. D., Wang, J., Fogelman, A. M., Martín, M. G., et al. (2018). Phospholipid remodeling and cholesterol availability regulate intestinal stemness and tumorigenesis. *Cell Stem Cell* 22, 206–220. E4. doi:10.1016/j.stem.2017.12.017

Wang, B., and Tontonoz, P. (2019). Phospholipid remodeling in Physiology and disease. *Annu. Rev. Physiol.* 81, 165–188. doi:10.1146/annurev-physiol-020518-114444

Wang, L., Qian, H., Nian, Y., Han, Y., Ren, Z., Zhang, H., et al. (2020). Structure and mechanism of human diacylglycerol O-acyltransferase 1. *Nature* 581, 329–332. doi:10.1038/s41586-020-2280-2

Wang, X., Reid Sutton, V., Omar Peraza-Llanes, J., Yu, Z., Rosetta, R., Kou, Y. C., et al. (2007). Mutations in X-linked porcn, A putative regulator of Wnt signaling, cause focal dermal hypoplasia. *Nat. Genet.* 39, 836–838. doi:10.1038/ng2057

Weiss, S. B., Kennedy, E. P., and Kiyasu, J. Y. (1960). The enzymatic synthesis of triglycerides. *J. Biol. Chem.* 235, 40–44. doi:10.1016/s0021-9258(18)69581-x

Weiss, S. B., and Kennedy, E. P. (1956). The enzymatic synthesis of triglycerides. *J. Of Am. Chem. Soc.* 78, 3550. doi:10.1021/ja01595a088

Weselake, R. J., Madhavji, M., Szarka, S. J., Patterson, N. A., Wiehler, W. B., Nykiforuk, C. L., et al. (2006). Acyl-coa-binding and self-associating properties of A recombinant 13.3 kda N-terminal fragment of diacylglycerol acyltransferase-1 from oilseed rape. *Bmc Biochem.* 7, 24. doi:10.1186/1471-2091-7-24

Willner, E. L., Tow, B., Buhman, K. K., Wilson, M., Sanan, D. A., Rudel, L. L., et al. (2003). Deficiency of acyl coa:cholesterol acyltransferase 2 prevents atherosclerosis in apolipoprotein E-deficient mice. *Proc. Of Natl. Acad. Of Sci.* 100, 1262–1267. doi:10.1073/pnas.0336398100

Wu, C. S., Wei, Q., Wang, H., Kim, D. M., Balderas, M., Wu, G., et al. (2020). Protective effects of ghrelin on fasting-induced muscle atrophy in aging mice. *J. Gerontol. A Biol. Sci. Med. Sci.* 75, 621–630. doi:10.1093/gerona/gly256

Wu, F., Zhang, Y., Sun, B., Mcmahon, A. P., and Wang, Y. (2017). Hedgehog signaling: From basic biology to cancer therapy. *Cell Chem. Biol.* 24, 252–280. doi:10.1016/j.chembiol.2017.02.010

Xie, L. Y., Huang, H. Y., Fang, T., Liang, J. Y., Hao, Y. L., Zhang, X. J., et al. (2022). A prognostic survival model of pancreatic adenocarcinoma based on metabolism-related gene expression. *Front. Genet.* 13, 804190. doi:10.3389/fgene.2022.804190

Yada, T., Damdindorj, B., Rita, R. S., Kurashina, T., Ando, A., Taguchi, M., et al. (2014). Ghrelin signalling in B-cells regulates insulin secretion and blood glucose. *Diabetes Obes. Metab.* 16 (1), 111–117. doi:10.1111/dom.12344

Yang, H., Bard, M., Bruner, D. A., Gleeson, A., Deckelbaum, R. J., Aljinovic, G., et al. (1996). Sterol esterification in yeast: A two-gene process. *Science* 272, 1353–1356. doi:10.1126/science.272.5266.1353

Yang, W., Bai, Y., Xiong, Y., Zhang, J., Chen, S., Zheng, X., et al. (2016). Potentiating the antitumour response of Cd8(+) T cells by modulating cholesterol metabolism. *Nature* 531, 651–655. doi:10.1038/nature17412

Yen, C. L., Monetti, M., Burri, B. J., and Farese, R. V., Jr. (2005). The triacylglycerol synthesis enzyme Dgat1 also catalyzes the synthesis of diacylglycerols, waxes, and retinyl esters. *J. Lipid Res.* 46, 1502–1511. doi:10.1194/jlr.M500036-JLR200

Yen, C. L., Stone, S. J., Koliwad, S., Harris, C., and Farese, R. V., Jr. (2008). Thematic review series: Glycerolipids. Dgat enzymes and triacylglycerol biosynthesis. *J. Lipid Res.* 49, 2283–2301. doi:10.1194/jlr.R800018-JLR200

Yu, C., Chen, J., Lin, S., Liu, J., Chang, C. C., and Chang, T. Y. (1999). Human acyl-coa:cholesterol acyltransferase-1 is A homotetrameric enzyme in intact cells and *in vitro*. *J. Biol. Chem.* 274, 36139–36145. doi:10.1074/jbc.274.51.36139

Yu, C., Kennedy, N. J., Chang, C. C., and Rothblatt, J. A. (1996). Molecular cloning and characterization of two isoforms of Saccharomyces cerevisiae acyl-coa:sterol acyltransferase. *J. Biol. Chem.* 271, 24157–24163. doi:10.1074/jbc.271.39.24157

Yu, J., Liao, P.-J., Xu, W., Jones, J. R., Everman, D. B., Flanagan-Steet, H., et al. (2021). Structural model of human porcn illuminates disease-associated variants and drug-binding sites. *J. Of Cell Sci.* 134, jcs259383. doi:10.1242/jcs.259383

Zallar, L. J., Farokhnia, M., Tunstall, B. J., Vendruscolo, L. F., and Leggio, L. (2017). The role of the ghrelin system in drug addiction. *Int. Rev. Neurobiol.* 136, 89–119. doi:10.1016/bs.irn.2017.08.002

Zhai, L., Chaturvedi, D., and Cumberledge, S. (2004). Drosophila wnt-1 undergoes A hydrophobic modification and is targeted to lipid rafts, A process that requires porcupine. *J. Of Biol. Chem.* 279, 33220–33227. doi:10.1074/jbc.M403407200

Zhang, C., Chen, X., Zhu, R. M., Zhang, Y., Yu, T., Wang, H., et al. (2012). Endoplasmic reticulum stress is involved in hepatic srebp-1c activation and lipid accumulation in fructose-fed mice. *Toxicol. Lett.* 212, 229–240. doi:10.1016/j.toxlet.2012.06.002

Zhang, Q., Yao, D., Rao, B., Jian, L., Chen, Y., Hu, K., et al. (2021). The structural basis for the phospholipid remodeling by lysophosphatidylcholine acyltransferase 3. *Nat. Commun.* 12, 6869. doi:10.1038/s41467-021-27244-1

Zhao, T. J., Liang, G., Li, R. L., Xie, X., Sleeman, M. W., Murphy, A. J., et al. (2010a). Ghrelin O-acyltransferase (goat) is essential for growth hormone-mediated survival of calorie-restricted mice. *Proc. Natl. Acad. Sci. U. S. A.* 107, 7467–7472. doi:10.1073/pnas.1002271107

Zhao, T. J., Sakata, I., Li, R. L., Liang, G., Richardson, J. A., Brown, M. S., et al. (2010b). Ghrelin secretion stimulated by {Beta}1-Adrenergic receptors in cultured ghrelinoma cells and in fasted mice. *Proc. Natl. Acad. Sci. U. S. A.* 107, 15868–15873. doi:10.1073/pnas.1011116107

Zhao, Y., Chen, Y. Q., Bonacci, T. M., Bredt, D. S., Li, S., Bensch, W. R., et al. (2008). Identification and characterization of A major liver lysophosphatidylcholine acyltransferase. *J. Biol. Chem.* 283, 8258–8265. doi:10.1074/jbc.M710422200

Zhou, X., Liu, K., Cui, J., Xiong, J., Wu, H., Peng, T., et al. (2021). Circ-Mboat2 knockdown represses tumor progression and glutamine catabolism by mir-433-3p/got1 Axis in pancreatic cancer. *J. Exp. Clin. Cancer Res.* 40, 124. doi:10.1186/s13046-021-01894-x

frontiers | Frontiers in Physiology

TYPE Review
PUBLISHED 30 May 2023
DOI 10.3389/fphys.2023.1166125

OPEN ACCESS

EDITED BY
Rebeca M. Mejias Estevez,
Sevilla University, Spain

REVIEWED BY
Shernaz Xerxes Bamji,
University of British Columbia, Canada
Gareth Thomas,
Temple University, United States
Tomaszq Wójtowicz,
Polish Academy of Sciences, Poland

*CORRESPONDENCE
Dale D. O. Martin,
dale.martin@uwaterloo.ca

RECEIVED 14 February 2023
ACCEPTED 12 May 2023
PUBLISHED 30 May 2023

CITATION
Ramzan F, Abrar F, Mishra GG, Liao LMQ and Martin DDO (2023), Lost in traffic: consequences of altered palmitoylation in neurodegeneration.
Front. Physiol. 14:1166125.
doi: 10.3389/fphys.2023.1166125

Lost in traffic: consequences of altered palmitoylation in neurodegeneration

Firyal Ramzan, Fatima Abrar, Gyana Gourab Mishra, Lucia Meng Qi Liao and Dale D. O. Martin*

NeurdyPhagy Lab, Department of Biology, Faculty of Science, University of Waterloo, Waterloo, ON, Canada

One of the first molecular events in neurodegenerative diseases, regardless of etiology, is protein mislocalization. Protein mislocalization in neurons is often linked to proteostasis deficiencies leading to the build-up of misfolded proteins and/or organelles that contributes to cellular toxicity and cell death. By understanding how proteins mislocalize in neurons, we can develop novel therapeutics that target the earliest stages of neurodegeneration. A critical mechanism regulating protein localization and proteostasis in neurons is the protein-lipid modification S-acylation, the reversible addition of fatty acids to cysteine residues. S-acylation is more commonly referred to as S-palmitoylation or simply palmitoylation, which is the addition of the 16-carbon fatty acid palmitate to proteins. Like phosphorylation, palmitoylation is highly dynamic and tightly regulated by writers (i.e., palmitoyl acyltransferases) and erasers (i.e., depalmitoylating enzymes). The hydrophobic fatty acid anchors proteins to membranes; thus, the reversibility allows proteins to be re-directed to and from membranes based on local signaling factors. This is particularly important in the nervous system, where axons (output projections) can be meters long. Any disturbance in protein trafficking can have dire consequences. Indeed, many proteins involved in neurodegenerative diseases are palmitoylated, and many more have been identified in palmitoyl-proteomic studies. It follows that palmitoyl acyl transferase enzymes have also been implicated in numerous diseases. In addition, palmitoylation can work in concert with cellular mechanisms, like autophagy, to affect cell health and protein modifications, such as acetylation, nitrosylation, and ubiquitination, to affect protein function and turnover. Limited studies have further revealed a sexually dimorphic pattern of protein palmitoylation. Therefore, palmitoylation can have wide-reaching consequences in neurodegenerative diseases.

KEYWORDS

palmitoylation, neurodegenenerative diseases, autophagy, posttranslational modification, sex differences

1 Introduction

Regardless of the etiology, one of the first insults in all neurodegenerative diseases is mislocalization of proteins. Protein mislocalization in neurons is often linked to proteostasis deficiencies, which can lead to a build-up of misfolded proteins or damaged organelles, ultimately resulting in cell death (Martin et al., 2015; Suk and Rousseaux, 2020). In this review, we discuss the contribution of palmitoylation to protein dysfunction related to

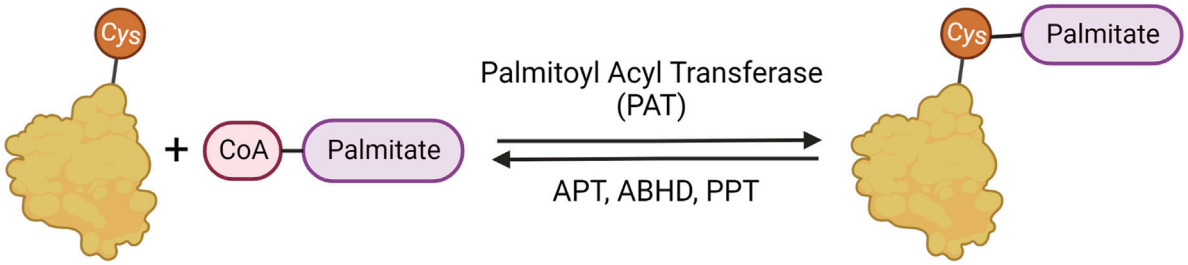

FIGURE 1
Palmitoylation mechanism. Palmitoylation involves the reversible addition of palmitate to cysteine residues through a labile thioester bond. The palmitate is added to proteins by palmitoylate acyl transferases (PATs) and removed by α/β serine hydrolases (ABHDs) and thioesterases (APTs and PPTs).

neurodegeneration. S-palmitoylation, the reversible addition of the lipid palmitate to specific cysteine residues via a labile thioester bond, helps to anchor proteins to membranes, allowing dynamic regulation of protein localization. Thus, the reversibility of S-palmitoylation allows soluble proteins to be directed to and from membranes throughout neurons, including synapses, dendrites, and axons. Palmitoylation can also occur on transmembrane proteins, dynamically regulating their function without affecting localization (Zaballa and van der Goot, 2018). Irreversible palmitoylation is less common but possible via a stable amide bond (N-palmitoylation) or ester bond (O-palmitoylation) (Buglino and Resh, 2008; Ji et al., 2016; Gao and Hannoush, 2018). In this review, however, palmitoylation refers to S-palmitoylation.

Palmitoylation is important in many cellular and metabolic processes and has been implicated in neurodegeneration and diseases of the nervous system (Resh, 1999; 2016; Linder and Deschenes, 2007; Sanders et al., 2015; Cho and Park, 2016) The addition of the 16-carbon fatty acid palmitate to cysteine residues is facilitated by palmitoyl acyl transferases (PATs) that are characterized by and named after their conserved Asp-His-His-Cys with Zinc fingers (ZDHHC) active site domains (Fukata et al., 2004; Roth et al., 2006; Hou et al., 2009). The removal of palmitate from proteins is facilitated by several classes of serine hydrolases (Figure 1), including acyl protein thioesterase (APTs), protein palmitoyl thioesterase (PPTs), and α/β-hydrolase domain (ABHD) proteins (Chen, Fan, and Boehning, 2021; Bononi et al., 2021; Hornemann, 2015; Lin and Conibear, 2015; Toyoda, Sugimoto, and Yamashita, 1999; Duncan and Gilman, 1998; Yokoi et al., 2016).

2 Going off course: dire consequences of altered palmitoylation in neurons

Palmitoylation regulates many aspects of neuronal protein trafficking and function (reviewed in Philippe and Jenkins, 2019; Petropavlovskiy et al., 2021). Neurons are polarized cells with long thin axons and shorter, thicker dendrites. Using action potentials that run from the cell body down the length of the axon, neurons communicate with each other through synapses, the connection points between axons and dendrites from different neurons (Bullock et al., 2005). At the synapse, distinct proteins and receptors localize to the post-synapse and pre-synapse. A recent compendium of 15 palmitoyl-proteome studies, found an enrichment of palmitoylation in the synaptic proteome (Sanders et al., 2015). Now, nearly 50% of synaptic proteins are considered to be palmitoylated (Petropavlovskiy et al., 2021). The reversibility of palmitoylation allows neurons to dynamically create and maintain this specific protein localization (Matt et al., 2019; Philippe and Jenkins, 2019). Thus, the quick reversibility of palmitoylation and its importance in regulating protein localization makes it a compelling candidate for functional regulation in neurodegenerative diseases.

Not surprisingly, a mammalian palmitoyl-proteome study identified numerous biomarker-based disease-association enrichments of neurodegenerative diseases and neurodevelopmental disorders (Sanders et al., 2015). These diseases and disorders include, but are not limited to, schizophrenia, chorea, Huntington Disease (HD), spinal cord diseases, Amyotrophic Lateral Sclerosis (ALS), and cranial nerve disease (Sanders et al., 2015). Indeed, key proteins involved in HD, ALS, and Alzheimer Disease (AD) have already been shown to have altered palmitoylation in disease states (Yanai et al., 2006; Cho and Park, 2016; Antinone et al., 2017).

Considering the enrichment of palmitoylated proteins and the dynamic role it plays in cells, palmitoylation has emerged as an attractive area of research in neurodegenerative diseases. The role of palmitoylating and depalmitoylating enzymes in neurodegenerative diseases is discussed in the next section. Importantly, palmitoylation acts as a mediator and modulator of numerous functions within the cell, but is best known for shuttling soluble proteins to membranes. However, palmitoylation does not act alone, but in concert with or in addition to other posttranslational modifications, discussed in section 4. The interplay of palmitoylation with other posttranslational modifications is tightly regulated and important for proteostasis, which is disrupted in numerous diseases (See section 5). Finally, there is growing evidence of sex differences in palmitoylation, indicating a role of palmitoylation in the regulation of sex differences in disease, discussed in section 6.

3 Putting together the ancestral puzzle of palmitoylation: Lessons from model organisms

Studying protein palmitoylation using lower model organisms like *Saccharomyces cerevisiae*, *Caenorhabditis elegans*, *Drosophila*

melanogaster and *Mus musculus* has immense potential to provide critical insights due to the conserved role of palmitoylation and associated pathological processes contributing to neurodegeneration (Hayashi, 2021). Studies have identified 7 PATs in *Saccharomyces cerevisiae*, 15 in *Caenorhabditis elegans*, 22 in *Drosophila melanogaster* and 24 in *Mus musculus* (Bannan et al., 2008; Edmonds and Morgan, 2014; Zaballa and van der Goot, 2018). All these PATs share the characteristic cysteine-rich domain (CRD) containing the "DHHC" motif unique to palmitoylating enzymes highlighting the conserved mechanisms PATs use in palmitoylating their substrates. Importantly, model organisms have and continue to serve as a valuable tool to decipher the role of palmitoylation in cellular function and pathogenesis by facilitating the ability of researchers to run a diverse set of genetic manipulation, localization studies, and behavioural assays.

3.1 Model organisms used in palmitoylation studies

Yeast was the first model system used to identify palmitoylation through the identification of zinc-finger-like CRD containing palmitoylating enzymes Akr1 and Erf2 (Lobo et al., 2002; Roth et al., 2002) that eventually led the way to the identification of a family of 23–24 ZDHHC isoforms in mammals (Fukata et al., 2004; Huang et al., 2004; Keller et al., 2004). Yeast has been an invaluable model organism to identify PAT interactors through high throughput knock-out studies, which has helped identify palmitoylation of various neurodegeneration proteins. The fruit fly model, *Drosophila melanogaster*, is emerging as another model organism for studying palmitoylation and has been key in modelling neurodegenerative diseases. Flies allow sophisticated genetic manipulation and molecular analysis at an organismal level that can be coupled with various behavioural assays (Lu and Vogel, 2009; Nitta and Sugie, 2022).

3.2 Uses of model organisms in high throughput studies

Apart from PAT substrate identification, yeast has provided a robust and efficient model for high throughput screening of the global S-palmitoyl-proteome under various nutrient conditions (Roth et al., 2006) as well as identification of palmitoylation inhibitors (Coronel Arrechea et al., 2021). Once validated, these inhibitors could be translated to higher model organisms and ultimately lead to palmitoylation-related therapeutic development for neurodegenerative diseases. While yeast has been an invaluable model to identify PATs, PAT substrates, establish high throughput approaches, and identify pharmacological inhibitors, they are unable to provide understanding of the nervous system. To inform the role of palmitoylation in the nervous system and organisms at a global scale, *Drosophila melanogaster* and *Mus musculus* have been used.

The Korey group (Bannan et al., 2008) was the first to identify all 22 PATs and their expression profile in flies. Many fly PATs are highly expressed in the nervous system, emphasizing palmitoylation's role in neuronal health and function. A recent S-palmitoyl-proteome study in *Drosophila*-derived S2R+ cells identified an estimated 3.5% of expressed genes in these cells to be palmitoylated. Interestingly, these palmitoylated proteins were found to be more conserved between flies and mammals compared to non-palmitoylated proteins (Porcellato et al., 2022). They also identified putative substrates and interaction partners of the various PATs through DHHC-BioID, a proximity biotinylation-based method, which they validated in larval and adult flies for a complete organismal study. Although the function of each PAT in fly neuronal health and their conservation to the mammalian system remains to be characterized, this work provides the foundation for more in-depth studies involving PATs in the nervous system and their roles in neurodegeneration.

The utilization of mice in recent RNA sequencing studies has resulted in the curation of a valuable resource for palmitoylation enzymes in the mouse brain, BrainPalmSeq (Wild et al., 2022). This resource combines information from numerous single-cell RNAseq studies, complemented with bulk and pooled-cell RNAseq studies which include a diversity of brain regions, and ages of tested mice. The authors revealed cell-type-specific and regional ZDHHC expression in the nervous system. They further found interrelated patterns of expression between ZDHHC enzymes and their substrates, as well as depalmitoylating enzymes and other brain-expressed genes (Wild et al., 2022). They recently expanded on this to create CellPalmSeq, a new interactive tool and RNAseq database for multiple human and laboratory cell lines (Wild et al., 2023). The same group identified substrates that are differentially palmitoylated and speculated based on co-localization analysis that the dynamic palmitoylation of a subset of these substrates was mediated by ZDHHCs 2, 5, and 8 (Nasseri et al., 2022) This suggests that palmitoylation in the brain is highly regulated and influenced by external stimuli. Thus, this information provides valuable insight into the roles of palmitoylating enzymes in the mammalian brain and nervous system.

3.3 Putting PATs in their place: how PATs fit in neurodegeneration

In this section, we outline the roles and contributions of specific PATs in mechanisms of neurodegeneration and diseases of the brain and nervous system as known in the current literature.

3.3.1 Huntington disease (ZDHHC17 and ZDHHC13)

Huntington Disease (HD) is an autosomal-dominant progressive neurodegenerative disease caused by a mutation in the *HTT* gene. This single mutation results in an expansion in the polyglutamine (polyQ or CAG repeat in the *HTT* gene) region at the N-terminus of the huntingtin (HTT) protein (The Huntington's Disease Collaborative Research Group, 1993). Repeats greater than 36 result in mutant huntingtin (mHTT) and increases the risk of developing HD. The larger the repeat region, the earlier the age of onset and the more severe the symptoms. In HD, mHTT has reduced palmitoylation compared to the wild-type form, which is linked to increased insoluble mHTT and decreased ZDHHC17 activity (Yanai et al., 2006; Huang et al., 2011).

Increasing brain palmitoylation in HD mouse models acts to rescue the phenotype and is emerging as a potential therapeutic approach (Lemarié et al., 2021; Virlogeux et al., 2021).

ZDHHC17 is the most well-conserved PAT, from yeast to humans (Young et al., 2012; Butland et al., 2014). Both ZDHHC17 and ZDHHC13 are unique among the PATS due to the presence of their N-terminal ankyrin-repeat domains (facing the cytosol), absent in other PATs (Mitchell et al., 2006; Tabaczar et al., 2017). Moreover, they have 6 predicted transmembrane domains as opposed to the typical 4, also reflected in the yeast ZDHHC17 homolog Akr1 (Politis, Roth, and Davis, 2005; Mitchell et al., 2006; Tabaczar et al., 2017). ZDHHC17 was initially discovered as an interactor protein of HTT *via* a yeast two-hybrid screen (Singaraja et al., 2002) and was initially named Huntingtin Interacting Protein 14 (HIP14). Due to its similarity to ZDHHC17, ZDHHC13 was named HIP14-Like or HIP14 L. The HTT–ZDHHC17 interaction is disrupted by the pathogenic expansion of the mHTT polyQ domain (128Q compared with 15Q for the wild-type protein) (Singaraja et al., 2002). The study was later validated in an HD mouse model, suggesting that defects in HTT palmitoylation could contribute to the disease (Yanai et al., 2006).

ZDHHC17 and ZDHHC13 are essential for regulating mHTT function in HD, specifically through palmitoylation (Huang et al., 2011). Further, in the presence of mHTT with an expanded polyQ tract in the YAC128 HD mouse model, there is reduced HTT palmitoylation and reduced interaction between HTT and ZDHHC17 (Singaraja et al., 2002; Huang et al., 2004; Yanai et al., 2006). In a mouse model expressing truncated ZDHHC13 that retains the N-terminal ankyrin repeat, mice have abnormalities in hair, skin, and bone, as well as reduced survival and increased amyloidosis, indicating a role of ZDHHC13 in regulating essential functions in multiple tissue and cell types, including neurons, epithelial, and bone (Saleem et al., 2010). Interestingly, a less severe phenotype is linked to *Zdhhc13* knockout. This may suggest that the ankyrin repeat has a dominant negative effect in the truncation model (Sutton et al., 2013). In contrast, mouse models of *Zdhhc17* deficiency or deletion have more severe phenotypes. In the constitutive *Zdhhc17* hypomorph model, the resulting behavioural and physiological deficits resemble those of an HD mouse model (Singaraja et al., 2011). In the conditional inducible *Zdhhc17* knockout mouse model, adulthood deletion of *Zdhhc17* resulted in sudden death due to rapidly progressing paralysis within 10 weeks post-induction (Sanders et al., 2016). These data suggest a significant role of ZDHHC17 in modulating pathology in HD, but also suggest that ZDHHC17 is an essential PAT, likely due to its many interactors and substrates (Butland et al., 2014). This may be linked to recently identified ZDHHC17 substrates dual leucine-zipper kinase (DLK) and nicotinamide mononucleotide adenylyltransferase-2 (NMNAT2) (Niu et al., 2020). DLK and NMNAT2 are involved in a compartmentalized retinal ganglion cell death model where these enzymes form a "trust but verify" system. Specifically, palmitoylated DLK is involved in conveying an axon-to-soma pro-degenerative signal in the event of a neuronal insult like axon injury, through upregulation of pro-apoptotic genes, while palmitoylated NMNAT2 is important in maintaining axon integrity through inhibition of Wallerian degeneration. Thus, ZDHHC17-mediated palmitoylation of DLK and NMNAT2 may be a critical regulator that decides neuronal cell fate (Niu et al., 2020).

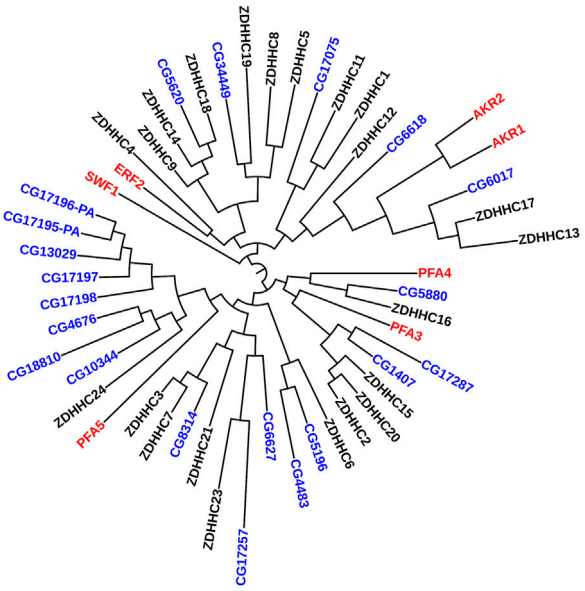

FIGURE 2
Phylogenetic Tree comparing PATs in yeast, flies, and humans. Maximum Likelihood midpoint-rooted phylogenetic tree of full-length ZDHHC proteins from *Saccharomyces cerevisiae* (red), *Drosophila melanogaster* (blue), and Homo sapiens (black) generated in Mega 11 software with 100 bootstrap replication and Jones-Taylor-Thornton model for amino acid substitution model (Tamura et al., 2021). The *Drosophila* PATs that cluster together (CG17196-PA–CG10344) are expressed only in fly testes.

Similar results have been recapitulated in flies. Presynaptic localization for dHIP14 (fruit fly orthologue for ZDHHC17) (CG6017 in Figure 2) has been reported in the central nervous system as well as the neuromuscular junction (Ohyama et al., 2007; Stowers and Isacoff, 2007). There, dHIP14 is involved in subcellular distribution of a variety of neuronal proteins in flies, including the synaptosomal associated protein of 25 kDa (SNAP-25) and cysteine string protein (CSP), and is required for photoreceptor synaptic transmission, thus suggesting palmitoylation as a possible mechanism to rapidly regulate synaptic efficiency. Indeed, dHIP14 was shown to be required for synaptic vesicle exocytosis and loss of dHIP14 led to mislocalization of SNAP25 and CSP. Moreover, dHIP14 mutants show exocytic defects at low-frequency stimulation and a nearly complete loss of synaptic transmission at higher temperatures, demonstrating the importance of dHIP14 in neurotransmitter release (Ohyama et al., 2007). This suggests that ZDHHC17's neuronal functions are conserved across species.

3.3.2 Alzheimer disease (ZDHHC12, ZDHHC7, and ZDHHC21)

Alzheimer Disease (AD) is a progressive neurodegenerative disorder resulting in brain atrophy and increased cell death, characterized by plaque formation within the brain, primarily consisting of the amyloid-beta (Aβ) protein. Aβ is formed by the sequential cleavage of amyloid precursor protein (APP) by β- and ɣ-secretases. Thus far, nearly all the primary players in AD have been shown to be palmitoylated, including APP (Bhattacharyya, Barren, and Kovacs, 2013), two ɣ-secretase subunits, APH1aL and Nicastrin

(Meckler et al., 2010), and β-secretase 1 (BACE1) (Benjannet et al., 2001).

AD is the most common form of progressive dementia characterized by the accumulation of Aβ or tau protein aggregates (Nah, Yuan, and Jung, 2015; W; Zhang et al., 2022). The Aβ peptides are generated as a cleavage product of the APP. APP palmitoylation at C186 and C187 by ZDHHC7 and ZDHHC21 is required for APP to exit the ER and its normal processing (Bhattacharyya, Barren, and Kovacs, 2013). Increased palmitoylation of APP improves targeting of APP to lipid rafts where APP is cleaved, forming increased levels of Aβ aggregates. While treatment with palmitoylation inhibitors reduced the presence of palmitoylated APP in lipid rafts as well as the Aβ aggregate production, thus suggesting a role of palmitoylation in AD disease pathogenesis (Bhattacharyya et al., 2016). APP is cleaved by BACE1, followed by subsequent cleavage by γ-secretase to produce Aβ fragments. BACE1 is palmitoylated at four sites; C478, C482, and C485 in the cytosolic region (Benjannet et al., 2001; Vetrivel et al., 2009; Motoki et al., 2012), and C474 in the transmembrane domain (Vetrivel et al., 2009; Motoki et al., 2012). Studies have reported contrasting effects of BACE1 palmitoylation on APP processing. Two separate studies by the Thinakaran and the Araki groups demonstrated that mutation of the four cysteines to alanine resulted in reduced lipid raft localization in heterologous cell lines and primary neuronal cultures (Vetrivel et al., 2009; Motoki et al., 2012). However, no loss in BACE1 protein stability or subcellular localization was observed (Vetrivel et al., 2009). The non-palmitoylated form of BACE1 did not affect the APP processing and Aβ production in comparison to the wild-type BACE1 despite the loss in lipid raft association. Thus, indicating that β-cleavage of APP by BACE1 is not influenced by lipid raft microdomains (Vetrivel et al., 2009; Motoki et al., 2012). Conversely, in 2011, the Thinakaran group demonstrated that BACE1 engineered to be localized onto the lipid rafts by the addition of glycosylphosphatidylinositol (GPI) led to improved Aβ production (Vetrivel et al., 2011). Since localization to the lipid raft was palmitoylation dependent, this indicates that BACE1 palmitoylation may be contributing to APP processing. An *in vivo* study conducted in a knock-in BACE1-palmitoylation deficient mouse model revealed that although lack of palmitoylation did not affect APP processing, the synaptic activity-dependent release of Aβ aggregates increased in BACE1 palmitoylation deficient mice compared to wild-type controls as determined by the analysis of brain interstitial fluid (Andrew et al., 2017). They further showed that lack of BACE1 palmitoylation reduced cerebral amyloid burden indicating that palmitoylation may be an important modulator of amyloid burden in AD (Andrew et al., 2017).

Lipid raft-associating subunits of the γ-secretase, Nicastrin and APH-1 are also known to be palmitoylated. Nicastrin is palmitoylated at transmembrane C689 while APH-1 is palmitoylated at cytosolic C182 and C245 sites (Cheng et al., 2009). Although palmitoylation defective forms of these proteins do not affect γ-secretase assembly and function, studies have shown that the palmitoylation of these proteins is necessary for their nascent stability as well as association with lipid rafts, suggesting a role of palmitoylation in protein stability and lipid raft localization (Cheng et al., 2009; Meckler et al., 2010). Transgenic AD mice co-expressing palmitoylation deficient forms of APH1aL, an isoform of APH-1 and Nicastrin had significantly reduced Aβ aggregate deposition in the frontal cortex compared to the ones expressing WT forms of the subunits (Meckler et al., 2010). Thus, suggesting that the palmitoylation status of these proteins can influence disease pathology in AD. ZDHHC12 is implicated in regulating palmitoylation of key proteins in AD. ZDHHC12 was initially found to inhibit APP metabolism and Aβ production in AD in mouse-derived neuroblastoma cells (N2A cells) (Mizumaru et al., 2009). In addition, a recent genome-wide association study found a significant association of ZDHHC12 in structural brain connectivity in a comparison of control patients, patients with mild cognitive impairment, and patients with AD, indicating a role of ZDHHC12 in alterations of AD brain segregation and integration (Elsheikh et al., 2020). Together with data from *in vitro* studies, this suggests ZDHHC12 may be involved in the early development of Aβ plaques in AD.

3.4 Depalmitoylation in neurodegenerative disease

In contrast to the PAT ZDHHC enzymes, Palmitoyl-protein thioesterase (PPT) and ABHD enzymes depalmitoylate proteins. Depalmitoylation and some of the enzymes that facilitate it have been implicated in neural diseases as well as neuronal functions.

3.4.1 Neuronal ceroid lipofuscinosis type 1 (PPT1)

Neuronal ceroid lipofuscinosis type 1 (CLN1), also known as infantile neuronal ceroid lipofuscinosis (INCL), is a rare (1 in 100,000 births), but one of the most lethal, inherited neurodegenerative lysosomal storage disorders caused by mutations in the *PPT1* gene resulting in PPT1 deficiency. PPT1 depalmitoylates proteins in the lysosome to facilitate protein degradation. Consequently, loss of PPT1 activity is toxic, resulting in the accumulation of pathological sphingolipids in patient cells and subsequent lysosomal enlargement (Tyynelä et al., 1993; Ahtiainen et al., 2006). Patients with CLN1 generally develop symptoms around 18 months of age, including visual defects, blindness, motor and cognitive deficits, seizures and death between 8–13 years of age (Santavuori, 1988).

Ppt1 function is well conserved from flies to humans; thus, the INCL pathologies may be due, in part, to the accumulation of various embryonic neural defects, similar to that of *Drosophila*, and may be relevant for understanding the developmental origin of neural deficiencies in INCL. Fly embryos bearing loss-of-function *Ppt1* mutations display numerous neural defects ranging from abnormal cell fate specification, missing and disorganized neurons, faulty motoneuronal axon trajectory, and mild to severe defects in the longitudinal axon bundles of the ventral nerve cord (Chu-LaGraff et al., 2010). Further, the two Ppt1 mutant strains with single point mutations (S77F and A179T) showed defects in the developing peripheral nervous system, specifically in the chordotonal neural cluster, with decreased number of sensory neurons and abnormal neuronal shapes with aberrant dendritic projections. Moreover, Ppt1 deficiency in adult flies leads to abnormal accumulation of lysosomal storage material, albeit in a different pattern than observed in human patient cells, and reduced lifespan (Hickey et al., 2006). A study overexpressing Ppt1 in the

visual system of adult transgenic flies linked Ppt1 function to synaptic vesicle cycling, endo-lysosomal trafficking, synaptic development, and activity-dependent remodelling of the synapse (Buff, Smith, and Korey, 2007). Together, these results suggest that Ppt1 is essential for synaptic and lysosomal activity, and for proper neuronal cell fates and organization in early development.

A study of brain tissue from INCL patients and a constitutive *Ppt1* knockout (*Ppt1*-KO) mouse model linked rapid neurodegeneration to increased apoptosis indicated by elevated levels of caspases 3 and 9 and cleaved poly-ADP ribose polymerase enzyme (PARP) (Kim et al., 2006). Levels of superoxide-dismutase 2 (SOD-2) in INCL patient hippocampus and *Ppt1*-KO mouse brains were also increased indicating elevated oxidative stress and generally associated with higher reactive oxygen species (ROS). This was confirmed in cultured neurospheres from *Ppt1*-KO and wild-type mice. *Ppt1*-KO neurospheres had elevated levels of ROS and SOD-2, as well as SOD-2 activity (Kim et al., 2006). Together, these results suggest the rapid neurodegeneration in INCL patients and in *Ppt1*-KO mice is likely caused, in part, by a combination of ER-stress-mediated caspase-12 activation (mediates caspase-3 activation and apoptosis (Zhang et al., 2006)) as well as elevated ROS production (causes destabilization of calcium homeostasis activating caspases-3, -9, and apoptosis) (Kim et al., 2006). Furthermore, a study using a *Ppt1*-KO mouse model found therapeutic potential in supplementing the lack of PPT1 function by using a depalmitoylation molecule, N-tert-butyl-hydroxylamine (NtBuHA). Specifically, NtBuHA crossed the blood-brain barrier, depleted lysosomal ceroid, suppressed neuronal apoptosis, slowed neurological deterioration, and extended lifespan (Sarkar et al., 2013). As such, the deficiency of PPT1's depalmitoylating activity is integral to the development of CLN1. Indeed, in a recent study, the same group found reduced ZDHHC5 and ZDHHC23 levels in the brains of the same *Ppt1* KO mouse model (Sadhukhan et al., 2021). Moreover, membrane-bound APT1 levels were suppressed, which stimulated microglia proliferation through increasing plasma-membrane H-Ras. In turn, this neuroinflammation phenotype was rescued by treatment with NtBuHA (Sadhukhan et al., 2021). These studies suggest that NtBuHA may be used as a therapeutic to lower palmitoylation in the brain, also indicating PPT1's depalmitoylating function in INCL. Furthermore, altered palmitoylation of substrates of PPT1, APT1, ZDHHC5 and ZDHHC23 likely contribute to CLN1 pathogenesis. Previously, PPT1's substrates were unknown. However, a recent study identified more than 100 novel PPT1 substrates, many of which have functions at the synapse, including channels and transporters, G-protein-associated molecules, endo/exocytic components, synaptic adhesion molecules, and mitochondrial proteins (Gorenberg et al., 2022). This indicates a role of PPT1-mediated depalmitoylation in synaptic and neuronal function and further supports PPT1's effects on neuronal function in CLN1.

3.4.2 Hereditary spastic paraplegia (ABHD16A)

ABHD16A, also known as Human Lymphocyte Antigen B-associated transcript 5 (BAT5), is a phosphatidylserine lipase recently identified as a novel protein depalmitoylating enzyme that has been linked to complex hereditary spastic paraplegia (HSP) (Lemire et al., 2021; Yahia et al., 2021; Miyake et al., 2022). ABHD16A is highly conserved in mammals, is composed of 558 residues in humans and mice, and was found to be genetically distant from other members of the ABHD family (Xu et al., 2018). ABHD16A exhibits ubiquitous expression with highest expression being in skeletal muscle and the brain (Xu et al., 2018). It is also palmitoylated (Martin and Cravatt, 2009) and localized in the plasma membranes in human platelets and mouse megakaryocytes (Senis et al., 2007).

HSP is a genetically and clinically heterogeneous group of inherited neurodegenerative diseases (Mackay-Sim, 2021). Patients with "complex" HSP display additional symptoms, including neuronal and non-neuronal features (Mackay-Sim, 2021). In one study of four patients from two Sudanese families, two *ABHD16A* null variants were identified to segregate in an autosomal recessive pattern of inheritance within these families, with a severe clinical presentation in the patients of developmental delay, intellectual impairment, spasticity, and skeletal deformities, similar to complex HSP (Yahia et al., 2021). The group further confirmed, in comparison to sibling controls, a lack of ABHD16A expression in patient fibroblasts (derived from 3 of the four patients) and found increased expression of the lipid phosphatidylserine with long-chain fatty acid, implicating ABHD16A's role in lipid metabolism in the disease (Yahia et al., 2021). In another study of 11 patients from 6 families with diverse origins, homozygous variants of ABHD16A were identified across the *ABHD16A* gene, leading to diverse complex forms of HSP in each of the studied patients, and confirmed a lack of ABHD16A expression in fibroblasts derived from 4 patients (Lemire et al., 2021). In a third study of two affected children from a Chilean family, researchers identified a homozygous *ABHD16A* variant to lead to HSP (Miyake et al., 2022). These studies suggest various mutations within the *ABHD16A* gene may lead to diverse forms of complex HSP, but it remains unclear if this is due to ABHD16A's role in lipid metabolism or protein depalmitoylation activity or perhaps both.

3.4.3 Other links between depalmitoylation and neuronal mechanisms

While some depalmitoylating enzymes have been implicated in specific neural diseases, in other instances either depalmitoylation or depalmitoylating enzymes have been linked to neuronal mechanisms that may be involved in disease. Post-synaptic density-95 (PSD95) undergoes rapid palmitoylation cycling to regulate its functions in neurons (El-Husseini et al., 2002). Increased PSD95 levels were found to prevent the effects of Aβ on synapses by preventing Aβ′s modification of the NMDA receptor C-terminal domain (CTD) conformation, its interaction with protein phosphatase 1 (PP1), and thus preventing synaptic weakening. By treating with palmostatin B, a depalmitoylation inhibitor, PSD95 levels were upregulated and Aβ′s interaction with the NMDAR and PP1 were prevented, having a protective effect (Dore et al., 2021). Similarly, inhibiting mHTT depalmitoylation using an APT1 inhibitor in mammalian cells has a protective effect against forming aggregates (Lemarié et al., 2021). Similar to mHTT, increasing PSD95 palmitoylation may be a therapeutic avenue of research in diseases associated with Aβ, such as AD. ABHD17A, 17B, and 17C were found to selectively depalmitoylate PSD95 in rat hippocampal neurons, and may

serve as potential therapeutic targets in conditions with Aβ dysfunction (Yokoi et al., 2016). APT1 and APT2 have both also been linked to regulate neuronal substrates (Milde and Coleman, 2014; Sadhukhan et al., 2021; Shen et al., 2022). Specifically, APT1 was found to depalmitoylate PSD-95 and glutamate receptors in rat hippocampal neurons, and also found to affect neuronal synaptic plasticity (Shen et al., 2022). Further, both APT1 and APT2 were found to depalmitoylate the axon survival factor NMNAT2 (Milde and Coleman, 2014).

4 Hitting the mark: interrelationship of palmitoylation and other PTMs

Posttranslational modifications (PTMs) govern many aspects of protein function and are strictly regulated. Therefore, it is not surprising that aberrant PTMs are intimately linked to neurodegenerative diseases (Ren et al., 2014; Didonna and Benetti, 2016). Despite in-depth studies of individual modifications in neurodegeneration, it remains a challenge to build a map of the complex interplay and regulation of all PTMs that are implicated in neurodegenerative diseases. However, it is important to recognize collective patterns of PTM combinations in different neurodegenerative diseases, referred to as the "PTM code" (Lothrop, Torres, and Fuchs, 2013). To date, a comprehensive overview of interactions in the context of palmitoylation within the PTM network has yet to be fully recorded. In this review, well-established PTMs that are involved in neurodegeneration will be of focus in examining crosstalk with palmitoylation (Calabrese, Molzahn, and Mayor, 2022; Didonna and Benetti, 2016; Ren et al., 2014).

4.1 Phosphorylation

The interaction of palmitoylation with phosphorylation has been studied to a greater extent than other PTMs in neurodegeneration. The combinatorial interplay of the two has an important role in protein trafficking and localization due to the reversibility of both modifications that can be rapidly and dynamically regulated (Stram and Payne, 2016; Zaballa and van der Goot, 2018). Studies have shown varied types of interactions including synergistic, reciprocal, and precursor regulation between the two PTMs (Salaun, Greaves, and Chamberlain, 2010; Shipston, 2011; Gauthier-Kemper et al., 2014; Moritz et al., 2015; Berg et al., 2016; Main and Fuller, 2022). The addition of the negatively charged phosphate group can modulate membrane binding by interacting with the positively charged head groups in the lipid bilayer or interrupt the interaction of polybasic domains of proteins with negatively charged head groups (Quatela et al., 2008; Vitrac et al., 2017). Palmitoylation also mediates membrane interactions for anchoring by increasing hydrophobicity (Zaballa and van der Goot, 2018). Therefore, it is not surprising that the two PTMs can operate synergistically. Indeed, the neuronal Growth Associated Protein 43 (GAP43), essential for axonal growth, requires both palmitoylation and phosphorylation for transport and association with the plasma membrane (Gauthier-Kemper et al., 2014). However, palmitoylation, not phosphorylation, was shown to be required for proper sorting from the soma to the tip of the growth cone, likely by facilitating active transport, as the non-palmitoylatable mutant remained diffuse in the cytosol (Gauthier-Kemper et al., 2014). Therefore, phosphorylation, in concert with palmitoylation, can regulate and promote protein trafficking and localization.

Reciprocal, or antagonistic, regulation has also been reported between phosphorylation and palmitoylation. Dopamine transporters are mutually regulated by protein kinase C (PKC)-mediated phosphorylation and palmitoylation where an increase in phosphorylation decreases palmitoylation, consequently down-regulating dopamine transport capacity, and *vice versa* (Moritz et al., 2015). This may contribute to the reduction in dopamine levels in Parkinson Disease (PD) (Bu, Farrer, and Khoshbouei, 2021). Similarly, synapsin 1, involved in regulating clustering of synaptic vesicles, is also antagonistically controlled where an increase in phosphorylation negatively regulates its palmitoylation, which is required for synaptic vesicle binding thereby hindering clustering at the synapse (Yan et al., 2022). This may contribute to the defects in *a*-synuclein synaptic vesicle docking observed in PD (Man et al., 2021; Zou, Tian, and Zhang, 2021).

In some cases, palmitoylation acts as a precursor for phosphorylation. For example, APT1-mediated depalmitoylation is required to precede phosphorylation within the Akt/mTOR/p70S6 signalling pathway (Berg et al., 2016). Regardless of the nature of regulation, aberrant phosphorylation is a prevalent characteristic of neurodegenerative diseases, particularly in those involving protein aggregation (Tenreiro, Eckermann, and Outeiro, 2014; Xia, Prokop, and Giasson, 2021). However, the crosstalk of palmitoylation and phosphorylation is highly variable; therefore, the relationship will need to be determined for individual proteins or diseases of interest. This suggests that palmitoylation should not be studied in isolation, but with the effects of other PTMs kept in mind.

4.2 Acetylation

Palmitoylation has been suggested to regulate acetylation in neural stem cell differentiation (Chen et al., 2016). Acetylation involves the transfer of an acetyl group from acetyl-CoA to lysines and is catalyzed by lysine acetyl transferases and de-acetylases, more commonly known as histone acetyl transferases (HATs) and histone de-acetylases (HDACs) (Didonna and Benetti, 2016). Disruptions in the balance between HAT/HDAC activity contribute to neurodegeneration. At the transcriptional level, histone hypo-acetylation at one or multiple genetic loci leads to lower expression and loss of function, or widespread transcriptional disruptions, respectively (Didonna and Benetti, 2016). At the protein level, several proteins in polyglutamine neurodegenerative diseases are acetylated and palmitoylated, including HTT in HD and ataxins in spinocerebellar ataxias. Here, protein acetylation was impeded by palmitoylation, *via* either inhibiting HAT or upregulating HDAC activity (Didonna and Benetti, 2016; Li et al., 2002; Sugars and Rubinsztein, 2003; Blanc et al., 2015; Yanai et al., 2006; Wei et al., 2014).

Similarly, tubulin acetylation may be regulated by palmitoylation. Tubulin is the structural subunit of microtubules

that is critical for axonal structure and transport. Consequently, disruptions in tubulin have been linked to several neurodegenerative diseases (Sferra et al., 2020; Santiago-Mujika et al., 2021). Acetylated tubulin requires palmitoylation to facilitate microtubule assembly and stability in cilia and other compartments in HEK293T cells, primary astrocytes, ependymal cells, and neurons derived from inducible pluripotent stem cells (Tripathi et al., 2021). Two acetylation sites have been identified in tubulin: *a*-subunit K40 that faces the microtubule lumen and mediates binding with microtubule associated proteins and β-subunit K252 at the interface of the two subunits, which is thought to regulate dimerization and microtubule assembly (LeDizet and Piperno, 1987; Chu et al., 2011; Wloga, Joachimiak, and Fabczak, 2017). Interestingly, K252 and C354 are in close physical proximity (PDB ID: 1TUB) (Nogales, Wolf, and Downing, 1998; Madej et al., 2014; Thinon et al., 2018), which may suggest a potential regulatory interaction of palmitoylation at C354 and K252 acetylation in microtubule assembly. Thus, altered tubulin palmitoylation may lead to mislocalization or decreased microtubule formation and contribute to disease pathogenesis (Nekooki-Machida and Hagiwara, 2020). Taken together, palmitoylation regulation or interference with acetylation may be a common mechanism in neurodegeneration.

4.3 S-nitrosylation

S-nitrosylation involves the reversible addition of a nitric oxide (NO) group to cysteines and has a wide range of crosstalk with other PTMs (Hess and Stamler, 2012). S-nitrosylation plays an important role in modulating signal transduction pathways (Anand and Stamler, 2012; Corpas et al., 2015). S-nitrosylation increases with age and aberrant S-nitrosylation has been reported in a number of key proteins and neurotoxic pathways involved in various neurodegenerative diseases, including AD, PD, and HD (Nakamura et al., 2015). Because S-nitrosylation and palmitoylation both occur on cysteines, their potential interrelationship in regulating protein function is particularly interesting, but has not been well-characterized. Moreover, S-nitrosylation can be detected by the commonly used acyl-exchange assays. Therefore, caution must be taken when studying the two PTMs using the acyl-exchange assays. A high-throughput study using a mass spectrometric approach found changes in the crosstalk of the S-nitrosylation and palmitoylation of many synaptic proteins upon stress induction, suggesting that this interaction is important in the brain (Zaręba-Kozioł et al., 2021).

There may be direct competition at the target residue or the presence of NO may be targeting the addition of the reactive cysteine to CoA and blocking the formation of fatty acyl-CoA needed for palmitoylation entirely, leaning towards competitive regulation, especially in synaptic proteins (Salaun, Greaves, and Chamberlain, 2010; Hess and Stamler, 2012). Consistent with this notion, NO agents that induce S-nitrosylation inhibit palmitoylation of SNAP-25 and GAP43, which are required for neuronal plasticity and growth (Hess et al., 1993; Matt et al., 2019). Similarly, PSD-95 is S-nitrosylated and palmitoylated on the same cysteines, while upregulation of one inhibits the other (Ho et al., 2011). Inhibitory effects have also been reported in other proteins. For example, NO inhibits the SARS-CoV spike protein palmitoylation and reduces binding to angiotensin-converting enzyme 2 receptor on the host cell, thereby affecting infectivity (Akerström et al., 2009). However, this may not always be the case as NO has been shown to increase palmitoylation of H-Ras (Baker, Booden, and Buss, 2000).

Conversely, palmitoylation also regulates nitric oxide synthase, which is a source of NO within the cell (Iwakiri et al., 2006). Given that NO synthesis is coupled to S-nitrosylation in mammals, palmitoylation and depalmitoylation may play a direct role in global S-nitrosylation as a whole (García-Cardeña et al., 1996; Yeh et al., 1999; Navarro-Lérida et al., 2004; Anand and Stamler, 2012).

For example, S-nitrosylation regulates phosphatase with sequence homology to Phosphatase and Tensin (PTEN)/Akt signaling, and consequently, either promotes neuroprotective processes *via* inhibition of PTEN and activation of Akt, or inhibiting protective pathways by S-nitrosylation of Akt directly (Numajiri et al., 2011; Nakamura et al., 2013). In line with this notion, aberrant S-nitrosylation of sequestosome 1 (SQSTM1), or p62, hinders the clearance of built-up protein by directly inhibiting autophagy in PD (Oh et al., 2022). Correspondingly, the protein misfolding repair activity of protein disulfide-isomerase (PDI), which mediates ER stress by suppressing the buildup of aberrant proteins, is compromised by S-nitrosylation (Uehara et al., 2006; Nakamura et al., 2013). It is important to note that almost all of the aforementioned S-nitrosylated proteins in neurodegeneration are predicted to be palmitoylated, with some experimentally validated (Blanc et al., 2015). If palmitoylation, in general, inhibits S-nitrosylation, this provides another means to target pathogenic processes in neurodegeneration.

Taken together, S-nitrosylation may play a mechanistic role in disrupting palmitoylation-mediated protein trafficking, proteostasis, and function, or may function downstream of palmitoylation. The potential inhibitory regulation of palmitoylation needs to be further examined in the study of protein S-nitrosylation in neurodegeneration.

4.4 Ubiquitination

Crosstalk between ubiquitin and other PTMs is important in maintaining proteostasis. Ubiquitination refers to the conjugation of ubiquitin to lysine or N-terminal methionine of target substrates, including ubiquitin itself (Sadowski et al., 2012). Ubiquitin can also be removed by deubiquitinases (Komander and Rape, 2012; Schmidt et al., 2021). Although ubiquitin can signal non-degradative processes, the primary function of ubiquitin conjugation is protein targeting and tagging for degradation through the ubiquitin-proteasome system (UPS), which is often impaired in neurodegenerative diseases, thus contributing to protein aggregation (Sadowski et al., 2012; Didonna and Benetti, 2016; Watanabe, Taguchi, and Tanaka, 2020). This mechanism involves a cascade of enzymes, namely, E1 ubiquitin-activating enzyme, E2 ubiquitin-conjugating enzymes and E3 ubiquitin ligases (Komander and Rape, 2012; Schmidt et al., 2021). Ubiquitin signalling is one of the most important mechanisms in the pathogenesis of neurodegenerative diseases (Le Guerroué and Youle, 2021).

In many cases, palmitoylation has been shown to antagonize ubiquitination by increasing protein stability and preventing

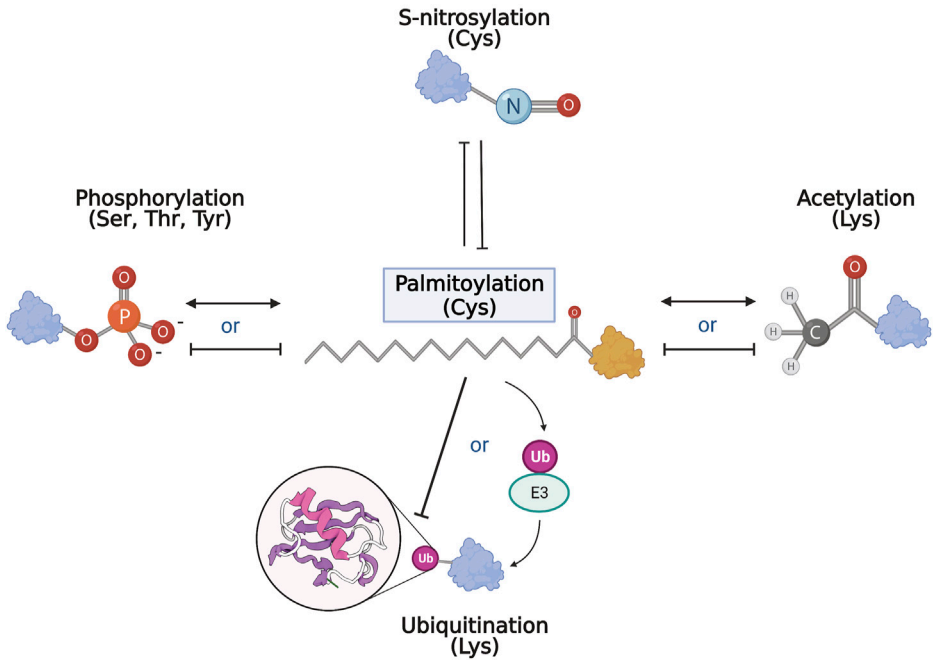

FIGURE 3
PTM network and palmitoylation. Schematic representation of the interrelationship of palmitoylation and other PTMs. Palmitoylation and S-nitrosylation mostly compete and inhibit each other on target cysteines. With phosphorylation and acetylation, both competitive and complementary interactions with palmitoylation have been recorded where palmitoylation may either inhibit or act synergistically with the other modification. Similarly, and perhaps paradoxically, palmitoylation can inhibit ubiquitination of target substrates, but is also required for activation and function of some E3 ubiquitin ligases.

degradation. For example, sortilin turnover is mediated by ubiquitination which has several implications in neurodegeneration (Carlo, Nykjaer, and Willnow, 2014). Sortilin is a lysosomal sorting receptor which binds apolipoprotein and amyloid complexes in AD (Carlo et al., 2013; Carlo, Nykjaer, and Willnow, 2014). It is also involved in the delivery of progranulin to the lysosome for degradation, therefore contributing to the loss of progranulin which leads to frontotemporal dementia and TDP-43 pathology in ALS (Hu et al., 2010; Kumar-Singh, 2011; Carlo, Nykjaer, and Willnow, 2014; Gan, Khan, and Gitcho, 2015). Sortilin itself is protected from degradation by palmitoylation as it shuttles between the Golgi and endosomes (Dumaresq-Doiron, Jules, and Lefrancois, 2013). Similarly, palmitoylation protects endosomal SNARE proteins that shuttle between endosomes and Golgi in yeast by preventing ubiquitin ligase recognition (Valdez-Taubas and Pelham, 2005; Greaves and Chamberlain, 2007). In addition, voltage-gated calcium channels required for neurotransmitter release, such as $Ca_v2.2$ (Saegusa et al., 2020), are also protected from degradation by palmitoylation (Page, Rothwell, and Dolphin, 2016).

On the other hand, palmitoylation plays an important role in the proper functioning of the UPS machinery. A number of E3 ubiquitin ligases themselves require palmitoylation. For example, palmitoylation of a rat E3 ubiquitin ligase enriched in the brain increases levels of overall polyubiquitination (Araki et al., 2003). In addition, E3 ubiquitin ligases, including Gp78, require palmitoylation in their canonical RING finger motifs for their enzymatic activity (Fairbank et al., 2012). Therefore, palmitoylation may protect proteins from degradation while trafficking within the cell, allowing them to carry out their functions. In contrast, aberrant palmitoylation can contribute to the ubiquitin-associated degradation or build-up of important proteins in neurodegeneration. Conversely, palmitoylation is implicated in defects within the UPS machinery, thus contributing to toxic protein build-up leading to cell death.

4.5 PTM network and palmitoylation

Taken together, palmitoylation is closely related to many PTMs that are disrupted in neurodegenerative diseases. Although few studies examine the co-regulatory relationship of palmitoylation and another PTM on target proteins, some commonalities and themes emerged (Figure 3). So far, palmitoylation has been shown to compete with S-nitrosylation and inhibit ubiquitination directly. In contrast, palmitoylation has also shown synergy with other PTMs such as phosphorylation. Palmitoylation may precede other PTMs by facilitating correct subcellular localization of specific proteins to enable further modifications. Alternatively, palmitoylation may in turn regulate the enzymatic machinery of PTMs, such as in phosphorylation and ubiquitination, affecting the modifications on a larger scale. Regardless of the affected pathway, aberrant palmitoylation has been shown to play an important role in the pathogenesis of neurodegenerative diseases, thus presenting the

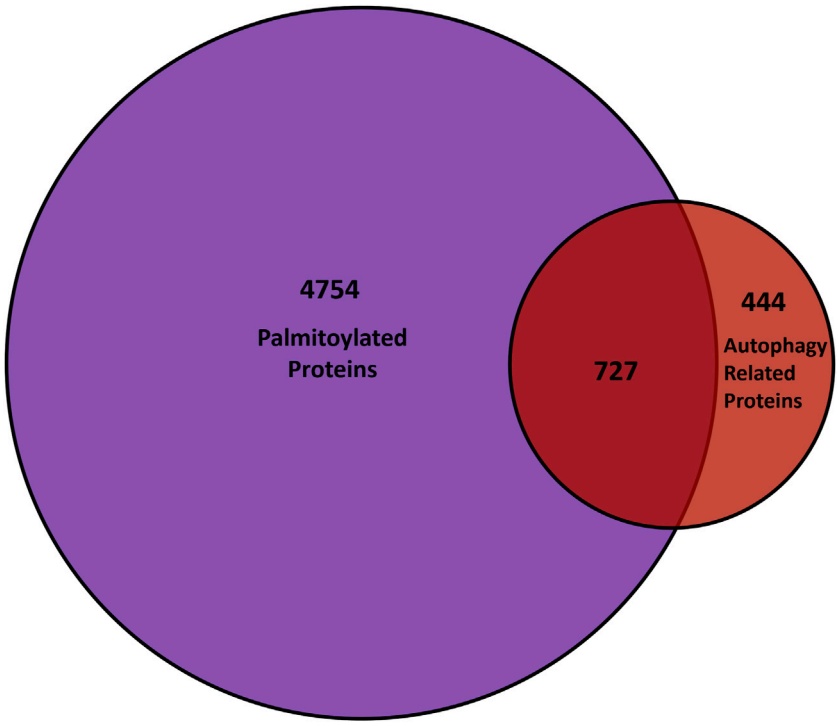

FIGURE 4
Comparison of palmitoyl-proteomes and autophagy network. The overlap between genes that encode palmitoylated proteins from the SwissPalm database (Blanc et al. 2015) and the core as well as regulatory autophagy proteins available on the Autophagy Regulatory Network (Türei et al. 2015) is represented in the Venn diagram.

need for more in-depth examinations of palmitoylation in the PTM network of neurodegeneration.

5 Traffic jam: palmitoylation regulates proteostasis

Following mislocalization, a primary hallmark of many neurodegenerative diseases is protein aggregation caused by deficiencies in protein turnover (Menzies et al., 2017; Ma, Attarwala, and Xie, 2019; Stavoe and Holzbaur, 2019). The cell has two primary methods to remove misfolded proteins; the UPS system, described above, and autophagy. Autophagy is an intracellular pathway responsible for the clearance of damaged organelles and toxic or aggregated proteins. The process is also important for neuronal health. With age, neuronal cells accumulate damaged organelles that can be toxic. Not surprisingly, dysfunctional autophagy has emerged as a common pathway in many neurodegenerative disorders (Nah, Yuan, and Jung, 2015).

Since neurons are terminally differentiated postmitotic cells that cannot replenish via cell division, autophagy plays an integral role in ensuring the removal of toxic cargo to maintain cellular homeostasis (reviewed in (Kulkarni and Maday, 2018; Stavoe and Holzbaur, 2019)). There are three types of autophagy pathways: microautophagy, macroautophagy, and chaperone-mediated autophagy (CMA). The best-characterized pathway is macroautophagy which will be the focus of this section, henceforth referred to as 'autophagy'. Autophagy begins with a double membrane precursor structure called a phagophore which engulfs the target waste, consisting of damaged organelles and toxic protein aggregates (Menzies et al., 2017). Phagophores mature and close, forming a double-membraned vesicle called the autophagosome. The cargo-carrying autophagosomes fuse with lysosomes for degradation (Martin et al., 2015; Menzies et al., 2017). The autophagy pathway is regulated by several autophagy-related proteins (ATG proteins). Microtubule light chain (LC3) is an important autophagy protein involved in autophagosome formation and elongation. p62 is an autophagy receptor that delivers toxic cargo to lysosomes for degradation of the toxic aggregates (Ma, Attarwala, and Xie, 2019). p62 binds to the ubiquitinylated proteins marked for degradation and directly interacts with LC3-II. The interaction of p62 and LC3-II results in the formation of cargo carrying autophagosomes, that later fuse with lysosomes for the removal of cellular waste (Menzies et al., 2017).

5.1 Palmitoylation and autophagy

Autophagy is a highly membrane-dependent process that requires proteins to quickly relocalize to membranes to initiate the formation of the autophagosome from donor membranes, inhibitory proteins need to translocate from membranes to the cytosol, and autophagosomes must fuse with lysosomes. Therefore, dynamic palmitoylation could provide a mechanism

for proteins to mediate these processes. As mentioned, proteostasis deficiencies was among the top diseases enriched in palmitoylated proteins, suggesting a role for palmitoylation in autophagy (Sanders et al., 2015). In turn, several autophagy-related proteins are predicted to be palmitoylated (Ren, Jhala, and Du, 2013), while a few have recently been validated, but not in the context of autophagy. Thus, we compared the known genes of proteins from mouse, rat, and humans provided by SwissPalm (Blanc et al., 2015) and autophagy core and regulatory proteins from the autophagy regulatory network (Türei et al., 2015) (Figure 4). Remarkably, over 60% (727/1171) of autophagy regulatory genes have a proteoform that is potentially palmitoylated.

Akt is a key autophagy regulator recently shown to be palmitoylated (Blaustein et al., 2021). Akt, or protein kinase B, is a serine-threonine kinase with three isoforms Akt1, Akt2, and Akt 3. Akt has multiple targets within the cell. One of the downstream targets of the Akt pathway is the mechanistic target of rapamycin (mTOR) which is a major kinase regulator of the autophagy pathway that receives signals from various signalling pathways (reviewed in (Heras-Sandoval et al., 2014)). Activation of the AKT/mTOR pathway inhibits autophagy by mTOR activation and therefore, protects and promotes cell survival. In a recent study, Akt1 and Akt2 were reported to be palmitoylated in heterologous cells (Blaustein et al., 2021). Furthermore, they confirmed that Akt1 is palmitoylated at C344. This study revealed that palmitoylation of Akt1 not only regulates its membrane association but also showed that phosphorylation at T308, required for activity of non-palmitoylated Akt1 mutant, was downregulated significantly. Thus, suggesting that palmitoylation of Akt1 is important for Akt activity during autophagy.

Both Akt and the multimeric complex mTOR complex 1 (mTORC1) are negative regulators of autophagy and Akt suppresses autophagy through downstream activation of mTORC1. mTORC1 is an important regulator for many cellular functions, including protein synthesis, autophagy, and neuronal cell development (Deleyto-Seldas and Efeyan, 2021) and was recently shown to contain palmitoylated components, including the catalytic subunit mTOR (Sanders, Simone, and Thomas, 2019). mTORC1 suppresses autophagy activation by phosphorylation-dependent inhibition of ULK1/2, TFEB, and Atg13 in the early stages of autophagy. This prevents the expression of lysosomal and autophagy genes, thus inhibiting lysosomal biogenesis. The activation of the complex depends on the recruitment of mTOR to lysosomes, where mTORC1 assembles. In turn, recruitment of LAMTOR1 to the lysosome is also required for mTORC1 signaling and is also palmitoylated (Sanders, Simone, and Thomas, 2019). Subsequently, LAMTOR1 has been shown to interact with ZDHHC3 (Tang et al., 2022). However, investigations involving palmitoylation-specific assays are required to confirm whether ZDHHC3 is the PAT regulating palmitoylation of LAMTOR1. Results from Sanders *et al.* suggest that the activity of mTORC1 is palmitoylation-dependent in heterologous cells and hippocampal neurons (Sanders, Simone, and Thomas, 2019). Although these studies did not look at autophagy specifically or neurodegeneration, this strongly suggests that mTORC signaling during autophagy likely requires palmitoylation, further confirming the role of palmitoylation of autophagy regulators in the nervous system. Altered palmitoylation may be linked to disruptions in the PI3K/AKT/mTOR pathway in AD and PD (reviewed in (Rai et al., 2019)).

5.2 PATs and proteostasis

Under nutrient starvation conditions, the Golgi complex disassembles and fragments. These fragments are delivered to autophagosomes for degradation by CALCOCO1 in a selective form of autophagy referred to as Golgiphagy (Nthiga et al., 2021). CALCOCO1 is localized to the Golgi through its interaction with ZDHHC17, via the zDHHC Ankyrin-repeat binding motif (zDABM). The Johansen group identified ZDHHC17 and ZDHHC13 as interactors of CALCOCO1 (Nthiga et al., 2021), which directly binds to ZDHHC17 on the Golgi and recruits the ATG8 family of proteins at its LC3-interacting region to promote autophagy-mediated degradation of Golgi. They also observed reduced degradation of the Golgi complex in CALCOCO1 KO HeLa cell lines that were supplemented with the mutant-zDABM CALCOCO1, incapable of interacting with ZDHHC17, suggesting an important role of ZDHHC17-CALCOCO1 interaction for degradation. They predict that since palmitoylation studies have not identified CALCOCO1 as a palmitoylation substrate, the ZDHHC17 regulation of Golgiphagy is likely palmitoylation-independent. However, it will be important to confirm and investigate the effect of palmitoylation on ZDHHC17-CALCOCO1 interaction during Golgiphagy.

That said, this is a particularly interesting new avenue of research connecting autophagy and PATs in a potentially palmitoylation-independent pathway. Although ZDHHC13 and ZDHHC17 are PATs, they have several palmitoylation-independent interactors, which remain to be characterized. For instance, ZDHHC17 binds another autophagy receptor, optineurin (OPTN), in a palmitoylation-independent manner (Butland et al., 2014). It is possible that the ZDHHC17-OPTN complex may regulate another form of selective autophagy.

5.3 Palmitoylation beyond huntingtin in Huntington Disease

HTT is a scaffold protein that is involved in various cellular processes, including autophagy (Ochaba et al., 2014; Gelman, Rawet-Slobodkin, and Elazar, 2015; Martin et al., 2015; Rui et al., 2015; Ashkenazi et al., 2017). The build-up of toxic mutant HTT (mHTT) aggregates has been suggested to stem from impaired autophagy that is disrupted at various stages in HD. One of the characteristics of HD is the accumulation of empty autophagosomes, which is linked to disrupted cargo recognition during autophagy (Martinez-Vicente et al., 2010). HTT is now known to play multiple roles in basal autophagy (Martin et al., 2014; 2015; Ochaba et al., 2014; Rui et al., 2015; Ashkenazi et al., 2017; Ehrnhoefer et al., 2018). HTT interacts with p62 and facilitates its association with LC3 thereby playing an integral role in autophagosome formation (Rui et al., 2015). All together, these reports now implicate a role for HTT in regulating basal autophagy independent from fasting-induced autophagy. Thus, many of the defects in autophagy in HD, may be due to a loss wildtype HTT function that is also disrupted by mutant HTT.

5.4 Palmitoylation of HTT

Although HD is caused by a polyQ expansion at the N-terminus of HTT, there is an enrichment of palmitoylated proteins in the HD-related proteins (Sanders et al., 2015), suggesting that this PTM may be playing an important role in disease pathogenesis. HTT is palmitoylated by ZDHHC17 at the C214 site (Yanai et al., 2006; Butland et al., 2014) and depalmitoylated by APT1 and APT2 (Lin and Conibear, 2015; Lemarié et al., 2021). It was recently reported that the palmitoylation of mHTT is reduced in HD mouse models which decreases further with age (Yanai et al., 2006; Lemarié et al., 2021). Importantly, treating mHTT-expressing cells with APT inhibitors can normalize mHTT palmitoylation levels. Moreover, improved palmitoylation levels reduced mHTT aggregation and cytotoxicity in COS-7 cells and cultured YAC128 mouse neurons (Lemarié et al., 2021). A similar study demonstrated that inhibition of depalmitoylation with the APT1 inhibitor ML348 restored neuropathology in HD CAG140 knock-in mice, suggesting that overall rescue of brain palmitoylation improves HD phenotype in the CAG140 mouse models (Virlogeux et al., 2021).

The increased clearance of mHTT promoted by inhibiting depalmitoylation may be linked to autophagy by making mHTT a better substrate or redirecting mHTT to the autophagosome while also aiding wildtype HTT regulate basal autophagy. Characterizing the role of palmitoylation in autophagy regulation is important and understanding this mechanism may provide a novel therapeutic target for HD. As such, further research in this area will shed light on the link between palmitoylation and autophagy in HD. A recent study has identified several new palmitoylation sites in full-length HTT, which may provide greater insight into how mHTT is targeted for degradation (Lemarié et al., 2023).

5.5 Autophagy dysregulation in Alzheimer Disease

Furthermore, several studies supporting the role of autophagy dysfunction in AD pathogenesis have been reported. The first evidence emerged in 2005 when the accumulation of autophagosomes was confirmed in AD patients' brains by immunogold fluorescence and electron microscopy techniques suggesting impairment of later stages of autophagy, particularly autophagosome to lysosome maturation (Nixon et al., 2005). This is associated with elevated p62 levels in AD patients (W. Zhang et al., 2022). It was previously reported that the purified autophagosomes from the liver of transgenic mice overexpressing APP were enriched in APP, Aβ, and proteases and secretases involved in APP cleavage (Yu et al., 2004). These findings link the build-up of Aβ aggregates with impaired autophagy. Recently, elevated p62 levels were detected in the cerebrospinal fluid (CSF) from AD and frontotemporal dementia patients, further providing evidence of autophagy dysregulation in AD (Rubino et al., 2022).

The Aβ aggregates are known to activate the mTORC1 pathway resulting in the inhibition of autophagy (Caccamo et al., 2011). Evidence so far suggests that palmitoylation plays an integral role in AD pathogenesis and mTORC1 localization and activity. Therefore, further investigations are necessary to understand the specific role of palmitoylation in autophagy regulation in AD pathogenesis.

5.6 Autophagy dysregulation in Parkinson Disease

A recent palmitoyl-proteome study revealed dysregulation of palmitoylation in the cortex of Parkinson Disease (PD) patients, suggesting a role of palmitoylation and protein mislocalization in PD pathophysiology (Cervilla-Martínez et al., 2022). PD is characterized by the accumulation of alpha-synuclein and ubiquitin in intracytoplasmic inclusions called Lewy bodies (Nah, Yuan, and Jung, 2015). While about 5% of PD cases are hereditary, mutations in *LRRK2* (Encoding leucine-rich repeat kinase 2, LRRK2) are considered to be one of the most common causes of genetic PD (Pang et al., 2022).

LRRK2 mutations lead to increased kinase activity (West et al., 2005) as well as the accumulation of autophagosomes (Alegre-Abarrategui et al., 2009; Bravo-San Pedro et al., 2013). Reduced co-localization of autophagosome and lysosomal markers suggests that LRRK2 mutations impair autophagosomal maturation to lysosomes (Sánchez-Danés et al., 2012). Interestingly, LRRK2 is predicted to be palmitoylated (Schapansky et al., 2014). Although they did not perform palmitoylation-specific assays, the group observed a decrease in dimerization of LRRK2 protein in total RAW264.7 cell lysates in response to treatment with 2-bromopalmitate, suggesting a potential role of palmitoylation in LRRK2 activity. Due to the broad off-target effects of 2-bromopalmitate, further investigations are necessary to characterize LRRK2 palmitoylation and its potential role in autophagy contributing to PD pathogenesis.

5.7 Autophagy dysregulation in ALS

Amyotrophic Lateral Sclerosis (ALS) is a fatal adult-onset progressive motor neuron disease characterized by the loss of upper (motor cortex, bulbar-onset) and lower (brainstem, spinal onset) motor neurons. About 5%–10% of ALS cases are inherited, categorized as familial ALS (fALS), while the remainder of ALS cases occur sporadically, referred to as sporadic ALS (sALS). Superoxide dismutase 1 (SOD1) was the first protein linked to ALS and mutations in the *SOD1* gene lead to 20% of fALS cases (Trojsi et al., 2020). A palmitoyl-proteomic study revealed an enrichment of palmitoylation in ALS biomarkers (Sanders et al., 2015). Indeed, palmitoylation of the fALS-linked mutant form of SOD1 (G93A-SOD1) is increased in HEK293 and motor neuron cell lines, while SOD1 palmitoylation is increased in ALS patient spinal cord tissues (Antinone et al., 2013; 2017). In cells, increased palmitoylation of G93A-SOD1 was associated with increased ER retention and decreased SOD1 maturation.

Treatment of G93A-SOD1 mice with rapamycin, an inhibitor of the mTOR pathway, leads to the accumulation of autophagosomes and yet fails to reduce levels of toxic SOD1 mutants (Zhang et al., 2011). This may be due the increased autophagosomes already detected in the spinal motor neurons of G93A-SOD1 mutant transgenic mouse models compared to age-matched controls (A. Li, Zhang, and Le, 2008) and increased autophagic flux in ALS patient lymphoblasts bearing the SOD1 mutation (Lastres-Becker et al., 2021). Since palmitoylation of SOD1 mutant is dysregulated in ALS, it will be worth investigating how palmitoylation may be regulating the autophagic flux in ALS disease.

Since the identification of SOD1's role in ALS, over 30 genes have now been linked to ALS, many of which are required for autophagy, while the vast majority have been identified in large palmitoyl-proteomic studies (Chen et al., 2012; Cirulli et al., 2015; Blanc et al., 2015; Sanders et al., 2015). In particular, the ZDHHC17 binding partner OPTN is highly associated with ALS. This provides another strong link to palmitoylation and ALS. Furthermore, a recent genome-wide meta-analysis reported a strong association between ALS and single nucleotide polymorphisms in *ZDHHC6* (Iacoangeli et al., 2020). However, the actual role of these PATs in ALS remains unknown, therefore, it is worth investigating the role of palmitoylation on regulating ALS disease progression.

6 Sex differences in palmitoylation and neurodegeneration

Many neurodegenerative diseases, including AD, PD, and ALS, demonstrate sex differential etiology and diagnoses (Hanamsagar and Bilbo, 2016; Ullah et al., 2019). These sex differences are generally understudied; indeed, many therapeutic strategies are often tested in one sex over the other. As such, therapeutic strategies and a holistic understanding of disease is lacking, thus requiring an understanding of the underlying causes of sex differences. There is evidence to suggest one of these underlying causes is fatty acylation. There is a demonstrable sex difference in palmitoylation in the nervous system (Hohoff et al., 2019; Zaręba-Kozioł et al., 2021). Specifically, in a mouse model of ZDHHC7 knockout, there is a sex difference in hippocampal structure and synaptic transmission in the medial prefrontal cortex (Hohoff et al., 2019). Additionally, ZDHHC7 KO reduced anxiety-related behaviours in female mice, with no effect in males (Hohoff et al., 2019). A follow-up study compared synaptoneurosomes from male and female ZDHHC7 knockout mice for palmitoylation using mass spectrometry. Here, they found sex specifically regulated substrates of ZDHHC7 and their resulting palmitoylation, suggesting that the observed sex differences may arise from divergent substrate specificity of ZDHHC7 in male and female synapses (Zaręba-Kozioł et al., 2021).

Palmitoylation plays an important role in regulating sex hormone activity, particularly through regulating sex steroid receptors, presenting another underlying mechanism for palmitoylation to act on sex differences (Pedram et al., 2007; 2012; Cohen et al., 2021). Sex steroid receptors are transcription factors that work by activating or inhibiting gene expression, with secondary activity on rapid cellular mechanisms through membrane-bound receptor subtypes (Michels and Hoppe, 2008). Notably, both the androgen and estrogen receptors undergo S-palmitoylation and N-myristoylation (Acconcia et al., 2004; Marino and Ascenzi, 2006; Marino, Ascenzi, and Acconcia, 2006; Pedram et al., 2007; La Rosa et al., 2012). Myristoylation is similar to palmitoylation, but involves the irreversible co-translational addition of the 14 carbon fatty acid myristate to N-terminal glycines (Martin, Beauchamp, and Berthiaume, 2011). Both ZDHHC7 and ZDHHC21 palmitoylate the sex receptors (Pedram et al., 2012). Functionally, palmitoylation directs the sex steroid receptors to the cell membrane, a required step for transcriptional activity (Pedram et al., 2007). At the cell membrane, sex steroid receptors can have rapid effects on cell signaling processes (Acconcia et al., 2004). Once sex steroid receptors are transported to the nuclear membrane, they can enter and bind to DNA, regulating transcription.

There is increasing evidence suggesting that palmitoylation-derived sex differences contribute to neurodegeneration. However, current evidence linking the two is limited and palmitoylation-induced sex differences need to be further explored as a source of sexually dimorphic disease phenotypes.

7 Conclusion

It will be important that palmitoylation continue to be studied in the context of neurodegenerative disease. Palmitoylation is particularly relevant in post-mitotic cells, such as neurons, due to its reversibility. This reversibility makes palmitoylation a prime candidate for treatment in neurodegenerative diseases. Importantly, palmitoylation can impact cellular functions and phenotypes in neurodegeneration through several pathways, particularly protein turnover and autophagy. Autophagy is dysregulated in many neurodegenerative diseases, and many proteins involved are predicted or confirmed to be palmitoylated. Palmitoylation also interacts with other posttranslational modifications, which is another potential target in neurodegeneration. The enzymes regulating palmitoylation and depalmitoylation are also potential targets in specific diseases. For example, DLK is required for the retrograde prodegenerative signal along axons after injury in a palmitoylation-dependent manner. As highlighted above, DLK is palmitoylated by ZDHHC17. Furthermore, inhibiting DLK kinase activity has emerged as a target in multiple neurodegenerative diseases and spinal cord injury and kinase inhibitors have moved into clinical trials. Recent work from the Thomas Group has shown that blocking DLK palmitoylation is as effective as inhibiting kinase activity itself (Holland et al., 2016), and have designed high throughput drug screens to identify novel small molecules that target DLK palmitoylation (Martin et al., 2019). Indeed, targeting kinase activity tends to lead to off-target inhibition of closely related kinases but targeting DLK palmitoylation may result in more specific inhibition. Thus, understanding the molecular mechanisms of palmitoylation in neurons is likely to lead to new therapeutics or targets in neurodegenerative diseases. Ravikumar et al., 2004, Tamura et al., 2021.

As the field of palmitoylation grows and we begin to match more palmitoylation substrates with their ZDHHCs, and better understand how the interrelationship of palmitoylation and other PTMs contribute to the pathogenesis in neurodegeneration, we will be able to fully identify novel therapeutic targets.

Author contributions

FR and DM conceived and developed the idea for the review. FR, FA, GM, LL, and DM drafted the manuscript. FR prepared Figure 1. FA did the analysis for and prepared Figure 4. GM did the analysis for and prepared Figure 2. LQ prepared Figure 3. FR and DM edited the final draft with contributions from all authors. All authors contributed to the article and approved the submitted version.

Funding

This work was supported by a Natural Sciences and Engineering Research Council (NSERC) Discovery Grant (RGPIN-2019-04617) to DM, Canadian Institutes of Health Research (CIHR 472640) Postdoctoral Award to FR, and ALS Canada Trainee Award to LL.

Acknowledgments

We would like to extend our gratitude to Shaun Sanders for comments and revisions, as well as to Andrew Doxey and Laura Hug for their feedback on Figure 2.

Conflict of interest

The authors declare that the research was conducted in the absence of any commercial or financial relationships that could be construed as a potential conflict of interest.

Publisher's note

References

Acconcia, F., Ascenzi, P., Fabozzi, G., Visca, P., and Marino, M. (2004). S-palmitoylation modulates human estrogen receptor-alpha functions. *Biochem. Biophysical Res. Commun.* 316 (3), 878–883. doi:10.1016/j.bbrc.2004.02.129

Ahtiainen, L., Luiro, K., Kauppi, M., Tyynelä, J., Kopra, O., and Jalanko, A. (2006). Palmitoyl protein thioesterase 1 (PPT1) deficiency causes endocytic defects connected to abnormal saposin processing. *Exp. Cell Res.* 312 (9), 1540–1553. doi:10.1016/j.yexcr.2006.01.034

Akerström, S., Gunalan, V., Tat Keng, C., Tan, Y.-J., and Ali, M. (2009). Dual effect of nitric oxide on SARS-CoV replication: Viral RNA production and palmitoylation of the S protein are affected. *Virology* 395 (1), 1–9. doi:10.1016/j.virol.2009.09.007

Alegre-Abarrategui, J., Christian, H., Michele, M., Lufino, P., Mutihac, R., Venda, L. L., et al. (2009). LRRK2 regulates autophagic activity and localizes to specific membrane microdomains in a novel human genomic reporter cellular model. *Hum. Mol. Genet.* 18 (21), 4022–4034. doi:10.1093/hmg/ddp346

Anand, P., and Stamler, J. S. (2012). Enzymatic mechanisms regulating protein S-nitrosylation: Implications in health and disease. *J. Mol. Med.* 90 (3), 233–244. doi:10.1007/s00109-012-0878-z

Andrew, R. J., Fernandez, C. G., Stanley, M., Jiang, H., Nguyen, P., Rice, R. C., et al. (2017). Lack of BACE1 S-palmitoylation reduces amyloid burden and mitigates memory deficits in transgenic mouse models of alzheimer's disease. *Proc. Natl. Acad. Sci.* 114 (45), E9665-E9674. doi:10.1073/pnas.1708568114

Antinone, S. E., Ghadge, G. D., Lam, T. T., Wang, L., Roos, R. P., and Green, W. N. (2013). Palmitoylation of superoxide dismutase 1 (SOD1) is increased for familial amyotrophic lateral sclerosis-linked SOD1 mutants. *J. Biol. Chem.* 288 (30), 21606–21617. doi:10.1074/jbc.M113.487231

Antinone, S. E., Ghadge, G. D., Ostrow, L. W., Roos, R. P., and Green, W. N. (2017). S-acylation of SOD1, CCS, and a stable SOD1-CCS heterodimer in human spinal cords from ALS and non-ALS subjects. *Sci. Rep.* 7 (1), 41141. doi:10.1038/srep41141

Araki, K., Kawamura, M., Suzuki, T., Matsuda, N., Kanbe, D., Ishii, K., et al. (2003). A palmitoylated RING finger ubiquitin ligase and its homologue in the brain membranes. *J. Neurochem.* 86 (3), 749–762. doi:10.1046/j.1471-4159.2003.01875.x

Arrechea, C., ConsueloGiolito, M. L., García, I. A., Soria, G., and Valdez Taubas, J. (2021). A novel yeast-based high-throughput method for the identification of protein palmitoylation inhibitors. *Open Biol.* 11 (8), 200415. doi:10.1098/RSOB.200415

Ashkenazi, A., Bento, C. F., Ricketts, T., Vicinanza, M., Siddiqi, F., Pavel, M., et al. (2017). Polyglutamine tracts regulate beclin 1-dependent autophagy. *Nature* 545 (7652), 108–111. doi:10.1038/nature22078

Baker, T. L., Booden, M. A., and Buss, J. E. (2000). S-nitrosocysteine increases palmitate turnover on ha-ras in NIH 3T3 cells. *J. Biol. Chem.* 275 (29), 22037–22047. doi:10.1074/jbc.M001813200

Bannan, B. A., Van Etten, J., Kohler, J. A., Tsoi, Y., Hansen, N. M., Sigmon, S., et al. (2008). The Drosophila protein palmitoylome: Characterizing palmitoyl-thioesterases and DHHC palmitoyl-transferases. *Fly* 2 (4), 198–214. doi:10.4161/FLY.6621

Benjannet, S., Elagoz, A., Wickham, L., Mamarbachi, M., Munzer, J. S., Basak, A., et al. (2001). Post-translational processing of beta-secretase (beta-amyloid-converting enzyme) and its ectodomain shedding. The pro- and transmembrane/cytosolic domains affect its cellular activity and amyloid-beta production. *J. Biol. Chem.* 276 (14), 10879–10887. doi:10.1074/jbc.M009899200

Berg, V., Baatout, D., Wendtner, C., Hallek, M., and Frenzel, L. P. (2016). APT1-Mediated cross-talk between palmitoylation and phosphorylation events of the BCR pathway sensitizes CLL cells towards BCR-associated kinase inhibitors. *Blood* 128 (22), 4361. doi:10.1182/blood.v128.22.4361.4361

Bhattacharyya, R., Barren, C., and DoraKovacs, M. (2013). Palmitoylation of amyloid precursor protein regulates amyloidogenic processing in lipid rafts. *J. Neurosci.* 33 (27), 11169–11183. doi:10.1523/JNEUROSCI.4704-12.2013

Bhattacharyya, R., Fenn, R. H., Barren, C., Tanzi, R. E., and Kovacs, D. M. (2016). Palmitoylated APP forms dimers, cleaved by BACE1. *PLoS ONE* 11 (11), e0166400. doi:10.1371/journal.pone.0166400

Blanc, M., David, F., Abrami, L., Migliozzi, D., Armand, F., Bürgi, J., et al. (2015). SwissPalm: Protein palmitoylation database. *F1000Research* 4, 261. doi:10.12688/f1000research.6464.1

Blaustein, M., Piegari, E., Calejman, C. M., Vila, A., Amante, A., Victoria Manese, M., et al. (2021). Akt is S-palmitoylated: A new layer of regulation for Akt. *Front. Cell Dev. Biol.* 9, 626404. doi:10.3389/fcell.2021.626404

Bononi, G., Tuccinardi, T., Rizzolio, F., and Granchi, C. (2021). α/β-Hydrolase domain (ABHD) inhibitors as new potential therapeutic options against lipid-related diseases. *J. Med. Chem.* 64 (14), 9759–9785. doi:10.1021/acs.jmedchem.1c00624

Bravo-San PedroJosé, M., Niso-Santano, M., Gómez-Sánchez, R., Pizarro-Estrella, E., Aiastui-Pujana, A., et al. (2013). The LRRK2 G2019S mutant exacerbates basal autophagy through activation of the MEK/ERK pathway. *Cell. Mol. Life Sci.* 70 (1), 121–136. doi:10.1007/s00018-012-1061-y

Bu, M., Farrer, M. J., and Khoshbouei, H. (2021). Dynamic control of the dopamine transporter in neurotransmission and homeostasis. *NPJ Park. Dis.* 7 (1), 22. doi:10.1038/s41531-021-00161-2

Buff, H., Smith, A. C., and Korey, C. A. (2007). Genetic modifiers of Drosophila palmitoyl-protein thioesterase 1-induced degeneration. *Genetics* 176 (1), 209–220. doi:10.1534/genetics.106.067983

Buglino, J. A., and Resh, M. D. (2008). Hhat is a palmitoylacyltransferase with specificity for N-palmitoylation of sonic hedgehog. *J. Biol. Chem.* 283 (32), 22076–22088. doi:10.1074/jbc.M803901200

Bullock, T. H., Bennett, M. V. L., Johnston, D., Josephson, R., Marder, E., and Douglas Fields, R. (2005). Neuroscience. The neuron doctrine, redux. *Science* 310 (5749), 791–793. doi:10.1126/science.1114394

Butland, S. L., Sanders, S. S., Schmidt, M. E., Riechers, S.-P., Lin, D. T. S., Martin, D. D., et al. (2014). The palmitoyl acyltransferase HIP14 shares a high proportion of interactors with huntingtin: Implications for a role in the pathogenesis of Huntington's disease. *Hum. Mol. Genet.* 23 (15), 4142–4160. doi:10.1093/hmg/ddu137

Caccamo, A., Maldonado, M. A., Majumder, S., Medina, D. X., Walter, H., Magrí, A., et al. (2011). Naturally secreted amyloid-β increases mammalian target of rapamycin (MTOR) activity via a PRAS40-mediated mechanism. *J. Biol. Chem.* 286 (11), 8924–8932. doi:10.1074/JBC.M110.180638

Calabrese, G., Molzahn, C., and Mayor, T. (2022). Protein interaction networks in neurodegenerative diseases: From physiological function to aggregation. *J. Biol. Chem.* 298 (7), 102062. doi:10.1016/j.jbc.2022.102062

Carlo, A.-S., Anders, N., and Willnow, T. E. (2014). Sorting receptor sortilin-a culprit in cardiovascular and neurological diseases. *J. Mol. Med.* 92 (9), 905–911. doi:10.1007/s00109-014-1152-3

Carlo, A.-S., Gustafsen, C., Guido, M., Nielsen, M., Kempa, S., Petersen, C. M., et al. (2013). The pro-neurotrophin receptor sortilin is a major neuronal APOE receptor for catabolism of amyloid-β peptide in the brain. *Mol. Neurodegener.* 8 (S1), P10. doi:10.1186/1750-1326-8-s1-p10

Cervilla-Martínez, J. F., Rodríguez-Gotor, J. J., Wypijewski, K. J., Fontán-Lozano, Á., Wang, T., Santamaría, E., et al. (2022). Altered cortical palmitoylation induces

widespread molecular disturbances in Parkinson's disease. *Int. J. Mol. Sci.* 23 (22), 14018. doi:10.3390/ijms232214018

Chen, J. J., Fan, Y., and Darren, B. (2021). Regulation of dynamic protein S-acylation. *Front. Mol. Biosci.* 8, 656440. doi:10.3389/fmolb.2021.656440

Chen, S., Zhang, X., Song, L., and Le, W. (2012). Autophagy dysregulation in amyotrophic lateral Sclerosis. *Brain Pathol.* 22, 110–116. doi:10.1111/j.1750-3639.2011.00546.x

Chen, X., Du, Z., Li, X., Wang, L., Wang, F., Shi, W., et al. (2016). Protein palmitoylation regulates neural stem cell differentiation by modulation of EID1 activity. *Mol. Neurobiol.* 53 (8), 5722–5736. doi:10.1007/s12035-015-9481-y

Cheng, H., Vetrivel, K. S., Drisdel, R. C., Meckler, X., Gong, P., Yoon Leem, J., et al. (2009). S-palmitoylation of γ-secretase subunits nicastrin and aph-1. *J. Biol. Chem.* 284 (3), 1373–1384. doi:10.1074/jbc.M806380200

Cho, E., and Park, M. (2016). Palmitoylation in alzheimer's disease and other neurodegenerative diseases. *Pharmacol. Res.* 111, 133–151. doi:10.1016/j.phrs.2016.06.008

Chu, C.-W., Hou, F., Zhang, J., Phu, L., Loktev, A. V., Kirkpatrick, D. S., et al. (2011). A novel acetylation of β-tubulin by san modulates microtubule polymerization via down-regulating tubulin incorporation. *Mol. Biol. Cell* 22 (4), 448–456. doi:10.1091/mbc.E10-03-0203

Chu-LaGraff, Q., Blanchette, C., O'Hern, P., and Denefrio, C. (2010). The Batten disease Palmitoyl Protein Thioesterase 1 gene regulates neural specification and axon connectivity during Drosophila embryonic development. *PLoS ONE* 5 (12), e14402. doi:10.1371/journal.pone.0014402

Cirulli, E. T., Lasseigne, B. N., Petrovski, S., Sapp, P. C. P. A. D., Claire, S. L., et al. (2015). Exome sequencing in amyotrophic lateral Sclerosis identifies risk genes and pathways. *Science* 347 (6229), 1436–1441. doi:10.1126/science.aaa3650

Cohen, D. J., ElBaradie, K., Boyan, B. D., and Schwartz, Z. (2021). Sex-specific effects of 17β-estradiol and dihydrotestosterone (DHT) on growth plate chondrocytes are dependent on both ERα and ERβ and require palmitoylation to translocate the receptors to the plasma membrane. *Biochimica Biophysica Acta (BBA) - Mol. Cell Biol. Lipids* 1866 (12), 159028. doi:10.1016/j.bbalip.2021.159028

Corpas, F. J., Begara-Morales, J. C., Sánchez-Calvo, B., Chaki, M., and Barroso, J. B. (2015). "Nitration and S-nitrosylation: Two post-translational modifications (PTMs) mediated by reactive nitrogen species (RNS) and their role in signalling processes of plant cells," in *Reactive oxygen and Nitrogen species signaling and communication in Plants* (Berlin, Germany: Springer International Publishing), 267–281.

Deleyto-Seldas, N., and Efeyan, A. (2021). The MTOR–autophagy Axis and the control of metabolism. *Front. Cell Dev. Biol.* 9, 1519. doi:10.3389/fcell.2021.655731

Didonna, A., and Benetti, F. (2016). Post-translational modifications in neurodegeneration. *AIMS Biophys.* 3 (1), 27–49. doi:10.3934/biophy.2016.1.27

Dore, K., Carrico, Z., Alfonso, S., Marino, M., Koymans, K., Kessels, H. W., et al. (2021). PSD-95 protects synapses from β-amyloid. *Cell Rep.* 35 (9), 109194. doi:10.1016/j.celrep.2021.109194

Dumaresq-Doiron, K., Jules, F., and Lefrancois, S. (2013). Sortilin turnover is mediated by ubiquitination. *Biochem. Biophys. Res. Commun.* 433 (1), 90–95. doi:10.1016/j.bbrc.2013.02.059

Duncan, J. A., and Gilman, A. G. (1998). A cytoplasmic acyl-protein thioesterase that removes palmitate from G protein alpha subunits and p21(RAS). *J. Biol. Chem.* 273 (25), 15830–15837. doi:10.1074/jbc.273.25.15830

Edmonds, M. J., and Morgan, A. (2014). A systematic analysis of protein palmitoylation in Caenorhabditis elegans. *BMC Genomics* 15, 1–16. doi:10.1186/1471-2164-15-841

Ehrnhoefer, D. E., Martin, D. D. O., Qiu, X., Ladha, S., Caron, N. S., Skotte, N. H., et al. (2018). Preventing mutant huntingtin proteolysis and intermittent fasting promote autophagy in models of Huntington disease. *Acta Neuropathol. Commun.* 6 (1), 16. doi:10.1186/s40478-018-0518-0

El-Husseini, E.-D. A., Schnell, E., Dakoji, S., Neal, S., Zhou, Q., et al. (2002). Synaptic strength regulated by palmitate cycling on PSD-95. *Cell* 108 (6), 849–863. doi:10.1016/S0092-8674(02)00683-9

Elsheikh, S. S. M., Chimusa, E. R., Mulder, N. J., and Crimi, A. (2020). Genome-wide association study of brain connectivity changes for alzheimer's disease. *Sci. Rep.* 10 (1), 1433. doi:10.1038/s41598-020-58291-1

Fairbank, M., Huang, K., El-Husseini, A., and Ivan, R. N. (2012). RING finger palmitoylation of the endoplasmic reticulum Gp78 E3 ubiquitin ligase. *FEBS Lett.* 586 (16), 2488–2493. doi:10.1016/j.febslet.2012.06.011

Fukata, M., Fukata, Y., Adesnik, H., Nicoll, R. A., and Bredt, D. S. (2004). Identification of PSD-95 palmitoylating enzymes. *Neuron* 44 (6), 987–996. doi:10.1016/J.NEURON.2004.12.005

Gan, K. A., Khan, K., and Gitcho, M. A. (2015). P2-039: Progranulin missense mutations causing frontotemporal lobar degeneration misregulate endogenous TDP-43. *Alzheimers* 11, P496. doi:10.1016/j.jalz.2015.06.575

Gao, X., and Hannoush, R. N. (2018). A decade of click chemistry in protein palmitoylation: Impact on Discovery and new Biology. *Cell Chem. Biol.* 25 (3), 236–246. doi:10.1016/j.chembiol.2017.12.002

García-Cardeña, G., Oh, P., Liu, J., Schnitzer, J. E., and Sessa, W. C. (1996). Targeting of nitric oxide synthase to endothelial cell caveolae via palmitoylation: Implications for nitric oxide signaling. *Proc. Natl. Acad. Sci. U. S. A.* 93 (13), 6448–6453. doi:10.1073/pnas.93.13.6448

Gauthier-Kemper, A., Igaev, M., Sündermann, F., Janning, D., Brühmann, J., Moschner, K., et al. (2014). Interplay between phosphorylation and palmitoylation mediates plasma membrane targeting and sorting of GAP43. *Mol. Biol. Cell* 25 (21), 3284–3299. doi:10.1091/mbc.E13-12-0737

Gelman, A., Rawet-Slobodkin, M., and Elazar, Z. (2015). Huntingtin facilitates selective autophagy. *Nat. Cell Biol.* 17 (3), 214–215. doi:10.1038/ncb3125

Gorenberg, E. L., Tieze, S. M., Yücel, B., Zhao, H. R., Chou, V., Tomita, S., et al. (2022). Identification of substrates of palmitoyl protein thioesterase 1 highlights roles of depalmitoylation in disulfide bond formation and synaptic function. *PLOS Biol.* 20 (3), e3001590. doi:10.1371/journal.pbio.3001590

Greaves, J., and Chamberlain, L. H. (2007). Palmitoylation-dependent protein sorting. *J. Cell Biol.* 176 (3), 249–254. doi:10.1083/jcb.200610151

Hanamsagar, R., and Bilbo, S. D. (2016). Sex differences in neurodevelopmental and neurodegenerative disorders: Focus on microglial function and neuroinflammation during development. *J. Steroid Biochem. Mol. Biol.* 160, 127–133. doi:10.1016/j.jsbmb.2015.09.039

Hayashi, T. (2021). Evolutionarily established palmitoylation-dependent regulatory mechanisms of the vertebrate glutamatergic synapse and diseases caused by their disruption. *Front. Mol. Neurosci.* 14, 796912. doi:10.3389/fnmol.2021.796912

Heras-Sandoval, D., JazminPérez-Rojas, M., Hernández-Damián, J., and Pedraza-Chaverri, J. (2014). The role of PI3K/AKT/MTOR pathway in the modulation of autophagy and the clearance of protein aggregates in neurodegeneration. *Cell. Signal.* 26, 2694–2701. doi:10.1016/j.cellsig.2014.08.019

Hess, D. T., Patterson, S. I., Smith, D. S., and Skene, J. H. (1993). Neuronal growth cone collapse and inhibition of protein fatty acylation by nitric oxide. *Nature* 366 (6455), 562–565. doi:10.1038/366562a0

Hess, T., Douglas, T., and Stamler, J. S. (2012). Regulation by S-nitrosylation of protein post-translational modification. *J. Biol. Chem.* 287 (7), 4411–4418. doi:10.1074/jbc.R111.285742

Hickey, A. J., Chotkowski, H. L., Singh, N., Ault, J. G., Korey, C. A., MacDonald, M. E., et al. (2006). Palmitoyl-protein thioesterase 1 deficiency in *Drosophila melanogaster* causes accumulation of abnormal storage material and reduced life span. *Genetics* 172 (4), 2379–2390. doi:10.1534/genetics.105.053306

Ho, G. P. H., Selvakumar, B., Mukai, J., Lynda, D. H., Wang, Y., Gogos, J. A., et al. (2011). S-nitrosylation and S-palmitoylation reciprocally regulate synaptic targeting of PSD-95. *Neuron* 71 (1), 131–141. doi:10.1016/j.neuron.2011.05.033

Hohoff, C., Zhang, M., Oliver, A., Kravchenko, M., Buschert, J., Kerkenberg, N., et al. (2019). Deficiency of the palmitoyl acyltransferase ZDHHC7 impacts brain and behavior of mice in a sex-specific manner. *Brain Struct. Funct.* 224 (6), 2213–2230. doi:10.1007/s00429-019-01898-6

Holland, S. M., Collura, K. M., Ketschek, A., Noma, K., Ferguson, T. A., Jin, Y., et al. (2016). Palmitoylation controls DLK localization, interactions and activity to ensure effective axonal injury signaling. *Proc. Natl. Acad. Sci.* 113 (3), 763–768. doi:10.1073/pnas.1514123113

Hornemann, T. (2015). Palmitoylation and depalmitoylation defects. *J. Inherit. Metabolic Dis.* 38 (1), 179–186. doi:10.1007/s10545-014-9753-0

Hou, H., Arun, T., Meiringer, C., Subramanian, K., Ungermann, C., and Peter, J. (2009). Analysis of DHHC acyltransferases implies overlapping substrate specificity and a two-step reaction mechanism. *Traffic* 10 (8), 1061–1073. doi:10.1111/j.1600-0854.2009.00925.x

Hu, F., Padukkavidana, T., Vægter, C. B., Brady, O. A., Zheng, Y., Mackenzie, I. R., et al. (2010). Sortilin-mediated endocytosis determines levels of the frontotemporal dementia protein, progranulin. *Neuron* 68 (4), 654–667. doi:10.1016/j.neuron.2010.09.034

Huang, K., Sanders, S. S., Kang, R., Carroll, J. B., Sutton, L., Wan, J., et al. (2011). Wild-type HTT modulates the enzymatic activity of the neuronal palmitoyl transferase HIP14. *Hum. Mol. Genet.* 20 (17), 3356–3365. doi:10.1093/hmg/ddr242

Huang, K., Yanai, A., Kang, R., Arstikaitis, P., Singaraja, R. R., Metzler, M., et al. (2004). Huntingtin-interacting protein HIP14 is a palmitoyl transferase involved in palmitoylation and trafficking of multiple neuronal proteins. *Neuron* 44 (6), 977–986. doi:10.1016/j.neuron.2004.11.027

Iacoangeli, A., Tian, L., Khleifat, A., Jones, A. R., Opie-Martin, S., Jonathan, R., et al. (2020). Genome-wide meta-analysis finds the ACSL5-ZDHHC6 locus is associated with ALS and links weight loss to the disease genetics. *Cell Rep.* 33 (4), 108323. doi:10.1016/j.celrep.2020.108323

Iwakiri, Y., Satoh, A., Chatterjee, S., Toomre, D. K., Chalouni, C. M., Fulton, D., et al. (2006). Nitric oxide synthase generates nitric oxide locally to regulate compartmentalized protein S-nitrosylation and protein trafficking. *Proc. Natl. Acad. Sci. U. S. A.* 103 (52), 19777–19782. doi:10.1073/pnas.0605907103

Ji, Y., Bachschmid, M. M., Costello, C. E., and Cheng, L. (2016). S- to N-palmitoyl transfer during proteomic sample preparation. *J. Am. Soc. Mass Spectrom.* 27 (4), 677–685. doi:10.1007/s13361-015-1319-3

Keller, C. A., Xu, Y., Panzanelli, P., Martin, M. L., Alldred, M., Sassoè-Pognetto, M., et al. (2004). The gamma2 subunit of GABA(A) receptors is a substrate for palmitoylation by GODZ. *J. Neurosci.* 24 (26), 5881–5891. doi:10.1523/JNEUROSCI.1037-04.2004

Kim, S.-J., Zhang, Z., Lee, Yi-C., and Mukherjee, A. B. (2006). Palmitoyl-protein thioesterase-1 deficiency leads to the activation of caspase-9 and contributes to rapid neurodegeneration in INCL. *Hum. Mol. Genet.* 15 (10), 1580–1586. doi:10.1093/hmg/ddl078

Komander, D., and Rape, M. (2012). The ubiquitin code. *Annu. Rev. Biochem.* 81 (1), 203–229. doi:10.1146/annurev-biochem-060310-170328

Kulkarni, V. V., and Maday, S. (2018). Compartment-specific dynamics and functions of autophagy in neurons: Dynamics and functions of neuronal autophagy. *Dev. Neurobiol.* 78 (3), 298–310. doi:10.1002/dneu.22562

Kumar-Singh, S. (2011). Progranulin and TDP-43: Mechanistic links and future directions. *J. Mol. Neurosci.* 45 (3), 561–573. doi:10.1007/s12031-011-9625-0

La Rosa, P., Pesiri, V., Guy, L., Marino, M., and Acconcia, F. (2012). Palmitoylation regulates 17β-estradiol-induced estrogen receptor-α degradation and transcriptional activity. *Mol. Endocrinol.* 26 (5), 762–774. doi:10.1210/me.2011-1208

Lastres-Becker, I., Gracia, P., Arribas-Blázquez, M., Maestro, I., Borrego-Hernández, D., Boya, P., et al. (2021). Molecular alterations in sporadic and sod1-als immortalized lymphocytes: Towards a personalized therapy. *Int. J. Mol. Sci.* 22 (6), 3007. doi:10.3390/ijms22063007

Le Guerroué, F., and Youle, R. J. (2021). Ubiquitin signaling in neurodegenerative diseases: An autophagy and proteasome perspective. *Cell Death Differ.* 28 (2), 439–454. doi:10.1038/s41418-020-00667-x

LeDizet, M., and Piperno, G. (1987). Identification of an acetylation site of chlamydomonas alpha-tubulin. *Proc. Natl. Acad. Sci. U. S. A.* 84 (16), 5720–5724. doi:10.1073/pnas.84.16.5720

Lemarié, F. L., Caron, N. S., Sanders, S. S., Schmidt, M. E., Nguyen, Y. T. N., Seunghyun, Ko, et al. (2021). Rescue of aberrant huntingtin palmitoylation ameliorates mutant huntingtin-induced toxicity. *Neurobiol. Dis.* 158, 105479. doi:10.1016/j.nbd.2021.105479

Lemarié, F. L., Sanders, S. S., Nguyen, Y. T. N., Martin, D. D. O., and Hayden, M. R. (2023). Full-length huntingtin is palmitoylated at multiple sites and post-translationally myristoylated following caspase-cleavage. *Front. Physiology* 14, 1086112. doi:10.3389/fphys.2023.1086112

Lemire, G., Ito, Y. A., Marshall, A. E., Chrestian, N., Stanley, V., Brady, L., et al. (2021). ABHD16A deficiency causes a complicated form of hereditary spastic paraplegia associated with intellectual disability and cerebral anomalies. *Am. J. Hum. Genet.* 108 (10), 2017–2023. doi:10.1016/j.ajhg.2021.09.005

Li, A., Zhang, X., and Le, W. (2008). Altered macroautophagy in the spinal cord of SOD1 mutant mice. *Autophagy* 4 (3), 290–293. doi:10.4161/auto.5524

Li, F., Todd, M., Pittman, R. N., and Chakravarti, D. (2002). Ataxin-3 is a histone-binding protein with two independent transcriptional corepressor activities. *J. Biol. Chem.* 277 (47), 45004–45012. doi:10.1074/jbc.M205259200

Linder, M. E., and Deschenes, R. J. (2007). Palmitoylation: Policing protein stability and traffic. *Nat. Rev. Mol. Cell Biol.* 8 (1), 74–84. doi:10.1038/nrm2084

Lin, D. T. S., and Conibear, E. (2015). ABHD17 proteins are novel protein depalmitoylases that regulate N-ras palmitate turnover and subcellular localization. *ELife* 4, e11306. doi:10.7554/eLife.11306

Lobo, S., Greentree, W. K., Linder, M. E., and Deschenes, R. J. (2002). Identification of a ras palmitoyltransferase in Saccharomyces cerevisiae. *J. Biol. Chem.* 277 (43), 41268–41273. doi:10.1074/JBC.M206573200

Lothrop, A. P., Adam, P., Torres, M. P., and Fuchs, S. M. (2013). Deciphering post-translational modification codes. *FEBS Lett.* 587 (8), 1247–1257. doi:10.1016/j.febslet.2013.01.047

Lu, B., and Vogel, H. (2009). *Drosophila* models of neurodegenerative diseases. *Annu. Rev. Pathology Mech. Dis.* 4 (1), 315–342. doi:10.1146/annurev.pathol.3.121806.151529

Ma, S., Attarwala, I. Y., and XiangXie, Q. (2019). SQSTM1/P62: A potential target for neurodegenerative disease. *ACS Chem. Neurosci.* 10, 2094–2114. doi:10.1021/acschemneuro.8b00516

Mackay-Sim, A. (2021). Hereditary spastic paraplegia: From genes, cells and networks to novel pathways for drug Discovery. *Brain Sci.* 11 (3), 403. doi:10.3390/brainsci11030403

Madej, T., Lanczycki, C. J., Zhang, D., Thiessen, P. A., Geer, R. C., Marchler-Bauer, A., et al. (2014). MMDB and VAST+: Tracking structural similarities between macromolecular complexes. *Nucleic Acids Res.* 42 (D1), D297–D303. doi:10.1093/nar/gkt1208

Main, A., and Fuller, W. (2022). Protein S-palmitoylation: Advances and challenges in studying a therapeutically important lipid modification. *FEBS J.* 289 (4), 861–882. doi:10.1111/febs.15781

Man, W. K., Tahirbegi, B., Vrettas, M. D., Preet, S., Ying, L., Vendruscolo, M., et al. (2021). The docking of synaptic vesicles on the presynaptic membrane induced by α-synuclein is modulated by lipid composition. *Nat. Commun.* 12 (1), 927. doi:10.1038/s41467-021-21027-4

Marino, M., Ascenzi, P., and Acconcia, F. (2006). S-palmitoylation modulates estrogen receptor alpha localization and functions. *Steroids* 71 (4), 298–303. doi:10.1016/j.steroids.2005.09.011

Marino, M., and Ascenzi, P. (2006). Steroid hormone rapid signaling: The pivotal role of S-palmitoylation. *IUBMB Life* 58 (12), 716–719. doi:10.1080/15216540601019485

Martin, B. R., and Cravatt, B. F. (2009). Large-scale profiling of protein palmitoylation in mammalian cells. *Nat. Methods* 6 (2), 135–138. doi:10.1038/nmeth.1293

Martin, D. D. O., Beauchamp, E., and Berthiaume, L. G. (2011). Post-translational myristoylation: Fat matters in cellular life and death. *Biochimie* 93 (1), 18–31. doi:10.1016/j.biochi.2010.10.018

Martin, D. D. O., Heit, R. J., Yap, M. C., Davidson, M. W., Hayden, M. R., and Berthiaume, L. G. (2014). Identification of a post-translationally myristoylated autophagy-inducing domain released by caspase cleavage of huntingtin. *Hum. Mol. Genet.* 23 (12), 3166–3179. doi:10.1093/hmg/ddu027

Martin, D. D. O., Kanuparthi, P. S., Holland, S. M., Sanders, S. S., Jeong, H. K., Einarson, M. B., et al. (2019). Identification of novel inhibitors of DLK palmitoylation and signaling by high content screening. *Sci. Rep.* 9 (1), 3632. doi:10.1038/s41598-019-39968-8

Martin, D. D. O., Ladha, S., Ehrnhoefer, D. E., and Hayden., M. R. (2015). Autophagy in Huntington disease and huntingtin in autophagy. *Trends Neurosci.* 38, 26–35. doi:10.1016/j.tins.2014.09.003

Martinez-Vicente, M., Talloczy, Z., Wong, E., Tang, G., Koga, H., Kaushik, S., et al. (2010). Cargo recognition failure is responsible for inefficient autophagy in Huntington's disease. *Nat. Neurosci.* doi:10.1038/nn.2528

Matt, L., Kim, K., Chowdhury, D., and Hell, J. W. (2019). Role of palmitoylation of postsynaptic proteins in promoting synaptic plasticity. *Front. Mol. Neurosci.* 12, 8. doi:10.3389/fnmol.2019.00008

Meckler, X., Roseman, J., Das, P., Cheng, H., Pei, S., Keat, M., et al. (2010). Reduced Alzheimer's disease ß-amyloid deposition in transgenic mice expressing S-palmitoylation-deficient APH1aL and nicastrin. *J. Neurosci.* 30 (48), 16160–16169. doi:10.1523/JNEUROSCI.4436-10.2010

Menzies, F. M., Fleming, A., Caricasole, A., Bento, C. F., Andrews, S. P., Ashkenazi, A., et al. (2017). Autophagy and neurodegeneration: Pathogenic mechanisms and therapeutic opportunities. *Neuron* 93, 1015–1034. doi:10.1016/j.neuron.2017.01.022

Michels, G., and Hoppe, U. C. (2008). Rapid actions of androgens. *Front. Neuroendocrinol.* 29 (2), 182–198. doi:10.1016/j.yfrne.2007.08.004

Milde, S., and Coleman, M. P. (2014). Identification of palmitoyltransferase and thioesterase enzymes that control the subcellular localization of axon survival factor nicotinamide mononucleotide adenylyltransferase 2 (NMNAT2). *J. Biol. Chem.* 289 (47), 32858–32870. doi:10.1074/jbc.M114.582338

Mitchell, D. A., Vasudevan, A., Linder, M. E., and Deschenes, R. J. (2006). Thematic review series: Lipid posttranslational modifications. Protein palmitoylation by a family of DHHC protein S-acyltransferases. *J. Lipid Res.* 47 (6), 1118–1127. doi:10.1194/jlr.R600007-JLR200

Miyake, N., Silva, S., Troncoso, M. ., Okamoto, N., Andachi, Y., Kato, M., et al. (2022). A homozygous *ABHD16A* variant causes a complex hereditary spastic paraplegia with developmental delay, absent speech, and characteristic face. *Clin. Genet.* 101 (3), 359–363. doi:10.1111/cge.14097

Mizumaru, C., Saito, Y., Ishikawa, T., Yoshida, T., Yamamoto, T., Nakaya, T., et al. (2009). Suppression of APP-containing vesicle trafficking and production of β-amyloid by AID/DHHC-12 protein. *J. Neurochem.* 111 (5), 1213–1224. doi:10.1111/j.1471-4159.2009.06399.x

Moritz, A. E., Rastedt, D. E., Stanislowski, D. J., Shetty, M., Smith, M. A., Vaughan, R. A., et al. (2015). Reciprocal phosphorylation and palmitoylation control dopamine transporter kinetics. *J. Biol. Chem.* 290 (48), 29095–29105. doi:10.1074/jbc.M115.667055

Motoki, K., Kume, H., Oda, A., Tamaoka, A., Ai, H., Kametani, F., et al. (2012). Neuronal B-amyloid generation is independent of lipid raft association of B-secretase BACE1: Analysis with a palmitoylation-deficient mutant. *Brain Behav.* 2 (3), 270–282. doi:10.1002/brb3.52

Nah, J., Yuan, J., and Jung, Y. K. (2015). Autophagy in neurodegenerative diseases: From mechanism to therapeutic approach. *Mol. Cells* 38, 381–389. doi:10.14348/molcells.2015.0034

Nakamura, T., Prikhodko, O. A., Pirie, E., Nagar, S., Akhtar, M. W., Oh, C.-Ki, et al. (2015). Aberrant protein S-nitrosylation contributes to the pathophysiology of neurodegenerative diseases. *Neurobiol. Dis.* 84, 99–108. doi:10.1016/j.nbd.2015.03.017

Nakamura, T., Tu, S., Akhtar, M. W., CarmenSunico, R., Okamoto, S.-I., and Lipton, S. A. (2013). Aberrant protein S-nitrosylation in neurodegenerative diseases. *Neuron* 78 (4), 596–614. doi:10.1016/j.neuron.2013.05.005

Nasseri, G. G., Matin, N., AngelaWild, R., Tosefsky, K., Flibotte, S., Stacey, R. G., et al. (2022). Synaptic activity–dependent changes in the hippocampal palmitoylome. *Sci. Signal.* 15 (763), eadd2519. doi:10.1126/scisignal.add2519

Navarro-Lérida, I., Corvi, M. M., Alvarez Barrientos, A., Gavilanes, F., Berthiaume, L. G., and Rodríguez-Crespo, I. (2004). Palmitoylation of inducible nitric-oxide synthase at cys-3 is required for proper intracellular traffic and nitric oxide synthesis. *J. Biol. Chem.* 279 (53), 55682–55689. doi:10.1074/jbc.M406621200

Nekooki-Machida, Y., and Hagiwara, H. (2020). Role of tubulin acetylation in cellular functions and diseases. *Med. Mol. Morphol.* 53 (4), 191–197. doi:10.1007/s00795-020-00260-8

Nitta, Y., and Sugie, A. (2022). Studies of neurodegenerative diseases using *Drosophila* and the development of novel approaches for their analysis. *Fly* 16 (1), 275–298. doi:10.1080/19336934.2022.2087484

Niu, J., Sanders, S. S., Jeong, H.-K., Holland, S. M., Sun, Y., Collura, K. M., et al. (2020). Coupled control of distal axon integrity and somal responses to axonal damage by the palmitoyl acyltransferase ZDHHC17. *Cell Rep.* 33 (7), 108365. doi:10.1016/j.celrep.2020.108365

Nixon, R. A., Wegiel, J., Kumar, A., Yu, W. H., Peterhoff, C., Cataldo, A., et al. (2005). Extensive involvement of autophagy in alzheimer disease: An immuno-electron microscopy study. *J. Neuropathology Exp. Neurology* 64 (2), 113–122. doi:10.1093/jnen/64.2.113

Nogales, E., Wolf, S. G., and Downing, K. H. (1998). Structure of the alpha beta tubulin dimer by electron crystallography. *Nature* 391 (6663), 199–203. doi:10.1038/34465

Nthiga, T. M., Shrestha, B. K., Bruun, J.-A., Larsen, K. B., Lamark, T., and Johansen, T. (2021). Regulation of Golgi turnover by CALCOCO1-mediated selective autophagy. *J. Cell Biol.* 220 (6), e202006128. doi:10.1083/jcb.202006128

Numajiri, N., Takasawa, K., Nishiya, T., Tanaka, H., Ohno, K., Hayakawa, W., et al. (2011). On-off system for PI3-kinase-akt signaling through S-nitrosylation of phosphatase with sequence homology to Tensin (PTEN). *Proc. Natl. Acad. Sci. U. S. A.* 108 (25), 10349–10354. doi:10.1073/pnas.1103503108

Ochaba, J., Lukacsovich, T., George, C., Zheng, S., Margulis, J., Salazar, L., et al. (2014). Potential function for the huntingtin protein as a scaffold for selective autophagy. *Proc. Natl. Acad. Sci. U. S. A.* 111 (47), 16889–16894. doi:10.1073/pnas.1420103111

Oh, C.-K., Dolatabadi, N., Cieplak, P., Diaz-Meco, M. T., Moscat, J., Nolan, J. P., et al. (2022). S-nitrosylation of P62 inhibits autophagic flux to promote α-synuclein secretion and spread in Parkinson's disease and Lewy body dementia. *J. Neurosci.* 42, 3011–3024. doi:10.1523/JNEUROSCI.1508-21.2022

Ohyama, T., Verstreken, P., Ly, C. V., Rosenmund, T., Rajan, A., Tien, A. C., et al. (2007). Huntingtin-interacting protein 14, a palmitoyl transferase required for exocytosis and targeting of CSP to synaptic vesicles. *J. Cell Biol.* 179 (7), 1481–1496. doi:10.1083/JCB.200710061

Page, K. M., Rothwell, S. W., and Dolphin, A. C. (2016). The CaVβ subunit protects the I-ii loop of the voltage-gated calcium channel CaV2.2 from proteasomal degradation but not oligoubiquitination. *J. Biol. Chem.* 291 (39), 20402–20416. doi:10.1074/jbc.M116.737270

Pang, S. Y. Y, Lo, R. C. N., Ho, P. W. L., Hui, F. L., Chang, E. S. S., Leung, C.T., et al. (2022). LRRK2, GBA and their interaction in the regulation of autophagy: Implications on therapeutics in Parkinson's disease. *Transl. Neurodegener.* 11 (1), 1–14. doi:10.1186/S40035-022-00281-6

Pedram, A., Razandi, M., Deschenes, R. J., and Levin, E. R. (2012). DHHC-7 and -21 are palmitoylacyltransferases for sex steroid receptors. *Mol. Biol. Cell* 23 (1), 188–199. doi:10.1091/mbc.e11-07-0638

Pedram, A., Razandi, M., Sainson, R.C. A., Kim, J. K., Hughes, C. C., and Levin., E. R. (2007). A conserved mechanism for steroid receptor translocation to the plasma membrane. *J. Biol. Chem.* 282 (31), 22278–22288. doi:10.1074/jbc.M611877200

Petropavlovskiy, A. A., Kogut, J. A., Leekha, A., Townsend, C. A., and Sanders, S. S. (2021). A sticky situation: Regulation and function of protein palmitoylation with a spotlight on the axon and axon initial segment. *Neuronal Signal.* 5 (4), NS20210005–22. doi:10.1042/NS20210005

Philippe, J. M., and Jenkins, P. M. (2019). Spatial organization of palmitoyl acyl transferases governs substrate localization and function. *Mol. Membr. Biol.* 35 (1), 60–75. doi:10.1080/09687688.2019.1710274

Politis, E. G., Roth, A. F., and Davis, N. G. (2005). Transmembrane topology of the protein palmitoyl transferase Akr1. *J. Biol. Chem.* 280 (11), 10156–10163. doi:10.1074/jbc.M411946200

Porcellato, E., González-Sánchez, J. C., Ahlmann-Eltze, C., Elsakka, M. A., Shapira, I., et al. (2022). The S-palmitoylome and DHHC-PAT interactome of Drosophila melanogaster S2R+ cells indicate a high degree of conservation to mammalian palmitoylomes. *PloS One* 17 (8), e0261543. doi:10.1371/JOURNAL.PONE.0261543

Quatela, S. E., PamelaSung, J., Ahearn, I. M., Bivona, T. G., and Philips, M. R. (2008). Analysis of K-ras phosphorylation, translocation, and induction of apoptosis. *Methods Enzym.* 439, 87–102. doi:10.1016/S0076-6879(07)00407-7

Rai, S. N., Dilnashin, H., Birla, H., Singh, S. S., Zahra, W., Singh Rathore, A., et al. (2019). The role of PI3K/Akt and ERK in neurodegenerative disorders. *Neurotox. Res.* 35, 775–795. doi:10.1007/s12640-019-0003-y

Ravikumar, B., Vacher, C., Berger, Z., Davies, J. E., Luo, S., Oroz, L. G., et al. (2004). Inhibition of MTOR induces autophagy and reduces toxicity of polyglutamine expansions in fly and mouse models of Huntington disease. *Nat. Genet.* 36 (6), 585–595. doi:10.1038/ng1362

Ren, Ru-J., Dammer, E. B., Wang, G., Seyfried, N. T., and Allan, I. L. (2014). Proteomics of protein post-translational modifications implicated in neurodegeneration. *Transl. Neurodegener.* 3 (1), 23. doi:10.1186/2047-9158-3-23

Ren, W., Jhala, U. S., and Du, K. (2013). Proteomic analysis of protein palmitoylation in adipocytes. *Adipocyte* 2 (1), 17–28. doi:10.4161/adip.22117

Resh, M. D. (1999). Fatty acylation of proteins: New insights into membrane targeting of myristoylated and palmitoylated proteins. *Biochimica Biophysica Acta (BBA) - Mol. Cell Res.* 1451 (1), 1–16. doi:10.1016/S0167-4889(99)00075-0

Resh, M. D. (2016). Fatty acylation of proteins: The long and the short of it. *Prog. Lipid Res.* 63, 120–131. doi:10.1016/j.plipres.2016.05.002

Roth, A. F., Feng, Y., Chen, L., and Davis, N. G. (2002). The yeast DHHC cysteine-rich domain protein Akr1p is a palmitoyl transferase. *J. Cell Biol.* 159 (1), 23–28. doi:10.1083/JCB.200206120

Roth, A. F., Junmei, W., Bailey, A. O., Sun, B., JasonKuchar, A., Green, W. N., et al. (2006). Global analysis of protein palmitoylation in yeast. *Cell* 125 (5), 1003–1013. doi:10.1016/J.CELL.2006.03.042

Rubino, E., Boschi, S., Roveta, F., Marcinnò, A., Cermelli, A., Borghese, C., et al. (2022). Investigating P62 concentrations in cerebrospinal fluid of patients with dementia: A potential autophagy biomarker *in vivo*? *Brain Sci.* 12 (10), 1414. doi:10.3390/brainsci12101414

Rui, N. Y., Ning, Y., Xu, Z., Patel, B., Chen, Z., Chen, D., et al. (2015). Huntingtin functions as a scaffold for selective macroautophagy. *Nat. Cell Biol.* 17 (3), 262–275. doi:10.1038/ncb3101

Sadhukhan, T., Bagh, M. B., Appu, A. P., Mondal, A., Zhang, W., Liu, A., et al. (2021). In a mouse model of INCL reduced S-palmitoylation of cytosolic thioesterase APT1 contributes to microglia proliferation and neuroinflammation. *J. Inherit. Metabolic Dis.* 44 (4), 1051–1069. doi:10.1002/jimd.12379

Sadowski, M., Suryadinata, R., Tan, A. R., Roesley, S. N. A., and Sarcevic, B. (2012). Protein monoubiquitination and polyubiquitination generate structural diversity to control distinct biological processes. *IUBMB Life* 64 (2), 136–142. doi:10.1002/iub.589

Saegusa, H., Xu, L., Wang, X., Kayakiri, M., and Tanabe, T. (2020). Knockdown of microglial Cav2.2 N-type voltage-dependent Ca2+ channel ameliorates behavioral deficits in a mouse model of Parkinson's disease. *FEBS Lett.* 594 (17), 2914–2922. doi:10.1002/1873-3468.13853

Salaun, C., Greaves, J., and Chamberlain, L. H. (2010). The intracellular dynamic of protein palmitoylation. *J. Cell Biol.* 191 (7), 1229–1238. doi:10.1083/jcb.201008160

Saleem, A. N., Yen-Hui, C., Jin Baek, H., Hsiao, Ya-W., Huang, H.-W., Kao, H.-J., et al. (2010). Mice with alopecia, osteoporosis, and systemic amyloidosis due to mutation in Zdhhc13, a gene coding for palmitoyl acyltransferase. *PLoS Genet.* 6 (6), e1000985. doi:10.1371/journal.pgen.1000985

Sánchez-Danés, A., Richaud-Patin, Y., Carballo-Carbajal, I., Jiménez-Delgado, S., Caig, C., Mora, S., et al. (2012). Disease-specific phenotypes in dopamine neurons from human IPS-based models of genetic and sporadic Parkinson's disease. *EMBO Mol. Med.* 4 (5), 380–395. doi:10.1002/emmm.201200215

Sanders, S. S., Simone, F. I., and Thomas, G. M. (2019). MTORC1 signaling is palmitoylation-dependent in hippocampal neurons and non-neuronal cells and involves dynamic palmitoylation of LAMTOR1 and MTOR. *Front. Cell. Neurosci.* 13, 115. doi:10.3389/fncel.2019.00115

Sanders, S. S., Martin, D. D. O., Butland, S. L., Lavallée-Adam, M., Calzolari, D., Kay, C., et al. (2015). Curation of the mammalian palmitoylome indicates a pivotal role for palmitoylation in diseases and disorders of the nervous system and cancers. *PLOS Comput. Biol.* 11 (8), e1004405. doi:10.1371/journal.pcbi.1004405

Sanders, S. S., Parsons, M. P., Mui, K. K. N., Southwell, A. L., Franciosi, S., Cheung, D., et al. (2016). Sudden death due to paralysis and synaptic and behavioral deficits when hip14/zdhhc17 is deleted in adult mice. *BMC Biol.* 14 (1), 108. doi:10.1186/s12915-016-0333-7

Santavuori, P. (1988). Neuronal ceroid-lipofuscinoses in childhood. *Brain Dev.* 10 (2), 80–83. doi:10.1016/S0387-7604(88)80075-5

Santiago-Mujika, E., Luthi-Carter, R., Giorgini, F., Kalaria, R. N., and Mukaetova-Ladinska, E. B. (2021). Tubulin and tubulin posttranslational modifications in alzheimer's disease and vascular dementia. *Front. Aging Neurosci.* 13, 730107. doi:10.3389/fnagi.2021.730107

Sarkar, C., Chandra, G., Peng, S., Zhang, Z., Liu, A., and AnilMukherjee, B. (2013). Neuroprotection and lifespan extension in Ppt1−/− mice by NtBuHA: Therapeutic implications for INCL. *Nat. Neurosci.* 16 (11), 1608–1617. doi:10.1038/nn.3526

Schapansky, J., Nardozzi, J. D., Felizia, F., and LaVoie, M. J. (2014). Membrane recruitment of endogenous LRRK2 precedes its potent regulation of autophagy. *Hum. Mol. Genet.* 23 (16), 4201–4214. doi:10.1093/hmg/ddu138

Schmidt, M. F., Gan, Z. Y., Komander, D., and Grant, D. (2021). Ubiquitin signalling in neurodegeneration: Mechanisms and therapeutic opportunities. *Cell Death Differ.* 28 (2), 570–590. doi:10.1038/s41418-020-00706-7

Senis, Y. A., Tomlinson, M. G., García, Á., Dumon, S., Herbert, J., Cobbold, S. P., et al. (2007). A comprehensive proteomics and genomics analysis reveals novel transmembrane proteins in human platelets and mouse megakaryocytes including G6b-B, a novel immunoreceptor tyrosine-based inhibitory motif protein. *Mol. Cell Proteomics* 6, 548–564. doi:10.1074/mcp.D600007-MCP200

Sferra, A., Nicita, F., and Bertini, E. (2020). Microtubule dysfunction: A common feature of neurodegenerative diseases. *Int. J. Mol. Sci.* 21 (19), 7354. doi:10.3390/ijms21197354

Shen, Z., Xia, Z., Liu, J., Zheng, J., Luo, Y., Yang, H., et al. (2022). APT1-Mediated depalmitoylation regulates hippocampal synaptic plasticity. *J. Neurosci.* 42 (13), 2662–2677. doi:10.1523/JNEUROSCI.1741-21.2022

Shipston, M. J. (2011). Ion Channel regulation by protein palmitoylation. *J. Biol. Chem.* 286 (11), 8709–8716. doi:10.1074/jbc.R110.210005

Singaraja, R. R., Hadano, S., Metzler, M., Scott, G., Wellington, C. L., Warby, S., et al. (2002). HIP14, a novel ankyrin domain-containing protein, links huntingtin to intracellular trafficking and endocytosis. *Hum. Mol. Genet.* 11 (23), 2815–2828. doi:10.1093/hmg/11.23.2815

Singaraja, R. R., Huang, K., Sanders, S. S., Milnerwood, A. J., Hines, R., Lerch, J. P., et al. (2011). Altered palmitoylation and neuropathological deficits in mice lacking HIP14. *Hum. Mol. Genet.* 20 (20), 3899–3909. doi:10.1093/hmg/ddr308

Stavoe, A. K. H., and Holzbaur, E. L. F. (2019). Autophagy in neurons. *Annu. Rev. Cell Dev. Biol.* 35 (1), 477–500. doi:10.1146/annurev-cellbio-100818-125242

Stowers, R. S., and Isacoff, E. Y. (2007). Drosophila huntingtin-interacting protein 14 is a presynaptic protein required for photoreceptor synaptic transmission and expression of the palmitoylated proteins synaptosome-associated protein 25 and cysteine string protein. *J. Neurosci. Official J. Soc. Neurosci.* 27 (47), 12874–12883. doi:10.1523/JNEUROSCI.2464-07.2007

Stram, A. R., and Payne, R. M. (2016). Post-translational modifications in mitochondria: Protein signaling in the powerhouse. *Cell. Mol. Life Sci.* 73 (21), 4063–4073. doi:10.1007/s00018-016-2280-4

Sugars, K. L., and Rubinsztein, D. C. (2003). Transcriptional abnormalities in Huntington disease. *Trends Genet.* 19 (5), 233–238. doi:10.1016/S0168-9525(03)00074-X

Suk, T. R., and Rousseaux, M. W. C. (2020). The role of TDP-43 mislocalization in amyotrophic lateral Sclerosis. *Mol. Neurodegener.* 15 (1), 45. doi:10.1186/s13024-020-00397-1

Sutton, L. M., Sanders, S. S., Butland, S. L., Singaraja, R. R., Franciosi, S., Southwell, A. L., et al. (2013). Hip14l-Deficient mice develop neuropathological and behavioural features of Huntington disease. *Hum. Mol. Genet.* 22 (3), 452–465. doi:10.1093/hmg/dds441

Tabaczar, S., Czogalla, A., Podkalicka, J., Biernatowska, A., and Sikorski, A. F. (2017). Protein palmitoylation: Palmitoyltransferases and their specificity. *Exp. Biol. Med.* 242 (11), 1150–1157. doi:10.1177/1535370217707732

Tamura, K., Stecher, G., and Kumar, S. (2021). MEGA11: Molecular evolutionary genetics analysis version 11. *Mol. Biol. Evol.* 38 (7), 3022–3027. doi:10.1093/molbev/msab120

Tang, M., Xia, Y., Xiao, T., Cao, R., Cao, Y., and Ouyang, B. (2022). Structural exploration on palmitoyltransferase DHHC3 from Homo sapiens. *Polymers* 14 (15), 3013. doi:10.3390/polym14153013

Tenreiro, S., Eckermann, K., and Outeiro, T. F. (2014). Protein phosphorylation in neurodegeneration: Friend or foe? *Front. Mol. Neurosci.* 7, 42. doi:10.3389/fnmol.2014.00042

The Huntington's Disease Collaborative Research Group (1993). A novel gene containing a trinucleotide repeat that is expanded and unstable on Huntington's disease chromosomes. The Huntington's Disease Collaborative Research Group. *Cell* 72 (6), 971–983. doi:10.1016/0092-8674(93)90585-E

Thinon, E., Fernandez, J. P., Molina, H., and Hang, H. C. (2018). Selective enrichment and direct analysis of protein S-palmitoylation sites. *J. Proteome Res.* 17 (5), 1907–1922. doi:10.1021/acs.jproteome.8b00002

Toyoda, T., Sugimoto, H., and Yamashita, S. (1999). Sequence, expression in Escherichia coli, and characterization of lysophospholipase II. *Biochimica Biophysica Acta (BBA) - Mol. Cell Biol. Lipids* 1437 (2), 182–193. doi:10.1016/S1388-1981(99)00007-4

Tripathi, P., Zhu, Z., Qin, H., Ahmed, E., Crivelli, S. M., Roush, E., et al. (2021). Palmitoylation of acetylated tubulin and association with ceramide-rich platforms is critical for ciliogenesis. *J. Lipid Res.* 62, 100021. doi:10.1194/jlr.RA120001190

Trojsi, F., D'Alvano, G., Bonavita, S., and Tedeschi, G. (2020). Genetics and sex in the pathogenesis of amyotrophic lateral Sclerosis (ALS): Is there a link? *Int. J. Mol. Sci.* 21 (10), 3647. doi:10.3390/ijms21103647

Türei, D., Földvári-Nagy, L., Fazekas, D., Módos, D., Kubisch, J., Kadlecsik, T., et al. (2015). Autophagy regulatory network — a systems-level bioinformatics resource for studying the mechanism and regulation of autophagy. *Autophagy* 11 (1), 155–165. doi:10.4161/15548627.2014.994346

Tyynelä, J., Palmer, D. N., Baumann, M., and Haltia, M. (1993). Storage of saposins A and D in infantile neuronal ceroid-lipofuscinosis. *FEBS Lett.* 330 (1), 8–12. doi:10.1016/0014-5793(93)80908-D

Uehara, T., Nakamura, T., Yao, D., Shi, Z.-Q., Gu, Z., Ma, Y., et al. (2006). S-nitrosylated protein-disulphide isomerase links protein misfolding to neurodegeneration. *Nature* 441 (7092), 513–517. doi:10.1038/nature04782

Ullah, M. F., Ahmad, A., Bhat, S. H., Abu-Duhier, F. M., Barreto, G. E., and Ghulam, Md A. (2019). Impact of sex differences and gender specificity on behavioral characteristics and pathophysiology of neurodegenerative disorders. *Neurosci. Biobehav. Rev.* 102, 95–105. doi:10.1016/j.neubiorev.2019.04.003

Valdez-Taubas, J., and Pelham, H. (2005). Swf1-Dependent palmitoylation of the SNARE Tlg1 prevents its ubiquitination and degradation. *EMBO J.* 24 (14), 2524–2532. doi:10.1038/sj.emboj.7600724

Vetrivel, K. S., Barman, A., Chen, Y., Nguyen, P. D., Wagner, S. L., Prabhakar, R., et al. (2011). Loss of cleavage at ß′-site contributes to apparent increase in β-amyloid peptide (Aβ) secretion by β-secretase (BACE1)-Glycosylphosphatidylinositol (GPI) processing of amyloid precursor protein. *J. Biol. Chem.* 286 (29), 26166–26177. doi:10.1074/JBC.M111.260471

Vetrivel, K. S., Meckler, X., Chen, Y., Nguyen, P. D., Seidah, N. G., Vassar, R., et al. (2009). Alzheimer disease Abeta production in the absence of S-palmitoylation-dependent targeting of BACE1 to lipid rafts. *J. Biol. Chem.* 284 (6), 3793–3803. doi:10.1074/JBC.M808920200

Virlogeux, A., Scaramuzzino, C., Lenoir, S., Carpentier, R., Louessard, M., Genoux, A., et al. (2021). Increasing brain palmitoylation rescues behavior and neuropathology in Huntington disease mice. *Sci. Adv.* 7 (14), eabb0799. doi:10.1126/sciadv.abb0799

Vitrac, H., MacLean, D. M., Karlstaedt, A., Taegtmeyer, H., Jayaraman, V., Bogdanov, M., et al. (2017). Dynamic lipid-dependent modulation of protein topology by post-translational phosphorylation. *J. Biol. Chem.* 292 (5), 1613–1624. doi:10.1074/jbc.M116.765719

Watanabe, Y., Taguchi, K., and Tanaka, M. (2020). Ubiquitin, autophagy and neurodegenerative diseases. *Cells* 9 (9), 2022. doi:10.3390/cells9092022

Wei, P. F., Zhang, Li, Nethi, S. K., Barui, A. K., Lin, J., Zhou, W., et al. (2014). Accelerating the clearance of mutant huntingtin protein aggregates through autophagy induction by europium hydroxide nanorods. *Biomaterials* 35 (3), 899–907. doi:10.1016/j.biomaterials.2013.10.024

West, A. B., Moore, D. J., Biskup, S., Bugayenko, A., Smith, W. W., Ross, C. A., et al. (2005). Parkinson's disease-associated mutations in leucine-rich repeat kinase 2 augment kinase activity. *Proc. Natl. Acad. Sci. U. S. A.* 102 (46), 16842–16847. doi:10.1073/pnas.0507360102

Wild, A. R., Hogg, P. W., Flibotte, S., Nasseri, G. G., Hollman, R. B., Abazari, D., et al. (2022). Exploring the expression patterns of palmitoylating and de-palmitoylating enzymes in the mouse brain using the curated RNA-seq database BrainPalmSeq. *ELife* 11, e75804. doi:10.7554/eLife.75804

Wild, A. R., Hogg, P. W., Flibotte, S., Kochhar, S., Hollman, R. B., Haas, K., et al. (2023). CellPalmSeq: A curated RNAseq database of palmitoylating and de-palmitoylating enzyme expression in human cell types and laboratory cell lines. *Front. Physiology* 14, 1110550. doi:10.3389/fphys.2023.1110550

Wloga, D., Joachimiak, E., and Hanna, F. (2017). Tubulin post-translational modifications and microtubule dynamics. *Int. J. Mol. Sci.* 18 (10), 2207. doi:10.3390/ijms18102207

Xia, Y., Prokop, S., and Giasson, B. I. (2021). 'Don't phos over tau': Recent developments in clinical biomarkers and therapies targeting tau phosphorylation in alzheimer's disease and other tauopathies. *Mol. Neurodegener.* 16 (1), 37. doi:10.1186/s13024-021-00460-5

Xu, J., Gu, W., Ji, K., Zhao, X., Zhu, H., and Zheng, W. (2018). Sequence analysis and structure prediction of ABHD16A and the roles of the ABHD family members in human disease. *Open Biol.* 8 (5), 180017. doi:10.1098/rsob.180017

Yahia, A., Elsayed, L. E. O., Valter, R., Hamed, A. A. A., Mohammed, I. N., Elseed, M. A., et al. (2021). Pathogenic variants in ABHD16A cause a novel psychomotor developmental disorder with spastic paraplegia. *Front. Neurology* 12, 720201. doi:10.3389/fneur.2021.720201

Yan, P., Liu, H., Zhou, T., Sun, P., Wang, Y., Wang, X., et al. (2022). Crosstalk of Synapsin1 palmitoylation and phosphorylation controls the dynamicity of synaptic vesicles in neurons. *Cell Death Dis.* 13 (9), 786. doi:10.1038/s41419-022-05235-4

Yanai, A., Huang, K., Kang, R., Singaraja, R. R., Arstikaitis, P., Gan, Lu., et al. (2006). Palmitoylation of huntingtin by HIP14 is essential for its trafficking and function. *Nat. Neurosci.* 9 (6), 824–831. doi:10.1038/NN1702

Yeh, D. C., Duncan, J. A., Yamashita, S., and Michel, T. (1999). Depalmitoylation of endothelial nitric-oxide synthase by acyl-protein thioesterase 1 is potentiated by Ca(2+)-calmodulin. *J. Biol. Chem.* 274 (46), 33148–33154. doi:10.1074/jbc.274.46.33148

Yokoi, N., Fukata, Y., Sekiya, A., Murakami, T., Kobayashi, K., and Fukata, M. (2016). Identification of PSD-95 depalmitoylating enzymes. *J. Neurosci.* 36 (24), 6431–6444. doi:10.1523/JNEUROSCI.0419-16.2016

Young, F. B., Butland, S. L., Sanders, S. S., Sutton, L. M., and Hayden., M. R. (2012). Putting proteins in their place: Palmitoylation in Huntington disease and other neuropsychiatric diseases. *Prog. Neurobiol.* 97 (2), 220–238. doi:10.1016/j.pneurobio.2011.11.002

Yu, W. H., Kumar, A., Peterhoff, C., Kulnane, L. S., Uchiyama, Y., Lamb, B. T., et al. (2004). Autophagic vacuoles are enriched in amyloid precursor protein-secretase activities: Implications for β-amyloid peptide over-production and localization in alzheimer's disease. *Int. J. Biochem. Cell Biol.* 36 (12), 2531–2540. doi:10.1016/j.biocel.2004.05.010

Zaballa, M., and van der Goot, G. F. (2018). The molecular era of protein S-acylation: Spotlight on structure, mechanisms, and dynamics. *Crit. Rev. Biochem. Mol. Biol.* 53 (4), 420–451. doi:10.1080/10409238.2018.1488804

Zaręba-Kozioł, M., Bartkowiak-Kaczmarek, A., Roszkowska, M., Bijata, K., Figiel, I., Halder, A. K., et al. (2021). S-palmitoylation of synaptic proteins as a novel mechanism underlying sex-dependent differences in neuronal plasticity. *Int. J. Mol. Sci.* 22 (12), 6253. doi:10.3390/ijms22126253

Zhang, W., Xu, C., Sun, J., Shen, H. M., Wang, J., and Yang, C. (2022). Impairment of the autophagy–lysosomal pathway in alzheimer's diseases: Pathogenic mechanisms and therapeutic potential. *Acta Pharm. Sin. B* 12, 1019–1040. doi:10.1016/j.apsb.2022.01.008

Zhang, X., Liang, L., Chen, S., Yang, D., Wang, Y., Zhang, X., et al. (2011). Rapamycin treatment augments motor neuron degeneration in SOD1 G93A mouse model of amyotrophic lateral Sclerosis. *Autophagy* 7 (4), 412–425. doi:10.4161/auto.7.4.14541

Zhang, Z., Lee, Yi-C., Kim, S.-Jo, Choi, M. S., Tsai, P.-C., Xu, Y., et al. (2006). Palmitoyl-protein thioesterase-1 deficiency mediates the activation of the unfolded protein response and neuronal apoptosis in INCL. *Hum. Mol. Genet.* 15 (2), 337–346. doi:10.1093/hmg/ddi451

Zou, L., Tian, Y., and Zhang, Z. (2021). Dysfunction of synaptic vesicle endocytosis in Parkinson's disease. *Front. Integr. Neurosci.* 15, 619160. doi:10.3389/fnint.2021.619160

Frontiers in Physiology

Understanding how an organism's components work together to maintain a healthy state

The second most-cited physiology journal, promoting a multidisciplinary approach to the physiology of living systems - from the subcellular and molecular domains to the intact organism and its interaction with the environment.

Discover the latest Research Topics

See more →

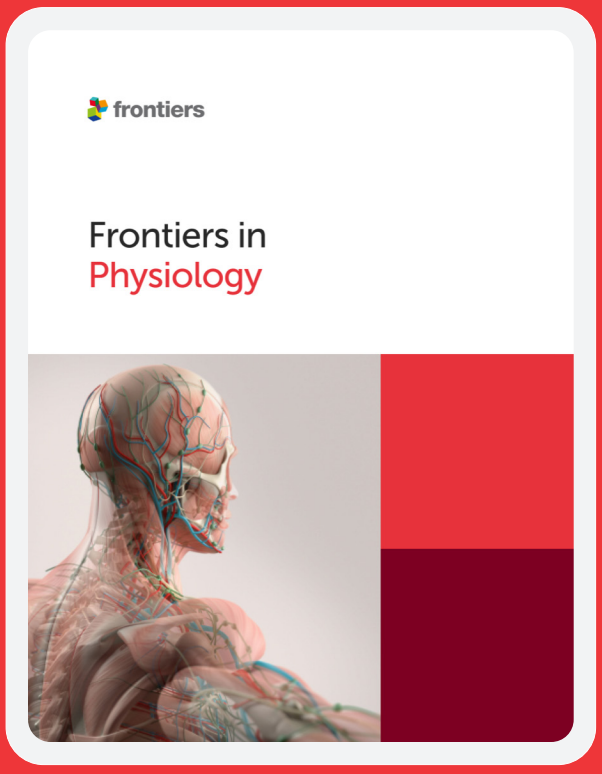

Frontiers

Avenue du Tribunal-Fédéral 34
1005 Lausanne, Switzerland
frontiersin.org

Contact us

+41 (0)21 510 17 00
frontiersin.org/about/contact